FROM STRUCTURE TO SIGNALOSOMES: NEW PERSPECTIVES ABOUT MEMBRANE RECEPTORS AND CHANNELS

EDITED BY: Yi Ma, Kai He and Gerald A. Berkowitz

PUBLISHED IN: Frontiers in Plant Science

frontiers Research Topics

frontiers

ISSN 1664-8714
ISBN 978-2-88945-973-5
DOI 10.3389/978-2-88945-973-5

About Frontiers

Frontiers is more than just an open-access publisher of scholarly articles: it is a pioneering approach to the world of academia, radically improving the way scholarly research is managed. The grand vision of Frontiers is a world where all people have an equal opportunity to seek, share and generate knowledge. Frontiers provides immediate and permanent online open access to all its publications, but this alone is not enough to realize our grand goals.

Frontiers Journal Series

The Frontiers Journal Series is a multi-tier and interdisciplinary set of open-access, online journals, promising a paradigm shift from the current review, selection and dissemination processes in academic publishing. All Frontiers journals are driven by researchers for researchers; therefore, they constitute a service to the scholarly community. At the same time, the Frontiers Journal Series operates on a revolutionary invention, the tiered publishing system, initially addressing specific communities of scholars, and gradually climbing up to broader public understanding, thus serving the interests of the lay society, too.

Dedication to Quality

Each Frontiers article is a landmark of the highest quality, thanks to genuinely collaborative interactions between authors and review editors, who include some of the world's best academicians. Research must be certified by peers before entering a stream of knowledge that may eventually reach the public - and shape society; therefore, Frontiers only applies the most rigorous and unbiased reviews.
Frontiers revolutionizes research publishing by freely delivering the most outstanding research, evaluated with no bias from both the academic and social point of view. By applying the most advanced information technologies, Frontiers is catapulting scholarly publishing into a new generation.

What are Frontiers Research Topics?

Frontiers Research Topics are very popular trademarks of the Frontiers Journals Series: they are collections of at least ten articles, all centered on a particular subject. With their unique mix of varied contributions from Original Research to Review Articles, Frontiers Research Topics unify the most influential researchers, the latest key findings and historical advances in a hot research area! Find out more on how to host your own Frontiers Research Topic or contribute to one as an author by contacting the Frontiers Editorial Office: researchtopics@frontiersin.org

FROM STRUCTURE TO SIGNALOSOMES: NEW PERSPECTIVES ABOUT MEMBRANE RECEPTORS AND CHANNELS

Topic Editors:
Yi Ma, University of Connecticut, United States
Kai He, Lanzhou University, China
Gerald A. Berkowitz, University of Connecticut, United States

Citation: Ma, Y., He, K., Berkowitz, G. A., eds. (2019). From Structure to Signalosomes: New Perspectives About Membrane Receptors and Channels. Lausanne: Frontiers Media. doi: 10.3389/978-2-88945-973-5

Table of Contents

frontiers in Plant Science

EDITORIAL
published: 22 May 2019
doi: 10.3389/fpls.2019.00682

Editorial: From Structure to Signalsomes: New Perspectives About Membrane Receptors and Channels

Yi Ma[1]*, *Kai He*[2] and *Gerald A. Berkowitz*[1]*

[1] Plant Science, University of Connecticut, Mansfield, CT, United States, [2] School of Life Sciences, Lanzhou University, Lanzhou, China

Keywords: ion channels, signalosome, stress response and growth, signal transduction, membrane receptors

OPEN ACCESS

Edited by:
Kendal Hirschi,
Baylor College of Medicine,
United States

Reviewed by:
Roberto Adrian Gaxiola,
Arizona State University, United States
June M. Kwak,
Daegu Gyeongbuk Institute of Science and Technology (DGIST), South Korea
Wayne Versaw,
Texas A&M University, United States

***Correspondence:**
Yi Ma
yi.ma@uconn.edu
Gerald A. Berkowitz
gerald.berkowitz@uconn.edu

Specialty section:
This article was submitted to Plant Traffic and Transport, a section of the journal Frontiers in Plant Science

Received: *09 April 2019*
Accepted: *06 May 2019*
Published: *22 May 2019*

Citation:
Ma Y, He K and Berkowitz GA (2019) Editorial: From Structure to Signalsomes: New Perspectives About Membrane Receptors and Channels. Front. Plant Sci. 10:682. doi: 10.3389/fpls.2019.00682

Editorial on the Research Topic

From Structure to Signalsomes: New Perspectives About Membrane Receptors and Channels

The plasma membrane (PM) forms a selective barrier between the interior of the cell and the external environment. The PM structure and constituents can act as a sentry to facilitate perception of changes in the environment to trigger intricate signaling cascades, leading to fine-tuned adaptive responses. The PM contains a plethora of proteins that are channels, transporters, receptors or enzymes. These proteins are involved in a number of cell activities such as the following: (a) transport of molecules or other substances across the plasma membrane, (b) perception of external environmental cues that cause perturbations in plant homeostasis (for example, temperature stress and salinity), and (c) patterning the cellular response to internal (plant) signal molecules such as hormones or peptides. In these cases of PM function, the transduction of signal perception orchestrates downstream events in the cytosol that modify cell function to respond to the signal (Palme, 2012). The proteins could function together as a signalosome in a discreet functional unit (a plasma membrane "nanodomain") to facilitate the signal transduction processes that are responsible for plant growth and development or defense responses (Tapken and Murphy, 2015).

This Frontiers Research Topic have compiled a collection of cutting-edge research articles and up to date reviews on the study of plasma membrane proteins that are involved in abiotic or biotic stress, cell growth and plant development. The article collection that composes this Research Topic includes 13 original research articles, one review and one perspective. Contributions were made by 115 authors from Australia, China, Denmark, Italy, Tunisia, United Arab Emirates, and the United States.

Regulation of plasma membrane transporters is crucial for ion homeostasis in plants under a variety of abiotic stress conditions. Hazzouri et al. identified the *HKT1;5* gene and its associated QTL in barley. This work provides new insights on the breeding of salt tolerant barley. Among the small grains, this crop is often grown in soil with saline stress. Another HKT member in rice, OsHKT2;4, was shown to be a low-affinity Mg^{2+} transporter that mediates Mg^{2+} homeostasis under high Mg^{2+} conditions (Zhang et al.). In addition, Yan et al. demonstrated that Mg^{2+} transporters MGT6 and MGT7 has additive dual functions in plant adaptation to a low Mg^{2+} environment and detoxification of excess Mg^{2+} under high Mg^{2+} conditions. Niu et al. showed that the lipid flippase activity of the P_4-type ATPase ALA6 plays a critical role for membrane stability under heat stress. Yu et al. demonstrated that overexpression of poplar ABA receptors *PtPYRL1* or *PtPYRL5* significantly enhanced cold, drought, and osmotic tolerance in poplar trees.

Cyclic nucleotide-gated ion channels (CNGCs) and Ca^{2+} have been shown to play vital roles in plant defense responses to various pathogens (Ma and Berkowitz, 2011; Moeder et al., 2011). Zhang et al. showed that silencing of tomato *CNGC1* and *CNGC14* enhanced *Xanthomonas oryzae* pv. *oryzicola* (*Xoc*) induced hypersensitive responses and non-host resistance to *Xoc*, suggesting a negative regulatory role of these CNGCs in non-host resistance and basal immune responses (also referred to as pathogen associated molecular pattern (PAMP)-triggered immunity). Studies have revealed contradictory roles of CNGCs in pathogen resistance; clearly this ion channel-mediated signal transduction system responding to pathogen perception should be the focus of further studies in the future to better understand how Ca^{2+} and CNGCs regulate plant immune defense responses to microbial pathogens.

Plasma membrane localized transporters and receptors regulate hormone mediated cell elongation. Among the transporters facilitating this signaling are the PIN-FORMED (PIN) family of auxin transporters. Ni et al. showed that *S*-nitrosoglutathione-regulated PIN2 endocytosis is important for root elongation. Some members of the large family of leucine-rich repeat receptor-like kinases (LRR-RLKs) act as receptors for hormones and peptides; in some cases these receptors can transduce developmental signals into altered cell growth. Among these LRR-RLKs involved in facilitating peptide signals and modulating growth is ERECTA. Qu et al. demonstrated that ERECTA regulates hypocotyl elongation by activating auxin biosynthesis. In another study of ERECTA, in this case focusing on shade avoidance, Du et al. showed that under shade, ERECTA-regulated hypocotyl elongation is controlled by both auxin and gibberellins.

Yang et al. and Li et al. employed transcriptomic approaches to reveal genes involved in Ca^{2+} regulated peanut pod development, which could also be regulated by hormonal signaling. Ca^{2+} signaling is involved as a secondary cytosolic messenger responding to ligand perception by cell membrane receptors in myriad signal transduction pathways, including those responding to pathogen perception during defense response, and in response to hormone/peptide cues patterning growth and development. One such signaling pathway that impacts cell expansion involves the tyrosine-sulfated pentapeptide phytosulfokine (PSK) acting as a peptide hormone signal that activates cell responses upon binding to its cognate LRR-RLK receptor PSKR1. Irving et al. focused on the signaling pathway activated by PSKR1 perception of the PSK ligand in a review of a subset of LRR-RLK cell membrane receptors. Irving et al. noted that, in addition to having cytosol kinase domains that facilitate downstream signaling, PSKR1 (and similar LRR-RLKs) also facilitate downstream signaling involving cGMP generation and CNGC activation which then leads to cytosolic Ca^{2+} elevation. Irving et al. provide some insightful context for signaling in presenting the PSK/PSKR1 interaction as impacting other membrane proteins beyond CNGCs. They point out that PSKR1 is thought to function as a complex with other proteins including the coreceptor BAK1, a CNGC, and the cell membrane proton pumps AHA1 and AHA2. These proteins might act as a unit, or signalosome in a nanodomain at the cell surface.

A peptide hormone/LRR-RLK cell membrane receptor signaling pathway similar to PSK/PSKR1 involves another tyrosine-sulfated peptide, PSY1, and its cognate receptor PSY1R. Oehlenschlæger et al. studied PSY1-dependent transphosphorylation of residues in the activation loop of PSY1R, which are critical for the activation of the receptor and downstream signaling. They demonstrated that PSY1R activation involves interaction (transphosphorylation) with the BAK1 coreceptor (and other members of the BAK1 membrane protein family) in a fashion similar to PSKR1. Intriguingly, signaling by the PSKR1 and PSY1R receptors also involves activation of a cell membrane proton pump [in this case, only AHA1; (Fuglsang et al., 2014)], and both receptors are involved in cell expansion activated during developmental programs in plants. The two pathways downstream from these receptors are also involved in signaling that leads to plant defense against pathogen invasion (Mosher and Kemmerling, 2013). Gao et al. studied another aspect of the coreceptor BAK1 involvement in immune signaling. In their study, they found that some signal associated with light interacts with programmed cell death; one possible downstream outcome from immune signaling. The immune responses involving BAK1 as an upstream component were found to involve proteins of the salicylic acid signaling pathway.

Gehring and Turek summarized the current progress of work on cyclic nucleotide monophosphates (cAMP and cGMP), which activate CNGCs. And, as mentioned above, Irving et al. provided a review and perspectives on the research of cyclic nucleotides using cGMP and PSKR1 as an example. Although the presence of plant nucleotide cyclases that synthesize cAMP and cGMP in plant cells is still controversial, more and more evidence supports their roles in numerous signal transduction pathways in plant cells; the focus of some of the contributions to this Research Topic.

More than 80% of the global population live in poverty; most of this problem can be attributed to adverse agricultural conditions such as salinity, drought, lack of nutrition, temperature stress or pathogen infection. The studies included in this Research Topic could provide new insights on how to solve or ameliorate such problems through the modifications of traits controlled by certain genes.

AUTHOR CONTRIBUTIONS

YM wrote the editorial article. GB edited and modified the article. KH proofread the article.

REFERENCES

Fuglsang, A. T., Kristensen, A., Cuin, T. A., Schulze, W. X., Persson, J. R., Thuesen, K. H., et al. (2014). Receptor kinase-mediated control of primary active proton pumping at the plasma membrane. *Plant J.* 80, 951–964. doi: 10.1111/tpj.12680

Ma, W., and Berkowitz, G. A. (2011). Ca^{2+} conduction by plant cyclic nucleotide-gated channels and associated signaling components in pathogen defense signal transduction cascades. *New. Phytol.* 190, 566–572. doi: 10.1111/j.1469-8137.2010.03577.x

Moeder, W., Urquhart, W., Ung, H., and Yoshioka, K. (2011). The role of cyclic nucleotide-gated ion channels in plant immunity. *Mol. Plant* 4, 442–452. doi: 10.1093/mp/ssr018

Mosher, S., and Kemmerling, B. (2013). PSKR1 and PSY1R-mediated regulation of plant defense responses. *Plant Signal. Behav.* 8:e24119. doi: 10.4161/psb.24119

Palme, K. (2012). *Signals and Signal Transduction Pathways in Plants*. Dordrecht: Springer. doi: 10.1007/978-94-011-0239-1

Tapken, W., and Murphy, A. S. (2015). Membrane nanodomains in plants: capturing form, function, and movement. *J. Expt. Bot.* 66, 1573–1586. doi: 10.1093/jxb/erv054

Conflict of Interest Statement: The authors declare that the research was conducted in the absence of any commercial or financial relationships that could be construed as a potential conflict of interest.

frontiers in Plant Science

PERSPECTIVE
published: 28 March 2018
doi: 10.3389/fpls.2018.00415

Moonlighting Proteins and Their Role in the Control of Signaling Microenvironments, as Exemplified by cGMP and Phytosulfokine Receptor 1 (PSKR1)

Helen R. Irving[1,2], David M. Cahill[3] and Chris Gehring[4]*

[1] Monash Institute of Pharmaceutical Sciences, Monash University, Melbourne, VIC, Australia, [2] La Trobe Institute for Molecular Science, La Trobe University, Bendigo, VIC, Australia, [3] Faculty of Science Engineering and Built Environment, Deakin University, Geelong, VIC, Australia, [4] Department of Chemistry, Biology and Biotechnology, University of Perugia, Perugia, Italy

Signal generating and processing complexes and changes in concentrations of messenger molecules such as calcium ions and cyclic nucleotides develop gradients that have critical roles in relaying messages within cells. Cytoplasmic contents are densely packed, and in plant cells this is compounded by the restricted cytoplasmic space. To function in such crowded spaces, scaffold proteins have evolved to keep key enzymes in the correct place to ensure ordered spatial and temporal and stimulus-specific message generation. Hence, throughout the cytoplasm there are gradients of messenger molecules that influence signaling processes. However, it is only recently becoming apparent that specific complexes involving receptor molecules can generate multiple signal gradients and enriched microenvironments around the cytoplasmic domains of the receptor that regulate downstream signaling. Such gradients or signal circuits can involve moonlighting proteins, so called because they can enable fine-tune signal cascades via cryptic additional functions that are just being defined. This perspective focuses on how enigmatic activity of moonlighting proteins potentially contributes to regional intracellular microenvironments. For instance, the proteins associated with moonlighting proteins that generate cyclic nucleotides may be regulated by cyclic nucleotide binding directly or indirectly. In this perspective, we discuss how generation of cyclic nucleotide-enriched microenvironments can promote and regulate signaling events. As an example, we use the phytosulfokine receptor (PSKR1), discuss the function of its domains and their mutual interactions and argue that this complex architecture and function enhances tuning of signals in microenvironments.

Keywords: calcium, cyclic nucleotides, cyclic GMP (cGMP), kinases, intracellular signals, microenvironment, molecular crowding, phytosulfokine receptor (PSKR1)

OPEN ACCESS

Edited by:
Yi Ma,
University of Connecticut,
United States

Reviewed by:
Ian Max Møller,
Aarhus University, Denmark
John Hancock,
University of the West of England,
United Kingdom

****Correspondence:***
Helen R. Irving
h.irving@latrobe.edu.au

Specialty section:
This article was submitted to Plant Traffic and Transport, a section of the journal Frontiers in Plant Science

Received: *21 August 2017*
Accepted: *14 March 2018*
Published: *28 March 2018*

Citation:
Irving HR, Cahill DM and Gehring C (2018) Moonlighting Proteins and Their Role in the Control of Signaling Microenvironments, as Exemplified by cGMP and Phytosulfokine Receptor 1 (PSKR1). Front. Plant Sci. 9:415. doi: 10.3389/fpls.2018.00415

INTRODUCTION

Often, despite the beautiful illustrations from Goodsell (1993, 2016), it is forgotten how crowded it is within the cytoplasmic space (Fulton, 1982). The term molecular crowding is used to indicate that 25 to 40% of space in the cytoplasm is occupied by many different, large biomolecules (**Figure 1A**). The number of individual biomolecules is estimated to range from 10 to 1000 molecules per cell

(Srere, 1967; Luby-Phelps, 2000; Ellis, 2001). Water is closely associated with the surface of large biomolecules while the flow apart from this encasing layer reflects diffusion (Srere, 1980, 1981, 2000; Saenger, 1987; Luby-Phelps, 2000, 2013; Ellis, 2001; Saxton, 2012; Phillip and Schreiber, 2013).

In plant cells, the cytoplasm is found in a relatively narrow layer between the plasma membrane and large organelles such as the vacuole, compounding the problem of molecular crowding. Underlying the plasma membrane is a network of cytoskeletal proteins that support and interact with other proteins, and are involved in organelle movement (Williamson, 1993; Shimmen, 2007; Goldstein and van de Meert, 2015). Cytoplasmic streaming involves various biophysical pathways resulting in movement that can be along cellular edges or alternatively create turbulence throughout the cytoplasm (Goldstein and van de Meert, 2015). Over short distances diffusion of small molecules is faster than cytoplasmic streaming (Vestergaard et al., 2012). However, if the small molecules have affinity to large biomolecules, they may have restricted capacity to diffuse (Geremia et al., 2006).

Molecular crowding occurs despite the limited copies of individual proteins present (Luby-Phelps, 2000, 2013; Ellis, 2001), so correct spatial arrangements of individual enzymes is necessary for signals to be relayed through signal networks to elicit cellular responses. Several metabolic pathways or metabolons employ molecular channeling to efficiently deliver the product from the first enzyme to form the substrate for the next enzyme (Srere, 1985, 2000; Miles et al., 1999; Winkel, 2004; Moller, 2010; Sweetlove and Fernie, 2013; Zhang et al., 2017). Correct positioning of individual enzymes and scaffold proteins enhances signal cascades via molecular channeling (Rohwer et al., 1998; Wheeldon et al., 2016). Positioning in this way creates subcellular microenvironments containing micro-cues of concentrated signaling molecules that in turn activate downstream points of signal cascades, thereby emphasizing the importance of spatial and temporal regulation of protein expression.

The crowded intracellular space combined with cellular compartmentalization and intracellular molecular gradients, have led biological systems toward microenvironments (or localized signaling circuits). We propose that a component of these signaling circuits are moonlighting proteins. In a general sense, moonlighting proteins are proteins that can perform more than one function and/or act in more than one spot in the cell (Jeffery, 2003, 2009, 2014). Examples of the latter type of moonlighting proteins include various mitochondrial proteins that also act in the nucleus (Monaghan and Whitmarsh, 2015) where they contribute to cellular signaling pathways. It is thought that during evolution, ancestral proteins have acquired additional functions including transcriptional regulation and signal transduction. For instance, it has been suggested that many of the newly emerging RNA-binding proteins are moonlighting as they have enzymatic activities, for example in metabolism, as well as functioning as regulators of transcription and RNA turnover (Hentze and Preiss, 2010; Marondedze et al., 2016b). In this perspective, we will concentrate on moonlighting proteins with roles in signal transduction. Many of these moonlighting proteins are receptor kinases that contain a cytosolic main function, a kinase, and an additional cryptic function, a cyclase (Wong and Gehring, 2013; Wong et al., 2015). The spatial arrangement of these two domains is somewhat unexpected and since both enzymatic activities are affected by second messengers such as calcium ions and the catalytic product of each domain, these moonlighting proteins are likely to serve as molecular tuners. For these reasons, we propose that such moonlighting signaling proteins are well-suited to operate in or generate subcellular microenvironments containing ions or small molecules that provide points of control in signal cascades (**Figure 1B**). Concepts of metabolons and molecular crowding are well-established while the concept of proteins generating their own small molecule microenvironmental regulatory milieu is less established. This perspective focuses on recent advances in cGMP signaling in plants, and how enigmatic activity of moonlighting proteins can contribute to regional intracellular microenvironments. First, we discuss the importance of small incremental changes in cGMP microenvironments and then we use the phytosulfokine receptor (PSKR1) as an example of a moonlighting protein that generates phospho- and cGMP-microenvinvironments.

SIGNAL STRENGTH AND SPECIFICITY

A considerable body of literature exists on the biological functions and mechanisms of action of cyclic nucleotide signaling in lower and higher eukaryotes (Lemtiri-Chlieh et al., 2011). In fact, cGMP and cAMP are accepted as key signaling molecules in developmental and environmental stress response cascades. However, acceptance that cyclic nucleotides have such a role in plant signaling was slow. One reason was that, in plants, cellular cyclic nucleotide levels seem generally lower than in

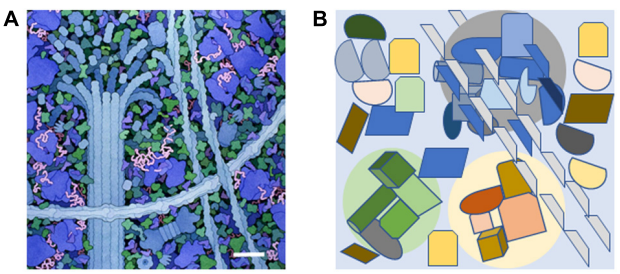

FIGURE 1 | The molecularly crowded cytoplasm and the presence of small signal-enriched microenvironments within the cytoplasm. **(A)** A small portion of the cytoplasm depicting molecular crowding as illustrated by David S. Goodsell, the Scripps Research Institute. Cytoskeletal components are shown along with ribosomes (large blue molecules). The scale bar = 30 nm and is based on the measured width of ribosomes (Haga et al., 1970). **(B)** Diagram showing how specific signal-enriched areas can occur in the cytoplasm. Three areas with different micro-enriched signals (gray, pale green, and pale yellow) are depicted that affect separate groups of proteins and represent areas with diameters of 100–200 nm. The microenvironments may be created by proteins within the group or generated from external sources such as ion fluxes from internal organelles or the extracellular environment.

animals or lower eukaryotes (Newton et al., 1999; Gehring, 2010; Marondedze et al., 2017). An additional reason for the initially reluctant acceptance of these signaling molecules in higher plants was that molecular evidence for mononucleotide cyclases in higher plants only came after the first plant draft genome was published in 2000 (Ludidi and Gehring, 2003). Since the publication of the first mononucleotide cyclase, the number of identified and experimentally tested mononucleotide cyclases has increased steadily and there are indications that there are >50 candidate cyclases in the *Arabidopsis thaliana* proteome and that they come in many different domain organizations (Meier et al., 2007; Wong and Gehring, 2013). The multitude of candidates and domain partners points to a diverse spectrum of biological functions for mononucleotide cyclases and their catalytic products.

Invariably the question of how a single messenger, like cAMP or cGMP, is capable of triggering highly specific responses to different developmental and/or environmental stimuli arises. It seems obvious that saturating the cell with either cAMP or cGMP cannot be the answer. To illustrate the point, such an approach would be like attempting to regulate traffic flow in a city with only one "gigantic traffic light" that is either red or green. Since the "gigantic traffic light" is unlikely to work, two solutions come to mind. One solution relies on strict compartmentalization of the messenger(s) and the other on the combination and integration of several messengers, e.g., cAMP/cGMP with cytoplasmic calcium ions and/or pH. A recent review has highlighted the interplay of calcium ion signatures with cGMP in plant–microbe interactions (Yuan et al., 2017). Specific response signatures and cooperation between messengers arises through spatial clustering of stimulus-dependent cyclases and their downstream signaling components and/or through the specific binding of the cyclic nucleotides to effector molecules such as kinases (Kwezi et al., 2011; Isner and Maathuis, 2016; Wheeler et al., 2017) or channel subunits (Hoshi, 1995; Zelman et al., 2012). A recent study using a constitutively expressed mammalian guanylate cyclase in Arabidopsis that produced intracellular cGMP levels >50-fold above normal resulted in mis-signaling and down-regulation of many proteins in systemic acquired resistance (Hussain et al., 2016). This study and others where calcium ion influxes flood intracellular compartments (Sanders et al., 2002; Yuan et al., 2017) highlight the need for transient and controlled levels of signaling molecules to generate appropriate responses to environmental and developmental stimuli within defined cytoplasmic areas or cellular compartments.

An affinity pull-down approach has been applied to obtain a cGMP-dependent interactome (Donaldson and Meier, 2013; Donaldson et al., 2016) where several of the cGMP-binding candidates have critical functions in the Calvin–Benson–Bassham cycle and the photorespiration pathway and they also contain cyclic nucleotide-binding domains. It is conceivable that the enzyme activity of these molecules may be directly or indirectly modified by cGMP. Since the Calvin–Benson–Bassham cycle is confined to the stroma of the chloroplast, we might imagine cGMP is generated specifically in the stroma to modulate these enzymes without affecting, for example, cGMP-dependent channels found in the plasma membrane of guard cells. Incidentally, it has also been demonstrated that the activity of the cGMP-binding photorespiration enzyme glycolate oxidase (GOX1) is dampened by cGMP and NO treatment. Since GOX1 produces H_2O_2 in response to *Pseudomonas* (Pst DC3000 AvrRpm1), it implicates cGMP-mediated processes in the cross-talk between NO and H_2O_2 signaling during defense responses (Donaldson et al., 2016).

If we agree that the "gigantic traffic light" does not work, we may find it easier to accept that small transients in cellular cAMP and cGMP are not a problem, but rather the solution to highly differentiated stimulus-specific cellular signaling in plants. The "gigantic traffic light" has additional implications; predominantly in relation to systems-based investigations of cAMP- and cGMP-dependent processes where the experimental set-up includes cell-permeant cyclic mononucleotides at high concentrations. Such investigations, particularly at the system level, can give insights into cyclic mononucleotide-dependent phosphoproteome (Marondedze et al., 2016a), but merely identify target rather than resolve stimulus-specific signaling cascades. In addition to the generators of the cyclic nucleotide signal, we must also consider the signal-off state. The role and, to this date, lack of genetic evidence for suitable phosphodiesterases that degrade cyclic nucleotides to mononucleotide phosphates has been excellently reviewed (Grosse and Durner, 2016). To generate greater insights into the formation of subcellular microenvironments, specific signaling pathways need to be examined in detail as complex interactions are likely between proteins and the immediate microenvironment (**Figure 1B**). Below we describe the evidence supporting the formation of a subcellular microenvironment surrounding the moonlighting phytosulfokine receptor (PSKR1) as an example of how plants may utilize enigmatic enzymatic centers in homeostatic function.

PSKR1 AND THE FORMATION OF MICROENVIRONMENTS

Phytosulfokine (PSK) was first discovered as a secreted sulfated pentapeptide promoting growth in cell cultures and the receptor via ligand-based affinity chromatography (Matsubayashi and Sakagami, 1996; Matsubayashi et al., 2002). Characterization of PSK:PSKR1 ligand-receptor interactions has shown that they have extensive roles in plant growth and development (Wheeler and Irving, 2010; Matsubayashi, 2014; Sauter, 2015). PSKR1 is a member of the leucine-rich repeat receptor like kinase family that typically contain a large extracellular ligand-binding domain composed of leucine-rich repeats, a single transmembrane spanning domain and an intracellular catalytic kinase domain (Matsubayashi et al., 2002). There are five genes encoding PSK that are expressed in different tissues of the plant (Matsubayashi et al., 2006). Active PSK needs to be sulfated and this is achieved by tyrosylprotein sulfotransferase (TPST) found in the Golgi apparatus. Genetic approaches have been a powerful tool used to study PSK:PSKR interactions in plants and much of this work has been carried out in Arabidopsis. All sulfated residues are removed in *tpst* mutants as TPST is the single enzyme catalyzing sulfation of tyrosine residues in Arabidopsis,

while triple knockouts of *pskr1*, *pskr2* and *pysr1* are used to create the null *pskr* receptor background. These plants show defects in growth and development. Specifically, the *pskr* null background has reduced root and shoot growth and revealed that the PSK:PSKR receptor system is involved in promoting root and shoot growth in addition to roles in development of xylem vessels and pollen tubes (Sauter, 2015). Analysis of plant pathogen interactions has revealed that PSKR also has roles in protecting plants. While plant growth is promoted by PSK, pattern-triggered immune responses such as those activated by the biotrophic bacteria *Pseudomonas syringae* are attenuated by PSK (Igarashi et al., 2012). Interestingly, although the *pskr* or *tpst* null mutants are more resistant to biotrophic pathogens such as *P. syringae*, the oomycete *Hyaloperonospora arabidopsidis* and the nematode *Meloidogyne incognita*, they are more susceptible to necrotrophic pathogens such as the fungus *Alternaria brassicicola* (Mosher et al., 2013; Rodiuc et al., 2016). One of the features biotrophic pathogens have in common is that on penetrations of host cells, they stimulate the formation of specialized cell structures (e.g., haustoria) and it appears that these pathogens have co-opted the PSK signaling system to promote cell differentiation (Rodiuc et al., 2016). Moreover, PSK is expressed in nodules in *Lotus japonicus* and application of exogenous PSK increases nodule numbers (Wang C. et al., 2015) where rhizobia may be co-opting PSK in the formation of the specialized nodule.

Binding of PSK to PSKR1 stimulates allosteric changes throughout the receptor resulting in heterodimerization interactions with other integral membrane proteins such as the somatic embryogenesis receptor-like kinase (SERKs) including BRI1-associated receptor kinase (BAK1)/SERK3 (Wang J. et al., 2015). Leucine-rich repeat receptor like kinase homo- and heterodimerization is well-established following the characterization of the brassinosteroid receptor brassinosteroid insensitive 1 (BRI1) (Clouse, 2011). Similarly, the damage ligand, AtPep1, binds to its leucine-rich repeat receptor like kinase, PEPR1, and causes heterodimerization with BAK1 (Tang et al., 2015). BAK1 is a promiscuous molecule that was first discovered associated with BRI1 but also interacts with many other LRR RLKs (Chinchilla et al., 2009). Life time fluorescence imaging revealed that PSKR1 interacted with H^+-ATPases AHA1 and AHA2 and also BAK1 to form a receptor complex (Ladwig et al., 2015). This complex involving PSKR1, BAK1, AHA1, and AHA2 also associates with the cyclic nucleotide-gated cation channel 17 (CNGC17) although PSKR1 does not directly bind to it (Ladwig et al., 2015). Since CNGC17 is regulated by calmodulin and cGMP (Zelman et al., 2012; Fischer et al., 2013, 2017), there is a possibility that a localized receptor complex microenvironment involving calcium ions and possibly cyclic nucleotides such as cGMP is generated (**Figure 2**).

In vitro studies provided the first clues that PSKR1 may form subcellular microenvironments containing cGMP. Within the kinase domain of PSKR1 is a sequence motif predictive of a guanylate cyclase center (Kwezi et al., 2007). Studies using recombinant cytoplasmic domains of PSKR1 revealed that the protein could indeed produce cGMP albeit at low levels that were enhanced with additional calcium ions (Kwezi et al., 2011; Muleya et al., 2014, 2016). Both BRI1 and PEPR1 also have a similar guanylate cyclase center that can generate cGMP (Kwezi et al., 2007; Qi et al., 2010; Wheeler et al., 2017). Initial studies used a small recombinant fragment of the BRI1 kinase domain containing the guanylate cyclase center that showed cGMP generation (Kwezi et al., 2007) although a later study using most of the kinase domain failed to show cGMP production (Bojar et al., 2014). However, a more sensitive detection method has since demonstrated cGMP production by the full length BRI1 kinase domain (Wheeler et al., 2017). Notably, this recombinant protein also contained the N and C terminal regions necessary for homodimerization (Bojar et al., 2014) that has been predicted to be necessary for the catalytic conversion of GTP to cGMP (Freihat et al., 2014; Muleya et al., 2016). Arabidopsis mesophyll protoplasts treated with exogenous application of PSK generated increased cGMP levels compared to the controls treated with the non-sulfated backbone PSK pentapeptide (Kwezi et al., 2011). Furthermore, transfection of protoplasts with full-length PSKR1 considerably raised basal levels of cGMP (Kwezi et al., 2011). In addition, the ligand for PEPR1, Pep1, stimulates intracellular increases in cGMP measured using an *in vivo* cGMP reporter in root cells (Ma et al., 2012). Within the catalytic guanylate cyclase center, G924 in PSKR1 is predicted to have roles in determining substrate specificity for GTP (Sunahara et al., 1998; Tucker et al., 1998; Wong and Gehring, 2013; Wong et al., 2015). When glycine is mutated to lysine (G924K), cGMP production is reduced *in vitro* (Kwezi et al., 2011; Muleya et al., 2014). Complementation studies with this full length mutant in the *pskr* null background showed that it could not restore root growth (Ladwig et al., 2015). However, although the G924K mutant did not significantly impair phosphorylation of the SOX substrate (Muleya et al., 2014), it was unable to phosphorylate myelin basic protein (Kaufmann et al., 2017), so questions arise about its ability to properly phosphorylate PSKR1 downstream substrates *in vivo*.

Phosphorylation has long been recognized as a means of regulation of proteins as the number and specific residues phosphorylated create ionic enriched micro-environments. Like BRI1, PSKR1 is a dual kinase with the ability to phosphorylate tyrosine as well as threonine and serine residues (Oh et al., 2009; Muleya et al., 2016) and has a complex autophosphorylation profile involving dimerization (Hartmann et al., 2015; Muleya et al., 2016). Complementation studies with the PSKR1 kinase inactive mutant K762E in the *pskr* null background demonstrated that kinase activity is essential for root and shoot growth (Hartmann et al., 2014). The phosphorylation status of PSKR1 is important in regulating the guanylate cyclase activity as well as its kinase activity. For instance, phosphorylated mimetic mutations of phosphorylated serine residues located at the juxtamembrane region enhance kinase activity *in vitro* and also have differential effects on growth, promoting growth in the root but not the shoot (Muleya et al., 2016; Kaufmann et al., 2017). Interestingly, the mimetic non-phosphorylated mutation decreases kinase activity and both mutations are associated with a lack of guanylate cyclase activity, whereas other mutations that modify kinase activity (Y888E or Y888F) have little effect on guanylate cyclase activity (Muleya et al., 2016). These differences may be related to the ability of the phospho-mimetic mutants to form homodimers,

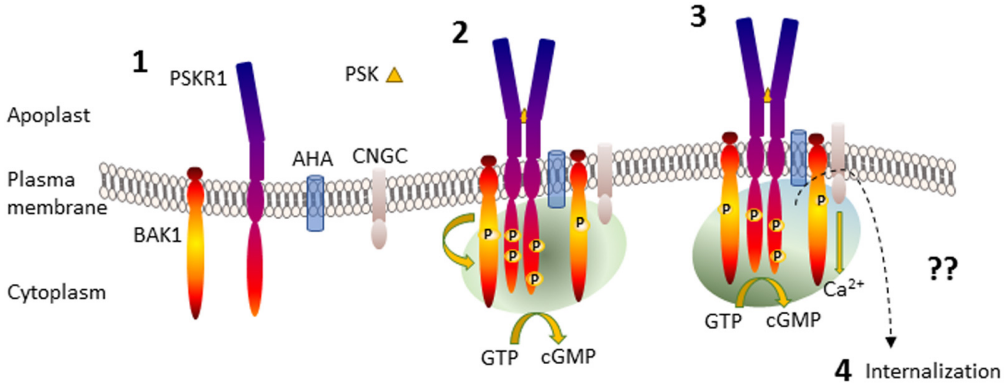

FIGURE 2 | Generation of PSKR1 activated subcellular cGMP enriched-microenvironment. Part 1 shows the anchoring of the proteins in the plasma membrane. Part 2 shows PSK binding to the ligand-binding domain of PSKR1 and receptor dimerization with BAK1 and phosphorylation, formation of an association with AHA and CNGC and the generation of a microenvironment containing cGMP generated via PSKR1 (green shading) although other sources are possible. Part 3 depicts the activation of CNGC and development of an additional calcium ion microenvironment surrounding the receptor complex (blue shading) that enhances cGMP production, which in turn inhibits kinase activity. Part 4 is not depicted and represents receptor deactivation possibly by endocytosis resulting in internalization as indicated by a dashed arrow. For further details see the text. AHA, H^+-ATPases; BAK1, BRI1 associated kinase; CNGC, cyclic nucleotide-gated channel; PSK, phytosulfokine; PSKR1, phytosulfokine receptor.

which are important at least in the tyrosine kinase activity and potentially in the guanylate cyclase activity (Muleya et al., 2016).

There appears to be considerable intramolecular crosstalk occurring as not only is kinase activity associated with specific residues being available for phosphorylation, but it is decreased by the guanylate cyclase product cGMP. Thus PSKR1 can generate an enriched environment of cGMP that in turn suppresses its predominant kinase function. The PSKR1 receptor complex also includes CNGC17 (Ladwig et al., 2015) which can be regulated by cGMP. Together these findings suggest that cGMP acts as a regional traffic signal within the PSKR1 receptor complex (**Figure 2**). BRI1 also displays a complex autophosphorylation status that impacts on its effects on growth (Clouse, 2011). Like PSKR1, cGMP inhibits kinase activity in BRI1 and certain kinase inactive mutants no longer generate any cGMP (Kwezi et al., 2011; Wheeler et al., 2017). To date, it is not known how cGMP inhibits kinase activity of PSKR1 or BRI1 but it is potentially by binding at intracellular allosteric sites on the receptors. Following activation of PSKR1 and PePR1 and association with BAK1, they are then internalized by a clathrin-dependent pathway that is important in sustaining immune responses (Mbengue et al., 2016; Rodiuc et al., 2016).

Intracellular calcium ion concentration is tightly controlled to ensure that cells can rapidly respond to specific patterns of spatial and temporal changes in calcium ion levels (Ehrhardt et al., 1996; Sanders et al., 2002; Kudla et al., 2010; Steinhorst and Kudla, 2013; Chen et al., 2015; Yuan et al., 2017). Changes in calcium ion concentration begin at localized points in the cell via influx from external sources that in turn can amplify release via both internal and further external sources generating calcium ion waves (Tuteja and Mahajan, 2007). Calcium ion concentration is returned to basal levels via various internalization mechanisms. *In vitro* studies have shown that PSKR1 can directly respond to physiological calcium ion concentrations of 0.1–10 μM via a reversible inhibition of kinase activity (Muleya et al., 2014). Notably at these same concentrations, guanylate cyclase activity is enhanced and this appears to be a reciprocal effect as lower calcium ion concentrations are associated with high kinase activity (Muleya et al., 2014). It is possible that even higher levels of calcium ions override this effect since 100 μM did not inhibit kinase activity using myelin basic protein as a substrate (Kaufmann et al., 2017). PSKR1 also contains a predicted calmodulin binding site within its kinase domain that interacts with calmodulins (Hartmann et al., 2014). Although complementation studies using PSKR1 W831S mutants in the *pskr* null background suggest that calmodulin binding is necessary for growth responses (Hartmann et al., 2014) it has since been identified that this mutation removes kinase activity (Kaufmann et al., 2017). There is a need to investigate if specific PSK signaling modulates changes in calcium ion concentrations and how these may affect the receptor and immediate surrounding microenvironment.

CONCLUSION AND FUTURE QUESTIONS

We argue that small amplitude signals have a critical part to play in plant homeostasis and that these begin with the development of micro-signaling environments within the cytoplasm that set up the potential for specific signal cascades. Such cascades are likely to exhibit skewed subcellular distribution of the moonlighting proteins and gradients of their small molecule products. Growing pollen tubes in fact have marked distribution gradients in calcium ions that are independent of cytoplasmic streaming and diffusion (Tuteja and Mahajan, 2007). Advances in spatial and concentration level detection methods will enable demonstration of the skewed distribution of the moonlighting proteins and their products which are restricted to small defined areas possibly due to affinity with other molecules that prevents their diffusion.

We have focused on how PSK signals via the PSKR1 receptor to generate a complex series of cross-talk situations on PSKR1 itself involving phosphorylation, cGMP and calcium ions that also influence other proteins such as CNGC17 present in the receptor complex (**Figure 2**). Ligand activated PSKR1 raises cGMP levels that in turn activate CNGC17 increasing calcium ion influx. The consequences of activating this moonlighting protein system are twofold. Firstly, increases in calcium ion concentration potentiate cGMP production amplifying the signal. Secondly, increases in calcium reduce kinase activity of PSKR1 (and its downstream signal cascades). However, there may be increases in activity of other kinases that are dependent on cGMP and/or calcium ion and/or calmodulin. If this is the case, then the moonlighting action of PSKR1 would be a tuner switch for two or more distinct kinase dependent cascades. How changes in calcium ions and cGMP modulate PSK signaling is not clear and will be subject of future investigation. An area that is particularly worth focusing on is how PSK signaling is modulated and switched from growth promotion, to specialized cell development and/or defense responses and the role of subcellular microenvironments in these pathways. In conjunction with these questions, we need to consider the role of phosphodiesterase and suppressors of other signaling molecules that contribute to changes in cellular microenvironments.

We predict that changes at the intracellular microenvironmental level are likely to affect more than homeostasis of individual proteins and will actually have an important part in initiating cellular signaling pathways to maintain plant function in response to rapidly changing environmental conditions and stresses. Understanding the roles of cellular microenvironments is a current focus in diverse research areas as it is now evident that the location of ribosomes influences the mRNA that will be translated and the post-translation modifications that follow (Shi et al., 2017; Simsek et al., 2017).

AUTHOR CONTRIBUTIONS

HI and CG conceived the perspective and drafted the manuscript. All authors revised the manuscript, agreed to content, and approved the final version.

REFERENCES

Bojar, D., Martinez, J., Santiago, J., Rybin, V., Bayliss, R., and Hothorn, M. (2014). Crystal structures of the phosphorylated BRI1 kinase domain and implications for brassinosteroid signal initiation. *Plant J.* 78, 31–43. doi: 10.1111/tpj.12445

Chen, J., Gutjahr, C., Bleckmann, A., and Dresselhaus, T. (2015). Calcium signaling during reproduction and biotrophic fungal interactions in plants. *Mol. Plant* 8, 595–611. doi: 10.1016/j.molp.2015.01.023

Chinchilla, D., Shan, L., He, P., de Vries, S., and Kemmerling, B. (2009). One for all: the receptor-associated kinase BAK1. *Trends Plant Sci.* 14, 535–541. doi: 10.1016/j.tplants.2009.08.002

Clouse, S. D. (2011). Brassinosteroid signal transduction: from receptor kinase activation to transcriptional networks regulating plant development. *Plant Cell* 23, 1219–1230. doi: 10.1105/tpc.111.084475

Donaldson, L., and Meier, S. (2013). An affinity pull-down approach to identify the plant cyclic nucleotide interactome. *Methods Mol. Biol.* 1016, 155–173. doi: 10.1007/978-1-62703-441-8_11

Donaldson, L., Meier, S., and Gehring, C. (2016). The Arabidopsis cyclic nucleotide interactome. *Cell Commun. Signal.* 14:10. doi: 10.1186/s12964-016-0133-2

Ehrhardt, D. W., Wais, R., and Long, S. R. (1996). Calcium spiking in plant root hairs responding to Rhizobium nodulation signals. *Cell* 85, 673–681. doi: 10.1016/S0092-8674(00)81234-9

Ellis, R. J. (2001). Macromolecular crowding: an important but neglected aspect of the intracellular environment. *Curr. Opin. Struct. Biol.* 11, 114–119. doi: 10.1016/S0959-440X(00)00172-X

Fischer, C., DeFalco, T. A., Karia, P., Snedden, W. A., Moeder, W., Yoshioka, K., et al. (2017). Calmodulin as a Ca2+-sensing subunit of Arabidopsis cyclic nucleotide-gated channel complexes. *Plant Cell Physiol.* 58, 1208–1221. doi: 10.1093/pcp/pcx052

Fischer, C., Kugler, A., Hoth, S., and Dietrich, P. (2013). An IQ domain mediates the interaction with calmodulin in a plant-cyclic nucleotide-gated channel. *Plant Cell Physiol.* 54, 573–584. doi: 10.1093/pcp/pct021

Freihat, L., Muleya, V., Manallack, D. T., Wheeler, J. I., and Irving, H. R. (2014). Comparison of moonlighting guanylate cyclases – roles in signal direction? *Biochem. Soc. Trans.* 42, 1773–1779. doi: 10.1042/BST20140223

Fulton, A. B. (1982). How crowded is the cytoplasm? *Cell* 30, 345–347. doi: 10.1016/0092-8674(82)90231-8

Gehring, C. (2010). Adenyl cyclases and cAMP in plant signaling - past and present. *Cell Commun. Signal.* 8:15. doi: 10.1186/1478-811X-8-15

Geremia, S., Campagnolo, M., Demitri, N., and Johnson, L. N. (2006). Simulation of diffusion time of small molecules in protein crystals. *Structure* 14, 393–400. doi: 10.1016/j.str.2005.12.007

Goldstein, R. E., and van de Meert, J.-W. (2015). A physical perspective on cytoplasmic streaming. *Interface Focus* 5:20150030. doi: 10.1098/rsfs.2015.0030

Goodsell, D. S. (1993). *The Machinery of Life*. Berlin: Springer-Verlag. doi: 10.1007/978-1-4757-2267-3

Goodsell, D. S. (2016). *Atomic Evidence: Seeing the Molecular Basis of Life*. Berlin: Springer. doi: 10.1007/978-3-319-32510-1

Grosse, I., and Durner, J. (2016). In search of enzymes with a role in 3',5'-cyclic guanosine monophosphate metabolism in plants. *Front. Plant Sci.* 7:576. doi: 10.3389/fpls.2016.00576

Haga, J. Y., Hamilton, M. G., and Petermann, M. L. (1970). Electron microscopic observations on the large subunit of the rat liver ribosome. *J. Cell Biol.* 47, 211–221. doi: 10.1083/jcb.47.1.211

Hartmann, J., Fischer, C., Dietrich, P., and Sauter, M. (2014). Kinase activity and calmodulin binding are essential for growth signaling by the phytosulfokine receptor PSKR1. *Plant J.* 78, 192–202. doi: 10.1111/tpj.12460

Hartmann, J., Linke, D., Bönniger, C., Tholey, A., and Sauter, M. (2015). Conserved phosphorylation sites in the activation loop of Arabidopsis phytosulokine receptor PSKR1 differentially affect kinase and receptor activity. *Biochem. J.* 472, 379–391. doi: 10.1042/BJ20150147

Hentze, M. W., and Preiss, T. (2010). The REM phase of gene regulation. *Trends Biochem. Sci.* 35, 423–426. doi: 10.1016/j.tibs.2010.05.009

Hoshi, T. (1995). Regulation of voltage dependence of the KAT1 channel by intracellular factors. *J. Gen. Physiol.* 105, 309–328. doi: 10.1085/jgp.105.3.309

Hussain, J., Chen, J., Locato, V., Sabetta, W., Behera, S., Cimini, S., et al. (2016). Constitutive cyclic GMP accumulation in Arabidopsis thaliana compromises systemic acquired resistance induced by an avirulent pathogen by modulating local signals. *Sci. Rep.* 6:36423. doi: 10.1038/srep36423

Igarashi, D., Tsuda, K., and Katagiri, F. (2012). The peptide growth factor, phytosulfokine, attenuates pattern-triggered immunity. *Plant J.* 71, 194–204. doi: 10.1111/j.1365-313X.2012.04950.x

Isner, J.-C., and Maathuis, F. J. M. (2016). cGMP signalling in plants: from enigma to main stream. *Funct. Plant Biol.* 45, 93–101. doi: 10.1071/FP16337

Jeffery, C. J. (2003). Moonlighting proteins: old proteins learning new tricks. *Trends Genet.* 19, 415–417. doi: 10.1016/S0168-9525(03)00167-7

Jeffery, C. J. (2009). Moonlighting proteins - an update. *Mol. Biosyst.* 5, 345–350. doi: 10.1039/b900658n

Jeffery, C. J. (2014). An introduction to protein moonlighting. *Biochem. Soc. Trans.* 42, 1679–1683. doi: 10.1042/BST20140226

Kaufmann, C., Motzkus, M., and Sauter, M. (2017). Phosphorylation of the phytosulokine peptide receptor PSKR1 controls receptor activity. *J. Exp. Bot.* 68, 1411–1423. doi: 10.1093/jxb/erx030

Kudla, J., Batistic, O., and Hashimoto, K. (2010). Calcium signals: the lead currency of plant information processing. *Plant Cell* 22, 541–563. doi: 10.1105/tpc.109.072686

Kwezi, L., Meier, S., Mungur, L., Ruzvidzo, O., Irving, H., and Gehring, C. (2007). The *Arabidopsis thaliana* brassinosteroid receptor (AtBRI1) contains a domain that functions as a guanylyl cyclase *in vitro*. *PLoS One* 2:e449. doi: 10.1371/journal.pone.0000449

Kwezi, L., Ruzvidzo, O., Wheeler, J. I., Govender, K., Iacuone, S., Thompson, P. E., et al. (2011). The phytosulfokine (PSK) receptor is capable of guanylate cyclase activity and enabling cyclic GMP-dependant signaling in plants. *J. Biol. Chem.* 286, 22580–22588. doi: 10.1074/jbc.M110.168823

Ladwig, F., Dahlke, R. I., Stuhrwohdldt, N., Hartmann, J., Harter, K., and Sauter, M. (2015). Phytosulfokine regulates growth in Arabidopsis through a response module at the plasma membrane that includes CYCLIC NUCLEOTIDE-GATED CHANNEL17, H-ATPase, and BAK1. *Plant Cell* 27, 1718–1729. doi: 10.1105/tpc.15.00306

Lemtiri-Chlieh, F., Thomas, L., Marondedze, C., Irving, H., and Gehring, C. (2011). "Cyclic nucleotides and nucleotide cyclases in plant stress responses," in *Abiotic Stress Response in Plants - Physiological, Biochemical and Genetic Perspectives*, eds A. Shanker and B. Venkateswarlu (London: InTech - Open Access Publisher).

Luby-Phelps, K. (2000). Cytoarchitecture and physical properties of cytoplasm: volume, viscosity, diffusion, intracellular surface area. *Int. Rev. Cytol.* 192, 189–221. doi: 10.1016/S0074-7696(08)60527-6

Luby-Phelps, K. (2013). The physical chemistry of cytoplasm and its influence on cell function: an update. *Mol. Biol. Cell* 24, 2593–2596. doi: 10.1091/mbc.E12-08-0617

Ludidi, N. N., and Gehring, C. (2003). Identification of a novel protein with guanylyl cyclase activity in *Arabidopsis thaliana*. *J. Biol. Chem.* 278, 6490–6494. doi: 10.1074/jbc.M210983200

Ma, Y., Walker, R. K., Zhao, Y., and Berkowitz, G. A. (2012). Linking ligand perception by PEPR pattern recognition receptors to cytosolic Ca2+ elevation and downstream immune signaling in plants. *Proc. Natl. Acad. Sci. U.S.A.* 109, 19852–19857. doi: 10.1073/pnas.1205448109

Marondedze, C., Groen, A., Thomas, L., Lilley, K. S., and Gehring, C. (2016a). A quantitative phosphoproteome analysis of cGMP-dependent cellular responses in *Arabidopsis thaliana*. *Mol. Plant* 9, 621–623. doi: 10.1016/j.molp.2015.11.007

Marondedze, C., Thomas, L., Serrano, N. L., Lilley, K. S., and Gehring, C. (2016b). The RNA-binding protein repertoire of *Arabidopsis thaliana*. *Sci. Rep.* 6:29766. doi: 10.1038/srep29766

Marondedze, C., Wong, A., Thomas, L., Irving, H., and Gehring, C. (2017). Cyclic nucleotide monophosphates in plants and plant signaling. handbook of experimental pharmacology. *Handb. Exp. Pharmacol.* 238, 87–103. doi: 10.1007/164_2015_35

Matsubayashi, Y. (2014). Posttranslationally modified small-peptide signals in plants. *Annu. Rev. Plant Biol.* 65, 385–413. doi: 10.1146/annurev-arplant-050312-120122

Matsubayashi, Y., Ogawa, M., Kihara, H., Niwa, M., and Sakagami, Y. (2006). Disruption and overexpression of Arabidopsis phytosulokine receptor gene affects cellular longevity and potential for growth. *Plant Physiol.* 142, 45–53. doi: 10.1104/pp.106.081109

Matsubayashi, Y., Ogawa, M., Morita, A., and Sakagami, Y. (2002). An LRR receptor kinase involved in perception of a peptide plant hormone, phytosulfokine. *Science* 296, 1470–1472. doi: 10.1126/science.1069607

Matsubayashi, Y., and Sakagami, Y. (1996). Phytosulfokine, sulfated peptides that induce the proliferation of single mesophyll cells of Asparagus officinales L. *Proc. Natl. Acad. Sci. U.S.A.* 93, 7623–7627. doi: 10.1073/pnas.93.15.7623

Mbengue, M., Bourdais, G., Gervasi, F., Beck, M., Zhou, J. M., Spallek, T., et al. (2016). Clathrin-dependent endocytosis is required for immunity mediated by pattern recognition receptor kinases. *Proc. Natl. Acad. Sci. U.S.A.* 113, 11034–11039. doi: 10.1073/pnas.1606004113

Meier, S., Seoighe, C., Kwezi, L., Irving, H., and Gehring, C. (2007). Plant nucleotide cyclases: an increasingly complex and growing family. *Plant Signal. Behav.* 2, 536–539. doi: 10.4161/psb.2.6.4788

Miles, E. W., Rhee, S., and Davies, D. R. (1999). The molecular basis of substrate channeling. *J. Biol. Chem.* 274, 12193–12196. doi: 10.1074/jbc.274.18.12193

Moller, B. L. (2010). Dynamic metabolons. *Science* 330, 1328–1329. doi: 10.1126/science.1194971

Monaghan, R. M., and Whitmarsh, A. J. (2015). Mitochondrial proteins moonlighting in the nucleus. *Trends Biochem. Sci.* 40, 728–735. doi: 10.1016/j.tibs.2015.10.003

Mosher, S., Seybold, H., Rodriguez, P., Stahl, M., Davies, K. A., Dayaratne, S., et al. (2013). The tyrosine-sulfated peptide receptors PSKR1 and PSY1R modify the immunity of Arabidopsis to biotrophic and necrotrophic pathogens in an antagonistic manner. *Plant J.* 73, 469–482. doi: 10.1111/tpj.12050

Muleya, V., Marondedze, C., Wheeler, J. I., Thomas, L., Mok, Y. F., Griffin, M. W. D., et al. (2016). Phosphorylation of the dimeric cytoplasmic domain of the phytosulfokine receptor, PSKR1. *Biochem. J.* 473, 3081–3098. doi: 10.1042/BCJ20160593

Muleya, V., Wheeler, J. I., Ruzvidzo, O., Freihat, L., Manallack, D. T., Gehring, C., et al. (2014). Calcium is the switch in the moonlighting dual function of the ligand-activated receptor kinase phytosulfokine receptor 1. *Cell Commun. Signal.* 12:60. doi: 10.1186/s12964-014-0060-z

Newton, R. P., Roef, L., Witters, E., and van Onckelen, H. (1999). Tansley Review No. 106. Cyclic nucleotides in higher plants: the enduring paradox. *New Phytol.* 143, 427–455. doi: 10.1046/j.1469-8137.1999.00478.x

Oh, M.-H., Wang, X., Kota, U., Goshe, M. B., Clouse, S. D., and Huber, S. C. (2009). Tyrosine phosphorylation of the BRI1 receptor kinase emerges as a component of brassinosteroid signaling in Arabidopsis. *Proc. Natl. Acad. Sci. U.S.A.* 106, 658–663. doi: 10.1073/pnas.0810249106

Phillip, Y., and Schreiber, G. (2013). Formation of protein complexes in crowded environments - from in vitro to in vivo. *FEBS Lett.* 587, 1046–1052. doi: 10.1016/j.febslet.2013.01.007

Qi, Z., Verma, R., Gehring, C., Yamaguchi, Y., Zhao, Y., Ryan, C. A., et al. (2010). Ca2+ signaling by plant *Arabidopsis thaliana* Pep peptides depends on AtPepR1, a receptor with guanylyl cyclase activity, and cGMP-activated Ca2+ channels. *Proc. Natl. Acad. Sci. U.S.A.* 107, 21193–21198. doi: 10.1073/pnas.1000191107

Rodiuc, N., Barlet, X., Hok, S., Perfus-Barbeoch, L., Allasia, V., Enger, G., et al. (2016). Evolutionary distant pathogens require the Arabidopsis phytosulfokine signalling pathway to establish disease. *Plant Cell Environ.* 39, 1396–1407. doi: 10.1111/pce.12627

Rohwer, J. M., Postma, P. W., Kholodenko, B. N., and Westerhoff, H. V. (1998). Implications of macromolecular crowding for signal transduction and metabolite channeling. *Proc. Natl. Acad. Sci. U.S.A.* 95, 10547–10552. doi: 10.1073/pnas.95.18.10547

Saenger, W. (1987). Structure and dynamics of water surrounding biomolecules. *Annu. Rev. Biophys. Biophys. Chem.* 16, 93–114. doi: 10.1146/annurev.bb.16.060187.000521

Sanders, D., Pelloux, J., Brownlee, C., and Harper, J. F. (2002). Calcium at the crossroads of signaling. *Plant Cell* 14(Suppl.), s401–s417. doi: 10.1105/tpc.002899

Sauter, M. (2015). Phytosulfokine peptide signaling. *J. Exp. Bot.* 66, 5161–5169. doi: 10.1093/jxb/erv071

Saxton, M. J. (2012). Wanted: a positive control for anomalous subdiffusion. *Biophys. J.* 103, 2411–2422. doi: 10.1016/j.bpj.2012.10.038

Shi, Z., Fujii, K., Kovary, K. M., Genuth, N. R., Rost, H. L., Teruel, M. N., et al. (2017). Heterogeneous ribosomes preferentially translate distinct subpools of mRNAs genome-wide. *Mol. Cell* 67, 1–13. doi: 10.1016/j.molcel.2017.05.021

Shimmen, T. (2007). The sliding theory of cytoplasmic streaming: fifty years of progress. *J. Plant Res.* 120, 31–43. doi: 10.1007/s10265-006-0061-0

Simsek, D., Tiu, G. C., Flynn, R. A., Byeon, G. W., Leppek, K., Xu, A. F., et al. (2017). The mammalian ribo-interactome reveals ribosome functional diversity and heterogeneity. *Cell* 169, 1051–1065. doi: 10.1016/j.cell.2017.05.022

Srere, P. A. (1967). Enzyme concentrations in tissues. *Science* 158, 936–937. doi: 10.1126/science.158.3803.936

Srere, P. A. (1980). The infrastructure of the mitochondrial matrix. *Trends Biochem. Sci.* 5, 120–121. doi: 10.1016/0968-0004(80)90051-1

Srere, P. A. (1981). Protein crystals as a model for mitochondrial matrix proteins. *Trends Biochem. Sci.* 6, 4–7. doi: 10.1016/0968-0004(81)90003-7

Srere, P. A. (1985). The metabolon. *Trends Biochem. Sci.* 10, 109–110. doi: 10.1016/0968-0004(85)90266-X

Srere, P. A. (2000). Macromolecular interactions: tracing the roots. *Trends Biochem. Sci.* 25, 150–153. doi: 10.1016/S0968-0004(00)01550-4

Steinhorst, L., and Kudla, J. (2013). Calcium - a central regulator of pollen germination and tube growth. *Biochim. Biophys. Acta* 1833, 1573–1581. doi: 10.1016/j.bbamcr.2012.10.009

Sunahara, R. K., Beuve, A., Tesmer, J. J. G., Sprang, S. R., Garbers, D. L., and Gilman, A. G. (1998). Exchange of substrate and inhibitor specification between adenylyl and guanylyl cyclases. *J. Biol. Chem.* 273, 16332–16338. doi: 10.1074/jbc.273.26.16332

Sweetlove, L. J., and Fernie, A. R. (2013). The spatial organization of metabolism within the plant cell. *Annu. Rev. Plant Biol.* 64, 723–746. doi: 10.1146/annurev-arplant-050312-120233

Tang, J., Han, Z., Sun, Y., Zhang, H., Gong, X., and Chai, J. (2015). Structural basis for recognition of an endogenous peptide by the pareceptor kinase PEPR1. *Cell Res.* 25, 110–120. doi: 10.1038/cr.2014.161

Tucker, C. L., Hurley, J. H., Miller, T. R., and Hurley, J. B. (1998). Two amino acid substitutions convert a guanylyl cyclase, RetGC-1, into an adenylyl cyclase. *Proc. Natl. Acad. Sci. U.S.A.* 95, 5993–5997. doi: 10.1073/pnas.95.11.5993

Tuteja, N., and Mahajan, S. (2007). Calcium signaling networks in plants: an overview. *Plant Signal. Behav.* 2, 79–85. doi: 10.4161/psb.2.2.4176

Vestergaard, C. L., Flyvbjerg, H., and Møller, I. M. (2012). Intracellular signaling by diffusion: can waves of hydrogen peroxide transmit intracellular information in plant cells. *Front. Plant Sci.* 3:295. doi: 10.3389/fpls.2012.00295

Wang, C., Yu, H., Zhang, Z., Yu, L., Xu, X., Hing, Z., et al. (2015). Phytosulfokine is involved in positive regulation of Lotus japonicus nodulation. *Mol. Plant Microbe Interact.* 28, 847–855. doi: 10.1094/MPMI-02-15-0032-R

Wang, J., Li, H., Han, Z., Zhang, H., Wang, T., Lin, G., et al. (2015). Allosteric receptor activation by the plant peptide hormone phytosulfokine. *Nature* 525, 265–268. doi: 10.1038/nature14858

Wheeldon, I., Minteer, S. D., Banta, S., Barton, S. C., Atanassov, P., and Sigman, M. (2016). Substrate channelling as an approach to cascade reactions. *Nat. Chem.* 8, 299–309. doi: 10.1038/nchem.2459

Wheeler, J. I., and Irving, H. R. (2010). Evolutionary advantages of secreted peptide signalling molecules. *Funct. Plant Biol.* 37, 382–394. doi: 10.1071/FP09242

Wheeler, J. I., Wong, A., Marondedze, C., Groen, A. J., Kwezi, L., Freihat, L., et al. (2017). The brassinosteroid receptor BRI1 can generate cGMP enabling cGMP-dependent downstream signaling. *Plant J.* 91, 590–600. doi: 10.1111/tpj.13589

Williamson, R. E. (1993). Organelle movements. *Annu. Rev. Plant Physiol. Plant Mol. Biol.* 44, 181–202. doi: 10.1146/annurev.pp.44.060193.001145

Winkel, B. S. J. (2004). Metabolic channeling in plants. *Annu. Rev. Plant Biol.* 55, 85–107. doi: 10.1146/annurev.arplant.55.031903.141714

Wong, A., and Gehring, C. (2013). The Arabidopsis thaliana proteome harbors undiscovered multi-domain molecules with functional guanylyl cyclase catalytic centers. *Cell Commun. Signal.* 11:48. doi: 10.1186/1478-811X-11-48

Wong, A., Gehring, C., and Irving, H. R. (2015). Conserved functional motifs and homology modeling to predict hidden moonlighting functional sites. *Front. Bioeng. Biotech.* 3:82. doi: 10.3389/fbioe.2015.00082

Yuan, P., Jauregui, E., Du, L., Tanaka, K., and Poovaiah, B. W. (2017). Calcium signatures and signaling events orchestrate plant-microbe interactions. *Curr. Opin. Plant Biol.* 38, 173–183. doi: 10.1016/j.pbi.2017.06.003

Zelman, A. K., Dawe, A., Gehring, C., and Berkowitz, G. A. (2012). Evolutionary and structural perspectives of plant cyclic nucleotide-gated cation channels. *Front. Plant Sci.* 3:95. doi: 10.3389/fpls.2012.00095

Zhang, Y., Beard, K. F. M., Swart, C., Bergmann, S., Krahnert, I., Nikoloski, Z., et al. (2017). Protein-protein interactions and metabolite channelling in the plant tricarboxylic acid cycle. *Nat. Commun.* 8:15212. doi: 10.1038/ncomms15212

Conflict of Interest Statement: The authors declare that the research was conducted in the absence of any commercial or financial relationships that could be construed as a potential conflict of interest.

frontiers in Plant Science

ORIGINAL RESEARCH
published: 12 March 2018
doi: 10.3389/fpls.2018.00274

Magnesium Transporter MGT6 Plays an Essential Role in Maintaining Magnesium Homeostasis and Regulating High Magnesium Tolerance in *Arabidopsis*

Yu-Wei Yan[1,2], Dan-Dan Mao[3,4], Lei Yang[3], Jin-Liang Qi[1,3], Xin-Xin Zhang[1,5], Qing-Lin Tang[1,6], Yang-Ping Li[1,2], Ren-Jie Tang[1] and Sheng Luan[1]**

[1] Department of Plant and Microbial Biology, University of California, Berkeley, Berkeley, CA, United States, [2] Key Laboratory of Biology and Genetic Improvement of Maize in Southwest Region, Maize Research Institute of Sichuan Agricultural University, Chengdu, China, [3] Nanjing University–Nanjing Forestry University Joint Institute for Plant Molecular Biology, State Key Laboratory for Pharmaceutical Biotechnology, College of Life Sciences, Nanjing University, Nanjing, China, [4] College of Life Sciences, Hunan Normal University, Changsha, China, [5] Key Laboratory of Saline-Alkali Vegetation Ecology Restoration in Oil Field, Ministry of Education, Alkali Soil Natural Environmental Science Center, Northeast Forestry University, Harbin, China, [6] Key Laboratory of Horticulture Science for Southern Mountainous Regions, Southwest University, Chongqing, China

OPEN ACCESS

Edited by:
Kai He,
Lanzhou University, China

Reviewed by:
Dai-Yin Chao,
Shanghai Institutes for Biological Sciences (CAS), China
Caiji Gao,
South China Normal University, China

***Correspondence:**
Ren-Jie Tang
rjtang@berkeley.edu
Sheng Luan
sluan@berkeley.edu

Specialty section:
This article was submitted to Plant Traffic and Transport, a section of the journal Frontiers in Plant Science

Received: 04 January 2018
Accepted: 16 February 2018
Published: 12 March 2018

Citation:
Yan Y-W, Mao D-D, Yang L, Qi J-L, Zhang X-X, Tang Q-L, Li Y-P, Tang R-J and Luan S (2018) Magnesium Transporter MGT6 Plays an Essential Role in Maintaining Magnesium Homeostasis and Regulating High Magnesium Tolerance in Arabidopsis. Front. Plant Sci. 9:274. doi: 10.3389/fpls.2018.00274

Magnesium (Mg) is one of the essential nutrients for all living organisms. Plants acquire Mg from the environment and distribute within their bodies in the ionic form via Mg^{2+}-permeable transporters. In *Arabidopsis*, the plasma membrane-localized magnesium transporter MGT6 mediates Mg^{2+} uptake under Mg-limited conditions, and therefore is important for the plant adaptation to low-Mg environment. In this study, we further assessed the physiological function of MGT6 using a knockout T-DNA insertional mutant allele. We found that MGT6 was required for normal plant growth during various developmental stages when the environmental Mg^{2+} was low. Interestingly, in addition to the hypersensitivity to Mg^{2+} limitation, *mgt6* mutants displayed dramatic growth defects when external Mg^{2+} was in excess. Compared with wild-type plants, *mgt6* mutants generally contained less Mg^{2+} under both low and high external Mg^{2+} conditions. Reciprocal grafting experiments further underpinned a role of MGT6 in a shoot-based mechanism for detoxifying excessive Mg^{2+} in the environment. Moreover, we found that *mgt6 mgt7* double mutant showed more severe phenotypes compared with single mutants under both low- and high-Mg^{2+} stress conditions, suggesting that these two MGT-type transporters play an additive role in controlling plant Mg^{2+} homeostasis under a wide range of external Mg^{2+} concentrations.

Keywords: Mg^{2+} transporter, Mg^{2+} homeostasis, *Arabidopsis*, MGT6, MGT7

INTRODUCTION

Magnesium (Mg) is an essential macronutrient for plants. Being the most abundant free divalent cation in living cells, Mg^{2+} serves as a counter ion for nucleotides and a central metal for chlorophylls, and acts as a cofactor for many enzymes in catalytic processes. Mg^{2+} also contributes to membrane stabilization and active conformation of macromolecules (Shaul, 2002).

Both low and high levels of Mg present in the soil are deleterious to plant growth, thus affecting crop production. Due to unbalanced application of chemical fertilizers, plants may exhibit Mg deficiency symptoms in the presence of high levels of other cations such as calcium (Ca^{2+}) and potassium (K^{+}) in the soil (Hermans et al., 2013). Moreover, excessive aluminum (Al^{3+}) in acidic soils or other heavy metals severely inhibit the uptake of Mg^{2+}, resulting in Mg deficiency in the plants. These problems lead to reduction in crop yield as well as higher susceptibility to some plant diseases. On the other hand, high levels of Mg are found in serpentine soils featuring a low Ca/Mg ratio (Brady et al., 2005). Genome sequencing of *Arabidopsis lyrata* plants grown in serpentine or non-serpentine habitats has identified a number of polymorphisms associated with Ca^{2+} and Mg^{2+} transport (Turner et al., 2010). Although it is critical for plant cells to maintain an optimal Mg^{2+} level for normal growth and development, the transport and regulatory mechanisms that govern Mg^{2+} acquisition, distribution, and reallocation are poorly understood (Tang and Luan, 2017).

In bacterial cells, there are at least three distinct types of membrane proteins CorA, MgtE, and MgtA/B that are capable of transporting Mg^{2+}. While the MgtE channel and the P-type ATPases MgtA/B do not seem to have any close homologs in plants, there is a major family of Mg^{2+} transporters (MGTs) related to bacterial CorA proteins (Li et al., 2001). They are also named as "MRS2s" based on the ability to rescue the yeast *mrs2* mutant lacking the Mrs2 protein, a yeast homolog of CorA-type transporter that mediates Mg^{2+} transport into the mitochondrial matrix (Schock et al., 2000). The CorA-family proteins feature a unique topology with two closely spaced, C-terminal transmembrane (TM) domains, the first of which contains a conserved GMN (Gly-Met-Asn) tripeptide motif that is essential for Mg^{2+} transport (Szegedy and Maguire, 1999). Crystal structure of the *Thermotoga maritima* CorA establishes the protein as a pentameric cone-shaped ion channel (Eshaghi et al., 2006; Lunin et al., 2006).

Several members of the *Arabidopsis* MGTs facilitate Mg^{2+} transport in bacteria or yeast (Li et al., 2001, 2008; Mao et al., 2008, 2014; Gebert et al., 2009). Genes coding for MGT-type transporters are widely expressed in various plant tissues and cell types in *Arabidopsis* (Li et al., 2001; Gebert et al., 2009) and the proteins are targeted to plasma membrane or intracellular membranes, implicating MGT members functioning in Mg^{2+} transport across multiple cellular membranes. MGT1 is mainly expressed in the root hair and the elongation zone as well as the vascular tissues and leaf trichomes (Gebert et al., 2009), suggesting a potential role in Mg^{2+} translocation in these particular cell types. MGT2 and MGT3 are associated with vacuolar membrane and possibly involved in Mg^{2+} homeostasis in leaf mesophyll cells (Conn et al., 2011). Quite a few MGTs including MGT4, MGT5, and MGT9 are highly expressed in pollen and anther cells, and are required for plant reproduction, suggesting that active Mg^{2+} transport is critical for pollen development (Li et al., 2008, 2015; Chen et al., 2009; Xu et al., 2015). MGT10 is localized in the chloroplast envelope, and is strongly expressed in the rosette and cauline leaves, indicating its possible function in Mg^{2+} translocation into chloroplasts (Drummond et al., 2006). Indeed, two recent studies confirmed that mutant plants lacking MGT10 show defects in chloroplast development and plant photosynthesis (Liang et al., 2017; Sun et al., 2017). In rice, OsMGT1 is localized to the plasma membrane and its rapid up-regulation upon Al^{3+} stress confers Al^{3+} tolerance on rice plants as a result of enhanced Mg^{2+} uptake (Chen et al., 2012). Interestingly, OsMGT1 plays a role in rice salt tolerance possibly through activating the transport activity of OsHKT1;5 (Chen et al., 2017).

Among all the MGT-type Mg^{2+} transporters in *Arabidopsis*, MGT6 and MGT7 are thought to be more directly involved in controlling cellular Mg^{2+} homeostasis because impairment of MGT6 or MGT7 function renders *Arabidopsis* plants hypersensitive to low-Mg conditions (Gebert et al., 2009; Mao et al., 2014; Oda et al., 2016). MGT6 appears to be localized to the plasma membrane and mediate the high-affinity Mg^{2+} uptake via roots (Mao et al., 2014). Consistent with this role, expression of *MGT6* is dramatically up-regulated at the transcriptional level when external Mg^{2+} becomes limited (Mao et al., 2014). MGT7 is preferentially expressed in roots, and also plays an important role for plant adaptation to low-Mg conditions although the mechanism is not clear (Gebert et al., 2009). In this study, we showed that MGT6 is equally important for controlling plant Mg^{2+} homeostasis under normal and high-Mg conditions. We uncovered a shoot-based mechanism that underlies MGT6 function in detoxifying excessive Mg^{2+}, in addition to its role in root Mg^{2+} uptake under Mg-limited conditions. Furthermore, by analyzing the *mgt6 mgt7* double mutant, we showed that these two Mg^{2+} transporters MGT6 and MGT7 play an overlapping role in maintaining essential Mg^{2+} homeostasis under a wide range of external Mg^{2+} concentrations.

MATERIALS AND METHODS

Plant Materials and Growth Conditions

Arabidopsis thaliana ecotype Col-0 was used in this study. T-DNA insertional mutant lines were obtained from the *Arabidopsis* Biological Resource Center. The seed stock IDs are as follows: SALK_205483 (*mgt6*) and SALK_064741 (*mgt7*). The double mutant *mgt6 mgt7* was generated by crossing *mgt7* to *mgt6* mutant, and progeny of F2 generation was screened for double homozygous mutations in *MGT6* and *MGT7* using a PCR-based genotyping approach.

Wild-type and mutant plants were grown in the soil at 22°C under the 16-h-light/8-h-dark condition in the greenhouse. Hydroponically grown plants were generally kept in the 1/6 strength MS solution under the short-day condition (8-h-light/16-h-dark) in the greenhouse. Fresh liquid solutions were replaced twice a week.

Phenotypic Assays

Arabidopsis seeds of different genotypes were sterilized with 10% bleach for 5 min and washed in sterilized water for 3 times. Seeds were sown on the solid plates supplemented with different concentrations of Mg^{2+}. The basal medium contained 1/6 strength of MS salt (Murashige and Skoog, 1962) in which $MgSO_4$

was replaced by the K_2SO_4. Different concentrations of $MgCl_2$ were added as the Mg^{2+} source. After 2-day stratification at 4°C, plates were vertically grown at 22°C in the growth chamber.

For the post-germination assay, seeds were first sown on MS medium solidified with 1% phytoagar. After germination, 5-day-old seedlings were transferred onto 1/6 Mg^{2+}-free MS medium (containing 1% sucrose, pH = 5.8, solidified with 0.8% agarose) supplemented with Mg^{2+} at the indicated concentrations.

For phenotypic assay in the hydroponics, 7-day-old seedlings were transferred to liquid solutions containing 1/6 MS salts supplemented with 1.25 mM $MgSO_4$. After 2-week culture, the plants were treated with solutions containing different concentrations of Mg^{2+}.

Functional Complementation

For complementation of the *mgt6* mutant, a 3.5-kb genomic fragment including the *MGT6* coding region as well as 1.5 kb of the 5′ flanking DNA upstream of the starting codon was amplified by PCR from *Arabidopsis* genomic DNA with forward (5′-AC GGATAAATGTGGGGATGCTTG-3′) and reverse (5′-CCAA ATCAAATCAACCCATAAAC-3′) primers. The PCR product was cloned into the SmaI site of the binary vector pCAMBIA1300. After sequencing, the construct was transformed into *Agrobacterium tumefaciens* strain GV3101 and introduced into *mgt6* mutant plants by the floral dip method (Clough and Bent, 1998). Transgenic seeds were screened on MS medium supplemented with 25 mg/L hygromycin. Resistant seedlings were transplanted to soil and grown in the greenhouse for seed propagation. T3 homozygous transgenic plants were subject to gene expression analysis and phenotypic assays together with wild-type plants and *mgt6* mutants.

RNA Isolation and Gene Expression Analysis

Total RNA was extracted from plant materials using the TRIzol reagent (Invitrogen). After being digested by DNase I (Invitrogen) to decontaminate DNA, cDNA was generated from RNA samples at 42°C using SuperScript II reverse transcriptase (Invitrogen). The resultant cDNA samples were used for PCR amplification with the gene-specific primers. Quantitative real-time PCR was performed on the DNA Engine Opticon System (MJ Research) using the SYBR Green Realtime PCR Master Mix to monitor double-stranded DNA products. Data were calculated based on the comparative threshold cycle method. The relative expression of each Mg-starvation marker gene was double-normalized using the housekeeping gene *ACTIN2* and using the control expression values measured in the wild type when external Mg^{2+} is 1.5 mM.

Grafting Experiments

Reciprocal grafting experiments were performed as previously described with minor modifications (Marsch-Martínez et al., 2013). Seeds were sown on MS medium containing 1% agar and 2% sucrose, and grown vertically in the growth chamber (22°C, 14-h-light/10-h-dark) after 2-day stratification at 4°C. Six-day-old *Arabidopsis* seedlings were transversely cut with a sharp blade in the middle position of the hypocotyl so that each individual seedling was divided into two parts. Subsequently, different parts of each material were re-assembled and grafted on half MS medium supplemented with 1.2% agar, 0.5% sucrose, 3 mg/L Benomyl [methyl 1-(butylcarbamoyl)-2-benzimidazolecarbamate], 0.02 mg/L IAA (indole acetic acid) and 0.04 mg/L 6-BA (6-benzylaminopurine). The grafted seedlings were grown vertically in the growth chamber for another 10 days to allow the formation of the graft union. Successfully unified seedlings with the same size and status were then transferred to the hydroponic culture for further experiments.

Measurement of the Mg and Ca Content

Plant samples were harvested from root and shoot tissues, respectively, and briefly washed with ddH_2O for 10 s. The samples were then thoroughly dried up in the oven at 80°C. The dry matters were collected in the 15 mL centrifuge tubes (ions free) and digested with 1 mL ultrapure HNO_3 (Sigma-Aldrich) in the water bath at 95°C for 4 h. Digested samples were diluted to the appropriate concentrations with ddH_2O, and the elemental concentrations were determined by inductively coupled plasma optical emission spectroscopy (ICP-OES; PerkinElmer, Waltham, MA, United States).

RESULTS

Knockout Mutation in MGT6 Leads to Plant Hypersensitivity to Mg Deficiency

In a previous study, we have shown that knock-down of *MGT6* in transgenic plants by RNA interference resulted in growth retardation under low-Mg conditions (Mao et al., 2014). To further address the physiological role of MGT6, we isolated a previously unidentified T-DNA insertional mutant from the SALK collection (SALK_203866), in which the T-DNA insertion is located in the third exon of *MGT6*, 39 base pair (bp) upstream of the stop codon (**Figure 1A**). RT-PCR analyses showed that full-length *MGT6* transcript was not detectable in the *mgt6* mutant, while *MGT4* gene located in the same chromosome is normally expressed (**Figure 1B**). Consistent with earlier findings, mutation in *MGT6* leads to hypersensitivity to Mg limitation in that the *mgt6* mutants experienced growth defects at the germination stage (**Figures 1C–F**). When germinated on the medium containing no Mg^{2+} or 0.01 mM Mg^{2+}, the *mgt6* mutants showed shorter roots and smaller and pale cotyledons (**Figures 1C,D**). In the presence of 0.25 mM Mg^{2+}, *mgt6* seedlings appeared more normal, albeit still smaller than the wild-type (**Figure 1E**). Early seedling establishment during germination became comparable between wild-type and mutant plants when external Mg^{2+} reached 1.5 mM (**Figure 1F**). Statistical analysis of root length (**Figure 1G**) and seedling fresh weight (**Figure 1H**) verified the hypersensitivity to Mg deficiency in the *mgt6* mutant.

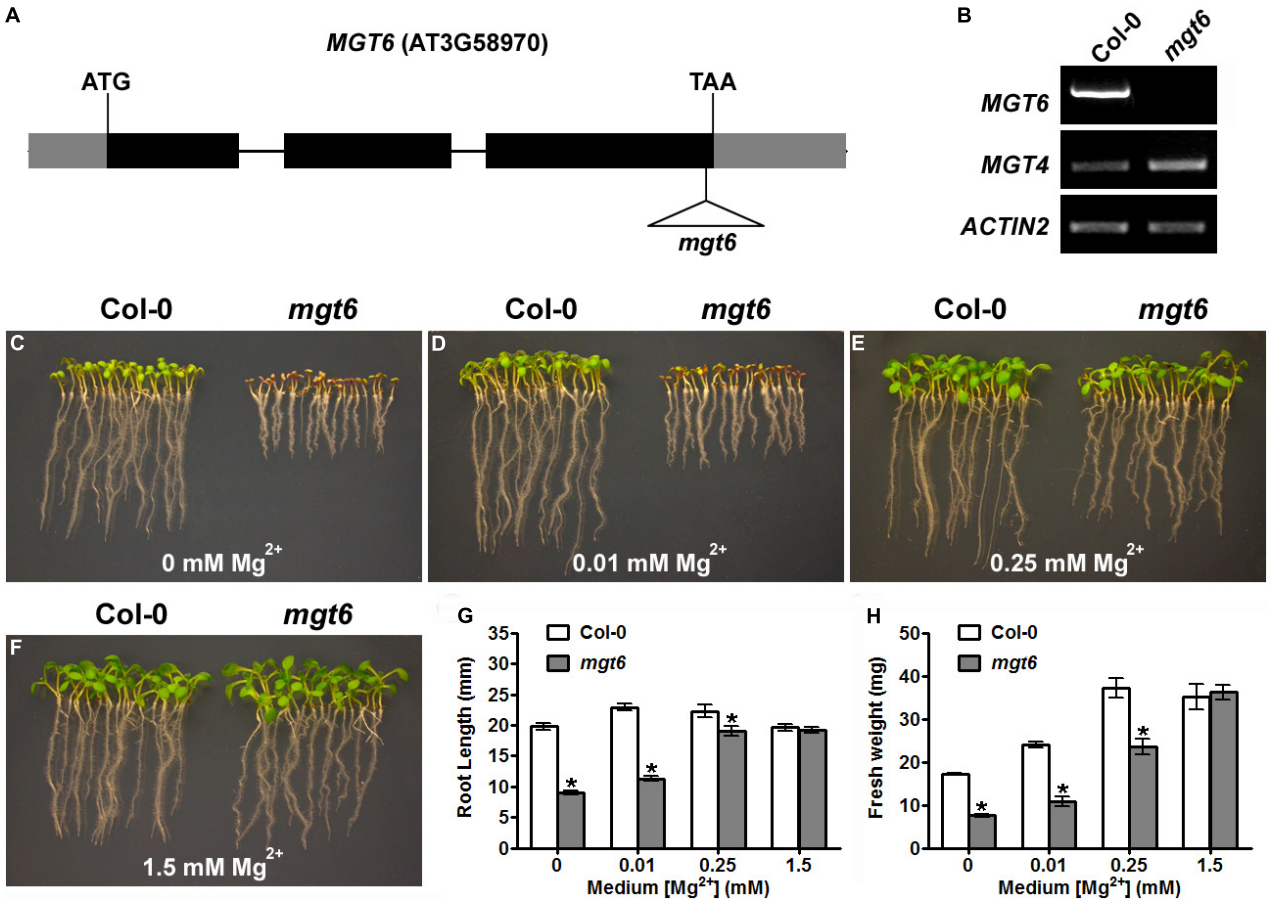

FIGURE 1 | The T-DNA insertional *mgt6* mutant is hypersensitive to Mg^{2+} deficiency. **(A)** Schematic diagram of the T-DNA insertion in the *mgt6* mutant. Exons and introns are depicted to scale by boxes and lines, respectively. The coding region of the gene is shown as black boxes while the 5′ and 3′ UTR of the cDNA is shown as light-shaded boxes. The position of the T-DNA is indicated by the triangle. **(B)** RT-PCR analysis of *MGT6* and *MGT4* in wild-type and *mgt6* seedlings. **(C–F)** Growth phenotype of young seedlings 6 days after seed germination on the medium supplemented with different concentrations of Mg^{2+}. **(G)** Quantification of root length of 7-day-old seedlings. **(H)** Quantification of seedling fresh weight. Data represent means ± SE of four replicate experiments. Asterisks indicate significant difference between the wild type and *mgt6* mutant (Student's *t*-test, $*P < 0.05$).

Because MGT-type transporters are capable of transporting several divalent cations in bacteria and yeast (Li et al., 2001; Mao et al., 2008), we examined the growth of *mgt6* mutant in the absence of other divalent cation nutrients. Whereas *mgt6* consistently displayed growth defects in the absence of Mg^{2+}, seedling growth appeared indistinguishable between wild type and *mgt6* on the medium lacking other divalent cations including Ca^{2+}, Fe^{2+}, Mn^{2+}, and Zn^{2+} (Supplementary Figure S1). These data suggest that under physiological conditions MGT6 may function in plants to cope with variable external Mg status, but is not relevant to other divalent cations.

MGT6 Is Required for Plant Growth in *Arabidopsis* Under a Wide Range of External Mg^{2+} Concentrations

To extend the phenotypic analysis of the *mgt6* mutant, we grew the seedlings of the mutant together with the wild-type plants on the plates containing various levels of Mg^{2+} in the post-germination assay. When grown on the low-Mg medium containing 0, 0.01, 0.05, or 0.25 mM Mg^{2+}, the *mgt6* mutant plants were clearly stunted as compared with Col-0 (**Figure 2A**); the primary roots were shorter (**Figure 2B**) and the seedling fresh weight was significantly reduced (**Figure 2C**). Because Mg^{2+} is the central structural cation for chlorophyll, we analyzed the chlorophyll content in the young leaves and found that the mutant had a lower chlorophyll level under extremely low-Mg conditions (0, 0.01, and 0.05 mM Mg^{2+}; **Figure 2D**). When the medium Mg^{2+} levels reached a moderate range (0.75, 1.25, and 3 mM), the growth of *mgt6* mutants appeared comparable to that of wild-type (**Figure 2A**), although primary root length or seedling fresh weight was slightly affected (**Figures 2B,C**). Notably, in the presence of 6 mM Mg^{2+} that is regarded as high, the *mgt6* seedlings exhibited a strong growth defect (**Figure 2A**), with much lower fresh weight (**Figure 2C**) and reduced chlorophyll content (**Figure 2D**) than wild-type plants. These data suggested that the *mgt6* mutant is not only

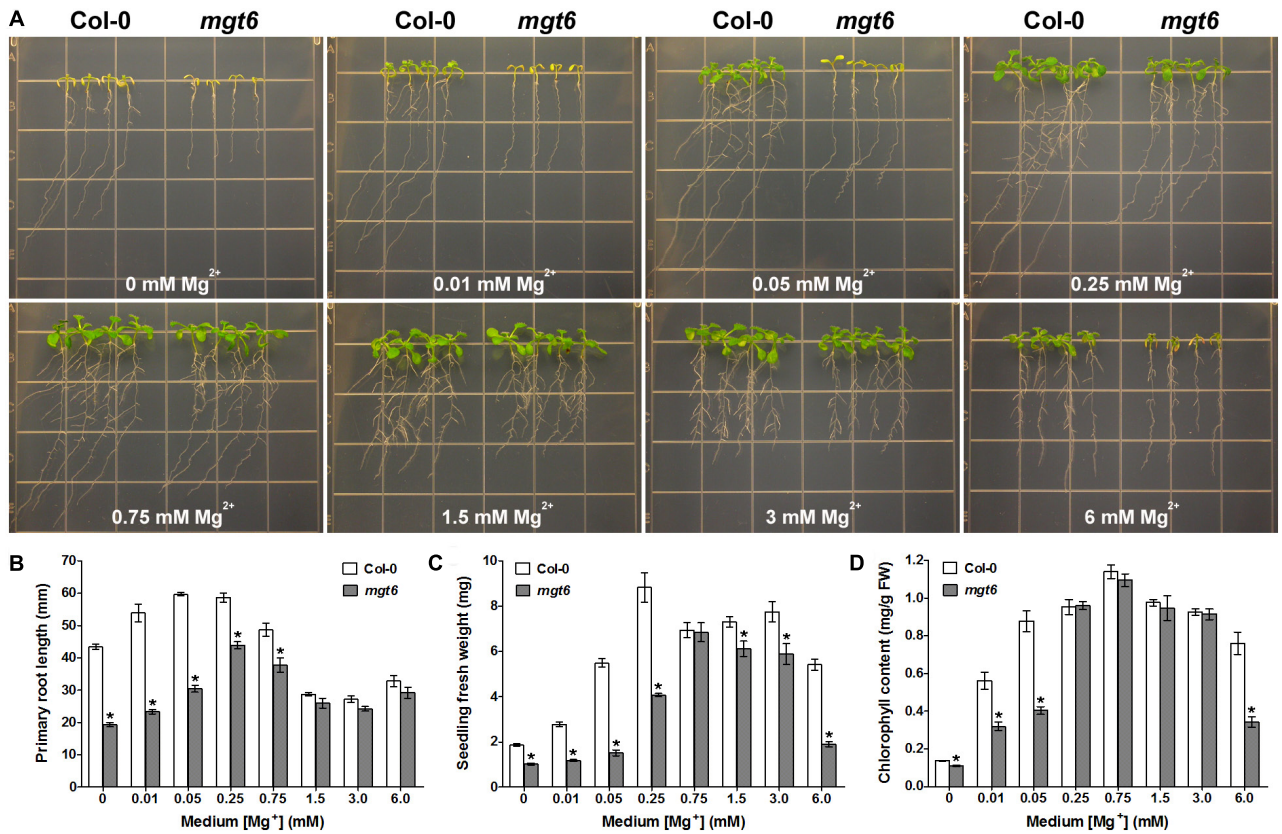

FIGURE 2 | *mgt6* mutant is hypersensitive to Mg^{2+} deficiency and excess. **(A)** Growth phenotype of 5-day-old young seedlings transferred onto the medium supplemented with indicated concentrations of Mg^{2+} for 10 days. **(B)** Quantification of primary root length of the seedlings at the end of treatment. **(C)** Quantification of seedling fresh weight. **(D)** Quantification of leaf chlorophyll content. Data represent means ± SE of four replicate experiments. Asterisks indicate significant difference between the wild type and *mgt6* mutant (Student's *t*-test, $^*P < 0.05$).

compromised under low-Mg levels but also hypersensitive to high-Mg stress.

To verify the observed phenotypes in the *mgt6* mutant resulted from *MGT6* mutation, we conducted a complementation test. A genomic fragment of *MGT6* was introduced into the *mgt6* mutant. Several homozygous transgenic lines with a similar *MGT6* transcript level to that in wild type were obtained (Supplementary Figure S2B). Phenotypic analysis of two representative lines showed that seedling growth defects were fully rescued under both low- and high-Mg conditions (Supplementary Figure S2), suggesting MGT6 is indeed required for plant adaptation to Mg deficiency as well as plant tolerance to high-Mg stress.

To assess the function of MGT6 in mature plants, we grew wild-type and *mgt6* plants to flowering stage in the hydroponic solutions with defined levels of external Mg^{2+}. We found that the *mgt6* plants showed compromised growth in all conditions tested (**Figure 3A**), but the growth difference was much more pronounced between wild-type and *mgt6* plants under extremely low (0.01 and 0.05 mM) and high-Mg^{2+} (10 mM) conditions, as revealed by the root and shoot biomass (**Figures 3B,C**). These results suggest that MGT6 is essential for plant growth at all developmental stages under a wide range of Mg^{2+} concentrations in the environment, and particularly plays an important role in plant adaption to low- and high-Mg^{2+} stresses.

MGT6 Controls Plant Mg^{2+} Homeostasis in Both Root and Shoot Tissues

In order to investigate how plant Mg^{2+} homeostasis is affected by loss of *MGT6* function under various conditions, we measured metal content in the roots and shoots of the wild type and *mgt6*. We first employed the plant materials cultivated *in vitro* after 2 weeks' growth on the plates. As expected, compared with wild-type plants, we observed a dramatic decrease in Mg content in both roots and shoots of *mgt6* mutants grown under low (0.01 mM) Mg conditions (**Figure 4A**). In the presence of normal (1.5 mM) and high (6 mM) external Mg^{2+} levels, *mgt6* mutants also contained less Mg in both roots and shoots than wild-type plants, when the seedlings were grown on the plates (**Figure 4A**). Because Ca is usually associated with Mg homeostasis, we also measured Ca content in the plants. While Ca content in the root of *mgt6* mutant was slightly higher, we surprisingly found that Mg deficiency resulted in a drastic reduction in shoot Ca compared with wild-type (**Figure 4B**). The Ca content, like other

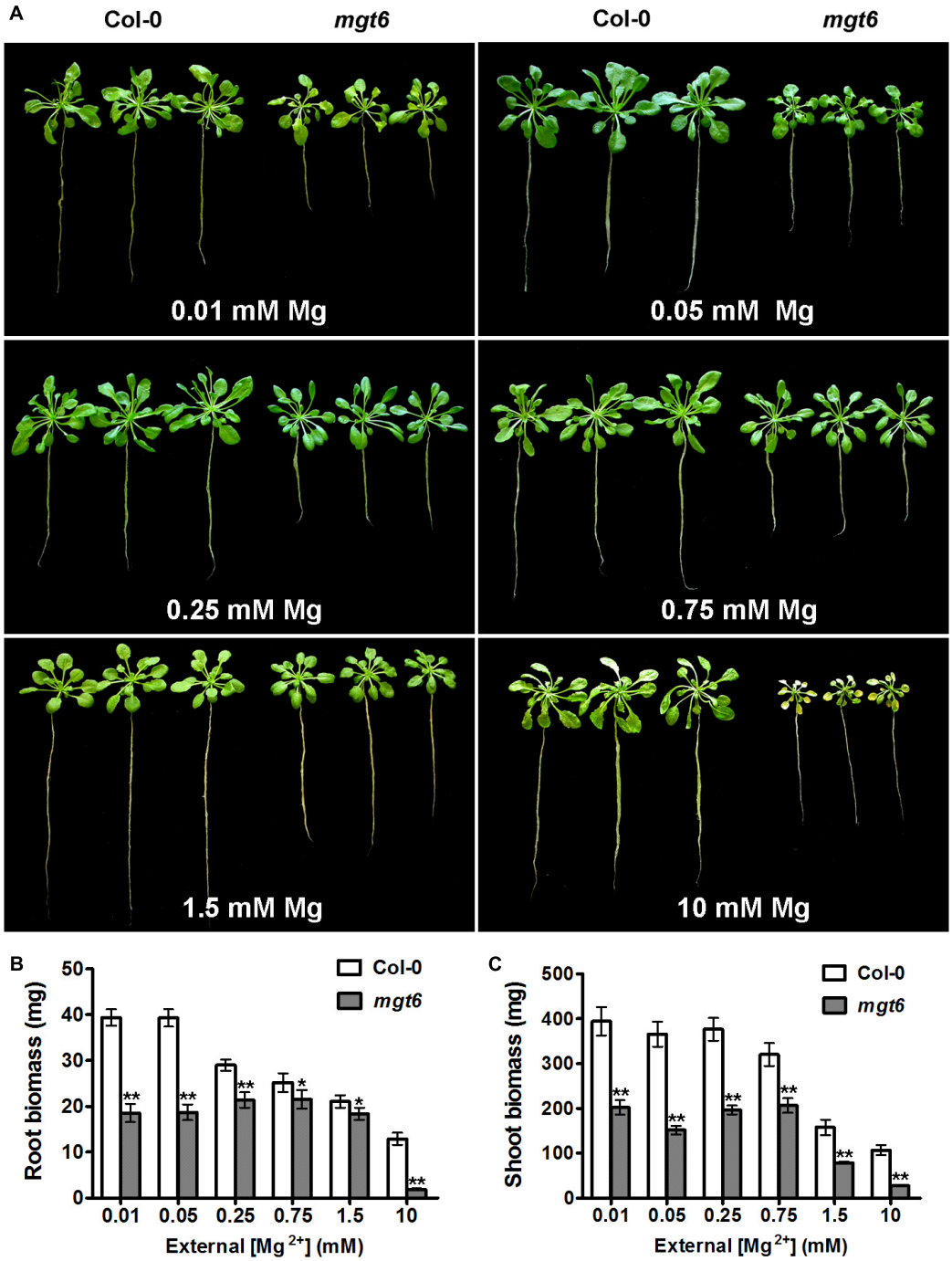

FIGURE 3 | Mature plant phenotypes of *mgt6* mutants in a range of different external Mg^{2+} concentrations. **(A)** Growth phenotypes of 1-month-old wild-type plants and *mgt6* mutants under hydroponic conditions containing indicated concentrations of Mg^{2+}. **(B)** Quantification of root biomass. **(C)** Quantification of shoot biomass. Data represent means ± SE of three replicate experiments. Asterisks indicate significant difference between the wild type and *mgt6* mutant (Student's *t*-test, $*P < 0.05$, $**P < 0.01$).

parameters of plant growth, was comparable between the wild-type and mutant plants grown under 1.5 mM Mg^{2+} (**Figure 4B**). The *mgt6* mutant retained significantly less Ca in the root and slightly decreased Ca content in the shoot tissue when plants were cultured in 6 mM Mg^{2+} (**Figure 4B**).

We further measured the Mg and Ca content in the hydroponically grown mature plants. As the external Mg^{2+} levels increased, wild-type plants accumulated elevated amount of Mg in both root and shoot tissues. The *mgt6* plants generally showed a significant reduction in root Mg content compared with

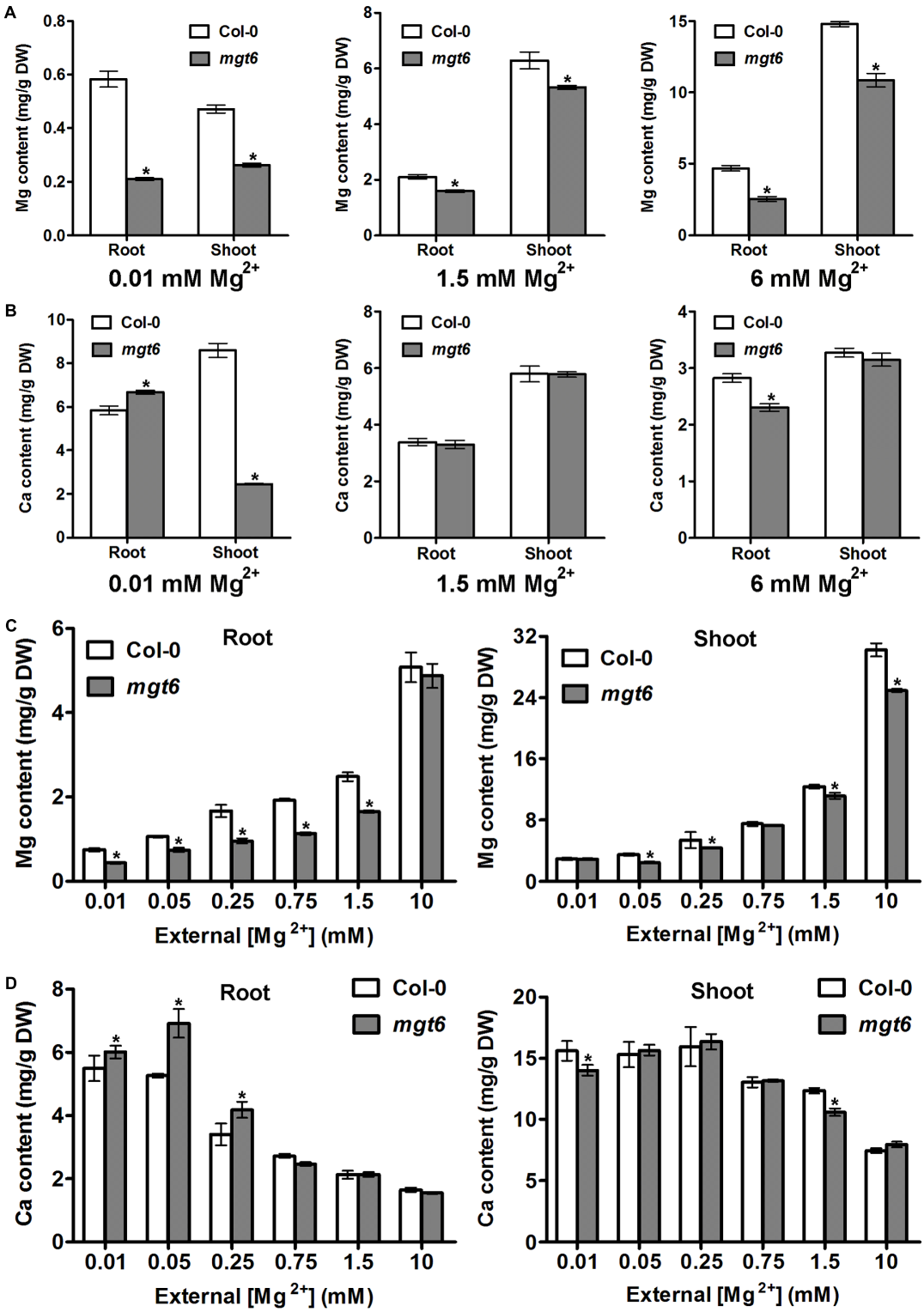

FIGURE 4 | Mg and Ca content in the *mgt6* mutant under various growth conditions. **(A)** Mg content in the root and shoot of 2-week-old wild-type and *mgt6* plants grown on the plates containing indicated concentrations of Mg^{2+}. **(B)** Ca content in the root and shoot of 2-week-old wild-type and *mgt6* plants grown on the plates containing indicated concentrations of Mg^{2+}. **(C)** Mg content in the root and shoot of 4-week-old wild-type and *mgt6* plants grown in the hydroponic solutions containing various concentrations of Mg^{2+}. **(D)** Ca content in the root and shoot of 4-week-old wild-type and *mgt6* plants grown in the hydroponic solutions containing various concentrations of Mg^{2+}. Data represent means ± SE of four replicate experiments. Asterisks indicate significant difference between the wild type and *mgt6* mutant (Student's *t*-test, $*P < 0.05$).

wild type, except under 10 mM Mg^{2+} (**Figure 4C**). However, the shoot Mg content between wild type and *mgt6* is most strikingly different under 10 mM Mg^{2+}, although under some other concentrations of Mg^{2+}, such as 0.05, 0.25, and 1.5 mM, *mgt6* mutant also contained lower Mg content in the shoot compared with wild type (**Figure 4C**). Plant Ca contents are negatively correlated with external Mg^{2+} levels. Under low-Mg conditions (0.01, 0.05, and 0.25 mM), an obvious elevation in root Ca was observed in the *mgt6* mutant (**Figure 4D**), presumably due to the antagonistic interaction between Mg and Ca. These results suggest MGT6 regulates plant Mg^{2+} homeostasis in both roots and shoots, and functions in a wide range of external Mg^{2+} concentrations at all developmental stages.

Grafting Assay Uncovers a Shoot-Based Mechanism for MGT6 Function in High-Mg Tolerance

While the low-Mg sensitive phenotype of *mgt6* can be explained by impaired Mg^{2+} uptake by root under Mg-limited conditions in the mutant, the high-Mg susceptibility of *mgt6* remains obscure. Since MGT6 controls both root and shoot Mg^{2+} homeostasis, we attempted to further investigate the mechanism by which MGT6 contributes to plant Mg^{2+} tolerance. Because MGT6 is widely expressed in plants, we decided to examine the relative contribution of MGT6 in roots versus in shoots through reciprocal grafting experiments between *mgt6* mutants and wild-type plants (**Figure 5**). When grown under low-Mg^{2+} conditions (0.01 mM), the shoots with wild-type scions and *mgt6* rootstocks appeared to be smaller than that of self-grafted wild-type plants, although the root looked similar. The grafted plants with *mgt6* scions and wild-type rootstocks were significantly smaller than wild-type self-grafted plants, but generally larger than *mgt6* self-grafted plants. Under the moderate level of Mg^{2+} (1.5 mM), both groups of the reciprocal grafted plants grew smaller than wild-type self-grafted plants. However, in the hydroponic culture containing 10 mM Mg^{2+}, which is considered to be a toxic concentration, the grafted plants with *mgt6* scions and wild-type rootstocks phenocopied the defects seen in the *mgt6* self-grafts, whereas the grafted plants with wild-type scions and *mgt6* rootstocks resembled the phenotype of wild-type self-grafted plants (**Figure 5A**). We measured root and shoot fresh weight quantitatively, which verified the growth phenotypes (**Figures 5B,C**). These observations suggested that MGT6 is important in both root and shoot tissues when external Mg^{2+} is low and moderate. Presumably, MGT6-mediated absorption of external Mg^{2+} represents the dominant role under these conditions. When the external Mg^{2+} is extremely high, MGT6 function in the shoot becomes critical to detoxify excessive Mg^{2+} at the whole plant level. Consistent with this notion, wild-type scions grafted on mgt6 rootstocks lead to significantly lower root Mg^{2+} content under 0.01 and 1.5 mM Mg^{2+} conditions (**Figures 6A,B**). In the presence of 10 mM external Mg^{2+}, shoots from *mgt6* grafted onto wild-type rootstocks retained much less Mg^{2+} in the shoot, similar to that observed in self-grafted *mgt6* plants (**Figure 6C**). This further supported the idea that MGT6 fulfills a shoot-based mechanism to detoxify excessive Mg^{2+}, which could involve vacuolar Mg^{2+} storage based on the observation of lower Mg content in the mutant shoots.

Functional Synergy of MGT6 and MGT7 in *Arabidopsis*

Arabidopsis MGT7 encodes a low-affinity Mg^{2+} transporter (Mao et al., 2008) and is indispensable for optimal plant growth under low-Mg^{2+} conditions (Gebert et al., 2009). To investigate the functional interaction between MGT6 and MGT7, we created a double mutant that lacks both *MGT6* and *MGT7* transcripts (Supplementary Figure S3A). We found that the *mgt6 mgt7* double mutant displayed pronounced growth retardation in the soil (Supplementary Figure S3B). Quantitative analysis indicated that the shoot fresh weight of the double mutant was only half of that of the wild type and single mutants (Supplementary Figure S3C).

We examined the growth phenotype of *mgt6 mgt7* double mutant under various external Mg^{2+} concentrations, in comparison with wild-type as well as the *mgt6* and *mgt7* single mutants. While *mgt6* single mutants exhibited very strong growth defects under both low- and high-Mg conditions, the phenotype of *mgt7* single mutant under the same condition was mild (**Figure 7A**). However, the *mgt6 mgt7* double mutant was significantly more sensitive to external Mg^{2+} than the *mgt6* single mutant (**Figure 7A**). The primary root of *mgt6 mgt7* was shorter than that of *mgt6* under low-Mg conditions (**Figure 7B**), although seedling fresh weight was comparable (**Figure 7C**). The leaf chlorophyll content in *mgt6 mgt7*was lower compared with *mgt6* when high Mg^{2+} is present in the medium (**Figure 7D**).

Gene expression analysis indicated that a handful of gene markers (Kamiya et al., 2012) were more responsive to Mg-starvation in the *mgt6* or *mgt7* mutant background than in the wild type, suggesting that the *mgt6* and *mgt7* mutants are impaired in low-Mg^{2+} adaptation. Consistent with the more severe phenotype, the *mgt6 mgt7* double mutant displayed enhanced expression of Mg-starvation marker genes compared with the single mutants (Supplementary Figure S4). Taken together, these results indicate both MGT6 and MGT7 are important for plant Mg homeostasis and their functions are additive in regulating Mg^{2+} transport under a wide range of external Mg^{2+} concentrations.

DISCUSSIONS

In addition to air and water, plant growth and development rely on mineral nutrients taken up by roots and translocated into the shoot tissues through apoplast and symplast pathways, which entail not only transpiration-driven mass flow but also active membrane transport processes facilitated by various ion channels and transporters. Mg is an essential macronutrient in plants with diverse biological functions. However, the molecular mechanisms for Mg transport and homeostasis in plant cells remain largely unknown. Genomes of many plants such as *Arabidopsis*, rice, and maize, encode homologs of the bacterial CorA-type proteins referred to as MGTs/MRS2s (Li et al., 2001, 2016; Saito et al., 2013). Some members of the MGT family have been functionally

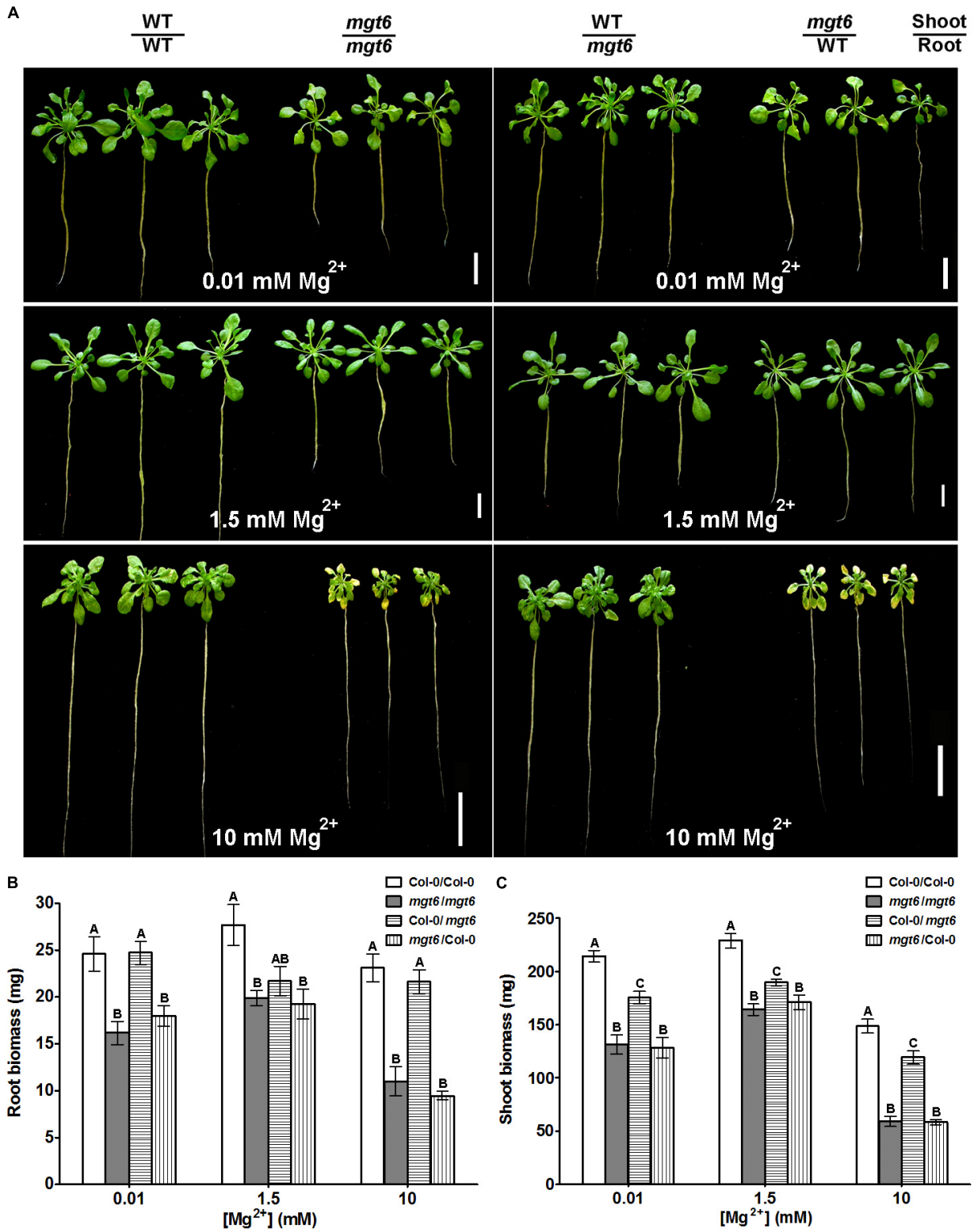

FIGURE 5 | Phenotypic analysis of reciprocal grafting of wild-type and *mgt6* plants. **(A)** Growth phenotypes of 1-month-old grafted plants with different combinations under hydroponic conditions containing indicated concentrations of Mg^{2+}. The genotype of the shoot scion is indicated in the upper part and the genotype of the rootstock is indicated in the lower part. Scale bar = 2 cm. **(B)** Quantification of root biomass. **(C)** Quantification of shoot biomass. Data represent means ± SE of three replicate experiments. Columns with different letters indicate significant difference (one-way ANOVA test, $P < 0.05$).

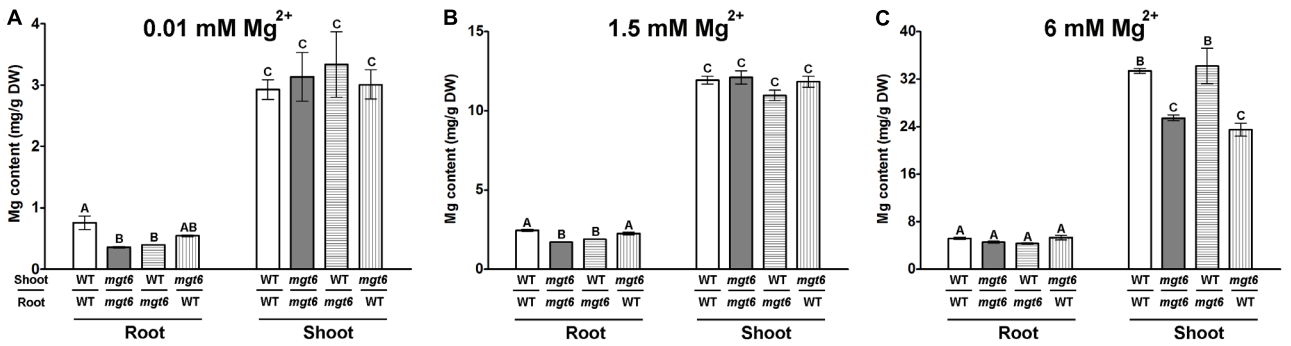

FIGURE 6 | Mg content in grafted plants under different external Mg^{2+} conditions. **(A–C)** Determination of Mg content in the root and shoot tissues of four types of grafted plants grown in the hydroponic solutions containing different concentrations of Mg^{2+} (0.01, 1.5, and 6 mM). Data represent means ± SE of four replicate experiments. Columns with different letters indicate significant difference (one-way ANOVA test, $P < 0.05$).

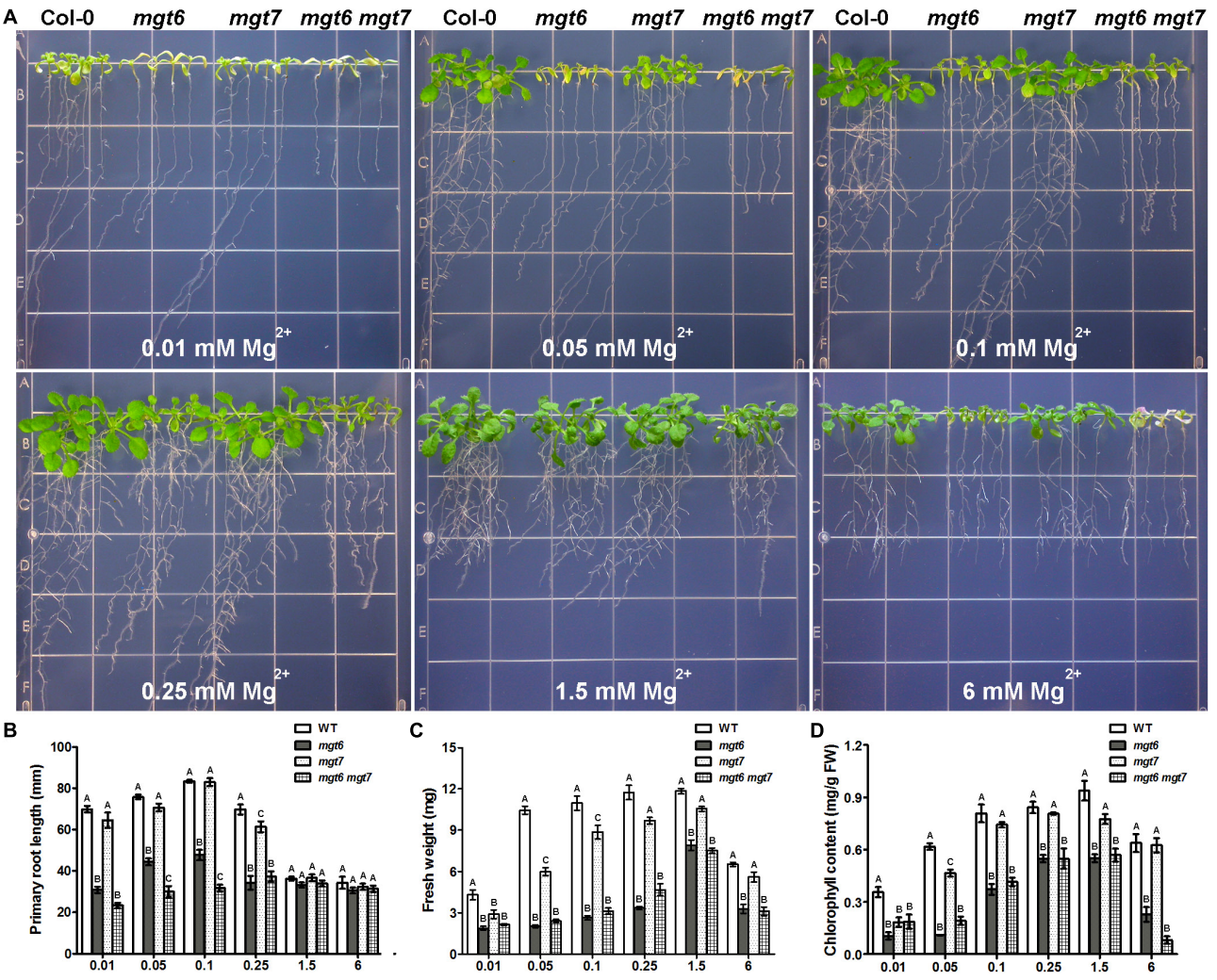

FIGURE 7 | The *mgt6 mgt7* double mutant shows enhanced sensitivity to low- and high-Mg stresses than the single mutants. **(A)** Growth phenotype of 5-day-old young seedlings transferred onto the medium supplemented with indicated concentrations of Mg^{2+} for 10 days. **(B)** Quantification of primary root length of 15-day-old seedlings at the end of treatment. **(C)** Quantification of seedling fresh weight. **(D)** Quantification of leaf chlorophyll content. Data represent means ± SE of four replicate experiments. Columns with different letters indicate significant difference (one-way ANOVA test, $P < 0.05$).

characterized, but the physiological roles of these transporters are not well understood. In *Arabidopsis*, we previously showed that MGT6 is capable of facilitating high-affinity Mg^{2+} uptake from the soil when external Mg^{2+} concentration is in the sub-millimolar range (Mao et al., 2014). Consistent with this role, expression of the *MGT6* gene is highly inducible in the root tissues in response to low Mg (Mao et al., 2014). In the present study, we not only corroborated earlier findings regarding the critical role of MGT6 in low-Mg adaptation, but also extended the function of MGT6 in controlling plant Mg^{2+} homeostasis within a wide range of external Mg^{2+} levels. The *mgt6* knock-out mutant displayed obvious phenotype under high-Mg conditions, suggesting MGT6 exerts physiological functions in plants other than Mg^{2+} absorption. In higher plants, after absorption from the soil solution by roots, Mg^{2+} is believed to be transported to the aerial parts via transpiration stream moving through the xylem vessels. However, little is known about the molecular identity of the transporters involved in this long-distance transport. MGT6 might fulfill such a role in the xylem transport of Mg^{2+}. Considering the negative membrane potential, Mg^{2+} is expected to be loaded passively into the pericycle cells. MGT6 may be responsible for Mg^{2+} import into pericycle and xylem parenchyma cells. On the other hand, the possibility that MGT6 serves as an "exporter" in this process cannot be excluded. It is generally believed that ion secretion occurs across plasmalemma of the parenchyma cells surrounding the xylem vessels (Clarkson, 1993; Gaymard et al., 1998). Interestingly, MGT5, the closest homolog of MGT6 in *Arabidopsis*, was shown to be a bidirectional Mg^{2+} carrier that operates in a concentration-dependent manner (Li et al., 2008). Therefore, it is possible that MGT6 might also function in Mg^{2+} efflux from xylem parenchyma cells, pushing Mg^{2+} influx into the xylem vessel. Future electrophysiological analysis of MGT6 conductance is required to test this hypothesis.

Although Mg^{2+} is an essential mineral, high levels of Mg^{2+}, such as those in the serpentine soils, could be toxic to plants. Recently we established that vacuolar sequestering of Mg^{2+}, regulated by the tonoplast CBL-CIPK signaling network, is crucial for plants to survive under high-Mg conditions (Tang et al., 2015). In the present work, we uncovered another component mainly fulfilled by MGT6 that underlies high-Mg tolerance at the whole plant level. Previous studies indicate that serpentine-adapted plants appear to efficiently transport Mg^{2+} from root to shoot, whereas the serpentine-sensitive counterparts are less capable of driving Mg^{2+} entry into the transpiration stream, resulting in a lower Mg^{2+} concentration in the shoot (Palm et al., 2012). Consistent with this finding, our physiological analysis of *mgt6* mutant under high-Mg conditions showed that *mgt6* retained considerably less Mg^{2+} in the shoot tissue compared to wild-type, accompanied by the growth retardation upon high-Mg stress. These data support the notion that long-distance Mg^{2+} transport mediated by MGT6 may play a critical role in protecting plants from Mg^{2+} toxicity at the whole plant level. More importantly, reciprocal grafting test indicated that MGT6 function in the shoot tissue is responsible for the high-Mg^{2+} tolerance. Considering the plasma membrane localization of MGT6, it is reasonable to speculate that MGT6 probably facilitates Mg^{2+} entry into the cytosol of leaf cells after the Mg^{2+} ions in the xylem unload into the apoplastic space. The excessive Mg^{2+} in the cytosol is subsequently sequestered into the central vacuole via tonoplast-localized Mg^{2+} transporters. This transport cascade is critical for detoxification of excessive Mg^{2+}, which is reminiscent of a recent model proposed for Ca^{2+} detoxification in plants (Wang et al., 2017).

Another notable finding in this study is that another MGT-type transporter MGT7 partially overlaps with the function of MGT6. With a preferential expression in the root, MGT7 was shown to be important for plant adaptation to low-Mg conditions (Gebert et al., 2009). In our study, we found that although MGT6 plays a more dominant role in low-Mg conditions, MGT7 seems to be additive to MGT6 function because *mgt6 mgt7* double mutant is more sensitive to low-Mg stress than the *mgt6* single mutant, which is also supported by the enhanced activation of Mg-starvation gene expression in the double mutant. Interestingly, under high-Mg conditions, mutation of MGT7 also significantly enhanced the sensitivity of *mgt6*, although single mutant of *mgt7* only exhibited a subtle phenotype under the same condition. These results suggest that MGT7 synergistically works together with MGT6 in the context of Mg^{2+} homeostasis at the whole plant level. Further investigations will sort out the mode of action for each of them to explain this functional synergy.

Subcellular localization of the MGT proteins may prove to be difficult to study. For instance, recent studies reported discrepant cellular localizations for MGT6 in the plasma membrane (Mao et al., 2014) and endoplasmic reticulum (ER; Oda et al., 2016), respectively. Several other MGT members such as MGT7 (Gebert et al., 2009) and MGT4 (Li et al., 2015) were also shown to be ER-associated, which needs to be re-evaluated because quite a few membrane proteins tend to be mis-targeted to ER, especially when overexpressed in a transient expression system (Denecke et al., 2012; Quattrocchio et al., 2013; Segami et al., 2014). Future studies using the native promoter, coupled with functional complementation in the mutant background as well as other approaches, are needed to verify the subcellular localization of MGT-type transporters *in situ*. It will also be interesting to examine if the targeting of MGT6 or MGT7 would be dynamically altered in different subcellular compartments in response to various Mg^{2+} concentrations.

As sessile organisms, plants have to cope with fluctuating concentrations of Mg^{2+} in nature. How plants maintain a balanced level of Mg^{2+} is not well understood. The present study as well as our previous work provides a working model in which MGT6 plays a dual role in controlling Mg^{2+} homeostasis. When external Mg^{2+} is limited, expression of *MGT6* is induced in root epidermal cells and root hairs, making this transporter primarily responsible for Mg^{2+} uptake from the soil. When external Mg^{2+} is sufficient or becomes excessive, MGT6 mediates Mg^{2+} loading into the shoot tissues, where leaf mesophyll cells can subsequently sequester extra amount of Mg^{2+} into large vacuoles via yet-unknown transporters. Future efforts

should be made in identifying uncharacterized Mg^{2+} transport proteins in plants. Furthermore, establishing the regulators and signaling pathways that fine-tune the expression and function of these transport systems will be a challenging but urgent task, which will ultimately lead to genetic manipulation of plants for precise adaption to the changing Mg^{2+} concentrations in the environment.

AUTHOR CONTRIBUTIONS

Y-WY and R-JT designed and conducted most of the experiments, interpreted the results, and wrote the draft of the manuscript. D-DM, X-XZ, Q-LT, and Y-PL assisted in some experiments and helped analyze the data. LY and J-LQ provided tools and reagents and made helpful discussions. SL supervised and conceptualized the study and finalized the paper. All the authors approved the final version of the manuscript.

FUNDING

This work was funded by National Science Foundation to SL and National Natural Science Foundation of China (31500200) to D-DM. Y-WY was in part supported by a fellowship from the China Scholarship Council.

SUPPLEMENTARY MATERIAL

The Supplementary Material for this article can be found online at: https://www.frontiersin.org/articles/10.3389/fpls.2018.00274/full#supplementary-material

REFERENCES

Brady, K. U., Kruckeberg, A. R., and Bradshaw, H. D. (2005). Evolutionary ecology of plant adaptation to serpentine soils. *Annu. Rev. Ecol. Evol. Syst.* 36, 243–266. doi: 10.1146/annurev.ecolsys.35.021103.105730

Chen, J., Li, L. G., Liu, Z. H., Yuan, Y. J., Guo, L. L., Mao, D. D., et al. (2009). Magnesium transporter AtMGT9 is essential for pollen development in *Arabidopsis*. *Cell Res.* 19, 887–898. doi: 10.1038/cr.2009.58

Chen, Z. C., Yamaji, N., Horie, T., Che, J., Li, J., An, G., et al. (2017). A Magnesium transporter *OsMGT1* plays a critical role in salt tolerance in rice. *Plant Physiol.* 174, 1837–1849. doi: 10.1104/pp.17.00532

Chen, Z. C., Yamaji, N., Motoyama, R., Nagamura, Y., and Ma, J. F. (2012). Up-regulation of a magnesium transporter gene OsMGT1 is required for conferring aluminum tolerance in rice. *Plant Physiol.* 159, 1624–1633. doi: 10.1104/pp.112.199778

Clarkson, D. T. (1993). Roots and the delivery of solutes to the xylem. *Philos. Trans. R. Soc. B* 341, 5–17. doi: 10.1098/rstb.1993.0086

Clough, S. J., and Bent, A. F. (1998). Floral dip: a simplified method for *Agrobacterium*-mediated transformation of *Arabidopsis thaliana*. *Plant J.* 16, 735–743. doi: 10.1046/j.1365-313x.1998.00343.x

Conn, S. J., Conn, V., Tyerman, S. D., Kaiser, B. N., Leigh, R. A., and Gilliham, M. (2011). Magnesium transporters, MGT2/MRS2-1 and MGT3/MRS2-5, are important for magnesium partitioning within *Arabidopsis thaliana* mesophyll vacuoles. *New Phytol.* 190, 583–594. doi: 10.1111/j.1469-8137.2010.03619.x

Denecke, J., Aniento, F., Frigerio, L., Hawes, C., Hwang, I., Mathur, J., et al. (2012). Secretory pathway research: the more experimental systems the better. *Plant Cell* 24, 1316–1326. doi: 10.1105/tpc.112.096362

Drummond, R. S. M., Tutone, A., Li, Y. C., and Gardner, R. C. (2006). A putative magnesium transporter AtMRS2-11 is localized to the plant chloroplast envelope membrane system. *Plant Sci.* 170, 78–89. doi: 10.1016/j.plantsci.2005.08.018

Eshaghi, S., Niegowski, D., Kohl, A., Molina, D. M., Lesley, S. A., and Nordlund, P. (2006). Crystal structure of a divalent metal ion transporter CorA at 2.9 angstrom resolution. *Science* 313, 354–357. doi: 10.1126/science.1127121

Gaymard, F., Pilot, G., Lacombe, B., Bouchez, D., Bruneau, D., Boucherez, J., et al. (1998). Identification and disruption of a plant shaker-like outward channel involved in K+ release into the xylem sap. *Cell* 94, 647–655. doi: 10.1016/S0092-8674(00)81606-2

Gebert, M., Meschenmoser, K., Svidova, S., Weghuber, J., Schweyen, R., Eifler, K., et al. (2009). A root-expressed magnesium transporter of the MRS2/MGT gene family in *Arabidopsis thaliana* allows for growth in low-Mg2+ environments. *Plant Cell* 21, 4018–4030. doi: 10.1105/tpc.109.070557

Hermans, C., Conn, S. J., Chen, J. G., Xiao, Q. Y., and Verbruggen, N. (2013). An update on magnesium homeostasis mechanisms in plants. *Metallomics* 5, 1170–1183. doi: 10.1039/c3mt20223b

Kamiya, T., Yamagami, M., Hirai, M. Y., and Fujiwara, T. (2012). Establishment of an *in planta* magnesium monitoring system using *CAX3* promoter-luciferase in *Arabidopsis*. *J. Exp. Bot.* 63, 355–363. doi: 10.1093/jxb/err283

Li, H. Y., Du, H. M., Huang, K. F., Chen, X., Liu, T. Y., Gao, S. B., et al. (2016). Identification, and functional and expression analyses of the CorA/MRS2/MGT-Type magnesium transporter family in maize. *Plant Cell Physiol.* 57, 1153–1168. doi: 10.1093/pcp/pcw064

Li, J., Huang, Y., Tan, H., Yang, X., Tian, L., Luan, S., et al. (2015). An endoplasmic reticulum magnesium transporter is essential for pollen development in *Arabidopsis*. *Plant Sci.* 231, 212–220. doi: 10.1016/j.plantsci.2014.12.008

Li, L., Tutone, A. F., Drummond, R. S., Gardner, R. C., and Luan, S. (2001). A novel family of magnesium transport genes in Arabidopsis. *Plant Cell* 13, 2761–2775. doi: 10.1105/tpc.13.12.2761

Li, L. G., Sokolov, L. N., Yang, Y. H., Li, D. P., Ting, J., Pandy, G. K., et al. (2008). A mitochondrial magnesium transporter functions in *Arabidopsis* pollen development. *Mol. Plant* 1, 675–685. doi: 10.1093/mp/ssn031

Liang, S., Qi, Y. F., Zhao, J., Li, Y. F., Wang, R., Shao, J. X., et al. (2017). Mutations in the Arabidopsis *AtMRS2-11/AtMGT10/VAR5* gene cause leaf reticulation. *Front. Plant Sci.* 8:2007. doi: 10.3389/fpls.2017.02007

Lunin, V. V., Dobrovetsky, E., Khutoreskaya, G., Zhang, R., Joachimiak, A., Doyle, D. A., et al. (2006). Crystal structure of the CorA Mg2+ transporter. *Nature* 440, 833–837. doi: 10.1038/nature04642

Mao, D., Chen, J., Tian, L., Liu, Z., Yang, L., Tang, R., et al. (2014). *Arabidopsis* transporter MGT6 mediates magnesium uptake and is required for growth under magnesium limitation. *Plant Cell* 26, 2234–2248. doi: 10.1105/tpc.114.124628

Mao, D. D., Tian, L. F., Li, L. G., Chen, J., Deng, P. Y., Li, D. P., et al. (2008). *AtMGT7*: an *Arabidopsis* gene encoding a low-affinity magnesium transporter. *J. Integr. Plant Biol.* 50, 1530–1538. doi: 10.1111/j.1744-7909.2008.00770.x

Marsch-Martínez, N., Franken, J., Gonzalez-Aguilera, K. L., De Folter, S., Angenent, G., and Alvarez-Buylla, E. R. (2013). An efficient flat-surface collar-free grafting method for *Arabidopsis thaliana* seedlings. *Plant Methods* 9:14. doi: 10.1186/1746-4811-9-14

Murashige, T., and Skoog, F. (1962). A revised medium for rapid growth and bioassays with tobacco tissue cultures. *Physiol. Plant* 15, 473–495. doi: 10.1111/j.1399-3054.1962.tb08052.x

Oda, K., Kamiya, T., Shikanai, Y., Shigenobu, S., Yamaguchi, K., and Fujiwara, T. (2016). The Arabidopsis Mg transporter, MRS2-4, is essential for Mg homeostasis under both low and high Mg conditions. *Plant Cell Physiol.* 57, 754–763. doi: 10.1093/pcp/pcv196

Palm, E., Brady, K., and Van Volkenburgh, E. V. (2012). Serpentine tolerance in *Mimulus guttatus* does not rely on exclusion of magnesium. *Funct. Plant Biol.* 39, 679–688. doi: 10.1007/s00442-009-1448-0

Quattrocchio, F. M., Spelt, C., and Koes, R. (2013). Transgenes and protein localization: myths and legends. *Trends Plant Sci.* 18, 473–476. doi: 10.1016/j.tplants.2013.07.003

Saito, T., Kobayashi, N. I., Tanoi, K., Iwata, N., Suzuki, H., Iwata, R., et al. (2013). Expression and functional analysis of the CorA-MRS2-ALR-type magnesium transporter family in rice. *Plant Cell Physiol.* 54, 1673–1683. doi: 10.1093/pcp/pct112

Schock, I., Gregan, J., Steinhauser, S., Schweyen, R., Brennicke, A., and Knoop, V. (2000). A member of a novel *Arabidopsis thaliana* gene family of candidate Mg2+ ion transporters complements a yeast mitochondrial group II intron-splicing mutant. *Plant J.* 24, 489–501. doi: 10.1046/j.1365-313x.2000.00895.x

Segami, S., Makino, S., Miyake, A., Asaoka, M., and Maeshima, M. (2014). Dynamics of vacuoles and H^+-pyrophosphatase visualized by monomeric green fluorescent protein in *Arabidopsis*: artifactual bulbs and native intravacuolar spherical structures. *Plant Cell* 26, 3416–3434. doi: 10.1105/tpc.114.127571

Shaul, O. (2002). Magnesium transport and function in plants: the tip of the iceberg. *Biometals* 15, 309–323. doi: 10.1023/A:1016091118585

Sun, Y., Yang, R. A., Li, L. G., and Huang, J. R. (2017). The magnesium transporter MGT10 is essential for chloroplast development and photosynthesis in *Arabidopsis thaliana*. *Mol. Plant* 10, 1584–1587. doi: 10.1016/j.molp.2017.09.017

Szegedy, M. A., and Maguire, M. E. (1999). The CorA Mg^{2+} transport protein of *Salmonella typhimurium* mutagenesis of conserved residues in the second membrane domain. *J. Biol. Chem.* 274, 36973–36979. doi: 10.1074/jbc.274.52.36973

Tang, R. J., and Luan, S. (2017). Regulation of calcium and magnesium homeostasis in plants: from transporters to signaling network. *Curr. Opin. Plant Biol.* 39, 97–105. doi: 10.1016/j.pbi.2017.06.009

Tang, R. J., Zhao, F. G., Garcia, V. J., Kleist, T. J., Yang, L., Zhang, H. X., et al. (2015). Tonoplast CBL-CIPK calcium signaling network regulates magnesium homeostasis in Arabidopsis. *Proc. Natl. Acad. Sci. U.S.A.* 112, 3134–3139. doi: 10.1073/pnas.1420944112

Turner, T. L., Bourne, E. C., Von Wettberg, E. J., Hu, T. T., and Nuzhdin, S. V. (2010). Population resequencing reveals local adaptation of *Arabidopsis lyrata* to serpentine soils. *Nat. Genet.* 42, 260–263. doi: 10.1038/ng.515

Wang, Y., Kang, Y., Ma, C., Miao, R., Wu, C., Long, Y., et al. (2017). CNGC2 is a Ca2+ influx channel that prevents accumulation of apoplastic Ca2+ in the leaf. *Plant Physiol.* 173, 1342–1354. doi: 10.1104/pp.16.01222

Xu, X. F., Wang, B., Lou, Y., Han, W. J., Lu, J. Y., Li, D. D., et al. (2015). *Magnesium transporter 5* plays an important role in Mg transport for male gametophyte development in *Arabidopsis*. *Plant J.* 84, 925–936. doi: 10.1111/tpj.13054

Conflict of Interest Statement: The authors declare that the research was conducted in the absence of any commercial or financial relationships that could be construed as a potential conflict of interest.

frontiers in Plant Science

ORIGINAL RESEARCH
published: 06 March 2018
doi: 10.3389/fpls.2018.00285

SlCNGC1 and *SlCNGC14* Suppress *Xanthomonas oryzae* pv. *oryzicola*-Induced Hypersensitive Response and Non-host Resistance in Tomato

*Xuan-Rui Zhang[1], You-Ping Xu[2] and Xin-Zhong Cai[1]**

[1] Institute of Biotechnology, College of Agriculture and Biotechnology, Zhejiang University, Hangzhou, China, [2] Center of Analysis and Measurement, Zhejiang University, Hangzhou, China

Mechanisms underlying plant non-host resistance to *Xanthomonas oryzae* pv. *oryzicola* (*Xoc*), the pathogen causing rice leaf streak disease, are largely unknown. Cyclic nucleotide-gated ion channels (CNGCs) are calcium-permeable channels that are involved in various biological processes including plant resistance. In this study, functions of two tomato *CNGC* genes *SlCNGC1* and *SlCNGC14* in non-host resistance to *Xoc* were analyzed. Silencing of *SlCNGC1* and *SlCNGC14* in tomato significantly enhanced *Xoc*-induced hypersensitive response (HR) and non-host resistance, demonstrating that both *SlCNGC1* and *SlCNGC14* negatively regulate non-host resistance related HR and non-host resistance to *Xoc* in tomato. Silencing of *SlCNGC1* and *SlCNGC14* strikingly increased *Xoc*-induced callose deposition and strongly promoted both *Xoc*-induced and flg22-elicited H_2O_2, indicating that these two *SlCNGCs* repress callose deposition and ROS accumulation to attenuate non-host resistance and PAMP-triggered immunity (PTI). Importantly, silencing of *SlCNGC1* and *SlCNGC14* apparently compromised cytosolic Ca^{2+} accumulation, implying that SlCNGC1 and SlCNGC14 function as Ca^{2+} channels and negatively regulate non-host resistance and PTI-related responses through modulating cytosolic Ca^{2+} accumulation. *SlCNGC14* seemed to play a stronger regulatory role in the non-host resistance and PTI compared to *SlCNGC1*. Our results reveal the contribution of CNGCs and probably also Ca^{2+} signaling pathway to non-host resistance and PTI.

Keywords: cyclic nucleotide-gated ion channel (CNGCs), *Xanthomonas oryzae* pv. *oryzicola*, PAMP-triggered immunity, non-host resistance, Ca^{2+} signaling

OPEN ACCESS

Edited by:
Gerald Alan Berkowitz, University of Connecticut, United States

Reviewed by:
Keiko Yoshioka, University of Toronto, Canada
Selena Gimenez-Ibanez, Centro Nacional de Biotecnología, Spain

****Correspondence:***
Xin-Zhong Cai
xzhcai@zju.edu.cn

Specialty section:
This article was submitted to Plant Traffic and Transport, a section of the journal Frontiers in Plant Science

Received: *31 August 2017*
Accepted: *19 February 2018*
Published: *06 March 2018*

Citation:
Zhang X-R, Xu Y-P and Cai X-Z (2018) SlCNGC1 and SlCNGC14 Suppress Xanthomonas oryzae pv. oryzicola-Induced Hypersensitive Response and Non-host Resistance in Tomato. Front. Plant Sci. 9:285. doi: 10.3389/fpls.2018.00285

INTRODUCTION

Each pathogen has its own host range. Non-host resistance is triggered when a non-adapted pathogen attempts to infect a plant species outside of its host range. Thus, non-host resistance is widely occurring, durable and broad-spectrum to non-adapted pathogens and is highly potential to be exploited in crop resistance engineering (Schulze-Lefert and Panstruga, 2011; Senthil-Kumar and Mysore, 2013). It has been clear that plant non-host resistance utilizes both preformed and induced defense mechanisms and frequently elicites hypersensitive response (HR)

(Mysore and Ryu, 2004; Senthil-Kumar and Mysore, 2013). The preformed mechanisms generally consist of plant physical and chemical barriers, including antibiotic compounds (Bednarek and Osbourn, 2009; Fan et al., 2011). The induced non-host resistance is elicited after the preformed defense is overcome. As observed for host resistance, pathogen-associated molecular pattern (PAMP)-triggered immunity (PTI) and effector-triggered immunity (ETI) are often initiated in this layer of defense (Niks and Marcel, 2009; Senthil-Kumar and Mysore, 2013). Efforts to identifiy non-host resistance-related genes resulted in the finding that some genes, such as *PLD*δ, *GOX*, *SGT1,* and *NHO1*, contribute to both host and non-host resistance in Arabidopsis (Lu et al., 2001; Maimbo et al., 2010; Rojas et al., 2012; Pinosa et al., 2013). Generally speaking, the mechanisms underlying plant non-host resistance are far from well understood.

Xanthomonas oryzae pv. *oryzae* (*Xoo*) and *X. oryzae* pv. *oryzicola* (*Xoc*) are two important pathovars of *X. oryzae*, causing bacterial blight and leaf streak diseases, respectively, in rice (*Oryza sativa*), which is a staple food in many countries and a model plant for cereal biology (Nino-Liu et al., 2006). It is notable that these two pathovars utilize distinct mechanisms to infect rice leaves. *Xoo* is a vascular pathogen that enters rice leaves via the hydathodes, while *Xoc* penetrates rice leaves mainly through stomata or wound sites and colonizes intercellular spaces in the mesophyll (Nino-Liu et al., 2006). During infection of their plant hosts, many strains secrete transcription activator-like (TAL) effectors, which enter the host cell nucleus and activate specific corresponding host genes at effector binding elements (EBEs) in the promoter (Boch et al., 2009; Moscou and Bogdanove, 2009). It has been established that host resistance to *Xoo* is mostly related to the action of TAL effectors, either by polymorphisms that prevent the induction of susceptibility (S) genes or by executor resistance (R) genes with EBEs embedded in their promoter, and that induce cell death and resistance (Bogdanove et al., 2010; Zhang et al., 2015). *Xoc* is known to suppress host resistance, and no host *R* gene has been identified against it (Cai et al., 2017). Compared with the host resistance (Zhang and Wang, 2013), non-host resistance to *Xoo* and *Xoc* is much less studied. We have previously identified seven genes required for non-host resistance to *Xoo* in *Nicotiana benthamiana*. Among them are a calreticulin and a peroxidase, indicating that oxidative burst and calcium-dependent signaling pathways play an important role in non-host resistance to *Xoo* (Li et al., 2012). However, molecular mechanisms underlying non-host resistance to *Xoc* remain largely unknown. Whether the oxidative burst and calcium signaling pathway contribute to the non-host resistance to *Xoc* as to *Xoo* awaits examination.

The cyclic nucleotide-gated ion channels (CNGCs) are suggested to be one of the important pathways for conducting Ca^{2+} ions in signaling transduction (Talke et al., 2003). They are ligand-gated Ca^{2+}-permeable divalent cation-selective channels that are often localized in plasma membrane, presumptively are activated by direct binding of cyclic nucleotides and are complexly regulated by binding of calmodulin (CaM) to the CaM Binding (CaMB) domain (Chin et al., 2009; Ma et al., 2009; Wang et al., 2013; Gao et al., 2014; DeFalco et al., 2016a,b; Fischer et al., 2017). The plant CNGCs are involved in numerous biological functions varying from plant development and stress tolerance to disease resistance (Kaplan et al., 2007; Qi et al., 2010; Ma and Berkowitz, 2011; Moeder et al., 2011). CNGCs are well conserved among plant species, comprising 20 members in Arabidopsis and 18 members in tomato (Saand et al., 2015a,b). Earlier studies revealed that *AtCNGC2*, *AtCNGC4*, *AtCNGC11,* and *AtCNGC12* and their homologs play an important role in disease resistance against various pathogens (Yu et al., 1998; Clough et al., 2000; Balagué et al., 2003; Jurkowski et al., 2004; Yoshioka et al., 2006; Ali et al., 2007; Ma and Berkowitz, 2011; Chin et al., 2013; Fortuna et al., 2015; Saand et al., 2015a). Later, other *CNGC* members such as *SlCNGC1* and *SlCNGC14* were also found to contribute to disease resistance (Saand et al., 2015a,b). We found that *SlCNGC1* and *SlCNGC14* play a negative role in non-host resistance to *Xoo* in tomato (Saand et al., 2015b). However, whether these *SlCNGCs* indeed encode functional CNGC channels and whether and how they function in non-host resistance to *Xoc* in tomato remains further study.

Our data in this study strongly indicate that SlCNGC1 and SlCNGC14 function as Ca^{2+} channels and negatively regulate tomato non-host resistance to *Xoc* through modulating ROS accumulation and callose deposition. Our results provide evidence for the contribution of CNGC-mediated Ca^{2+} signaling pathway to non-host resistance.

MATERIALS AND METHODS

Plant Growth and Inoculation

Tomato (cv. Money Maker) plants were grown in growth room at 21°C with16 h light/8 h dark photoperiod. For disease resistance evaluation analyses, tomato plants were inoculated with *X. oryzae* pv. *oryzicola* (*Xoc*). After single colony propagation culture in NA medium, the *Xoc* bacterial cells were collected and resuspended in ddH_2O to 1×10^8 cfu mL^{-1}. The bacterial suspension was then infiltrated into leaves with sterilized needleless syringe. The infiltration zones were marked immediately after infiltration. The inoculated plants were grown in growth room at 26°C with16 h light/8 h dark photoperiod.

Gene Silencing Analyses

The virus-induced gene silencing (VIGS) target fragments of SlCNGC1 (Solyc01g095770.2) and SlCNGC14 (Solyc03g114110.2) were amplified by RT-PCR with gene-specific primers (Supplementary Table S1) and ligated into the TRV-based VIGS vector pYL156, which was subsequently electroporated into *Agrobacterium tumefaciens* strain GV3101 for VIGS analyses. VIGS analyses were conducted with vacuum infiltration delivery approach as described using recombinant pYL156 with insertion of an eGFP fragment instead of an empty pYL156 as control to alleviate viral symptom (Saand et al., 2015a). At about 3 weeks post agro-infiltration, plants were inoculated with *Xoc* as described above.

Detection of Callose Deposition

Callose deposition were stained with aniline blue and visualized in fluorescence microscope. Briefly, the collected leaves were

washed twice with ddH_2O and ethanol, respectively, and cleared in acetic acid-ethanol (1:3) for 4 h. After washed twice with ddH2O, the leaves were incubated in aniline blue solution [150 mM KH_2PO_4, 0.1% (w/v) aniline blue, pH 9.5] for 1 h. The stained leaves were washed with ddH_2O and observed in 30% glycerol by fluorescence microscopy.

Bacterial Number Counting Assays

Bacterial numbers in *Xoc*-infiltrated leaves of silenced plants were determined as previously reported (Li et al., 2012).

Detection of ROS

Xoc-inoculated leaves of tomato plants were detached and stained with 3,3-diamino benzidine hydrochloride (DAB) (1mg/mL) as described (Li et al., 2015). Quantitative determination of PAMP-elicited H_2O_2 was conducted using a luminol-based approach (Saand et al., 2015a). For each experiment, six tomato leaf disks of 3 mm at diameter from three plants were dipped in distilled water in the light over night. The leaf disks were then transferred into 50 μL of distilled water in a 96-well plate. After addion of the same volume mixture which contains 200 nM luminol (Sigma-Aldrich), 20 μg of horseradish peroxidase and 200 nM flg22, H_2O_2 were measured for 35 min as luminescence using a Microplate Luminometer (Titertek Berthold, Germany).

Calcium Assay

Transient increase of cytosolic Ca^{2+} concentration was monitored in the Aequarin transgenic tomato lines. For each experiment, six leaf disks were punched from three plants and vacuum-infiltrated in 12.5 μM coelenterazin h (Sigma) on a 96-well plate for 1 min and then set for 2 h at room temperature. Before measurement, the coelenterazin solution was gently removed and 200 μL of PAMP solution (100 nM flg22) was added to the wells. Luminescence was measured using a Microplate Luminometer (Titertek Berthold, Germany).

Gene Expression Analyses by qRT-PCR

Five defense-related Ca^{2+} signaling genes SlCDPK10 (Solyc11g018610.1), SlCAMTA3 (Solyc04g056270.2), SlCBP60G (Solyc01g100240.2), SlCAM2 (Solyc10g081170.1) and SlCAM6 (Solyc03g098050.2) were subjected to gene expression analyses (Zhao et al., 2013; Rahman et al., 2016b; Wang et al., 2016). Total RNA was isolated by Trizol (TaKaRa, Japan) extraction according to the manufacture's instructions. RNAs were treated with DNase I (TaKaRa, Japan) and then reverse transcribed. Quantitative real time PCR (qRT-PCR) was performed as previously described using the StepOne Real-Time PCR system (Applied Biosystems, United States) with SYBR Green PCR Master Mix (TaKaRa, Japan) (Saand et al., 2015a). 18s rDNA was used as internal control. The accession number and the specific primers for amplification of the analyzed genes were listed (Supplementary Table S1). The expression of target genes relative to control was calculated based on a value of $2^{-\Delta\Delta Ct}$ as recommended by the manufacturer. Meanwhile, semi-qRT-PCR for these genes were conducted in parallel and obtained PCR products were analyzed by agarose gel electrophoresis.

Statistical Analyses of Data

All experiments were conducted three times independently. The quantitative measurement data were statistically analyzed using SPSS software and represent means ± standard error. Significant difference between mean values was determined with DMRT ($p < 0.05$).

RESULTS

Silencing of *SlCNGC1* and *SlCNGC14* Enhanced *Xoc*-Induced Hypersensitive Response and Non-host Resistance

In order to dissect the function of *SlCNGC1* and *SlCNGC14* in *Xoc*-induced HR and non-host resistance, we used TRV-based VIGS vector to perform VIGS analyses for these genes. Transcripts of *SlCNGC1* and *SlCNGC14* genes accumulated to only about 20% of the eGFP silencing control (**Figure 1A**), indicating that *SlCNGC1* and *SlCNGC14* genes had been effictiently silenced in these plants. Inoculation assays with *Xoc* in these silencing plants demonstrated that *SlCNGC1*- and *SlCNGC14*-silenced leaves showed more severe *Xoc*-induced HR than the eGFP control leaves. *SlCNGC1*- and *SlCNGC14*-silenced leaves showed obvious HR necrosis at 3 h post *Xoc* inoculation, and exhibited strong HR necrosis at 9 hpi, especially *SlCNGC14*-silenced leaves, which had turned into desiccative, while the eGFP control plants displayed barely visible and weak HR necrosis at 3 and 9 hpi, respectively (**Figure 1B**). This result indicated that silencing of *SlCNGC1* and *SlCNGC14* enhanced *Xoc*-induced HR.

We further counted *Xoc* bacterial number in the infiltrated leaf areas. The result showed that compared with the eGFP controls, *Xoc* bacterial number in *SlCNGC1*- and *SlCNGC14*-silenced plants decreased significantly by 0.7 orders of magnitude at 9 hpi (**Figure 1C**), indicating that silencing of *SlCNGC1* and *SlCNGC14* enhanced non-host resistance to *Xoc*.

Collectively, these results implied that both *SlCNGC1* and *SlCNGC14* might negatively regulate non-host resistance related HR cell death and non-host resistance to *Xoc* in tomato.

Silencing of *SlCNGC1* and *SlCNGC14* Increased *Xoc*-Induced Callose Deposition

To probe the mechanisms underlying *SlCNGC1*- and *SlCNGC14*-dependent regulation of non-host resistance against *Xoc*, effect of these *CNGC* genes on callose deposition upon pathogen infection was examined. Callose deposition was visible in the aniline blue-stained leaves under the fluorescence microscopy. Microscopic observation result showed that *SlCNGC1*- and *SlCNGC14*-silenced leaves deposited much more callose than eGFP control leaves (**Figure 2A**). Further quantification revealed that callose deposits in *SlCNGC1*- and *SlCNGC14*-silenced leaves was 5.9- and 7.3-fold respectively, as many as in the eGFP control leaves at 4 hpi (**Figure 2B**). This result demonstrates that *SlCNGC1* and *SlCNGC14* repress the callose deposition upon

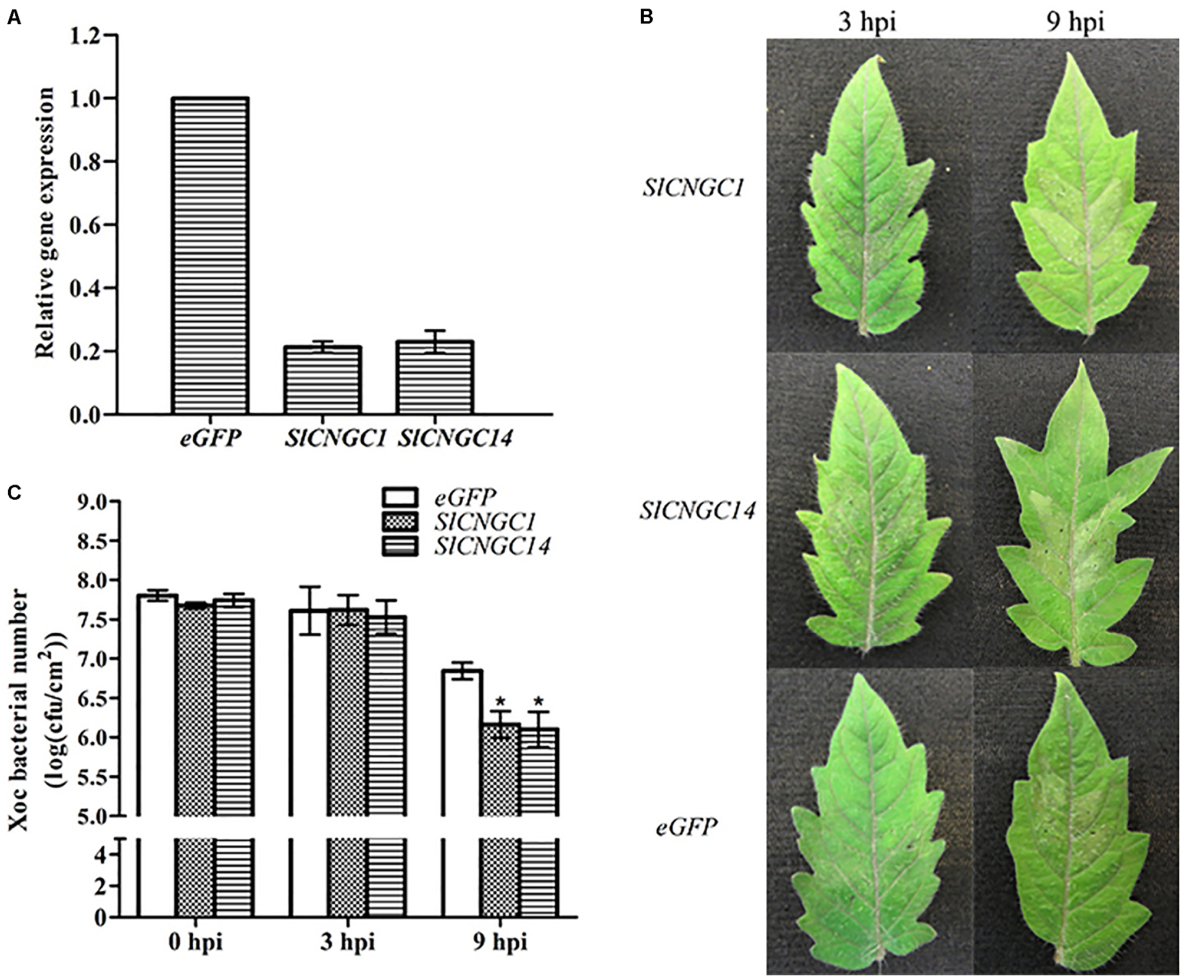

FIGURE 1 | Silencing of *SlCNGC1* and *SlCNGC14* enhanced HR and non-host resistance to *Xoc* in tomato. **(A)** Silencing efficiency analysis. Plants infiltrated with *Agrobacterium* suspensions carrying an eGFP-control vector served as control plants. Accumulation level of *SlCNGC1* and *SlCNGC14* transcript in VIGS-treated plants and the eGFP-control plants was detected by qRT-PCR analyses. **(B)** *Xoc*-induced hypersensitive response (HR). Photographs were taken at 3 and 9 hpi. **(C)** *Xoc* bacterial number counting. *Xoc* bacterial numbers were counted in leaf areas that were inoculated with bacterium at 3 and 9 hpi. At least five leaves were tested for each treatment, and the data represent means ± standard error (SE). Significant differences between treatments and the control are indicated by an asterisk ($p < 0.05$).

pathogen infection to alleviate non-host resistance to *Xoc* in tomato.

Silencing of *SlCNGC1* and *SlCNGC14* Promoted ROS Accumulation

Reactive oxygen species (ROS) is indispensable to *X. oryzae* pv. *oryzae* (*Xoo*)-induced HR and non-host resistance (Li et al., 2015). Thus, we analyzed the effect of *SlCNGC1* and *SlCNGC14* on the production of hydrogen peroxide (H_2O_2), one of the primary species of ROS. DAB staining result demonstrated that infiltration areas of *SlCNGC1*- and *SlCNGC14*-silenced leaves showed significantly stronger DAB staining than those of control (**Figure 3A**), implying that silencing of *SlCNGC1* and *SlCNGC14* increased the production of H_2O_2.

Effect of *SlCNGC1* and *SlCNGC14* on the PAMP (flg22)-elicited H_2O_2 accumulation was further examined using leaf disk assays and was indicated as relative luminescence (RLU). The luminol-based assay showed that flg22-induced H_2O_2 in *SlCNGC1*- and *SlCNGC14*-silenced leaves culminated to over 4100 RLU, while that in eGFP control leaves was peaked only to 940 RLU (**Figure 3B**), demonstrating that silencing of *SlCNGC1* and *SlCNGC14* promoted the production of flg22-elicited H_2O_2.

Together, these results suggest that *SlCNGC1* and *SlCNGC14* supress the ROS accumulation to attenuate non-host resistance and PTI.

Silencing of *SlCNGC1* and *SlCNGC14* Compromised Cytosol Ca^{2+} Influx

Some Arabidopsis CNGCs have been proved to be functional Ca^{2+} channels (Gao et al., 2014; Wang et al., 2017). To examine whether SlCNGC1 and SlCNGC14 function as Ca^{2+} channels,

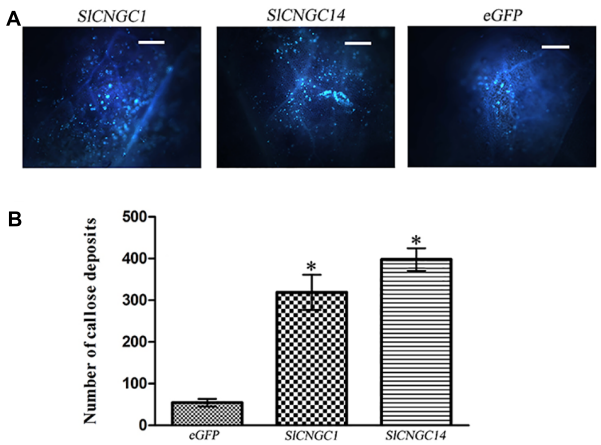

FIGURE 2 | Silencing of *SlCNGC1* and *SlCNGC14* increased *Xoc*-induced callose deposition. Leaves inoculated with *Xoc* at 4 hpi were stained with aniline blue and visualized in fluorescence microscope. A typical staining result **(A)** and its quantification result **(B)** were shown. Significant differences between treatments and the control are indicated by an asterisk ($p < 0.05$).

effect of silencing of these genes on accumulation of cytosolic Ca^{2+} elicited by the PAMP flg22 was monitored through leaf disk assays using aequorin transgenic tomato lines. In eGFP control aequorin transgenic plants, flg22-triggered Ca^{2+} increased rapidly and peaked to 192 RLU, while those in *SlCNGC1*- and *SlCNGC14*-silenced aequorin transgenic plants strongly decreased with the peak value drop to only 97 and 39 RLU, respectively (**Figure 4**). This result indicates that SlCNGC1 and SlCNGC14 function as Ca^{2+} channels and negatively regulate non-host resistance and PTI through modulating cytosolic Ca^{2+} accumulation.

Silencing of *SlCNGC1* and *SlCNGC14* Altered Expression of Defense-Related Ca^{2+} Signaling Genes

To obtain a clue to understand how *SlCNGC1* and *SlCNGC14* genes, as Ca^{2+} channel genes, regulate plant disease resistance, we examined effect of silencing of these genes on expression of a set of defense-related Ca^{2+} signaling genes to probe the possibility of their involvement in *SlCNGC1*- and *SlCNGC14*-mediated resistance regulation. The genes under this expression analysis included two CaM genes *SlCaM2* and *SlCaM6*, a tomato homolog (*SlCDPK10*) of Arabidopsis calcium-dependent protein kinase gene *AtCDPK11*, and the tomato homologs (*SlCBP60g* and *SlCAMTA3*) of two Arabidopsis CaM-binding transcription factors *AtCBP60g* and *AtCAMTA3*. All these genes play an important role in regulating disease resistance (Du et al., 2009; Wang et al., 2009, 2011; Boudsocq et al., 2010; Zhao et al., 2013; Sun et al., 2015; Rahman et al., 2016a,b; Wang et al., 2016). Result of qRT-PCR showed that at 4 h after inoculation with *Xoc*, *SlCNGC1*- and *SlCNGC14*-silenced leaves reduced expression of the negative defense regulatory gene *SlCAMTA3* by 2.5-fold, and generally increased expression of the positive defense regulatory genes *SlCaM6*, *SlCDPK10*, and *SlCBP60g* to different extent, which was much higher in *SlCNGC14*-silenced leaves than *SlCNGC1*-silenced leaves. Expression of *SlCaM6*, *SlCDPK10* and *SlCBP60g* genes in *SlCNGC1*-silenced leaves was 4.3-, 1.5- and 2.5-fold, respectively, as high as that in the eGFP controls, while these folds were 34.0,

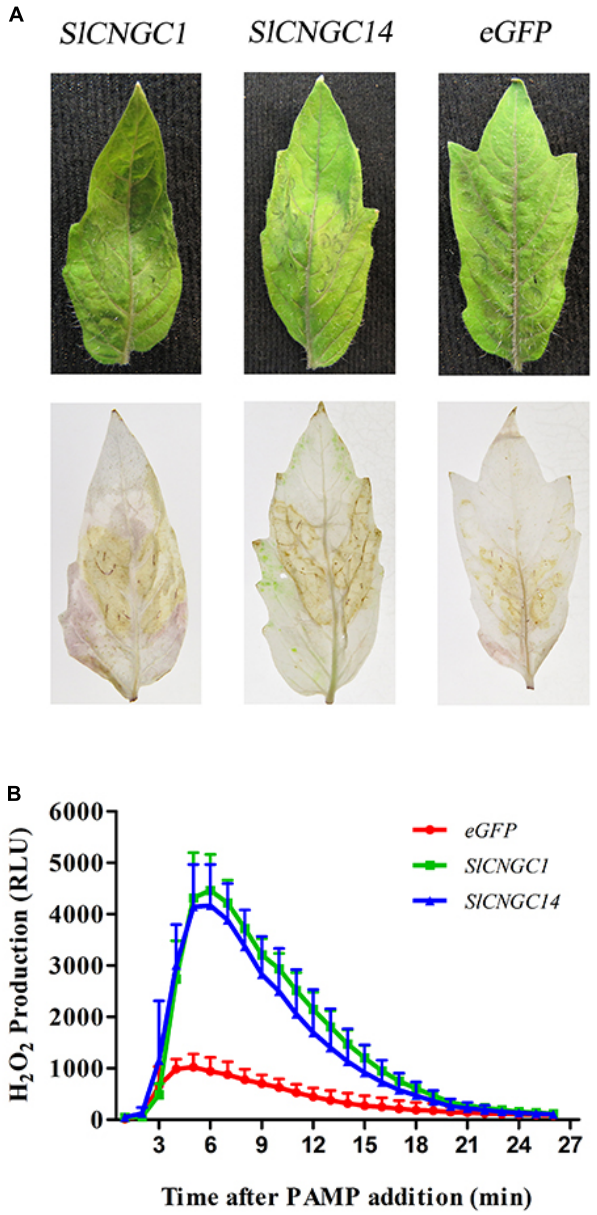

FIGURE 3 | Silencing of *SlCNGC1* and *SlCNGC14* promoted *Xoc*-induced and flg22-elicited ROS accumulation. **(A)** *Xoc*-induced ROS assay. Hydrogen peroxide (H_2O_2) accumulation at 4 hpi was detected through Diaminobenzidine (DAB) staining analysis. The *Xoc*-infiltrated leaves before (Up panel) and after (Down panel) staining analyses were presented. **(B)** flg22-elicited ROS assay. Production of H_2O_2 induced by 100 nM flg22 was detected using a luminol-based assay in leaf disks of *SlCNGC1*-, *SlCNGC14*-silenced plants and the eGFP non-silenced control plants. Data are shown as relative luminol units (RLUs) and represent the mean ± SE of three independent experiments.

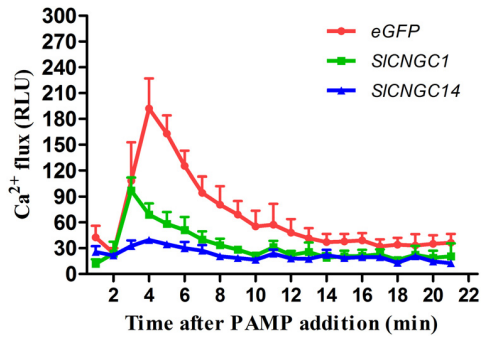

FIGURE 4 | Silencing of *SlCNGC1* and *SlCNGC14* compromised cytosolic Ca^{2+} accumulation. Production of Ca^{2+} flux elicited by 100 nM flg22 was detected using a luminescence-based assay in leaf disks of *SlCNGC1*-, *SlCNGC14*-silenced plants and the eGFP non-silenced control plants of the aequorin transgenic tomato lines. Data are shown as relative luminescence units (RLU) and represent the mean ± SE of three independent experiments.

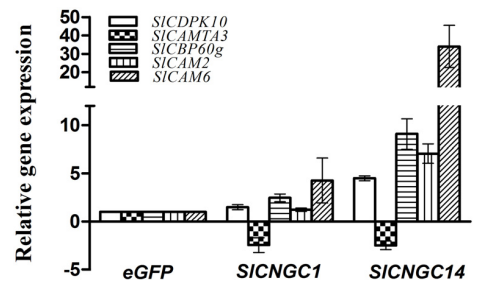

FIGURE 5 | Silencing of *SlCNGC1* and *SlCNGC14* altered expression of defense-related Ca^{2+} signaling genes. Expression of defense-related Ca^{2+} signaling genes *SlCAM2*, *SlCAM6*, *SlCDPK10*, *SlCAMTA3,* and *SlCBP60g* were examined for *SlCNGC1*-, *SlCNGC14*-silenced plants relative to the eGFP non-silenced control plants after inoculation with *Xoc* at 4 hpi by qRT-PCR with 18s rDNA gene serving as a loading control gene. Data represent the mean ± SE of three independent experiments.

4.5, and 9.1 for that in *SlCNGC14*-silenced leaves (**Figure 5**). This result implies that *SlCNGC1* and *SlCNGC14* might modulate the expression of these Ca^{2+} signaling genes.

DISCUSSION

We previously found that two tomato *CNGC* genes *SlCNGC1* and *SlCNGC14* play an important role in tomato HR elicited by the rice bacterial blight pathogen *X. oryzae* pv. *oryzae* (*Xoo*) (Saand et al., 2015a). Here, we further reveal that these two *CNGC* genes likely encode functional Ca^{2+} channels and negatively affect tomato non-host resistance to the rice bacterial leaf streak pathogen *Xoc*, through modulating ROS accumulation and callose deposition. The role of Ca^{2+} signaling pathway in non-host resistance to *Xoc* is previously unknown. Our results provide evidence for the contribution of *CNGC*-mediated Ca^{2+} signaling pathway to this non-host resistance.

In plants, only a few CNGCs such as AtCNGC2 and AtCNGC18 have been proved to function as Ca^{2+} channels (Gao et al., 2014; Wang et al., 2017). Whether the tomato *CNGC* genes encode functional Ca^{2+} channels remain to be verified. In this study, we demonstrated that silencing of *SlCNGC1* and *SlCNGC14* significantly reduced or almost abolished cytosolic Ca^{2+} accumulation (**Figure 4**). Thus, SlCNGC1 and SlCNGC14 likely function as Ca^{2+} channels. Further electrophysiological studies are required to provide more evidences to verify it.

It is recently reported that Arabidopsis *cngc2* mutant overaccumulates Ca^{2+} in apoplastic compartment and increased HR and resistance (Wang et al., 2017). Similarly, in this study, we found that silencing of *SlCNGC1* and *SlCNGC14* significantly reduced cytosolic Ca^{2+} accumulation and enhanced HR and non-host resistance to *Xoc* and PTI. Whether silencing of *SlCNGC1* and *SlCNGC14* results in overaccumulation of Ca^{2+} in apoplastic compartment as observed in *Atcngc2* mutant (Wang et al., 2017) requires further confirmation.

ROS is the well-known master signal in plant immunity and is indispensable to *Xoo*-induced HR and non-host resistance (Li et al., 2015). Thus, it is considerable that regulation of ROS accumulation represents one of the essential mechanisms underlying *SlCNGC1*- and *SlCNGC14*-dependent regulation of HR and non-host resistance to *Xoc* and PTI. How *SlCNGC1* and *SlCNGC14* negatively regulate ROS accumulation remains an intriguing question to be addressed. NADPH oxidase encoded by *RBOH* genes is the key enzyme to generate ROS during plant-pathogen interactions. Interestingly, Ca^{2+} affects the activity of this enzyme which contains EF-hands to bind Ca^{2+}. Moreover, *AtCPK28*, a calcium-dependent protein kinase gene, negatively regulate ROS accumulation during PTI (Monaghan et al., 2014). In this context, it is notable that silencing of *SlCNGC1* and *SlCNGC14* strongly represses cytosolic Ca^{2+} accumulation and expression of a set of denfense-related Ca^{2+} signaling genes including *SlCaM6*, *SlCDPK10* and *SlCBP60g* (**Figures 4**, **5**). Whether and how these changes affect NADPH oxidase thereby modulate ROS accumulation deserves further investigation.

SlCNGC1 and SlCNGC14 belong to group I and group III of tomato CNGC family. They function similarly in negative modulation of tomato HR and non-host resistance to *Xoc*. Both of them suppress ROS accumulation and callose deposition and alter expression of a same set of defense-related Ca^{2+} signaling genes including *SlCaM6*, *SlCDPK10* and *SlCBP60g*. However, the degree of effect in resistance responses by silencing SlCNGC1 and SlCNGC14 varies (**Figures 1–5**), indicating the difference of their involvement in this non-host resistance although it can be the consequence of difference of silencing degree. In animal, CNGC often forms homo- or hetero-oligomer to function (Kaupp and Seifert, 2002). Furthermore, some plant CNGC isoforms, such as AtCNGC2 and AtCNGC4, have been reported to be able to homo- or hetero-complex *in planta* (Chin et al., 2013). In this context, whether SlCNGC1 and SlCNGC14 form oligomer to regulate HR and plant immunity is worth further clarifying. Additionally, cellular localization of plant CNGCs other than long expected plasma membrane have been reported recently (DeFalco et al., 2016b). Whether the cellular localization and accumulation of SlCNGC1 and SlCNGC14 differ awaits further study.

Roles of CNGCs in plant disease resistance seem to be complex. Results from previous studies using Ca^{2+} channel blockers indicated that cytosolic Ca^{2+} elevation in response to PAMPs such as flg22 is required for PAMP induced defense resposnes including ROS burst (Jeworutzki et al., 2010; Ranf et al., 2011; Segonzac et al., 2011), suggesting a positive role of the possibly involved CNGCs in PTI defenses. However, CNGC genes likely play different roles in various types of resistance. For instance, T-DNA insertion knockout mutants for *AtCNGC11* and *AtCNGC12* exhibit unaffected flg22 induced PTI responses but show a partial breakdown of resistance against avirulent, but not virulent *Hyaloperonospora arabidopsidis* and *Pseudomonas syringae*, indicating that both *AtCNGC11* and *AtCNGC12* might be not involved in PTI but act as positive regulators of *R* gene-mediated resistance responses (Yoshioka et al., 2006; Moeder et al., 2011). Differently, null mutants for *AtCNGC2* and *AtCNGC4* display impaired HR cell death, while maintaining resistance against avirulent pathogens, exhibiting enhanced broad-spectrum resistance against virulent pathogens, elevated levels of SA, and constitutive expression of PR genes (Yu et al., 1998; Clough et al., 2000; Yu et al., 2000; Balagué et al., 2003; Jurkowski et al., 2004; Genger et al., 2008), and thus these AtCNGCs seem to play positive role in HR while have negative role in *R* gene-mediated resistance and basal resistance. Additionally, *AtCNGC2* was reported to positively contribute to Pep-elicited immunity (Qi et al., 2010; Ma et al., 2012, 2013) and LPS-triggered Ca^{2+} influx that led to nitric oxide production and consequent HR formation (Ali et al., 2007; Ma et al., 2007), but might be not involved in flg22-triggered immunity (Jeworutzki et al., 2010). In this study, we found the negative role of *SlCNGC1* and *SlCNGC14* in *Xoc*-induced HR and non-host resistance, adding further complexity to the function of plant CNGCs. It is likely that different members of CNGC family might have different roles in resistance and at least some CNGCs are multifunctional and differentially regulate various types of resistance against different pathogens. *SlCNGC1* and *SlCNGC14*, which exhibit similar function in *Xoc*-induced HR and non-host resistance, belong to different groups of CNGCs, with *SlCNGC1* to group I as *AtCNGC11* and *AtCNGC12*, while *SlCNGC14* to group III, indicating that the function of CNGCs is not group-dependent, as we suggested previously (Saand et al., 2015b). Mechanisms underlying plant CNGC-mediated resistance againt various pathogens await further elucidation.

CONCLUSION

Gene silencing analyses demonstrated that *SlCNGC1* and *SlCNGC14* negatively regulate non-host resistance related HR cell death and non-host resistance to *X. oryzae* pv. *oryzicola* (*Xoc*) in tomato. These two *SlCNGCs* repress callose deposition and ROS accumulation to alleviate non-host resistance and likely also PTI. Silencing of *SlCNGC1* and *SlCNGC14* strongly reduced cytosolic Ca^{2+} accumulation, suggesting that SlCNGC1 and SlCNGC14 function as Ca^{2+} channels and negatively regulate non-host resistance and PTI through modulating cytosolic Ca^{2+} accumulation. *SlCNGC14* likely played a stronger regulatory role in the non-host resistance and PTI than *SlCNGC1*. Our results reveal the contribution of CNGC-mediated Ca^{2+} signaling pathway to non-host resistance and PTI.

AUTHOR CONTRIBUTIONS

The project was coordinated by X-ZC. X-RZ conducted the gene silencing analyses. X-RZ and Y-PX carried out the gene expression, designed and analyzed all statistical data. X-ZC conceived of the study, and participated in its design and coordination. X-ZC and X-RZ prepared the manuscript. All authors read and approved the final manuscript.

FUNDING

This work was financially supported by grants from the Zhejiang Provincial Natural Science Foundation of China (No. LZ18C140002), the Genetically Modified Organisms Breeding Major Projects (No. 2014ZX0800905B), the National Natural Science Foundation of China (No. 31672014), and the National Key Research and Development Project (No. 2017YFD020 0602).

ACKNOWLEDGMENTS

We are grateful to Prof. Gerald Alan Berkowitz, Department of Plant Science and Landscape Architecture, Agricultural Biotechnology Laboratory, University of Connecticut, United States, for providing seeds of aequorin transgenic tomato lines.

SUPPLEMENTARY MATERIAL

The Supplementary Material for this article can be found online at: https://www.frontiersin.org/articles/10.3389/fpls.2018.00285/full#supplementary-material

REFERENCES

Ali, R., Ma, W., Lemtiri-Chlieh, F., Tsaltas, D., Leng, Q., von Bodman, S., et al. (2007). Death don't have no mercy and neither does calcium: *Arabidopsis* CYCLIC NUCLEOTIDE GATED CHANNEL2 and innate immunity. *Plant Cell* 19, 1081–1095. doi: 10.1105/tpc.106.045096

Balagué, C., Lin, B., Alcon, C., Flottes, C., Malmström, M., Köhler, C., et al. (2003). HLM1, an essential signaling component in the hypersensitive response, is a member of the cyclic nucleotide–gated channel ion channel family. *Plant Cell* 15, 365–379. doi: 10.1105/tpc.006999

Bednarek, P., and Osbourn, A. (2009). Plant-microbe interactions: chemical diversity in plant defense. *Science* 324, 746–748. doi: 10.1126/science.1171661

Boch, J., Scholze, H., Schornack, S., Landgraf, A., Hahn, S., Kay, S., et al. (2009). Breaking the code of DNA binding specificity of TAL-type III effectors. *Science* 326, 1509–1512. doi: 10.1126/science.1178811

Bogdanove, A. J., Schornack, S., and Lahaye, T. (2010). TAL effectors: finding plant genes for disease and defense. *Curr. Opin. Plant Biol.* 13, 394–401. doi: 10.1016/j.pbi.2010.04.010

Boudsocq, M., Willmann, M. R., Mccormack, M., Lee, H., Shan, L., He, P., et al. (2010). Differential innate immune signalling via Ca^{2+} sensor protein kinases. *Nature* 464, 418–422. doi: 10.1038/nature08794

Cai, L., Cao, Y., Xu, Z., Ma, W., Zakria, M., Zou, L., et al. (2017). A transcription activator-like effector Tal7 of *Xanthomonas oryzae* pv. *oryzicola* activates rice gene *Os09g29100* to suppress rice immunity. *Sci. Rep.* 7:5089. doi: 10.1038/s41598-017-04800-8

Chin, K., DeFalco, T. A., Moeder, W., and Yoshioka, K. (2013). The Arabidopsis cyclic nucleotide-gated ion channels AtCNGC2 and AtCNGC4 work in the same signaling pathway to regulate pathogen defense and floral transition. *Plant Physiol.* 163, 611–624. doi: 10.1104/pp.113.225680

Chin, K., Moeder, W., and Yoshioka, K. (2009). Biological roles of cyclic-nucleotide-gated ion channels in plants: what we know and don't know about this 20 member ion channel family. *Botany* 87, 668–677. doi: 10.1139/B08-147

Clough, S. J., Fengler, K. A., Yu, I. C., Lippok, B., Smith, R. K. Jr., and Bent, A. F. (2000). The *Arabidopsis dnd1* "defense, no death" gene encodes a mutated cyclic nucleotide-gated ion channel. *Proc. Natl. Acad. Sci. U.S.A.* 97, 9323–9328. doi: 10.1073/pnas.150005697

DeFalco, T. A., Marshall, C. B., Munro, K., Kang, H. G., Moeder, W., Ikura, M., et al. (2016a). Multiple calmodulin-binding sites positively and negatively regulate Arabidopsis CYCLIC NUCLEOTIDE-GATED CHANNEL12. *Plant Cell* 28, 1738–1751. doi: 10.1105/tpc.15.00870

DeFalco, T. A., Moeder, W., and Yoshioka, K. (2016b). Opening the gates: insights into cyclic nucleotide-gated channel-mediated signaling. *Trends Plant Sci.* 21, 903–906. doi: 10.1016/j.tplants.2016.08.011

Du, L., Ali, G. S., Simons, K. A., Hou, J., Yang, T., Reddy, A. S., et al. (2009). Ca^{2+}/calmodulin regulates salicylic-acid-mediated plant immunity. *Nature* 457, 1154–1158. doi: 10.1038/nature07612

Fan, J., Crooks, C., Creissen, G., Hill, L., Fairhurst, S., Doerner, P., et al. (2011). *Pseudomonas sax* genes overcome aliphatic isothiocyanate–mediated non-host resistance in *Arabidopsis*. *Science* 331, 1185–1188. doi: 10.1126/science.1201477

Fischer, C., DeFalco, T. A., Karia, P., Snedden, W. A., Moeder, W., Yoshioka, K., et al. (2017). Calmodulin as a Ca^{2+}-sensing subunit of Arabidopsis cyclic nucleotide-gated channel complexes. *Plant Cell Physiol.* 58, 1208–1221. doi: 10.1093/pcp/pcx052

Fortuna, A., Lee, J., Ung, H., Chin, K., Moeder, W., and Yoshioka, K. (2015). Crossroads of stress responses, development and flowering regulation–the multiple roles of Cyclic Nucleotide Gated Ion Channel 2. *Plant Signal. Behav.* 10:e989758. doi: 10.4161/15592324.2014.989758

Gao, Q. F., Fei, C. F., Dong, J. Y., Gu, L. L., and Wang, Y. F. (2014). Arabidopsis CNGC18 is a Ca^{2+}-permeable channel. *Mol. Plant* 7, 739–743. doi: 10.1093/mp/sst174

Genger, R. K., Jurkowski, G. I., McDowell, J. M., Lu, H., Jung, H. W., Greenberg, J. T., et al. (2008). Signaling pathways that regulate the enhanced disease resistance of Arabidopsis '*defense, no death*' mutants. *Mol. Plant Microbe Interact.* 10, 1285–1296. doi: 10.1094/MPMI-21-10-1285

Jeworutzki, E., Roelfsema, M. R., Anschutz, U., Krol, E., Elzenga, J. T., Felix, G., et al. (2010). Early signaling through the Arabidopsis pattern recognition receptors FLS2 and EFR involves Ca^{2+}-associated opening of plasma membrane anion channels. *Plant J.* 62, 367–378. doi: 10.1111/j.1365-313X.2010.04155.x

Jurkowski, G. I., Smith, R. K. Jr., Yu, I. C., Ham, J. H., Sharma, S. B., Klessig, D. F., et al. (2004). *Arabidopsis DND2*, a second cyclic nucleotide-gated ion channel gene for which mutation causes the "*defense, no death*" phenotype. *Mol. Plant Microbe Interact.* 17, 511–520. doi: 10.1094/MPMI.2004.17.5.511

Kaplan, B., Sherman, T., and Fromm, H. (2007). Cyclic nucleotide-gated channels in plants. *FEBS Lett.* 581, 2237–2246. doi: 10.1016/j.febslet.2007.02.017

Kaupp, U. B., and Seifert, R. (2002). Cyclic nucleotide-gated ion channels. *Physiol. Rev.* 82, 769–824. doi: 10.1146/annurev.cellbio.19.110701.154854

Li, W., Xu, Y. P., Yang, J., Chen, G. Y., and Cai, X. Z. (2015). Hydrogen peroxide is indispensable to *Xanthomonas oryzae* pv. *oryzae*-induced hypersensitive response and nonhost resistance in *Nicotiana benthamiana*. *Australas. Plant Pathol.* 44, 611–617. doi: 10.1007/s13313-015-0376-1

Li, W., Xu, Y. P., Zhang, Z. X., Cao, W. Y., Li, F., Zhou, X., et al. (2012). Identification of genes required for nonhost resistance to *Xanthomonas oryzae* pv. *oryzae* reveals novel signaling components. *PLoS One* 7:e42796. doi: 10.1371/journal.pone.0042796

Lu, M., Tang, X., and Zhou, J. M. (2001). Arabidopsis *NHO1* is required for general resistance against *Pseudomonas* bacteria. *Plant Cell* 13, 437–447.

Ma, W., and Berkowitz, G. A. (2011). Ca^{2+} conduction by plant cyclic nucleotide gated channels and associated signaling components in pathogen defense signal transduction cascades. *New Phytol.* 190, 566–572. doi: 10.1111/j.1469-8137.2010.03577.x

Ma, W., Qi, Z., Smigel, A., Walker, R. K., Verma, R., and Berkowitz, G. A. (2009). Ca2+, cAMP, and transduction of non-self perception during plant immune responses. *Proc. Natl. Acad. Sci. U.S.A.* 106, 20995–21000. doi: 10.1073/pnas.0905831106

Ma, W., Yoshioka, K., and Berkowitz, G. (2007). Cyclic nucleotide gated channels and Ca^{2+}-mediated signal transduction during plant innate immune response to pathogens. *Plant Signal. Behav.* 2, 548–550. PMID: 19704555; PMCID: PMC2634365

Ma, Y., Walker, R. K., Zhao, Y., and Berkowitz, G. A. (2012). Linking ligand perception by PEPR pattern recognition receptors to cytosolic Ca^{2+} elevation and downstream immune signaling in plants. *Proc. Natl. Acad. Sci. U.S.A.* 109, 19852–19857. doi: 10.1073/pnas.1205448109

Ma, Y., Zhao, Y., Walker, R. K., and Berkowitz, G. A. (2013). Molecular steps in the immune signaling pathway evoked by plant elicitor peptides: Ca^{2+}-dependent protein kinases, nitric oxide, and reactive oxygen species are downstream from the early Ca^{2+} signal. *Plant Physiol.* 163, 1459–1471. doi: 10.1104/pp.113.226068

Maimbo, M., Ohnishi, K., Hikichi, Y., Yoshioka, H., and Kiba, A. (2010). S-glycoprotein-like protein regulates defense responses in *Nicotiana* plants against *Ralstonia solanacearum*. *Plant Physiol.* 152, 2023–2035. doi: 10.1104/pp.109.148189

Moeder, W., Urquhart, W., Ung, H., and Yoshioka, K. (2011). The role of cyclic nucleotide-gated ion channels in plant immunity. *Mol. Plant* 4, 442–452. doi: 10.1093/mp/ssr018

Monaghan, J., Matschi, S., Shorinola, O., Rovenich, H., Matei, A., Segonzac, C., et al. (2014). The calcium-dependent protein kinase CPK28 buffers plant immunity and regulates BIK1 turnover. *Cell Host Microbe* 16, 605–615. doi: 10.1016/j.chom.2014.10.007

Moscou, M. J., and Bogdanove, A. J. (2009). A simple cipher governs DNA recognition by TAL effectors. *Science* 326:1501. doi: 10.1126/science.1178817

Mysore, K. S., and Ryu, C. M. (2004). Nonhost resistance: How much do we know? *Trends Plant Sci.* 9, 97–104. doi: 10.1016/j.tplants.2003.12.005

Niks, R. E., and Marcel, T. C. (2009). Nonhost and basal resistance: How to explain specificity? *New Phytol.* 182, 817–828. doi: 10.1111/j.1469-8137.2009.02849.x

Nino-Liu, D. O., Ronald, P. C., and Bogdanove, A. (2006). *Xanthomonas oryzae* pathovars: model pathogens of a model crop. *Mol. Plant Pathol.* 7, 303–324. doi: 10.1111/j.1364-3703.2006.00344.x

Pinosa, F., Buhot, N., Kwaaitaal, M., Fahlberg, P., Thordal-Christensen, H., Ellerström, M., et al. (2013). Arabidopsis phospholipase Dδ is involved in basal defense and nonhost resistance to powdery mildew fungi. *Plant Physiol.* 163, 896–906. doi: 10.1104/pp.113.223503

Qi, Z., Verma, R., Gehring, C., Yamaguchi, Y., Zhao, Y., Ryan, C. A., et al. (2010). Ca^{2+} signaling by plant *Arabidopsis thaliana* Pep peptides depends on AtPepR1, a receptor with guanylyl cyclase activity, and cGMP-activated Ca^{2+} channels. *Proc. Natl. Acad. Sci. U.S.A.* 107, 21193–21198. doi: 10.1073/pnas.1000191107

Rahman, H., Xu, Y. P., Zhang, X. R., and Cai, X. Z. (2016a). *Brassica napus* genome possesses extraordinary high number of CAMTA genes and CAMTA3 contributes to PAMP-triggered immunity and resistance to *Sclerotinia sclerotiorum*. *Front. Plant Sci.* 7:581. doi: 10.3389/fpls.2016.00581

Rahman, H., Yang, J., Xu, Y. P., Munyampundu, J. P., and Cai, X. Z. (2016b). Phylogeny of plant CAMTAs and role of AtCAMTAs in nonhost resistance to *Xanthomonas oryzae* pv. *oryzae*. *Front. Plant Sci.* 7:117. doi: 10.3389/fpls.2016.00177

Ranf, S., Eschen-Lippold, L., Pecher, P., Lee, J., and Scheel, D. (2011). Interplay between calcium signalling and early signalling elements during defence responses to microbe- or damage-associated molecular patterns. *Plant J.* 68, 100–113. doi: 10.1111/j.1365-313X.2011.04671.x

Rojas, C. M., Senthil-Kumar, M., Wang, K., Ryu, C. M., Kaundal, A., and Mysore, K. S. (2012). Glycolate oxidase modulates reactive oxygen species–mediated

signal transduction during nonhost resistance in *Nicotiana benthamiana* and *Arabidopsis*. *Plant Cell* 24, 336–352. doi: 10.1105/tpc.111.093245

Saand, M. A., Xu, Y. P., Li, W., Wang, J. P., and Cai, X. Z. (2015a). Cyclic nucleotide gated channel gene family in tomato: genome-wide identification and functional analyses in disease resistance. *Front. Plant Sci.* 6:303. doi: 10.3389/fpls.2015.00303

Saand, M. A., Xu, Y. P., Munyampundu, J. P., Li, W., Zhang, X. R., and Cai, X. Z. (2015b). Phylogeny and evolution of plant cyclic nucleotide-gated ion channel (CNGC) gene family and functional analyses of tomato CNGCs. *DNA Res.* 22, 471–483. doi: 10.1093/dnares/dsv029

Schulze-Lefert, P., and Panstruga, R. (2011). A molecular evolutionary concept connecting nonhost resistance, pathogen host range, and pathogen speciation. *Trends Plant Sci.* 16, 117–125. doi: 10.1016/j.tplants.2011.01.001

Segonzac, C., Feike, D., Gimenez-Ibanez, S., Hann, D. R., Zipfel, C., and Rathjen, J. P. (2011). Hierarchy and roles of pathogen-associated molecular pattern-induced responses in *Nicotiana benthamiana*. *Plant Physiol.* 156, 687–699. doi: 10.1104/pp.110.171249

Senthil-Kumar, M., and Mysore, K. S. (2013). Nonhost resistance against bacterial pathogens: retrospectives and prospects. *Annu. Rev. Phytopathol.* 51, 407–427. doi: 10.1146/annurev-phyto-082712-102319

Sun, T., Zhang, Y., Li, Y., Zhang, Q., Ding, Y., and Zhang, Y. (2015). ChIP-seq reveals broad roles of SARD1 and CBP60g in regulating plant immunity. *Nat. Commun.* 6:10159. doi: 10.1038/ncomms10159

Talke, I. N., Blaudez, D., Maathuis, F. J., and Sanders, D. (2003). CNGCs: prime targets of plant cyclic nucleotide signalling? *Trends Plant Sci.* 8, 286–293. doi: 10.1016/S1360-1385(03)00099-2

Wang, J. P., Xu, Y. P., Munyampundu, J. P., Liu, T. Y., and Cai, X. Z. (2016). Calcium-dependent protein kinase (CDPK) and CDPK-related kinase (CRK) gene families in tomato: genome-wide identification and functional analyses in disease resistance. *Mol. Genet. Genomics* 291, 661–676. doi: 10.1007/s00438-015-1137-0

Wang, L., Tsuda, K., Sato, M., Cohen, J. D., Katagiri, F., and Glazebrook, J. (2009). Arabidopsis CaM binding protein CBP60g contributes to MAMP-induced SA accumulation and is involved in disease resistance against *Pseudomonas syringae*. *PLoS Pathog.* 5:e1000301. doi: 10.1371/journal.ppat.1000301

Wang, L., Tsuda, K., Truman, W., Sato, M., Nguyen, L. V., Katagiri, F., et al. (2011). CBP60g and SARD1 play partially redundant, critical roles in salicylic acid signaling. *Plant J.* 67, 1029–1041. doi: 10.1111/j.1365-313X.2011.04655.x

Wang, Y., Kang, Y., Ma, C., Miao, R., Wu, C., Long, Y., et al. (2017). CNGC2 is a Ca^{2+} influx channel that prevents accumulation of apoplastic Ca^{2+} in the leaf. *Plant Physiol.* 173, 1342–1354. doi: 10.1104/pp.16.01222

Wang, Y. F., Munemasa, S., Nishimura, N., Ren, H. M., Robert, N., Han, M., et al. (2013). Identification of cyclic GMP-activated nonselective Ca^{2+}-permeable cation channels and associated *CNGC5* and *CNGC6* genes in Arabidopsis guard cells. *Plant Physiol.* 163, 578–590. doi: 10.1104/pp.113.225045

Yoshioka, K., Moeder, W., Kang, H. G., Kachroo, P., Masmoudi, K., Berkowitz, G., et al. (2006). The chimeric *Arabidopsis* CYCLIC NUCLEOTIDE-GATED ION CHANNEL11/12 activates multiple pathogen resistance responses. *Plant Cell* 18, 747–763. doi: 10.1105/tpc.105.038786

Yu, I. C., Fengler, K. A., Clough, S. J., and Bent, A. F. (2000). Identification of Arabidopsis mutants exhibiting an altered hypersensitive response in gene-for-gene disease resistance. *Mol. Plant Microbe Interact.* 13, 227–286. doi: 10.1094/MPMI.2000.13.3.277

Yu, I. C., Parker, J., and Bent, A. F. (1998). Gene-for-gene disease resistance without the hypersensitive response in *Arabidopsis dnd1* mutant. *Proc. Natl. Acad. Sci. U.S.A.* 95, 7819–7824. PMID: 9636234; PMCID: PMC22769

Zhang, H., and Wang, S. (2013). Rice versus *Xanthomonas oryzae* pv. *oryzae*: a unique pathosystem. *Curr. Opin. Plant Biol.* 16, 188–195. doi: 10.1016/j.pbi.2013.02.008

Zhang, J., Yin, Z., and White, F. (2015). TAL effectors and the executor *R* genes. *Front. Plant Sci.* 6:641. doi: 10.3389/fpls.2015.00641

Zhao, Y., Liu, W., Xu, Y. P., Cao, J. Y., Braam, J., and Cai, X. Z. (2013). Genome-wide identification and functional analyses of calmodulin genes in Solanaceous species. *BMC Plant Biol.* 13:70. doi: 10.1186/1471-2229-13-70

Conflict of Interest Statement: The authors declare that the research was conducted in the absence of any commercial or financial relationships that could be construed as a potential conflict of interest.

frontiers in Plant Science

ORIGINAL RESEARCH
published: 19 February 2018
doi: 10.3389/fpls.2018.00156

Mapping of *HKT1;5* Gene in Barley Using GWAS Approach and Its Implication in Salt Tolerance Mechanism

Khaled M. Hazzouri[1,2], Basel Khraiwesh[3], Khaled M. A. Amiri[1,4], Duke Pauli[5], Tom Blake[6], Mohammad Shahid[7], Sangeeta K. Mullath[8], David Nelson[2], Alain L. Mansour[9], Kourosh Salehi-Ashtiani[3], Michael Purugganan[2] and Khaled Masmoudi[8]**

[1] Khalifa Center for Genetic Engineering and Biotechnology, United Arab Emirates University, Al Ain, United Arab Emirates, [2] Center for Genomics and Systems Biology, New York University of Abu Dhabi, Abu Dhabi, United Arab Emirates, [3] Laboratory of Algal and Systems Biology, New York University of Abu Dhabi, Abu Dhabi, United Arab Emirates, [4] Department of Biology, College of Science, United Arab Emirates University, Al Ain, United Arab Emirates, [5] Plant Breeding and Genetics, School of Integrative Plant Science, Cornell University, Ithaca, NY, United States, [6] Department of Plant Sciences and Plant Pathology, Montana State University, Bozeman, MT, United States, [7] International Center for Biosaline Agriculture, Dubai, United Arab Emirates, [8] Department of Arid Land Agriculture, College of Food and Agriculture, United Arab Emirates University, Al Ain, United Arab Emirates, [9] Date Palm Tissue Culture, United Arab Emirates University, Al Ain, United Arab Emirates

OPEN ACCESS

Edited by:
Gerald Alan Berkowitz, University of Connecticut, United States

Reviewed by:
Ahmad Arzani, Isfahan University of Technology, Iran
Wei Li, China Agricultural University, China

***Correspondence:**
Khaled Masmoudi
khaledmasmoudi@uaeu.ac.ae
Khaled M. Hazzouri
hazzourik@nyu.edu;
khaled_hazzouri@uaeu.ac.ae

Specialty section:
This article was submitted to Plant Traffic and Transport, a section of the journal Frontiers in Plant Science

Received: *04 September 2017*
Accepted: *29 January 2018*
Published: *19 February 2018*

Citation:
Hazzouri KM, Khraiwesh B, Amiri KMA, Pauli D, Blake T, Shahid M, Mullath SK, Nelson D, Mansour AL, Salehi-Ashtiani K, Purugganan M and Masmoudi K (2018) Mapping of HKT1;5 Gene in Barley Using GWAS Approach and Its Implication in Salt Tolerance Mechanism. Front. Plant Sci. 9:156. doi: 10.3389/fpls.2018.00156

Sodium (Na^+) accumulation in the cytosol will result in ion homeostasis imbalance and toxicity of transpiring leaves. Studies of salinity tolerance in the diploid wheat ancestor *Triticum monococcum* showed that *HKT1;5*-like gene was a major gene in the QTL for salt tolerance, named *Nax2.* In the present study, we were interested in investigating the molecular mechanisms underpinning the role of the *HKT1;5* gene in salt tolerance in barley (*Hordeum vulgare*). A USDA mini-core collection of 2,671 barley lines, part of a field trial was screened for salinity tolerance, and a Genome Wide Association Study (GWAS) was performed. Our results showed important SNPs that are correlated with salt tolerance that mapped to a region where *HKT1;5* ion transporter located on chromosome four. Furthermore, sodium (Na^+) and potassium (K^+) content analysis revealed that tolerant lines accumulate more sodium in roots and leaf sheaths, than in the sensitive ones. In contrast, sodium concentration was reduced in leaf blades of the tolerant lines under salt stress. In the absence of NaCl, the concentration of Na^+ and K^+ were the same in the roots, leaf sheaths and leaf blades between the tolerant and the sensitive lines. In order to study the molecular mechanism behind that, alleles of the *HKT1;5* gene from five tolerant and five sensitive barley lines were cloned and sequenced. Sequence analysis did not show the presence of any polymorphism that distinguishes between the tolerant and sensitive alleles. Our real-time RT-PCR experiments, showed that the expression of *HKT1;5* gene in roots of the tolerant line was significantly induced after challenging the plants with salt stress. In contrast, in leaf sheaths the expression was decreased after salt treatment. In sensitive lines, there was no difference in the expression of *HKT1;5* gene in leaf sheath under control and saline conditions, while a slight increase in the expression was observed in roots after salt treatment. These results provide stronger evidence that

HKT1;5 gene in barley play a key role in withdrawing Na^+ from the xylem and therefore reducing its transport to leaves. Given all that, these data support the hypothesis that *HKT1;5* gene is responsible for Na^+ unloading to the xylem and controlling its distribution in the shoots, which provide new insight into the understanding of this QTL for salinity tolerance in barley.

Keywords: GWAS, barley, salinity tolerance, *HKT1;5* gene, sodium transport

INTRODUCTION

The world's land area affected by salinized soil and water is approximately 7%, and according to the FAO Land and Plant Nutrition Management service, most of the world's land is not cultivated, but a significant proportion of irrigated land is salt-affected. In arid and semi-arid regions, soil salinization is a major threat to agriculture, where water scarcity and inadequate irrigation management will severely reduce crop yield (FAO, 2008). Accumulation of sodium in the cytosol of plants is toxic due to imbalance of ions in the transpiring leaves. There are two major mechanisms of salinity stress at the whole plant level that are advanced so far: a rapid and early osmotic stress which reduces shoot growth, and a slower accumulating ionic stress which accelerates senescence of older leaves (Sahi et al., 2006; Munns and Tester, 2008). Osmotic stress affects the plant's water relations due to reduced availability of water from the soil solution (Munns, 2005), which in turn disturbs the growth of the plant by reducing cell expansion and elongation rates. This mechanism will lead to smaller and thicker leaves, reducing photosynthesis by stomatal closure, and limiting water uptake (Fricke et al., 2004). To minimize the toxic effects of ionic Na^+ stress, plants employ different mechanisms to adapt and tolerate saline conditions. The most important ones to minimize the harmful effects of ionic Na^+ stress include immediate Na^+ exclusion from uptake, limit of xylem Na^+ loading and/or retranslocation from the shoot; efficient compartmentalization of Na^+ mainly into vacuoles, cytosolic K^+ homeostasis and preservation in root and mesophyll cells, efficient osmotic adjustment by a decrease of water loss and an increase of water uptake, and last but not least a ROS detoxification (Blumwald, 2000; Zhu, 2003; Munns and Tester, 2008). To tolerate salinity, plants deploy a variety of traits to control the function and development of the cell that relies on signal perception, signal integration and processing. Therefore, adaptation to salinity stress is a quantitative character, which is controlled by different genetic pathways, where multiple genes are implicated in salinity tolerance (DeRose-Wilson and Gaut, 2011).

Barley (*Hordeum vulgare*) is the major and most salt tolerant cereal crop worldwide (Munns and Tester, 2008). It can tolerate up to 250 mM NaCl (equivalent to 40% seawater), beyond which the survival rates drop drastically. Cultivated barley, its wild ancestor (*Hordeum vulgare subp. Spontaneum*) and domesticated barley are originated from the Fertile Crescent and Tibet (Kilian et al., 2006; Dai et al., 2012). Genetic diversity and adaptation of barley to extreme conditions resulted in a rich pool of genetic variation (Nevo and Chen, 2010). However, breeding efforts to select high yield and stability genotype of barley plants in marginal environment have met with limited success (Flowers and Flowers, 2005). Indeed, modern cultivated barely varieties share 15–40% of all alleles within the barley gene pool, which indicate that only a small fraction of barley genetic resource has been used to improve salinity tolerance (Long et al., 2013). Salinity tolerance in plants is under complex polygenic trait controlled by numerous quantitative trait loci (QTLs) and several genes have been proposed to be involved (Flowers, 2004). High-Affinity K^+ Transporter (*HKT*) genes encode Na^+ and/or K^+ transport systems, active at the plasma membrane (Almeida et al., 2013; Véry et al., 2014). While weakly represented in dicot species genomes (e.g., one single HKT gene in Arabidopsis and poplar), the *HKT* family comprises more members displaying a large functional diversity in monocots, including cereals. For instance, rice (*Oryza sativa*) possesses 9 *HKT* genes (Garciadeblás et al., 2003), and barley (*Hordeum vulgare*) and wheat (*Triticum aestivum*) have been deduced from southern blot analyses to possess 5 to 11 *HKT* genes per genome, respectively (Huang et al., 2008). Based on phylogenetic and functional analyses, plant *HKT* genes have been divided into two subfamilies (Platten et al., 2006). Subfamily 1 *HKT* (present in all higher plant species) encode Na^+-selective transporters, while subfamily 2 ones (monocot specific) encodes systems permeable to both Na^+ and K^+ (Jabnoune et al., 2009; Munns et al., 2012; Sassi et al., 2012; Ben Amar et al., 2014; Suzuki et al., 2016).

In durum wheat, two QTLs (*Nax1* and *Nax2*) were found to be involved in salinity tolerance. The *Nax2* region corresponds to the *HKT1;5* locus, which encodes a selective Na^+ transporter. The *Nax2* locus on the 5AL chromosome is homologous to *Kna1* located on chromosome 4DL carrying the major QTL for Na^+ exclusion in common wheat (Byrt et al., 2007; James et al., 2011; Arzani and Ashraf, 2016). Moreover, *HKT* genes shown to be associated to QTLs of salt tolerance belong to subfamily 1. They have been shown to play crucial roles in salinity tolerance in different plant species (Munns et al., 2012; Asins et al., 2013, 115; Arzani and Ashraf, 2016).

A wide range of physiological and agronomic traits was used as selection criteria to map QTL for salinity tolerance in barley. Among these, we can enumerate plant survival (Zhou et al., 2012; Fan et al., 2015), stomatal size, frequency, and photosynthesis parameters (Liu et al., 2017), yield and agronomic traits (Xue et al., 2009), seed germination and seedling growth stage (Witzel et al., 2010; Ahmadi-Ochtapeh et al., 2015), Na^+ exclusion (Shavrukov et al., 2010), tissue ion content (Xue et al., 2009), water soluble carbohydrate and chlorophyll content (Siahsar and Narouei, 2010). In previous study, Salinity tolerance in barely was assessed through a combination of plant survival and leaf wilting (Zhou et al., 2012; Fan et al., 2015).

These two major symptoms caused by salt stress had been used for evaluating salinity tolerance of barley through QTL mapping.

To uncover and elucidate the genetic basis of complex agronomic traits, genome-wide association studies (GWAS) have been increasingly used. To elucidate the genetic basis of plant height and inflorescence architecture in sorghum, GWAS was performed using genome-wide map of SNP variation that allowed to map several classical loci of plant height, candidate genes for inflorescence architecture (Morris et al., 2013). In rice, GWAS was implemented to identify loci controlling salinity tolerance. Depending on 6,000 SNPs in many stress-responsive genes, Infinium high-throughput assay was used to genotype 220 rice accessions. In addition to *saltol*, a major QTL, identified to control salinity tolerance at seedling stage, GWAS peaks representing new QTLs was found on chromosome 4, 6, and 7 (Kumar et al., 2015). In wheat, the analysis of the *Nax2*, which corresponds to *TmHKT1;5*-type gene, suggests that this gene display distinctive expression pattern in roots.

Here, we present a genome-wide association study (GWAS) in the USDA barley core collection. This population comprising 2,671 lines collected worldwide, selected to represent the entire 30,000 lines of the USDA collection, was evaluated for different agronomic characters performance and yield in the field in order to identify loci associated with salinity tolerance using single nucleotide polymorphism (SNP) data and to study the molecular mechanism underpinning the role of the *HKT1;5* ion transporter gene in slat tolerance in barley. Real time PCR experiments allowed to compare the expression patterns of *HKT1;5* gene in roots, leaves and leaf sheaths in tolerant and sensitive barley lines.

MATERIALS AND METHODS

Barley Germplasm

A total of 2,671 barley accessions collected worldwide, selected to represent the entire 30,000 lines of the USDA barley collection (**Figure 1A**), was evaluated for salinity response to map the locations of genes contributing to low flag leaf Na^+/K^+ ratio under saline production environment using association analysis.

Field Trials and Evaluation of Salinity Tolerance

Field trial was implemented at the International Center for Biosaline Agriculture (ICBA), Dubai, United Arab Emirates (25° 05′ 40.8″ N 55° 23′ 23. 5″ E), from November 2012 to May 2013.

The surface soil texture at ICBA field experimental station is composed of 98% sand, 1% silt, and 1% clay. The native soil is non saline, where the electrical conductivity of its saturated extract is 1.2 dS m^{-1}). It is moderately alkaline (pH 8.22), strongly calcareous, porous (45% porosity), and the organic matter content is very low (<0.5%). The saturation percentage of the soil is 26 and has a high drainage capacity. ICBA soil is classified as Typic Torripsamments, carbonatic, and hyperthermic (Shahid et al., 2014). Soil amendment provided by the company Koblenz compost organic fertilizer (manufactured by Tadweer waste Treatment LLC, Dubai, UAE), was supplemented to the top of the soil at a rate of 40 tons FW. ha^{-1} (at 85% moisture) to increase the soil water-holding capacity and to deliver some of the deficient and required nutrients, such as nitrogen (N), potassium (K), sulfur (S), and micro-nutrients. The field was irrigated with fresh water and fertilization with phosphorous was conducted 2 weeks before sowing using a single supply of 45 kg P_2O_5 ha^{-1}. Granular urea nitrogen (N) fertilizer was applied once at a rate of 30 kg N ha^{-1}, 3 weeks after planting. An application of NPK fertilizer (20-20-20) at a rate of 30 kg ha^{-1} was also given 6 weeks after planting by fertilization.

The 2,671 barley lines were sown in plots of one row of 2 m length each. Plots were randomized in an augmented design, and salt tolerant check line (58/1A) was sown every 50 plots. Two rows of a local barley cultivar (cv. Omani) were sown around the experimental area to reduce edge effects. Approximately 50 seeds per line were hand sown at 2 cm spacing and 1 cm depth per row. The space between rows was 25 cm as per the drip irrigation system design. As we are dealing with sandy soil with very poor water holding capacity and the evapotranspiration was very high, all plots were irrigated twice per day for 5 min each time. Each plot received 4.4 L water per day. The USDA barley core collection was evaluated for different traits related to agronomic performance and yield, but in this paper we will focus only on Na^+ and K^+ content in the flag leaf as an indice of salinity tolerance. Plants were irrigated with fresh water (< 1 dS m^{-1}), referred to hereafter as the control condition, or with saline ground water (≈23 dS m^{-1}), referred to hereafter as saline condition. Saline plots were irrigated with ground water (≈23 dS m^{-1}) for the entire growing period, starting from the third week after germination and until the physiological maturity of the spikes. The distribution of drippers was homogenous and the distance between drippers allowed the overlapping of wetting fronts. Flag leaf was harvested during the heading time from all lines from the control and saline conditions. The electrical conductivity of the saturated soil extract at harvesting time was 16.8 dS m^{-1}. Na^+ and K^+ content was determined from samples of 1 g flag leaf digested with 2% nitric acid in ultrapure Milli Q water. After complete digestion, the filtrate was analyzed by the Inductively Coupled Plasma Emission Optical Spectrophotometer (ICP-OES, Perkin Elmer) to determine Na^+ and K^+ concentrations in the flag leaf.

Genotyping of the USDA Barley Core Collection

The USDA Barley core collection, a sub-sample of 2,671 lines chosen to represent the genotypic and phenotypic variability within the entire USDA collection of 30,000 accessions, was genotyped using the Illumina 9K single nucleotide polymorphism (SNP) array (Comadran et al., 2012). Briefly, this SNP array was constructed from a combination of the existing Barley Oligo Pool Assay (BOPA) SNPs (Close et al., 2009) and SNPs discovered from RNA-seq analyses as described by Comadran et al. (2012). To generate the called SNPs from the RNA-seq data, short-read data from 10 common cultivars (Barke, Betzes, Bowman, Derkado, Intro, Morex, Optic, Quench,

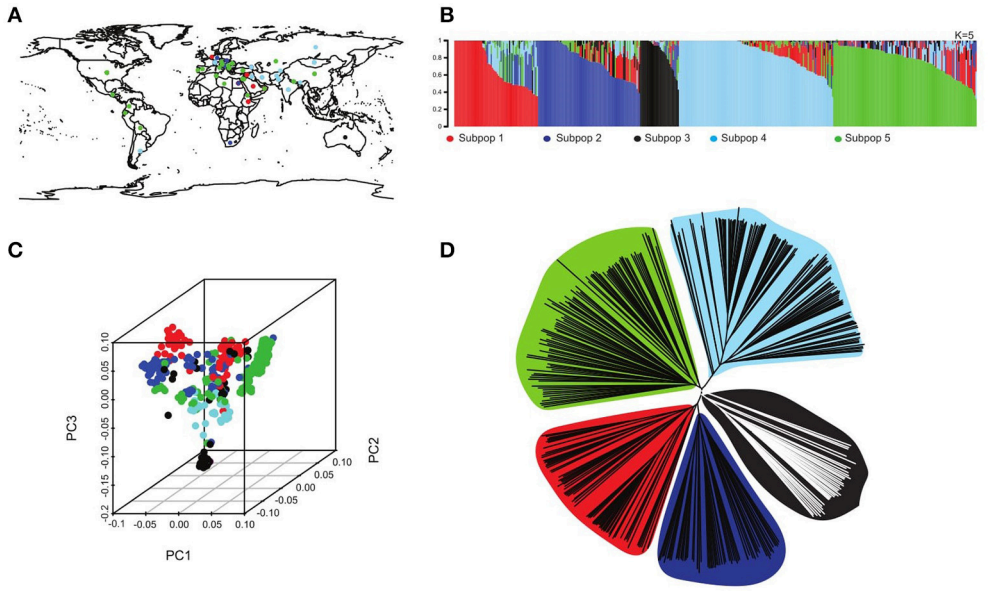

FIGURE 1 | Population structure in the USDA core collection. **(A)** Geographical distribution of the different lines represented in the core collection, colors refer to the five different subpopulations. **(B)** Population structure run using the software STRUCTURE (Pritchard et al., 2000) of the 2761 accession depicting five subpopulations ($K = 5$) each represented with a different color with shared colors represent admixture group. **(C)** 3D principal component diagram showing the five subpopulations in different colors clustering consistent with the neighboring joining tree. **(D)** A neighboring joining tree showing the five different subpopulations.

Sergeant, and Tocada) were aligned onto the Harvest 35 reference sequences (available at http://harvest-web.org/hweb/mainmenu.wc). These putative SNPs were then further processed through quality control measures including removing minor alleles, selecting those SNPs with adequate read depth, and removing duplicate SNPs so that there was only a single SNP per unigene. From the initial 31,616 SNP candidates, 5,010 SNPs were selected for their coverage, information content, and technical performance. These SNPs were combined with the existing 2,832 BOPA SNPs to construct the Illumina 9K array. Of the 7,842 SNPs, 3,968 have been genetically mapped using 360 individuals from a F_6 RIL population derived from the F_1 progeny of a cross between Morex and Barke (complete information regarding the SNP assay development can be found in Comadran et al. (2012) and at http://bioinf.hutton.ac.uk/iselect/app/, verified 8 Aug. 2017. All genotypic data used in this work is available from The Triticeae Toolbox (https://triticeaetoolbox.org/, verified 8 Aug. 2017).

Population Structure and Kinship Analysis

Population structure was investigated using a Bayesian model-based approach of clustering implemented in STRUCTURE (Pritchard et al., 2000) to assign individuals to subpopulations. A clustering was run from $K = 2$ to $K = 10$ with 20 iterations with 10,000 burning period and 10,000 MCMC (Markov Chain Monte Carlo) for each value of K clusters and the logarithm of the data was estimated using an admixture model with correlated allele frequency. The optimal K was determined based on the likelihood model across 20 runs using the Evanno method (Evanno et al., 2005). The membership coefficient for the optimal K was permutated to match the various replicates for that value of K using CLUMPP (Jakobsson and Rosenberg, 2007). For visualization, we used the plotting function implemented in DISTRUCT software (Rosenberg, 2004). Using the method of Ritland (1996), we estimated kinship (K) using the software SPAGeDi (Hardy and Vekemans, 2002).

Genome Wide Association Analysis

The genome-wide association study was performed on the content of flag leaf sodium, potassium and their ratio using 3,968 genome-wide SNP markers. The association analysis was performed using the Genome Association and Prediction Integrated Tool package (GAPIT) (Zhang et al., 2010; Lipka et al., 2012), using the optimum compression mixed linear model and P3D options to increase speed and statistical power. To control for population structure and relatedness, the mixed model incorporated principal components (Price et al., 2006) and a kinship matrix (Ritland, 1996). The amount of phenotypic variation explained by the model was assessed using the R^2 statistics. To correct for multiple testing problem, the procedure by Benjamini and Hochberg (1995) was used at a false discovery rates (FDRs) of 5%. A neighboring joining (NJ) tree was generated using the R package ape (Paradis et al., 2004). Principal component was plotted with the R package scatterplot3D (Ligges and Mächler, 2003). Linkage disequilibrium analysis was performed using HAPLOVIEW v.4.2 (Barrett et al., 2005) and the candidate genes located within and/or adjacent to the associated SNPs were identified using the website Barleymap

(http://floresta.eead.csic.es/barleymap/) using the Morex genome annotation data.

Evaluation of Salinity Tolerance of Selected Sensitive and Tolerant Lines in Hydroponics

Based on the field trial screening of the USDA barley core collection for salinity tolerance and ICP for the estimation of sodium and potassium content in the flag leaf, our results showed that the maintenance of K^+ with exclusion of Na^+ from the flag leaf was highly correlated with salt tolerance. The relationship to discriminate between sodium and potassium and for which a simple index, the Na^+/K^+ ratio was strong enough to be exploited as a selection tool to screen for salinity tolerance. In fact, *Saltol* QTL was reported as a major association with Na^+/K^+ ratio measured at reproduction stage in mapping salinity tolerance in rice. Using this index, we selected five barley lines showing the lowest Na^+/K^+ ratio and accumulate less Na^+ in the flag leaf, along with five sensitive lines for deep characterization of the maintenance of K^+ acquisition with exclusion of Na^+ from the flag leaf, which has been found highly correlated with plant salt tolerance in the field trial. The experiment was designed to conduct plant growth in hydroponic culture conditions onto half-strength Hoagland's solution (Davenport et al., 2005) under greenhouse conditions and in triplicate for each treatment. Salt treatment (0, 7, and 15 dS m^{-1}) was applied at the early three-leaf stage and was maintained until the end of the plant growth cycle. Leaf, leaf sheath and root samples were harvested after 2 weeks of performing salt treatment for Na^+ and K^+ analysis. Scoring symptoms of survival, wilting, chlorosis, senescence, and death of the plants assessed salinity tolerance.

Molecular Cloning of the *HKT1;5* Alleles

DNA was isolated from the flag leaf of the panel of 5 tolerant and 5 sensitive barely accessions, using the CTAB method. PCR amplification of the *HKT1;5* gene was accomplished with *Pfu* DNA polymerase (Promega) and specific primers (forward: 5′-CTAGCGCAGCTGTCGCTCTT-3′; and reverse: 5′-ACGTTGAAGTTGAGTGGGTC-3′). The PCR protocol consisted of an initial denaturation at 95°C for 3 min, followed by 30 cycles comprising a first step at 95°C for 30 S, an annealing step at 56°C for 30 S and an elongation step at 72°C for 3 min, and a final extension at 72°C for 5 min. Purified amplified products were cloned into the PCR cloning vector pSC-A-amp/kan from StrataClone, according to the manufacturer's protocol, and sequenced. The sequences were polished and aligned to each other, to other *Hordeum* and *Triticum* species.

Real Time PCR

Total RNA from 2 tolerant and 2 sensitive barely accessions under control and salt treatment (200 mM NaCl) was isolated with RNeasy plant mini kit (Qiagen). The remaining genomic DNA was removed by treating RNA with DNase-RNase free (Promega). The first strand cDNA was synthesized from 1 μg of total RNA, using the SuperScript kit (Invitrogen), according to the manufacturer's protocol.

Real-time PCR was performed in 384-well plates with the Light Cycler ® 480 Real-Time PCR System (Roche) using SYBR Green I (Roche). Oligonucleotides were designed using Primer 3. Primers were used for *HKT1;5* gene (forward, 5′-tcgtgcatagccatcttcgt-3′, and reverse 5′-GATGCTGAGGACGTTGAAGT-3′). Actin gene from barley was used as a housekeeping gene, to calculate a normalization factor. Primers used for the actin gene were (forward: 5′-CAATGTTCCTGCCATGTACG-3′, and reverse: 5′-ATGAGGAAGGGCGTATCCTT-3′). PCR reactions were performed in a 10 μl final volume, containing 3 μl cDNA (40 ng of cDNA), 0.5 μl of each primer (at 10 μM), 5 μL 2x SYBR Green I master mix and 1 μl of RNase-free water (Sigma). The reaction consisted of an initial denaturation at 94°C for 10 min followed by 45 cycles at 94°C for 10 s, 60°C for 10 s, and 72°C for 15 s. three biological repetitions were performed to calculate the expression level.

RESULTS

Salinity Tolerance of the USDA Barley Core Collection

The barley core collection tested in the field exhibited significant difference in salinity tolerance. Traits were mapped at the heading stage for flag leaf length, width, weight, Na^+ and K^+ content, and at the maturity stage for grain yield. The scores were presented in **Supplementary Figure 1** and show the density distribution of the phenotypic variation for the different traits measured.

Seeds from the five tolerant and five sensitive lines were sown in perlite and the experiment was designed to conduct plant growth in hydroponics system with half-strength Hoagland's solution under greenhouse conditions and in triplicate for each treatment. Salt treatment (0, 7, and 15 dS m^{-1}) was applied at the stage of three leaves and was maintained until the end of the plant cycle. The sensitive lines exhibited severe symptoms of toxicity and senescence when plants are challenged with 15 dS m^{-1} of salt, while the tolerant lines exhibited moderate symptoms of toxicity and senescence (**Figure 2A**).

The tolerant and sensitive lines showed no significant difference in unidirectional root uptake of sodium under control and salt stress conditions at 7 and 15 dS m^{-1} (**Figure 2B**). However, the capacity of the leaf sheath in the tolerant lines to extract and sequester sodium as it entered the leaf was higher when the plants were challenged with salt stress. The sensitive lines were leaking sodium to the upper shoots and accumulate more sodium in their flag leaf. In contrast, the tolerant lines showed the lowest Na^+/K^+ ratio in their flag leaf, suggesting a lower rate of transfer of sodium from the roots to the shoots (**Figure 2B**). Statistical analysis was done using the Dunn (1964) Kruskal-Wallis multiple comparison with *p*-value adjusted with the false discovery rate method using an R package (see **Supplementary Table 1**). Our results are consistent with the finding of James et al. (2006), where the lower rates of net Na^+ loading of the xylem is due to lower rates of Na^+ transport from

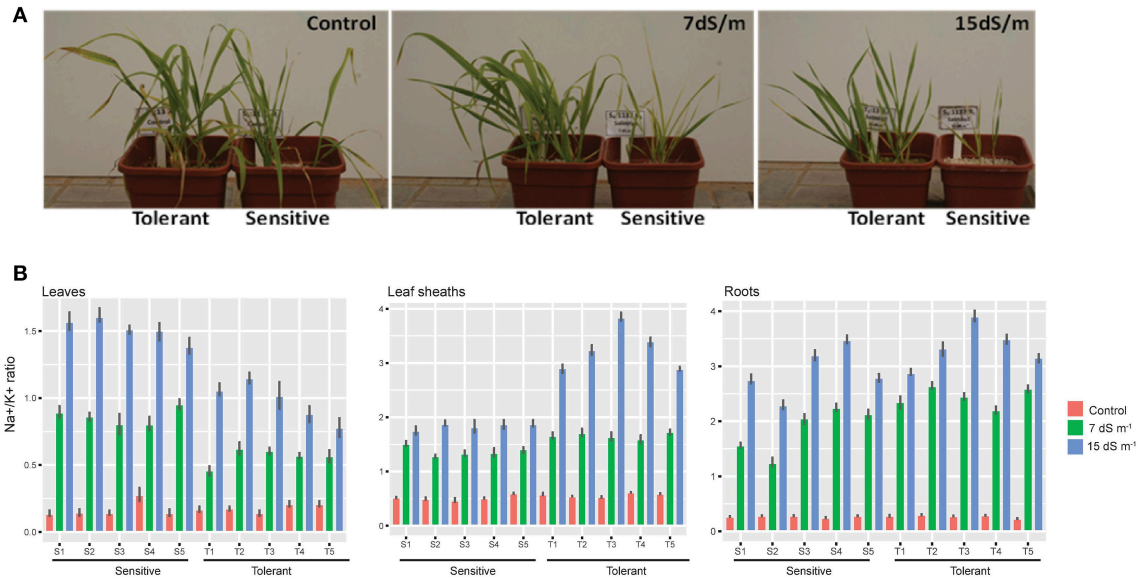

FIGURE 2 | Na^+ measures in different barely tissues. **(A)** A photograph of barely plants tolerant and sensitive subjected to Control, 7 and 15 ds m^{-1}. **(B)** Five tolerant and five sensitive barely plants subjected to 7 and 15 ds m^{-1} compared to a control. Measures of Na^+ in Leaf, leaf sheath and roots shown in barplot with mean ± standard error ($P < 0.05$), in salt tolerant and sensitive compared to control are shown.

roots to shoots, and not to lower rates of net uptake of Na^+ from the soil solution or higher rates of retranslocation in the phloem.

Population Structure

The population structure analysis assigned the genotypes to five subpopulations $K = 5$ with some admixture individuals in each subpopulation (**Figure 1B**), using a probability of membership $P \geq 0.8$. This result is consistent with previous studies using the same USDA barley core collection (Muñoz-Amatriaín et al., 2014). At the contrary, this is not consistent with Fan et al. (2016), may be due to an arbitrary threshold of membership they consider in their analysis. Our structure analysis is consistent with the 3D principal Components analysis as well as the neighboring joining tree (NJ) that shows five clusters representing the five subpopulations (**Figures 1C,D**).

Genome Wide Association Analysis

The genetic basis of salt tolerance in *Hordeum vulgare* was examined using a unified mixed model that controls for population structures and kinship. At least four SNPs were most significant for the Na^+ trait as well as the ratio K^+/Na^+ at a genome-wide Bonferroni-corrected threshold that was estimated based on the effective number of independent tests (**Table 1**). No significant SNPs were found for the potassium K^+ trait. Given the complex architecture of the salt tolerance trait, the most significant SNPs using this unified mixed model for both Na^+ and K^+/Na^+ were located within 2 Mb region on the distal part of chromosome four (**Figures 3A,B**, **Table 2**). There are four SNPs that are significant (**Table 1**). Two of the SNPs (11_11186 and 11_20272) were significantly associated with the low accumulation of Na^+ in the leaves. On average, the lines carrying the major frequency allele of the peak SNPs (11_11186 and 11_20272) were accumulating 15.5 mmoles more than with the alternative allele, and their effects were in the opposite direction. The other two SNPs (11_10610 and 12_30476) are associated with the trait and the allelic effect estimate is in the same direction (**Supplementary Figure 2**). The SNPs individually in both traits accounted from 16 to 28% of the total phenotypic variation elucidated by the traits and they are in linkage disequilibrium (LD) ($r^2 = 0.72$–0.83) with each other (**Figure 3C**).

Co-localization of Candidate Genes Associated with SNPs

Four significant SNPs were shown to be around an important *HKT 1;5* gene, which is a known major player in salt tolerance in wheat, rice and Arabidopsis. The SNP 12_30476 is around 0.5 Mb away from this transporter. There are multiple genes (**Table 2**) that are in the region that are part or adjacent to those significant SNPs. Genes contained in this region with significant SNPs association with reduce accumulation of Na^+ from the Manhattan location also have some predicted functions such as lipid-transfer protein, flavin-containing monooxygenase family protein, zinc finger protein, Protein NRT1/ PTR FAMILY 6.3 and expansin B2. The ortholog of these genes was shown to play a role in salt tolerance in other species (Chen et al., 2012; Jülke and Ludwig-Müller, 2015; Kong et al., 2016; Zhang et al., 2016).

Molecular Cloning of the *HKT1;5* Alleles

Isolation of the barley *HKT1;5* transporter gene from the tolerant and sensitive lines was attempted, considering the availability of the full length *HKT1;5* gene sequence in the Genbank

TABLE 1 | Significant SNPs in Na^+ and K^+/Na^+ ratio trait from the GWAS analysis.

Na^+ (SNPs)	Chromosome	Position	*P*-values	MAF[a]	R^2 (%)[b]	FDR_adjusted_Pvalues[c]
11_20272	4	639755066	6.73E-22	0.274	18.2	1.56E-18
11_11186	4	639392844	2.44E-18	0.435	17.6	2.83E-15
11_10610	4	638202331	2.71E-15	0.435	17.12	2.10E-12
12_30476	4	638223459	1.53E-13	0.455	16.8	8.88E-11
K^+/Na^+ (SNPs)	4					
11_11186	4	639392844	1.29E-18	0.435	28.2	3.01E-15
11_20272	4	639755066	4.04E-18	0.274	28.2	4.69E-15
11_10610	4	638202331	3.67E-13	0.435	27.4	2.84E-10
12_30476	4	638223459	1.34E-11	0.455	27.2	7.78E-09

[a] *Minor allele frequency*
[b] *percent phenotypic variation explained by the trait*
[c] *False discovery rate adjusted p-value*

(accession # DQ912169.1). The reference sequence was used to design primers for amplification by PCR of the barley *HKT1;5* genomic DNA. Eight alleles of the *HKT1;5* gene were amplified, cloned, sanger sequenced and aligned. A midpoint rooted phylogenetic tree showing the relationship between the different lines (tolerant and sensitive) along with the *HKT1;5* reference sequence for barley and other species was generated (**Supplementary Figure 3**). The assembled sequences from the tolerant and sensitive lines did not show any allelic variation that is linked to function. We could not find any nucleotide substitution in the coding region that differentiate the tolerant from the sensitive ones. Moreover, the analysis of cis-elements of 1 kb fragment from the *HKT1;5* promoter sequence (using http://bioinformatics.psb.ugent.be/webtools/plantcare/html/) gene between the tolerant (1_kb_PI138711.2_tolerant; 1_kb_PI21378_tolerant) and sensitive (1_kb_Chlo6091.2_sensitive; 1_kb_PI467358_sensitive) lines did not show any differences. A total of 28 cis-elements were distributed along the sequence (**Supplementary Table 3**). These cis-elements don't show any direct relation to regulation of genes under salt stress. However, we can't rule out that these cis-elements could modulate in a positive and indirect way the expression of *HKT1;5* gene in the leaf sheath of the tolerant compared to the sensitive lines. Further analysis is needed in this perspective.

Real Time PCR

Expression of the *HKT 1;5* gene in the salt sensitive barley leaf compared to the control showed after 72 h of salt treatment a significant increase ($p < 0.05$) in the expression than the control plants that are not subjected to salt stress. In contrast, the salt tolerant barley leaf showed a significant decrease in expression ($p < 0.05$) than the control plants (**Figure 4**). Expression of the *HKT 1;5* gene in the salt sensitive barley roots as well as in the salt tolerant ones compared to the control showed a significant ($p < 0.05$) increase in the expression level (**Figure 4**). Expression of the *HKT 1;5* gene in the salt sensitive barley leaf sheaths compared to the control plants showed no significant increase in the expression. At high concentration of salt (200 mM NaCl), the reduction of the expression level of *HKT1;5* gene in leaf sheath of the tolerant line is correlated with increases in Na^+ accumulation in this tissue. This is reflecting that *HKT1;5* gene play an important role in restricting the transport of Na^+ from leaf sheath to the upper leaves. The range of expression level (means ± SD, $n = 3$ biological replicates) in each line and tissue was analyzed with a *t*-student test with reported *P*-value (<0.05) (**Supplementary Table 2**).

DISCUSSION

Salinity tolerance involves a complex of responses at molecular, cellular and whole plant levels and is governed by the action of multiple genes that are highly affected by the environment, and genotype-by-environment (G × E) interactions (Arzani and Ashraf, 2016). Sodium exclusion play a major contributor of the mechanism conferring salt tolerance (Munns et al., 2006). Salt tolerance in plants was shown to depend on *HKT* transporters, which mediate Na^+-specific transport or Na^+- K^+ co-transport and illustrate a key role in regulation of Na^+ homeostasis (Rodríguez-Navarro and Rubio, 2006). For instance, a source of sodium exclusion named *Nax2*, found in the diploid ancestral wheat relative, *Triticum monococcum*, confers a decreased rate of Na^+ transport from roots to shoots by retrieving Na^+ from the root xylem into xylem parenchyma cells (Davenport et al., 2005; James et al., 2006). A candidate gene in the *Nax2* locus from *T. monococcum* (*TmHKT1;5-A)* and a major salt tolerance locus from bread wheat *Kna1* (*TaHKT1;5-D*), encode a Na^+-selective transporter, expressed in stellar root cells surrounding xylem vessels, and therefore can limit the amount of Na^+ that is translocated in the xylem to the leaf tissues (Munns et al., 2012; Byrt et al., 2014).

A new QTL for salinity tolerance in barley was identified through GWAS study (Fan et al., 2016). Association mapping for salinity tolerance was performed on 206 barley accessions and 408 DArT markers. Only two significant marker-trait associations for one QTL were detected on 4H. The authors showed that QTL on 4H with the nearest marker of bPb-9668 was the most significant, consistently detected in all methods. In the present study, using GWAS we mapped important SNPs that are located within 0.5 Mb from an important *HKT1;5* gene

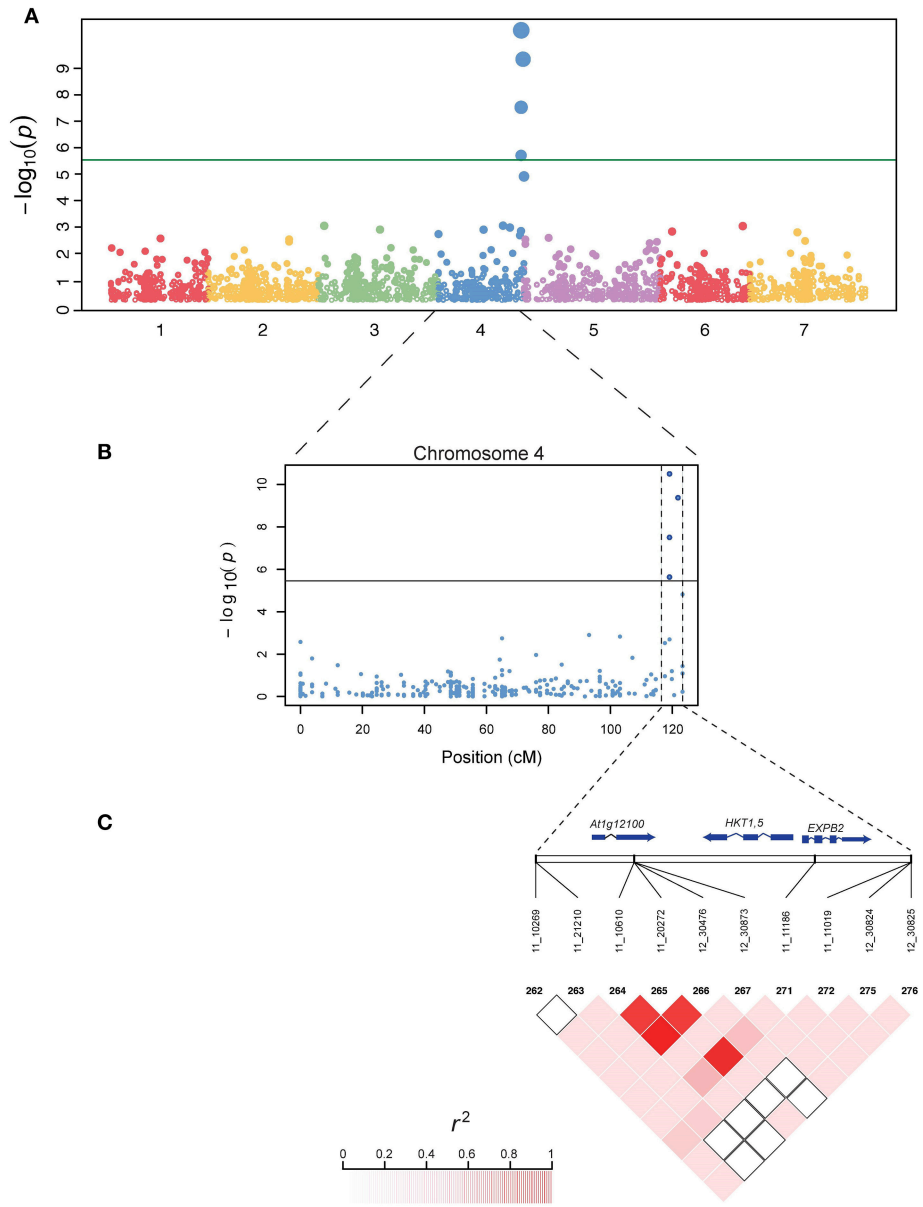

FIGURE 3 | Genome wide association (GWAS) study in barley. **(A)** A Manhattan plot generated showing the seven barley chromosomes and the significant SNPs on the chromosome 4. The y-axis is the negative $\log_{10}$ transformed *p*-values of SNP from a genome-wide association analysis for Na^+ plotted against the genetic distance in cM. **(B)** A zoom view of chromosome 4 with the bottom showing the candidate range for the gene *HKT1;5* associated with low Na+ accumulation in barley using the Morex annotation genome. **(C)** A panel depicting the extent of linkage disequilibrium in this region based on r^2. The r^2 values are indicated using color intensity at the left bottom. A region of 1.5 Mb associated with *HKT1;5* including other genes are indicated using two vertical dashed lines. Genes are represented in the middle panel.

in barley, which may play a significant role in reducing Na+ concentration in the leaves. Since we don't have the sequence that expand this region in all the lines, more sequencing could be done across the majority of the barely accession (tolerant and sensitive) for better quantification. Other genes co-localizing in this region that have orthologs involved in salinity stress tolerance in other species could also play potential candidates for future validation. The application of linked SNP molecular markers for salinity tolerance in barley would be suitable to relevant crosses within the barley breeding program. They have the ability to cost effectively enable breeders to select germplasm and breeding lines using a simple DNA test without the need of a lot of phenotypic variation.

In rice and Arabidopsis, allelic variation for *OsHKT1;5* and *AtHKT1;5* was shown to be linked to the function of the gene (Ren et al., 2005; Rus et al., 2006). Our result in barley for

TABLE 2 | Positions of the significant markers on the morex genome.

Marker	Chr	Start	End	Strand	Other alignments	Gene_class	Description	InterPro	GeneOntologies	PFAM
HORVU4Hr1G087760	Chr4H	638201783	638202868	+	No	HC_G	Bifunctional Inhibitor/lipid-transfer protein/seed storage 25 albumin superfamily protein	IPR016140 IPR027923		PF14547
11_10610	Chr4H	638202331	638202332	+	No					
HORVU4Hr1G087780	Chr4H	638223190	638275418	-	No	HC_G	Bifunctional Inhibitor/lipid transfer protein/seed storage 25 albumin superfamily protein	IPR016140 IPR027923		PF14547
HORVU4Hr1G087790	Chr4H	638223364	638224442	+	No	LC_u	Unpredicted protein			
12_30476	Chr4H	638223459	638223460	+	No					
HORVU4Hr1G087960	Chr4H	638634849	638636785	-	No					
HORVU4Hr1G087960	Chr4H	638634849	638636785	-	No	HC_G	Sodium transporter HKT1	IPR003445	GO: 0006812 GO: 0008324 GO: 0055085	PF02386
11_11186	Chr4H	639392844	639392845	+	No					
HORVU4Hr1G088140	Chr4H	639752735	639755477	+	No	HC_G	Expansin B2	IPR007118 IPR009009 IPR005795 IPR007112 IPR007117	GO: 0005576 GO: 0019953	PF01357 PF03330
11_20272	Chr4H	639755066	639755067	+	No					
HORVU4Hr1G089510	Chr4H	642560530	642564723	-	No	HC_G	Beta-amylase 5	IPR017853 IPR018238 IPR001371 IPR001554 IPR013781	GO: 0000272 GO: 0005975 GO: 0016161	PF01373
11_11019	Chr4H	642560940	642560941	+	No					

Annotation of the genes anchored close to those markers are summarized with emphasize on the HKT1;5 ge

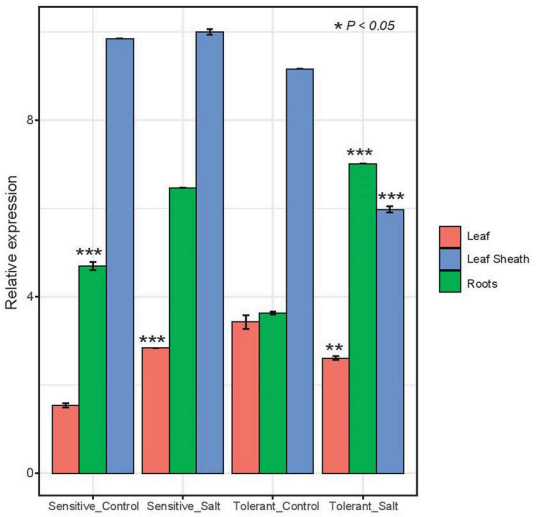

FIGURE 4 | Expression analysis of HKT 1;5 by real time RT-PCR. Amplification of RNA from leaf, leaf sheath and root tissues of two barley salt tolerant and two salt sensitive lines. Sampling was done in triplicates after 48 h of growing the plants under salt stress condition (200 mM NaCl). A house keeping gene actin from barely was used for control and the data was normalized to 0 mM NaCl. The range of expression level (means ± SD, $n = 3$ biological replicates) in each line and tissue was analyzed with a *t*-student test and significance was reported (*$P < 0.05$; **$P < 0.005$; ***$P < 0.0005$).

5 tolerant and 5 sensitive lines showed no allelic variation for the *HKT1;5* gene that is correlated with the phenotype, which is similar to what has been identified in wheat (Byrt et al., 2007). This result seems to suggest that difference in leaf Na^+ concentration between the tolerant and sensitive lines, is mostly due to expression variation of this gene, rather than allelic variation.

The exclusion of Na^+ is an important strategy employed by plants to prevent any shoot damage induced by Na^+ accumulation. In barley, Na^+ exclusion is an important salt tolerance strategy (Chen et al., 2007) as in wheat, however barley can tolerate more Na^+ accumulated in the shoot than wheat (Munns and James, 2003; Colmer et al., 2005). This will suggest that tissue tolerance of Na^+ in barley is a unique feature for salt tolerance. As an evidence of this, a recent study showed a constitutive overexpression of *HKT2;1* gene that increased salt tolerance in barley, showed an increase in the level of Na^+ concentration in the shoots (Mian et al., 2011).

HKT1;5 gene expression in the sensitive leaf sheath was the highest and did not change upon salt stress. However, Na^+ accumulation in leaf sheath was much lower than in the tolerant line and there is no evidence of removal of Na^+ from xylem in the leaf sheath of the sensitive line and Na^+ is leaking to the upper shoots. In the tolerant line, *HKT1;5* gene expression was decreased upon salt treatment and Na^+ accumulation in this tissue was higher than in the sensitive line, reducing its transport to the upper shoots. Similarly, reduced expression level of Na^+ transporter, *TaHKT1;5* gene by gene silencing in transgenic bread wheat lines, increases Na^+ accumulation in the leaves which reflecting that *TaHKT1;5* has in important role in restricting the transport of Na^+ from the root to the leaves in bread wheat and showed the potentiality to increase salinity tolerance in bread wheat by the manipulation of *HKT1;5* gene (Byrt et al., 2014). In roots, there is an increase in the expression of *HKT1;5* gene in both tolerant and sensitive lines and no significant effect on root Na^+ accumulation was observed. The precise control of Na^+/K^+ selective accumulation in leaf, leaf sheath and root tissues is an essential mechanism to maintain cellular homeostasis in the presence of imposed high salt concentration in the growth solution. It was shown in bread wheat that *TaHKT1;5* confers the essential salinity tolerance mechanism associated with the *Kna1* locus via shoot Na^+ exclusion and is critical in maintaining a high K^+/Na^+ ratio in the leaves (Byrt et al., 2014). In rice, it was shown that *OsHKT1;5* plays a major role in the removal of Na^+ from the xylem sap into the surrounding xylem parenchyma cells, thereby protecting leaves from Na^+ toxicity (Ren et al., 2005). Possible roles of known HKT transporters in controlling Na^+ flux in barley could function as an Na^+ uptake system in the epidermal cortical cells and their expression could be down-regulated in conditions of salinity. This was shown to be the case for *OsHKT2;1*, which mediates the transport of Na^+ into roots of K^+-starved plants and was down-regulated when plants were exposed to salinity (Horie et al., 2007). In addition, comparative analysis using salt-tolerant and sensitive rice varieties have led to the hypothesis that *OsHKT1;4* restricts leaf-sheath-to blade Na^+ transfer in rice plants under salinity stress (Cotsaftis et al., 2012). This mechanism is consistent with tissue specific expression of this gene that is regulating the transport of Na^+ from root to leaves. In previous reports, it was demonstrated that *HKT* genes from *Arabidopsis thaliana* and rice, *AtHKT1;1* and *OsHKT1;5*, reduce transport of Na^+ to the upper shoot and increase tolerance of the plant to salinity (Møller et al., 2009; Plett et al., 2010). Moreover, Munns et al. (2012) reported that *TmHKT1;5* encoding a Na^+-selective transporter located on the plasma membrane of root cells surrounding xylem vessels, was perfectly localized to withdraw Na^+ from the xylem and therefore reduce its transport to leaves. In accordance with the expression results, our data related to Na^+ and K^+ content analysis showed that the ratio Na^+/K^+ was associated with a higher root Na^+ concentration in both tolerant and sensitive lines, while in leaf sheath there was a higher Na^+ concentration than in leaf blade of the tolerant lines.

Our results support what has been known about *HKT 1;5* transporter gene and salt tolerance in barely, but it is the first time, that this gene is mapped using a GWAS approach. The question next is to test the function of this gene and its transport properties by performing electrophysiological recordings in Xenopus oocytes. We will design in the future an RNA interference experiment to knock down the gene in a tissue specific manner, study the transcript accumulation and see if the transgenic lines will accumulate more Na^+ in their leaves. Similar work has been done in bread wheat, where *TaHKT1;5-D* expression was predominantly observed within the stele, particularly within xylem parenchyma and pericycle cells, which are adjacent to the xylem vessels, whereas *TaHKT1;5-D* transcripts was reduced in roots of transgenic lines containing an

RNAi construct, increasing leaf Na^+ concentration (Byrt et al., 2014).

Few data allowing to understand the different wheat and rice salt tolerance QTL linked to *HKT1;5* transporter genes are available so far. Indeed, the *Kna1* QTL involving the bread wheat D genome *TaHKT1;5* gene could certainly be explained by the low level of expression of the durum wheat *HKT1;5* genes as compared to *TaHKT1;5-D* (Byrt et al., 2014). The *Nax2* QTL, which has a similar mechanism to *Kna1* in bread wheat, involving *T. monococcum TmHKT1;5-A* gene might be similarly explained by higher expression of the *TmHKT1;5* gene as compared to durum wheat ones (Byrt et al., 2007, 2014; Munns et al., 2012). In rice, it was demonstrated that Na^+ exclusion in the leaf was influenced by *OsHKT1;5* transcript abundance and that functional differences between the *OsHKT1;5* allele from salt-tolerant rice variety, Nona Bokra, and an allele from the salt-sensitive variety, Koshihikari, were referred to four amino acid substitutions (Ren et al., 2005; Cotsaftis et al., 2012). So far, 15 different *OsHKT1;5* alleles in rice showed a strong association with leaf Na^+ concentrations (Negrão et al., 2013; Platten et al., 2013).

The present data of this work indicates that *HKT1;5* gene from barley has a higher expression in roots and therefore limiting the amount of Na^+ transported in the xylem to the leaf tissues. Moreover, in previous work we demonstrated that alleles in the *Nax1* locus from durum wheat, *TdHKT1;4-1* and *TdHKT1;4-2* encode Na+ selective transporters and are effective in limiting Na^+ accumulation in the leaves (Ben Amar et al., 2014).

CONCLUSION

New insights into understanding the role of *HKT1;5* transporter gene in salt tolerance in barley was achieved. Using GWAS approach, we mapped for the first time *HKT1;5* gene from barley. Important SNPs markers were mapped and are located within 0.5 Mb from the *HKT1;5* gene and may play a significant role in reducing Na^+ concentration in the leaves. Sequence analysis of *HKT1;5* alleles from tolerant and sensitive barley lines did not show any allelic variation that is linked to function and correlated with the phenotype. This is similar to what was found in wheat (Byrt et al., 2007). This seems to suggest that difference in leaf Na^+ concentration between tolerant and sensitive lines, is mostly due to expression variation of *HKT1;5* gene, rather than allelic variation. The expression pattern of *HKT1;5* gene in barley revealed through real time PCR suggests that exclusion of Na^+ from the roots is happening in the salt tolerant line due to the higher expression of the *HKT1;5* gene in the roots, but the accumulation of Na^+ in the leaf sheath in the tolerant lines is consistent with the decrease in expression of *HKT1;5* gene in the leaf sheath and leaf to compensate the increase of expression in roots, which imply that the Na^+ is going to accumulate less in the leaves of the tolerant lines than the sensitive. This mechanism is consistent with tissue specific expression of this gene that is regulating the exclusion of Na^+ from the leaves. Ultimately, to study the function of *HKT1;5* gene in barley, knock down experiment via CRISPR-Cas9 technology or RNA interference will be applied in a tissue specific manner to study the accumulation of Na^+ in leaves and the tolerance phenotype.

AUTHOR CONTRIBUTIONS

KH, KA, and KM did the design of the paper and the analysis. BK did the real time PCR. DP and TB provided the SNP arrays and MS did the field testing. SM and DN did some laboratory work related to real time PCR. AM and KS-A discussed the manuscript. MP improved the manuscript.

FUNDING

This research work was supported by funding from the United Arab Emirates University to KM under grant number 31F096. We are grateful to the International Center for Biosaline Agriculture team for phenotyping the barley USDA core collection in their field experimental station and evaluation of the salinity tolerance.

SUPPLEMENTARY MATERIAL

The Supplementary Material for this article can be found online at: https://www.frontiersin.org/articles/10.3389/fpls.2018.00156/full#supplementary-material

Supplementary Figure 1 | Histogram plot of the phenotypic variation of the different traits (grain yield, average flag leaf width, average flag leaf length) measured. Wide dashed line represents the density distribution, while narrow ones represent the normal fitted distribution.

Supplementary Figure 2 | Phenotypic differences between lines carrying different alleles of the four SNPs (11_10610; 12_30476; 11_11186; 11_20272) associated with salt concentration (Na^+) showing allelic estimate and directionality. The boxplot shows the differences of Na^+ concentration for the four SNPs showing the different alleles of the SNP locus. The box shows the first, second and third quartile. The width of the box is proportional to the square root of the number of individuals for each allele. The difference of mean (Δm) and the Pearson correlation (r) between the genotype and phenotype values as well as the P value of the correlation is shown on the side of the boxplots.

Supplementary Figure 3 | A midpoint rooted phylogenetic tree showing the relationship between the different lines (tolerant and sensitive) along with the *HKT1;5* reference sequence for barley and other species was generated. The accession numbers are as follows: *Oryza_indica* (HQ162137.1), *Oryza_glaberrima* (JQ695813.1), *Oryza_japonica* (AP014957.1), *Oryza_rufipogon* (JQ695808.1), *Oryza_sativa* (JQ695818.1), *Triticum monococcum* (DQ646332.1), *Triticum_aestivum_cultivar Kharchia* (KU212875.1), *Hordeum_marinum_Subsp_marinum* (KF606928.1), *Hordeum_marinum_Subsp_gussoneanum* (KF606929.1), *Horedum_vulgare* (DQ912169.1).

Supplementary Table 1 | Statistical analysis using the Dunn (1964) Kruskal-Wallis multiple comparison with *p*-value adjusted with the false discovery rate method for Na^+/K^+ ratio in roots, leaf sheaths and leaves at 0, 7, and 15 dSm^{-1}.

Supplementary Table 2 | Statistical analysis using the *t*-student test comparing the range of expression level (means ± SD, $n = 3$ biological replicates) in tolerant and sensitive lines and tissues (roots, sheaths and leaves) and *P*-value was reported (<0.05).

Supplementary Table 3 | A summary of the putative 28 cis-elements along the 1 Kb sequence promoter of the *HKT1;5* gene in two tolerant and two sensitive lines using the PlantCARE database.

REFERENCES

Ahmadi-Ochtapeh, H., Soltanloo, H., Ramezanpour, S. S., Naghavi, M. R., Nikkhah, H. R., and Yoosefi Rad, S. (2015). QTL mapping for salt tolerance in barley at seedling growth stage. *Biol. Plant.* 59, 283–290. doi: 10.1007/s10535-015-0496-z

Almeida, P., Katschnig, D., and de Boer, A. H. (2013). HKT transporters-state of the art. *Int. J. Mol. Sci.* 14, 20359–20385. doi: 10.3390/ijms141020359

Arzani, A., and Ashraf, M. (2016). Smart engineering of genetic resources for enhanced salinity tolerance in crop plants. *Crit. Rev. Plant Sci.* 35, 146–189. doi: 10.1080/07352689.2016.1245056

Asins, M. J., Villalta, I., Aly, M. M., Olias, R., Alvarez de Morales, P., Huertas, R., et al. (2013). Two closely linked tomato HKT coding genes are positional candidates for the major tomato QTL involved in Na^+/K^+ homeostasis. *Plant Cell Environ.* 36, 1171–1191. doi: 10.1111/pce.12051

Barrett, J. C., Fry, B., Maller, J., and Daly, M. J. (2005). Haploview: analysis and visualization of LD and haplotype maps. *Bioinformatics* 21, 263–265. doi: 10.1093/bioinformatics/bth457

Ben Amar, S., Brini, F., Sentenac, H., Masmoudi, K., and Véry, A. A. (2014). Functional characterization in *Xenopus* oocytes of Na+ transport systems from durum wheat reveals diversity among two *HKT1;4* transporters. *J. Exp. Bot.* 65, 213–222. doi: 10.1093/jxb/ert361

Benjamini, Y., and Hochberg, Y. (1995). Controlling the false discovery rate: a practical and powerful approach to multiple testing. *J. R. Stat. Soc. Series B* 57, 289–300.

Blumwald, E. (2000). Sodium transport and salt tolerance in plants. *Curr. Opin. Cell Biol.* 12, 431–434. doi: 10.1016/S0955-0674(00)00112-5

Byrt, C. S., Platten, J. D., Spielmeyer, W., James, R. A., Lagudah, E. S., Dennis, E. S., et al. (2007). *HKT1;5*-like cation transporters linked to Na^+ exclusion loci in wheat, *Nax2* and *Kna1*. *Plant Physiol.* 143, 1918–1928. doi: 10.1104/pp.106.093476

Byrt, C. S., Xu, B., Krishnan, M., Lightfoot, D. J., Athman, A., Jacobs, A. K., et al. (2014). The Na^+ transporter, *TaHKT1;5*-D, limits shoot Na^+ accumulation in bread wheat. *Plant J.* 80, 516–526. doi: 10.1111/tpj.12651

Chen, C. Z., Lv, X. F., Li, J. L., Yi, H. Y., and Gong, J. M. (2012). Arabidopsis NRT1.5 is another essential component in the regulation of nitrate reallocation and stress tolerance. *Plant Physiol.* 159, 1582–1590. doi: 10.1104/pp.112.199257

Chen, Z., Pottosin, I. I., Cuin, T. A., Fuglsang, A. T., Tester, M., Jha, D., et al. (2007). Root plasma membrane transporters controlling K^+/Na^+ homeostasis in salt-stressed barley. *Plant Physiol.* 145, 1714–1725. doi: 10.1104/pp.107.110262

Close, T. J., Bhat, P. R., Lonardi, S., Wu, Y., Rostoks, N., Ramsay, L., et al. (2009). Development and implementation of high-throughput SNP genotyping in barley. *BMC Genomics* 10:582. doi: 10.1186/1471-2164-10-582

Colmer, T. D., Munns, R., and Flowers, T. J. (2005). Improving salt tolerance of wheat and barley: future prospects. *Aust. J. Exp. Agric.* 45, 1425–1443. doi: 10.1071/EA04162

Comadran, J., Kilian, B., Russell, J., Ramsay, L., Stein, N., Ganal, M., et al. (2012). Natural variation in a homolog of Antirrhinum CENTRORADIALIS contributed to spring growth habit and environmental adaptation in cultivated barley. *Nat. Genet.* 44, 1388–1392. doi: 10.1038/ng.2447

Cotsaftis, O., Plett, D., Shirley, N., Tester, M., and Hrmova, M. (2012). A two-staged model of Na+ exclusion in rice explained by 3D modelling of HKT transporters and alternative splicing. *PLoS ONE* 7:e39865. doi: 10.1371/journal.pone.0039865

Dai, F., Nevo, E., Wu, D. Z., Comadran, J., Zhou, M. X., Qiu, L., et al. (2012). Tibet is one of the centers of domestication of cultivated barley. *Proc. Natl. Acad. Sci. U.S.A.* 109, 16969–16973. doi: 10.1073/pnas.1215265109

Davenport, R., James, R. A., Zakrisson-Plogander, A., Tester, M., and Munns, R. (2005). Control of sodium transport in durum wheat. *Plant Physiol.* 137, 807–818. doi: 10.1104/pp.104.057307

DeRose-Wilson, L., and Gaut, B. S. (2011). Mapping salinity tolerance during *Arabidopsis thaliana* germination and seedling growth. *PLoS ONE* 6:e22832. doi: 10.1371/journal.pone.0022832

Dunn, O. J. (1964). Multiple comparisons using rank sums. *Technometrics* 6, 241–252. doi: 10.1080/00401706.1964.10490181

Evanno, G., Regnaut, S., and Goudet, J. (2005). Detecting the number of clusters of individuals using the software STRUCTURE: a simulation study. *Mol. Ecol.* 14, 2611–2620. doi: 10.1111/j.1365-294X.2005.02553.x

Fan, Y., Shabala, S., Ma, Y. L., Xu, R. G., and Zhou, M. X. (2015). Using QTL mapping to investigate the relationships between abiotic stress tolerance (drought and salinity) and agronomic and physiological traits. *BMC Genomics* 16:43. doi: 10.1186/s12864-015-1243-8

Fan, Y., Zhou, G., Shabala, S., Chen, Z. H., Cai, S., Li, C., et al. (2016). Genome-Wide Association Study Reveals a New QTL for Salinity Tolerance in Barley (*Hordeum vulgare* L.). *Front. Plant Sci.* 7:946. doi: 10.3389/fpls.2016.00946

FAO (2008). *FAO Land and Plant Nutrition Management Service*. Available online at: http://www.fao.org/ag/agl/agll/spush.

Flowers, T. J. (2004). Improving crop salt tolerance. *J. Exp. Bot.* 55, 307–319. doi: 10.1093/jxb/erh003

Flowers, T. J., and Flowers, S. A. (2005). Why does salinity pose such a difficult problem for plant breeders? *Agric. Water Manag.* 78, 15–24. doi: 10.1016/j.agwat.2005.04.015

Fricke, W., Akhiyarova, G., Veselov, D., and Kudoyavova, G. (2004). Rapid and tissue-specific changes in ABA and in growth rate in response to salinity in barley leaves. *J. Exp. Bot.* 55, 1115–1123. doi: 10.1093/jxb/erh117

Garciadeblás, B., Senn, M. E., Bañuelos, M. A., and Rodríguez-Navarro, A. (2003). Sodium transport and HKT transporters: the rice model. *Plant J.* 34, 788–801. doi: 10.1046/j.1365-313X.2003.01764.x

Hardy, O. J., and Vekemans, X. (2002). SPAGEDi: a versatile computer program to analyze spatial genetic structure at the individual or population levels. *Mol. Ecol. Notes* 2, 618–620. doi: 10.1046/j.1471-8286.2002.00305.x

Horie, T., Costa, A., Kim, T. H., Han, M. J., Horie, R., Leung, H. Y., et al. (2007). Rice *OsHKT2;1* transporter mediates large Na+ influx component into K+-starved roots for growth. *EMBO J.* 26, 3003–3014. doi: 10.1038/sj.emboj.7601732

Huang, S., Spielmeyer, W., Lagudah, E. S., and Munns, R. (2008). Comparative mapping of *HKT* genes in wheat, barley and rice, key determinants of Na+ transport and salt tolerance. *J. Exp. Bot.* 59, 927–937. doi: 10.1093/jxb/ern033

Jabnoune, M., Espeout, S., Mieulet, D., Fizames, C., Verdeil, J.-L., Conéjéro, G., et al. (2009). Diversity in expression patterns and functional properties in the rice HKT transporter family. *Plant Physiol.* 150, 1955–1971. doi: 10.1104/pp.109.138008

Jakobsson, M., and Rosenberg, N. A. (2007). CLUMPP: a cluster matching and permutation program for dealing with label switching and multimodality in analysis of population structure. *Bioinformatics* 23, 1801–1806. doi: 10.1093/bioinformatics/btm233

James, R. A., Blake, C., Byrt, C., and Munns, R. (2011). Major genes for Na^+ exclusion, *Nax1* and *Nax2* (wheat *HKT1;4* and *HKT1;5*) decrease Na^+ accumulation in bread wheat leaves under saline and waterlogged conditions. *J. Exp. Bot.* 62, 2939–2947. doi: 10.1093/jxb/err003

James, R. A., Davenport, R. J., and Munns, R. (2006). Physiological characterization of two genes for Na^+ exclusion in durum wheat, *Nax1* and *Nax2*. *Plant Physiol.* 142, 1537–1547. doi: 10.1104/pp.106.086538

Kilian, B., Ozkan, H., Kohl, J., vonHaeseler, A., Barale, F., Deusch, O., et al. (2006). Haplotype structure at seven barley genes: relevance to gene pool bottlenecks, phylogeny of ear type and site of barley domestication. *Mol. Genet. Genom.* 276, 230–241. doi: 10.1007/s00438-006-0136-6

Kong, W., Li, J., Yu, Q., Cang, W., Xu, R., Wang, Y., et al. (2016). Two Novel flavin-containing monooxygenases involved in biosynthesis of aliphatic glucosinolates. *Front. Plant Sci.* 7:1292. doi: 10.3389/fpls.2016.01292

Kumar, V., Singh, A., Mithra, S. V. A., Krishnamurthy, S. L., Parida, S. K., Jain, S., et al. (2015). Genome-wide association mapping of salinity tolerance in rice (*Oryza sativa*). *DNA Res.* 22, 133–145. doi: 10.1093/dnares/dsu046

Ligges, U., and Mächler, M. (2003). Scatterplot3d - an R Package for visualizing multivariate data. *J. Stat. Softw.* 8, 1–20. doi: 10.18637/jss.v008.i11

Lipka, A. E., Tian, F., Wang, Q. S., Peiffer, J., Li, M., Bradbury, P. J., et al. (2012). GAPIT: genome association and prediction integrated tool. *Bioinformatics* 28, 2397–2399. doi: 10.1093/bioinformatics/bts444

Liu, X., Fan, Y., Mak, M., Holford, P., Wang, F., Chen, G., et al. (2017). QTLs for stomatal and photosynthetic traits related to salinity tolerance in barley. *BMC Genomics* 18:9. doi: 10.1186/s12864-016-3380-0

Long, N. V., Dolstra, O., Malosetti, M., Kilian, B., Graner, A., Visser, R. G., et al. (2013). Association mapping of salt tolerance in barley (*Hordeum vulgare* L.). *Theor. Appl. Genet.* 126, 2335–2351. doi: 10.1007/s00122-013-2139-0

Mian, A., Oomen, R. J., Isayenkov, S., Sentenac, H., Maathuis, F. J., and Véry, A.-A. (2011). Over- expression of an Na^+- and K^+-permeable

HKT transporter in barley improves salt tolerance. *Plant J.* 68, 468–479. doi: 10.1111/j.1365-313X.2011.04701.x

Møller, I. S., Gilliham, M., Jha, D., Mayo, G. M., Roy, S. J., Coates, J. C., et al. (2009). Shoot Na+ exclusion and increased salinity tolerance engineered by cell type-specific alteration of Na+ transport in Arabidopsis. *Plant Cell* 21, 2163–2178. doi: 10.1105/tpc.108.064568

Morris, G. P., Ramu, P., Deshpande, S. P., Hash, T., Shah, T., Upadhyaya, H. D., et al. (2013). Population genomic and genome-wide association studies of agroclimatic traits in sorghum. *Proc. Natl. Acad. Sci. U.S.A.* 110, 453–458. doi: 10.1073/pnas.1215985110

Munns, R. (2005). Genes and salt tolerance: bringing them together. *New Phytol.* 167, 645–663. doi: 10.1111/j.1469-8137.2005.01487.x

Munns, R., and James, R. (2003). Screening methods for salinity tolerance: a case study with tetraploid wheat. *Plant Soil* 253, 201–218. doi: 10.1023/A:1024553303144

Munns, R., James, R. A., and Läuchli, A. (2006). Approaches to increasing the salt tolerance of wheat and other cereals. *J. Exp. Bot.* 57, 1025–1043. doi: 10.1093/jxb/erj100

Munns, R., James, R. A., Xu, B., Athman, A., Conn, S. J., Jordans, C., et al. (2012). Wheat grain yield on saline soils is improved by an ancestral Na transporter gene. *Nat. Biotech.* 30, 360–366. doi: 10.1038/nbt.2120

Munns, R., and Tester, M. (2008). Mechanisms of salinity tolerance. *Annu. Rev. Plant Biol.* 59, 651–681. doi: 10.1146/annurev.arplant.59.032607.092911

Muñoz-Amatriaín, M., Cuesta-Marcos, A., Endelman, J. B., Comadran, J., Bonman, J. M., Bockelman, H. E., et al. (2014). The USDA barley core collection: genetic diversity, population structure, and potential for genome-wide association studies. *PLoS ONE* 9:e94688. doi: 10.1371/journal.pone.0094688

Negrão, S., Almadanim, C. M., Pires, I. S., Abreu, I. A., Maroco, J., Courtois, B., et al. (2013). New allelic variants found in key rice salt-tolerance genes: an association study. *Plant Biotech. J.* 11, 87–100. doi: 10.1111/pbi.12010

Nevo, E., and Chen, G. X. (2010). Drought and salt tolerances in wild relatives for wheat and barley improvement. *Plant Cell Environ.* 33, 670–685. doi: 10.1111/j.1365-3040.2009.02107.x

Paradis, E., Claude, J., and Strimmer, K. (2004). APE: analyses of phylogenetics and evolution in R language. *Bioinformatics* 20, 289–290. doi: 10.1093/bioinformatics/btg412

Platten, J. D., Cotsaftis, O., Berthomieu, P., Bohnert, H., Davenport, R., Fairbairn, D., et al. (2006). Nomenclature for HKT transporters, key determinants of plant salinity tolerance. *Trends Plant Sci.* 11, 372–374. doi: 10.1016/j.tplants.2006.06.001

Platten, J. D., Egdane, J. A., and Ismail, A. M. (2013). Salinity tolerance, Na+ exclusion and allele mining of *HKT1;5* in *Oryza sativa* and *O. glaberrima*: many sources, many genes, one mechanism? *BMC Plant Biol.* 13:32. doi: 10.1186/1471-2229-13-32

Plett, D., Safwat, G., Gilliham, M., Møller, I. S., Roy, S., Shirley, N., et al. (2010). Improved salinity tolerance of rice through cell-type-specific expression of *AtHKT1;1*. *PLoS ONE* 5:e12571. doi: 10.1371/journal.pone.0012571

Price, A. L., Patterson, N. J., Plenge, R. M., Weinblatt, M. E., Shadick, N. A., and Reich, D. (2006). Principal components analysis corrects for stratification in genome-wide association studies. *Nat. Genet.* 38, 904–909. doi: 10.1038/ng1847

Pritchard, J. K., Stephens, M., and Donnelly, P. (2000). Inference of population structure using multilocus genotype data. *Genetics* 155, 945–959.

Ren, Z. H., Gao, J. P., Li, L. G., Cai, X. L., Huang, W., Chao, D. Y., et al. (2005). A rice quantitative trait locus for salt tolerance encodes a sodium transporter. *Nature Genet.* 37, 1141–1146. doi: 10.1038/ng1643

Ritland, K. (1996). Estimators for pairwise relatedness and individual inbreeding coefficients. *Genet. Res.* 67, 175–185. doi: 10.1017/S0016672300033620

Rodríguez-Navarro, A., and Rubio, F. (2006). High-affinity potassium and sodium transport systems in plants. *J. Exp. Bot.* 57, 1149–1160. doi: 10.1093/jxb/erj068

Rosenberg, N. A. (2004). Distruct: a program for the graphical display of population structure. *Mol. Ecol. Notes* 4, 137–138. doi: 10.1046/j.1471-8286.2003.00566.x

Rus, A., Baxter, I., Muthukumar, B., Gustin, J., Lahner, B., Yakubova, E., et al. (2006). Natural variants of AtHKT1 enhance Na^+ accumulation in two wild population of Arabidopsis. *PLoS Genet.* 2:e210. doi: 10.1371/journal.pgen.0020210

Jülke, S., and Ludwig-Müller, J. (2015). Response of Arabidopsis thaliana roots with altered lipid transfer protein (ltp) gene expression to the clubroot disease and salt stress. *Plants* 5:2. doi: 10.3390/plants5010002

Sahi, C., Singh, A., Blumwald, E., and Grover, A. (2006). Beyond osmolytes and transporters: novel plant salt-stress tolerance-related genes from transcriptional profiling data. *Physiol. Plant.* 127, 1–9. doi: 10.1111/j.1399-3054.2005.00610.x

Sassi, A., Mieulet, D., Khan, I., Moreau, B., Gaillard, I., Sentenac, H., et al. (2012). The rice monovalent cation transporter OsHKT2;4: revisited ionic selectivity. *Plant Physiol.* 160, 498–510. doi: 10.1104/pp.112.194936

Shahid, S. A., Abdelfattah, M. A., Wilson, M. A., Kelly, J. A., and Chiaretti, J. V. (2014). *United Arab Emirates Keys to Soil Taxonomy*. Abu Dhabi: Springer science + Business Media Dordrecht.

Shavrukov, Y., Gupta, N. K., Miyazaki, J., Baho, M. N., Chalmers, K. J., Tester, M., et al. (2010). HvNax3- a locus controlling shoot sodium exclusion derived from wild barley (*Hordeum vulgare* ssp. spontaneum). *Funct. Integr. Genom.* 10, 277–291. doi: 10.1007/s10142-009-0153-8

Siahsar, B. A., and Narouei, M. (2010). Mapping QTLs of physiological traits associated with salt tolerance in 'Steptoe 'x' Morex' doubled haploid lines of barley at seedling stage. *J. Food Agric. Environ.* 8, 751–759.

Suzuki, K., Yamaji, N., Costa, A., Okuma, E., Kobayashi, N. I., Kashiwagi, T., et al. (2016). OsHKT1;4-mediated Na+ transport in stems contributes to Na^+ exclusion from leaf blades of rice at the reproductive growth stage upon salt stress. *BMC Plant Biol.* 16:22. doi: 10.1186/s12870-016-0709-4

Véry, A.-A., Nieves-Cordones, M., Daly, M., Khan, I., Fizames, C., and Sentenac, H. (2014). Molecular biology of K+ transport across the plant cell membrane: what do we learn from comparison between plant species? *J. Plant Physiol.* 9, 748–769. doi: 10.1016/j.jplph.2014.01.011

Witzel, K., Weidner, A., Surabhi, G. K., Varshney, R. K., Kunze, G., Buck-Sorlin, G. H., et al. (2010). Comparative analysis of the grain proteome fraction in barley genotypes with contrasting salinity tolerance during germination. *Plant Cell Environ.* 33, 211–222. doi: 10.1111/j.1365-3040.2009.02071.x

Xue, D. W., Huang, Y. Z., Zhang, X. Q., Wei, K., Westcott, S., Li, C. D., et al. (2009). Identification of QTLs associated with salinity tolerance at late growth stage in barley. *Euphytica* 169, 187–196. doi: 10.1007/s10681-009-9919-2

Zhang, A., Liu, D., Hua, C., Yan, A., Liu, B., and Wu, M. (2016). The Arabidopsis Gene zinc finger protein 3 (ZFP3) is involved in salt stress and osmotic stress response. *PLoS ONE* 11:e0168367. doi: 10.1371/journal.pone.0168367

Zhang, Z., Ersoz, E., Lai, C. Q., Todhunter, R. J., Tiwari, H. K., and Gore, M. A. (2010). Mixed linear model approach adapted for genome-wide association studies. *Nat. Genet.* 42, 355–360. doi: 10.1038/ng.546

Zhou, G. F., Johnson, P., Ryan, P. R., Delhaize, E., and Zhou, M. X. (2012). Quantitative trait loci for salinity tolerance in barley (*Hordeum vulgare* L.). *Mol. Breed.* 29, 427–436. doi: 10.1007/s11032-011-9559-9

Zhu, J. K. (2003). Regulation of ion homeostasis under salt stress. *Curr. Opin. Plant Biol.* 6, 441–445. doi: 10.1016/S1369-5266(03)00085-2

Conflict of Interest Statement: The authors declare that the research was conducted in the absence of any commercial or financial relationships that could be construed as a potential conflict of interest.

frontiers in Plant Science

ORIGINAL RESEARCH
published: 07 February 2018
doi: 10.3389/fpls.2018.00124

Auxin and Gibberellins Are Required for the Receptor-Like Kinase ERECTA Regulated Hypocotyl Elongation in Shade Avoidance in Arabidopsis

Junbo Du[1,2,3†], Hengke Jiang[1,2,3†], Xin Sun[1,2,3†], Yan Li[1,2,3†], Yi Liu[1], Mengyuan Sun[1,2,3], Zhou Fan[1], Qiulin Cao[1], Lingyang Feng[1,2,3], Jing Shang[1,2], Kai Shu[1,2,3], Jiang Liu[1,2,3], Feng Yang[1,2,3], Weiguo Liu[1,2,3], Taiwen Yong[1,2,3], Xiaochun Wang[1,2,3], Shu Yuan[4], Liang Yu[1,2,3], Chunyan Liu[1,2,3] and Wenyu Yang[1,2,3*]*

[1] College of Agronomy, Sichuan Agricultural University, Chengdu, China, [2] Sichuan Engineering Research Center for Crop Strip Intercropping System, Sichuan Agricultural University, Chengdu, China, [3] Key Laboratory of Crop Ecophysiology and Farming System in Southwest China – Ministry of Agriculture, Sichuan Agricultural University, Chengdu, China, [4] College of Resources, Sichuan Agricultural University, Chengdu, China

Plants use shade avoidance strategy to escape the canopy shade when grown under natural conditions. Previous studies showed that the Arabidopsis receptor-like kinase ERECTA (ER) is involved in shade avoidance syndrome. However, the mechanisms of ER in modulating SAR by promoting hypocotyl elongation are unknown yet. Here, we report that ER regulated hypocotyl elongation in shade avoidance requires auxin and gibberellins (GAs). The T-DNA insertional *ER* mutant *er-3* shows a less hypocotyl length than that in Col-0 wild type. Promoter::GUS staining analysis shows that *ER* and its paralogous genes *ERECTA-LIKE1* (*ERL1*) and *ERECTA-LIKE2* (*ERL2*) are differentially expressed in the seedlings, of which only *ER* is most obviously upregulated in the hypocotyl by shade treatment. Exogenous feeding assay by using media-application with vertical-grown of Arabidopsis seedlings showed that the hypocotyl length of *er-3* is partially promoted by indol-3-acetic acid (IAA), while it is relatively insensitive of *er-3* to various concentrations of IAA than that of Col-0. Hypocotyl elongation of *er-3* is promoted similar to that of Col-0 by high temperature in the white light condition, but the elongation was not significantly affected by the treatment of the auxin transport inhibitor 1-*N*-naphthylphthalamic acid (NPA). Exogenous GA3 increased the hypocotyl elongation of both *er-3* and the wild type in the shade condition, and the GA3 biosynthesis inhibitor paclobutrazol (PAC) severely inhibits the hypocotyl elongation of Col-0 and *er-3*. Further analysis showed that auxin biosynthesis inhibitors yucasin and L-kynurenine remarkably inhibited the hypocotyl elongation of *er-3* while yucasin shows a more severe inhibition to *er-3* than Col-0. Relative expression of genes regulating

OPEN ACCESS

Edited by:
Kai He,
Lanzhou University, China

Reviewed by:
Joshua Blakeslee,
The Ohio State University, United States
Yingfang Zhu,
Purdue University, United States

***Correspondence:**
Junbo Du
junbodu@hotmail.com
Wenyu Yang
mssiyangwy@sicau.edu.cn

† These authors have contributed equally to this work.

Specialty section:
This article was submitted to Plant Traffic and Transport, a section of the journal Frontiers in Plant Science

Received: *30 June 2017*
Accepted: *23 January 2018*
Published: *07 February 2018*

Citation:
Du J, Jiang H, Sun X, Li Y, Liu Y, Sun M, Fan Z, Cao Q, Feng L, Shang J, Shu K, Liu J, Yang F, Liu W, Yong T, Wang X, Yuan S, Yu L, Liu C and Yang W (2018) Auxin and Gibberellins Are Required for the Receptor-Like Kinase ERECTA Regulated Hypocotyl Elongation in Shade Avoidance in Arabidopsis. Front. Plant Sci. 9:124. doi: 10.3389/fpls.2018.00124

auxin homeostasis and signaling, and GA homeostasis is less in *er-3* than that in Col-0. Furthermore, genetic evidences show that *ER* regulated hypocotyl elongation is dependent of PHYTOCHROME B (PHYB). Overall, we propose that ER regulated shade avoidance by promoting hypocotyl elongation is PHYB-dependent and requires auxin and GAs.

Keywords: ERECTA, receptor-like kinase, shade avoidance, auxin, GA

INTRODUCTION

Light is one of the most important factors for plant survival and production. In a natural environment, plants always grow closely to one another. Under these conditions, red light wavelengths is been absorbed while the far red light wavelengths is reflected by the leaves of the neighboring plants, resulting in reduction of red:far red (R:FR) light ratio and light intensity, referred to as shade condition. Plants have evolved sophisticated mechanisms which involves architecture and physiological process including increase of the hypocotyl and stem length, hyponasty, early flowering and yield reduction, which is referred to as shade avoidance syndrome (SAR) (Casal, 2013; Wit et al., 2016). In the shade, plants must accelerate their growth in order to maintain their height at least as tall as their neighboring plants to succeed in light sensing competition conditions (Ballaré, 1999). In this process, plants have to expend more energy to support their elongation growth at the expense of leaf development, seed number and yield reduction. Arabidopsis and most crops show typical phenotypes of SAR, while some other plants display shade tolerance phenotype mimicking the phenotypes of the plants in the white light condition (Valladares and Niinemets, 2008; Carriedo et al., 2016).

Upon sensing the canopy shade by the neighboring plants, phytochromes in plant cells would perceive the changes of R:FR light condition and rapidly evoke cascades of actions. Of all the five phytochromes, phytochrome A (PHYA), phytochrome B (PHYB), phytochrome C (PHYC), phytochrome D (PHYD), and phytochrome E (PHYE) in Arabidopsis, PHYB was found to play dominant roles in shade avoidance (Ballaré, 1999; Ruberti et al., 2012; Casal, 2013; Wit et al., 2016). When plants were under shade conditions, PHYB releases the binding of phytochrome interacting factor (PIF) transcription factors and facilitates their entry into the nucleus to bind the promoters of the target genes to trigger the expression of genes in regulating phytohormone levels and signaling pathways (Lorrain et al., 2008; Casal, 2013). Most phytohormones which are found to participate in several aspects of the shade avoidance signaling pathways, auxin and gibberellins (GAs) are best established to be essential for elongation-promoting of plant hypocotyls, stems and petioles (Wit et al., 2016; Yang and Li, 2017). In Arabidopsis and *Brassica rapa* seedlings, auxins are biosynthesized in the cotyledon when suffered to shade and cotyledon-synthesized auxins are then transported to promote the hypocotyl elongation (Tao et al., 2008; Procko et al., 2014). In these processes, genes related to plant growth and development, and adaptation are largely expressed.

Indol-3-acetic acid (IAA) is the predominant naturally occurring auxin in plants (Zhao, 2010, 2012). In higher plants, auxin biosynthesis is likely extremely complex in plants, which includes *de novo* auxin production and the release from auxin conjugates (Zhao, 2010, 2012, 2014). IAA exists in two forms, the free IAA and conjugated IAA, the free IAA can be converted from the conjugated IAA, which is considered as the storage forms or the intermediates for degradation (Woodward and Bartel, 2005; Ludwig-Müller, 2011; Zhao, 2014). Previous isotope-labeling experiment and genetic evidence demonstrated that auxin principally biosynthesized via tryptophan (Trp)-dependent and Trp-independent pathways to coordinately regulate plant growth and development (Wright et al., 1991; Normanly et al., 1993; Woodward and Bartel, 2005; Wang et al., 2015). More evidence showed that several Trp-dependent auxin biosynthesis pathways contribute predominantly to IAA levels referring to the indole-3-acetaldoxime (IAOx) pathway, indoleacetamine (IAM) pathway, and the indole-3-pyruvic acid (IPA) pathway, of which the IPA pathways is the well studied pathway up to date (Korasick et al., 2013; Tivendale et al., 2014; Zhao, 2014). IAA biosynthesized from the Trp by using the IPA as intermediate by a two-step pathway is the best completely established pathway (Zhao, 2012, 2014). In this pathway, Trp is first converted to IPA by TAA1/TARs and IPA is subsequently catalyzed by YUCCAs (YUCs) into IAA (Zhao et al., 2001; Tao et al., 2008). In recent years, more and more compelling evidence showed that, in addition to auxin biosynthesis, auxin transport and metabolism are also essential to hypocotyl elongation in shade avoidance (Pierik et al., 2009; Keuskamp et al., 2010; Zhao, 2010; Yang and Li, 2017). Several studies have demonstrated that auxin transport is important in hypocotyl elongation in etiolated growth, photomorphogenesis, and phototropism similar to shade avoidance response (Jensen et al., 1998; Wu et al., 2016).

When plants are exposed to the adverse environment, the external stimuli will activate the cell membrane-located receptor molecules and initiate the changes of conformation of the receptors. Receptor-like kinases (RLKs) are a set of single transmembrane proteins located on the plasma membrane which involve in sensing the environmental changes including cell-to-cell and cell-to-environment communications (Becraft, 2002; Li, 2010). A typical RLK contains an extracellular domain for signal perception, a transmembrane domain for membrane anchoring and an intercellular Ser/Thr/Tyr kinase domain for signal transduction via phosphorylation (Walker and Zhang, 1990; Shiu and Li, 2004; Oh et al., 2009; Li, 2010; Oh et al., 2010). The first plant RLK was identified from maize by using degenerate PCR primers to the protein kinase domain

(Walker and Zhang, 1990). More than 610 RLKs have been found in Arabidopsis in recent years (Shiu and Bleecker, 2001; Shiu et al., 2004). Up to date, more and more RLKs have been found to function in many aspects of plant growth and development, cell death and defense (Li and Chory, 1997; Li et al., 2002; Nam and Li, 2002; Zipfel et al., 2006; Chinchilla et al., 2007; He et al., 2007; Du et al., 2012). For instance, the BRI1 was found as a receptor of brassinosteroids (BRs) (Li and Chory, 1997), BAK1 is a co-receptor of BRI1 in BR signaling pathways in regulating plant growth and development (Li et al., 2002; Nam and Li, 2002). Furthermore, BAK1 was also found as a co-receptor of FLS2 and EFR in pathogen perception and defense pathways (Zipfel et al., 2006; Chinchilla et al., 2007). ERECTA (ER) was firstly found in 1957 by using X-ray irradiated Arabidopsis Landsberg ecotype (Rédei et al., 1992). ER and its functional paralogs ERL1 and ERL2 not only control multiple aspects of plant morphology, but also regulate plant responses to environmental changes (Shpak et al., 2004). Genetic analysis has shown that the *er* mutant displays compact inflorescence and short blunt silique phenotypes due to the decrease in cell proliferation and growth (Shpak et al., 2003). In addition, ERL1 and ERL2 were found to play a redundant role in cell proliferation of organ growth and patterning (Shpak et al., 2004). Furthermore, ER was found to regulate transpiration efficiency in Arabidopsis (Masle et al., 2005). Overexpression of truncated Arabidopsis ER in tomato decreased water loss and enhanced drought tolerance (Villagarcia et al., 2012). Overexpression of Arabidopsis ER in Arabidopsis, rice and tomato increased plant biomass and improved thermal tolerance independent of water content (Shen et al., 2015). Single nucleotide polymorphism (SNP) analysis has shown that an ER homologous gene might be associated with drought adaptation between wild and common bean (Blair et al., 2016).

In recent studies, Patel et al. demonstrated that ER regulates petiole angle and elongation in the shade particularly at cool temperatures in Landsberg ecotype (Patel et al., 2013). It is possible that ER stimulate petiole elongation by promoting the cell expansion in the petioles. Another study also showed that ER makes an important contribution to the shade avoidance syndrome in some stages during plant development against light fluctuations (Kasulin et al., 2013). However, the mechanisms of ER in modulating the SAR are not clear yet, which needs further investigation.

Here, we report our identification of ER in regulating Arabidopsis hypocotyl elongation in the shade in Col-0 background. The results show that loss-of-function of *ER* displays a shorter hypocotyl length than that of Col-0 wild type in the shade condition. Promoter::GUS analyses show that the expression of *ER* is remarkably induced in the hypocotyl by shade treatment. Further investigation show that ER regulated hypocotyl elongation is probably via actions of auxin and GAs, and is dependent of PHYB. Our data supplied a new identification of ER in shade avoidance and detailed a possible mechanism of ER regulated shade avoidance underlying the involvement of auxin homeostasis and signaling pathways, as well as GA homeostasis, which provides new evidence and mechanisms for ER regulated shade avoidance.

MATERIALS AND METHODS

Plant Materials and Growth Conditions

All the Arabidopsis seeds used in these studies were Col-0 ecotype. Seeds of *er-3* (SALK_044110) (Durbak and Tax, 2011), *phyB* (SALK_022035C) were ordered from Arabidopsis Biological Resource Center (ABRC). Plants were grown at 22°C in a long-day growth condition (16 h of light and 8 h of dark) in a greenhouse except those for special treatments.

Arabidopsis seeds were surface-sterilized and grown in the soil or on the 1/2 Murashige and Skoog (MS) media (pH 5.7) supplemented with 1% sucrose and 0.8% agar. For shade treatment of soil-grown plants, 10-day-old Arabidopsis Col-0 and *er-3* single mutant grown in a normal light condition (16 h of light and 8 h of dark) with PAR of 65 μmol m^{-2} s^{-1} and R/FR of 1.3) in a greenhouse and then transferred to a green filter (type No. 122 with a transmittance of 45.6%[1], England) with PAR of 31 μmol m^{-2} s^{-1} and R/FR of 0.5 for another 15 days. For shade treatment of media-grown plants, plants were grown in normal light condition for 3 days and then treated with the green filter for another 5 days. Plants were then used for further analyses. Unless it is specially stated that, the plants were grown on slightly vertical 1/2 MS media.

Semi-quantitative Reverse Transcription (RT)-PCR and Quantitative PCR (qPCR) Analyses

Two micrograms of total RNA were extracted by using an RNAprep pure Plant Kit (Tiangen Biotech) used for reverse transcription with M-MLV (Invitrogen). The first strand of cDNAs was used for semi-quantitative reverse transcription PCR (RT-PCR) analyses with *ExTaq* DNA polymerase (TaKaRa) according to previous studies (Du et al., 2012). Real-time PCR was employed with SYBR® Premix Ex Taq™ II (TaKaRa) and relative expression of genes compared to *ACT2* was calculated using $\Delta\Delta$Ct method. Primers used in this study are listed in **Supplementary Table S1**.

Promoter::GUS Construction of ER Family Genes and GUS Staining

Promoters of *ER*, *ERL1* and *ERL2* with 1.5 kb were amplified from genomic DNA and cloned with a Gateway® Cloning technology (Invitrogen). The genes were recombined into a binary vector *pBASTA-GWR-GUS* and the destination plasmids were then overexpressed in Col-0 with *Agrobacterium*-mediated transformation. Surface-sterilized seeds of homozygous transgenic plants harboring promoter-GUS were grown on 1/2 MS media. After stratification for 2 days at 4°C, the plates were grown vertically at 22°C in white light for 3 days, and then transferred to white light or shade conditions for another 5 days for GUS staining. For GUS staining, ER, ERL1, or ERL2 promoter-GUS transgenic seedlings were stained according to previous studies (Guo et al., 2010). The stained plants were observed and for photo-capture under a Leica M165C digital

[1]www.q-max.net

stereo microscope, the images were subsequently arranged by using the Adobe Photoshop CS6 software.

Treatment of Phytohormones and the Biosynthesis Inhibitors

Surface-sterilized seeds were grown on 1/2 MS plates supplemented with 1% sucrose, 0.8% agar and different concentrations of IAA (Sangon), GA3 (Sangon), the auxin biosynthesis inhibitors yucasin and L-kynurenine (kyn) (Sigma-Aldrich), and the GA biosynthesis inhibitor paclobutrazol (PAC) (Sangon). The seedlings were grown at a slight angle with the hypocotyl touching the media. Stock solutions of the phytohormones and the inhibitors were dissolved as follows: 20 mM of IAA were dissolved in ethanol, 20 mM of GA3 in methanol, 500 mM of yucasin in DMSO, 100 mM of kyn in 0.5 M HCl and 5 mM PAC in methanol, respectively. ddH_2O was used for dilution for the working concentrations. The hypocotyl length was measured with ImageJ 1.6 and analyzed with Graphpad 5.0.

RESULTS

Loss-of-Function of *ER* Is Shade Insensitive in Hypocotyl Elongation

To understand whether ER regulates hypocotyl elongation in shade response, *er-3* (Durbak and Tax, 2011), a T-DNA insertional loss-of-function mutant of *ER*, was used to assess the shade response. After 3-day white-light growth, Col-0 and *er-3* were then moved to the shade condition for another 5 days. The results showed that the hypocotyl length of *er-3* were significantly less sensitive to shade treatment than that of Col-0 in our shade condition (**Figures 1A,B**). To further confirm the shade response phenotypes of *er* mutant, we grew the Col-0 and *er-3* seeds in the soil and covered a green filter for shade treatment. In the shade condition, both soil-grown Col-0 and *er* showed a typical shade avoidance response including petiole elongation (**Figures 1C,D**). Nevertheless, the petiole elongation was shorter in *er-3* single mutant than that in Col-0 in the shade, indicating that petiole elongation of *er-3* is relatively insensitive to shade, which is consistent with other *er* alleles in previous studies (Patel et al., 2013). These results suggest that ER in Col-0 ecotype makes a contribution to shade avoidance syndrome.

Expression of *AtER* in Hypocotyl Is Upregulated by Shade

To examine whether the transcript level of *ER* in the hypocotyl of Arabidopsis responds to shade, we performed RT-PCR analysis to check gene expression by the time-course shade treatment. The results showed that the shade inducible gene *PIL1* was upregulatedly expressed in the hypocotyls of Col-0 after 30 min by shade treatment and increased as time rises (**Supplementary Figure S1**), indicating that our shade condition is reliable for study on the shade avoidance syndrome. Under this shade condition, we further found that the expression of *ER* was upregulated in the hypocotyls of Col-0 after 30 min and reached

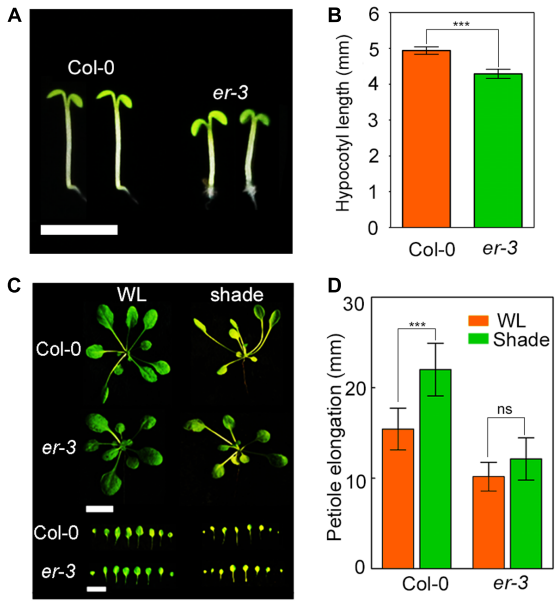

FIGURE 1 | Phenotypes of Col-0 and *er-3* single mutant in shade avoidance. **(A)** Phenotypes of Col-0 and *er-3* grown on MS media under the shade conditions. Scale bar represents 5 mm. **(B)** Statistical data of hypocotyl length of Col-0 and *er-3* under white light and shade conditions. At least 30 seedlings were measured for each genotype. Error bars represent SE. **(C)** Phenotypes of Col-0 and *er-3* grown in the soil under white light and shade conditions. Scale bars represent 10 mm. **(D)** Statistical data of petiole length of Col-0 and *er-3* grown in the soil under white light and shade conditions. At least 30 seedlings were measured for each genotype. Error bars represent SE. Student's *t*-test indicated the differences are statistically significant (***$P < 0.001$).

at a highest level after 2 h of shade treatment (**Supplementary Figure S1**). These results indicate that *ER* is responsive to shade at the transcription level, suggesting that *ER* might function in shade avoidance pathways in the hypocotyl of Arabidopsis.

ER Family Genes Are Differentially Responsive to Shade

There are three *ER* family genes, *ER* and its paralogous genes *ERL1* and *ERL2* in the Arabidopsis genome. To investigate whether ER family members are responsive to shade stress, we constructed expression vectors harboring a GUS reporter gene driven by the native promoters of *ER* family genes. As shown in **Figure 2**, *ER* is principally expressed in the young tissues and the hypocotyls when grown in the white light, whereas slightly expressed in the cotyledons. However, *ER* shows a higher expression level in the cotyledon, petiole and hypocotyl in the shade condition. *ERL1* is slightly expressed on the leaf margin, petiole and meristem, and its expression is remarkably induced in the meristem by shade but only slightly induced in the hypocotyl. The expression of *ERL2* is mainly distributed on the leaf margin and the meristem of the seedling, whereas downregulated by shade in the leaves and obviously upregulated in the meristem. These results indicate that *ER* family genes differentially respond to shade stress and only the expression of *ER* is most obviously

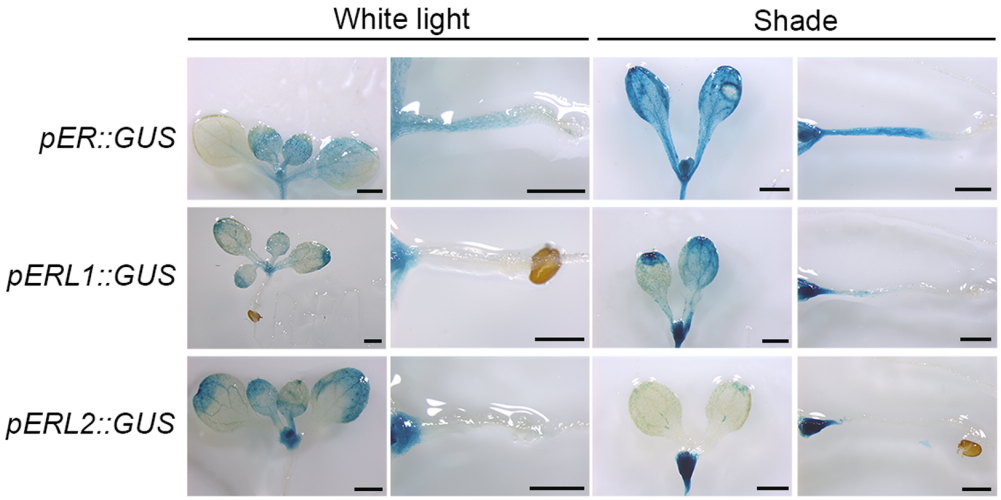

FIGURE 2 | Spatiotemporal expression pattern of *ER* family genes in the white light and shade. Scale bars represent 0.5 mm. pER::GUS staining of 5-day shade treated seedlings show differential expression of *ER*, *ERL1* and *ERL2* under white and shade conditions.

increased in the hypocotyls, suggesting that ER might contribute more to shade avoidance rather than ERL1 and ERL2 in the hypocotyls.

Exogenous Auxin Promoted the Hypocotyl Length of *er-3* in Shade Response

To examine whether *er-3* inhibited hypocotyl elongation in the shade is impaired in auxin biosynthesis, we determined the response of *er-3* to indole-3-acetic acid (IAA), the main natural auxin. As shown in **Figure 3**, 0.1 and 0.5 μM of IAA remarkably promoted the hypocotyl elongation of both Col-0 and *er-3*, and 0.5 μM of IAA fully rescued the hypocotyl length of *er-3* than that of Col-0 without IAA treatment. The results indicate that IAA is essential for ER regulated hypocotyl elongation and IAA biosynthesis might be impaired in *er-3* in the shade. Further, higher concentrations of IAA inhibit the elongation of both Col-0 and *er-3*, but *er-3* shows a shorter hypocotyl phenotype than that of Col-0 by the same concentration of IAA treatment (**Figures 3A,B**), implying that auxin signaling is also diminished in the *er-3* mutant. These results suggested that both auxin biosynthesis and signaling pathways might be impaired in the *er-3* mutant in the shade condition.

Genetic and physiological evidences show that IAA is principally biosynthesized from the precursor tryptophan via TRYPTOPHAN AMINOTRANSFERASE of ARABIDOPSIS/SHADE AVOIDANCE 3 (TAA1/SAV3), which catalyzes the production of IPA from L-tryptophan (L-Trp), then the IPA is as the substrate of YUC proteins to produce IAA (Zhao et al., 2001; Tao et al., 2008; Dai et al., 2013). Chemical library screening assay showed that kyn is a Trp analog as an effective competitive inhibitor of TAA1/TARs (TRYPTOPHAN AMINOTRANSFERASE RELATEDs) in Arabidopsis, which can effectively block the steps of Trp to IPA (He et al., 2011). In IPA to IAA steps, yucasin was recently found as a potent inhibitor of YUC enzymes in the major IAA biosynthesis pathways (Nishimura et al., 2014). To further understand whether ER regulated shade avoidance is deficient in auxin biosynthesis and in which step of auxin biosynthesis pathways, the effects of kyn and yucasin on Col-0 and *er-3* single mutant were investigated. In the shade condition, the results showed that the hypocotyl elongation of both vertically grown Col-0 and *er-3* at a slight angle are inhibited by both kyn and yucasin treatment (**Supplementary Figures S2A,B**). However, elongation of *er-3* shows less sensitive to kyn and yucasin than that of the wild type (**Supplementary Figures S2A,B**), suggesting that ER regulated hypocotyl elongation might depend on conversion of both Trp to IPA and IPA to IAA. It is reported that in some growth conditions, the plant appears thigmotropic response (Meng et al., 2012). To clarify that whether the inhibition of hypocotyl elongation by kyn and yucasin is resulted from the thigmotropism, we also test the horizontal growth of the plants on agar plates (0.5% agar) feeding by IAA biosynthesis inhibitors in the shade condition. Plants showed a similar inhibition of the hypocotyl elongation of Col-0 and *er-3* by both kyn and yucasin to that grown vertically at a slight angle (**Supplementary Figures S2A,C**). The inhibition of the hypocotyl elongation of Col-0 and *er-3* by IAA biosynthesis inhibitor therefore seems to be independent of thigmotropism. These results indicate that auxin biosynthesis is essential for the hypocotyl elongation of Col-0 and *er-3* stimulated by shading.

High Temperature Increases Shade-Stimulated Hypocotyl Elongation of *er-3*

Previous studies demonstrated that high temperature can increase the endogenous free auxin levels to promote the hypocotyl elongation (Gray et al., 1998). To test whether *er-3* regulated hypocotyl elongation in the shade is dependent on endogenous auxin levels, we tested the hypocotyl elongation

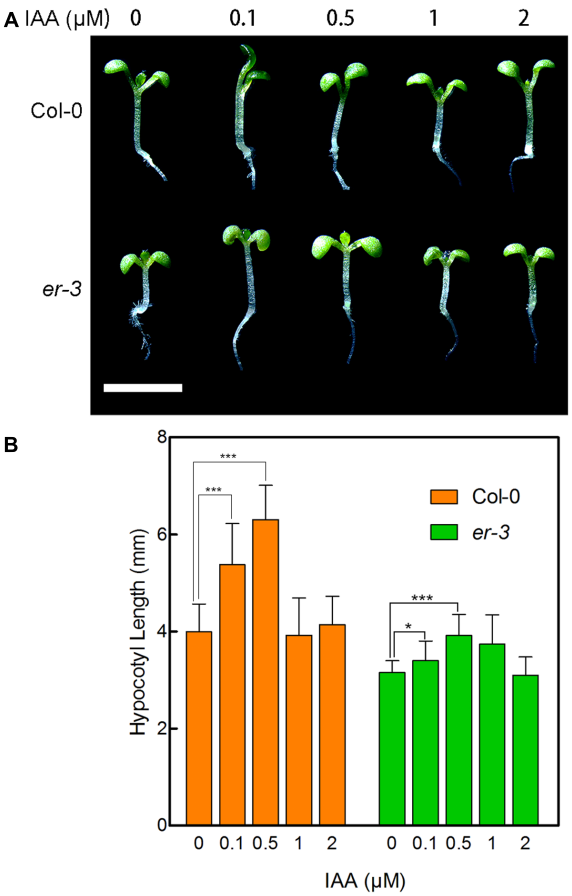

FIGURE 3 | Hypocotyl phenotypes of Col-0 and *er-3* in response to IAA. **(A)** Hypocotyl phenotypes Col-0 and *er-3* seedlings with different concentrations of IAA treatment. **(B)** Statistical data of hypocotyl length of Col-0 and *er-3* by IAA treatment under shade conditions. Student's *t*-test indicated the differences are statistically significant (*$P < 0.05$; ***$P < 0.001$). At least 10 seedlings were measured for each genotype. Error bars represent SE. Scale bars represent 0.5 cm.

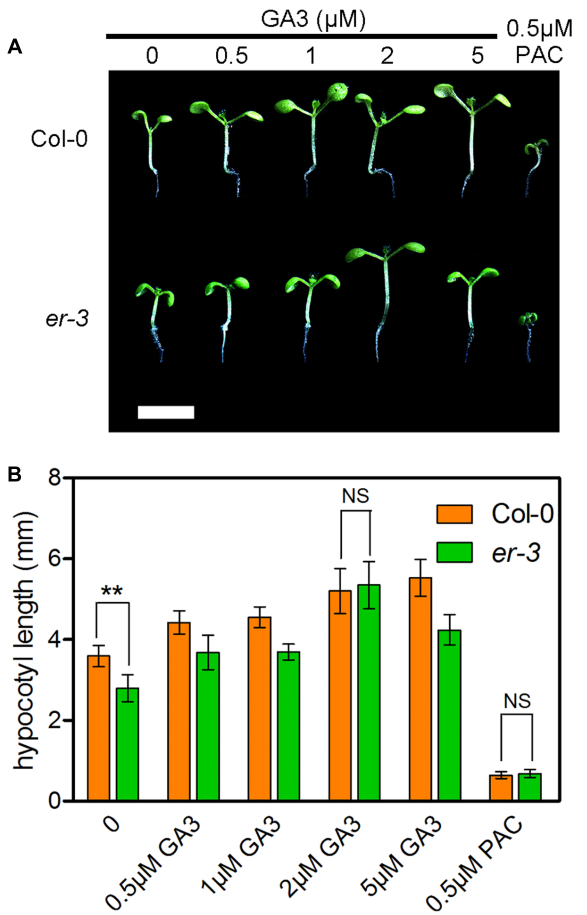

FIGURE 4 | Exogenous feeding of GA3 enhanced the hypocotyl elongation of both Col-0 and *er-3* in the shade. **(A)** Hypocotyl phenotypes of Col-0 and *er-3* by different concentrations of GA3 and PAC treatment. Scale bar represents 0.5 cm. **(B)** Statistical data of hypocotyl length of Col-0 and *er-3* by treatment of GA3 and PAC under shade conditions. Student's *t*-test indicated the differences are statistically significant (**$P < 0.01$). At least 10 seedlings were measured for each genotype. Error bars represent SE.

response of *er-3* to a high temperature of 30°C. The results showed that, similar to shade avoidance syndrome, hypocotyl elongation of both Col-0 and *er-3* is enhanced by high temperature even in the white light condition, and hypocotyl length of *er-3* is rescued similar to that of Col-0 by the same high temperature treatment, indicating that endogenous auxin level is essential for ER-modulated hypocotyl elongation. To further investigate that whether auxin transport is also essential for promoting the hypocotyl elongation of *er-3* by endogenous IAA increase, we use a polar auxin transport inhibitor 1-*N*-naphthylphthalamic acid (NPA) treatment at 30°C. As shown in **Supplementary Figure S3**, NPA could slightly inhibit the hypocotyl length of both Col-0 and *er-3* that increased by high temperature in the white light, while the hypocotyl length shows no significance between Col-0 and *er-3* by 5 μM of NPA treatment. These results suggest that ER-mediated hypocotyl elongation is dependent on endogenous auxin levels but not remarkably depends on auxin transport.

Exogenous GA3 Increased the Hypocotyl Length of *er* in the Shade

Gibberellins are another important group of phytohormones required to regulate the hypocotyl elongation in shade avoidance. To understand whether ER modulated hypocotyl elongation is deficient in GA biosynthesis, the effects of various concentrations of GA3 on the hypocotyl elongation of *er-3* and Col-0 were investigated (**Figure 4**). The results showed that lower concentrations of GA3 can promote the hypocotyl elongation of both Col-0 and *er-3*, and the promotion of the hypocotyl length in *er-3* is less than that in Col-0 by concentrations of 0.5 and 1 μM of GA3 (**Figures 4A,B**). However, 2 μM of GA3 can stimulate the hypocotyl elongation of *er-3* similar to that of Col-0 (**Figures 4A,B**), indicating that the ER regulated hypocotyl elongation is partially dependent of GAs. Furthermore, the hypocotyl elongation of both Col-0 and *er-3* are impaired to the similar length by the GA biosynthesis inhibitor PAC

(**Figures 4A,B**), indicating that GAs are important, but not only specific, for ER-mediated shade avoidance. These results suggest that GA level is an important regulator for hypocotyl growth for both the wild type and *er-3* mutant in the shade.

Auxin- and GA-Related Genes Are Differentially Regulated by ER in the Shade

To further elucidate the molecular mechanisms of ER modulated hypocotyl growth, genes related to auxin and GA biosynthesis and signaling pathways were examinated. Auxin biosynthesis gene *YUC9* and auxin-responsive genes, *IAA29* and *SAUR68*, whose expression is also rapidly upregulated by shade (Tao et al., 2008; Galstyan et al., 2011), are upregulated in both Col-0 and *er-3* under shade condition, and that the expression level is higher in Col-0 than that in *er-3*, suggesting that *ER* mutation impairs the expression level of auxin biosynthesis gene *YUC9* and auxin response might be impaired in *er-3* in the shade. Previous studies revealed that *VAS2*, encoding an IAA-amido synthetase Gretchen Hagen 3 (GH3).17, is expressed predominantly in the hypocotyl and plays important role in conversion of free IAA to IAA-Glu (IAA-glutamate) independent of IPA-mediated IAA biosynthesis (Zheng et al., 2016). To test whether ER regulated hypocotyl elongation in the shade is dependent on *VAS2*, we checked the expression level of *VAS2* in Col-0 and *er-3*. The results showed that relative expression of *VAS2* is decreased in Col-0 by shading compared to that in the white light condition. While *VAS2* is significantly upregulated in shade-treated *er-3* compared to that in *er-3* grown in the white light, and is much higher in expression than that of Col-0 in the shade condition. These results indicate that *VAS2* might also contribute to ER-regulated hypocotyl elongation in the shade.

The GA biosynthetic genes *GA20OX1*, *GA3OX1*, and *GA1* were induced in the shade treated both Col-0 and *er-3*, respectively. While expression of *GA3OX1* is less in *er-3* than that in Col-0, indicating that GA biosynthesis might be diminished in the conversion of GA9/GA20 to GA4/GA1. Expression of *GA1* is induced in both Col-0 and *er-3* by shade, whereas the expression level is lower in *er-3* than that in Col-0 (**Figure 5**). However, the expression of the GA catabolic gene, *GA2OX1* is sharply decreased in both shade treated Col-0 and *er-3* than that in white light-treated plants. *GA2OX1* exhibit a slightly less expression in shade treated *er-3* than that in shade-treated Col-0, suggesting that conversion of copalyl diphosphate (CPP) from geranylgeranyl diphosphate (GGPP) in GA biosynthesis might be impaired in *er-3*. However, significant changes in expression of GA biosynthesis and catabolic genes were not more remarkable than that of genes in auxin homeostasis and signaling pathways, implying that auxin might contribute more to ER-regulated hypocotyl elongation than GA in the shade.

ER Regulated Hypocotyl Elongation in Response to Shade Is Dependent of PHYB

Pants use red and far-red light-absorbing phytochromes A and B to sense the changes of R:FR ratio, of which phytochrome B (PHYB) play dominant role in shade avoidance inhibition. To determine whether ER-controlled hypocotyl elongation is via PHYB, we crossed *er-3* with a T-DNA insertional mutant *phyB* to generate an *er-3 phyB* double mutant (**Figure 6A**). In the white light condition, Col-0 and *er-3* single mutant show a hypocotyl inhibition phenotype, and *phyB* single mutant shows a hypocotyl elongation phenotype compared with that of Col-0 and *er-3* single mutant. However, *er-3 phyB* double mutant displays a hypocotyl elongation phenotype mimicking *phyB* single mutant but *ER* mutation significantly reduced hypocotyl elongation of *phyB* (**Figures 6A,B**). These results indicate that PHYB inhibited hypocotyl elongation in the white light is ER dependent. In the shade condition, *er-3* single mutant shows a shade avoidance phenotype in the hypocotyl, but elongation of the hypocotyl of *er-3* was significantly insensitive to shade compared with Col-0. Hypocotyls of both *phyB* and *er phyB* mutants also elongated in the shade condition. However, *er-3 phyB* is less sensitive to shade compared to the *phyB* single mutant, but *er-3 phyB* double mutant shows more sensitive in hypocotyl elongation compared to that of *er* single mutant, indicating that ER promoted hypocotyl elongation depends on PHYB (**Figures 6A,B**).

DISCUSSION

Hypocotyl growth is stimulated by various factors from internal signals and surrounding environment and controlled by complicated signaling networks. Plant receptor-like kinases play critical roles in perception of environmental signals. However, researches on RLK-mediated shade avoidance are seldom reported. Previous studies demonstrated that the leucine-rich repeat receptor-like kinase ER not only regulates Arabidopsis growth and development, but also plays a role in response to environmental stimuli (Torii et al., 1996; van Zanten et al., 2009; Shpak, 2013). Our study demonstrated that a T-DNA insertional mutation of Arabidopsis *ER* in Clo-0 background inhibits hypocotyl elongation in shade avoidance. Previous studies showed that Arabidopsis ER regulates petiole elongation and leaf hyponasty response in shade avoidance in a temperature-dependent manner in the Arabidopsis Landsberg ecotype (Patel et al., 2013). Another study from an independent group showed that ER contributes to hypocotyl, petiole and lamina elongation, hyponastic growth and flowering time in response to end-of-day far-red (R/FR) light in a genetic background-dependent manner (Kasulin et al., 2013). However, mechanisms of ER controlled shade avoidance are unknown yet.

Our physiological evidence revealed that ER regulates hypocotyl elongation in shade avoidance probably via auxin homeostasis and signaling pathways, and GA homeostasis pathways. Firstly, expression pattern analyses showed the expression of *ER*, but not its homologs *ERL1* and *ERL2*, which is specifically induced by shade in the Arabidopsis hypocotyl, suggesting that ER might play roles in hypocotyls in shade avoidance distinct from ERL1 and ERL2. Moreover, a cis-acting regulatory element prediction of the ER promoter region by PlantCARE showed that 14 light responsive elements are found

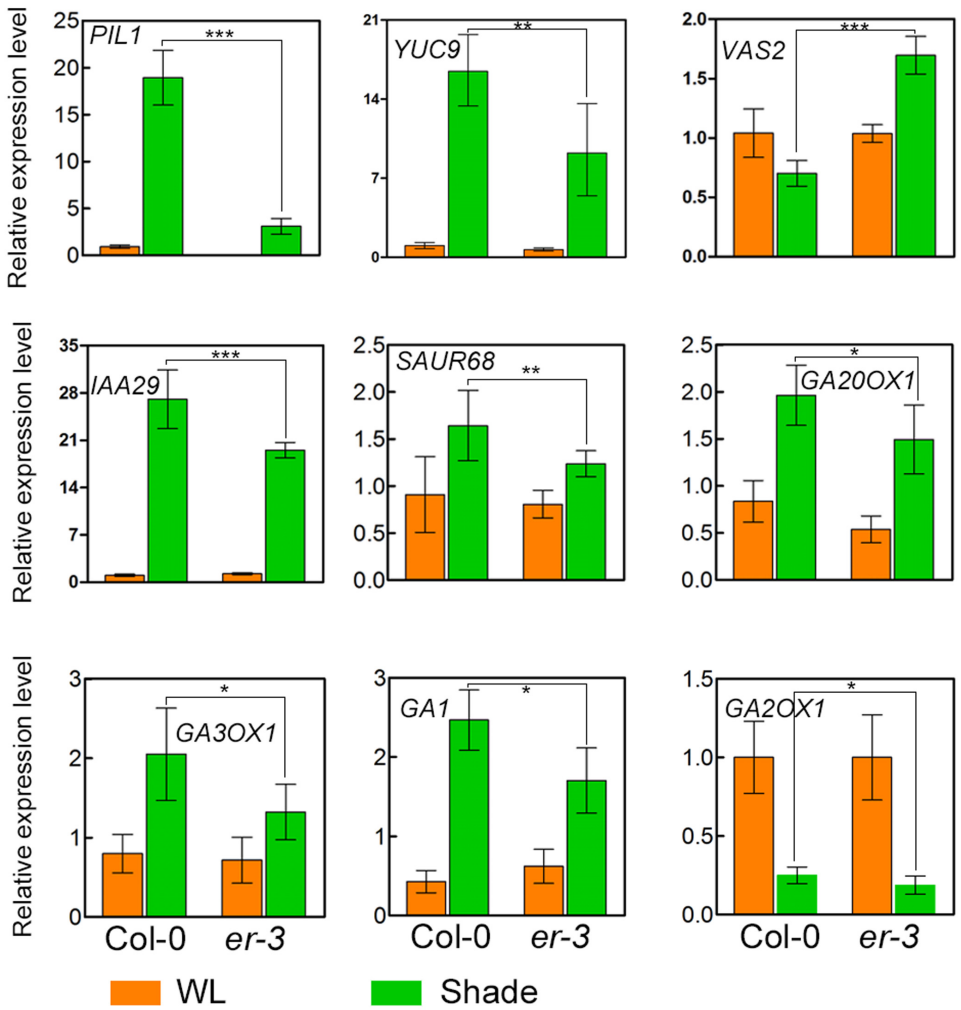

FIGURE 5 | Relative expression of genes in Col-0 and *er-3* under white light and shade conditions. Expression of the shade-inducible gene *PIL1*, auxin biosynthesis gene *YUC9*, auxin homeostasis gene *VAS2*, auxin signaling gene *IAA29* and *SAUR68*, GA biosynthesis gene *GA20OX1*, *GA3OX1* and *GA1* and GA catabolism gene *GA2OX1* were examined by using real time PCR analysis. Similar results from two biological repeats were obtained and at least three technical repeats in each biological assay were performed for the gene expression analysis and a presentative one is shown. Student's *t*-test indicated the differences are statistically significant (*$P < 0.05$; **$P < 0.01$; ***$P < 0.001$).

in the promoter of *ER* (**Supplementary Figure S4**), providing a clue that ER might involve in light responsiveness. Secondly, exogenous IAA feeding promoted the hypocotyl elongation of both Col-0 and *er-3* in the shade, while exogenous IAA only partially promoted the hypocotyl elongation of *er-3* comparing to that of the wild type, suggesting that ER-mediated hypocotyl elongation might be partially dependent of auxin biosynthesis. Nevertheless, *er-3* was relatively insensitive to IAA treatment than the wild type in the same concentration of IAA in the shade (**Figure 3**), implying that the auxin signaling pathways might be also impaired in the *er-3* mutant compared to the wild type in the shade. Previous studies showed that indole-3-pyruvic acid (IPyA) pathway is a major IAA biosynthesis pathway from tryptophan in Arabidopsis, in which the tryptophan aminotransferase SAV3/TAA1 and YUC enzymes play principal roles (Zhao et al., 2001; Tao et al., 2008; Dai et al., 2013). By using a chemical biology approach, Nishimura et al. discovered a potent IAA biosynthesis inhibitor, 5-(4-chlorophenyl)-4H-1,2,4-triazole-3-thiol (yucasin), which can effectively inhibit the activities of YUC thus impaired IAA production *in planta* (Nishimura et al., 2014). Another study showed that kyn is a tryptophan analog which can effectively inhibit Arabidopsis SAV3/TAA1/TARs identified from a chemical library screen (He et al., 2011). Our results showed that both yucasin and kyn can effectively inhibit the hypocotyl elongation of Col-0 and *er-3*, suggesting that both yucasin and kyn are potent inhibitors for Arabidopsis in the shade. Thirdly, it is known that high temperature can increase the endogenous auxin levels to promote the hypocotyl elongation of Arabidopsis and the expression of auxin biosynthesis gene *YUC9* is also induced by shade (Gray et al., 1998; Müller-Moulé et al., 2016), our results revealed that high temperature can enhance the hypocotyl

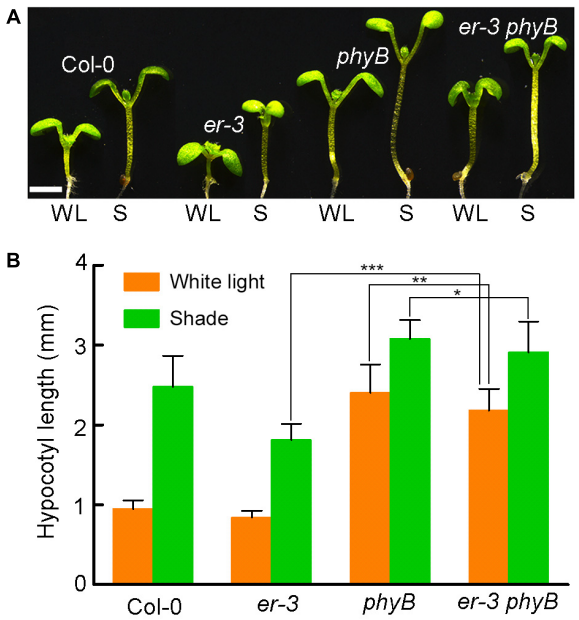

FIGURE 6 | ER promoted hypocotyl elongation is dependent of PHYB in the shade. **(A)** Phenotypes of Col-0, single and double mutants of *er-3* and *phyB* grown in white light and shade conditions. Scale bar represents 1 mm. **(B)** Statistical data of hypocotyl length of Col-0, *er-3* and *phyB* mutants in white light and shade conditions. Student's *t*-test indicated the differences are statistically significant (*$P < 0.05$; **$P < 0.01$; ***$P < 0.001$). At least 10 seedlings were measured for each genotype. Error bars represent SE.

elongation of *er-3* similar to that of Col-0 in the white light condition (**Supplementary Figure S3**) and auxin biosynthesis gene *YUC9* is less induced by shade in *er-3* than that in Col-0 (**Figure 5**), indicating that endogenous auxin homeostasis makes an important contribution to ER-mediated hypocotyl elongation in the shade. This conclusion also supported by another recent study which revealed that auxin biosynthesis is essential for ER regulated cell elongation in the hypocotyl under white light (Qu et al., 2017). It is reported that VAS2 controls the endogenous free IAA levels by conversion from IAA-Glu in the hypocotyl epidermis to promote the hypocotyl elongation (Zheng et al., 2016). Our qPCR results showed that relative expression of *VAS2* is down-regulated in Col-0 but upregulated in *er-3* by shading (**Figure 5**), suggesting that auxin metabolism might also contribute to ER-mediate shade avoidance in hypocotyl elongation. Auxin transport also plays roles in plant hypocotyl elongation in the white light condition (Jensen et al., 1998; Wu et al., 2016), our results indicated that auxin transport might be not essential for ER-regulated hypocotyl elongation, in that NPA treatment cannot cause the significant reduce in hypocotyl elongation of *er-3* compared to that of Col-0 in white light with high temperature conditions. These results suggested that auxin transport seems to be less important than auxin homeostasis in ER-mediated hypocotyl elongation in shade avoidance.

To date, the mechanisms of actions for auxin transport inhibitors have remained poorly understood (Teale and Palme, 2017). Although our physiological assays suggested that auxin transport inhibitors did not directly significantly affect the hypocotyl growth of *er-3* than that of Col-0, previous studies reported that long-term application of high concentrations of auxin to the roots leads to changes of auxin transport probably through auxin-dependent transcriptional control (Sieberer et al., 2000; Vieten et al., 2005; Vanneste and Friml, 2009). Moreover, high temperature is able to impact on membrane fluidity vesicular trafficking, and other hormonal responses (Kim and Portis, 2005; Asensi-Fabado et al., 2013; Hanzawa et al., 2013). For this reason, we speculate that it is also probably that high temperature induced auxin maxima in the roots or other processes and thus resulted in changes of auxin transport. In addition, several evidences has revealed that NPA probably binds either directly to the auxin efflux carrier including PIN and ABC-transporters (Rubery, 1979; Sussman and Goldsmith, 1981) or to auxin efflux-related regulatory proteins and cytoskeleton (Cox and Muday, 1994; Bailly et al., 2008) to inhibit auxin transport, but it has also been proposed that NPA may have other effects independent of auxin transport (Hössel et al., 2005). Altogether, we could not rule out that auxin balance in the hypocotyl of *er-3* might be neither affected by a loss or accentuation of an auxin maxima in the root, leading to alteration of auxin transport, nor affected by other biological processes, which might finally result in changes of ER-mediated hypocotyl elongation. In the future, more molecular and physiological evidences are required to uncover whether and how auxin transportation involving auxin transporters contributes in ER-regulated hypocotyl growth in shade avoidance.

Our exogenous GA3 feeding increased the hypocotyl length of *er-3* to the length of the wild type in the shade, suggesting that GA3 biosynthesis might be diminished in *er-3* under shade condition. Relative expression of genes in GA biosynthesis and catabolism pathways in *er-3* are less than that in the wild type, suggesting that ER modulates hypocotyl elongation might depend on GA homeostasis. Nevertheless, more genetic and biochemical evidences need to be done to elucidate the detailed mechanisms underlying the crosstalk between auxin and GA in ER regulated shade avoidance in the future. PHYB is the main photoreceptor in perception of changes of light quality of red to far-red light wave length. Previous studies show that ER modulates low light intensity induced petiole elongation independent of PHYB (van Zanten et al., 2010). Our genetic evidence shows that loss-of-function of *PHYB* can promote the hypocotyl elongation of *er-3*, whereas the hypocotyl length of the double mutant of *er-3 phyB* is shorter than that of *phyB* single mutant, suggesting that ER regulated hypocotyl elongation depends on PHYB, and *phyB*-mediated promotion of hypocotyl elongation is partially dependent of ER. However, the detailed molecular mechanisms of how does PHYB function in ER-mediated shade avoidance pathways needs further investigation. Interestingly, protein–protein interaction analyses by Search Tool for the Retrieval of Interacting Genes/Proteins (STRING[2]) show that ER and PHYB are in the same protein complex (**Supplementary Figure S5**), thus we speculate that it is probably ER and PHYB function together in hypocotyl

[2]http://string-db.org

elongation in a same protein complex. Furthermore, extensive evidence showed that RLKs play roles in plant growth and development, and defense with their co-receptors as receptor complex in previous studies. For instance, the BR receptor BRASSINOSTEROID INSENSITIVE 1 (BRI1) interacts with its co-receptors SOMATIC EMBRYOGENESIS RECEPTOR KINASEs (SERKs) to perceive and transduce BR signals to regulate plant growth and development (Li et al., 2002; Nam and Li, 2002; Gou et al., 2012). EF-TU RECEPTOR (EFR) and FLAGELLIN-SENSING 2 (FLS2) interacts with SERKs to sense the flagellin22 in plant defense signaling pathways (Zipfel et al., 2006; Chinchilla et al., 2007; Roux et al., 2011; Stegmann et al., 2017). ER family receptors interact with a receptor-like protein TOO MANY MOUTH (TMM) to form a homo- and heterodimer receptor complex to regulate stomatal development (Shpak et al., 2005). Receptor-like kinases FERONIA and THESEUS1 were found to control the shoot elongation of *Geranium pyrenaicum* identified by transcriptome analyses (Gommers et al., 2017). We therefore hypothesize that ER may function with unknown co-receptors to regulate hypocotyl elongation in shade avoidance by regulating the auxin homeostasis and signaling and GA homeostasis related networks. Further studies will focus on disclosing the detailed molecular mechanisms, including the crosstalk of auxin and GA in ER regulated hypocotyl elongation in shade avoidance.

AUTHOR CONTRIBUTIONS

JD and WY designed the experiments. JD, HJ, XS, YaL, MS, YiL, ZF, QC, LF, JS, KS, JL, WL, FY, TY, XW, SY, LY, and CL performed the experiments. JD, HJ, XS, and YaL analyzed the data. JD, HJ, XS, and YaL wrote the manuscript.

FUNDING

This work was supported by the National Natural Science Foundation of China grants 31401308, 31671445, and 31371555.

ACKNOWLEDGMENTS

The authors thank Dr. Tomokazu Koshiba at Tokyo Metropolitan University for generously providing yucasin and Mr. George Bawa and Muhmmad Ahsan Asghar for reading and commenting the manuscript. They are also grateful to the Arabidopsis Biological Resource Center (ABRC) for providing some of the T-DNA insertional mutant seeds.

SUPPLEMENTARY MATERIAL

The Supplementary Material for this article can be found online at: https://www.frontiersin.org/articles/10.3389/fpls.2018.00124/full#supplementary-material

FIGURE S1 | Time course of gene expression in Col-0 induced by shade. *ER* and the shade inducible genes *PIL1* and *XTR7* were upregulated in the shade. *ACT2* was amplified for 23 cycles as an internal control.

FIGURE S2 | Exogenous feeding of kyn and yucasin can inhibit shade stimulated hypocotyl elongation. **(A)** Phenotypes of Col-0 and *er-3* seedlings vertically with a slight angle or horizontally grown with treatment of different concentrations of kyn and yucasin in the shade. Scale bar represents 1 cm. **(B)** Statistical data of hypocotyl length of vertically grown Col-0 and *er-3* with a slight angle treated by kyn and yucasin under shade condition. **(C)** Statistical data of hypocotyl length of horizontally grown Col-0 and *er-3* treated by kyn and yucasin under shade condition. Student's *t*-test indicated the differences are statistically significant (***$P < 0.001$). At least 15 seedlings were measured for each genotype. Error bars represent SE.

FIGURE S3 | High temperature promoted hypocotyl elongation of both Col-0 and *er-3*. **(A)** Phenotype of Col-0 and *er-3* treated with 22°C and 30°C in the while light or shade conditions. 5 μM of NPA feeding were used at 30°C in the shade. **(B)** Statistical data for Col-0 *er-3* with/without NPA treatment grown at 22°C and 30°C in the while light or shade conditions.

FIGURE S4 | Motif prediction of the promoter of *ER* by PlantCARE (http://bioinformatics.psb.ugent.be/webtools/plantcare/html/). The yellow boxes show the motifs are light responsive elements.

FIGURE S5 | Prediction of interacting proteins of PHYB and ER in Arabidopsis by STRING (http://string-db.org/).

TABLE S1 | Primers used in this study.

REFERENCES

Asensi-Fabado, M. A., Oliván, A., and Munné-Bosch, S. (2013). A comparative study of the hormonal response to high temperatures and stress reiteration in three Labiatae species. *Environ. Exp. Bot* 94(Suppl. C), 57–65. doi: 10.1016/j.envexpbot.2012.05.001

Bailly, A., Sovero, V., Vincenzetti, V., Santelia, D., Bartnik, D., Koenig, B., et al. (2008). Modulation of P-glycoproteins by auxin transport inhibitors is mediated by interaction with immunophilins. *J. Biol. Chem.* 283, 21817–21826. doi: 10.1074/jbc.M709655200

Ballaré, C. L. (1999). Keeping up with the neighbours: phytochrome sensing and other signalling mechanisms. *Trends Plant Sci.* 4, 97–102. doi: 10.1016/S1360-1385(99)01383-7

Becraft, P. W. (2002). Receptor kinase signaling in plant development. *Annu. Rev. Cell Dev. Biol.* 18, 163–192. doi: 10.1146/annurev.cellbio.18.012502.083431

Blair, M., Cortes, A., and This, D. (2016). Identification of an *ERECTA* gene and its drought adaptation associations with wild and cultivated common bean. *Plant Sci.* 242, 250–259. doi: 10.1016/j.plantsci.2015.08.004

Carriedo, L. G., Maloof, J. N., and Brady, S. M. (2016). Molecular control of crop shade avoidance. *Curr. Opin. Plant Biol.* 30, 151–158. doi: 10.1016/j.pbi.2016.03.005

Casal, J. J. (2013). Photoreceptor signaling networks in plant responses to shade. *Annu. Rev. Plant Biol.* 64, 403–427. doi: 10.1146/annurev-arplant-050312-120221

Chinchilla, D., Zipfel, C., Robatzek, S., Kemmerling, B., Nurnberger, T., and Jones, J. D. G. (2007). A flagellin-induced complex of the receptor FLS2 and BAK1 initiates plant defence. *Nature* 448, 497–500. doi: 10.1038/nature05999

Cox, D., and Muday, G. (1994). NPA binding activity is peripheral to the plasma membrane and is associated with the cytoskeleton. *Plant Cell* 6, 1941–1953. doi: 10.1105/tpc.6.12.1941

Dai, X., Mashiguchi, K., Chen, Q., Kasahara, H., Kamiya, Y., Ojha, S., et al. (2013). The biochemical mechanism of auxin biosynthesis by an *Arabidopsis* YUCCA Flavin-containing Monooxygenase. *J. Biol. Chem.* 288, 1448–1457. doi: 10.1074/jbc.M112.424077

Du, J., Yin, H., Zhang, S., Wei, Z., Zhao, B., Zhang, J., et al. (2012). Somatic embryogenesis receptor kinases control root development mainly via

brassinosteroid-independent actions in *Arabidopsis thaliana*. *J. Integr. Plant Biol.* 54, 388–399. doi: 10.1111/j.1744-7909.2012.01124.x

Durbak, A. R., and Tax, F. E. (2011). CLAVATA signaling pathway receptors of *Arabidopsis* regulate cell proliferation in fruit organ formation as well as in meristems. *Genetics* 189, 177–194. doi: 10.1534/genetics.111.130930

Galstyan, A., Cifuentes-Esquivel, N., Bou-Torrent, J., and Martinez-Garcia, J. F. (2011). The shade avoidance syndrome in Arabidopsis: a fundamental role for atypical basic helix-loop-helix proteins as transcriptional cofactors. *Plant J.* 66, 258–267. doi: 10.1111/j.1365-313X.2011.04485.x

Gommers, C. M. M., Keuskamp, D. H., Buti, S., van Veen, H., Koevoets, I. T., Reinen, E., et al. (2017). Molecular profiles of contrasting shade response strategies in wild plants: differential control of immunity and shoot elongation. *Plant Cell* 29, 331–344. doi: 10.1105/tpc.16.00790

Gou, X., Yin, H., He, K., Du, J., Yi, J., Xu, S., et al. (2012). Genetic evidence for an indispensable role of somatic embryogenesis receptor kinases in brassinosteroid signaling. *PLOS Genet.* 8:e1002452. doi: 10.1371/journal.pgen.1002452

Gray, W. M., Östin, A., Sandberg, G., Romano, C. P., and Estelle, M. (1998). High temperature promotes auxin-mediated hypocotyl elongation in *Arabidopsis*. *Proc. Natl. Acad. Sci. U.S.A.* 95, 7197–7202. doi: 10.1073/pnas.95.12.7197

Guo, Z., Fujioka, S., Blancaflor, E. B., Miao, S., Gou, X., and Li, J. (2010). TCP1 modulates brassinosteroid biosynthesis by regulating the expression of the key biosynthetic gene *DWARF4* in *Arabidopsis thaliana*. *Plant Cell* 22, 1161–1173. doi: 10.1105/tpc.109.069203

Hanzawa, T., Shibasaki, K., Numata, T., Kawamura, Y., Gaude, T., and Rahman, A. (2013). Cellular auxin homeostasis under high temperature is regulated through a sorting NEXIN1-dependent endosomal trafficking pathway. *Plant Cell* 25, 3424–3433. doi: 10.1105/tpc.113.115881

He, K., Gou, X., Yuan, T., Lin, H., Asami, T., Yoshida, S., et al. (2007). BAK1 and BKK1 regulate brassinosteroid-dependent growth and brassinosteroid-independent cell-death pathways. *Curr. Biol.* 17, 1109–1115. doi: 10.1016/j.cub.2007.05.036

He, W., Brumos, J., Li, H., Ji, Y., Ke, M., Gong, X., et al. (2011). A small-molecule screen identifies L-kynurenine as a competitive inhibitor of TAA1/TAR activity in ethylene-directed auxin biosynthesis and root growth in *Arabidopsis*. *Plant Cell* 23, 3944–3960. doi: 10.1105/tpc.111.089029

Hössel, D., Schmeiser, C., and Hertel, R. (2005). Specificity patterns indicate that auxin exporters and receptors are the same proteins. *Plant Biol.* 7, 41–48. doi: 10.1055/s-2004-830475

Jensen, P. J., Hangarter, R. P., and Estelle, M. (1998). Auxin Transport is required for hypocotyl elongation in light-grown but not dark-grown Arabidopsis. *Plant Physiol.* 116, 455–462. doi: 10.1104/pp.116.2.455

Kasulin, L., Agrofoglio, Y., and Botto, J. F. (2013). The receptor-like kinase ERECTA contributes to the shade-avoidance syndrome in a background-dependent manner. *Ann. Bot.* 111, 811–819. doi: 10.1093/aob/mct038

Keuskamp, D. H., Pollmann, S., Voesenek, L. A. C. J., Peeters, A. J. M., and Pierik, R. (2010). Auxin transport through PIN-FORMED 3 (PIN3) controls shade avoidance and fitness during competition. *Proc. Natl. Acad. Sci. U.S.A.* 107, 22740–22744. doi: 10.1073/pnas.1013457108

Kim, K., and Portis, J. A. R. (2005). Temperature dependence of photosynthesis in Arabidopsis plants with modifications in rubisco activase and membrane fluidity. *Plant Cell Physiol.* 46, 522–530. doi: 10.1093/pcp/pci052

Korasick, D. A., Enders, T. A., and Strader, L. C. (2013). Auxin biosynthesis and storage forms. *J. Exp. Bot.* 64, 2541–2555. doi: 10.1093/jxb/ert080

Li, J. (2010). Multi-tasking of somatic embryogenesis receptor-like protein kinases. *Curr. Opin. Plant Biol.* 13, 509–514. doi: 10.1016/j.pbi.2010.09.004

Li, J., and Chory, J. (1997). A putative leucine-rich repeat receptor kinase involved in brassinosteroid signal transduction. *Cell* 90, 929–938. doi: 10.1016/S0092-8674(00)80357-8

Li, J., Wen, J., Lease, K. A., Doke, J. T., Tax, F. E., and Walker, J. C. (2002). BAK1, an Arabidopsis LRR receptor-like protein kinase, interacts with BRI1 and modulates brassinosteroid signaling. *Cell* 110, 213–222. doi: 10.1016/S0092-8674(02)00812-7

Lorrain, S., Allen, T., Duek, P. D., Whitelam, G. C., and Fankhauser, C. (2008). Phytochrome-mediated inhibition of shade avoidance involves degradation of growth-promoting BHLH transcription factors. *Plant J.* 53, 312–323. doi: 10.1111/j.1365-313X.2007.03341.x

Ludwig-Müller, J. (2011). Auxin conjugates: their role for plant development and in the evolution of land plants. *J. Exp. Bot.* 62, 1757–1773. doi: 10.1093/jxb/erq412

Masle, J., Gilmore, S. R., and Farquhar, G. D. (2005). The *ERECTA* gene regulates plant transpiration efficiency in *Arabidopsis*. *Nature* 436, 866–870. doi: 10.1038/nature03835

Meng, L., Buchanan, B. B., Feldman, L. J., and Luan, S. (2012). CLE-like (CLEL) peptides control the pattern of root growth and lateral root development in Arabidopsis. *Proc. Natl. Acad. Sci. U.S.A.* 109, 1760–1765. doi: 10.1073/pnas.1119864109

Müller-Moulé, P., Nozue, K., Pytlak, M. L., Palmer, C. M., Covington, M. F., Wallace, A. D., et al. (2016). *YUCCA* auxin biosynthetic genes are required for Arabidopsis shade avoidance. *PeerJ* 4:e2574. doi: 10.7717/peerj.2574

Nam, K. H., and Li, J. (2002). BRI1/BAK1, a receptor kinase pair mediating brassinosteroid signaling. *Cell* 110, 203–212. doi: 10.1016/S0092-8674(02)00814-0

Nishimura, T., Hayashi, K. I., Suzuki, H., Gyohda, A., Takaoka, C., Sakaguchi, Y., et al. (2014). Yucasin is a potent inhibitor of YUCCA, a key enzyme in auxin biosynthesis. *Plant J.* 77, 352–366. doi: 10.1111/tpj.12399

Normanly, J., Cohen, J. D., and Fink, G. R. (1993). *Arabidopsis thaliana* auxotrophs reveal a tryptophan-independent biosynthetic pathway for indole-3-acetic acid. *Proc. Natl. Acad. Sci. U.S.A.* 90, 10355–10359. doi: 10.1073/pnas.90.21.10355

Oh, M.-H., Wang, X., Kota, U., Goshe, M. B., Clouse, S. D., and Huber, S. C. (2009). Tyrosine phosphorylation of the BRI1 receptor kinase emerges as a component of brassinosteroid signaling in *Arabidopsis*. *Proc. Natl. Acad. Sci. U.S.A.* 106, 658–663. doi: 10.1073/pnas.0810249106

Oh, M.-H., Wang, X., Wu, X., Zhao, Y., Clouse, S. D., and Huber, S. C. (2010). Autophosphorylation of Tyr-610 in the receptor kinase BAK1 plays a role in brassinosteroid signaling and basal defense gene expression. *Proc. Natl. Acad. Sci. U.S.A.* 107, 17827–17832. doi: 10.1073/pnas.0915064107

Patel, D., Basu, M., Hayes, S., Majláth, I., Hetherington, F. M., Tschaplinski, T. J., et al. (2013). Temperature-dependent shade avoidance involves the receptor-like kinase ERECTA. *Plant J.* 73, 980–992. doi: 10.1111/tpj.12088

Pierik, R., Djakovic-Petrovic, T., Keuskamp, D. H., de Wit, M., and Voesenek, L. A. C. J. (2009). Auxin and ethylene regulate elongation responses to neighbor proximity signals independent of gibberellin and DELLA proteins in Arabidopsis. *Plant Physiol.* 149, 1701–1712. doi: 10.1104/pp.108.133496

Procko, C., Crenshaw, C. M., Ljung, K., Noel, J. P., and Chory, J. (2014). Cotyledon-generated auxin is required for shade-induced hypocotyl growth in *Brassica rapa*. *Plant Physiol.* 165, 1285–1301. doi: 10.1104/pp.114.241844

Qu, X., Zhao, Z., and Tian, Z. (2017). ERECTA regulates cell elongation by activating auxin biosynthesis in *Arabidopsis thaliana*. *Front. Plant Sci.* 8:1688. doi: 10.3389/fpls.2017.01688

Rédei, G. P., Koncz, C., Chua, N. H., and Schell, J. (1992). *A Heuristic Glance at the Past of Arabidopsis Genetics*. Singapore: World Scientific. doi: 10.1142/9789814439701_0001

Roux, M., Schwessinger, B., Albrecht, C., Chinchilla, D., Jones, A., Holton, N., et al. (2011). The *Arabidopsis* leucine-rich repeat receptor–like kinases BAK1/SERK3 and BKK1/SERK4 are required for innate immunity to hemibiotrophic and biotrophic pathogens. *Plant Cell* 23, 2440–2455. doi: 10.1105/tpc.111.084301

Ruberti, I., Sessa, G., Ciolfi, A., Possenti, M., Carabelli, M., and Morelli, G. (2012). Plant adaptation to dynamically changing environment: the shade avoidance response. *Biotechnol. Adv.* 30, 1047–1058. doi: 10.1016/j.biotechadv.2011.08.014

Rubery, P. (1979). The effects of 2,4-dinitrophenol and chemical modifying reagents on auxin transport by suspension-cultured crown gall cells. *Planta* 144, 173–178. doi: 10.1007/BF00387267

Shen, H., Zhong, X., Zhao, F., Wang, Y., Yan, B., Li, Q., et al. (2015). Overexpression of receptor-like kinase ERECTA improves thermotolerance in rice and tomato. *Nat. Biotechnol.* 33, 996–1003. doi: 10.1038/nbt.3321

Shiu, S. H., and Bleecker, A. B. (2001). Plant receptor-like kinase gene family: diversity, function, and signaling. *Sci. STKE* 2001:re22. doi: 10.1126/stke.2001.113.re22

Shiu, S. H., Karlowski, W. M., Pan, R., Tzeng, Y. H., Mayer, K. F., and Li, W. H. (2004). Comparative analysis of the receptor-like kinase family in Arabidopsis and rice. *Plant Cell* 16, 1220–1234. doi: 10.1105/tpc.020834

Shiu, S. H., and Li, W. H. (2004). Origins, lineage-specific expansions, and multiple losses of tyrosine kinases in eukaryotes. *Mol. Biol. Evol.* 21, 828–840. doi: 10.1093/molbev/msh077

Shpak, E. D. (2013). Diverse roles of ERECTA family genes in plant development. *J. Integr. Plant Biol.* 55, 1238–1250. doi: 10.1111/jipb.12108

Shpak, E. D., Berthiaume, C. T., Hill, E. J., and Torii, K. U. (2004). Synergistic interaction of three ERECTA-family receptor-like kinases controls *Arabidopsis* organ growth and flower development by promoting cell proliferation. *Development* 131, 1491–1501. doi: 10.1242/dev.01028

Shpak, E. D., McAbee, J. M., Pillitteri, L. J., and Torii, K. U. (2005). Stomatal patterning and differentiation by synergistic interactions of receptor kinases. *Science* 309, 290–293. doi: 10.1126/science.1109710

Shpak, E. D., Lakeman, M. B., and Torii, K. U. (2003). Dominant-negative receptor uncovers redundancy in the arabidopsis ERECTA leucine-rich repeat receptor-like kinase signaling pathway that regulates organ shape. *Plant Cell* 15, 1095–1110. doi: 10.1105/tpc.010413

Sieberer, T., Seifert, G., Hauser, M., Grisafi, P., Fink, G., and Luschnig, C. (2000). Post-transcriptional control of the *Arabidopsis* auxin efflux carrier EIR1 requires AXR1. *Curr. Biol.* 10, 1595–1598. doi: 10.1016/S0960-9822(00)00861-7

Stegmann, M., Monaghan, J., Smakowska-Luzan, E., Rovenich, H., Lehner, A., Holton, N., et al. (2017). The receptor kinase FER is a RALF-regulated scaffold controlling plant immune signaling. *Science* 355, 287–289. doi: 10.1126/science.aal2541

Sussman, M., and Goldsmith, M. (1981). The action of specific inhibitors of auxin transport on uptake of auxin and binding of N-1-naphthylphthalamic acid to a membrane site in maize coleoptiles. *Planta* 152, 13–18. doi: 10.1007/BF00384978

Tao, Y., Ferrer, J.-L., Ljung, K., Pojer, F., Hong, F., Long, J. A., et al. (2008). Rapid synthesis of auxin via a new tryptophan-dependent pathway is required for shade avoidance in plants. *Cell* 133, 164–176. doi: 10.1016/j.cell.2008.01.049

Teale, W., and Palme, K. (2017). Naphthylphthalamic acid and the mechanism of polar auxin transport. *J. Exp. Bot.* 69, 303–312. doi: 10.1093/jxb/erx323

Tivendale, N. D., Ross, J. J., and Cohen, J. D. (2014). The shifting paradigms of auxin biosynthesis. *Trends Plant Sci.* 19, 44–51. doi: 10.1016/j.tplants.2013.09.012

Torii, K. U., Mitsukawa, N., Oosumi, T., Matsuura, Y., Yokoyama, R., and Whittier, R. F. (1996). The Arabidopsis ERECTA gene encodes a putative receptor protein kinase with extracellular leucine-rich repeats. *Plant Cell* 8, 735–746. doi: 10.1105/tpc.8.4.735

Valladares, F., and Niinemets, Ü (2008). Shade tolerance, a key plant feature of complex nature and consequences. *Annu. Rev. Ecol. Evol. Syst.* 39, 237–257. doi: 10.1146/annurev.ecolsys.39.110707.173506

van Zanten, M., Snoek, L. B., Proveniers, M. C., and Peeters, A. J. (2009). The many functions of ERECTA. *Trends Plant Sci.* 14, 214–218. doi: 10.1016/j.tplants.2009.01.010

van Zanten, M., Snoek, L. B., van Eck-Stouten, E., Proveniers, M. C. G., Torii, K. U., Voesenek, L. A. C. J., et al. (2010). ERECTA controls low light intensity-induced differential petiole growth independent of Phytochrome B and Cryptochrome 2 action in *Arabidopsis thaliana*. *Plant Signal. Behav.* 5, 284–286. doi: 10.4161/psb.5.3.10706

Vanneste, S., and Friml, J. (2009). Auxin: a trigger for change in plant development. *Cell* 136, 1005–1016. doi: 10.1016/j.cell.2009.03.001

Vieten, A., Vanneste, S., Wisniewska, J., Benková, E., Benjamins, R., Beeckman, T., et al. (2005). Functional redundancy of PIN proteins is accompanied by auxin-dependent cross-regulation of PIN expression. *Development* 132, 4521–4531. doi: 10.1242/dev.02027

Villagarcia, H., Morin, A.-C., Shpak, E., and Khodakovskaya, M. V. (2012). Modification of tomato growth by expression of truncated ERECTA protein from *Arabidopsis thaliana*. *J. Exp. Bot.* 63, 6493–6504. doi: 10.1093/jxb/ers305

Walker, J. C., and Zhang, R. (1990). Relationship of a putative receptor protein kinase from maize to the S-locus glycoproteins of *Brassica*. *Nature* 345, 743–746. doi: 10.1038/345743a0

Wang, B., Chu, J., Yu, T., Xu, Q., Sun, X., Yuan, J., et al. (2015). Tryptophan-independent auxin biosynthesis contributes to early embryogenesis in *Arabidopsis*. *Proc. Natl. Acad. Sci. U.S.A.* 112, 4821–4826. doi: 10.1073/pnas.1503998112

Wit, M. D., Galvão, V. C., and Fankhauser, C. (2016). Light-mediated hormonal regulation of plant growth and development. *Annu. Rev. Plant Biol.* 67, 513–537. doi: 10.1146/annurev-arplant-043015-112252

Woodward, A. W., and Bartel, B. (2005). Auxin: regulation. *Action Interact. Ann. Bot.* 95, 707–735. doi: 10.1093/aob/mci083

Wright, A. D., Sampson, M. B., Neuffer, M. G., Michalczuk, L., Slovin, J. P., and Cohen, J. D. (1991). Indole-3-acetic acid biosynthesis in the mutant maize orange pericarp, a tryptophan auxotroph. *Science* 254, 998–1000. doi: 10.1126/science.254.5034.998

Wu, G., Carville, J. S., and Spalding, E. P. (2016). ABCB19-mediated polar auxin transport modulates Arabidopsis hypocotyl elongation and the endoreplication variant of the cell cycle. *Plant J.* 85, 209–218. doi: 10.1111/tpj.13095

Yang, C., and Li, L. (2017). Hormonal regulation in shade avoidance. *Front. Plant Sci.* 8:1527. doi: 10.3389/fpls.2017.01527

Zhao, Y. (2010). Auxin biosynthesis and its role in plant development. *Annu. Rev. Plant Biol.* 61, 49–64. doi: 10.1146/annurev-arplant-042809-112308

Zhao, Y. (2012). Auxin biosynthesis: a simple two-step pathway converts tryptophan to indole-3-acetic acid in plants. *Mol. Plant* 5, 334–338. doi: 10.1093/mp/ssr104

Zhao, Y. (2014). Auxin biosynthesis. *Am. Soc. Plant Biol.* 12:e0173. doi: 10.1199/tab.0173

Zhao, Y., Christensen, S. K., Fankhauser, C., Cashman, J. R., Cohen, J. D., Weigel, D., et al. (2001). A role for flavin monooxygenase-like enzymes in auxin biosynthesis. *Science* 291, 306–309. doi: 10.1126/science.291.5502.306

Zheng, Z., Guo, Y., Novák, O., Chen, W., Ljung, K., Noel, J. P., et al. (2016). Local auxin metabolism regulates environment-induced hypocotyl elongation. *Nat. Plants* 2:16025. doi: 10.1038/nplants.2016.25

Zipfel, C., Kunze, G., Chinchilla, D., Caniard, A., Jones, J. D., Boller, T., et al. (2006). Perception of the bacterial PAMP EF-Tu by the receptor EFR restricts agrobacterium-mediated transformation. *Cell* 125, 749–760. doi: 10.1016/j.cell.2006.03.037

Conflict of Interest Statement: The authors declare that the research was conducted in the absence of any commercial or financial relationships that could be construed as a potential conflict of interest.

frontiers in Plant Science

ORIGINAL RESEARCH
published: 27 November 2017
doi: 10.3389/fpls.2017.02005

Activation of the LRR Receptor-Like Kinase PSY1R Requires Transphosphorylation of Residues in the Activation Loop

Christian B. Oehlenschlæger[1], Lotte B. A. Gersby[1], Nagib Ahsan[2†], Jesper T. Pedersen[1†], Astrid Kristensen[1], Tsvetelina V. Solakova[1], Jay J. Thelen[2] and Anja T. Fuglsang[1]*

[1] Department of Plant and Environmental Sciences, Faculty of Science, University of Copenhagen, Copenhagen, Denmark, [2] Christopher S. Bond Life Sciences Center, Department of Biochemistry, University of Missouri, Columbia, MO, United States

PSY1R is a leucine-rich repeat (LRR) receptor-like kinase (RLK) previously shown to act as receptor for the plant peptide hormone PSY1 (peptide containing sulfated tyrosine 1) and to regulate cell expansion. PSY1R phosphorylates and thereby regulates the activity of plasma membrane-localized H^+-ATPases. While this mechanism has been studied in detail, little is known about how PSY1R itself is activated. Here we studied the activation mechanism of PSY1R. We show that full-length PSY1R interacts with members of the SERK co-receptor family *in planta*. We identified seven *in vitro* autophosphorylation sites on serine and threonine residues within the kinase domain of PSY1R using mass spectrometry. We furthermore show that PSY1R autophosphorylation occurs *in trans* and that the initial transphosphorylation takes place within the activation loop at residues Ser951, Thr959, and Thr963. While Thr959 and Thr963 are conserved among other related plant LRR RLKs, Ser951 is unique to PSY1R. Based on homology modeling we propose that phosphorylation of Ser951 stabilize the inactive conformation of PSY1R.

Keywords: receptor kinase, phosphorylation, mass spectrometry, PSY1 peptide, signaling peptides, LRR, activation loop

OPEN ACCESS

Edited by:
Yi Ma,
University of Connecticut,
United States

Reviewed by:
Jian Huang,
University of Wisconsin–Milwaukee,
United States
Yukihiro Ito,
Tohoku University, Japan

****Correspondence:***
Anja T. Fuglsang
atf@plen.ku.dk

†Present address:
Nagib Ahsan,
Division of Biology and Medicine, Brown University, Providence, RI, United States;
Center for Cancer Research Development, Proteomics Core Facility, Rhode Island Hospital, Providence, RI, United States
Jesper T. Pedersen,
Institute of Environmental Medicine, Karolinska Institutet, Stockholm, Sweden

Specialty section:
This article was submitted to Plant Traffic and Transport, a section of the journal Frontiers in Plant Science

Received: *01 September 2017*
Accepted: *10 November 2017*
Published: *27 November 2017*

Citation:
Oehlenschlæger CB, Gersby LBA, Ahsan N, Pedersen JT, Kristensen A, Solakova TV, Thelen JJ and Fuglsang AT (2017) Activation of the LRR Receptor-Like Kinase PSY1R Requires Transphosphorylation of Residues in the Activation Loop. Front. Plant Sci. 8:2005. doi: 10.3389/fpls.2017.02005

INTRODUCTION

As multicellular organisms, plants rely on a fine-tuned cell-to-cell communication system to coordinate growth responses. At the core of this system are members of the receptor-like kinase (RLK) superfamily. This massive family of plant proteins, which is implicated in both plant development (De Smet et al., 2009; Murphy et al., 2012) and plant innate immunity (Schwessinger and Ronald, 2012; Tang et al., 2017), maintains an appropriate balance between growth and defense. Plant RLKs belong to the RLK/Pelle class of protein kinases, which is composed of over 600 members in Arabidopsis (Gish and Clark, 2011), and are related to the mammalian Receptor Tyrosine Kinases (RTKs) (Shiu and Bleecker, 2001; Belkhadir et al., 2014). Most plant RLKs share the overall architecture of RTKs, with an extracellular ligand-binding domain, a single transmembrane-spanning domain, and a conserved intracellular kinase domain (KD).

Until recently, it was believed that most plant cell-to-cell communication was mediated by small lipophilic compounds, such as phytohormones and steroids, only. However, plant peptide hormones, which are expressed as precursor peptides (pre-pro-peptides) and undergo

post-translational modification followed by secretion via the secretory pathway, are emerging as important players in this process (Matsubayashi, 2011; Murphy et al., 2012). Plant peptide containing sulfated tyrosine 1 (PSY1; Amano et al., 2007) and phytosulfokine (PSK; Matsubayashi and Sakagami, 1996) are plant peptide hormones responsible for cell elongation activity in the elongation/differentiation zone of the root (Sauter et al., 2009; Matsubayashi et al., 2010) and hypocotyl (Stührwohldt et al., 2011; Fuglsang et al., 2014). The receptors for PSY1 and PSK, termed PSY1R and PSKR1 and PSKR2, respectively, form a small family of redundant RLKs (Matsubayashi et al., 2002; Amano et al., 2007) that are members of the leucine-rich repeat (LRR) RLK subclass of plant RLKs, which is encoded by 216 genes in Arabidopsis. The downstream signaling events of PSY1R and PSKR have not been fully characterized; however, PSKR contains a guanylate cyclase catalytic center in its KD, which enables signaling through the formation of the secondary messenger cyclic guanosine monophosphate (cGMP) (Kwezi et al., 2011). PSY1R was recently shown to regulate cell expansion by phosphorylating the plant plasma membrane H^+-ATPase (AHA2) and thereby promoting proton pumping (Fuglsang et al., 2014). Proton pumping is observed upon addition of PSY1 peptide and is dependent on the presence of PSY1R (Fuglsang et al., 2014). Interestingly, the growth-promoting effects of PSK do not require extracellular acidification by plasma membrane H^+-ATPases (Stührwohldt et al., 2011) and PSKR1 does not interact with AHA2 in a Bimolecular Fluorescence Complementation (BiFC) assay (Fuglsang et al., 2014), but the two proteins do co-localize in the plasma membrane (Ladwig et al., 2015).

The plant RLK activation mechanism differs from the activation mechanism of mammalian RTKs. In the classical RTK activation known from the mammalian field, ligand-induced RTK homodimerization brings the intracellular KDs into proximity, which thereby allows for intermolecular transphosphorylation and concomitant activation of the KDs and downstream signaling (Lemmon and Schlessinger, 2010). Transphosphorylation within the activation loop is also a central regulatory element of plant RLKs, as demonstrated in phosphorylation studies (Oh et al., 2000; Karlova et al., 2009) and further supported by crystal structures of plant RLK KDs containing phosphorylated residues (Yan et al., 2012; Bojar et al., 2014). Homodimerization, in some cases ligand-induced, has also been observed for a number of plant RLKs, including the *S*-locus Receptor Kinase (SRK) (Giranton et al., 2000), Brassinosteroid Insensitive 1 (BRI1) (Wang et al., 2005b), Flagellin Sensing 2 (FLS2) (Sun et al., 2012), and the CLV/BAM family (Guo et al., 2010).

However, about a decade ago, an interaction partner of BRI1 was identified and named BRI1-Associated Kinase 1 (BAK1) (Li et al., 2002; Nam and Li, 2002). Sequential transphosphorylation within the BRI1/BAK1 complex was demonstrated, showing that BRI1 is fully activated by BAK1 transphosphorylation within the juxtamembrane and C-terminal domains (Wang et al., 2008). BAK1 is also known as Somatic Embryogenesis Receptor-like Kinase 3 (SERK3) and belongs to a small family of SERK proteins consisting of five members (SERK1–5), each containing five LRRs in the extracellular domain (Hecht et al., 2001). SERK proteins are implicated in a range of diverse processes, including plant cell differentiation, growth, and immunity (Ma et al., 2016).

Additionally it has been found that SERKs acts as co-receptors for a range of LRR-RLKs. Each ligand-binding receptor seems to only interact with a limited number of SERK proteins (Ma et al., 2016). For example, BRI1 is regulated by SERK1, SERK4, and BAK1 (SERK3), whereas PSKR1 is regulated by SERK1, SERK2, and BAK1 (Wang et al., 2015). SERK proteins positively modulate the activity of its interaction partners by transphosphorylation (Schulze et al., 2010).

In this study, we investigated the transactivation mechanism of PSY1R and identified its *in vitro* autophosphorylation sites. By homology modeling to known structures of BRI1 and SIRK1 we propose how these residues are involved in stabilization of the activation loop in the active and inactive state, respectively. We furthermore showed that PSY1R interacted with members of the SERK family *in planta*.

MATERIALS AND METHODS

DNA Cloning

A list of primers and plasmids used in this study can be found in the Supplementary Tables 1 and 2. Full-length *SERK2*, *SERK4*, and *SERK5* cDNAs were amplified from an *Arabidopsis thaliana* Col-0 cDNA preparation. A cDNA clone of SERK1 was kindly provided by Professor S. C. de Vries (University of Wageningen). The PCR fragments were subcloned into Gateway pENTR/D-TOPO vector (Invitrogen Life Technologies). The BAK1 cDNA clone in the pCR8/GW/TOPO vector was obtained from Arabidopsis Biological Resource Center (ABRC) (clone CIW00115). The *SERK*, and *BAK1* genes were cloned into Gateway-compatible BiFC vectors by LR recombination using LR Clonase II Enzyme Mix (Invitrogen Life Technologies) to yield C-terminal fusions to cCFP or nYFP expressed from the 35S promoter. The PSY1R BiFC constructs were used in a previous study (Fuglsang et al., 2014) and the PSY1R K831A mutation, corresponding to the invariant lysine residue present in the protein kinase catalytic domain (Carrera et al., 1993), was generated through QuikChange Site Directed Mutagenesis (Agilent Technologies).

To generate constructs for expression in *E. coli*, the region of *PSY1R* encoding the entire intracellular domain of PSY1R was amplified with gene-specific primers carrying a 5′ CACC overhang for subcloning in the Gateway pENTR/D-TOPO vector (Invitrogen Life Technologies). Mutations and stop codons were introduced through QuikChange Site Directed Mutagenesis. The constructs were transferred into pDEST15 and pDEST17 (Invitrogen Life Technologies) through the LR reaction. All constructs were sequenced by Eurofins MWG Operon.

Transient Expression in *Nicotiana benthamiana*

Transformed *Agrobacterium tumefaciens* strain C58C1 was grown overnight in liquid YEP medium containing 25 μg/mL gentamicin and 50 μg/mL spectinomycin. Cells were washed and

resuspended in infiltration solution (10 mM $MgCl_2$, 100 μM acetosyringone), and diluted to an OD_{600} of 0.05, before mixing the transformed cells in the combinations to be tested. *N. benthamiana* leaves were infiltrated with the *A. tumefaciens* mix using a needleless syringe. Fluorescence was monitored approximately 48 h after infiltration.

Confocal Microscopy

A Leica SP5 confocal laser-scanning microscope with a 20 × 0.7 numerical aperture water-immersion objective was used to examine the lower epidermis of the infiltrated tobacco leaves. The complemented YFP/CFP fluorescence was excited at 448 nm and emission was detected at 515–540 nm. The gain was fixed in all samples to ensure that the emission intensity was comparable. Interaction was tested using both combinations of fusion proteins with similar results.

Expression and Purification of Recombinant Protein in *E. coli*

GST-tagged proteins were expressed either from the pGEX-4T-1 vector (GE Healthcare Life Sciences) in BL21(DE3) cells or from the pDEST15 vector in BL21-AI cells (Invitrogen Life Technologies). Briefly, LB medium was inoculated with an overnight LB + 100 μg/mL ampicillin culture to a start OD_{600} of 0.1 and grown at 37°C until the OD_{600} reached 0.5–0.7. Expression from the pDEST15 plasmid in BL21-AI cells was induced by the addition of L-(+)-arabinose to a final concentration of 0.2% (w/v) and the culture was incubated at 20°C overnight. Expression from the pGEX-4T-1 vector in BL21(DE3) cells was induced by the addition of 100 μM IPTG and the culture was incubated at 28°C for 3–4 h. In both cases, the cells were harvested at 14,000×*g* for 10 min, washed in cold H_2O, and pelleted again. The cells were resuspended in P-buffer (50 mM Tris–HCl, 150 mM NaCl, pH 7.5) containing 1 mM PMSF, 0.01% (w/v) DNase I, and 0.01% (w/v) lysozyme and lysed by sonication. The cell debris was collected by centrifugation at 15,000×*g* for 30 min and the lysate was incubated with Glutathione Sepharose 4B (GE Healthcare) for 2 h at 4°C. The resin was washed three times with P-buffer before eluting the protein with 50 mM L-glutathione in P-buffer, adjusted to pH 8.0. His-tagged proteins were expressed from the pDEST17 plasmid in BL21-AI cells as described above. The cells were harvested as described above, resuspended in lysis buffer (50 mM Na-phosphate, 300 mM NaCl, 10 mM imidazole, pH 8.0) containing 1 mM PMSF, 0.01% (w/v) DNase I, and 0.01% (w/v) lysozyme and opened by sonication. The cell lysate was collected as described above and incubated with Ni-NTA agarose (Qiagen) for 2 h at 4°C. The resin was washed three times with wash buffer (as lysis buffer, but containing 60 mM imidazole) before eluting the protein with elution buffer (as lysis buffer, but containing 250 mM imidazole).

Phosphorylation Assays

In a radiometric assay, purified kinase was incubated for 30 min at 30°C in kinase assay buffer (50 mM HEPES-NaOH pH 7.2, 150 mM NaCl, 10 mM $MgCl_2$, 1 mM DTT) with 50 μM ATP and 5 μCi γ-^{32}P-ATP (PerkinElmer) in a volume of 50 μL. The reaction was stopped by the addition of 10 μL 100% (w/v) TCA. The TCA-precipitated protein was dissolved in twofold concentrated Laemmli buffer and proteins were separated on a 10% SDS-PAGE gel. After the gel was stained and dried, it was exposed to a phosphor screen for 3 days and phosphorylation was detected using a Storm 860 scanner (Molecular Dynamics).

For detection of phosphorylated proteins with phosphoamino acid-specific antibodies, purified kinase was incubated for 1 h at 30°C in kinase assay buffer with 500 μM ATP. As above, the reaction was stopped by TCA precipitation and proteins were separated by SDS-PAGE. The protein bands were blotted onto a nitrocellulose membrane and the membrane was blocked with 3% (w/v) BSA. Rabbit polyclonal phosphoserine (Invitrogen Life Technologies, 61-8100, 1:200) and phosphothreonine (Invitrogen Life Technologies, 71-8200, 1:1000) antibodies were used as primary antibodies and polyclonal goat anti-rabbit alkaline phosphatase-coupled immunoglobulin (DAKO, D0487, 1:2000) were used as secondary antibody. The immunoblot was developed using NBT/BCIP substrate (Promega, S3771).

Homology Model of PSYR1 Kinase Domain

Modeller v9.19 software[1] (Sali and Blundell, 1993) was used to generate the homology models with maize SIRK1 KD (PDB ID: SIRK1) and BRI1 KD (PDB ID: 5LPV) as templates. The templates were alignment with the KD of PSY1R (residue 781–1079) individually and as a multiple alignment with both templates. Models were initially evaluated using discrete optimized protein energy (DOPE) score and using energy plots that show problematic regions. The generated models were further evaluated and energy refined using the SAVES[2] and GALAXY (Heo et al., 2013) server, respectively. Final models were visualized using PyMOL (The PyMOL Molecular Graphics System, Version 1.8 Schrödinger, LLC) and the inhibitor AMP-PNP and Mg^{2+} were modeled into the homology models to visualize the catalytic ATP binding site. The energy plots were visualized using Gnuplot 5.0.

MS/MS Detection of Phosphosites

Auto- and transphosphorylated sites of the intracellular domain of PSY1R were detected using a LTQ Orbitrap XL ETD mass spectrometer (Thermo Fisher Scientific, San Jose, CA, United States). Full-length recombinant proteins were digested in-solution and/or in-gel with sequencing grade trypsin (Promega, Madison, WI, United States). Freeze-dried tryptic peptides were dissolved by adding 40 μL of 0.1% formic acid and subjected to MS analysis. Ten microliters of each sample was resolved using a Finnigan Surveyor liquid chromatography system interfaced with the mass spectrometer. Tryptic peptides were fragmented using either collision-induced dissociation (CID) or "decision tree" methods that utilize both CID and electron-transfer dissociation (Swaney et al., 2008).

[1] http://www.salilab.org

[2] https://services.mbi.ucla.edu/SAVES/

The MS RAW files were searched against the TAIR10 database combined with a decoy database containing the randomized sequences of the original database. The search parameters, described in detail previously (Ahsan et al., 2013), were briefly as follows: the mass type, average precursor plus fragment; dynamic modifications, phosphorylation of Ser/Thr/Tyr (+79.9799 Da) and oxidation of Met (+15.9994 Da); and the static modification, Cys-carboxyamidomethylation.

Identification data were evaluated using the XCorr function of SEQUEST, and phosphorylation-site localization was accomplished using phosphoRS (Proteome Discoverer, v. 1.0.3, Thermo Fisher Scientific). The XCorr values for each charge state were set to default, and no decoy hits were allowed. Peptide mass deviation was 10 ppm and two peptides/protein were used to further filter the data. Phosphopeptides with a pRS score of ≥50 and a pRS site probability of ≥50% were considered as high-confidence phosphosites. For final validation, each spectrum was inspected manually and accepted only when the phosphopeptide had the highest pRS site probability, pRS score, XCorr value, and site-determining fragment ions allowed for unambiguous localization of the phosphorylation site.

RESULTS

Identification of PSY1R *in Vitro* Autophosphorylation Sites

We set out to investigate the autophosphorylation mechanism of PSY1R. The cytosolic KD of PSY1R (residues 741–1095; kPSY1R) were expressed in *E. coli* as GST-fused protein (**Figure 1**). An inactive variant of the kinase were generated by mutating the lysine residue in the catalytic domain to an alanine (kPSY1R K831A). Recombinant kPSY1R were incubated in an *in vitro* kinase assay in the absence or presence of ATP and phosphorylated amino acids were detected with phosphoamino acid-specific antibodies. As seen in **Figure 1**, phosphoserine (pSer) and phosphothreonine (pThr) antibodies reacted with the active kPSY1R protein, but weakly or not at all with the inactive kPSY1R K831A. This implies that PSY1R autophosphorylates on Ser and Thr residues. The addition of ATP to the kinase reaction assay increased the phosphorylation level especially of Thr residues. The presence of phosphorylated residues in samples without ATP indicates the kinase is active and autophosphorylated when expressed in *E. coli*. The detected phosphorylation of kPSY1R is, however, true autophosphorylation, since phosphorylation of the inactive kPSY1R K831A was nearly undetectable.

We then mapped the autophosphorylation sites of the intracellular domain of PSY1R. We incubated kPSY1R in the absence or presence of ATP to allow autophosphorylation. Afterward the proteins were digested with trypsin. The tryptic peptides were analyzed by LTQ-Orbitrap high-resolution mass spectrometry (MS/MS) to map phosphorylation events. Examples of MS/MS spectra for two of the determined autophosphorylation sites are shown in **Figure 2A**. These spectra presented evidence for phosphorylation of the peptides AKHENLVALQGYCVHDsAR and DIKSsNILLDGNFK

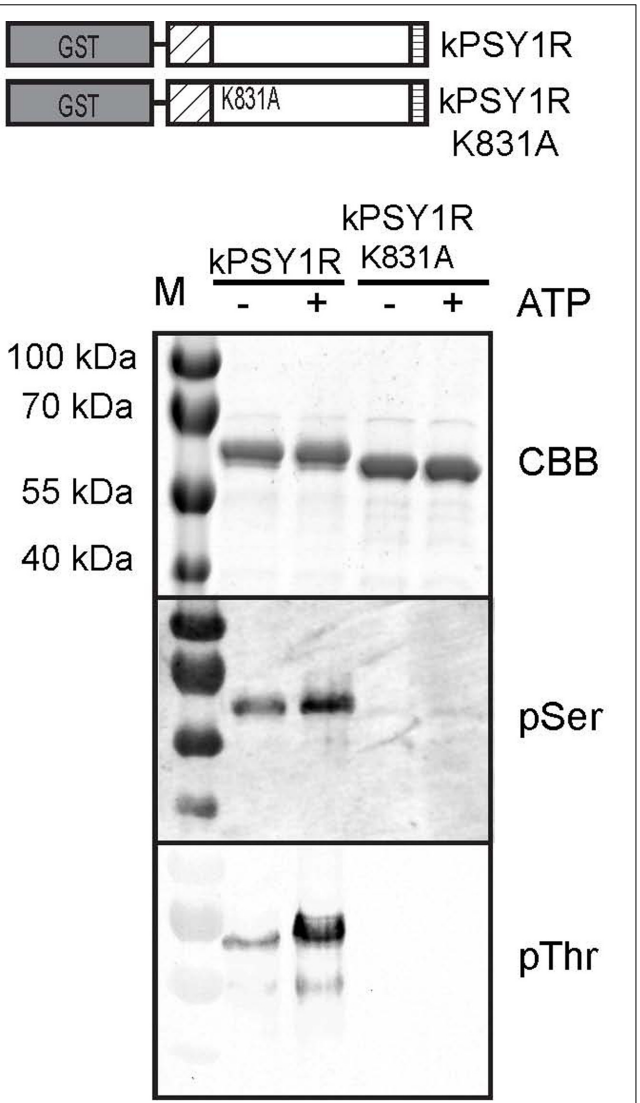

FIGURE 1 | PSY1R autophosphorylates on serine and threonine residues. The intracellular domain of PSY1R, was expressed in *E. coli* with a GST tag at the N-terminal end (kPSY1R). The kPSY1R K831A variant harbors the K831A mutation, which renders the kinase inactive. GST-purified kPSY1R or kPSY1RK831A was incubated in the presence or absence of ATP in an *in vitro* kinase assay and phosphorylation of the proteins was probed with phosphoamino acid-specific antibodies.

(lowercase letters denote phosphorylated residues), which contain the Ser870 and Ser933 phosphosites, respectively. We unambiguously identified seven total autophosphorylation sites (**Figure 2B**), including three threonine and four serine residues, each of which were located within the KD. Detailed information on the identified phosphopeptides is listed in **Table 1**. The PSY1R intracellular domain contains 12 possible phosphorylation targets within the juxtamembrane domain (JMD) (8 Ser, 2 Thr, and 2 Tyr), 35 possible targets within the KD (13 Ser, 11 Thr, and 11 Tyr), and 1 possible target within the C-terminal domain (1 Thr). However, autophosphorylation of JMD or C-terminal domain residues was not detected in our MS analysis. Spectral

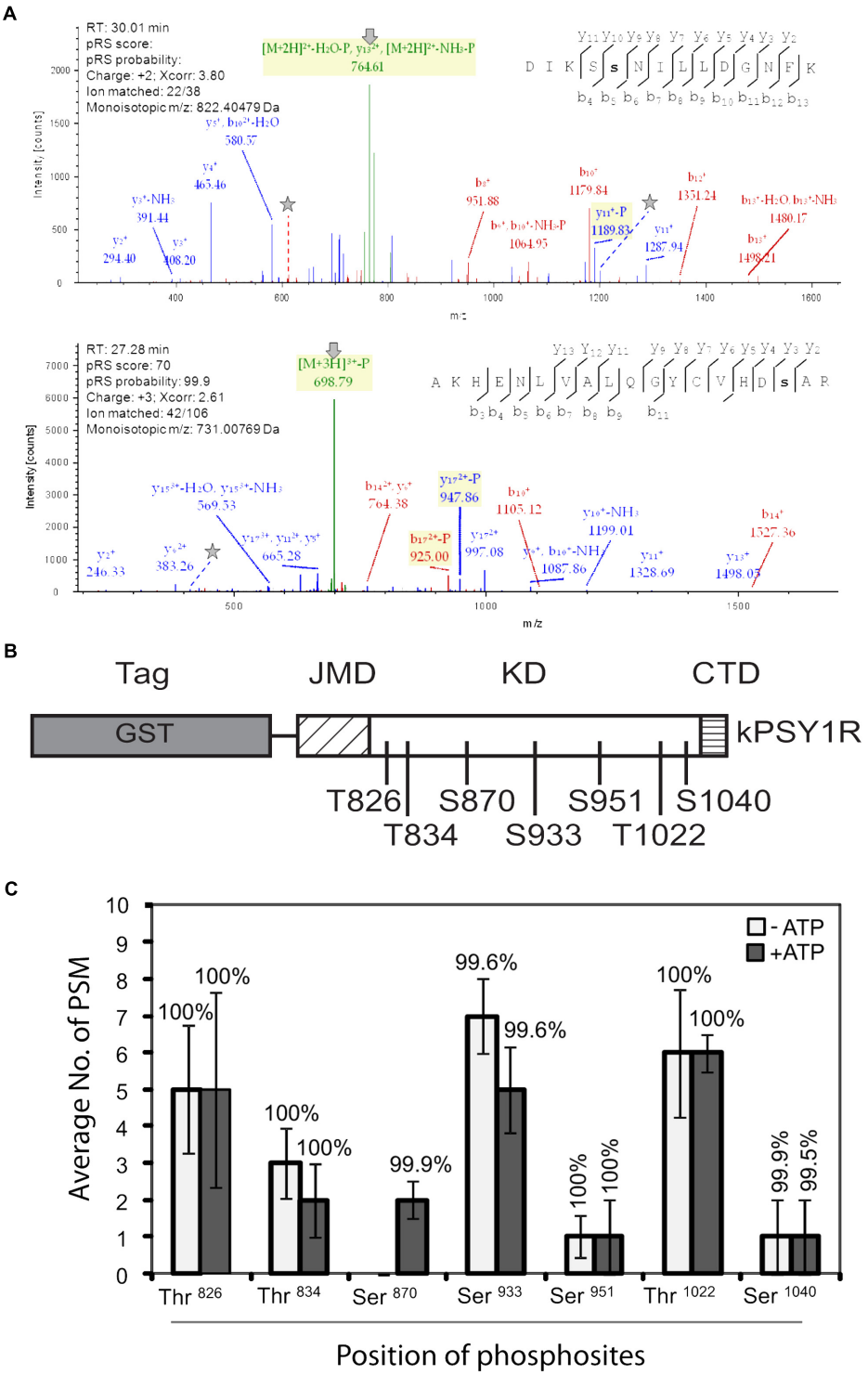

FIGURE 2 | Mapping of autophosphorylation sites in recombinant kPSY1R. **(A)** Upper panel: The MS/MS spectrum of the doubly charged phosphopeptide DIKSsNILLDGNFK provides evidence of phosphorylation of Ser933, which is found in the Ser/Thr protein kinase active site signature. Lower panel: The MS/MS spectrum of the triple charged peptide AKHENLVALQGYCVHDsAR provides evidence for phosphorylation of Ser870 within the kinase domain. N-terminal and C-terminal peptide sequence ions are indicated with b_i and y_i, respectively. In the spectra, lines and stars indicate the neutral loss of the phosphate on fragments or precursor ions and the phosphorylated residues, respectively. **(B)** Linear domain structure of the intracellular domain of PSY1R revealing the localization of the seven autophosphorylation sites in the kinase domain identified by MS. **(C)** Quantitative MS analysis of the autophosphorylation sites. Spectral count data (peptide spectral matches, PSM) are the means of four replicates. Percentages above the data bars indicate the pRS site probability for each amino acid. Solid and empty bars represent the presence and absence of ATP, respectively. Error bars represent means ± SE of four independent replicates.

TABLE 1 | Mass spectrometry data on the peptides carrying the PSY1R *in vitro* autophosphorylation sites.

Phosphosite	Phosphopeptide identified	Δ*M* (ppm)	pRS score[a]	pRS site probability[b]	XCorr	Charge	*m/z* (Da)	Ions matched
Thr826	ATLDNGpTKLAVK	1.63	80	T(2): 0.0; T(7): 100.0	3.76	2	1310.6694	23/32
Thr834	KLpTGDYGMMEK	0.87	163	T(3):100.0; Y(6): 0.0	3.97	2	1352.5615	26/29
Ser870	AKHENLVALQGYCVHDpSAR	1.36	70	Y(12): 0.1; S(17): 99.9	2.61	3	2191.0085	42/106
Ser933	DIKSpSNILLDGNFK	0.58	127	S(4): 95.3; S(5): 4.7	4.41	2	1643.8031	28/38
Ser951	AYVADFGLpSR	1.03	150	Y(2): 0.0; S(9): 100.0	3.64	2	1178.5230	25/26
Thr1022	ELVAWVHpTMKR	1.59	113	T(8): 100.0	2.71	2	1449.7050	24/29
Ser1040	DGKPEEVFDTLLREpSGNEEAMLR	0.02	70	T(10): 0.1; S(15): 99.9	3.09	3	2715.2332	47/130

[a]*pRS score. This peptide score is based on the cumulative binomial probability that the observed match is a random event. The value of the pRS score strongly depends on the data scored, but usually scores of above 50 give good evidence for a good PSM.* [b]*pRS site probabilities. For each phosphorylation site this is an estimation of the probability for the respective site being truly phosphorylated.*

count analyses revealed that the addition of ATP during the *in vitro* kinase assay enhanced autophosphorylation of Ser870, whereas the remaining six phosphosites were also identified in the control lacking ATP (**Figure 2C**).

Autophosphorylation of PSY1R Occurs *in Trans*

Since the full-length LRR RLK PSY1R protein was previously shown to form homodimers, we were prompted to ask whether the intracellular kinase activation mechanism involved inter- or intramolecular phosphorylation, i.e., *trans*- or *cis*-phosphorylation. To investigate this, we constructed a hexahistidine-tagged inactive variant of the intracellular domain of PSY1R (H_6-kPSY1R K831A, **Figure 3A**) and incubated it with the active kPSY1R protein. Interestingly, the inactive intracellular domain was phosphorylated in the presence of the active kPSY1R, but not when it was incubated alone (**Figure 3B**, phosphorimage), which demonstrates that *in vitro* autophosphorylation of the intracellular domain occurs *in trans*. Transphosphorylation of the inactive H_6-kPSY1R K831A by the active kPSY1R was detected when using the pThr antibody, but not with the pSer antibody (**Figure 3B**).

First Phase Transphosphorylation Sites Include Residues within the Kinase Activation Loop

To examine the transphosphorylation mechanism of kPSY1R in detail, we mapped the transphosphorylation sites of kPSY1R by MS. We incubated the inactive H_6-kPSY1R K831A with ATP in the presence or absence of active kPSY1R (GST-tagged) to allow for transphosphorylation. MS analysis identified three phosphorylated sites, Ser951, Thr959, and Thr963, within the KD of H_6-kPSY1R K831A after incubation with kPSY1R (**Figure 3B**). No phosphorylated sites were detected in H_6-kPSY1R K831A incubated without kPSY1R. Detailed data for the three phosphopeptides AYVADFGLsR, tHVTTELVGTLGYIPPEYGQAWVATLR, and LILPYRTHVTtELVGTLGYIPPEYGQAWVATLR harboring Ser951, Thr959, and Thr963, respectively, are provided in **Table 2**. Interestingly, all three transphosphorylation sites are located within the kinase activation loop, which was previously shown to carry phosphosites important for catalytic kinase activity in other kinases (Huse and Kuriyan, 2002). Spectral count analysis demonstrated that the phosphorylation level of Thr959 and Thr963 was higher than that of Ser951 (**Figure 3C**). This explains why transphosphorylated Ser951 is not detected by the pSer antibody (**Figure 3B**), as this residue has low phosphorylation levels compared to Thr959 and Thr963. Alignment of the activation loops from a number of plant LRR RLKs, showed that residues corresponding to Thr959 and Thr963 are conserved within in the activation loop whereas the Ser951 residue is unique for PSY1R (**Figure 3D**).

To verify the transphosphorylation sites identified by MS, we created a new construct (H_6-kPSY1R K831A-3x) in which all three proposed transphosphorylation sites (Ser951, Thr959, and Thr963) were mutated to alanine. We then asked whether the active kPSY1R could transphosphorylate H_6-kPSY1R K831A-3x. As shown in **Figure 3B**, transphosphorylation of threonine residues was completely abolished in H_6-kPSY1R K831A-3x. This indicates that Thr959 and Thr963 are exclusive first-phase transphosphorylation sites.

Residue Thr968 Is Indispensable for kPSY1R Kinase Activity, While Ser951 Is a Possible Negative Regulatory Phosphorylation Site

To evaluate the *in vitro* function of each possible autophosphorylation site on the activity of kPSY1R, we generated a series of point mutations. Each of the autophosphorylation sites identified by MS as well as all possible phosphorylation sites within the activation loop were mutated individually to alanine residues in wild-type kPSY1R, thereby preventing phosphorylation at the corresponding residue. As shown in **Figure 4A**, only mutation of residue T968 in the activation loop affected the autophosphorylation severely, resulting in a nearly inactive kinase. By contrast, mutation of S951 led to an increased autophosphorylation level, suggesting that phosphorylation of S951 negatively regulates kPSY1R activity (**Figure 4**).

To visualize and to identify a possible structural explanation for this positive and negative regulation by Ser/Thr phosphorylation we used Modeller 9.19 to predict a homology model of PSY1R KD (**Figure 5**). PSY1R was modeled in the active conformation using the crystal structure of phosphorylated BRI1 KD as template (Bojar et al., 2014). To predict PSY1R in the

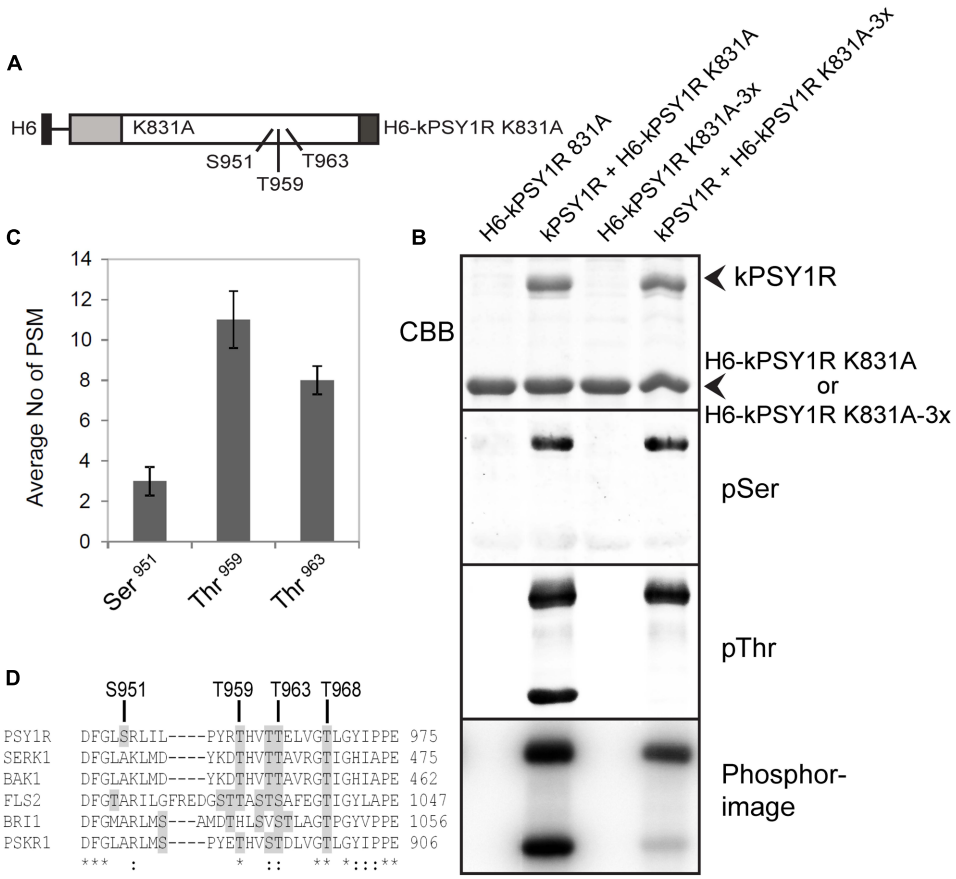

FIGURE 3 | First phase transphosphorylation sites of kPSY1R. **(A)** Linear domain structure of the intracellular domain of the H_6-kPSY1R K831A inactive mutant revealing the localization of the three transphosphorylation sites identified by MS. Juxtamembrane domain (JMD) is indicated by gray and C-terminal domain by dark gray shading. **(B)** The GST-tagged kPSY1R is able to transphosphorylate the inactive His-tagged kPSY1R K831A in an *in vitro* kinase assay with radiolabeled ATP. Transphosphorylation of H_6-kPSY1R K831A studied using a combination of phosphoserine and phosphothreonine antibodies and radiolabeled ATP. Mutation of the three transphosphorylation sites (3x = S951A, T959A, and T963A) identified by MS prevents transphosphorylation on threonine residues while overall transphosphorylation is reduced markedly as detected with radiolabeled ATP. **(C)** Average phosphopeptide spectral matches (PSM) identified for each phosphosite. The data represent the means ± SE of two independent replicates. **(D)** Amino acid sequence alignment of the kinase activation loop of selected plant LRR receptor-like kinases. The activation loop begins at the DFG motif and ends with the A/PPE motif. Serine and threonine residues are shaded in gray. The location of the transphosphorylated sites in PSY1R are indicated above the alignment. Asterisks denote conserved residues, while colons denote partially conserved or similar residues at the indicated position.

TABLE 2 | Mass spectrometry data on the peptides carrying the PSY1R *in vitro* transphosphorylation sites.

Phosphosite	Phosphopeptide identified	Δ*M* (ppm)	pRS score[a]	pRS site probability[b]	XCorr	Charge	*m/z* (Da)	Ions matched
Ser951	AYVADFGLpSR	3.22	138	Y(2): 0.0; S(9): 100.0	2.69	2	589.7676	22/26
Thr959	pTHVTTELVGTLGYIPPEYGQ-AWVATLR	3.13	90	T(1): 68.6; T(5): 10.5	4.98	3	1018.1807	63/208
Thr963	LILPYRTHVTpTELVGTLGYIP-PEYGQAWVATLR	3.82	53	T(7): 5.0; T(11): 40.0	4.22	4	952.7563	65/285

[a]*pRS score. This peptide score is based on the cumulative binomial probability that the observed match is a random event. The value of the pRS score strongly depends on the data scored, but usually scores of above 50 give good evidence for a good PSM.* [b]*pRS site probabilities. For each phosphorylation site this is an estimation of the probability for the respective site being truly phosphorylated.*

inactive conformation the recently published crystal structure of the maize SIRK1 KD was used as template (Aquino et al., 2017). However, as the sequence identity between the KDs of SIRK1 and PSY1R is relatively low (34%) and the energy plot (Supplementary Figure 1) indicated several problematic regions the crystal structure of BRI1 was included as template. The model based on the two templates showed a significantly better energy plot than models build on SIRK1 alone as seen in Supplementary Figure 1. The inactive conformation of LRR-RLKs is characterized by a structured activation loop

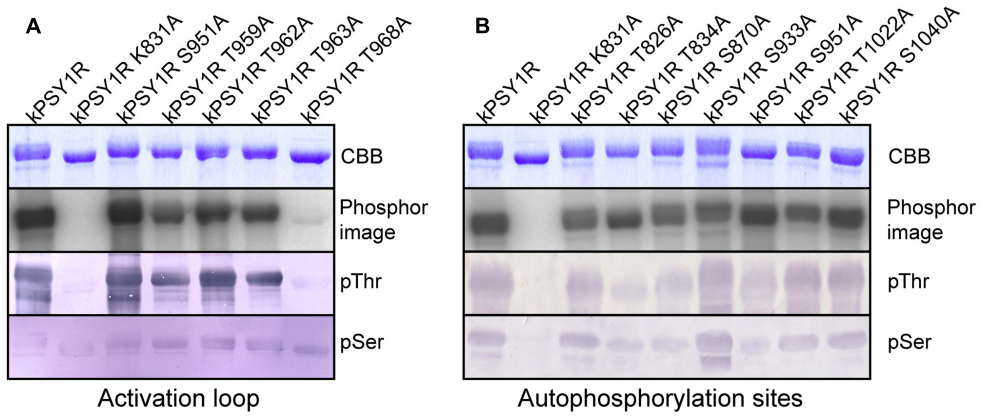

FIGURE 4 | Identification of possible phosphorylation sites that regulate PSY1R kinase activity. The autophosphorylation activity of different mutants of the intracellular domain of PSY1R was evaluated in an *in vitro* kinase assay with ^{32}P-labeled ATP. **(A)** Serine and threonine residues within the activation loop were mutated individually to alanine and the autophosphorylation activity of each mutant was compared to that of the wild type (kPSY1R) and inactive kinase mutant (kPSY1R K831A). **(B)** Serine and threonine residues identified as autophosphorylation sites by MS analysis were mutated individually to alanine and the autophosphorylation activity of each mutant was compared to that of the wild type (kPSY1R) and inactive K831A mutant (kPSY1R K831A).

(**Figure 5A**) (Aquino et al., 2017). As seen in **Figure 5A**, the homology model based on the two templates shows a much more structured activation loop than the model based on BRI1 alone indicating that the model is in the inactive conformation. We next added a phosphate group to Ser-951, Thr-963, and Thr-968 to see whether phosphorylation stabilizes either the active or inactive conformation. As seen in **Figure 5B**, addition of phosphate to the two threonine residues results in two possible salt bridges that can stabilize the active conformation whereas phosphorylation in the inactive conformation did not give rise to any stabilizing interactions (Supplementary Figure 2). In contrast, phosphorylation of Ser-951 seems to stabilize the inactive conformation only as the phosphate group can interact with both the backbone of Thr-963 and Arg-923. These observations support that phosphorylation of Thr-968 leads to increased autophosphorylation whereas Ser-951 seems to be a negative regulatory phosphorylation site.

kPSY1R Interacts with Members of the SERK Family

BAK1 and other members of the SERK family were previously shown to act as co-receptors for LRR-RLKs such as BRI1 and FLS2. To test whether SERK proteins could regulate PSY1R activity through phosphorylation, we created GST-tagged constructs of the intracellular domain of the SERK proteins (kSERK and kBAK) and tested whether these were able to transphosphorylate the inactive H6-kPSY1R K831A protein. In this case, we used the pThr antibody to detect transphosphorylation. As shown in **Figure 6A**, the intracellular domains of SERK1, SERK2, BAK1, and SERK4 were all able to transphosphorylate H_6-kPSY1R K831A, whereas kSERK5 exhibited weak autophosphorylation activity and did not transphosphorylate H_6-kPSY1R K831A. In the *Col*-0 accession, SERK5 harbors an R401L mutation in the otherwise conserved HRD motif of the KD, which could explain the lack of autophosphorylation activity observed in our assay. To test the ability of kPSY1R to transphosphorylate a SERK protein, we constructed an inactive H_6-tagged version of the intracellular domain of BAK1, H_6-mBAK1 K317A. As seen in **Figure 6B**, kPSY1R was able to transphosphorylate H_6-BAK1 K317A. Taken together, these results suggest that one or more of the SERK proteins act as co-receptors for PSY1R via a trans-activation mechanism.

PSY1R Can Form Homo- and Heterodimers *in Planta*

Using a BiFC assay, we evaluated the ability of full-length PSY1R and PSY1R mutants to dimerize *in planta*. As seen in **Figure 6C**, full-length PSY1R forms homodimers *in planta*, as we reported previously (Fuglsang et al., 2014). PSYR1 protein, harboring a K831A mutation in the KD (*psy1r*K831A) resulting in loss of kinase activity, also forms homodimers *in planta* (**Figure 6C**).

We further investigated whether PSY1R also forms complexes with SERK proteins. As shown in **Figure 6D**, PSY1R interacts with SERK5, even though SERK5 seems inactive, and to a lesser extent with BAK1, SERK1, and SERK2, whereas PSY1R barely interacted with SERK4 in the employed BiFC assay. All the interactions take place at the plasma membrane as expected. We did not detect homodimerization of any of the SERK members. Furthermore, PSY1R K831A forms a strong complex with BAK1.

DISCUSSION

Taken together, we identified three residues within the activation loop of PSY1R, which are part of the first phase transphosphorylation mechanism. By homology modeling to known structures of BRI1 and SIRK1 we demonstrated how these residues are involved in stabilization of the activation loop in the active and inactive state, respectively. Finally we demonstrated

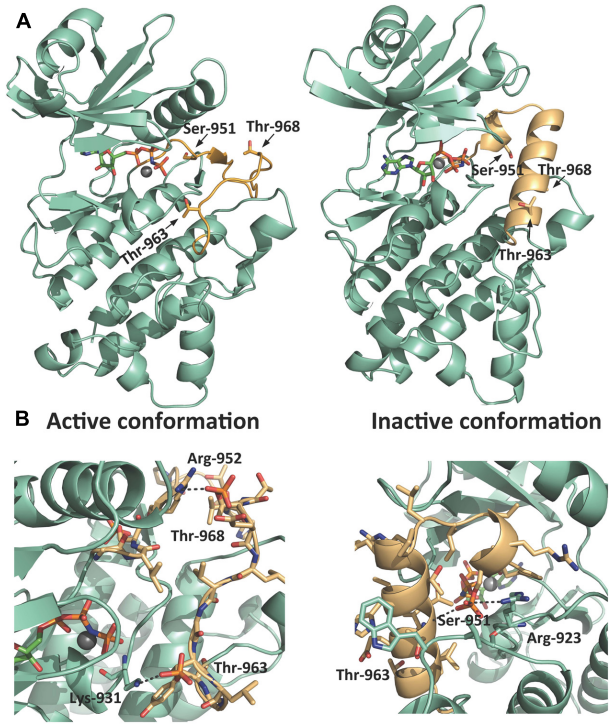

FIGURE 5 | Homology model of PSY1R kinase domain. A homology model of PSY1R kinase domain in both the active (left) and inactive (right) conformation. **(A)** The activation loop (light orange) starting from the conserved DFG motif contains multiple phosphorylation sites. Whereas the overall fold of the rest of the kinase domain (green cyan) is conserved between the two activation states, the active conformation of the activation loop is less structured compared to the inactive kinase. **(B)** Phosphorylation of the two threonine residues give rise to possible salt bridges between the phosphate groups and Lys-931 and Arg-952 that may stabilize the active kinase (left figure). Phosphorylation of Ser-951 stabilizes in contrast the inactive conformation (right figure) through a hydrogen bond between the phosphate and the backbone of Thr-963 and a possible salt bridge to Arg-923. The active site in all models is marked with the ATP analog AMP-PNP and Mg^{2+} modeled from the template structures (PDB-id 5LPV and 5UV4).

that PSY1R interacts with co-receptors from the SERK family and that kPSY1R are target for SERK kinases.

Mapping of the PSY1R autophosphorylation sites by MS revealed a total of seven autophosphorylation sites, four serine and three threonine residues, all located within the KD, including a single phosphosite (Ser951) within the activation loop. It is surprising that we did not detect any phosphorylation sites within the JMD previously reported to be important for the function of plant RLKs (Yoshida and Parniske, 2005; Xu et al., 2006; Petutschnig et al., 2010; Meyer et al., 2013). The *in vivo* phosphorylation site database PhosPhAt 4.0 (Durek et al., 2010) contains two PSY1R phosphorylation sites, Ser8 and Ser10, which are probably not authentic PSY1R autophosphorylation sites, as they are located within the predicted signal sequence.

Here we have demonstrated that PSY1R first-phase transphosphorylation occurs within the activation loop, specifically at residues Ser951, Thr959, and Thr963. Phosphorylation of Thr959 and Thr963 were only found in the transphosphorylation experiments and not in the initial mapping of phosphosites. This indicates that these sites are only transiently phosphorylated during the catalytic cycle and therefore caught in the inactive mutant; alternatively a full-length receptor protein is required in order to maintain the conformation with these sites phosphorylated. As seen from an alignment of the activation loops of a number of plant LRR RLKs (**Figure 3D**), the Ser951 residue is not conserved among the aligned RLKs and is unique for PSY1R. Based on homology modeling we propose that the phosphorylated Ser951 stabilizes the inactive conformation of PSY1R. In addition to Ser951, PSY1R contains four threonine residues, Thr959, Thr962, Thr963, and Thr968, which are conserved among the plant RLKs shown here. The residues within the activation loop of plant RLKs are key phosphorylation sites that are important for kinase activity (Oh et al., 2000; Shah et al., 2001; Wang et al., 2005a; Karlova et al., 2009). In the crystal structure of the BAK1 KD, all four threonine residues within the activation loop are phosphorylated and are involved in electrostatic interactions that maintain the conformation of the activation and catalytic loop (Yan et al., 2012). Structurally, the most important residue in BAK1 is Thr450, as it plays a role analogous to the single threonine residue (Thr197) within the activation loop of the mammalian kinase Protein Kinase A (Johnson et al., 1996). Interestingly, we found that the residue in PSY1R that corresponds to BAK1 Thr450, the Thr963 residue, was one of the initial transphosphorylation sites. Based on homology modeling, we speculate that the phosphorylated PSY1R Thr963 residue plays an important role in maintaining the active conformation of an activation loop.

Plant RLKs are categorized into two groups based on whether they are activated through intermolecular *trans*-phosphorylation or intramolecular *cis*-phosphorylation. Members of the former group are able to transphosphorylate an inactive version of the KD and show second order kinetics with respect to the kinase concentration and include BRI1 (Wang et al., 2005b), CLV1 (Williams et al., 1997), SERK1 (Shah et al., 2001), and HAESA (Horn and Walker, 1994; Taylor et al., 2013). Members of the latter group do not transphosphorylate an inactive KD and exhibit first order kinetics with respect to kinase concentration and include AtACR4 (Meyer et al., 2011), CrRLK1 (Schulze-Muth et al., 1996), and Xa21 (Liu et al., 2002). In our study, we observed that the KD of PSY1R transphosphorylated the inactive mutant PSY1R K831A. Therefore, we speculate that transphosphorylation is an important event in PSY1R signaling analogous to the proposed activation mechanism of BRI1 (Wang et al., 2008). BRI1 is first partially activated through transphosphorylation within the activation loop. The partially activated BRI1 receptor interacts with and phosphorylates BAK1, which in turn phosphorylates BRI1 on residues within the JMD and C-terminal domain, which fully activates BRI1 (Oh et al., 2014).

It is tempting to speculate that PSY1R is fully activated by SERK phosphorylation, analogous to BRI1. The requirement for a co-receptor would also explain the lack of detected phosphosites

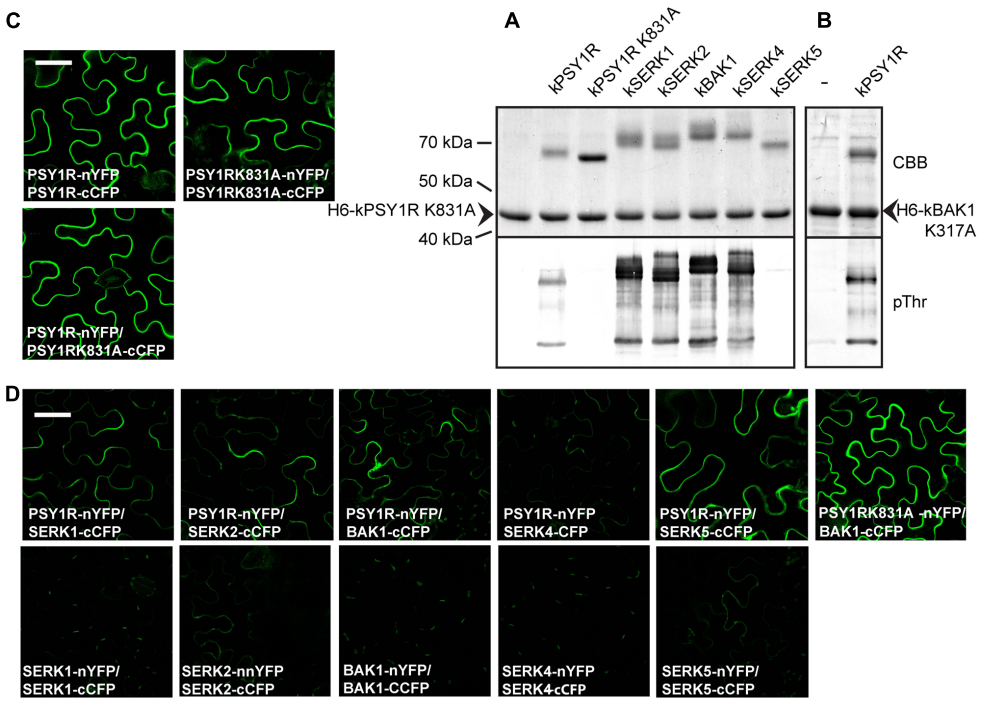

FIGURE 6 | Members from the SERK family transphosphorylate kPSY1R. **(A)** The GST-tagged kPSY1R is able to transphosphorylate the inactive His-tagged kPSY1R K831A in an *in vitro* kinase assay with radiolabeled ATP. Upper panel: CBB stained; Lower panel: Phosphor image. **(B)** Transphosphorylation between intracellular domains of PSY1R and members of the SERK family. SERK1, 2, and 4 and BAK1 transphosphorylate kPSY1R K831A and kPSY1R transphosphorylates kBAK1 K317A *in vitro*. SERK5 exhibits low autophosphorylation activity and does not transphosphorylate kPSY1R. Upper panel: CBB staining; Lower panel: Anti-phosphothreonine blot. **(C,D)** BiFC analysis of PSY1R and SERK interactions in *N. benthamiana* leaves. The proteins are fused to either the N-terminal part of YFP (nYFP) or the C-terminal part of CFP (cCFP) as indicated on the figure. All pictures are taken with the same magnification, scale bar = 50 μm. **(C)** PSY1R and PSY1R K831A form homodimers. **(D)** PSY1R interacts with members of the SERK family to varying degrees. Interaction between PSY1R and BAK1 is not dependent on PSY1R kinase activity. The SERK proteins do not form or only form weak homodimers in this assay. All pictures are taken with the same magnification, scale bar = 50 μm.

in the PSY1R JMD, as this would require the presence of a co-receptor in the *in vitro* assay applied for MS studies. In the crystal structure of the closely related PSK receptor PSKR1, a co-receptor is not required for ligand binding but the potential involvement of a co-receptor for the complex activation was suggested and it was found that PSK induces the heterodimerization of PSKR1 with SERK1, SERK2, and SERK3 *in planta* (Wang et al., 2015).

Additionally, we demonstrated *in planta* interactions between PSY1R and members of the SERK family, which act as co-receptors and regulate distinct signaling pathways (Chinchilla et al., 2009; Li, 2010). SERK proteins are implicated in controlling the balance between growth and defense, as they regulate the activity of receptors involved in plant development and in plant immunity. Our results suggest that SERK proteins also regulate PSY1R signaling. Based on BiFC analyses, we observed differences in the fluorescence intensity of the signal when testing for interactions between PSY1R and different SERK members. This might indicate differences in the stability of the interaction. Interestingly we observe a very strong interaction between the inactive PSY1R K831A mutant and BAK1 as well as between the inactive SERK5 and PSY1R. This shows that protein kinase activity is not required for the interaction, as previously observed within this family (Karlova et al., 2009). Also it could indicate that the interaction between the two kinases is less transient, compared to a situation with two active kinases, which therefore results in formation of more fluorescent molecules. Future studies will reveal whether the interactions between PSY1R and members of the SERK family are of functional relevance *in vivo*.

CONCLUSION

Our study has revealed details of the regulation of the kinase activity of PSY1R. Future studies will reveal the *in vivo* function of the identified autophosphorylation sites and how the interaction with the SERK co-receptor proteins fine-tunes PSY1R signaling.

AUTHOR CONTRIBUTIONS

CO and AF designed the study. CO, LG, and TS performed the kinase phosphorylation analysis. CO and AK performed the BiFC analysis. NA performed the MS analysis. JP performed the structural analysis. CO, JT, and AF supervised the project.

CO and AF wrote the manuscript. All authors reviewed the results and approved the final version of the manuscript.

FUNDING

This work was supported by the UNIK research initiative of the Danish Ministry of Science, Technology, and Innovation through the "Center for Synthetic Biology" at University of Copenhagen and by the Danish National Research Foundation through the PUMPKIN Center of Excellence.

SUPPLEMENTARY MATERIAL

The Supplementary Material for this article can be found online at: https://www.frontiersin.org/articles/10.3389/fpls.2017.02005/full#supplementary-material

REFERENCES

Ahsan, N., Huang, Y., Tovar-Mendez, A., Swatek, K. N., Zhang, J., Miernyk, J. A., et al. (2013). A versatile mass spectrometry-based method to both identify kinase client-relationships and characterize signaling network topology. *J. Proteome Res.* 12, 937–948. doi: 10.1021/pr3009995

Amano, Y., Tsubouchi, H., Shinohara, H., Ogawa, M., and Matsubayashi, Y. (2007). Tyrosine-sulfated glycopeptide involved in cellular proliferation and expansion in *Arabidopsis*. *Proc. Natl. Acad. Sci. U.S.A.* 104, 18333–18338. doi: 10.1073/pnas.0706403104

Aquino, B., Counago, R. M., Verza, N., Ferreira, L. M., Massirer, K. B., Gileadi, O., et al. (2017). Structural characterization of maize SIRK1 kinase domain reveals an unusual architecture of the activation segment. *Front. Plant Sci.* 8:852. doi: 10.3389/fpls.2017.00852

Belkhadir, Y., Yang, L., Hetzel, J., Dangl, J. L., and Chory, J. (2014). The growth-defense pivot: crisis management in plants mediated by LRR-RK surface receptors. *Trends Biochem. Sci.* 39, 447–456. doi: 10.1016/j.tibs.2014.06.006

Bojar, D., Martinez, J., Santiago, J., Rybin, V., Bayliss, R., and Hothorn, M. (2014). Crystal structures of the phosphorylated BRI1 kinase domain and implications for brassinosteroid signal initiation. *Plant J.* 78, 31–43. doi: 10.1111/tpj.12445

Carrera, A. C., Alexandrov, K., and Roberts, T. M. (1993). The conserved lysine of the catalytic domain of protein-kinases is actively involved in the phosphotransfer reaction and not required for anchoring ATP. *Proc. Natl. Acad. Sci. U.S.A.* 90, 442–446. doi: 10.1073/pnas.90.2.442

Chinchilla, D., Shan, L., He, P., De Vries, S., and Kemmerling, B. (2009). One for all: the receptor-associated kinase BAK1. *Trends Plant Sci.* 14, 535–541. doi: 10.1016/j.tplants.2009.08.002

De Smet, I., Voss, U., Jurgens, G., and Beeckman, T. (2009). Receptor-like kinases shape the plant. *Nat. Cell Biol.* 11, 1166–1173. doi: 10.1038/ncb1009-1166

Durek, P., Schmidt, R., Heazlewood, J. L., Jones, A., Maclean, D., Nagel, A., et al. (2010). PhosPhAt: the *Arabidopsis thaliana* phosphorylation site database. An update. *Nucleic Acids Res.* 38, D828–D834. doi: 10.1093/nar/gkp810

Fuglsang, A. T., Kristensen, A., Cuin, T. A., Schulze, W. X., Persson, J. R., Thuesen, K. H., et al. (2014). Receptor kinase-mediated control of primary active proton pumping at the plasma membrane. *Plant J.* 80, 951–964. doi: 10.1111/tpj.12680

Giranton, J. L., Dumas, C., Cock, J. M., and Gaude, T. (2000). The integral membrane S-locus receptor kinase of *Brassica* has serine/threonine kinase activity in a membranous environment and spontaneously forms oligomers *in planta*. *Proc. Natl. Acad. Sci. U.S.A.* 97, 3759–3764. doi: 10.1073/pnas.97.7.3759

Gish, L. A., and Clark, S. E. (2011). The RLK/Pelle family of kinases. *Plant J.* 66, 117–127. doi: 10.1111/j.1365-313X.2011.04518.x

Guo, Y., Han, L., Hymes, M., Denver, R., and Clark, S. E. (2010). CLAVATA2 forms a distinct CLE-binding receptor complex regulating Arabidopsis stem cell specification. *Plant J.* 63, 889–900. doi: 10.1111/j.1365-313X.2010.04295.x

Hecht, V., Vielle-Calzada, J. P., Hartog, M. V., Schmidt, E. D. L., Boutilier, K., Grossniklaus, U., et al. (2001). The Arabidopsis *SOMATIC EMBRYOGENESIS RECEPTOR KINASE 1* gene is expressed in developing ovules and embryos and enhances embryogenic competence in culture. *Plant Phys.* 127, 803–816. doi: 10.1104/pp.010324

Heo, L., Park, H., and Seok, C. (2013). GalaxyRefine: protein structure refinement driven by side-chain repacking. *Nucleic Acids Res.* 41, W384–W388. doi: 10.1093/nar/gkt458

Horn, M. A., and Walker, J. C. (1994). Biochemical properties of the autophosphorylation of RLK5, a receptor-like protein kinase from *Arabidopsis thaliana*. *Biochim. Biophys. Acta* 1208, 65–74. doi: 10.1016/0167-4838(94)90160-0

Huse, M., and Kuriyan, J. (2002). The conformational plasticity of protein kinases. *Cell* 109, 275–282. doi: 10.1016/S0092-8674(02)00741-9

Johnson, L. N., Noble, M. E., and Owen, D. J. (1996). Active and inactive protein kinases: structural basis for regulation. *Cell* 85, 149–158. doi: 10.1016/S0092-8674(00)81092-2

Karlova, R., Boeren, S., Van Dongen, W., Kwaaitaal, M., Aker, J., Vervoort, J., et al. (2009). Identification of in vitro phosphorylation sites in the *Arabidopsis thaliana* somatic embryogenesis receptor-like kinases. *Proteomics* 9, 368–379. doi: 10.1002/pmic.200701059

Kwezi, L., Ruzvidzo, O., Wheeler, J. I., Govender, K., Iacuone, S., Thompson, P. E., et al. (2011). The phytosulfokine (PSK) receptor is capable of guanylate cyclase activity and enabling cyclic GMP-dependent signaling in plants. *J. Biol. Chem.* 286, 22580–22588. doi: 10.1074/jbc.M110.168823

Ladwig, F., Dahlke, R. I., Stuhrwohldt, N., Hartmann, J., Harter, K., and Sauter, M. (2015). Phytosulfokine regulates growth in Arabidopsis through a response module at the plasma membrane that includes cyclic nucleotide-gated channel17, H^+-ATPase, and BAK1. *Plant Cell* 27, 1718–1729. doi: 10.1105/tpc.15.00306

Lemmon, M. A., and Schlessinger, J. (2010). Cell signaling by receptor tyrosine kinases. *Cell* 141, 1117–1134. doi: 10.1016/j.cell.2010.06.011

Li, J. (2010). Multi-tasking of somatic embryogenesis receptor-like protein kinases. *Curr. Opin. Plant Biol.* 13, 509–514. doi: 10.1016/j.pbi.2010.09.004

Li, J., Wen, J., Lease, K. A., Doke, J. T., Tax, F. E., and Walker, J. C. (2002). BAK1, an *Arabidopsis* LRR receptor-like protein kinase, interacts with BRI1 and modulates brassinosteroid signaling. *Cell* 110, 213–222. doi: 10.1016/S0092-8674(02)00812-7

Liu, G. Z., Pi, L. Y., Walker, J. C., Ronald, P. C., and Song, W. Y. (2002). Biochemical characterization of the kinase domain of the rice disease resistance receptor-like kinase XA21. *J. Biol. Chem.* 277, 20264–20269. doi: 10.1074/jbc.M110999200

Ma, X., Xu, G., He, P., and Shan, L. (2016). SERKing coreceptors for receptors. *Trends Plant Sci.* 21, 1017–1033. doi: 10.1016/j.tplants.2016.08.014

Matsubayashi, Y. (2011). Post-translational modifications in secreted peptide hormones in plants. *Plant Cell Phys.* 52, 5–13. doi: 10.1093/pcp/pcq169

Matsubayashi, Y., Matsuzaki, Y., Ogawa-Ohnishi, M., and Mori, A. (2010). Secreted peptide signals required for maintenance of root stem cell niche in *Arabidopsis*. *Science* 329, 1065–1067. doi: 10.1126/science.1191132

Matsubayashi, Y., Ogawa, M., Morita, A., and Sakagami, Y. (2002). An LRR receptor kinase involved in perception of a peptide plant hormone, phytosulfokine. *Science* 296, 1470–1472. doi: 10.1126/science.1069607

Matsubayashi, Y., and Sakagami, Y. (1996). Phytosulfokine, sulfated peptides that induce the proliferation of single mesophyll cells of *Asparagus officinalis* L. *Proc. Natl. Acad. Sci. U.S.A.* 93, 7623–7627. doi: 10.1073/pnas.93.15.7623

Meyer, M. R., Lichti, C. F., Townsend, R. R., and Rao, A. G. (2011). Identification of *in vitro* autophosphorylation sites and effects of phosphorylation on the *Arabidopsis* CRINKLY4 (ACR4) receptor-like kinase intracellular domain: insights into conformation, oligomerization, and activity. *Biochemistry* 50, 2170–2186. doi: 10.1021/bi101935x

Meyer, M. R., Shah, S., and Rao, A. G. (2013). Insights into molecular interactions between the juxtamembrane and kinase subdomains of the *Arabidopsis* Crinkly-4 receptor-like kinase. *Arch. Biochem. Biophys.* 535, 101–110. doi: 10.1016/j.abb.2013.03.014

Murphy, E., Smith, S., and De Smet, I. (2012). Small signaling peptides in *Arabidopsis* development: how cells communicate over a short distance. *Plant Cell* 24, 3198–3217. doi: 10.1105/tpc.112.099010

Nam, K. H., and Li, J. (2002). BRI1/BAK1, a receptor kinase pair mediating brassinosteroid signaling. *Cell* 110, 203–212. doi: 10.1016/S0092-8674(02)00814-0

Oh, M. H., Ray, W. K., Huber, S. C., Asara, J. M., Gage, D. A., and Clouse, S. D. (2000). Recombinant brassinosteroid insensitive 1 receptor-like kinase autophosphorylates on serine and threonine residues and phosphorylates a conserved peptide motif in vitro. *Plant Physiol.* 124, 751–766. doi: 10.1104/pp.124.2.751

Oh, M. H., Wang, X., Kim, S. Y., Wu, X., Clouse, S. D., and Huber, S. C. (2014). The Carboxy-terminus of BAK1 regulates kinase activity and is required for normal growth of *Arabidopsis*. *Front. Plant Sci.* 5:16. doi: 10.3389/fpls.2014.00016

Petutschnig, E. K., Jones, A. M., Serazetdinova, L., Lipka, U., and Lipka, V. (2010). The lysin motif receptor-like kinase (LysM-RLK) CERK1 is a major chitin-binding protein in *Arabidopsis thaliana* and subject to chitin-induced phosphorylation. *J. Biol. Chem.* 285, 28902–28911. doi: 10.1074/jbc.M110.116657

Sali, A., and Blundell, T. L. (1993). Comparative protein modelling by satisfaction of spatial restraints. *J. Mol. Biol.* 234, 779–815. doi: 10.1006/jmbi.1993.1626

Sauter, M., Kutschmar, A., Rzewuski, G., Stuhrwohldt, N., Beemster, G. T. S., and Inze, D. (2009). PSK-alpha promotes root growth in Arabidopsis. *New Phytol.* 181, 820–831. doi: 10.1111/j.1469-8137.2008.02710.x

Schulze, B., Mentzel, T., Jehle, A. K., Mueller, K., Beeler, S., Boller, T., et al. (2010). Rapid heteromerization and phosphorylation of ligand-activated plant transmembrane receptors and their associated kinase BAK1. *J. Biol. Chem.* 285, 9444–9451. doi: 10.1074/jbc.M109.096842

Schulze-Muth, P., Irmler, S., Schroder, G., and Schroder, J. (1996). Novel type of receptor-like protein kinase from a higher plant (*Catharanthus roseus*). cDNA, gene, intramolecular autophosphorylation, and identification of a threonine important for auto- and substrate phosphorylation. *J. Biol. Chem.* 271, 26684–26689. doi: 10.1074/jbc.271.43.26684

Schwessinger, B., and Ronald, P. C. (2012). Plant innate immunity: perception of conserved microbial signatures. *Annu. Rev. Plant Biol.* 63, 451–482. doi: 10.1146/annurev-arplant-042811-105518

Shah, K., Vervoort, J., and De Vries, S. C. (2001). Role of threonines in the *Arabidopsis thaliana* somatic embryogenesis receptor kinase 1 activation loop in phosphorylation. *J. Biol. Chem.* 276, 41263–41269. doi: 10.1074/jbc.M102381200

Shiu, S. H., and Bleecker, A. B. (2001). Receptor-like kinases from *Arabidopsis* form a monophyletic gene family related to animal receptor kinases. *Proc. Natl. Acad. Sci. U.S.A.* 98, 10763–10768. doi: 10.1073/pnas.181141598

Stührwohldt, N., Dahlke, R. I., Steffens, B., Johnson, A., and Sauter, M. (2011). Phytosulfokine-α controls hypocotyl length and cell expansion in *Arabidopsis thaliana* through Phytosulfokine receptor 1. *PLOS ONE* 6:e21054. doi: 10.1371/journal.pone.0021054

Sun, W., Cao, Y., Jansen Labby, K., Bittel, P., Boller, T., and Bent, A. F. (2012). Probing the *Arabidopsis* flagellin receptor: FLS2-FLS2 association and the contributions of specific domains to signaling function. *Plant Cell* 24, 1096–1113. doi: 10.1105/tpc.112.095919

Swaney, D. L., Mcalister, G. C., and Coon, J. J. (2008). Decision tree-driven tandem mass spectrometry for shotgun proteomics. *Nat. Methods* 5, 959–964. doi: 10.1038/nmeth.1260

Tang, D., Wang, G., and Zhou, J. M. (2017). Receptor kinases in plant-pathogen interactions: more than pattern recognition. *Plant Cell* 29, 618–637. doi: 10.1105/tpc.16.00891

Taylor, I., Seitz, K., Bennewitz, S., and Walker, J. C. (2013). A simple *in vitro* method to measure autophosphorylation of protein kinases. *Plant Methods* 9:22. doi: 10.1186/1746-4811-9-22

Wang, J. Z., Li, H. J., Han, Z. F., Zhang, H. Q., Wang, T., Lin, G. Z., et al. (2015). Allosteric receptor activation by the plant peptide hormone phytosulfokine. *Nature* 525, 265–268. doi: 10.1038/nature14858

Wang, X., Goshe, M. B., Soderblom, E. J., Phinney, B. S., Kuchar, J. A., Li, J., et al. (2005a). Identification and functional analysis of in vivo phosphorylation sites of the Arabidopsis BRASSINOSTEROID-INSENSITIVE1 receptor kinase. *Plant Cell* 17, 1685–1703.

Wang, X., Kota, U., He, K., Blackburn, K., Li, J., Goshe, M. B., et al. (2008). Sequential transphosphorylation of the BRI1/BAK1 receptor kinase complex impacts early events in brassinosteroid signaling. *Dev. Cell* 15, 220–235. doi: 10.1016/j.devcel.2008.06.011

Wang, X., Li, X., Meisenhelder, J., Hunter, T., Yoshida, S., Asami, T., et al. (2005b). Autoregulation and homodimerization are involved in the activation of the plant steroid receptor BRI1. *Dev. Cell* 8, 855–865.

Williams, R. W., Wilson, J. M., and Meyerowitz, E. M. (1997). A possible role for kinase-associated protein phosphatase in the *Arabidopsis* CLAVATA1 signaling pathway. *Proc. Natl. Acad. Sci. U.S.A.* 94, 10467–10472. doi: 10.1073/pnas.94.19.10467

Xu, W. H., Wang, Y. S., Liu, G. Z., Chen, X., Tinjuangjun, P., Pi, L. Y., et al. (2006). The autophosphorylated Ser686, Thr688, and Ser689 residues in the intracellular juxtamembrane domain of XA21 are implicated in stability control of rice receptor-like kinase. *Plant J.* 45, 740–751. doi: 10.1111/j.1365-313X.2005.02638.x

Yan, L., Ma, Y., Liu, D., Wei, X., Sun, Y., Chen, X., et al. (2012). Structural basis for the impact of phosphorylation on the activation of plant receptor-like kinase BAK1. *Cell Res.* 22, 1304–1308. doi: 10.1038/cr.2012.74

Yoshida, S., and Parniske, M. (2005). Regulation of plant symbiosis receptor kinase through serine and threonine phosphorylation. *J. Biol. Chem.* 280, 9203–9209. doi: 10.1074/jbc.M411665200

Conflict of Interest Statement: The authors declare that the research was conducted in the absence of any commercial or financial relationships that could be construed as a potential conflict of interest.

frontiers in Plant Science

ORIGINAL RESEARCH
published: 23 November 2017
doi: 10.3389/fpls.2017.01988

Excessive Cellular *S*-nitrosothiol Impairs Endocytosis of Auxin Efflux Transporter PIN2

Min Ni[1†], *Lei Zhang*[1†], *Ya-Fei Shi*[1†], *Chao Wang*[2†], *Yiran Lu*[1], *Jianwei Pan*[1,2] *and Jian-Zhong Liu*[1*]

[1] College of Chemistry and Life Sciences, Zhejiang Normal University, Jinhua, China, [2] Ministry of Education Key Laboratory of Cell Activities and Stress Adaptations, School of Life Sciences, Lanzhou University, Lanzhou, China

S-nitrosoglutathione reductase (GSNOR1) is the key enzyme that regulates cellular levels of *S*-nitrosylation across kingdoms. We have previously reported that loss of GSNOR1 resulted in impaired auxin signaling and compromised auxin transport in Arabidopsis, leading to the auxin-related morphological phenotypes. However, the molecular mechanism underpinning the compromised auxin transport in *gsnor1-3* mutant is still unknown. Endocytosis of plasma-membrane (PM)-localized efflux PIN proteins play critical roles in auxin transport. Therefore, we investigate whether loss of GSNOR1 function has any effects on the endocytosis of PIN-FORMED (PIN) proteins. It was found that the endocytosis of either the endogenous PIN2 or the transgenically expressed PIN2-GFP was compromised in the root cells of *gsnor1-3* seedlings relative to Col-0. The internalization of PM-associated PIN2 or PIN2-GFP into Brefeldin A (BFA) bodies was significantly reduced in *gsnor1-3* upon BFA treatment in a manner independent of *de novo* protein synthesis. In addition, the exogenously applied GSNO not only compromised the endocytosis of PIN2-GFP but also inhibited the root elongation in a concentration-dependent manner. Taken together, our results indicate that, besides the reduced PIN2 level, one or more compromised components in the endocytosis pathway could account for the reduced endocytosis of PIN2 in *gsnor1-3*.

Keywords: endocytosis, nitric oxide, PIN-FORMED (PIN) proteins, polar auxin transport, *S*-nitrosoglutathione reductase

OPEN ACCESS

Edited by:
Kai He,
Lanzhou University, China

Reviewed by:
Frantisek Baluska,
University of Bonn, Germany
Norbert Rolland,
Centre National de la Recherche Scientifique (CNRS), France

***Correspondence:**
Jian-Zhong Liu
jzliu@zjnu.cn

[†] *These authors have contributed equally to this work.*

Specialty section:
This article was submitted to Plant Traffic and Transport, a section of the journal Frontiers in Plant Science

Received: *06 July 2017*
Accepted: *03 November 2017*
Published: *23 November 2017*

Citation:
Ni M, Zhang L, Shi Y-F, Wang C, Lu Y, Pan J and Liu J-Z (2017) Excessive Cellular S-nitrosothiol Impairs Endocytosis of Auxin Efflux Transporter PIN2. Front. Plant Sci. 8:1988. doi: 10.3389/fpls.2017.01988

INTRODUCTION

Nitric oxide (NO) is a reactive free radical gaseous molecule that is involved in battery of biological processes both in animals and plants (Wendehenne et al., 2014). In plants, NO participates in biological processes such as stomatal closure, cell death and disease resistance, abiotic stress, flowering, and many other processes (Durner et al., 1998; Klessig et al., 2000; Neill et al., 2002; Lamattina et al., 2003; He et al., 2004, 2012; Wendehenne et al., 2004, 2014; Zeidler et al., 2004; Lee et al., 2008; Xuan et al., 2010; Fan and Liu, 2012; Lin et al., 2012; Ye et al., 2012; Mur et al., 2013).

S-nitrosylation, adding NO moiety to a protein, is a novel mechanisms by which NO regulates protein functions (Hess and Stamler, 2012; Wendehenne et al., 2014). This non-enzymatic reversible protein modification is analogous to protein phosphorylation (Stamler et al., 1992; Hess et al., 2005). Many proteins have been identified as targets of *S*-nitrosylation and their functions

are regulated by this modification (Lindermayr et al., 2005; Forrester et al., 2009; Hess and Stamler, 2012; Yang et al., 2015). In plants, the target cysteine residues of some *S*-nitrosylated proteins have been identified and the functional importance of this modification is unraveled (Lindermayr et al., 2006, 2010; Belenghi et al., 2007; Romero-Puertas et al., 2007; Serpa et al., 2007; Tada et al., 2008; Chen et al., 2009; Wang et al., 2009, 2015; Yun et al., 2011; Astier et al., 2012; Feng et al., 2013; Yang et al., 2015; Hu et al., 2017; Liu et al., 2017).

The level of cellular protein *S*-nitrosylation is dynamic and governed by NO levels and de-nitrosylation catalyzed by *S*-nitrosoglutathione reductase (GSNOR) (Liu et al., 2001; Feechan et al., 2005) and thioredoxin (Tada et al., 2008; Benhar et al., 2009; Sengupta and Holmgren, 2012). GSNOR is the key enzyme controlling *S*-nitrosoglutathione (GSNO) levels by reducing GSNO to oxidized GSH and NH_3 and thus indirectly controls the cellular levels of *S*-nitrosylated proteins (Liu et al., 2001, 2004; Feechan et al., 2005).

Auxin is one of mostly studied plant hormone that plays diverse roles in development (Teale et al., 2006). Auxin gradients, which are created and maintained by groups of transporters localized on plasma membrane (PM) are critical to auxin functions in the regulation of stem cell differentiation, the initiation of lateral organs and gravitropic responses (Woodward and Bartel, 2005; Leyser, 2006; Petrásek and Friml, 2009). One of the most important transporters is the PIN-FORMED (PIN) family of auxin efflux proteins (Chen et al., 1998; Galweiler et al., 1998; Muller et al., 1998; Geldner et al., 2001; Blilou et al., 2005; Wisniewska et al., 2006; Pan et al., 2009).

Clathrin-mediated endocytosis (CME) is an evolutionally conserved pathway that plays a critical role in determining protein abundance at the PM and/or the trans-Golgi network (TGN) during signaling transductions and retargeting/degradation of proteins at PM (Chen et al., 2011; McMahon and Boucrot, 2011; Wang et al., 2013). CME is the predominant pathway for the internalization of numerous membrane-localized proteins including PINs (Paciorek et al., 2005). By inhibiting the endocytosis of PIN, auxin increases levels of various PINs at the PM (Paciorek et al., 2005). As a result, auxin promotes its own efflux by vesicle-trafficking-dependent mechanism (Paciorek et al., 2005). In addition to CME, a BFA-insensitive and clathrin-independent endocytic route has also been reported for PM resident proteins (Beck et al., 2012).

We have previously reported that loss of GSNOR1 function in Arabidopsis impairs both auxin signaling and polar auxin transport and thereby the *gsnor1-3* mutant displays multiple auxin-related morphological defects including short and highly branched statures, short primary roots, and lack of lateral roots. The compromised polar auxin transport in *gsnor1-3* is due to universally reduced levels of auxin efflux transporters PIN proteins at the plasma membrane (PM) (Shi et al., 2015). However, whether loss of GSNOR1 inhibits polar auxin transport exclusively through reducing the abundance of PINs at PM or additional mechanisms are also involved, are largely unknown. Here, we showed that loss of GSNOR1 inhibited the internalization of either the transgenically expressed PIN2-GFP or the endogenous PIN2 independent of *de novo* protein synthesis and this inhibition could be recapitulated by exogenously applied GSNO. Furthermore, similar to loss of GSNOR1, exogenously applied GSNO inhibited the root elongation in a concentration dependent manner. Together, our results reveal an additional layer of complex roles of NO in regulating plant growth and development through modulating internalization of auxin efflux transporter.

Abbreviations: 2,4-D, 2,4-dichloropheenoxyacetic; CME, Clathrin-mediated endocytosis; CHX, cycloheximide; NO, Nitric oxide; GSNO, *S*-nitrosoglutathione; GSNOR1, *S*-nitrosoglutathione reductase 1; SNO, *S*-nitrosothiol; TGN, Trans-Golgi network.

RESULTS

Loss of GSNOR1 Results in Reduced Internalization of Transgenically Expressed PIN2-GFP

To examine the effect of NO signaling on the internalization of the PM-associated PIN proteins, we used Brefeldin A (BFA; 50 μM), a vesicle trafficking inhibitor (Geldner et al., 2001), to visualize the PIN2-GFP internalization in the wild-type and *gsnor1-3* seedlings that express the *PIN2-GFP* driven by its native promoter (*ProPIN2:PIN2-GFP*). Consistent with our previous report (Shi et al., 2015), the intensity of the PIN2-GFP fluorescence at the PM was significantly reduced in *gsnor1-3* mutants relative to the wild-type cells under mock conditions (compare **Figures 1A,D;** and **Figure 1G**). As expected, both the numbers and the relative intensities of the PIN2-GFP-labeled BFA bodies were also significantly reduced in the *gsnor1-3* compared to the wild-type cells (compare white arrow-pointed BFA bodies in **Figures 1B,E**; and see statistical data in **Figures 1H,I**), indicating that the internalization of the PIN2-GFP was reduced in the *gsnor1-3* mutants. To dissect whether the reduced numbers and intensities of the BFA-induced PIN2-GFP fluorescent bodies in *gsnor1-3* is exclusively resulted from the reduced levels of PIN2-GFP at the PM, we further analyzed the ratios of GFP signals in BFA bodies to those at the PM both in Col-0 and *gsnor1-3*, respectively, after BFA treatment. As shown in **Figure 1J**, the GFP signal ratio of BFA bodies/PM was significantly lower in *gsnor1-3* mutants than in the wild-type cells, indicating that, besides the reduced level of the PIN2-GFP at the PM, PIN2-GFP internalization itself is also compromised in the *gsnor1-3* mutant seedlings.

Auxin inhibits internalization of PM proteins (Paciorek et al., 2005). To address whether auxin inhibitory effect on PIN2 endocytosis is altered in the *gsnor1-3* mutants, we treated the transgenic seedlings expressing the PIN2-GFP both in the Col-0 and the *gsnor1-3* firstly with 10 μM 2,4-D for 30 min and followed by treatment with 10 μM 2,4-D plus 50 μM BFA for additional 60 min as described (Wang et al., 2013). As shown in **Figure 1**, 2,4-D similarly blocked the PIN2-GFP internalization both in the wild-type and the mutant cells (compare 1C and 1F), indicating that auxin inhibition of PIN2 internalization is not significantly impaired in the *gsnor1-3* mutant.

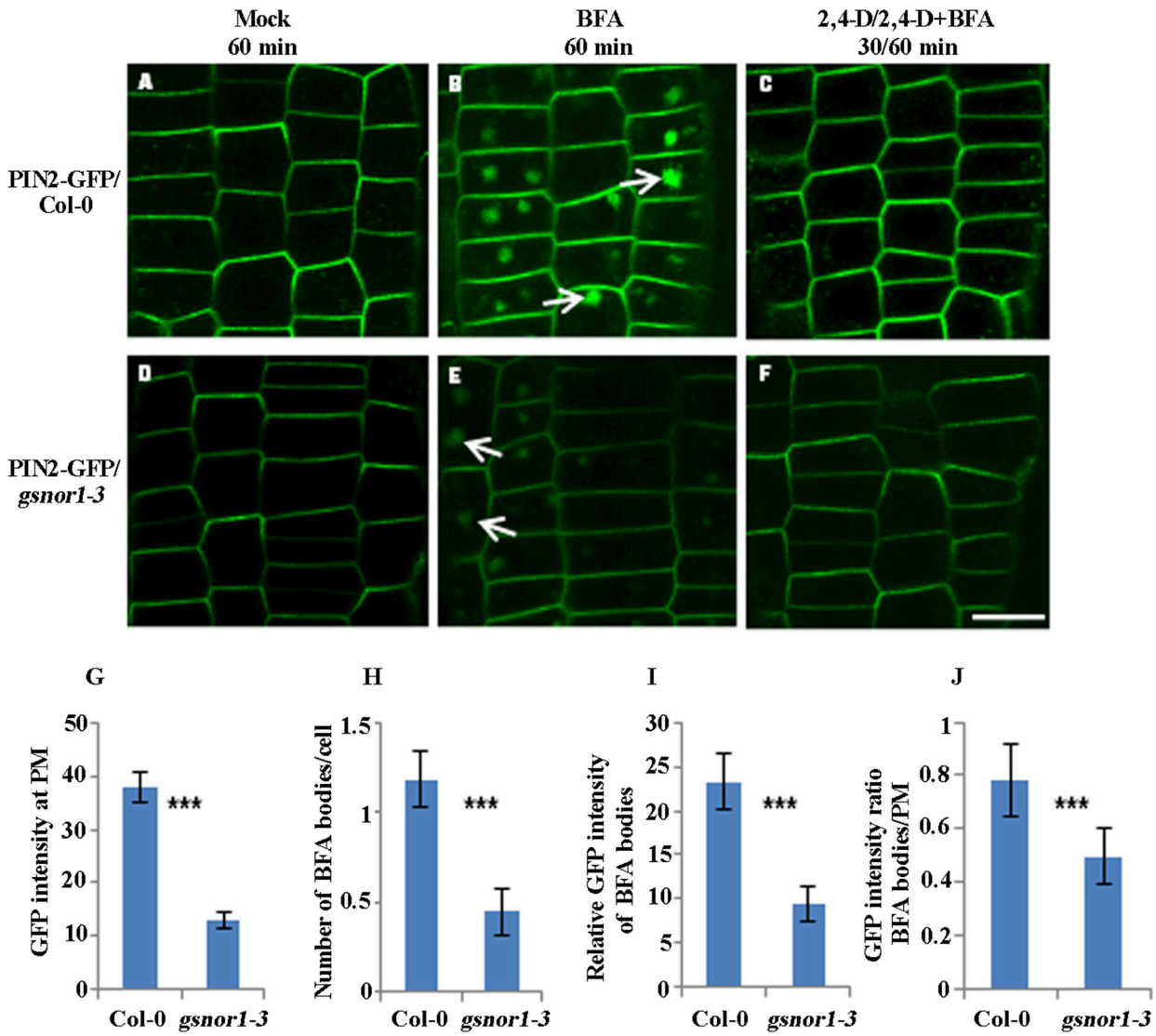

FIGURE 1 | The internalization and not the auxin inhibition of internalization of the transgenically expressed PIN2-GFP is impaired in *gsnor1-3* mutant. Six-day-old *ProPIN2:PIN2-GFP*-expressing transgenic seedlings either in Col-0 or in *gsnor1-3* background were treated with Mock **(A,D)**, 50 μM BFA for 60 min **(B,E),** and with 10 μM 2, 4-D for 30 min, followed by treatment with 50 μM BFA+ 10 μM 2, 4-D for additional 60 min **(C,F)**. Images were captured by confocal laser scanning microscopy (CLSM, Leica TCS SP5 AOBS). The numbers of BFA bodies (see white arrows) were counted and the fluorescence intensities both at the BFA bodies and at the PM were measured, respectively, using Image J (http://rsb.info.nih.gov/ij) and the statistical data were summarized **(G–J)**. **(G)** GFP intensity at the PM; **(H)** Number of BFA bodies per cell; **(I)** Relative GFP intensities of the BFA bodies; **(J)** The GFP intensity ratios of the BFA bodies/PM. Bar = 50 μm. ***Indicates significant differences between Col-0 and *gsnor1-3* by Student's *t*-test at 0.001 level.

Loss of GSNOR1 Results in Reduced Internalization of the Endogenous PIN2

Next, to test whether the internalization of endogenous PIN2 is similarly impaired as PIN2-GFP in the *gsnor1-3* mutant, we performed immunofluorescence microscopy analysis using affinity-purified anti-PIN2-specific antibodies (Wang et al., 2013). Similar to the PIN2-GFP shown in **Figure 1**, the level of the PM-localized endogenous PIN2 was significantly reduced in the *gsnor1-3* cells compared to the wild-type cells under the mock conditions (compare **Figures 2A,D** and **Figure 2G**). Similarly, the numbers and the relative intensities of PIN2-labeled BFA bodies (compare the white arrow-pointed BFA bodies in **Figures 2B,E**; also see statistical data in **Figures 2H,I**) and the fluorescence intensity ratio of BFA bodies/PM of the endogenous PIN2 (**Figure 2J**) were all significantly decreased in the *gsnor1-3* mutant compared to the wild-type cells. Again, the inhibition of the PIN2 internalization in the presence of 2,4-D was not significantly altered in the *gsnor1-3* mutant compared to the Col-0 cells (**Figures 2C,F**, no visible BFA bodies). These results confirmed the conclusions drawn from

the studies using the *ProPIN2:PIN2-GFP*-expressing transgenic seedlings (**Figure 1**), suggesting that the transgenic expressed PIN2-GFP driven by its own promoter can recapitulate the endogenous PIN2.

Loss of GSNOR1 Results in the Reduced Endocytosis of PIN2-GFP in the Absence of *de novo* Protein Synthesis

To accurately assess the effect of loss of GSNOR1 on the internalization of PM-localized PIN2-GFP, the interference of the newly synthesized PIN2-GFP on the level of PM-localized PIN2-GFP must be excluded. To do so, we firstly treated the 6-day-old seedlings with cycloheximide (CHX; 50 μM), an inhibitor of *de novo* protein synthesis, and followed by washout with CHX plus BFA. As shown in **Figure 3**, the GFP intensity on the PM, the number of BFA bodies per cell and the relative GFP intensity of BFA bodies were all significantly reduced in *gsnor1-3* mutant seedlings relative to the wild-type cells after treatment with CHX for 30 min and followed by washout with CHX and BFA for additional 15 min or 60 min (Compare **Figure 3A** and **Figure 3D**; **Figure 3B** and **Figure 3E**; **Figure 3C** and **Figure 3F**; and see statistical data shown in **Figures 3G–I**). Consistent with the results obtained without CHX treatment (**Figure 1I**), the GFP intensity ratio of BFA bodies/PM was significantly reduced in the *gsnor1-3* mutant cells relative to the wild-type cells after CHX and BFA co-treatment (**Figure 3J**). Accordingly, the relative level of the PM-localized GFP signal was higher in the *gsnor1-3* than in Col-0 after CHX and BFA co-treatment (**Figure 3K**). These results again indicate that the PIN2-GFP internalization is impaired in the *gsnor1-3* even without *de novo* protein synthesis.

The Exogenously Applied GSNO Recapitulates the Loss of GSNOR1 in Inhibiting PIN2-GFP Internalization

We reasoned that if the impaired internalization of the PIN2-GFP or PIN2 observed in the *gsnor1-3* (**Figures 1–3**) is indeed resulted from over-accumulation of cellular SNO, the exogenously applied GSNO should have a similar inhibitory effect on PIN2 internalization. To test this hypothesis, we tested the effect of exogenous GSNO treatment on the PIN2-GFP internalization in the wild-type cells. Consistent with the results obtained using the *gsnor1-3* mutant (**Figures 1**, **2**), exogenously applied GSNO not only reduced the level of the PM-localized PIN2-GFP (**Figures 4A–C**) but also inhibited the PIN2-GFP internalization in the presence of BFA in a concentration-dependent manner (**Figures 4E–G**, and statistical data in **Figures 4I,J**). These results suggest that the impaired polar auxin transport observed in the *gsnor1-3* mutant seedlings (Shi et al., 2015) could be resulted at least partially from the reduced internalization of PIN2 (**Figures 4D,H–J**).

Exogenous GSNO Inhibits Root Elongation in a Concentration Dependent Manner

Our previous studies have shown that loss of GSNOR1 impairs auxin signaling and transport and the *gsnor1-3* mutant plants display a wide range of auxin-related morphological defects including a short root phenotype (Shi et al., 2015). We postulated that if the short root phenotype observed in the *gsnor1-3* mutant seedlings is indeed a consequence of cellular SNO over-accumulation, the exogenously applied GSNO could mimic the effects of the loss-of-function mutant of GSNOR1. To test this postulation, we treated the Col-0 seedlings with different concentrations of GSNO and used the *gsnor1-3* mutant seedlings as a control. As expected, the exogenously applied GSNO inhibited the root elongation of the wild type seedlings in a concentration-dependent manner (**Figures 5A–C**), confirming that the excessive cellular SNO is at least partially, if not fully, responsible for the short root phenotype of the *gsnor1-3* mutant seedlings (**Figures 5D,E**, and Shi et al., 2015).

DISCUSSION

It is not an uncommon phenomenon that phytohormones play roles in regulating CME. It has been reported that strigolactones affect shoot branching by modulating the endocytosis of PIN1 (Shinohara et al., 2013), and salicylic acid (SA) represses endocytosis of different PM-associated proteins by blocking clathrin recruitment at the PM (Du et al., 2013). Auxin inhibits the CME of several PM-localized proteins, including several PIN proteins (Paciorek et al., 2005). As a result, auxin promotes its own efflux by inhibiting the internalization of PINs and increases various PIN levels at the PM (Paciorek et al., 2005). In this report, we provided evidence that NO, the other phytohormone, also play a role in the regulation of PIN2 endocytosis.

Our previous results have shown that even though the transcript level of *PIN2-GFP* was higher in the *gsnor1-3* mutant than in the wild type Col-0, the intensity of PIN2-GFP at the PM was significantly reduced in the *gsnor1-3* mutant relative to the wild-type plants (Shi et al., 2015). Likely, the reduced accumulation of PIN2 at the PM in the *gsnor1-3* could be partially resulted from compromised protein synthesis and/or stability and the reduced levels of the various PIN proteins in the *gsnor1-3* could be the primary cause of the compromised polar auxin transport (Shi et al., 2015). However, our present data uncover that, in addition to the reduced level of PIN2 at the PM, the internalizations of PIN2 was also compromised in the *gsnor1-3* mutant seedlings (**Figures 1–3**). Post-translational modifications play critical roles in regulating endocytosis. Both mono- and poly-ubiquitylation of single lysine is associated with cargo internalization and the intracellular sorting and targeting of PM proteins to the vacuole/lysosome rely on K63-linked ubiquitylation (Luschnig and Vert, 2014). PIN2 is modified by K63-linked poly-ubiquitin chains, which dependent on a class of ring-domain E3 ligase (RGLGs) (Yin et al., 2007; Leitner et al., 2012). Protein phosphorylation has been identified as a major determinant of PIN sorting and the sorting decision is dependent on the phosphorylation status of PINs and the activity of the serine/threonine protein kinase PINOID (PID) and its related proteins impact polar PIN distribution (Friml et al., 2004). As NO can also regulate protein functions by *S*-nitrosylation, it is highly possible that NO regulates internalization either directly by *S*-nitrosylating PINs or indirectly by *S*-nitrosylating the other key

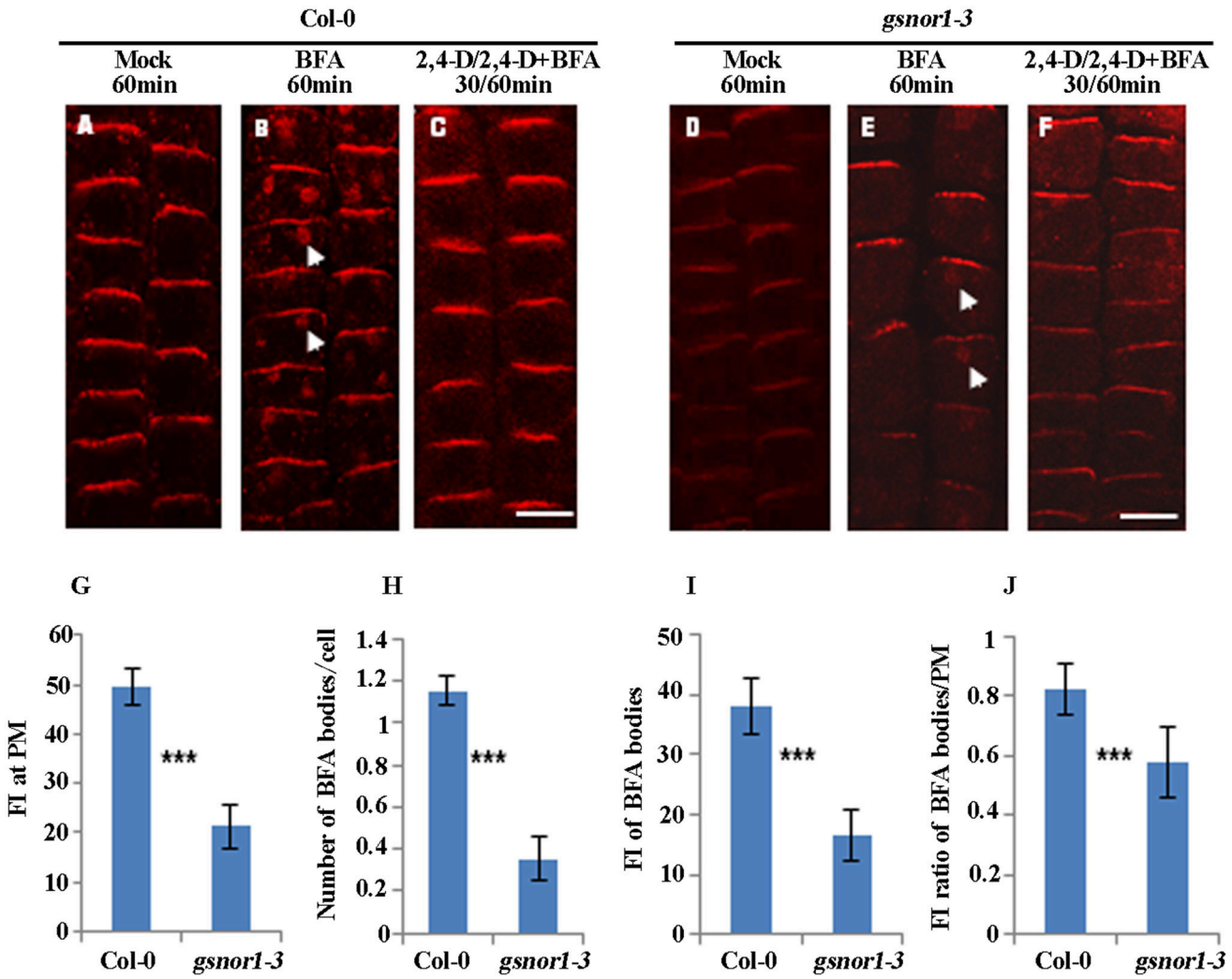

FIGURE 2 | The internalization and not the auxin inhibition of internalization of the endogenous PIN2 is impaired in *gsnor1-3* mutant. The immunolocalizations were performed using PIN2-specific antibodies (Wang et al., 2013) and Cy3-labeled anti-rabbit secondary antibodies (Sigma-Aldrich) on the primary roots of 6-day-old seedlings treated with Mock **(A,D)**, 50 μM BFA for 60 min **(B,E)** or with 10 μM 2, 4-D for 30 min, followed by treatment with 50 μM BFA+ 10 μM 2, 4-D for additional 60 min **(C,F)**. Images were captured using CLSM (Leica TCS SP5 AOBS). The numbers of BFA bodies (see white arrows) were counted and the fluorescence intensities (FI) at the BFA bodies and at the PM were measured, respectively, using Image J (http://rsb.info.nih.gov/ij) and the statistical data were summarized **(G–J)**. **(G)** Fluorescence intensity (FI) at the PM; **(H)** Number of BFA bodies per cell; **(I)** Relative fluorescence intensities (FI) of the BFA bodies; **(J)** The fluorescence intensity (FI) ratios of the BFA bodies/PM. Bar = 50 μm. ***Indicates significant differences between Col-0 and *gsnor1-3* by Student's *t*-test at 0.001 level.

proteins in the endocytic pathways. This statement is supported by the facts that the activities of many PM-resident ion channels in animals, including Na^+ and Ca^{2+} channels, are regulated by *S*-nitrosylation (Xu et al., 1998; Renganathan et al., 2002) and *S*-nitrosylation is invloved in modification of an outward-rectifying K^+ channel in *Vicia faba* (Sokolovski and Blatt, 2004).

Theoretically, the relatively enhanced level of PIN2-GFP at PM could relatively enhance the auxin polar transport (Paciorek et al., 2005). However, we observed a much reduced polar auxin transport in the *gsnor1-3* mutant primarily because of the universally reduced levels of PINs (Shi et al., 2015). One possibility is that the positive contribution of the relatively enhanced PM-localized PIN2, as a result of impaired internalizations, to polar auxin transport is masked by the inhibition resulted from the overall reduced level of PIN2 (**Figures 1**, **2**; Shi et al., 2015). The other possibility is that, even though the relative level of PM-localized PIN2 is enhanced in the *gsnor1-3* mutant relative to WT, the function of the PM-localized PIN2 is impaired under the excessive SNO condition, probably by *S*-nitrosylation. The functional endocytosis/exocytosis is required for replenishing the non-functional PM-localized PIN2 with newly synthesized functional PIN2 at PM. As a result, the reduced level of PIN2 and the compromised internalization of PIN2 (**Figures 1–3**) could contribute additively to the impaired polar auxin transport in the *gsnor1-3* mutant and thus its auxin-related morphological phenotypes.

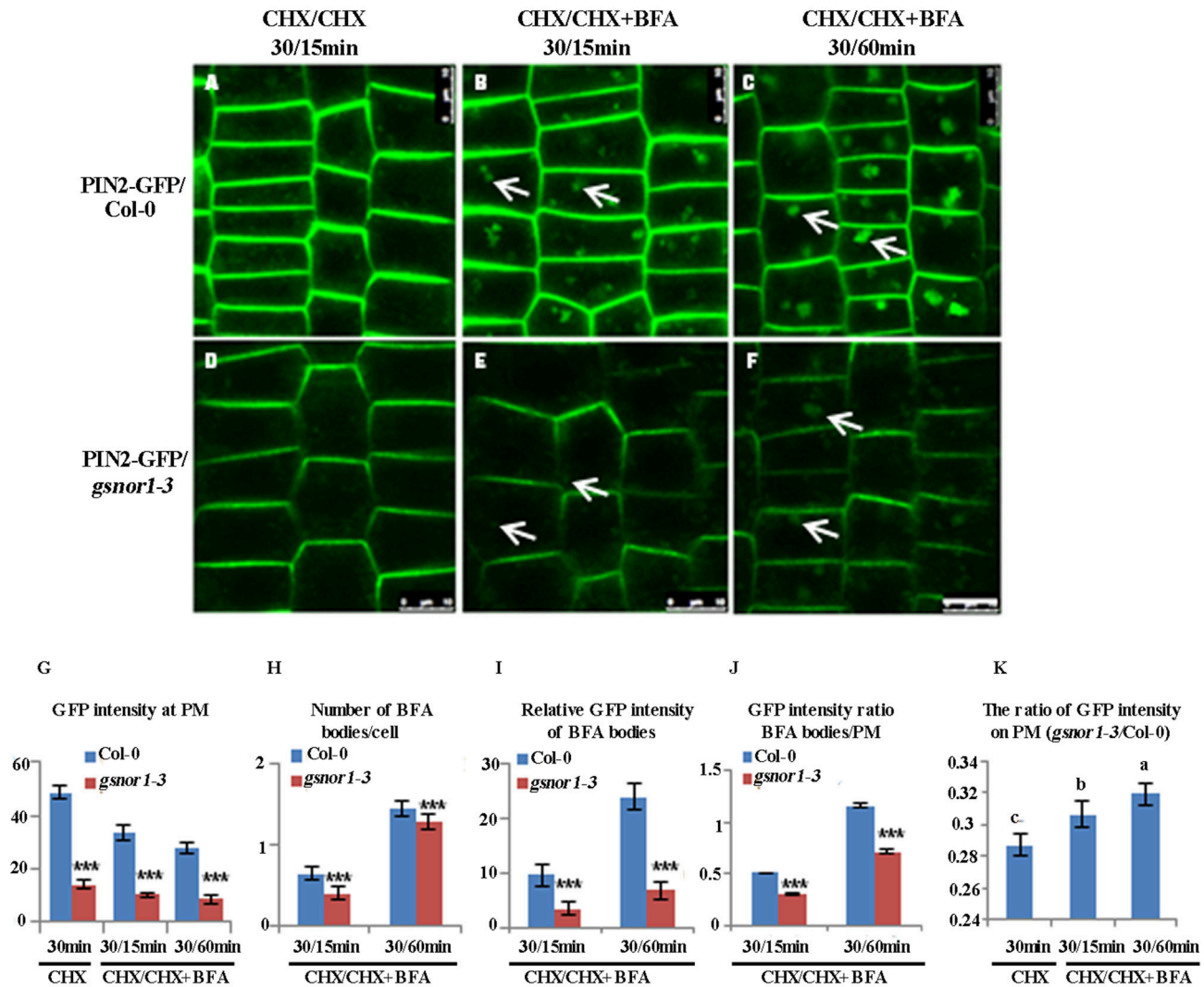

FIGURE 3 | The internalization of PIN2-GFP is reduced in *gsnor1-3* in the absence of *de novo* protein synthesis. *ProPIN2:PIN2-GFP* transgenic Col-0 and *gsnor1-3* mutant seedlings (6-day-old) were treated with cycloheximide (CHX) for 30 min first, followed by CHX alone for 15 min **(A,D)** or co-treatment with CHX+BFA for 15 **(B,E)** or 60 min **(C,F)**. Images were captured by confocal laser scanning microscopy (CLSM, Leica TCS SP5 AOBS). The numbers of BFA bodies (see white arrows) were counted and the fluorescence intensities at the BFA bodies as well as at the PM were measured, respectively, using Image J (http://rsb.info.nih.gov/ij) and the statistical data were summarized **(G–K)**. **(G)**. GFP intensity at the PM; **(H)** Number of BFA bodies per cell; **(I)** Relative GFP intensities of the BFA bodies; **(J)** GFP intensity ratios of the BFA bodies/PM; **(K)** GFP intensity ratios on PM (*gsnor1-3*/Col-0). Bar = 50 μm. ***Indicates significant differences between Col-0 and *gsnor1-3* by Student's *t*-test at 0.001 level. a, b, and c Indicate significant differences between the treatments by Student's *t*-test.

Even though the auxin signaling is significantly impaired in the *gsnor1-3* (Shi et al., 2015), the auxin inhibition of either the transgenically expressed PIN2-GFP or the endogenous PIN2 internalization is not affected in the *gsnor1-3* (**Figures 1C,F**, **2C,F**), suggesting that auxin signaling does not play a critical role in the inhibition of PIN2 internalization. In agreement with this, it has been shown that differential auxin regulation of CLC and CHC membrane association is ABP1-dependent but TIR1/AFB-independent (Wang et al., 2013) and the role of ABP1 in auxin signaling is questionable (Gao et al., 2015; Liu, 2015). Given that the clathrin are required for the auxin inhibition of the PIN2-GFP internalization (Wang et al., 2013) and the auxin inhibition of PIN2-GFP is not affected in *gsnor1-3* mutant (**Figures 1C,F**, **2C,F**), it is suggested that the reduced internalization of PIN2-GFP or endogenous PIN2 (**Figures 1**, **2**) may not be clathrin-dependent. In supporting this, it has been reported previously that the same PM protein could traffic through distinct endocytic routes (Beck et al., 2012). The activated FLS2 triggered by flg22 recognition at PM is targeted to the intracellular compartments for degradation via an ESCRT1-dependent, but BFA-insensitive route to prevent excessive and constitutive activation of defense signaling, whereas the non-activated or newly synthesized FLS2 is shuttled between PM and cytoplasm via a BFA-sensitive route (Robatzek et al., 2006; Beck et al., 2012; Spallek et al., 2013).

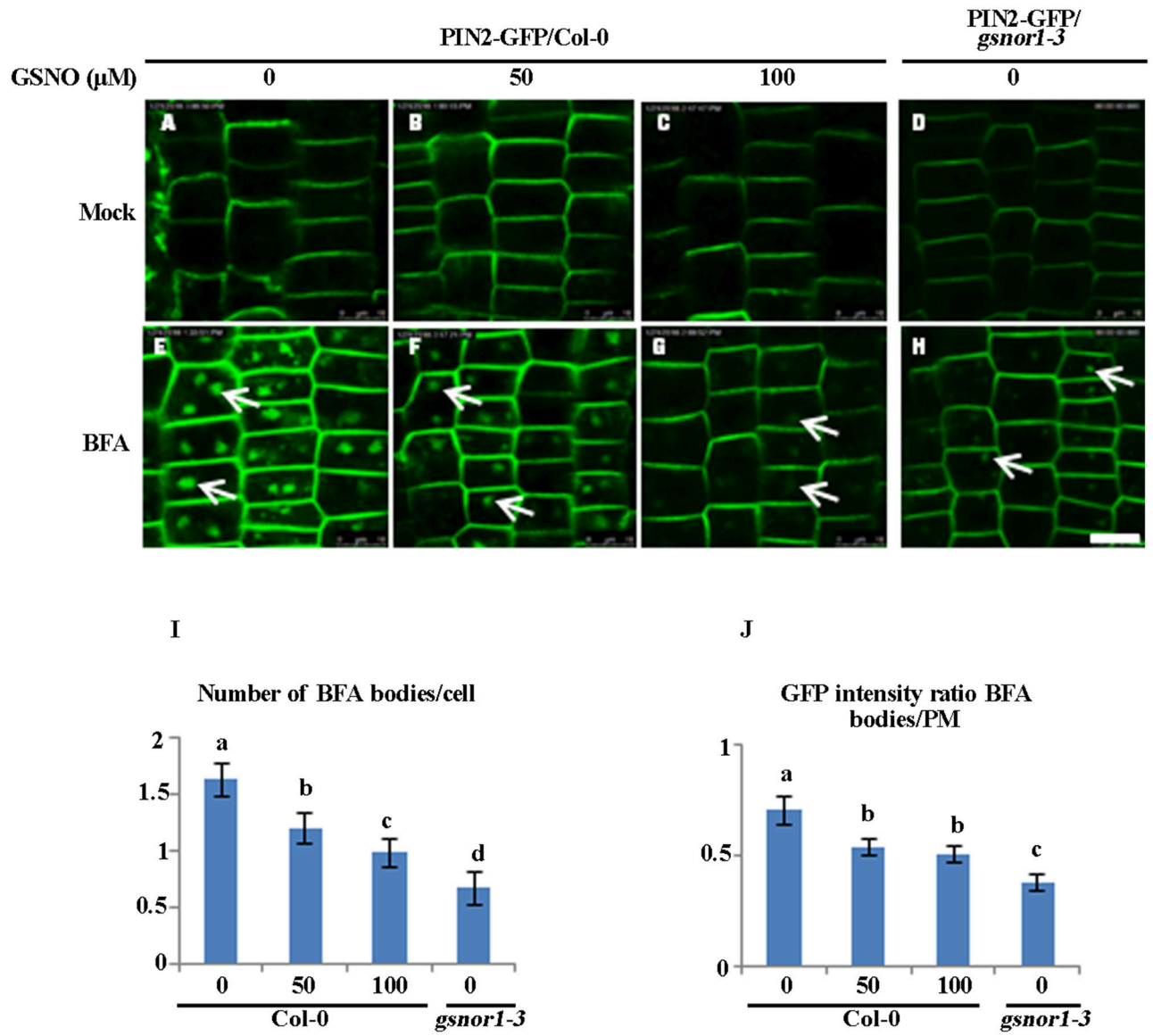

FIGURE 4 | Exogenously applied GSNO reduces both the internalization and the PM-associated level of PIN2-GFP in the Col-0 seedlings in a concentration-dependent manner. The 2-day-old wild type Col-0 seedlings grown on ½ MS agar plates were transferred onto the agar plates containing different concentration of GSNO **(A–C)**, or different concentration of GSNO plus 50 μM BFA **(E–G)** for additional 4 day. The *gsnor1-3* mutant is used as a control **(D,H)**. The images were captured by confocal laser scanning microscopy (CLSM, Leica TCS SP5 AOBS). The numbers of BFA bodies (see white arrows) were counted **(I)** and the fluorescence intensities of the BFA bodies and at the PM were measured, respectively, using Image J (http://rsb.info.nih.gov/ij). The GFP intensity ratios of BFA bodies to PM were measured and the statistical data were presented in **(J)**. Bar = 50 μm. a, b, c, and d indicate significant differences between the treatments by Student's *t*-test.

One may argue that the fluorescence intensity of some BFA bodies in *gsnor1-3* mutant (**Figures 1E**, **2E**) could be below the detection threshold under our Confocal settings, and therefore could have an impact on the fluorescence intensity ratio of BFA bodies/PM in the mutant. If that is really the case, the average fluorescence intensity of the BFA bodies within a cell or in a given captured image (5–20 root cells/image) of *gsnor1-3* root should be lower, and thus the fluorescence intensity ratio of BFA bodies/PM in the mutant should be lower than shown in **Figures 1J**, **2J**. As a result, the detection thresholds issue would not change our final conclusion that the internalization of either the transgenically expressed PIN2-GFP or the endogenous PIN2 was compromised in the *gsnor1-3* mutant.

In this report, we provided genetic and pharmaceutical evidence that the NO signaling plays an inhibitory role in PIN2 internalization. However, the molecular mechanism underlying the inhibition still remains unanswered. The questions like how NO signaling inhibits PIN2 internalization and what

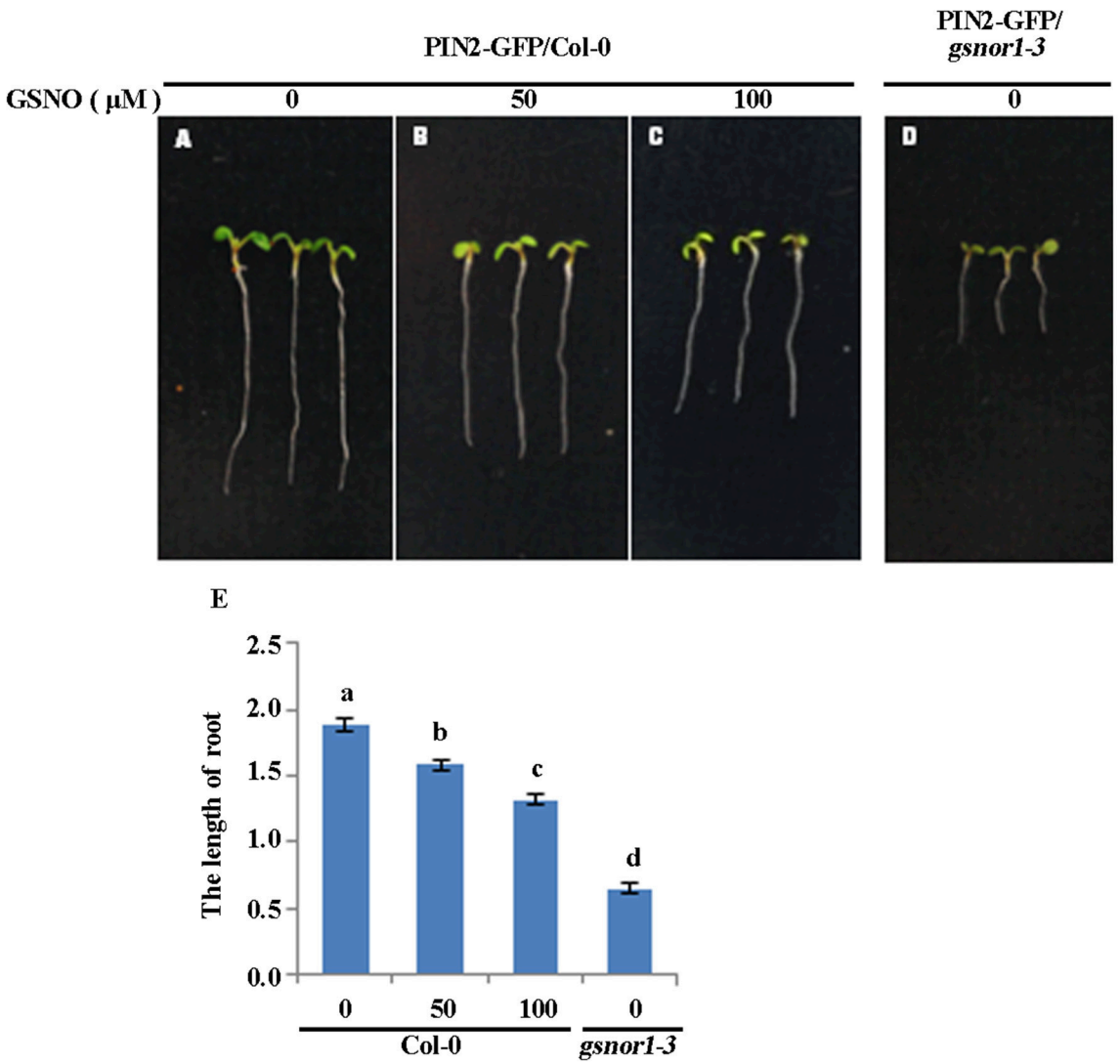

FIGURE 5 | Exogenously applied GSNO inhibits the root elongation of the Col-0 seedlings in a concentration-dependent manner. The 2-day-old seedlings of wide type Col-0 grown on ½ MS agar plates were transferred onto the agar plates supplied with 0 **(A),** 50 **(B)**, and 100 μM GSNO **(C)**. The *gsnor1-3* seedlings grown on the agar plates without containing GSNO used as a control **(D)**. The photos were taken 4 days after transfer. The root lengths were measured and listed in **(E)**. a, b, c, and d indicate significant differences between the treatments by Student's *t*-test.

is the causal relationship between the NO-inhibited PIN2 internalization and polar auxin transport need to be addressed in the future. Nonetheless, our results reveal an additional layer of complex roles of NO in regulating plant growth and development through modulating internalization of auxin efflux transporter.

MATERIALS AND METHODS

Arabidopsis Lines and Growth Conditions

Arabidopsis Col-0 and *gsnor1-3* (Feechan et al., 2005), the ProPIN2:PIN2-GFP transgenic line (Xu and Scheres, 2005) were used in this study. The ProPIN2:PIN2-GFP transgene was introgressed into the *gsnor1-3* background by crossing. The homozygous *gsnor1-3* line that expresses the *ProPIN2:PIN2-GFP* transgene was identified by the genomic PCR in combination of phenotype characterization among F3 population. These plants were grown under 16 h-light (22°C) /8h-dark (18°C). Seedlings were grown on 1/2 MS medium containing 1.0% sucrose (pH 5.7). Healthy six-day-old seedlings were used in this study.

Chemical Solutions

The stock solutions of CHX (50 mM, Sigma-Aldrich), BFA (50 mM; Invitrogen) and GSNO (100 mM, Sigma-Aldrich) were prepared in DMSO. 2,4-D (10 mM, Sigma-Aldrich) was firstly dissolved in 1 M KOH and then diluted with water as described (Wang et al., 2013).

Chemical Treatments

All chemical pretreatments except GSNO were for 30 min, and chemical treatment time is indicated in the text. For GSNO treatment, 2-day-old seedlings were transferred from GSNO-free 1/2 MS agar plates (containing 1.0% sucrose, pH 5.7) into agar plates containing different concentrations of GSNO as indicated in the text for additional 3-4 days. All seedlings were grown on MS basal salts with minimal organics (Sigma Aldrich) supplemented with 1% (w/v) Sucrose and 0.05% (w/v) MES-KOH, pH 5.6 (0.5 3 x MS), liquid medium, except otherwise specified. The final pH of the medium was 5.6–5.7.

Polyclonal Antibody and Immunofluorescence Microscopic Analysis

Polyclonal antibody, anti-AtPIN2, was raised in rabbits as described using a synthesized peptide (Wang et al., 2013) coupled with keyhole limpet hemocyanin containing an additional N-terminal Cys (Huabio). Immunofluorescence microscopic analysis was performed as described (Wang et al., 2013). The primary PIN2 antibody was detected using Cy3-labeled anti-rabbit secondary antibodies (Sigma-Aldrich). Fluorescence images were captured using CLSM (Leica TCS SP5 AOBS). Excitation wavelengths for GFP and Cy3 were 488 nm (argon laser) and 561 nm (diode laser), respectively. The emission wavelengths were 496–532 nm for GFP and 550–570 nm for Cy3, respectively. For the purpose of direct comparisons of fluorescence intensities, laser, pinhole, and gain settings of the confocal microscope were set exactly identical when capturing the images from the seedlings of different genotypes or treatments. The intensities of fluorescence signals both at the PM and the cytoplasmic vesicles were quantified on the captured digital images using Image J (http://rsb.info.nih.gov/ij) and the relative fluorescence intensities were presented as percentages of mock controls as described (Sauer et al., 2006; Robert et al., 2010). For the measurement of the fluorescence levels at the PM, optimal sections of the root cells were used for measurements. Using Image-J, PM regions of a captured images (over 20 cells for **Figure 1**; 5–10 cells for **Figures 2–4**) were selected with the rectangle tool. The mean pixel intensity readings (total intensity readings/area) for the selected PM regions were recorded and the average values were calculated subsequently. The data shown in **Figures 1**, **3**, **4** were averages from the different images captured at least from 30 individual roots. The data shown in **Figure 2** were averages from the different images captured at least from 10 individual roots. The experiments were repeated three times with similar results.

For the measurement of the fluorescence levels at the BFA bodies, the regions of the visible BFA bodies in a single cell of the captured images (over 20 cells for **Figure 1**; 5–10 cells for **Figures 2–4**) were selected with the oval tool of Image J. The mean pixel intensity readings (total intensity readings/area) for the selected regions in a single cell were recorded and the mean value of the fluorescence intensity of the BFA bodies in a single cell was calculated by dividing the number of BFA bodies in the single cell (the sum of mean values/the number of BFA bodies). The average fluorescence intensity of the BFA bodies in a captured image were calculated subsequently by dividing the number of cells in the captured image (the sum of average fluorescence intensity of the BFA bodies in a single cell/the number of cells in a captured image). The data shown in **Figures 1**, **3**, **4** were averages from different images captured from at least 30 individual roots. The data shown in **Figure 2** were averages from the different images captured at least from 10 individual roots. The experiments were repeated three times with similar results.

For calculation of the fluorescence intensity ratio of BFA/PM, the average fluorescence intensity of the BFA bodies measured in a captured image was divided by the average fluorescence intensity at the PM of the same image. The data shown in **Figures 1**, **3**, **4** were mean values of the images captured from at least 30 individual roots. The data shown in **Figure 2** were the mean values from the images captured at least from 10 individual roots. The experiments were repeated three times with similar results.

The BFA-induced internalization of PM-localized proteins was presented as the average number of fluorescence-labeled BFA bodies per cell (Robert et al., 2010). For all the quantitative data, a Student's *t* test (paired with two-tailed distribution) was used in statistical analysis.

Root Elongation Assay

The 2-day-old Col-0 seedlings grown on the 1/2 MS agar plates were transferred onto the 1/2 MS agar plates containing different concentration of GSNO for additional 3–4 days. The root length was measured under dissecting microscopy using Image J (http://rsb.info.nih.gov/ij).

AUTHOR CONTRIBUTIONS

J-ZL and JP designed the experiments. MN, LZ, Y-FS, CW and YL performed the experiments. J-ZL and JW wrote the manuscript.

FUNDING

This work was supported by the National Natural Science Foundation of China (31371401 and 31571423 to J-ZL; and 31370313 to JP), and Xin Miao Talent Program of Zhejiang Province (2016R404009).

ACKNOWLEDGMENTS

The authors thank Dr. Gary Loake for providing the *gsnor1-3* mutant. We also thank Mr. Zhen-Chao Li for his technical help in preparation of the figures.

REFERENCES

Astier, J., Kulik, A., Koen, E., Besson-Bard, A., Bourque, S., Jeandroz, S., et al. (2012). Protein S-nitrosylation: what's going on in plants? *Free Radic. Biol. Med.* 53, 1101–1110. doi: 10.1016/j.freeradbiomed.2012.06.032

Beck, M., Zhou, J., Faulkner, C., MacLean, D., and Robatzek, S. (2012). Spatio-temporal cellular dynamics of the Arabidopsis flagellin receptor reveal activation status-dependent endosomal sorting. *Plant Cell* 24, 4205–4219. doi: 10.1105/tpc.112.100263

Belenghi, B., Romero-Puertas, M. C., Vercammen, D., Brackenier, A., Inzé, D., Delledonne, M., et al. (2007). Metacaspase activity of *Arabidopsis thaliana* is regulated by S-nitrosylation of a critical cysteine residue. *J. Biol. Chem.* 282, 1352–1358. doi: 10.1074/jbc.M608931200

Benhar, M., Forrester, M. T., and Stamler, J. S. (2009). Protein denitrosylation: enzymatic mechanisms and cellular functions. *Nat. Rev. Mol. Cell Biol.* 10, 721–732. doi: 10.1038/nrm2764

Blilou, I., Xu, J., Wildwater, M., Willemsen, V., Paponov, I., Friml, J., et al. (2005). The PIN auxin efflux facilitator network controls growth and patterning in Arabidopsis roots. *Nature* 433, 39–44. doi: 10.1038/nature03184

Chen, R., Hilson, P., Sedbrook, J., Rosen, E., Caspar, T., and Masson, P. H. (1998). The *Arabidopsis thaliana* AGRAVITROPIC 1 gene encodes a component of the polar-auxin-transport efflux carrier. *Proc. Natl. Acad.Sci. U.S.A.* 95, 15112–15117. doi: 10.1073/pnas.95.25.15112

Chen, R., Sun, S., Wang, C., Li, Y., Liang, Y., An, F., et al. (2009). The Arabidopsis PARAQUAT RESISTANT2 gene encodes an S-nitrosoglutathione reductase that is a key regulator of cell death. *Cell Res.* 19, 1377–1387. doi: 10.1038/cr.2009.117

Chen, X., Irani, N. G., and Friml, J. (2011). Clathrin-mediated endocytosis: the gateway into plant cells. *Curr. Opin. Plant Biol.* 14, 674–682. doi: 10.1016/j.pbi.2011.08.006

Du, Y., Tejos, R., Beck, M., Himschoot, E., Li, H., Robatzek, S., et al. (2013). Salicylic acid interferes with clathrin-mediated endocytic protein trafficking. *Proc. Natl. Acad. Sci. U.S.A.* 110, 7946–7951. doi: 10.1073/pnas.1220205110

Durner, J., Wendehenne, D., and Klessig, D. F. (1998). Defense gene induction in tobacco by nitric oxide, cyclic GMP, and cyclic ADPribose. *Proc. Natl. Acad. Sci. U.S.A.* 95, 10328–10333. doi: 10.1073/pnas.95.17.10328

Fan, Q. J., and Liu, J. H. (2012). Nitric oxide is involved in dehydration/drought tolerance in *Poncirus trifoliata* seedlings through regulationof antioxidant systems and stomatal response. *Plant Cell Rep.* 31, 145–154. doi: 10.1007/s00299-011-1148-1

Feechan, A., Kwon, E., Yun, B. W., Wang, Y., Pallas, J. A., and Loake, G. J. (2005). A central role for S-nitrosothiols in plant disease resistance. *Proc. Natl. Acad. Sci. U.S.A.* 102, 8054–8059. doi: 10.1073/pnas.0501456102

Feng, J., Wang, C., Chen, Q., Chen, H., Ren, B., Li, X., et al. (2013). S-Nitrosylation of phosphotransfer proteins represses cytokinin signaling. *Nat. Commun.* 4:1529. doi: 10.1038/ncomms2541

Forrester, M. T., Thompson, J. W., Foster, M. W., Nogueira, L., Moseley, M. A., and Stamler, J. S. (2009). Proteomic analysis of Snitrosylation and denitrosylation by resin-assisted capture. *Nat. Biotechnol.* 27, 557–559. doi: 10.1038/nbt.1545

Friml, J., Yang, X., Michniewicz, M., Weijers, D., Quint, A., Tietz, O., et al. (2004). A PINOID-dependent binary switch in apical-basal PIN polar targeting directs auxin efflux. *Science* 306, 862–865. doi: 10.1126/science.1100618

Gälweiler, L., Guan, C., Müller, A., Wisman, E., Mendgen, K., Yephremov, A., et al. (1998). Regulation of polar auxin transport by AtPIN1 in Arabidopsis vascular tissue. *Science* 282, 2226–2230. doi: 10.1126/science.282.5397.2226

Gao, Y., Zhang, Y., Zhang, D., Dai, X., Estelle, M., and Zhao, Y. (2015). Auxin binding protein 1 (ABP1) is not required for either auxin signaling or Arabidopsis development. *Proc. Natl. Acad. Sci. U.S.A.* 112, 2275–2280. doi: 10.1073/pnas.1500365112

Geldner, N., Friml, J., Stierhof, Y. D., Jürgens, G., and Palme, K. (2001). Auxin transport inhibitors block PIN1 cycling and vesicle trafficking. *Nature* 413, 425–428. doi: 10.1038/35096571

He, Y., Tang, R. H., Hao, Y., Stevens, R. D., Cook, C. W., Ahn, S. M., et al. (2004). Nitric oxide represses the Arabidopsis floral transition. *Science* 305, 1968–1971. doi: 10.1126/science.1098837

He, H., Zhan, J., He, L., and Gu, M. (2012). Nitric oxide signaling in aluminum stress in plants. *Protoplasma* 249, 483–492. doi: 10.1007/s00709-011-0310-5

Hess, D. T., and Stamler, J. S. (2012). Regulation by S-nitrosylation of protein post-translational modification. *J. Biol. Chem.* 287, 4411–4418. doi: 10.1074/jbc.R111.285742

Hess, D. T., Matsumoto, A., Kim, S. O., Marshall, H. E., and Stamler, J. S. (2005). Protein S-nitrosylation: purview and parameters. *Nat. Rev. Mol. Cell Biol.* 6, 150–166. doi: 10.1038/nrm1569

Hu, J., Yang, H., Mu, J., Lu, T., Peng, J., Deng, X., et al. (2017). Nitric oxide regulates protein methylation during stress responses in plants. *Mol. Cell* 67, 702–710. doi: 10.1016/j.molcel.2017.06.031

Klessig, D. F., Durner, J., Noad, R., Navarre, D. A., Wendehenne, D., Kumar, D., et al. (2000). Nitric oxide and salicylic acid signaling in plant defense. *Proc. Natl. Acad. Sci. U.S.A.* 97, 8849–8855. doi: 10.1073/pnas.97.16.8849

Lamattina, L., García-Mata, C., Graziano, M., and Pagnussa, G. (2003). Nitric oxide: the versatility of an extensive signal molecule. *Annu. Rev. Plant Biol.* 54, 109–136. doi: 10.1146/annurev.arplant.54.031902.134752

Lee, U., Wie, C., Fernandez, B. O., Feelisch, M., and Vierling, E. (2008). Modulation of nitrosative stress by S-nitrosoglutathione reductase is critical for thermotolerance and plant growth in Arabidopsis. *Plant Cell* 20, 786–802. doi: 10.1105/tpc.107.052647

Leitner, J., Petrášek, J., Tomanov, K., Retzer, K., Parezova, M., Korbei, B., et al. (2012). Lysine63-linked ubiquitylation of PIN2 auxin carrier protein governs hormonally controlled adaptation of Arabidopsis root growth. *Proc. Natl. Acad. Sci. U.S.A.* 109, 8322–8327. doi: 10.1073/pnas.1200824109

Leyser, O. (2006). Dynamic integration of auxin transport and signalling. *Curr. Biol.* 16, R424–R433. doi: 10.1016/j.cub.2006.05.014

Lin, A., Wang, Y., Tang, J., Xue, P., Li, C., Liu, L., et al. (2012). Nitric oxide and protein Snitrosylation are integral to hydrogen peroxide-induced leaf cell death in rice. *Plant Physiol.* 158, 451–464. doi: 10.1104/pp.111.184531

Lindermayr, C., Saalbach, G., and Durner, J. (2005). Proteomic identification of S-nitrosylated proteins in Arabidopsis. *Plant Physiol.* 137, 921–930. doi: 10.1104/pp.104.058719

Lindermayr, C., Saalbach, G., Bahnweg, G., and Durner, J. (2006). Differential inhibition of Arabidopsis methionine adenosyltransferases by protein S-nitrosylation. *J. Biol. Chem.* 281, 4285–4291. doi: 10.1074/jbc.M511635200

Lindermayr, C., Sell, S., Müller, B., Leister, D., and Durner, J. (2010). Redox regulation of the NPR1-TGA1 system of *Arabidopsis thaliana* by nitric oxide. *Plant Cell* 22, 2894–2907. doi: 10.1105/tpc.109.066464

Liu, C. (2015). Auxin Binding Protein 1 (ABP1): a matter of fact. *J. Integr. Plant Biol.* 57, 234–235. doi: 10.1111/jipb.12339

Liu, J. Z., Duan, J., Ni, M., Liu, Z., Qiu, W. L., Whitham, S. A., et al. (2017). S-nitrosylation inhibits the kinase activity of tomato phosphoinositide-dependent kinase 1 (PDK1). *J. Biol. Chem.* doi: 10.1074/jbc.M117.803882. [Epub ahead of print].

Liu, L., Hausladen, A., Zeng, M., Que, L., Heitman, J., and Stamler, J. S. (2001). A metabolic enzyme for S-nitrosothiol conserved from bacteria to humans. *Nature* 410, 490–494. doi: 10.1038/35068596

Liu, L., Yan, Y., Zeng, M., Zhang, J., Hanes, M. A., Ahearn, G., et al. (2004). Essential roles of S-nitrosothiols in vascular homeostasis and endotoxic shock. *Cell* 116, 617–628. doi: 10.1016/S0092-8674(04)00131-X

Luschnig, G., and Vert, G. (2014). The dynamics of plant plasma membrane proteins: PINs and beyond. *Development* 141, 2924–2938. doi: 10.1242/dev.103424

McMahon, H. T., and Boucrot, E. (2011). Molecular mechanism and physiological functions of clathrin-mediated endocytosis. *Nat. Rev. Mol. Cell Biol.* 12, 517–533. doi: 10.1038/nrm3151

Muller, A., Guan, C., Gälweiler, L., Tänzler, P., Huijser, P., Marchant, A., et al. (1998). AtPIN2 defines a locus of Arabidopsis for root gravitropism control. *EMBO J.* 17, 6903–6911. doi: 10.1093/emboj/17.23.6903

Mur, L. A., Mandon, J., Persijn, S., Cristescu, S. M., Moshkov, I. E., Novikova, G. V., et al. (2013). Nitric oxide in plants: an assessment of the current state of knowledge. *AoB Plants* 5:pls052. doi: 10.1093/aobpla/pls052

Neill, S. J., Desikan, R., Clarke, A., and Hancock, J. T. (2002). Nitric oxide is a novel component of abscisic acid signaling in stomatal guard cells. *Plant Physiol.* 128, 13–16. doi: 10.1104/pp.010707

Paciorek, T., Zazímalová, E., Ruthardt, N., Petrásek, J., Stierhof, Y. D., Kleine-Vehn, J., et al. (2005). Auxin inhibits endocytosis and promotes its own efflux from cells. *Nature* 435, 1251–1256. doi: 10.1038/nature03633

Pan, J., Fujioka, S., Peng, J., Chen, J., Li, G., and Chen, R. (2009). The E3 ubiquitin ligase SCFTIR1/AFB and membrane sterols play key roles in auxin regulation of endocytosis, recycling, and plasma membrane accumulation of the auxin efflux transporter PIN2 in *Arabidopsis thaliana*. *Plant Cell* 21, 568–580. doi: 10.1105/tpc.108.061465

Petrásek, J., and Friml, J. (2009). Auxin transport routes in plant development. *Development* 136, 2675–2688. doi: 10.1242/dev.030353

Renganathan, M., Cummins, T. R., and Waxman, S. G. (2002). Nitric oxide blocks fast, slow, and persistent Na^+ channels in C-type DRG neurons by S-nitrosylation. *J. Neurophysiol.* 87, 761–775. doi: 10.1152/jn.00369.2001

Robatzek, S., Chinchilla, D., and Boller, T. (2006). Ligand-induced endocytosis of the pattern recognition receptor FLS2 in Arabidopsis. *Genes Dev.* 20, 537–542. doi: 10.1101/gad.366506

Robert, S., Kleine-Vehn, J., Barbez, E., Sauer, M., Paciorek, T., Baster, P., et al. (2010). ABP1 mediates auxin inhibition of clathrin-dependent endocytosis in Arabidopsis. *Cell* 143, 111–121. doi: 10.1016/j.cell.2010.09.027

Romero-Puertas, M. C., Laxa, M., Mattè, A., Zaninotto, F., Finkemeier, I., Jones, A. M., et al. (2007). S-nitrosylation of peroxiredoxin II E promotes peroxynitrite-mediated tyrosine nitration. *Plant Cell* 19, 4120–4130. doi: 10.1105/tpc.107.055061

Sauer, M., Paciorek, T., Benková, E., and Friml, J. (2006). Immunocytochemical techniques for whole-mount in situ protein localization in plants. *Nat. Protoc.* 1, 98–103. doi: 10.1038/nprot.2006.15

Sengupta, R., and Holmgren, A. (2012). Thioredoxin and thioredoxin reductase in relation to reversible S-nitrosylation. *Antioxid. Redox Signal.* 18, 259–269. doi: 10.1089/ars.2012.4716

Serpa, V., Vernal, J., Lamattina, L., Grotewold, E., Cassia, R., and Terenzi, H. (2007). Inhibition of AtMYB2 DNA-binding by nitric oxide involves cysteine S-nitrosylation. *Biochem. Biophys. Res. Commun.* 361, 1048–1053. doi: 10.1016/j.bbrc.2007.07.133

Shi, Y. F., Wang, D. L., Wang, C., Culler, A. H., Kreiser, M. A., Suresh, J., et al. (2015). Loss of GSNOR1 function leads to compromised auxin signaling and polar auxin transport. *Mol. Plant* 8, 1350–1365. doi: 10.1016/j.molp.2015.04.008

Shinohara, N., Taylor, C., and Leyser, O. (2013). Strigolactone can promote or inhibit shoot branching by triggering rapid depletion of the auxin efflux protein PIN1 from the plasma membrane. *PLoS Biol.* 11:e1001474. doi: 10.1371/journal.pbio.1001474

Sokolovski, S., and Blatt, M. R. (2004). Nitric oxide block of outwardrectifying K^+ channels indicates direct control by protein nitrosylation in guard cells. *Plant Physiol.* 136, 4275–4284. doi: 10.1104/pp.104.050344

Spallek, T., Beck, M., Ben Khaled, S., Salomon, S., Bourdais, G., et al. (2013). ESCRT-I Mediates FLS2 endosomal sorting and plant immunity. *PLoS Genet.* 9:e1004035. doi: 10.1371/journal.pgen.1004035

Stamler, J. S., Simon, D. I., Osborne, J. A., Mullins, M. E., Jaraki, O., Michel, T., et al. (1992). S-nitrosylation of proteins with nitric oxide: synthesis and characterization of biologically active compounds. *Proc. Natl. Acad. Sci. U.S.A.* 89, 444–448. doi: 10.1073/pnas.89.1.444

Tada, Y., Spoel, S. H., Pajerowska-Mukhtar, K., Mou, Z., Song, J., Wang, C., et al. (2008). Plant immunity requires conformational changes [corrected] of NPR1 via S-nitrosylation and thioredoxins. *Science* 321, 952–956. doi: 10.1126/science.1156970

Teale, W. D., Paponov, I. A., and Palme, K. (2006). Auxin in action: signalling, transport and the control of plant growth and development. *Nat. Rev. Mol. Cell Biol.* 7, 847–859. doi: 10.1038/nrm2020

Wang, C., Yan, X., Chen, Q., Jiang, N., Fu, W., Ma, B., et al. (2013). Clathrin light chains regulate clathrin-mediated trafficking, auxin signaling,and development in Arabidopsis. *Plant Cell* 25, 499–516. doi: 10.1105/tpc.112.108373

Wang, P., Du, Y., Hou, Y. J., Zhao, Y., Hsu, C. C., Yuan, F., et al. (2015). Nitric oxide negatively regulates abscisic acid signaling in guard cells by S-nitrosylation of OST1. *Proc. Natl. Acad. Sci. U.S.A.* 112, 613–618. doi: 10.1073/pnas.1423481112

Wang, Y. Q., Feechan, A., Yun, B. W., Shafiei, R., Hofmann, A., Taylor, P., et al. (2009). S-Nitrosylation of AtSABP3 antagonizes the expression of plant immunity. *J. Biol. Chem.* 284, 2131–2137. doi: 10.1074/jbc.M806782200

Wendehenne, D., Durner, J., Klessig, D. F. (2004). Nitric oxide: a new player in plant signalling and defence responses. *Curr. Opin. Plant Biol.* 7, 449–455.

Wendehenne, D., Gao, Q. M., Kachroo, A., and Kachroo, P. (2014). Free radical-mediated systemic immunity in plants. *Curr. Opin. Plant Biol.* 20C, 127–134. doi: 10.1016/j.pbi.2014.05.012

Wisniewska, J., Xu, J., Seifertová, D., Brewer, P. B., Ruzicka, K., Blilou, I., et al. (2006). Polar PIN localization directs auxin flow in plants. *Science* 312:883. doi: 10.1126/science.1121356

Woodward, A. W., and Bartel, B. (2005). Auxin: regulation, action, and interaction. *Ann. Bot.* 95, 707–735. doi: 10.1093/aob/mci083

Xu, J., and Scheres, B. (2005). Dissection of Arabidopsis ADPRIBOSYLATION FACTOR 1 function in epidermal cell polarity. *Plant Cell* 17, 525–536. doi: 10.1105/tpc.104.028449

Xu, L., Eu, J. P., Meissner, G., and Stamler, J. S. (1998). Activation of the cardiac calcium release channel (ryanodine receptor) by poly-Snitrosylation. *Science* 279, 234–237. doi: 10.1126/science.279.5348.234

Xuan, Y., Zhou, S., Wang, L., Cheng, Y., and Zhao, L. (2010). Nitric oxide functions as a signal and acts upstream of AtCaM3 in thermotolerance in Arabidopsis seedlings. *Plant Physiol.* 153, 1895–1906. doi: 10.1104/pp.110.160424

Yang, H., Mu, J., Chen, L., Feng, J., Hu, J., Li, L., et al. (2015). S-nitrosylation positively regulates ascorbate peroxidase activity during plant stress responses. *Plant Physiol.* 167, 1604–1615. doi: 10.1104/pp.114.255216

Ye, Y., Li, Z., and Xing, D. (2012). Sorting out the role of nitric oxide in cadmium-induced *Arabidopsis thaliana* programmed cell death. *Plant Signal. Behav.* 7, 1493–1494. doi: 10.4161/psb.21893

Yin, X. J., Volk, S., Ljung, K., Mehlmer, N., Dolezal, K., Ditengou, F., et al. (2007). Ubiquitin lysine 63 chain forming ligases regulate apical dominance in Arabidopsis. *Plant Cell* 19, 1898–1911. doi: 10.1105/tpc.107.052035

Yun, B. W., Feechan, A., Yin, M., Saidi, N. B., Le Bihan, T., Yu, M., et al. (2011). S-Nitrosylation of NADPH oxidase regulates cell death in plant immunity. *Nature* 478, 264–268. doi: 10.1038/nature10427

Zeidler, D., Zähringer, U., Gerber, I., Dubery, I., Hartung, T., Bors, W., et al. (2004). Innate immunity in *Arabidopsis thaliana*: lipopolysaccharides activate nitric oxide synthase (NOS). *Proc. Natl. Acad. Sci. U.S.A.* 101, 15811–15816. doi: 10.1073/pnas.0404536101

Conflict of Interest Statement: The authors declare that the research was conducted in the absence of any commercial or financial relationships that could be construed as a potential conflict of interest.

The handling Editor declared a shared affiliation, though no other collaboration, with several of the authors CW and JP.

frontiers in Plant Science

ORIGINAL RESEARCH
published: 24 October 2017
doi: 10.3389/fpls.2017.01823

The Rice High-Affinity K^+ Transporter OsHKT2;4 Mediates Mg^{2+} Homeostasis under High-Mg^{2+} Conditions in Transgenic *Arabidopsis*

Chi Zhang[1], Hejuan Li[1], Jiayuan Wang[1], Bin Zhang[1], Wei Wang[2], Hongxuan Lin[2], Sheng Luan[3], Jiping Gao[2] and Wenzhi Lan[1]**

[1] State Key Laboratory for Pharmaceutical Biotechnology, NJU–NFU Joint Institute for Plant Molecular Biology, College of Life Sciences, Nanjing University, Nanjing, China, [2] National Key Laboratory of Plant Molecular Genetics, Institute of Plant Physiology and Ecology, Shanghai Institutes for Biological Sciences, Chinese Academy of Sciences, Shanghai, China, [3] Department of Plant and Microbial Biology, University of California, Berkeley, Berkeley, CA, United States

OPEN ACCESS

Edited by:
Kai He,
Lanzhou University, China

Reviewed by:
Kendal Hirschi,
Baylor College of Medicine, United States
Fouad Lemtiri-Chlieh,
King Abdullah University of Science and Technology, Saudi Arabia
Tamara Pecenkova,
Institute of Experimental Botany (ASCR), Czechia

***Correspondence:**
Jiping Gao
jpgao@sibs.ac.cn
Wenzhi Lan
lanw@nju.edu.cn

Specialty section:
This article was submitted to Plant Traffic and Transport, a section of the journal Frontiers in Plant Science

Received: 27 July 2017
Accepted: 10 October 2017
Published: 24 October 2017

Citation:
Zhang C, Li H, Wang J, Zhang B, Wang W, Lin H, Luan S, Gao J and Lan W (2017) The Rice High-Affinity K^+ Transporter OsHKT2;4 Mediates Mg^{2+} Homeostasis under High-Mg^{2+} Conditions in Transgenic Arabidopsis. Front. Plant Sci. 8:1823. doi: 10.3389/fpls.2017.01823

Rice (*Oryza sativa*; background Nipponbare) contains nine *HKT* (high-affinity K^+ transport)-like genes encoding membrane proteins belonging to the superfamily of Ktr/TRK/HKT. OsHKTs have been proposed to include four selectivity filter-pore-forming domains homologous to the bacterial K^+ channel KcsA, and are separated into OsHKT1s with Na^+-selective activity and OsHKT2s with Na^+-K^+ symport activity. As a member of the OsHKT2 subfamily, OsHKT2;4 renders Mg^{2+} and Ca^{2+} permeability for yeast cells and *Xenopus laevis* oocytes, besides K^+ and Na^+. However, physiological functions related to Mg^{2+} *in planta* have not yet been identified. Here we report that OsHKT2;4 from rice (*O. sativa*; background Nipponbare) functions as a low-affinity Mg^{2+} transporter to mediate Mg^{2+} homeostasis in plants under high-Mg^{2+} environments. Using the functional complementation assay in Mg^{2+}-uptake deficient *Salmonella typhimurium* strains MM281 and electrophysiological analysis in *X. laevis* oocytes, we found that OsHKT2;4 could rescue the growth of MM281 in Mg^{2+}-deficient conditions and induced the Mg^{2+} currents in oocytes at millimolar range of Mg^{2+}. Additionally, overexpression of OsHKT2;4 to *Arabidopsis* mutant lines with a knockout of *AtMGT6*, a gene encoding the transporter protein necessary for Mg^{2+} adaptation in *Arabidopsis*, caused the Mg^{2+} toxicity to the leaves under the high-Mg^{2+} stress, but not under low-Mg^{2+} environments. Moreover, this Mg^{2+} toxicity symptom resulted from the excessive Mg^{2+} translocation from roots to shoots, and was relieved by the increase in supplemental Ca^{2+}. Together, our results demonstrated that OsHKT2;4 is a low-affinity Mg^{2+} transporter responsible for Mg^{2+} transport to aerials in plants under high-Mg^{2+} conditions.

Keywords: *Arabidopsis*, HKT transporter, MGT transporter, Mg^{2+} permeable, rice

INTRODUCTION

Apart from atmospheric oxygen and soil-derived water, plants require a range of minerals for their growth and development. As two major essential mineral nutrients for plant growth, K and Mg are available to plants in the ionic form (K^+ and Mg^{2+}), and are transported into root cells by the plasma membrane-localized channels and transporters. Up to now, most studies are focused on identifying the active, high-affinity channels and transporters, which function in K^+ and Mg^{2+} uptake from the nutrient-deficient environments (Hirsch et al., 1998; Li et al., 2001; Chérel et al., 2014; Mao et al., 2014). However, large majority of channels and transporters necessary for plants adaptation to nutrient-enriched conditions remain unknown.

Due to its key role in salt tolerance, high-affinity K^+ transporters (HKTs) family has been widely studied and most of its members are characterized as being permeable for specific ions in heterologous expression systems (Uozumi et al., 2000; Horie et al., 2001; Mäser et al., 2002b; Garciadeblas et al., 2003; Yao et al., 2010). HKTs in plants and their K^+ transporter (Trk and Ktr) counterparts in fungi and bacteria form a HKT/Trk/Ktr superfamily (Rodriguez-Navarro, 2000; Corratgé-Faillie et al., 2010; Yamaguchi et al., 2013). Plant HKT transporters are divided into two subgroups based on phylogenetic analyses to date (Mäser et al., 2002a; Platten et al., 2006; Horie et al., 2009; Hauser and Horie, 2010). Group I HKT members (HKT1s) are associated with retrieval of Na^+ from xylem in root or sheath restricting transport and accumulation of salt in sensitive leaf tissues (Davenport et al., 2007; Munns and Tester, 2008). Grass species evolved a second class of HKT proteins, and comprehensive analysis of this group II HKTs (HKT2s) has been made in rice (*Oryza sativa L.*) with up to four members, OsHKT2;1, OsHKT2;2, OsHKT2;3, and OsHKT2;4 characterized for the structure, expression, and function (Ariyarathna et al., 2016). Most of HKT2s members function as Na^+/K^+ transporters with a role in maintaining Na^+/K^+ homeostasis in plants (Horie et al., 2007, 2011; Lan et al., 2010; Yao et al., 2010; Nieves-Cordones et al., 2016). OsHKT2;4 seems to be an exception as it exhibited permeability to a wide range of cations, including Ca^{2+} and Mg^{2+} when it was expressed in *Xenopus laevis* oocytes (Lan et al., 2010; Horie et al., 2011). However, its physiological function in rice is still unknown.

The *Arabidopsis* genome contains a single *HKT* homolog, *AtHKT1;1*, which functions as a Na^+-selective uniporter and is not permeable to Ca^{2+} and Mg^{2+} (Davenport et al., 2007; Møller et al., 2009; Lan et al., 2010), suggesting that there are alternative transporters responsible for Ca^{2+} and Mg^{2+} transport in *Arabidopsis*. Ca^{2+} and Mg^{2+} are two of the most abundant divalent cations in living plant cells. Ca^{2+} is utilized to strengthen cell walls and a versatile messenger in almost all physiological processes in plants (Tang and Luan, 2017). The prominent role of Mg^{2+} is as the central atom of the chlorophyll molecule (Larkin, 2016), and it also participates in cation balance and activation of various enzymes in many fundamental processes (Shaul, 2002; Knoop et al., 2005; Bose et al., 2013). Although Ca^{2+} and Mg^{2+} are essential macronutrients required for plant growth, their overdose in the environment is toxic to plants (Tang et al., 2015; Oda et al., 2016). Thus, the transporters responsible for Ca^{2+} and Mg^{2+} homeostasis is of great importance for plant survival under low or high Ca^{2+} and Mg^{2+} conditions (Miedema et al., 2001; Li et al., 2008; Hermans et al., 2013; Mao et al., 2014; Oda et al., 2016). In contrast to the ambiguous research in Ca^{2+} transport, a family of Mg^{2+} transporters in *Arabidopsis* named as AtMGT (Li et al., 2001) or AtMRS2 (Gebert et al., 2009) has been studied extensively, and is found to play pivotal roles in Mg^{2+} transport and homeostasis in *Arabidopsis*. One of its members, AtMGT6/MRS2-4, is a high-affinity Mg^{2+} transporter, and loss-of-function of AtMGT6/MRS2-4 caused the severe growth retardation of *Arabidopsis* plants under low-Mg^{2+} conditions (Mao et al., 2014). Interestingly, AtMGT6/MRS2-4 also confers plants adaptation to high-Mg^{2+} conditions (Oda et al., 2016). Thus, *atmgt6* plant with loss-of-function of AtMGT6/MRS2-4 displays the deficient Mg^{2+} transport under wide range of Mg^{2+} concentrations, and is a promising expression system to examine whether the potential transporters possess physiological functions relevant to Mg^{2+} in plants.

Although OsHKT2;4 was demonstrated to be permeable for Mg^{2+} in *X. laevis* oocytes (Lan et al., 2010; Horie et al., 2011), this has been challenged in an independent study (Sassi et al., 2012). Here, we applied the *Salmonella typhimurium* MM281, a bacteria mutant lacking Mg^{2+} transport capacity useful for identifying the Mg^{2+} transport activities of potential transporters (Li et al., 2001; Gebert et al., 2009), to analyze the possible Mg^{2+} transport through OsHKT2;4. Furthermore, its function on Mg^{2+} homeostasis was also explored in *X. laevis* oocytes and transgenic *atmgt6 Arabidopsis* lines. Our results revealed that OsHKT2;4 is an effective Mg^{2+} transporter in maintaining Mg^{2+} homeostasis, probably through functional coordination with MGT-type transporters *in planta*.

MATERIALS AND METHODS

Plant Materials and Growth Conditions

Arabidopsis thaliana Columbia (Col-0) ecotype was used in this study. The T-DNA insertion mutant *atmgt6* (SALK_203866) was obtained from the *Arabidopsis* Biological Resource Center. Homozygous individuals of *atmgt6* were screened by PCR using primers listed in Supplementary Table 1. For on-plate growth assays, seeds were sterilized with 75% ethanol for 2 min, washed three times, and sown on half-strength Murashige and Skoog (MS) medium containing 0.75 mM Mg^{2+}, 1.5 mM Ca^{2+}, 1% sucrose (Sigma) and solidified with 0.8% phytoblend (Caisson Labs). The plates were kept at 4°C for 2 days and then were placed vertically in growth chamber under 90 $\mu mol \cdot m^{-2} \cdot s^{-1}$ light intensity with a 16 h light/8 h dark photoperiod. Three-day-old seedlings were transferred onto media containing various ions as indicated in the figure legends. For hydroponic cultures, 7-day-old seedlings germinated in half-strength MS (1/2 MS) were transferred to one-sixth-strength (1/6 MS) hydroponic medium containing 0.25 mM Mg^{2+} and 0.5 mM Ca^{2+} without sucrose for another 7 days. Plants were then transferred to hydroponic 1/6 MS media containing various contents of Mg^{2+}. Plant materials were harvested for further analyses 2 days after treatment.

Functional Complementation of Mg^{2+}-Transport by *Salmonella typhimurium* Mutant Strain MM281

The *S. typhimurium* mutant MM281, which lacks the Mg^{2+} transporter-*CorA*, *MgtA*, and *MgtB*, is used as a system for functional complementation analysis of candidate Mg^{2+}-transporter genes. MM281 competent cells were transformed with empty pTrc99A vector, *AtMGT10*-pTrc99A or *OsHKT2;4*-pTrc99A plasmid by electroporation. Cells were plated onto LB medium containing 10 mM Mg^{2+} and indicated antibiotics (34 $\mu g \cdot mL^{-1}$ chloramphenicol and 100 $\mu g \cdot mL^{-1}$ ampicillin), and incubated at 37°C overnight. The transformants were confirmed by PCR amplification and individual positive ones were grown in liquid LB medium containing 10 mM Mg^{2+} and antibiotics as indicated above. Fifty micrometer IPTG was applied for the induction of protein expression. The liquid cultures were adjusted to $OD_{600} = 1.0$, diluted in a 10-fold series, and spotted 3 μL onto N-minimal medium supplemented with different concentrations of $MgSO_4$ and the antibiotics. Growth of different strains was pictured after incubation at 37°C for 2 days. The growth rate of the three strains in liquid medium was also monitored as previously described (Mao et al., 2014). After growing in liquid LB medium to OD_{600} of 0.6–0.8, cells were harvested by centrifugation at 5000 × *g* for 10 min, washed twice with distilled water to remove excess Mg^{2+}, and resuspended in distilled water. N-minimal medium was prepared with various concentrations of $MgSO_4$ (0.1, 0.5, 1, and 10 mM). Cells were then adjusted to a final OD_{600} of 0.001–0.002. The growth of the cultures was monitored and was plotted as a function of growth time.

Plasmid Construction and Plant Transformation

For the constructs used in functional complementation assay in MM281 strain, the *OsHKT2;4* cDNA fragment was amplified using the primers *OsHKT2;4*-FC and *OsHKT2;4*-RC and ligated to the pTrc99A vector. For overexpressing *OsHKT2;4* in wild type and the *atmgt6* mutant, the genomic fragment (containing a 1.92 kb promoter region upstream of the *ATG* starting codon and 1731 bp coding region of *OsHKT2;4*) was amplified using primer pair *OsHKT2;4*-OE-F and *OsHKT2;4*-OE-R and cloned into pCAMBIA1300 vector. This construct was introduced into *Agrobacterium tumefaciens* strain GV3101 by electroporation and was selected on 1/2 MS medium containing kanamycin. The selected positive transformant was used to transform developing floral tissues of 4-week-old *atmgt6* plants using the flora dip method (Clough and Bent, 1998). For expression in *X. laevis* oocytes, *OsHKT2;4* cDNA was cloned into the pGEMHE vector downstream from the T7 promoter using primers *OsHKT2;4*-FP and *OsHKT2;4*-RP. All primer pairs were listed in Supplementary Table 1.

Gene Expression Analysis

Total RNA was extracted from rosette leaves using the TRizol Reagent (Invitrogen), and the first-strand cDNA was synthesized by M-MLV Reverse Transcriptase (Promega) following the manufacturer's instructions. The semi-quantitative RT-PCR analysis of gene expression using cDNA of Col-0, *atmgt6*, OE29, and OE24 followed by a 26 cycles of PCR amplification. *AtActin2* (AT3G18780) was used as the internal reference. Primers used are listed in the Supplementary Table 1.

Expression in *Xenopus laevis* Oocytes and Two-Electrode Voltage Clamp

cRNA was synthesized from 1 μg linearized DNA template using a mMessage mMachine *in vitro* transcription kit (Ambion) according to the manufacturer's recommendations and stored at −80°C. Stage V to VI *X. laevis* oocytes were harvested, defolliculated, and cultured in ND96 solution containing 96 mM NaCl, 2 mM KCl, 1.8 mM $CaCl_2$, 1 mM $MgCl_2$, 25 $\mu g \cdot mL^{-1}$ gentamicin, pH 7.4 adjusted with 5 mM HEPES/NaOH. Approximately 50 ng of cRNA, in a total volume of 23 nL, was injected into each *X. laevis* oocyte. Oocytes of 2 days after injection were used for two-electrode voltage-clamp analysis. The perfusion solution was used as described previously (Lan et al., 2010) with some modifications. The perfusion solution contained (in mM) 1 K-gluconate, 1 Na-gluconate, 185 mannitol, and 10 Mes-Tris (pH 7.4). The recording pipette contained 3 M KCl. The currents were recorded by hyperpolarized pulses of a 0.2 s prepulse at −40 mV followed by voltage steps of 60 to −150 mV (in 15 mV decrements, 1.8 s duration) followed by a 1.5 s deactivation at 0 mV. The current-voltage (*I-V*) curves plot current values at the end of each voltage-clamp episode ($t = 2$ s, $n = 6$ for each group).

Ion Content Measurement

Two-week-old hydroponically grown plants were exposed to solution containing different concentrations of Mg^{2+}. After 2-day exposure, both the roots and shoots were harvested and sampled for analysis. The dry weight (DW) of the samples was measured after drying for 48 h at 60°C. Subsequently, the samples were digested in 0.5 ml of 70% HNO_3 at 100°C for 30 min on a digester (DigiBlock ED16, LabTech). Ion concentration was measured by Inductively Coupled Plasma-Mass Spectrometry (ICP-MS) (PerkinElmer NexION 300).

RESULTS

OsHKT2;4 Rescued the Growth of Bacterial Strain MM281 in the Mg^{2+}-Deficient Medium

To determine whether OsHKT2;4 functions in Mg^{2+} transport, a cDNA fragment containing the complete open reading frame with 1530 bases encoded a protein of 509 residues was cloned and expressed in *S. typhimurium* mutant strain MM281. MM281 is incapable of loading Mg^{2+} into cellular compartment, as it lacks three functional Mg^{2+} transporters *CorA*, *MgtA,* and *MgtB*, and its growth is retarded or arrested when the culture medium contains less than 10 mM Mg^{2+} (Townsend et al., 1995; Li et al., 2001). Therefore, complementation of this strain has proved useful in identifying and developing information about potential

Mg^{2+} transporters, including AtMGTs (Li et al., 2001, 2008; Hicks et al., 2003; Mao et al., 2008; Chen et al., 2009; Mao et al., 2014).

We used *AtMGT10* (AT5G22830), also named as *AtMRS2-11*, as the positive control in the complementation assay of MM281 due to its high affinity in Mg^{2+} transport in MM281 system (Li et al., 2001). As shown in **Figure 1A**, the MM281 mutant strains exogenously expressing empty vector pTrc99A, *AtMGT10*-pTrc99A, or *OsHKT2;4*-pTrc99A grew normally in the medium with 10 mM Mg^{2+}. The strains expressing *OsHKT2;4*-pTrc99A exhibited faster growth than those expressing the empty pTrc99A vector in the media containing low concentrations of Mg^{2+} (1 and 2 mM), and still grew but to a less extent in the media containing 500 and 100 μM Mg^{2+}, while the control did not grow at these conditions (**Figure 1A**), suggesting that OsHKT2;4 renders the mutant strains more tolerant to Mg^{2+} deficiency by enhancing the Mg^{2+} transport activity. However, OsHKT2;4 was less effective to restore the growth of mutant strains compared with AtMGT10 in the media containing insufficient Mg^{2+}. For example, AtMGT10 rescued MM281 growth in medium containing 10 μM Mg^{2+} (**Figure 1A**), as shown before (Li et al., 2001), while OsHKT2;4 did not (**Figure 1A**). These results indicated that although OsHKT2;4 had the Mg^{2+} transport activity similar to AtMGT10, it might have the kinetic property with lower affinity to Mg^{2+} in heterologous MM281 system.

To further verify the complementation of OsHKT2;4 for the growth of MM281 tested in the agar plates (**Figure 1A**), the bacteria were cultured in the liquid media containing 0.1, 0.5, 1, or 10 mM Mg^{2+}, and their growth curves were established within 24 h after cultured. As shown in **Figure 1B**, the strain expressing AtMGT10 grew the most rapidly at these Mg^{2+} concentrations, supporting that AtMGT10 is a high-affinity Mg^{2+} transporter. In addition, MM281 expressing OsHKT2;4 displayed faster growth than those with empty vector pTrc99A under the conditions in which the Mg^{2+} concentration was 1 or 10 mM. By contrast, in the presence of 0.1 or 0.5 mM Mg^{2+}, the strains expressing OsHKT2;4 displayed the similar rate of growth to the strains expressing empty vector pTrc99A. These results were consistent with the ones observed on the agar plates, and demonstrated that OsHKT2;4 might mediate low-affinity Mg^{2+} uptake *in vivo*.

Mg^{2+}-Dependent Currents Generated by OsHKT2;4 Expressing *X. laevis* Oocytes under High-Mg^{2+} Conditions

To further assess the transporting properties of OsHKT2;4 under different Mg^{2+} concentrations, two-electrode voltage-clamp experiment using *X. laevis* oocytes was performed. OsHKT2;4-dependent currents were recorded from the oocytes injected with OsHKT2;4 cRNA or the oocytes injected with water perfused with different Mg^{2+} concentrations. The oocytes injected with water produced small endogenous currents in perfusion medium with 6 mM Mg^{2+} (**Figures 2A-a**). In contrast, *OsHKT2;4*-expressing oocytes generated the larger currents in the solutions containing 1.2, 6, and 20 mM Mg^{2+} (**Figures 2A-b–d**). The current-voltage relationship displayed the currents from *OsHKT2;4*-expressing oocytes perfused with 6 or 20 mM Mg^{2+} were significantly larger than those from *OsHKT2;4*-expressing oocytes perfused with 0.3 or 1.2 mM Mg^{2+}. It was noteworthy that the currents from OsHKT2;4-expressing oocytes perfused with 0.3 mM Mg^{2+} were similar to those with 1.2 mM Mg^{2+}, implying they might not be Mg^{2+} sensitive under low-Mg^{2+} conditions (**Figure 2B**).

To test this possibility, we compared the amplitude and reversal potential of the currents generated from the oocytes perfused with 0, 0.3, 1.2, 6, or 20 mM Mg^{2+}. The currents generated from the oocytes expressing OsHKT2;4 perfused with 0.3 or 1.2 mM Mg^{2+} displayed the similar levels of the amplitudes and reversal potentials, even were similar to those without Mg^{2+} (**Figures 2C,D**). These Mg^{2+} insensitive currents were larger than the currents from the oocytes injected with water (**Figure 2C**), and thus they may result from other ions, such as Na^+ or K^+ currents generated by OsHKT2;4, as suggested by the previous studies (Lan et al., 2010; Horie et al., 2011). By contrast, in the presence of 6 or 20 mM Mg^{2+}, the oocytes expressing OsHKT2;4 produced the currents with larger amplitudes and less negative reversal potentials compared with the others (**Figures 2C,D**). Thus, these results further supported the hypothesis that OsHKT2;4 exhibits permeability for Mg^{2+} only under the conditions containing high-Mg^{2+} concentrations.

Overexpression of OsHKT2;4 Enhanced the Sensitivity of *atmgt6* to High Mg^{2+} But Not to Low Mg^{2+}

We have shown previously that AtMGT6, a Mg^{2+} deficiency-induced Mg^{2+} transporter, mediates directly Mg^{2+} uptake in roots and is required for plant adaptation to low-Mg^{2+} environment (Mao et al., 2014). An independent study reported ethyl methanesulfonate (EMS)-mutagenized *AtMGT6*, or named as *AtMRS2-4*, caused plant growth defects under both low and high-Mg^{2+} conditions (Oda et al., 2016). Considering the critical role of AtMGT6 in Mg^{2+} acquisition, we suggested the activity of Mg^{2+} transport conducted by OsHKT2;4 might be covered by this transporter, and thus generated transgenic *OsHKT2;4 Arabidopsis* lines with the disruption of *AtMGT6* to examine the potential relevance of OsHKT2;4 to Mg^{2+} responses *in planta*. We used an *Arabidopsis* T-DNA insertion line (SALK_203866), in which T-DNA was inserted into the third exon of *AtMGT6* gene (**Figure 3A**). Transcript of *AtMGT6* in the line SALK_203866 was not detected by RT-PCR (**Figure 3C**), indicating that the T-DNA insertion line was a knockout allele, and referred to as *atmgt6* line hereafter. We then expressed the coding region of *OsHKT2;4* into *atmgt6* line driven by its native promoter (**Figure 3B**). The transformants were screened by hygromycin, and were further analyzed for the expression levels of *OsHKT2;4* by RT-PCR. We selected two of them as the representative transgenic lines due to their relatively high *OsHKT2;4* expression levels, and referred to as OE29 and OE34, respectively, to perform subsequent experiments (**Figure 3C**).

We examined the growth of the Col-0, *atmgt6*, and transgenic lines OE29 and OE34 in Mg^{2+}-depleted medium supplemented

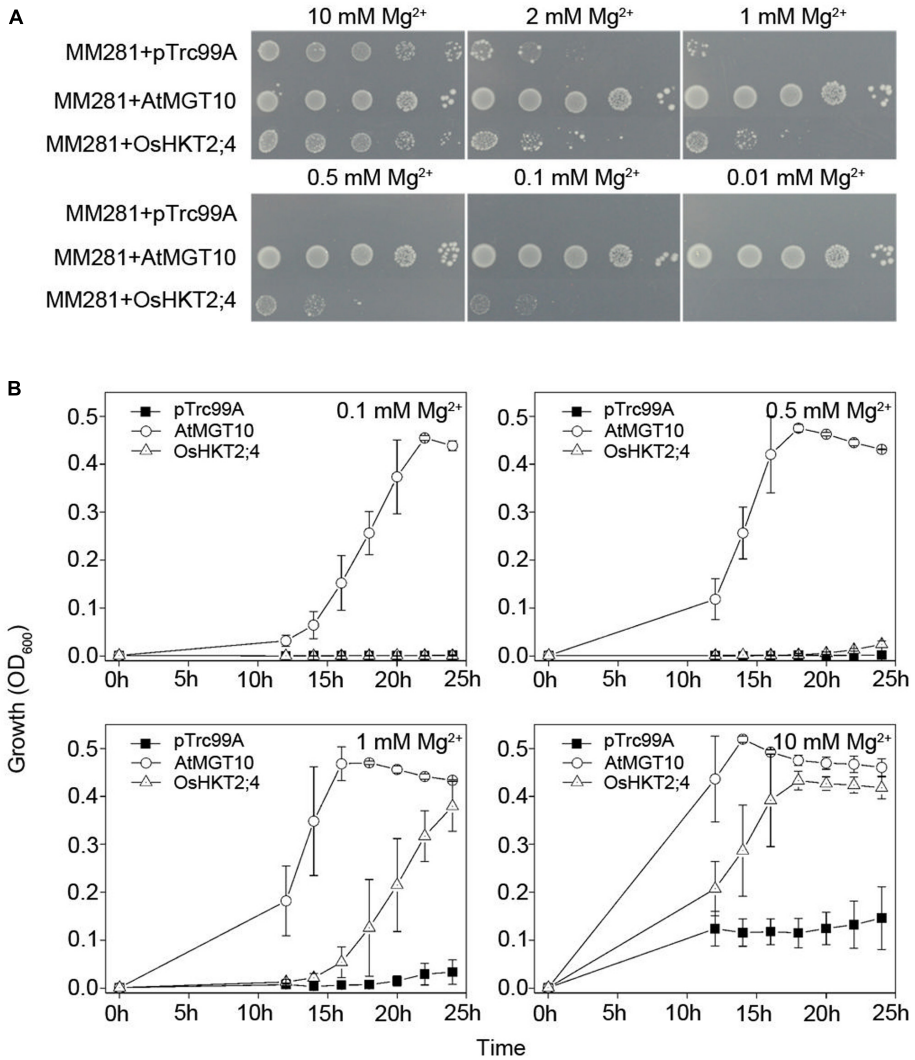

FIGURE 1 | Complementation of growth defects of bacterial mutant strains MM281 by OsHKT2;4 under the low-Mg^{2+} conditions. **(A)** Growth of bacterial strains on N-minimal medium containing 0.01, 0.1, 0.5, 1, 2, or 10 mM Mg^{2+}. The strains used in this assay were the strains MM281 transformed with the empty pTrc99A vector only (MM281+pTrc99A), coding sequence of *MGT10* in the pTrc99A vector (MM281+MGT10), or coding sequence of *OsHKT2;4* in pTrc99A vector (MM281+OsHKT2;4). From left to right is a 10-fold dilution series of bacterial cultures. **(B)** Growth curves of bacterial strains in liquid cultures. Bacterial cells described in **(A)** were grown in N-minimal liquid medium containing increasing concentrations of Mg^{2+} from 0.1 to 10 mM. Aliquots of the cultures were taken and monitored every 2 h by OD_{600} readings for the cell density from 10 to 24 h. Data are represented as the mean ± SD, $n = 3$.

with various contents of Mg^{2+} as indicated in **Figure 3D**. The mutant *atmgt6* exhibited growth defects in the medium containing 0, 0.01, 0.1, or 0.25 mM Mg^{2+}, and had lower fresh weight and shorter roots than those of the Col-0 plants, while the growth retardation could be rescued in the Mg^{2+}-sufficient medium (2 mM Mg^{2+}) (**Figure 3D**), consistent with the idea that *AtMGT6* confers low-Mg^{2+} tolerance for *Arabidopsis* (Mao et al., 2014; Oda et al., 2016). However, OsHKT2;4 overexpression could not rescue the growth deficiency of *atmgt6* in low-Mg^{2+} conditions as expected, as transgenic lines OE29 and OE34 displayed the similar growth phenotype to *atmgt6* with no significant differences on fresh weight and root length under these tested conditions (**Figures 3D–F**). These results suggested that OsHKT2;4 might not function in low-Mg^{2+} conditions *in planta*.

As shown in the experiments *in vitro*, OsHKT2;4 exhibiting Mg^{2+} transport activity in both heterologous MM281 system and *X. laevis* oocytes happened only at high external Mg^{2+} concentrations (**Figures 1**, **2**). Therefore, we presumed that OsHKT2;4 might mediate Mg^{2+} transport when plants were cultivated under the Mg^{2+} abundant conditions, though it was unable to function in low-Mg^{2+} conditions *in planta* (**Figures 3D–F**). To conduct assessment of the sensitivity to high-Mg^{2+} condition of OsHKT2;4, we used 1/6 MS medium supplemented with several concentrations of Mg^{2+} (2, 4, 6, 8, and 10 mM) for growth assays. After growing on 1/6 MS for

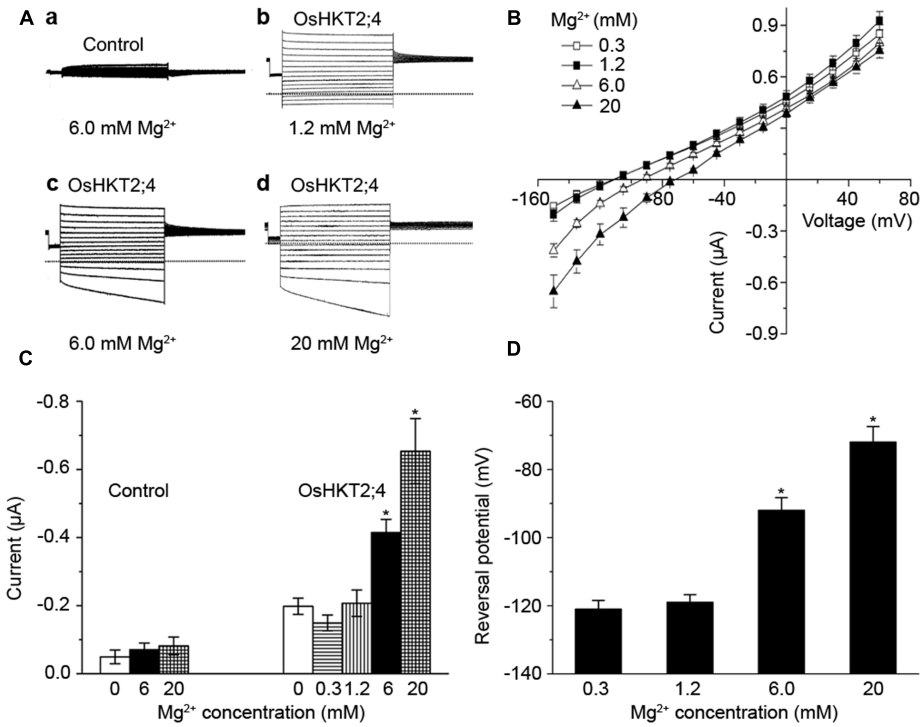

FIGURE 2 | The oocytes expressing OsHKT2;4 produced Mg^{2+} currents under the high-Mg^{2+} conditions. **(A)** The typical current traces generated from the oocytes injected with water perfused with **(a)** 6 mM Mg^{2+} (Control) and from the oocytes expressing OsHKT2;4 (OsHKT2;4) perfused with **(b)** 1.2 mM, **(c)** 6 mM or **(d)** 20 mM Mg^{2+}. Dotted lines represent the zero current level. **(B)** The current-voltage relationships deduced from the oocytes expressing OsHKT2;4 perfused with 0.3, 1.2, 6 or 20 mM Mg^{2+}. Summarized current data are from 8 cells/condition. **(C)** The current amplitudes at –150 mV recorded from the oocytes injected with water (Control) and oocytes expressing OsHKT2;4 (OsHKT2;4) perfused with different Mg^{2+} concentrations. **(D)** Reversal potentials of currents generated from the oocytes expressing OsHKT2;4 in the presence of various concentrations of Mg^{2+} as indicated in the figure. Data in **Figure 2** are presented as representative recordings or as mean ± SE of *n* (*n* = 6) observations with three repetitions, in which *n* is the number of samples. Asterisks indicate statistically significant differences compared with data from oocytes expressing OsHKT2;4 perfused with 1.2 mM Mg^{2+} (Unpaired student's *t*-test, $*P < 0.05$).

2 weeks, both the root length and fresh weight of transgenic lines OE29 and OE34 were comparable to those of *atmgt6* under the normal condition. However, addition of 2 mM Mg^{2+} resulted in growth arrest of OE29 and OE34 compared with *atmgt6*. Further increases of extra Mg^{2+} (up to 10 mM) demonstrated a consistent dosage-dependent inhibitory manner (**Figure 4A**). Quantitative analysis of root length (**Figure 4B**) and fresh weight (**Figure 4C**) indicated that, compared with Col-0 and *atmgt6*, the aerial parts of OE29 and OE34 exhibited a more severe growth retardation in Mg^{2+}-abundant conditions, while their root length were not altered. Taken together, these results demonstrated that OsHKT2;4 results in Mg toxicity on aerial tissues in high-Mg^{2+} conditions in *Arabidopsis*, supporting the idea of low-affinity Mg^{2+} uptake of OsHKT2;4.

To examine whether the high-Mg^{2+} toxic phenotype is a consequence of the ectopic expression of OsHKT2;4 in OE lines, we conducted an RT-PCR analysis to verify the expression of OsHKT2;4 under a high-Mg^{2+} condition supplemented with 6 mM Mg^{2+}. As demonstrated in Supplementary Figure 5, OsHKT2;4 was mainly expressed in shoot tissues under normal growth conditions, consistent with the previous report in rice (Lan et al., 2010). Moreover, the expression of *OsHKT2;4* in the shoots was not significantly induced by 6 mM Mg^{2+}, and even decreased after 24 h′ treatment with 6 mM Mg^{2+}. However, expression of *OsHKT2;4* in the roots was dramatically induced after 4 h′ treatment with 6 mM Mg^{2+}, and became even stronger after 24 h of this treatment (Supplementary Figure 5). The oppose effect on *OsHKT2;4* expression roots and shoots upon high Mg^{2+} suggested a disturbance on Mg^{2+} balance between roots and shoots under the high-Mg^{2+} conditions.

Overexpression of OsHKT2;4 Affected Mg^{2+} Homeostasis in the *atmgt6* Lines

To probe the reason responsible for the increased sensitivity to high external Mg^{2+} in the OE plants, Mg^{2+} concentration of the *atmgt6* and OsHKT2;4 overexpression lines was determined using ICP-MS. Plants were grown hydroponically for 2 weeks and then transferred to a fresh hydroponic medium containing 0, 0.25 (referred to as "Control" in **Figure 5**), and 6 mM Mg^{2+} for another 2 days before the roots and shoots were harvested, respectively, for analysis. As shown in **Figure 5A**, Mg^{2+} content was consistently higher in the OE lines than *atmgt6* in shoot tissues when plants grown in all Mg^{2+} regimes tested (0, 0.25, and 6 mM). In analysis of Mg^{2+} content of root tissues among different plants, although they exhibited similar and incremental

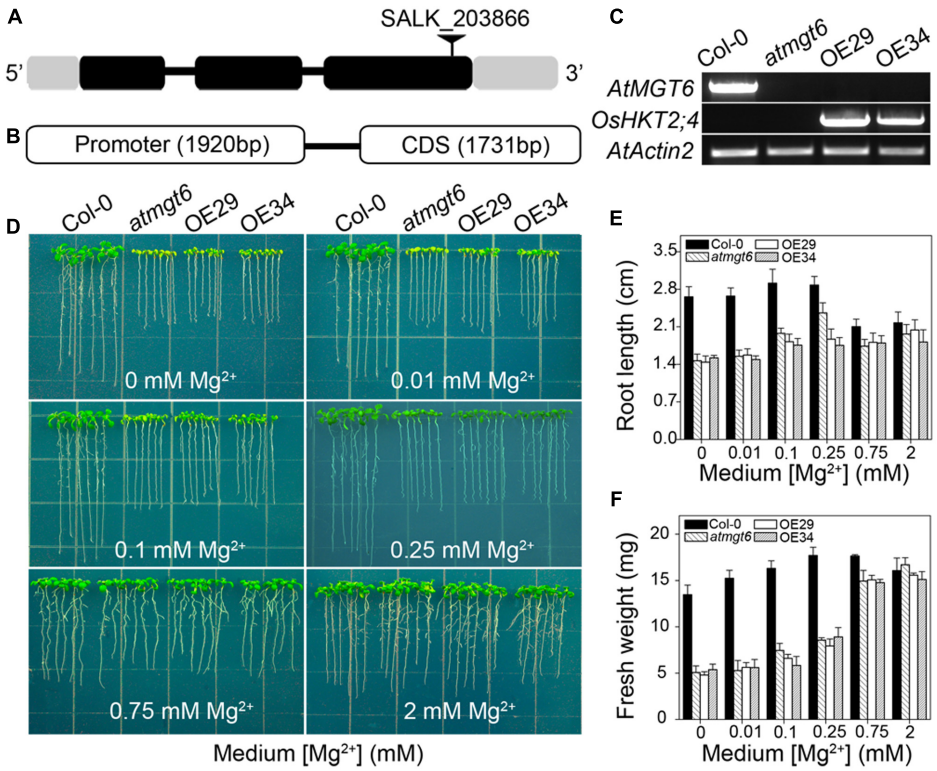

FIGURE 3 | Genetic characterization and phenotypic analysis of *atmgt6* mutant lines and their OsHKT2;4 overexpressed lines in low-Mg^{2+} conditions. **(A)** Scheme of *AtMGT6* gene structure and position of the T-DNA insertion of SALK_203866. The gray boxes indicate 5′ and 3′ untranslated regions, and black boxes and lines indicate exons and introns, respectively. The T-DNA insertion is shown as the triangle above the gene diagram. **(B)** Gene fragment of *OsHKT2;4*, including its promoter and CDS region that was introduced into *atmgt6* lines. **(C)** Semi-quantitative mRNA levels of *AtMGT6* and *OsHKT2;4* by RT-PCR analysis in wild type (Col-0), *AtMGT6* knockout mutant (*atmgt6*), and two *atmgt6* lines overexpressing OsHKT2;4 (OE29 and OE34). *AtActin2* was used as the internal standard. **(D)** The growth of Col-0, *atmgt6*, OE29, and OE34 under the Mg^{2+}-deficient conditions. After planted in half-strength Murashige and Skoog (1/2 MS) medium for 3 days, Col-0, *atmgt6*, OE29, and OE34 were transferred to one-sixth-strength MS (1/6 MS) medium containing 0, 0.01, 0.1, 0.25, 0.75, and 2 mM Mg^{2+} in total, and were photographed after growing for 7 days. Quantitative analyses of primary root length **(E)** and whole-plant fresh weight **(F)** of Col-0, *atmgt6*, OE29, and OE34 under the Mg^{2+}-deficient conditions described in **(D)**. Six independent 10-day-old seedlings of each genotype were gathered as one biological repeat for root length and fresh weight measurement. Data are represented as the mean ± SD, $n = 3$, in which n is the number of biological repeat.

Mg^{2+} content in the Mg^{2+}-deficient and normal medium, the OE lines contained ∼30% less Mg^{2+} compared with the *atmgt6* plants in 6 mM Mg^{2+} condition (**Figure 5B**). These results indicated an altered Mg^{2+} distribution ratio in shoot and root. We thus analyzed the Mg^{2+} partitioning between shoots and roots in *atmgt6* and OE lines, and noticed that as the Mg^{2+} level elevated, more Mg^{2+} sequestered in root tissues than in low-Mg^{2+} condition. In medium containing 6 mM Mg^{2+}, the shoots of *atmgt6* accumulated ∼37%, while the OE lines accumulated over ∼50% of the total Mg^{2+} enclosed in plants (**Figure 5C**), further confirming the critical role of OsHKT2;4 in the Mg^{2+} allocation between shoots and roots.

Increased Sensitivity of *atmgt6* Lines Expressing OsHKT2;4 to Excess Mg^{2+} Was Alleviated by Adding Ca^{2+}

Due to the similar physical properties, Ca^{2+} and Mg^{2+} compete for the same sites of substrates (Yermiyahu et al., 1994), and the balance of Ca^{2+} and Mg^{2+} is an important factor for plant growth. Previously, evidence was presented that OsHKT2;4 acts as a channel for the transport of both Ca^{2+} and Mg^{2+} (Lan et al., 2010; Horie et al., 2011). To examine whether Ca^{2+} affects the high Mg^{2+}-sensitive phenotype in OsHKT2;4 overexpressing lines, we assessed the growth of Col-0, *atmgt6*, *atmgt6* overexpressing OsHKT2;4 lines (OE29 and OE34) on Mg^{2+}-abundant 1/6 MS medium supplemented with different concentrations of excess Ca^{2+}.

In normal 1/6 MS medium, OE29 and OE34 exhibited the similar growth as *atmgt6*. As the concentration of external Mg^{2+} increased, OE29 and OE34 started to show a more severe growth arrest than *atmgt6* (**Figure 4A**). However, increasing Ca^{2+} improved the plant growth (**Figure 6A**) of all genotypes, and the improvement was more obvious in the OE29 and OE34 lines (Supplementary Figure 2). For example, fresh weight of OE lines was ∼50% of that in *atmgt6* in 1/6 MS medium with extra 8 mM Mg^{2+} ("basal medium" in **Figure 6**), however, when 1 mM Ca^{2+} was added to this basal medium, the fresh weight of OE lines was restored and reached to ∼80% to that in *atmgt6*. Moreover, when 3 mM

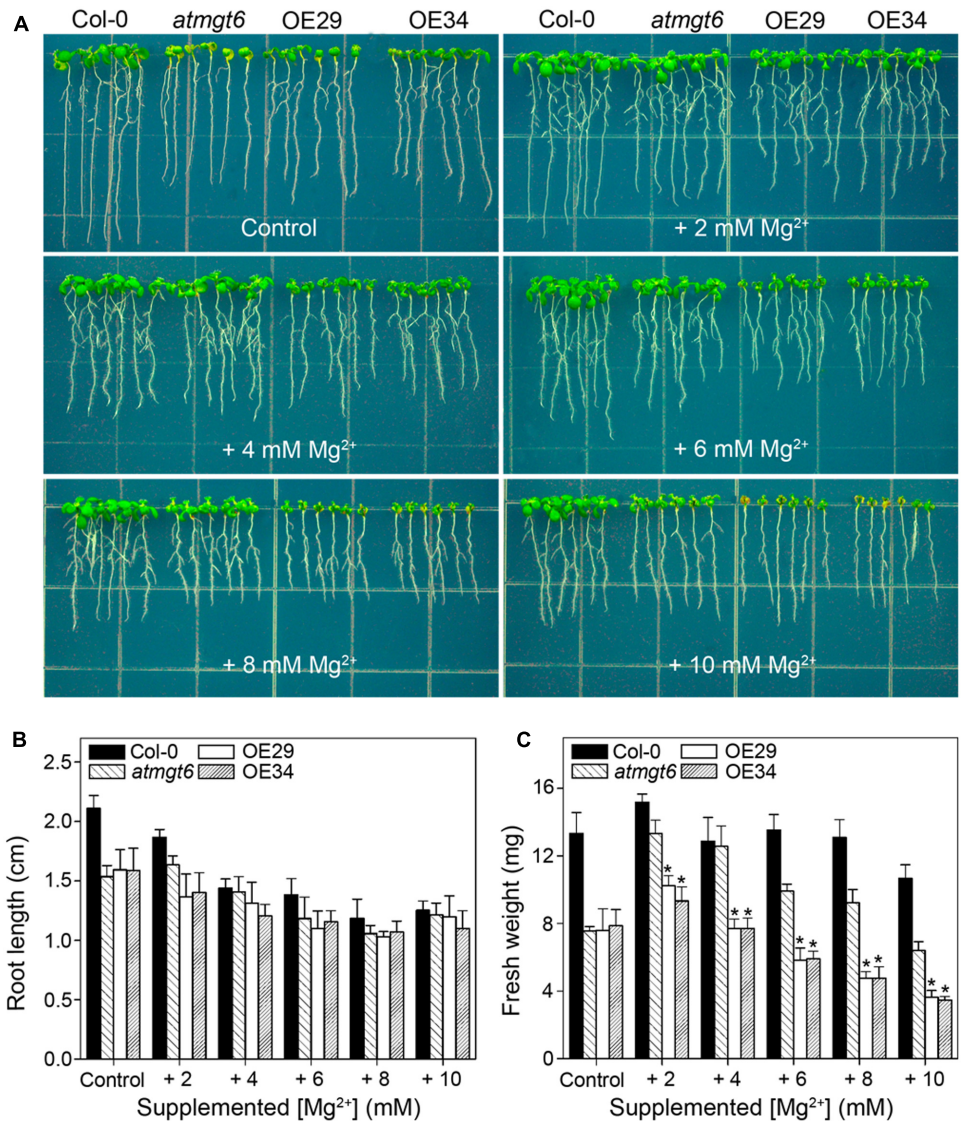

FIGURE 4 | Growth phenotype of *atmgt6* and transgenic *OsHKT2;4*-overexpression *atmgt6* lines in high-Mg^{2+} conditions. **(A)** The growth of Col-0, *atmgt6*, OE29, and OE34 under the Mg^{2+}-abundant conditions. After planted in half-strength MS (1/2 MS) medium for 3 days, Col-0, *atmgt6*, OE29, and OE34 were transferred to one-sixth-strength MS (1/6 MS, referred to as "Control" in the figure) containing a basal 0.25 mM Mg^{2+} and 1/6 MS medium supplemented with extra 2, 4, 6, 8, and 10 mM Mg^{2+}. Plants were photographed after growing for another 7 days. Quantitative analyses of primary root length **(B)** and whole-plant fresh weight **(C)** of Col-0, *atmgt6*, OE29, and OE34 under the Mg^{2+}-abundant conditions described in **(A)**. Six independent 10-day-old seedlings of each genotype were gathered as one biological repeat for root length and fresh weight measurement. Data are represented as the mean ± SD, $n = 3$, in which n is the number of biological repeat. Asterisks indicate statistically significant differences compared with *atmgt6* (Student's *t*-test, $^*P < 0.05$).

Ca^{2+} were added to the basal medium, both root length and fresh weight of OE29 and OE34 were recovered to almost an identical level with that of *atmgt6* (**Figures 6B,C** and Supplementary Figure 2), supporting the notion of Ca^{2+}-Mg^{2+} antagonism.

It has been reported that low Ca^{2+} in the medium triggered the increase of Mg^{2+} concentration, mimicking high-Mg^{2+} conditions (Rios et al., 2012). To analyze further whether Ca^{2+} deficiency is also responsible for the phenotype induced by high Mg^{2+}, we thus tested the sensitivity among different plants to low-Ca^{2+} conditions. In Ca^{2+}-depleted 1/6 MS medium ("basal medium" in **Figure 7**), similar phenotype was observed in *atmgt6* and OE lines, suggesting that OsHKT2;4 is not responsible for Ca^{2+} deficiency. On the contrary, as the increasing content of extra Mg^{2+} (2, 4, 6, and 8 mM) was added to the basal medium, differences of fresh weight between *atmgt6* and OE lines started to occur (**Figure 7** and Supplementary Figure 3). These results demonstrated that high Mg^{2+}, rather than Ca^{2+} deficiency, is the primary factor that caused growth defects in the OE lines than *atmgt6*.

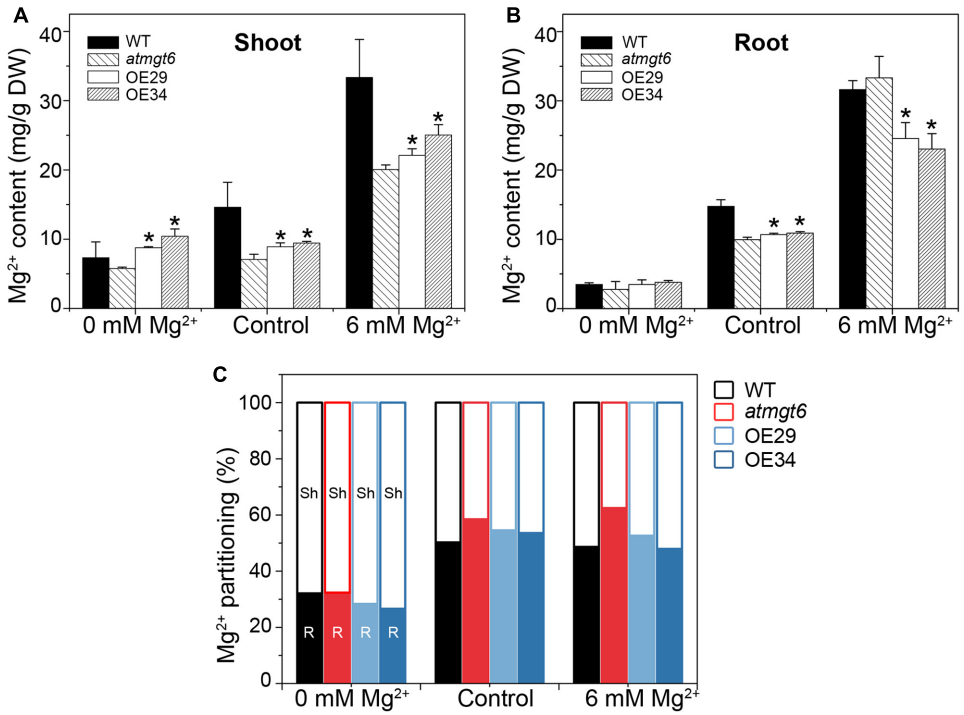

FIGURE 5 | Mg^{2+} content and its partitioning in shoots and roots of *atmgt6* and transgenic *OsHKT2;4*-overexpression *atmgt6* lines. Inductively Coupled Plasma-Mass Spectrometry (ICP-MS) analysis of Mg^{2+} contents in shoots **(A)** and roots **(B)** of Col-0, *atmgt6* and two transgenic *OsHKT2;4*-overexpression *atmgt6* lines, OE29 and OE34. After planted in the hydroponic medium containing 0.25 mM Mg^{2+} for 2 weeks, Col-0, *atmgt6*, OE29, and OE34 were transferred to the hydroponic medium containing 0, 0.25 (Control), or 6 mM Mg^{2+}, and were harvested for elemental analysis of roots and shoots after growing for 2 days. Data are represented as the mean ± SD, $n = 3$. Asterisks indicate statistically significant differences compared with *atmgt6* (Student's *t*-test, $*P < 0.05$). **(C)** Altered Mg^{2+} partitioning between shoot (Sh) and root (R) in Col-0, *atmgt6*, OE29, and OE34. Values are deduced from **(A,B)**.

DISCUSSION

Mg^{2+} is an essential macronutrient for plant growth, development and reproductive success (Li et al., 2001; Hermans et al., 2013; Mao et al., 2014), while it could be detrimental at high concentrations (Visscher et al., 2010). Plants possess specific Mg^{2+} transport systems that can function under a wide range of concentrations to secure intracellular Mg^{2+} homeostasis. Despite several transporters have been shown to function in Mg^{2+} uptake and distribution in *Arabidopsis*, including the AtMGT/AtMRS2-type transporters (Li et al., 2001) and Mg^{2+}/H^{+} antiporter AtMHX (Shaul et al., 1999), little is known about the transporters responsible for Mg^{2+} homeostasis in rice. OsHKT2;4 has been reported to function as a non-selective transporter for diverse cations, including Mg^{2+} and Ca^{2+}. Our study here provided further evidence that OsHKT2;4 exhibits characteristics of low-affinity transport of Mg^{2+}, and plays a key role in Mg^{2+} homeostasis for plant's adaptation to high-Mg^{2+} conditions.

Rice contains up to nine *HKT* genes (depending on variety), and OsHKT2;4 is the member of class II HKTs with the conserved Gly residues at the four P-loop filter positions (Mäser et al., 2002b). OsHKT2;4 is localized at the plasma membrane of rice cells, and its exogenous expression caused *X. laevis* oocytes to produce large currents when the extracellular Mg^{2+} concentrations were at the range of millimolar levels (Lan et al., 2010; Horie et al., 2011). *Triticum aestivum* HKT2;1 (TaHKT2;1) was also found to result in robust Mg^{2+} permeability of the oocytes, although to a lesser degree (Horie et al., 2011). OsHKT2;4-mediated currents exhibited the shifts to positive reversal potentials upon increased Mg^{2+} concentration from 5 to 50 mM (Horie et al., 2011). The present study further analyzed the capability of Mg^{2+}-uptake of OsHKT2;4 in three systems, the oocytes, bacteria, and *Arabidopsis* under the conditions containing high-Mg^{2+} concentrations. The current amplitudes and reversal potentials in the oocytes expressing OsHKT2;4 were not changed when the extracellular Mg^{2+} concentration was less than 1.2 mM, until its concentration reached 6 mM (**Figure 2**). Similarly, the expression of OsHKT2;4 rescued growth defects of MM281 bacteria cells that are deficient in Mg^{2+} uptake in the presence of relatively high-Mg^{2+} concentration, but the rescuing effect was much less than MGT10, the high-affinity Mg^{2+} transporter (**Figure 1**). Complementary to the observations in the oocytes and bacteria, the phenotype relating to Mg^{2+} stress in transgenic OsHKT2;4-overexpressed *atmgt6* lines happened at the Mg^{2+}-abundant (**Figure 4**), but not at Mg^{2+}-deficient conditions (**Figure 4**). Taken together, our findings showed that OsHKT2;4 has a distinct low-affinity Mg^{2+} transportation, and confirm Mg^{2+} permeability of OsHKT2;4 as reported (Lan et al., 2010; Horie et al., 2011). It is worth mentioning that OsHKT2;4

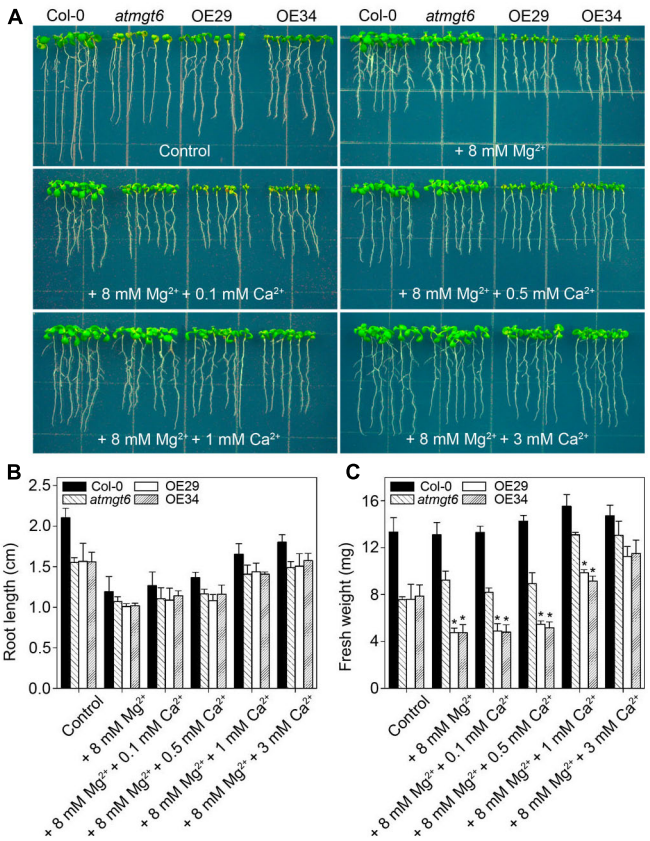

FIGURE 6 | Effects of high Ca^{2+} additions on the growth of *atmgt6* and transgenic *OsHKT2;4*-overexpression *atmgt6* lines in the Mg^{2+}-abundant medium. **(A)** The growth of Col-0, *atmgt6* and two transgenic *OsHKT2;4* overexpression *atmgt6* lines (OE29 and OE34) in 1/6 MS (Control) and the Mg^{2+}-abundant medium (1/6 MS with extra 8 mM Mg^{2+}, referred to as "+8 mM Mg^{2+}" in the figure) containing different extra Ca^{2+} concentrations. After planted in 1/2 MS medium for 3 days, Col-0, *atmgt6*, OE29, and OE34 were transferred to the 1/6 MS medium (containing a basal 0.25 mM Mg^{2+} and 0.5 mM Ca^{2+}), or the Mg^{2+}-abundant medium with 0, 0.1, 0.5, 1, or 3 mM extra Ca^{2+}. Plants were photographed after growing for another 7 days. Quantitative analyses of primary root length **(B)** and whole-plant fresh weight **(C)** of Col-0, *atmgt6*, OE29, and OE34 under the conditions described in **(A)**. Six independent 10-day-old seedlings of each genotype were gathered as one biological repeat for root length and fresh weight measurement. Data are represented as the mean ± SD, $n = 3$, in which n is the number of biological repeat. Asterisks indicate statistically significant differences compared with *atmgt6* (Student's *t*-test, $^*P < 0.05$).

was reported to be impermeable to Mg^{2+} when it was expressed in the oocytes by an independent study (Sassi et al., 2012). Due to the genetic diversity in rice during evolution and amino acid variation of HKTs among *Oryza* accessions (Horie et al., 2001; Ren et al., 2005), the differences might result from the sources of OsHKT2;4 from different rice varieties. In the previous studies (Lan et al., 2010; Horie et al., 2011) and the present study, genetically tractable rice (*O. sativa*; background Nipponbare) was used.

Mg^{2+} is taken up from the soil by the plant root system, which is likely to be mediated by AtMGT6/MRS2-4. AtMGT6/MRS2-4 is located in the plasma membrane or the endoplasmic reticulum and highly expressed in the root epidermal cells, and its disruption resulted in growth retardation of *Arabidopsis* under the low-Mg^{2+} condition (Mao et al., 2014; Oda et al., 2016). OsHKT2;4 might not be a key factor for roots to uptake Mg^{2+} from the low-Mg^{2+} environment as its overexpression did not cause the changed growth phenotype of transgenic lines (**Figure 3**), fitting the idea of its low-affinity Mg^{2+} transportation. After satisfying the needs of the roots, the rest of the Mg^{2+} will be transported to the shoot through the process involving AtMGT6/MRS2-4 activity (Oda et al., 2016). However, plants will display Mg^{2+} toxicity symptom when Mg^{2+} is over accumulated in the shoot. To deal with this toxicity, plants might restrain the Mg^{2+} distribution in shoot or sequester the excess intracellular Mg^{2+} into the vacuoles (Hermans et al., 2013; Tang et al., 2015). The OE lines had higher Mg^{2+} content in shoot compared with *atmgt6* under both low-Mg^{2+} and normal conditions (**Figure 5**), indicating the expression level of *OsHKT2;4* was high enough to drive transportation of Mg^{2+} from root to shoot. However, once the expression level of *OsHKT2;4* was further enhanced under high-Mg^{2+} conditions (Supplementary Figure 5), the Mg^{2+} transportation to shoot was also strengthened, thus leading to an increased Mg^{2+} distribution ratio of shoot to root and enhanced sensitivities of OE lines to high-Mg^{2+} conditions. Therefore, we suggested that OsHKT2;4 plays a key role in Mg^{2+} homeostasis and might control the Mg^{2+} translocation between roots and shoots under the high-Mg^{2+} conditions.

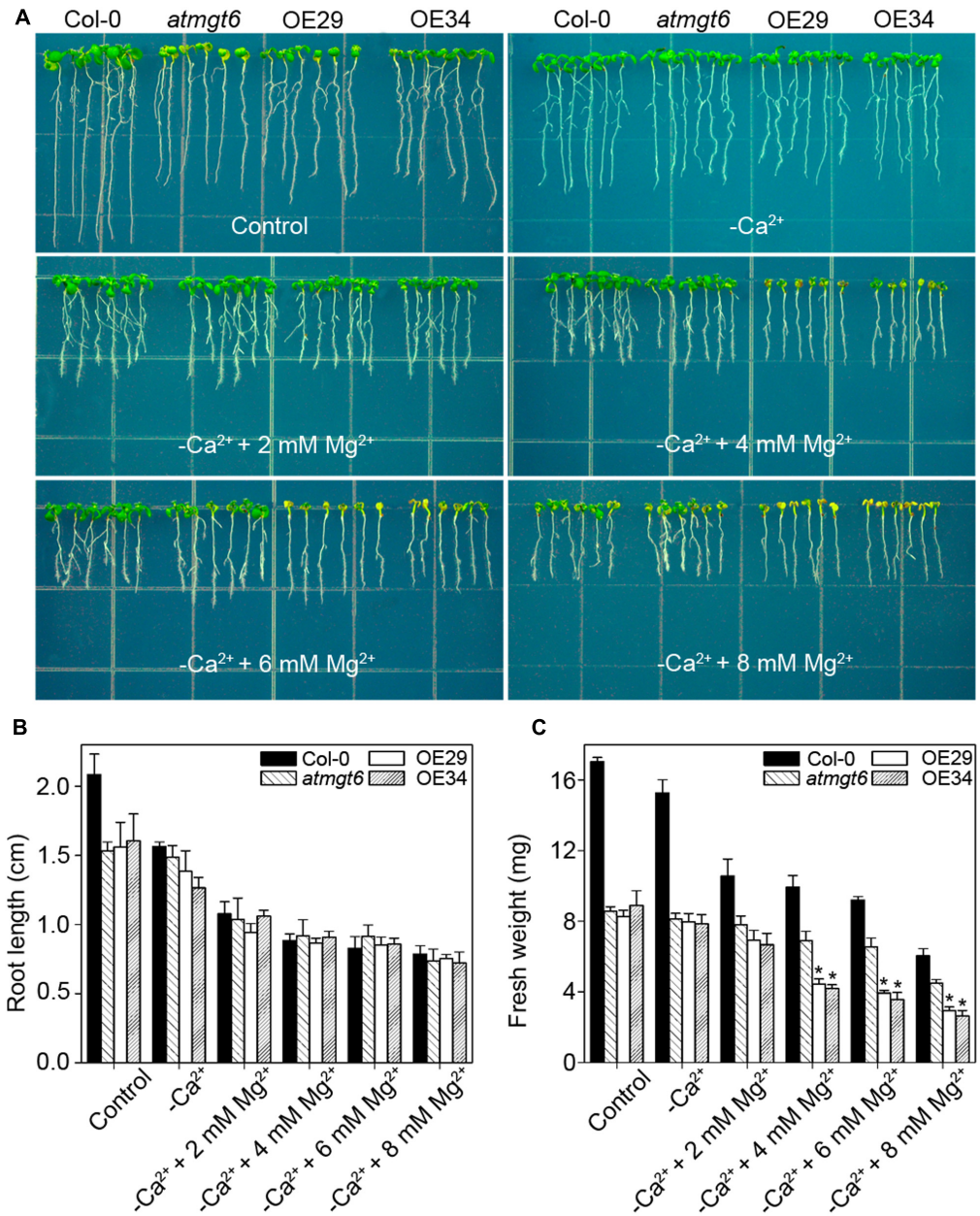

FIGURE 7 | Effects of the Ca^{2+} depletion on the growth of *atmgt6* and transgenic *OsHKT2;4*-overexpression *atmgt6* lines in the Mg^{2+}-abundant medium. **(A)** The growth of Col-0, *atmgt6* and transgenic two *OsHKT2;4* overexpression *atmgt6* lines (OE29 and OE34) in 1/6 MS (Control) and the 1/6 MS medium depleted of Ca^{2+} ($-Ca^{2+}$). After planted in 1/2 MS medium for 3 days, Col-0, *atmgt6*, OE29, and OE34 were transferred to the 1/6 MS medium (containing a basal 0.25 mM Mg^{2+} and 0.5 mM Ca^{2+}), or the 1/6 MS medium depleted of Ca^{2+} and supplemented with extra 2, 4, 6, or 8 mM Mg^{2+}. Plants were photographed after growing for another 7 days. Quantitative analyses of primary root length **(B)** and whole-plant fresh weight **(C)** of Col-0, *atmgt6*, OE29, and OE34 under the conditions described in **(A)**. Six independent 10-day-old seedlings of each genotype were gathered as one biological repeat for root length and fresh weight measurement. Data are represented as the mean ± SD, $n = 3$, in which n is the number of biological repeat. Asterisks indicate statistically significant differences compared with *atmgt6* (Student's *t*-test, $^*P < 0.05$).

Although roles of Ca^{2+} and Mg^{2+} are distinct in diverse physiological and biochemical processes, they may play an antagonistic function in plants. (Tang and Luan, 2017). For example, growth retardations induced by individual knockouts of genes in AtMRS2/AtMGT family under low Mg^{2+} could be ameliorated when Ca^{2+} concentrations were concomitantly lowered (Lenz et al., 2013). Mutation of *AtCAX1*, which encodes a vacuolar Ca^{2+}/H^+ exchanger, resulted in reduction of Ca^{2+} in the vacuole, thus leading to more Ca^{2+} retaining in the cytosol to counteract

with excess Mg^{2+} (Cheng et al., 2003; Bradshaw, 2005). Consistently, our study demonstrated that addition of Ca^{2+} to the high-Mg^{2+} medium could partially rescue the Mg^{2+}-induced growth defect of *atmgt6* and the OsHKT2;4-overexpressed lines to a wild type level (**Figure 6**), which is also a supportive evidence for the antagonistic interaction between Ca^{2+} and Mg^{2+} *in planta*. However, Mg^{2+} currents through OsHKT2;4 in oocytes were not inhibited and their reversal potentials were not significantly shifted in the presence of 1.8 mM Ca^{2+} in the perfusion solution (Supplementary Figure 4), indicating that Ca^{2+} did not inhibit Mg^{2+} uptake in oocytes expressing OsHKT2;4. Thus, the effects of changes in Ca^{2+} additions on Mg^{2+} toxicity might result from the physiological antagonism between Ca^{2+} and Mg^{2+} *in planta* (Bradshaw, 2005; Tang et al., 2015), although further evidence is needed.

In our previous study, we found that OsHKT2;4 had the diverse expression pattern in rice plants, including leaves, stems and primary/lateral roots, and was highly expressed at xylem and phloem of epidermis (Lan et al., 2010). However, the homozygous lines of *Tos*-tagged *oshkt2;4* rice lines behaved similarly to wild-type plants (Lan et al., 2010; Horie et al., 2011), and contained similar content of cations, including Mg^{2+} and Ca^{2+} (Lan et al., 2010). The absence of a phenotypic change in these rice lines suggested that OsHKT2;4 is functionally redundant with other transporters. Indeed, we found OsHKT2;4 rendered *Arabidopsis* Mg^{2+} sensitivity when *atmgt6* was knockout (**Figure 4**). Rice (*O. sativa*; background Nipponbare) is predicted to have nine AtMGT orthologs based on the BLAST search (Gebert et al., 2009), and Os10g0545000, the closest one to AtMGT6, is also widely expressed in rice according to the microarray gene expression data collected by Genevestigator[1] (Supplementary Figure 1). Elucidation of the functional relationships between MGT-type transporters and OsHKT2;4 will be a critical next step toward assessing their biological functions in rice.

[1] www.genevestigator.com

AUTHOR CONTRIBUTIONS

CZ, BZ, HL, JG, and WL designed the study. CZ, HL, BZ, and WL performed experiments. CZ, HL, JW, BZ, WW, JG, and WL analyzed and interpreted the data. CZ, HL, BZ, and WL wrote the manuscript. CZ, BZ, HL, SL, JG, and WL revised the manuscript critically. All authors read and approved the final manuscript.

FUNDING

This research was supported by the National Natural Science Foundation of China (31271626 and 31271682).

ACKNOWLEDGMENT

We thank Jiangsu Collaborative Innovation Center for Modern Crop Production for technical support.

SUPPLEMENTARY MATERIAL

The Supplementary Material for this article can be found online at: https://www.frontiersin.org/articles/10.3389/fpls.2017.01823/full#supplementary-material

REFERENCES

Ariyarathna, H. A., Oldach, K. H., and Francki, M. G. (2016). A comparative gene analysis with rice identified orthologous group II *HKT* genes and their association with Na^+ concentration in bread wheat. *BMC Plant Biol.* 16:21. doi: 10.1186/s12870-016-0714-7

Bose, J., Babourina, O., Shabala, S., and Rengel, Z. (2013). Low-pH and aluminum resistance in *Arabidopsis* correlates with high cytosolic magnesium content and increased magnesium uptake by plant roots. *Plant Cell Physiol.* 54, 1093–1104. doi: 10.1093/pcp/pct064

Bradshaw, H. D. Jr. (2005). Mutations in *CAX1* produce phenotypes characteristic of plants tolerant to serpentine soils. *New Phytol.* 167, 81–88. doi: 10.1111/j.1469-8137.2005.01408.x

Chen, J., Li, L. G., Liu, Z. H., Yuan, Y. J., Guo, L. L., Mao, D. D., et al. (2009). Magnesium transporter AtMGT9 is essential for pollen development in *Arabidopsis*. *Cell Res.* 19, 887–898. doi: 10.1038/cr.2009.58

Cheng, N. H., Pittman, J. K., Barkla, B. J., Shigaki, T., and Hirschi, K. D. (2003). The *Arabidopsis cax1* mutant exhibits impaired ion homeostasis, development, and hormonal responses and reveals interplay among vacuolar transporters. *Plant Cell* 15, 347–364. doi: 10.1105/tpc.007385

Chérel, I., Lefoulon, C., Boeglin, M., and Sentenac, H. (2014). Molecular mechanisms involved in plant adaptation to low K^+ availability. *J. Exp. Bot.* 65, 833–848. doi: 10.1093/jxb/ert402

Clough, S. J., and Bent, A. F. (1998). Floral dip: a simplified method for *Agrobacterium*-mediated transformation of *Arabidopsis thaliana*. *Plant J.* 16, 735–743. doi: 10.1046/j.1365-313x.1998.00343.x

Corratgé-Faillie, C., Jabnoune, M., Zimmermann, S., Véry, A. A., Fizames, C., and Sentenac, H. (2010). Potassium and sodium transport in non-animal cells: the Trk/Ktr/HKT transporter family. *Cel. Mol. Life Sci.* 67, 2511–2532. doi: 10.1007/s00018-010-0317-7

Davenport, R. J., Munoz-Mayor, A., Jha, D., Essah, P. A., Rus, A., and Tester, M. (2007). The Na^+ transporter AtHKT1;1 controls retrieval of Na^+ from the xylem in *Arabidopsis*. *Plant Cell Environ.* 30, 497–507. doi: 10.1111/j.1365-3040.2007.01637.x

Garciadeblas, B., Senn, M. E., Banuelos, M. A., and Rodriguez-Navarro, A. (2003). Sodium transport and HKT transporters: the rice model. *Plant J.* 34, 788–801. doi: 10.1046/j.1365-313X.2003.01764.x

Gebert, M., Meschenmoser, K., Svidova, S., Weghuber, J., Schweyen, R., Eifler, K., et al. (2009). A root-expressed magnesium transporter of the *MRS2/MGT* gene family in *Arabidopsis thaliana* allows for growth in low-Mg^{2+} environments. *Plant Cell* 21, 4018–4030. doi: 10.1105/tpc.109.070557

Hauser, F., and Horie, T. (2010). A conserved primary salt tolerance mechanism mediated by HKT transporters: a mechanism for sodium exclusion and maintenance of high K^+/Na^+ ratio in leaves during salinity stress. *Plant Cell Environ.* 33, 552–565. doi: 10.1111/j.1365-3040.2009.02056.x

Hermans, C., Conn, S. J., Chen, J., Xiao, Q., and Verbruggen, N. (2013). An update on magnesium homeostasis mechanisms in plants. *Metallomics* 5, 1170–1183. doi: 10.1039/c3mt20223b

Hicks, D. B., Wang, Z., Wei, Y., Kent, R., Guffanti, A. A., Banciu, H., et al. (2003). A tenth *atp* gene and the conserved *atpI* gene of a *Bacillus atp* operon have a role in Mg^{2+} uptake. *Proc. Natl. Acad. Sci. U.S.A.* 100, 10213–10218. doi: 10.1073/pnas.1832982100

Hirsch, R. E., Lewis, B. D., Spalding, E. P., and Sussman, M. R. (1998). A role for the AKT1 potassium channel in plant nutrition. *Science* 280, 918–921. doi: 10.1126/science.280.5365.918

Horie, T., Brodsky, D. E., Costa, A., Kaneko, T., Lo Schiavo, F., Katsuhara, M., et al. (2011). K^+ transport by the OsHKT2;4 transporter from rice with atypical Na^+ transport properties and competition in permeation of K^+ over Mg^{2+} and Ca^{2+} ions. *Plant Physiol.* 156, 1493–1507. doi: 10.1104/pp.110.168047

Horie, T., Costa, A., Kim, T. H., Han, M. J., Horie, R., Leung, H. Y., et al. (2007). Rice OsHKT2;1 transporter mediates large Na^+ influx component into K^+-starved roots for growth. *EMBO J.* 26, 3003–3014. doi: 10.1038/sj.emboj.7601732

Horie, T., Hauser, F., and Schroeder, J. I. (2009). HKT transporter-mediated salinity resistance mechanisms in *Arabidopsis* and monocot crop plants. *Trends Plant Sci.* 14, 660–668. doi: 10.1016/j.tplants.2009.08.009

Horie, T., Yoshida, K., Nakayama, H., Yamada, K., Oiki, S., and Shinmyo, A. (2001). Two types of HKT transporters with different properties of Na^+ and K^+ transport in *Oryza sativa*. *Plant J.* 27, 129–138. doi: 10.1046/j.1365-313x.2001.01077.x

Knoop, V., Groth-Malonek, M., Gebert, M., Eifler, K., and Weyand, K. (2005). Transport of magnesium and other divalent cations: evolution of the 2-TM-GxN proteins in the MIT superfamily. *Mol. Genet. Genomics* 274, 205–216. doi: 10.1007/s00438-005-0011-x

Lan, W. Z., Wang, W., Wang, S. M., Li, L. G., Buchanan, B. B., Lin, H. X., et al. (2010). A rice high-affinity potassium transporter (HKT) conceals a calcium-permeable cation channel. *Proc. Natl. Acad. Sci. U.S.A.* 107, 7089–7094. doi: 10.1073/pnas.1000698107

Larkin, R. M. (2016). Tetrapyrrole signaling in plants. *Front. Plant Sci.* 7:1586. doi: 10.3389/fpls.2016.01586

Lenz, H., Dombinov, V., Dreistein, J., Reinhard, M. R., Gebert, M., and Knoop, V. (2013). Magnesium deficiency phenotypes upon multiple knockout of *Arabidopsis thaliana* MRS2 clade B genes can be ameliorated by concomitantly reduced calcium supply. *Plant Cell Physiol.* 54, 1118–1131. doi: 10.1093/pcp/pct062

Li, L., Tutone, A. F., Drummond, R. S., Gardner, R. C., and Luan, S. (2001). A novel family of magnesium transport genes in *Arabidopsis*. *Plant Cell* 13, 2761–2775. doi: 10.1105/tpc.010352

Li, L. G., Sokolov, L. N., Yang, Y. H., Li, D. P., Ting, J., Pandy, G. K., et al. (2008). A mitochondrial magnesium transporter functions in *Arabidopsis* pollen development. *Mol. Plant* 1, 675–685. doi: 10.1093/mp/ssn031

Mao, D., Chen, J., Tian, L., Liu, Z., Yang, L., Tang, R., et al. (2014). *Arabidopsis* transporter MGT6 mediates magnesium uptake and is required for growth under magnesium limitation. *Plant Cell* 26, 2234–2248. doi: 10.1105/tpc.114.124628

Mao, D. D., Tian, L. F., Li, L. G., Chen, J., Deng, P. Y., Li, D. P., et al. (2008). AtMGT7: an *Arabidopsis* gene encoding a low-affinity magnesium transporter. *J. Integr. Plant Biol.* 50, 1530–1538. doi: 10.1111/j.1744-7909.2008.00770.x

Mäser, P., Eckelman, B., Vaidyanathan, R., Horie, T., Fairbairn, D. J., Kubo, M., et al. (2002a). Altered shoot/root Na^+ distribution and bifurcating salt sensitivity in *Arabidopsis* by genetic disruption of the Na^+ transporter *AtHKT1*. *FEBS Lett.* 531, 157–161. doi: 10.1016/S0014-5793(02)03488-9

Mäser, P., Hosoo, Y., Goshima, S., Horie, T., Eckelman, B., Yamada, K., et al. (2002b). Glycine residues in potassium channel-like selectivity filters determine potassium selectivity in four-loop-per-subunit HKT transporters from plants. *Proc. Natl. Acad. Sci. U.S.A.* 99, 6428–6433. doi: 10.1073/pnas.082123799

Miedema, H., Bothwell, J. H., Brownlee, C., and Davies, J. M. (2001). Calcium uptake by plant cells–channels and pumps acting in concert. *Trends Plant Sci.* 6, 514–519. doi: 10.1016/S1360-1385(01)02124-0

Møller, I. S., Gilliham, M., Jha, D., Mayo, G. M., Roy, S. J., Coates, J. C., et al. (2009). Shoot Na^+ exclusion and increased salinity tolerance engineered by cell type-specific alteration of Na^+ transport in *Arabidopsis*. *Plant Cell* 21, 2163–2178. doi: 10.1105/tpc.108.064568

Munns, R., and Tester, M. (2008). Mechanisms of salinity tolerance. *Annu. Rev. Plant Biol.* 59, 651–681. doi: 10.1146/annurev.arplant.59.032607.092911

Nieves-Cordones, M., Martinez, V., Benito, B., and Rubio, F. (2016). Comparison between *Arabidopsis* and rice for main pathways of K^+ and Na^+ uptake by roots. *Front. Plant Sci.* 7:992. doi: 10.3389/fpls.2016.00992

Oda, K., Kamiya, T., Shikanai, Y., Shigenobu, S., Yamaguchi, K., and Fujiwara, T. (2016). The *Arabidopsis* Mg transporter, MRS2-4, is essential for Mg homeostasis under both low and high Mg conditions. *Plant Cell Physiol.* 57, 754–763. doi: 10.1093/pcp/pcv196

Platten, J. D., Cotsaftis, O., Berthomieu, P., Bohnert, H., Davenport, R. J., Fairbairn, D. J., et al. (2006). Nomenclature for HKT transporters, key determinants of plant salinity tolerance. *Trends Plant Sci.* 11, 372–374. doi: 10.1016/j.tplants.2006.06.001

Ren, Z. H., Gao, J. P., Li, L. G., Cai, X. L., Huang, W., Chao, D. Y., et al. (2005). A rice quantitative trait locus for salt tolerance encodes a sodium transporter. *Nat. Genet.* 37, 1141–1146. doi: 10.1038/ng1643

Rios, J. J., Lochlainn, S. O., Devonshire, J., Graham, N. S., Hammond, J. P., King, G. J., et al. (2012). Distribution of calcium (Ca) and magnesium (Mg) in the leaves of *Brassica rapa* under varying exogenous Ca and Mg supply. *Ann. Bot.* 109, 1081–1089. doi: 10.1093/aob/mcs029

Rodriguez-Navarro, A. (2000). Potassium transport in fungi and plants. *Biochim. Biophys. Acta.* 1469, 1–30. doi: 10.1016/S0304-4157(99)00013-1

Sassi, A., Mieulet, D., Khan, I., Moreau, B., Gaillard, I., Sentenac, H., et al. (2012). The rice monovalent cation transporter OsHKT2;4: revisited ionic selectivity. *Plant Physiol.* 160, 498–510. doi: 10.1104/pp.112.194936

Shaul, O. (2002). Magnesium transport and function in plants: the tip of the iceberg. *Biometals* 15, 307–321. doi: 10.1023/A:1016091118585

Shaul, O., Hilgemann, D. W., de-Almeida-Engler, J., Van Montagu, M., Inz, D., and Galili, G. (1999). Cloning and characterization of a novel Mg^{2+}/H^+ exchanger. *EMBO J.* 18, 3973–3980. doi: 10.1093/emboj/18.14.3973

Tang, R. J., and Luan, S. (2017). Regulation of calcium and magnesium homeostasis in plants: from transporters to signaling network. *Curr. Opin. Plant Biol.* 39, 97–105. doi: 10.1016/j.pbi.2017.06.009

Tang, R. J., Zhao, F. G., Garcia, V. J., Kleist, T. J., Yang, L., Zhang, H. X., et al. (2015). Tonoplast CBL-CIPK calcium signaling network regulates magnesium homeostasis in Arabidopsis. *Proc. Natl. Acad. Sci. U.S.A.* 112, 3134–3139. doi: 10.1073/pnas.1420944112

Townsend, D. E., Esenwine, A. J., Rd, G. J., Bross, D., Maguire, M. E., and Smith, R. L. (1995). Cloning of the *mgtE* Mg^{2+} transporter from *Providencia stuartii* and the distribution of *mgtE* in gram-negative and gram-positive bacteria. *J. Bacteriol.* 177, 5350–5354. doi: 10.1128/jb.177.18.5350-5354.1995

Uozumi, N., Rubio, F., Kim, E. J., Yamaguchi, T., Muto, S., Tsuboi, A., et al. (2000). The *Arabidopsis HKT1* gene homolog mediates inward Na^+ currents in *Xenopus laevis* oocytes and Na^+ uptake in *Saccharomyces cerevisiae*. *Plant Physiol.* 122, 1249–1259. doi: 10.1104/pp.122.4.1249

Visscher, A. M., Paul, A. L., Kirst, M., Guy, C. L., Schuerger, A. C., and Ferl, R. J. (2010). Growth performance and root transcriptome remodeling of *Arabidopsis* in response to Mars-like levels of magnesium sulfate. *PLOS ONE* 5:e12348. doi: 10.1371/journal.pone.0012348

Yamaguchi, T., Hamamoto, S., and Uozumi, N. (2013). Sodium transport system in plant cells. *Front. Plant Sci.* 4:410. doi: 10.3389/fpls.2013.00410

Yao, X., Horie, T., Xue, S., Leung, H. Y., Katsuhara, M., Brodsky, D. E., et al. (2010). Differential sodium and potassium transport selectivities of the rice OsHKT2;1 and OsHKT2;2 transporters in plant cells. *Plant Physiol.* 152, 341–355. doi: 10.1104/pp.109.145722

Yermiyahu, U., Nir, S., Benhayyim, G., and Kafkafi, U. (1994). Quantitative competition of calcium with sodium or magnesium for sorption sites on plasma membrane vesicles of melon (*Cucumis melo* L.) root cells. *J. Membr. Biol.* 138, 55–63. doi: 10.1007/BF00211069

Conflict of Interest Statement: The authors declare that the research was conducted in the absence of any commercial or financial relationships that could be construed as a potential conflict of interest.

frontiers in Plant Science

ORIGINAL RESEARCH
published: 13 October 2017
doi: 10.3389/fpls.2017.01752

Overexpression of Pyrabactin Resistance-Like Abscisic Acid Receptors Enhances Drought, Osmotic, and Cold Tolerance in Transgenic Poplars

Jingling Yu[1†], Haiman Ge[1†], Xiaokun Wang[1], Renjie Tang[2], Yuan Wang[1], Fugeng Zhao[1], Wenzhi Lan[1], Sheng Luan[1,2]* and Lei Yang[1]**

[1] State Key Laboratory for Pharmaceutical Biotechnology, NJU–NFU Joint Institute for Plant Molecular Biology, College of Life Sciences, Nanjing University, Nanjing, China, [2] Department of Plant and Microbial Biology, University of California, Berkeley, Berkeley, CA, United States

OPEN ACCESS

Edited by:
Kai He,
Lanzhou University, China

Reviewed by:
Frantisek Baluska,
University of Bonn, Germany
Tamara Pecenkova,
Institute of Experimental Botany (ASCR), Czechia

***Correspondence:**
Wenzhi Lan
lanw@nju.edu.cn
Sheng Luan
sluan@berkeley.edu
Lei Yang
leiyang@nju.edu.cn

† These authors have contributed equally to this work.

Specialty section:
This article was submitted to Plant Traffic and Transport, a section of the journal Frontiers in Plant Science

Received: 22 July 2017
Accepted: 25 September 2017
Published: 13 October 2017

Citation:
Yu J, Ge H, Wang X, Tang R, Wang Y, Zhao F, Lan W, Luan S and Yang L (2017) Overexpression of Pyrabactin Resistance-Like Abscisic Acid Receptors Enhances Drought, Osmotic, and Cold Tolerance in Transgenic Poplars. Front. Plant Sci. 8:1752. doi: 10.3389/fpls.2017.01752

Abscisic acid (ABA) has been known participate in a wider range of adaptive responses to diverse environmental abiotic stresses such as drought, osmosis, and low temperatures. ABA signaling is initiated by its receptors PYR/PYL/RCARs, a type of soluble proteins with a conserved START domain which can bind ABA and trigger the downstream pathway. Previously, we discovered that poplar (*Populus trichocarpa*) genome encodes 14 PYR/PYL/RCAR orthologs (PtPYRLs), and two of them, PtPYRL1 and PtPYRL5 have been functionally characterized to positively regulate drought tolerance. However, the physiological function of these ABA receptors in poplar remains uncharacterized. Here, we generated transgenic poplar plants overexpressing PtPYRL1 and PtPYRL5 and found that they exhibited more vigorous growth and produced greater biomass when exposed to drought stress. The improved drought tolerance was positively correlated with the key physiological responses dictated by the ABA signaling pathway, including increase in stomatal closure and decrease in leaf water loss. Further analyses revealed that overexpression lines showed improved capacity in scavenging reactive oxygen species and enhanced the activation of antioxidant enzymes under drought stress. Moreover, overexpression of *PtPYRL1* or *PtPYRL5* significantly increased the poplar resistance to osmotic and cold stresses. In summary, our results suggest that constitutive expression of *PtPYRL1* and *PtPYRL5* significantly enhances the resistance to drought, osmotic and cold stresses by positively regulating ABA signaling in poplar.

Keywords: *Populus*, ABA receptor, drought, cold stress, osmotic stress, resistance

INTRODUCTION

Plants, as sessile organisms, have evolved sophisticated developmental and physiological strategies to adapt to the unfavorable and changing environments such as drought, high salinity, and temperature fluctuations. Drought has particularly been considered as one of the most serious natural hazards for agriculture due to the increasing water scarcity (Liu et al., 2015). Numerous

studies showed that drought stress exerts many negative effects on plant growth, photosynthesis, biomass accumulation, and ecosystem carbon cycling (Liu et al., 2011; Zhou et al., 2015). Desiccation results in the production of reactive oxygen species (ROS), the production of which, in turn, serves as an important indicator to multiple abiotic stresses (Apel and Hirt, 2004; Contreras-Porcia et al., 2011). Normally, ROS are rapidly scavenged as a result of the activation of an efficient antioxidant system involved in various drought-induced signaling pathways, which are modulated by abscisic acid (ABA) (Jiang and Zhang, 2002; Contreras-Porcia et al., 2011).

The physiological functions of ABA has been extensively investigated in plants since it was identified in the 1960s as an endogenous plant hormone which regulates many essential processes, including seed germination, stomatal movement, plant development and adaptive responses, to multiple environmental stresses, such as drought, extreme temperatures, hyperosmolarity, and salinity (Finkelstein et al., 2002; Park et al., 2009). Many key components in ABA signaling pathway have been identified at the molecular level (Finkelstein et al., 2002), including ABA receptors (Shen et al., 2006; Liu et al., 2007; Pandey et al., 2009), the group A type 2 C protein phosphatases (PP2Cs) that negatively regulate ABA signaling at an early step in the pathway (Allen et al., 1999), the SnRK2 kinases that are positive regulators (Mustilli et al., 2002; Yoshida et al., 2002; Fujii et al., 2007), transcription factors (Seki et al., 2002; Himmelbach et al., 2003) and ion channels (Lee et al., 2009).

As the initial sensor of ABA signaling pathway, 14 genes designated as *Pyr1* and *Pyl1-Pyl13* (for *PYR1-Like*) have been identified in the *Arabidopsis* genome and encode proteins belonging to members of the cyclase subfamily of the START/Bet v I superfamily, which share a conserved hydrophobic ligand-binding pocket (Ma et al., 2009; Park et al., 2009). In presence of ABA, these proteins perceive ABA, then undergo conformation changes, and subsequently bind to clade A subfamily of PP2Cs, thus de-repressing the inactivation of the downstream SNF1-related protein kinase 2 (SnRK2) kinases. The PYR/PYL/RCAR-PP2C-SnRK2 signaling module is conserved across land plants.

Genetic evidence suggested that higher-order mutants lacking multiple ABA receptors in *Arabidopsis* (*Pyr1;Pyl1;Pyl2;Pyl4;Pyl5;Pyl8*) exhibit severe ABA insensitive phenotypes, establishing their critical physiological roles in ABA signaling (Gonzalez-Guzman et al., 2012). *PYL5* over-expression in *Arabidopsis* led to a globally enhanced response to ABA and enhanced drought resistance (Santiago et al., 2009). Constitutive overexpression of PYL8/RCAR3 confers ABA hypersensitivity in *Arabidopsis* seeds (Saavedra et al., 2010). Overexpression of *NtPYL4* in tobacco hairy roots resulted in a reprogramming of the cellular metabolism that is represented by a decreased alkaloid accumulation and conferred ABA sensitivity to the production of alkaloids (Lackman et al., 2011).

Tree species in the genus *Populus* spp., commonly known as poplars, aspens, and cottonwoods, are widespread in the northern hemisphere with nutrient-poor environments, and are increasingly important for bioenergy, wood products, and environmental services (Doty et al., 2016). Most of the poplar cultivation and distribution area are in the desolate lands on the earth where it is usually cold and dry in winter, causing the restriction of poplar forestry. Therefore, it is very critical to improve the resistance of poplars to abiotic stresses, including drought-resistance and cold-resistance. We have previously shown that PtPYRL1 and PtPYRL5 (poplar AtPYR1-like 1 and 5) physically interacted with PP2Cs, which interacted with SnRK2 kinase, suggesting they might act as the ABA receptors in mediating ABA signal transduction through phosphorylation and dephosphorylation (Yu et al., 2016). Furthermore, overexpression of *PtPYRL1* or *PtPYRL5* in *Arabidopsis* enhanced ABA sensitivity and drought-resistance. However, it is still unknown if they also play a similar function in poplars which protect against drought stress. Here, we report that the overexpression of *PtPYRL1* and *PtPYRL5* in poplar enhances resistance to drought, osmosis, and cold, the abiotic stresses that poplar frequently encounters. Our results also provide a potential biotechnological tool in engineering stress-resistant poplar cultivars.

MATERIALS AND METHODS

Plant Materials and Growth Conditions

The sterile wild-type and transgenic hybrid poplar (*Populus davidiana* × *Populus bolleana*) were amplified by micropropagation with leaf bud explants and kept under a 16-h-light/8-h-dark photoperiod (120 $\mu mol \cdot m^{-2} \cdot s^{-1}$) at 21–24°C. The plantlets were sub-cultured onto fresh 1/2 Murashige and Skoog (MS) medium supplemented with 0.1 $mg \cdot L^{-1}$ naphthaleneacetic acid (NAA) and 1% (w/v) agar. Two-week-old wild type (WT) or transgenic hybrid poplars with new roots were transferred to 7.5 cm-width pots containing nutrient soil. The plants were grown in greenhouse under a 16-h-light/8-h-dark (120 $\mu mol \cdot m^{-2} \cdot s^{-1}$) at 21–24°C.

Poplar Transformation

To construct the pCAMBIA1301S2-*PtPYRL1* (or *PtPYRL5*) plasmid, the entire coding region of *PtPYRL1* (or *PtPYRL5*) was amplified by PCR with *Xba I-Sal I* (or *BamH I-Sal I*) linker primers and cloned into modified pCAMBIA1301S2 with the 2×CaMV 35S promoter via the *Xba I-Sal I* (or *BamH I-Sal I*) site (**Supplementary Figure S1**). The hybrid poplars (*Populus davidiana* × *Populus bolleana*) were transformed using *Agrobacterium tumefaciens* (EHA105 strain) infection method. Briefly, leave explants excised from 1- to 2-month-old were inoculated in the EHA105 culture resuspended with liquid MS for 10 min and then were plated on solid MS medium containing 0.4 $mg \cdot L^{-1}$ 6-BA, 0.1 $mg \cdot L^{-1}$ NAA and 0.01 $mg \cdot L^{-1}$ TDZ. After 2 days of co-cultivation with *Agrobacterium*, the explants were transferred onto fresh MS medium containing 400 $mg \cdot L^{-1}$ timentin, and 10 $mg \cdot L^{-1}$ hygromycin for selective regeneration. When regenerated shoots reached 1 cm tall, they were excised and placed on rooting medium. Then, the rooted seedlings were transferred into soil and grown in the greenhouse. The presence of transgene was verified by PCR from genomic DNA, using primers specific for P35S and *PtPYRL1*-RT-R or *PtPYRL5*-RT-R.

Histochemical GUS Analysis

Detection of β-glucuronidase (GUS) activity was performed as described by Jefferson et al. (1987) with some modifications: leaf explants were incubated in GUS assay buffer (50 mM sodium phosphate, pH 7.0, 0.1% [v/v] Triton X-100, 0.5 mM ferricyanide, 0.5 mM ferrocyanide, and 2 mM 5-bromo-4-chloro-3-indolyl-β-D-glucuronide) for 12 h at 37°C. Then the plant tissues were decolorized in 75% ethanol for three times. The samples were photographed after treatment.

Quantitative Real-time PCR Analysis

Total RNA was extracted from various samples using TRIzol reagent (Invitrogen, Carlsbad, CA, United States), which was sequentially treated with DNase I (Invitrogen) and reverse transcribed by M-MLV reverse transcriptase (Promega). In semi-quantitative RT-PCR and qRT-PCR assays, the poplar elongation factor gene *EF1*β was used as an internal reference. qRT-PCR was performed with a CFX Connect Real-Time System (Bio-Rad). The relative expression of series indicated genes was calculated based on the comparative threshold cycle method using *EF1*β as a control and normalized to the WT hybrid poplars (under normal conditions). All primers used in this study were listed in Supplementary Table S1.

Drought–Rehydration Experiments

Two-week-old WT or transgenic poplars were transplanted to each 7.5 cm-width pot containing 50 g nutrient soil for greenhouse cultivation. We chose the 2-month-old WT or transgenic poplar seedlings with the same height to perform the drought and rehydration experiments. As the control, half of WT and transgenic poplar seedlings were normally watered, and the rest of these seedlings were not watered. After 1 week, the plantlets were watered again. After 3 days, the re-watered plants were photographed.

Water Potential Determination

Leaf water potential was measured on the same location of the blade with a WP4-T Dew point PotentiaMeter (Decagon Devices, Inc., United States). Five individual plants from WT or different transgenic poplars were measured after drought treatment for 5 days.

Measurement of Contents of H_2O_2, MDA, and Proline

H_2O_2 in fresh leaves was analyzed using the method reported by Hu et al. (2012). The absorbance was recorded at 390 nm with the spectrophotometer (Biomate 3S, Thermo). Malondialdehyde (MDA) content was quantified using the method reported by Heath and Packer (1968), which is related with the level of lipid peroxidation in the leaves. The absorbance was read at 532 and 600 nm by the spectrophotometer (Biomate 3S, Thermo) with thiobarbituric acid (1%) in 20% trichloroacetic acid as control. The Proline content in leaves was quantified using the method by Bates et al. (1973). The absorbance was measured spectrophotometrically (Biomate 3S, Thermo) at 520 nm and toluene was used as blank.

Extraction and Assay of Antioxidant Enzymes

Fresh leaves (0.5 g/sample) were homogenized in presence of 100 mM Tris-HCl (5.0 ml, pH 7.5), 3.0 mM β-mercaptoethanol, 1.0 mM EDTA (ethylenediaminetetraacetic acid), and 1.5% polyvinylpyrrolidone-40. The mixture was better supplemented with serine and cysteine proteinase inhibitors [1.0 mM phenylmethanesulfonyl fluoride (PMSF) + 1.0 $\mu g \cdot mL^{-1}$ aprotinin]. The homogenate was centrifuged at 10,000 × *g* for 15 min (4°C) after the filtration through cheese cloth. The supernatants were collected and served as the crude enzyme for determination of SOD (EC1.15.1.1), CAT (EC1.11.1.6), and POD (EC 1.11.1.7) activities. For the determination of APX activity, leaf sample was separately grounded in a homogenizing medium supplemented with 2.0 mM ascorbic acid (AsA) to maintain the enzyme stability. SOD activity was analyzed after the photoreduction of nitroblue tetrazolium (NBT) according to the method of Giannopolitis and Ries (1977). The absorbance was recorded spectrophotometrically (Biomate 3S, Thermo) at 560 nm. One unit of SOD is the quantity of protein that hampers 50% photoreduction of NBT and the activity was expressed as enzyme unit (EU)$\cdot mg^{-1}$ protein. The method of Chance and Maehly (1955) was employed to analyze CAT activity. The absorbance was read at 240 nm through a UV-Visible spectrophotometer (Biomate 3S, Thermo) and EU$\cdot mg^{-1}$ protein represented the CAT activity. The method of Nakano and Asada (1981) was used for the APX activity (EC1.11.1.11) measurement. The absorbance was recorded at 290 nm each 30 s for 3 min spectrophotometrically (Biomate 3S, Thermo). The POD activity was determined by examining the absorbance of reaction buffer at 420 nm based on guaiacol oxidation (Maehly and Chance, 1954). APX activity was calculated by

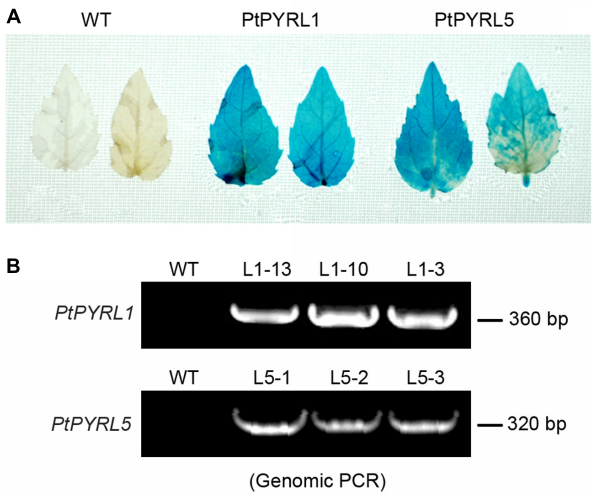

FIGURE 1 | Identification of transgenic poplar plants. **(A)** Histochemical analysis of GUS histochemical in *PtPYRL1* and *PtPYRL5* transgenic poplar leaves. **(B)** PCR analysis of genomic DNA from different independently regenerated hygromycin resistant lines using 35S and *PtPYRL1* and *PtPYRL5* specific primers.

the consumption rate of ASC using the ASC extinction molar coefficient ($e = 2.8\ mM^{-1}{\cdot}cm^{-1}$). APX activity was expressed with $EU{\cdot}mg^{-1}$ protein. One unit of APX is the quantity of protein used to break down 1.0 μmol of substrate per min at 25°C. The activity of GR (EC 1.6.4.2) and GPX (EC 1.11.1.9) was determined using GR Assay Kit (S0055, Beyotime, China) and Total GPX Assay Kit (S0058, Beyotime, China), respectively, according to the manufacturer's instructions. The absorbance was read at 340 nm with spectrophotometer (Biomate 3S, Thermo). GR activity was expressed as μmol NADPH oxidized min^{-1} ($EU{\cdot}mg^{-1}$ protein) (Carlberg and Mannervik, 1985). The GPX activity was calculated by measuring the reduction of NADPH to $NADP^+$ at 340 nm of absorbance.

Analysis of Relative Water Content (RWC)

The extent of desiccation in WT and transgenic poplars aboveground part was indicated with RWC (%) following the formula RWC % = $(W_{de} - W_{dr})/(W_f - W_{dr}) \times 100$, where W_f is the wet weight of fully hydrated aboveground part, W_{de} is the dehydrated weight after desiccation for a period of time, and W_{dr} is the dry weight determined after 48 h of drying at 80°C. Through this, the RWC reflects the extent of desiccation, with a fully hydrated shoot having a RWC of 100% and a fully dehydrated shoot having a RWC close to 0%. A lower RWC indicates higher desiccation.

Stomatal Aperture Measurements

To measure stomatal aperture in response to ABA, epidermal peels of the leaves in the same location were floated on a stomatal opening medium containing 50 mM KCl, 10 mM MES-KOH (pH 6.15), and 0.1 mM $CaCl_2$ and incubated in a growth chamber under white light (150 $\mu mol{\cdot}m^{-2}{\cdot}s^{-1}$) for 2 h. The epidermal strips were transferred to the opening medium with 0 or 20 μM ABA and incubated for a further 2 h before stomatal apertures were measured.

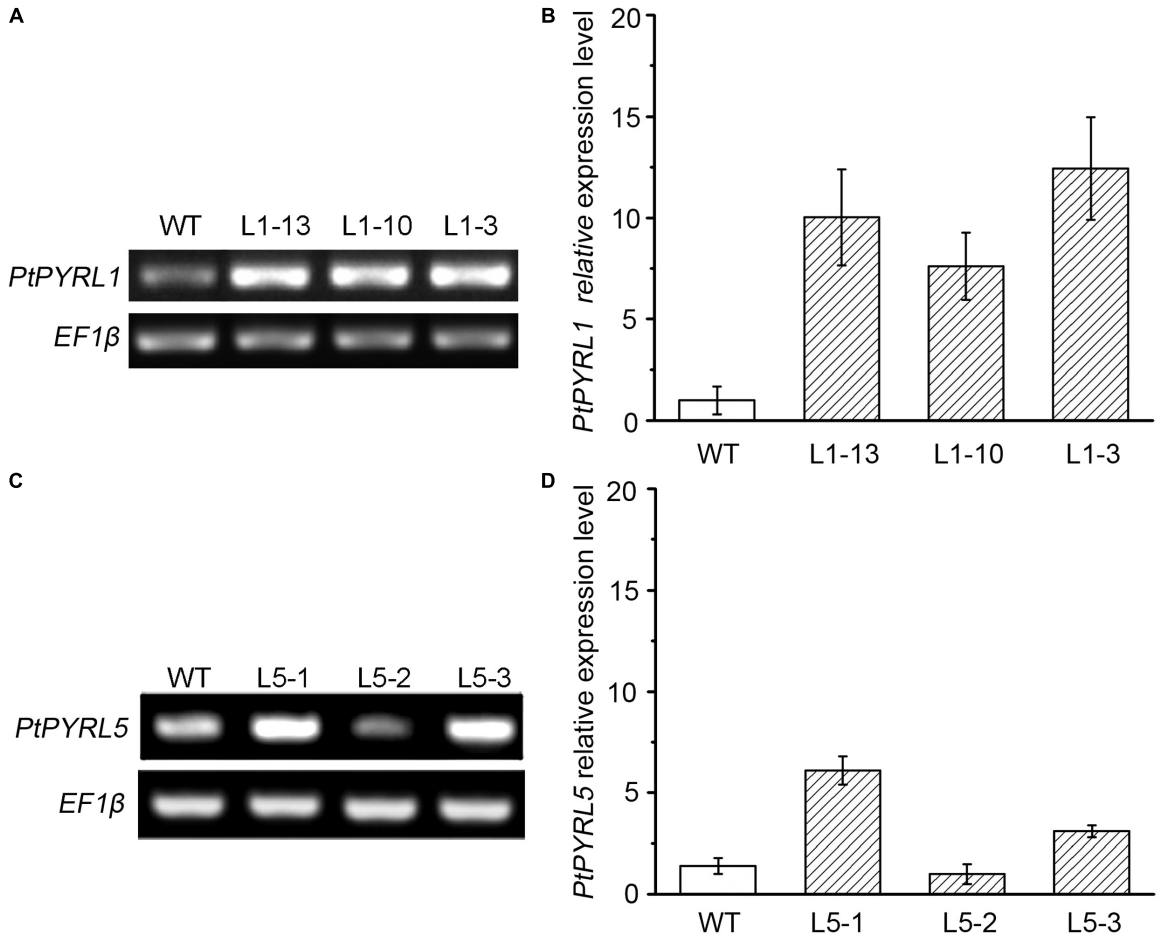

FIGURE 2 | Expression of *PtPYRL1* or *PtPYRL5* in wild type (WT) and transgenic hybrid poplars. Expression of *PtPYRL1* **(A)** or *PtPYRL5* **(C)** in 2-month-old WT and transgenic hybrid poplars (L1-13, L1-10, and L1-3) grown at normal medium. The level was detected using gene-specific primers after 26 PCR cycles. *EF1β* was used as endogenous control in all cDNA samples. Relative levels of *PtPYRL1* transcripts **(B)** or *PtPYRL5* transcripts **(D)** in three transgenic lines by qRT-PCR. Total RNA was isolated from 2-month-old leaves grown at normal medium. The relative expression level was calculated as the ratio of *PtPYRL* level to endogenous control *EF1β* level.

Hyperosmotic Stress Treatment

The 5 cm apical shoot segments of WT and transgenic poplars were transferred into the 1/2 solid Murashige and Skoog (MS) medium containing 0.1 mg·L^{-1} naphthaleneacetic acid and 1% (w/v) agar supplemented with 0, 200, or 300 mM mannitol. The photos were taken at the 30th day after mannitol treatment. The experiments were repeated three times.

H_2O_2 Staining

H_2O_2 in leaves was visualized by 3,3-diaminobenzidine (DAB). *Populus* leaves were cut at the leaf base and infiltrated in 1 mg/mL DAB solution (50 mM Tris-HAC, pH 5.0) for 2–8 h. Samples were then decolorized in 95% ethanol at 80°C for 2 h. Brown flecks indicate the accumulation of H_2O_2 (Yang et al., 2004). The leaves were observed and photographed under stereomicroscope.

Statistical Analysis

The experiments were repeated three times and all comparisons of average values were analyzed using one-way ANOVA test. *Post hoc* comparisons were performed by applying least significant difference test. Significant differences were indicated with the threshold of $P < 0.05$.

RESULTS

Molecular Characterization of the Transgenic *PtPYRLs* Poplar Plants

To obtain transgenic poplar lines that overexpress the ABA receptors *PtPYRL1* and *PtPYRL5* genes under the control of the CaMV 35S promoter were introduced into the leaf explants from

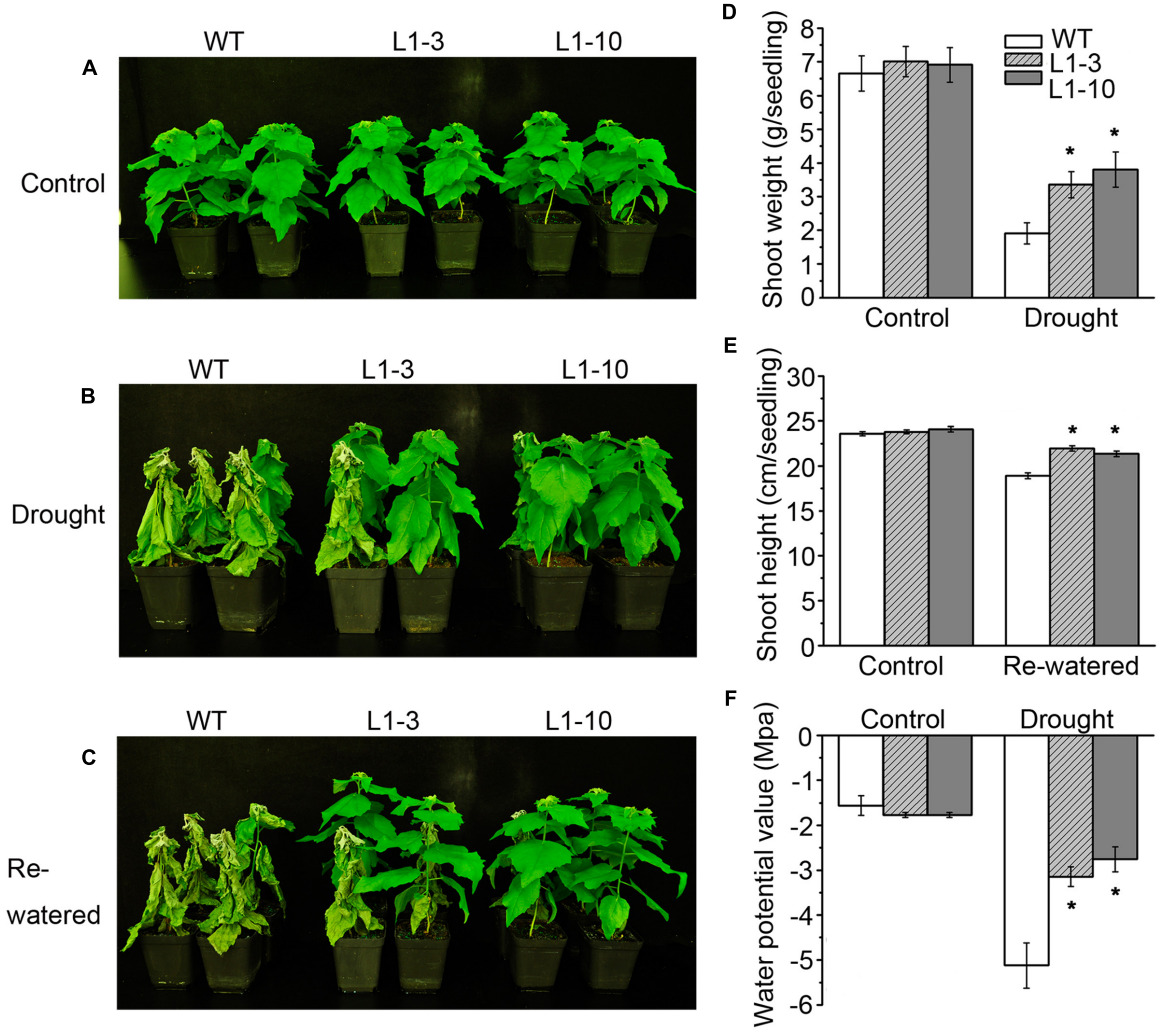

FIGURE 3 | Overexpression of poplar ABA receptor *PtPYRL1* in poplars enhanced drought-stress resistance. **(A)** Two-month-old WT (non-transgenic hybrid poplars) and transgenic poplars (L1-3 and L1-10) were cultured in the greenhouse with normal watering. **(B)** WT and transgenic hybrid poplars were not watered for 5 days. **(C)** After drought, WT and transgenic hybrid poplars were then re-watered for 3 days. The shoot weight after drought stress treatment **(D)**, shoot height after re-watered for 3 days **(E)**, water potential value **(F)** of WT and transgenic hybrid poplars were measured. Values are means ± standard deviation (SD) (one-way ANOVA test; *$P < 0.05$ as compared to WT).

a hybrid poplar cultivar (*Populus davidiana* × *Populus bolleana*), respectively. After cultured in the medium containing timentin and hygromycin, shoots were regenerated from some transfected explants (**Supplementary Figure S2A**). Partial regenerated shoots formed roots when they were placed on rooting medium (**Supplementary Figure S2B**), and these rooted plantlets were selected to analyze *35S-PtPYRL1* or *35S-PtPYRL5* insertion by PCR analysis of genomic DNA. A reporter gene encoding GUS was co-transferred into the leaf explants via the same vector, to authenticate the transgene expression in the putative transgenic lines. The GUS staining analysis revealed that all rooted seedlings expressed GUS activity properly (**Figure 1A**), confirming the integration and expression of the transgene in the genome of the transformants (**Figure 1B**). More than 10 independent lines were obtained for each of transgenes, including the lines L1-3, L1-10, and L1-13 expressing *PtPYRL1*, and the lines L5-1, L5-2, and L5-3 expressing *PtPYRL5* (**Figure 1B**). After the rooted seedlings were transferred into soil, the survival seedlings were selected for further analysis of the differential expression levels of *PtPYRLs* by RT-PCR (**Figures 2A,C**) and qRT-PCR (**Figures 2B,D**). Among of them, Lines L1-3, L1-10, and L1-13 had over eightfold increment of the relative expression level of *PtPYRL1* than in WT (**Figure 2B**), and lines L5-1 and L5-3 had over threefold increment of the relative expression level of *PtPYRL5* compared with WT (**Figure 2D**). Thus, two lines with high level of *PtPYRL1* (L1-3 and L1-10) or of *PtPYRL5* (L5-1 and L5-3) were used for subsequent physiological analysis.

Overexpression of Poplar ABA Receptors Enhanced Drought Tolerance in Transgenic Poplar Plants

To investigate the role of *PtPYRLs* in drought tolerance, 2-month-old wild-type, *PtPYRL1* transgenic plants (L1-3 and L1-10), and *PtPYRL5* transgenic plants (L5-1 and L5-3) were subjected to water withhold for 5 days and then re-watered for 3 days. After 5 days of water deprivation, wild-type plants began to wilt, while most of transgenic plants remained fresh and alive (**Figure 3B**), similar to those grown under the watering condition (**Figure 3A**). When plants were re-watered for 3 days,

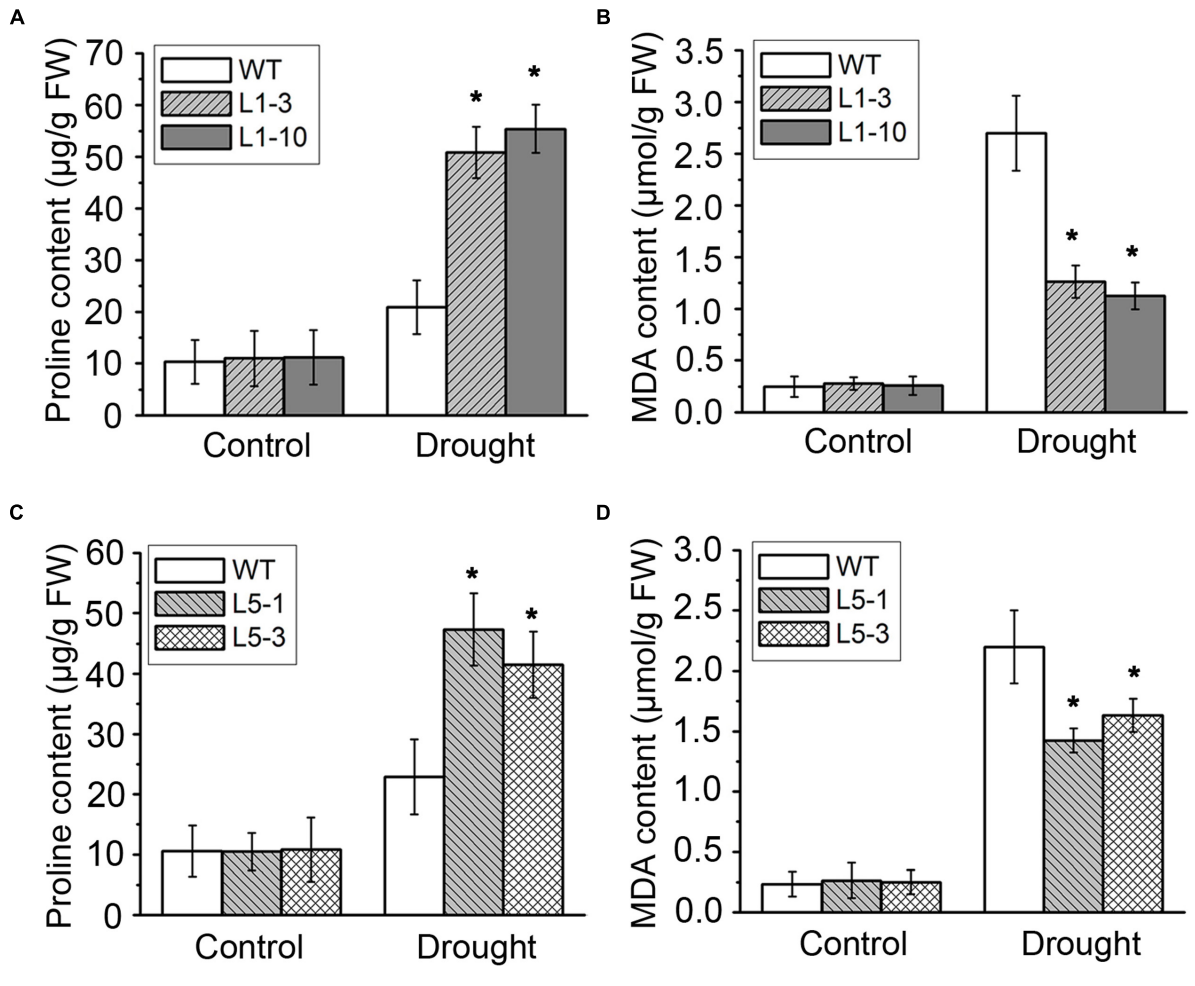

FIGURE 4 | Proline **(A,C)** and MDA **(B,D)** contents were measured in WT and PtPYRL1 or PtPYRL5 transgenic hybrid poplars after drought treatment. Values are means ± SD (one-way ANOVA test; $*P < 0.05$ as compared to WT).

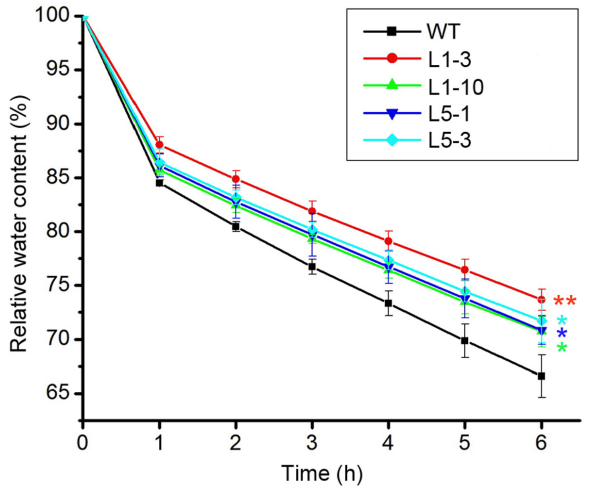

FIGURE 5 | Relative water content (RWC) of WT and *PtPYRL1*, *PtPYRL5* overexpressing poplars after exposure in the air. RWC during a 6-h period from the detached shoot of the WT, *PtPYRL1*- and *PtPYRL5*-overexpressing hybrid poplars. Each value is the mean ± SD of three biological determinations. One-way ANOVA test was used to compare the RWC of each transgenic poplar with those of the WT (with significant differences at $*P < 0.05$ as compared to WT; $**P < 0.01$ as compared to WT).

WT became wilted permanently and eventually died, whereas transgenic plants showed less damaged and most of them recovered growth (**Figure 3C**). Similarly, *PtPYRL5* transgenic plants [L5-1 and L5-3 and another two *PtPYRL1* transgenic lines (L1-8 and L1-5)] displayed a healthier growth compared with the WT after rewatering (**Supplementary Figures S3A–C**). Furthermore, transgenic poplars overexpressing *PtPYRL1* or *PtPYRL5* showed more shoot biomass (**Figure 3D** and **Supplementary Figures S3D, S4D**) and shoot height (**Figure 3E** and **Supplementary Figures S3E, S4E**) than WT. They also had higher leaf water potential Ψ than WT (**Figure 3F** and **Supplementary Figures S3F, S4F**), indicating the leaves of transgenic lines retained more water during the stress.

Drought stress severely impairs the cellular lipid structure and function in tree species (Štajner et al., 2011), and thus the corresponding products proline and MDA were measured in these poplars. Though the proline and MDA contents in both WT and transgenic poplars were increased after drought stress treatment, the transgenic poplars contained higher proline level (**Figures 4A,C**) and less MDA content (**Figures 4B,D**) than WT. It is noteworthy that the changes of biomass, water potential, proline, and MDA in the transgenic *PtPYRL5* lines (L5-1 and L5-3) were less significant than the transgenic *PtPYRL1* lines (L1-3 and L1-10), suggesting that PtPYRL1 may be more potent than PtPYL5 in inducing the downstream protective responses. Moreover, relative water content (RWC) of detached leaves was higher from transgenic *PtPYRL1* lines (L1-3 and L1-10) than from WT plants after exposed in air for 6 h (**Figure 5**). Taken together, these results indicated that overexpression of *PtPYRL1* or *PtPYRL5* in poplars enhanced the resistance to drought stress, probably by reducing water loss rate.

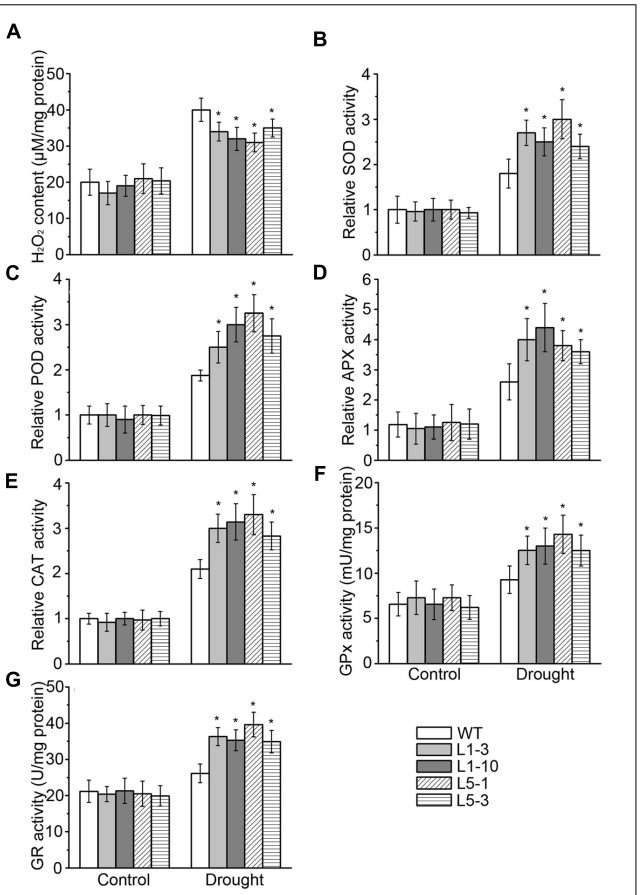

FIGURE 6 | H_2O_2 content **(A)**, SOD **(B)**, POD **(C)**, APX **(D)**, CAT **(E)**, GPx **(F),** and GR **(G)** activities assay of WT, *PtPYRL1,* and *PtPYRL5* overexpressing poplars under drought conditions. 2-month-old WT and transgenic hybrid poplars (L1-3, L1-10, L5-1, and L5-3) were watered regularly, drought stress was performed on these poplars withholding water for additional 5 days, and the leaves were collected. Values for enzyme activities such as SOD, POD, APX, and CAT were normalized to those for the WT hybrid poplars grown under well-watered conditions, which were set at one. Error bars show standard deviations ($n = 12$, one-way ANOVA test; $*P < 0.05$ as compared to WT).

Effects of *PtPYRLs* Overexpression on Antioxidant Metabolism in Poplars under Drought Stress

Lipid hydroperoxidation is considered as the biochemical indicator of cellular oxidative damage, which is induced by excessive accumulation of the reactive oxidative species (e.g., superoxide and H_2O_2) in plant cells (Yoshimura et al., 2004; Sochor et al., 2012). Therefore, we measured H_2O_2 content in the leaves of WT and transgenic plants. In parallel with the increase in MDA contents indicated in **Figure 4**, cellular H_2O_2 levels were also increased by drought stress in the WT and transgenic *PtPYRL1* or *PtPYRL5* plants. However, H_2O_2 level was significantly lower in these transgenic hybrid poplars than that in the WT leaves (**Figure 6A**). Correspondingly, the activity of the key enzymes controlling ROS

scavenging, including superoxide dismutase (SOD), peroxidase (POD), ascorbate peroxidases (APX), and catalase (CAT), were analyzed in these poplars under drought stress. Indeed, the activity of SOD, POD, APX, and CAT were remarkably enhanced in transgenic hybrid poplars compared with the WT (**Figures 6B–E**). Besides these antioxidant enzymes, plants have several non-enzymatic antioxidants important for redox equilibrium, such as glutathione (GSH) (Cao et al., 2009). GSH content is controlled by glutathione reductase (GR), which has an important role in maintaining the level of glutathione, and by glutathione peroxidases (GPx), which can catalyze the reduction of lipid peroxide through glutathione. Upon drought stress, transgenic hybrid poplars had higher activity of GR and GPx than WT (**Figures 6F,G**). These results indicated that overexpression of *PtPYRL1* and *PtPYRL5* resulted in greater stimulation of the activity of enzymes responsible for ROS and GSH metabolism in poplars upon drought stress.

Overexpression of *PtPYRL1* or *PtPYRL5* Accelerated Stomatal Closure Induced by ABA

The stomatal movement is one of the most important responses in plants under drought stress, and stomatal behavior is highly controlled by ABA. ABA was thus applied to assess the potential difference in stomatal movement between the WT and the transgenic *PtPYRLs* poplars. Without any treatment, even though overexpressing lines have more closed stomata, the difference was not significant, as shown by ANOVA test. With 20 μM ABA treatment, a significant decrease in stomatal aperture was found for both WT and the transgenic *PtPYRLs* poplars (**Figure 7A**). There was a significant difference between WT-mock and WT-ABA using ANOVA test. Stomatal apertures in the *PtPYRL1*- and *PtPYRL5*-overexpressing lines L1-3, L1-10, L5-1, and L5-3 reduced to 0.394, 0.395, 0.387, and 0.392, respectively, while stomatal aperture of WT became 0.490 (**Figure 7B**), which was significantly larger than that of *PtPYRL1*- and *PtPYRL5*-overexpressing lines. These results indicate that the overexpression of *PtPYRL1* and *PtPYRL5* enhanced poplar stomatal closure in response to ABA, which might be the cause of the enhanced drought tolerance of transgenic plants.

Overexpression of *PtPYRL1* or *PtPYRL5* Enhanced Osmotic Stress Resistance

Osmotic damage is a major consequence of drought stress in plants, and ABA signaling contributes to damage reduction (Skirycz and Inzé, 2010). Overexpression of *PtPYRL1* or *PtPYRL5* enhanced resistance to water deficit (**Figure 3** and **Supplementary Figures S3, S4**), which suggested a possible role of *PtPYRL1* or *PtPYRL5* in high osmotic stress resistance. To confirm this possibility, wild-type and transgenic shoots were cultured on 1/2 MS supplemented with 200 or 300 mM mannitol. The supplementation of mannitol inhibited the growth of WT and transgenic poplars (**Figure 8A**). At the presence of 300 mM mannitol, the WT plants did not even survive and their leaves show yellowish and withered, while young leaves of transgenic plants overexpressing *PtPYRL1* or *PtPYRL5* kept green and some

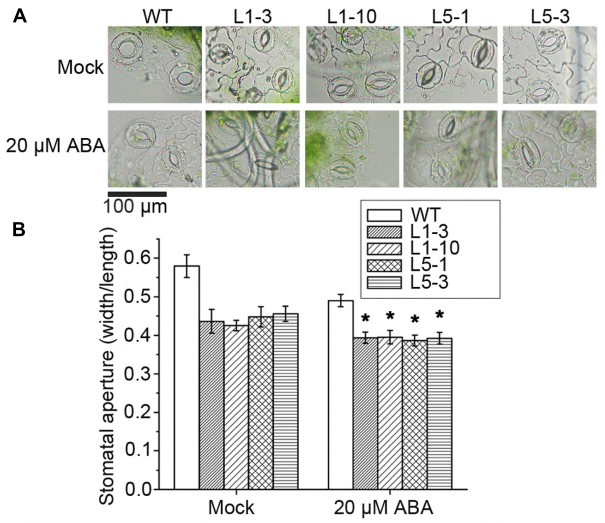

FIGURE 7 | Stomatal movement in WT and *PtPYRL1*, *PtPYRL5* overexpressing hybrid poplars under ABA treatment. **(A)** The representative images of stomata shape of WT and transgenic seedlings in the presence or absence of ABA. The 2-month-old WT and transgenic seedlings L1-3, L1-10, L5-1, and L5-3 were treated with stomata opening buffer (mock) (upper), or with 20 μM ABA (lower). Pictures were taken 2 h after ABA treatment in Olympus BX51 microscope in 40× magnification. Scale bar is 100 μm. **(B)** Stomatal aperture of WT and transgenic seedlings at 2 h after treatment with stomatal opening buffer (mock) or with 20 μM ABA. Stomatal aperture was calculated as the ratio of stomatal width to length. About 200 stomata were analyzed for each genotype. Bars represent mean ± SEM of three independent experiments and significant differences are indicated as $^*P < 0.05$.

old leaves displayed yellowish at leaf edge (**Figures 8A,B**). In addition, unlike WT plants, all transgenic plants generated new roots successfully in 1/2 MS medium supplemented with 300 mM mannitol (**Figures 8A,B**). According to the statistical analysis shown in **Figure 8C**, transgenic plants overexpressing PtPYRL1 or PtPYRL5 had roots with an average length of around 4.5 cm, while the WT did not have visible roots. These results indicated that the transgenic poplar overexpressing *PtPYRL1* or *PtPYRL5* improved the resistance to hyperosmotic stress.

Overexpression of *PtPYRL1* or *PtPYRL5* Reduced the Injury Induced by Low Temperature

We also subjected WT and transgenic *PtPYRL1* or *PtPYRL5* poplars to low temperature which is a common stress in poplars growth and found that *PtPYRL1* and *PtPYRL5* transgenic poplars displayed the increased resistance under chilling stress (**Figure 9**). After 4°C treatment for 5 days, the apical young leaves of WT were damaged more severely with leaf wilting and necrosis than that of transgenic poplars (**Figure 9A**). Furthermore, the leaves of WT had a higher accumulation of hydrogen peroxide visualized by 3,3-diaminobenzidine (DAB) (**Figure 9B**). Meanwhile, the

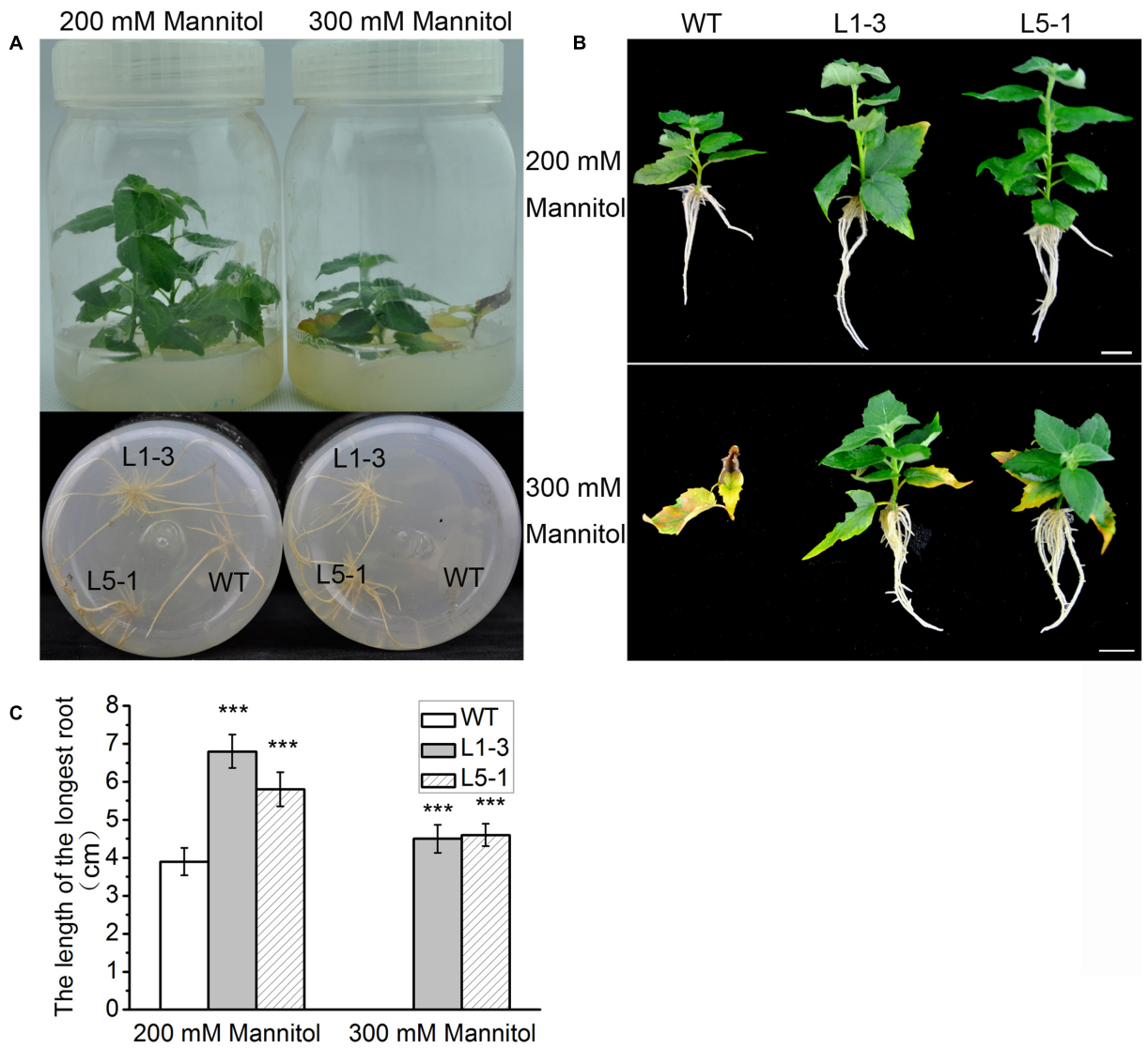

FIGURE 8 | Overexpression of *PtPYRL1/5* in hybrid poplar improved resistance to hyperosmotic stress. **(A)** Short shoot segments (upper) and new fibrous roots (down) grown for 5 days on 1/2 MS medium supplemented with mannitol (200 and 300 mM). Under 200 and 300 mM mannitol treatment, in comparison to the transgenic poplars, the damage to apical leaves bud and new roots of WT is more serious. **(B)** Outgrowth of fibrous roots of shoot segments from poplars overexpressing *PtPYRL1/5* (L1-3 and L5-1) is not inhibited by 300 mM mannitol, however, outgrowth of fibrous roots of shoot segments from WT poplars is inhibited by 300 mM mannitol. Bars represent 1 cm. **(C)** The length of the fibrous root of shoot segments in **(B)**. Values are the mean ± SD of three independent experiments (n = 10 shoots segments, $^{***}P < 0.001$ as compared to WT).

leaves of WT contained less proline accumulation, a key anti-freeze component (**Figure 9C**). These results suggested that overexpression of *PtPYRL1* or *PtPYRL5* alleviated the injury induced by low temperature in poplars.

DISCUSSION

As initial factors in triggering ABA signaling, the physiological function of PYR/PYL/RCARs family is supposed to be critical in the evolution from aquatic to terrestrial plants. *PYR/PYL/RCAR* genes have been reported to be present as 13–14 members in the genome of *Arabidopsis*, rice and *Populus* (Ma et al., 2009; Tian et al., 2015; Yu et al., 2016). As a class of ubiquitous soluble protein, the *PYR/PYL/RCARs* family plays a critical role in ABA response and signal transduction in plants. Overexpression of *Arabidopsis PYR/PYL/RCAR* receptors is known to enhance ABA response and plant drought tolerance (Santiago et al., 2009; Saavedra et al., 2010; Pizzio et al., 2013). Our previous study showed the transgenic *Arabidopsis* overexpressing *PtPYRL1* or *PtPYRL5* were both hypersensitive to ABA and enhanced drought resistance (Yu et al., 2016). In the present study, we further provide evidence that these two PtPYRL*s* are very important in poplars to confer tolerance to diverse environmental

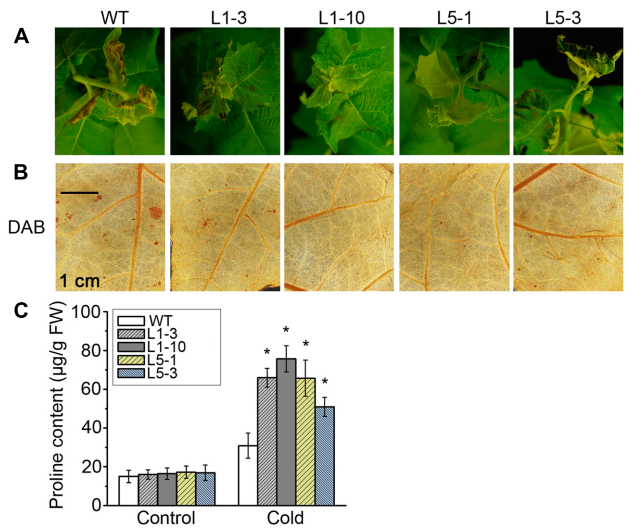

FIGURE 9 | Cell viability, contents of hydrogen peroxide, and osmolytes in leaves of WT and *PtPYRL1*, *PtPYRL5*- overexpressing poplars under low temperature treatments. **(A)** The phenotype of WT and transgenic hybrid poplars (L1-3, L1-10, L5-1, and L5-3) under cold stress treatments. Hydrogen peroxide in leaves were visualized by DAB **(B)**, respectively. **(C)** Proline content of WT and *PtPYRL1*- or *PtPYRL5*- overexpressing hybrid poplars. Values are means ± SD of three independent experiments (*$P < 0.05$ as compared to WT).

abiotic stresses, including drought, hyper-osmosis, and low temperature.

The *PYR/PYL/RCAR* genes have been shown to enhance drought tolerance in *Arabidopsis*, rice, and tomato (González-Guzmán et al., 2014; Kim et al., 2014; Zhao et al., 2016). But the evidence of functional studies in the woody plants are still lacking. In our study, hybrid poplar *Populus davidiana* × *Populus bolleana* was transformed with the *PtPYRL1* or *PtPYRL5* gene and WT hybrid poplar served as control. We did not observe any phenotypic changes in *PtPYRL1/5* overexpression transgenic poplars under normal growth conditions. Compared with WT poplars, overexpression of *PtPYRL1* or *PtPYRL5* enhanced drought tolerance. The shoot weight, leaf water potential, and proline concentration were obviously increased, and MDA content was markedly reduced in transgenic poplars under drought condition, resulted in rapid recovery with higher shoot height after drought and re-watering treatment. Low water availability in the dry soil limited evaporation and made water potential in the cell drop, these changes were associated with reduction in the leaf RWC. The overexpression of *PtPYRL1* or *PtPYRL5* in poplars showed larger leaf water potential (Ψ) after drought treatment, probably due to increased water retention capacity of the cells, lower water loss rate as well as more adaptive stomatal movement during the stress (Leung and Giraudat, 1998; Zhu, 2002; Souza et al., 2004; Kwak et al., 2008). As showed in **Figure 7**, exogenous ABA promoted the stomata closure, *PtPYRL1* or *PtPYRL5* overexpressing transgenic poplars were more sensitive to ABA. Hereafter, recovery will be described as the visual evidence of new above ground development and growth, according to previous studies (Brodribb and Cochard, 2009; Petrov et al., 2015), which defined the process of recovery as a process of reactivated physiological processes and meristematic activity. *PtPYRL1* or *PtPYRL5* overexpressing transgenic poplars were taller and better recovered than WT poplars after drought and re-watering treatment (**Figure 3E**). Our findings supported the earlier finding that drought causes hydraulic restriction, with the subsequent development of high tension in the xylem water column and the closure of stomata (Tyree and Sperry, 1988). Larger aboveground biomass indicated better survival in the drought stressed *PtPYRL1* or *PtPYRL5* overexpressing transgenic poplars, while more proline accumulation resulted in the better water status maintenance (Bajji et al., 2001) and less MDA concentration led to better protection of the cell membrane structures in the drought treated *PtPYRL1* or *PtPYRL5* overexpressing transgenic poplars. The results presented here indicated that PtPYRL1/5 positively regulates ABA-related response to drought stress.

Drought commonly results in oxidative stress due to the over-production and over-accumulation of ROS derived from inefficient dissipation of excessive excitation energy (Shanker et al., 2014). The over-accumulation of ROS may lead to biochemical disruption of membranes and result in mortality (Suzuki et al., 2012; Petrov et al., 2015). ROS scavenging systems of plants detoxify ROS to minimize and/or prevent oxidative damage in cells by increasing the activity of ROS scavenging enzymes such as SOD, CAT, APX, POD, GR, and GPx (Gill and Tuteja, 2010). In the present study, the content of H_2O_2 was significantly lower in the *PtPYRL1*- and *PtPYRL5*-overexpressing poplars than in WT under drought stress (**Figure 6A**). Consistent with this phenomenon, all of the measured antioxidant enzyme activities showed notably increased in transgenic poplars after drought treatment (**Figures 6B–G**). It was proposed that the antioxidant protection is related to higher leaf water potential Ψ (**Figure 3F** and **Supplementary Figures S3F, S4F**) (Menconi et al., 1995). These results demonstrated that overexpression of *PtPYRL1* or *PtPYRL5* increased the antioxidant enzyme activities protecting transgenic poplars against the oxidative damage.

Consistently, osmotic stress significantly suppressed wild-type poplars roots development and leaf growth compared with *PtPYRL1* or *PtPYRL5* overexpressing poplars (**Figure 8**). The increased root growth rate of transgenic poplars (**Figure 8C**) has to be coupled with a mechanism that alleviates the physiological growth retardation consequences of the osmotic stress. In *PtPYRL1* or *PtPYRL5* overexpressing poplars, roots had increased the low water availability, as their rapid root growth resulted in more water absorption. Since the osmotic stress has been suggested to increase the ABA levels in plant cells (Zeevaart and Creelman, 1998), transgenic poplars might perceive ABA more rapidly and might trigger more efficiently the downstream responses. The phenotype of transgenic poplars under osmotic stress indicated that *PtPYRL1* or *PtPYRL5* increased the tolerance to hyperosmotic stress.

Another common environmental stress, a low temperature, severely inhibits plant growth and development. A recent study illustrated that co-overexpression of two genes, a bZIP

transcription factor (*OsbZIP46CA1*) and a protein kinase (*SAPK6*) involved in the ABA signaling pathway, showed improved tolerance to heat and cold stresses in rice (Chang et al., 2017). In order to enhance plant adaptability to low temperature, lipids, amino acid, membrane components, and other molecules in the cell are produced to promote cell membrane fluidity and structural rearrangement (Maruyama et al., 2014; Wu et al., 2016). Balance of the cellular ROS homeostasis also contributes to the tolerance to temperature stresses (Wang et al., 2017). Our results showed that the *PtPYRL1* or *PtPYRL5* overexpressing poplars enhanced low temperature stress tolerance (**Figure 9**), associated with more efficient ROS scavenging (**Figure 9B**) and more proline accumulation to maintain membrane integrity (**Figure 9C**). On the other hand, it is well known that phytohormone ABA activates a cascade of downstream signaling events in response to cold exposure (Knight et al., 2004). Further studies are required to investigate how PtPYRL1 and PtPYRL5 mediates adaptive responses to cold at the molecular level. Moreover, though our data showed that both ABA receptors are over-expressed in transgenic poplar plants at the mRNA level, it would be interesting to test their protein accumulation in future studies, since it has been suggested that PYR/PYL receptors undergo regulation at protein level by 26S proteasome pathway in *Arabidopsis* (Bueso et al., 2014; Irigoyen et al., 2014).

Populus is a perennial woody model plant and also economically important tree. Most *Populus* are sensitive to environmental factors, which considerably affects their productivities. As we know, arid and semi-arid regions account for approximately 30% of the worldwide area (Sivakumar et al., 2005). Meanwhile, the climate in poplars cultivated land of China is mostly dry and frigid. Therefore, breeding high drought- and cold-tolerant poplar cultivars is very necessary for improving land use efficiency and poplar forestry development. In our study, transgenic poplar overexpressing *PtPYRL1* or *PtPYRL5* was found to be significantly more drought and chilling tolerant than WT plants. We hope that the transgenic poplars generated in this study can be used for cultivating in cold as well as arid and semi-arid areas.

AUTHOR CONTRIBUTIONS

LY, RT, and SL designed the study. LY, WL, HG, and JY revised the manuscript critically. LY, JY, RT, YW, XW, and FZ performed experiments, analyzed and interpreted the data, and wrote the manuscript.

FUNDING

This study was supported by the Fundamental Research Funds for the Central Universities (020814380062) and the Natural Science Foundation of Jiangsu Province of China (BK2012306).

ACKNOWLEDGMENT

We gratefully acknowledge Hongxia Zhang for poplar material and pCAMBIA1301S2 plasmid.

SUPPLEMENTARY MATERIAL

The Supplementary Material for this article can be found online at: https://www.frontiersin.org/articles/10.3389/fpls.2017.01752/full#supplementary-material

FIGURE S1 | The pCAMBIA1301S2-*PtPYRL1* (or *PtPYRL5*) Vector map.

FIGURE S2 | Transformants selection. **(A)** Adventitious bud regenerated from selection medium. **(B)** Transgenic shoots formed roots on selection medium.

FIGURE S3 | Overexpression of poplar ABA receptor *PtPYRL5* in poplars enhanced drought-stress resistance. **(A)** 2-month-old WT (non-transgenic hybrid poplars) and transgenic poplars (L5-1 and L5-3) were cultured in the greenhouse with normal watering. **(B)** WT and transgenic hybrid poplars were not watered for 5 days. **(C)** After drought, WT and transgenic hybrid poplars were then re-watered for 3 days. The shoot weight after drought stress treatment **(D)**, shoot height after re-watered for 3 days **(E)**, water potential value **(F)** of WT and transgenic hybrid poplars were measured. Values are means ± SD (one-way ANOVA test; $^*P < 0.05$ as compared to WT).

FIGURE S4 | Overexpression of poplar ABA receptor PtPYRL1 in poplars enhanced drought-stress resistance. **(A)** 2-month-old WT (non-transgenic hybrid poplars) and transgenic poplars (L1-8 and L1-5) were cultured in the greenhouse with normal watering. **(B)** WT and transgenic hybrid poplars were not watered for 5 days. **(C)** After drought, WT and transgenic hybrid poplars were then re-watered for 3 days. The shoot weight after drought stress treatment **(D)**, shoot height after re-watered for 3 days **(E)**, water potential value **(F)**, proline content **(G)** and MDA content **(H)** of WT and transgenic hybrid poplars were measured. Values are means ± SD ($n = 18$, three independent experiments, one-way ANOVA test; $^*P < 0.05$).

REFERENCES

Allen, G. J., Kuchitsu, K., Chu, S. P., Murata, Y., and Schroeder, J. I. (1999). *Arabidopsis abi1-1* and *abi2-1* phosphatase mutations reduce abscisic acid-induced cytoplasmic calcium rises in guard cells. *Plant Cell* 11, 1785–1798. doi: 10.2307/3871054

Apel, K., and Hirt, H. (2004). Reactive oxygen species: metabolism, oxidative stress, and signal transduction. *Annu. Rev. Plant Biol.* 55, 373–399. doi: 10.1146/annurev.arplant.55.031903.141701

Bajji, M., Kinet, J.-M., and Lutts, S. (2001). The use of the electrolyte leakage method for assessing cell membrane stability as a water stress tolerance test in durum wheat. *Plant Growth Regul.* 36, 61–70. doi: 10.1023/A:1014732714549

Bates, T. R., Rosenberg, H. A., and Tembo, A. V. (1973). Inconsistencies in rationale underlying official USP dissolution rate specifications for nitrofurantoin. *J. Pharm. Sci.* 62, 2057–2058. doi: 10.1002/jps.2600621241

Brodribb, T. J., and Cochard, H. (2009). Hydraulic failure defines the recovery and point of death in water-stressed conifers. *Plant Physiol.* 149, 575–584. doi: 10.1104/pp.108.129783

Bueso, E., Rodriguez, L., Lorenzo-Orts, L., Gonzalez-Guzman, M., Sayas, E., Muñoz-Bertomeu, J., et al. (2014). The single-subunit RING-type E3 ubiquitin ligase RSL1 targets PYL4 and PYR1 ABA receptors in plasma membrane to modulate abscisic acid signaling. *Plant J.* 80, 1057–1071. doi: 10.1111/tpj.12708

Cao, Y., Zhang, Z. W., Xue, L. W., Du, J. B., Shang, J., Xu, F., et al. (2009). Lack of salicylic acid in *Arabidopsis* protects plants against moderate salt stress. *Z. Naturforsch. C* 64, 231–238. doi: 10.1515/znc-2009-3-414

Carlberg, I., and Mannervik, B. (1985). Glutathione reductase. *Methods Enzymol.* 113, 484–490. doi: 10.1016/S0076-6879(85)13062-4

Chance, M., and Maehly, A. C. (1955). The assay of catalases and peroxidases. *Methods Enzymol.* 2, 764–817. doi: 10.1016/S0076-6879(55)02300-8

Chang, Y., Nguyen, B. H., Xie, Y., Xiao, B., Tang, N., Zhu, W., et al. (2017). Co-overexpression of the constitutively active form of OsbZIP46 and ABA-activated protein kinase SAPK6 improves drought and temperature stress resistance in rice. *Front. Plant Sci.* 8:1102. doi: 10.3389/fpls.2017.01102

Contreras-Porcia, L., Thomas, D., Flores, V., and Correa, J. A. (2011). Tolerance to oxidative stress induced by desiccation in *Porphyra columbina* (Bangiales, Rhodophyta). *J. Exp. Bot.* 62, 1815–1829. doi: 10.1093/jxb/erq364

Doty, S. L., Sher, A. W., Fleck, N. D., Khorasani, M., Bumgarner, R. E., Khan, Z., et al. (2016). Variable nitrogen fixation in wild *Populus*. *PLOS ONE* 11:e0155979. doi: 10.1371/journal.pone.0155979

Finkelstein, R. R., Gampala, S. S., and Rock, C. D. (2002). Abscisic acid signaling in seeds and seedlings. *Plant Cell* 14(Suppl.), S15–S45. doi: 10.1105/tpc.010441

Fujii, H., Verslues, P. E., and Zhu, J. K. (2007). Identification of two protein kinases required for abscisic acid regulation of seed germination, root growth, and gene expression in *Arabidopsis*. *Plant Cell* 19, 485–494. doi: 10.1105/tpc.106.048538

Giannopolitis, C. N., and Ries, S. K. (1977). Superoxide dismutases occurrence in higher plants. *Plant Physiol.* 59, 309–314. doi: 10.1104/pp.59.2.309

Gill, S. S., and Tuteja, N. (2010). Reactive oxygen species and antioxidant machinery in abiotic stress tolerance in crop plants. *Plant Physiol. Biochem.* 48, 909–930. doi: 10.1016/j.plaphy.2010.08.016

Gonzalez-Guzman, M., Pizzio, G. A., Antoni, R., Vera-Sirera, F., Merilo, E., Bassel, G. W., et al. (2012). *Arabidopsis* PYR/PYL/RCAR receptors play a major role in quantitative regulation of stomatal aperture and transcriptional response to abscisic acid. *Plant Cell* 24, 2483–2496. doi: 10.1105/tpc.112.098574

González-Guzmán, M., Rodríguez, L., Lorenzo-Orts, L., Pons, C., Sarrión-Perdigones, A., Fernández, M. A., et al. (2014). Tomato PYR/PYL/RCAR abscisic acid receptors show high expression in root, differential sensitivity to the abscisic acid agonist quinabactin, and the capability to enhance plant drought resistance. *J. Exp. Bot.* 65, 4451–4464. doi: 10.1093/jxb/eru219

Heath, R. L., and Packer, L. (1968). Photoperoxidation in isolated chloroplasts. I. Kinetics and stoichiometry of fatty acid peroxidation. *Arch. Biochem. Biophys.* 125, 189–198. doi: 10.1016/0003-9861(68)90654-1

Himmelbach, A., Yang, Y., and Grill, E. (2003). Relay and control of abscisic acid signaling. *Curr. Opin. Plant Biol.* 6, 470–479. doi: 10.1016/S1369-5266(03)00090-6

Hu, L., Li, H., Pang, H., and Fu, J. (2012). Responses of antioxidant gene, protein and enzymes to salinity stress in two genotypes of perennial ryegrass (*Lolium perenne*) differing in salt tolerance. *J. Plant Physiol.* 169, 146–156. doi: 10.1016/j.jplph.2011.08.020

Irigoyen, M. L., Iniesto, E., Rodriguez, L., Puga, M. I., Yanagawa, Y., Pick, E., et al. (2014). Targeted degradation of abscisic acid receptors is mediated by the ubiquitin ligase substrate adaptor DDA1 in *Arabidopsis*. *Plant Cell* 26, 712–728. doi: 10.1105/tpc.113.122234

Jefferson, R. A., Kavanagh, T. A., and Bevan, M. W. (1987). GUS fusions: beta-glucuronidase as a sensitive and versatile gene fusion marker in higher plants. *EMBO J.* 6, 3901–3907.

Jiang, M., and Zhang, J. (2002). Role of abscissic acid in water stress-induced antioxidant defense in leaves of maize seedlings. *Free Radic. Res.* 36, 1001–1015. doi: 10.1080/1071576021000006563

Kim, H., Lee, K., Hwang, H., Bhatnagar, N., Kim, D. Y., Yoon, I. S., et al. (2014). Overexpression of *PYL5* in rice enhances drought tolerance, inhibits growth, and modulates gene expression. *J. Exp. Bot.* 65, 453–464. doi: 10.1093/jxb/ert397

Knight, H., Zarka, D. G., Okamoto, H., Thomashow, M. F., and Knight, M. R. (2004). Abscisic acid induces *CBF* gene transcription and subsequent induction of cold-regulated genes via the *CRT* promoter element. *Plant Physiol.* 135, 1710–1717. doi: 10.1104/pp.104.043562

Kwak, J. M., Mäser, P., and Schroeder, J. I. (2008). The clickable guard cell, version II: interactive model of guard cell signal transduction mechanisms and pathways. *Arabidopsis Book* 6:e0114. doi: 10.1199/tab.0114

Lackman, P., González-Guzmán, M., Tilleman, S., Carqueijeiro, I., Pérez, A. C., Moses, T., et al. (2011). Jasmonate signaling involves the abscisic acid receptor *PYL4* to regulate metabolic reprogramming in *Arabidopsis* and tobacco. *Proc. Natl. Acad. Sci. U.S.A.* 108, 5891–5896. doi: 10.1073/pnas.1103010108

Lee, S. C., Lan, W. Z., Buchanan, B. B., and Luan, S. (2009). A protein kinase-phosphatase pair interacts with an ion channel to regulate ABA signaling in plant guard cells. *Proc. Natl. Acad. Sci. U.S.A.* 106, 21419–21424. doi: 10.1073/pnas.0910601106

Leung, J., and Giraudat, J. (1998). Abscisic acid signal transduction. *Annu. Rev. Plant Physiol Plant Mol. Biol.* 49, 199–222. doi: 10.1146/annurev.arplant.49.1.199

Liu, C. C., Liu, Y. G., Guo, K., Fan, D. Y., Li, G. Q., Zheng, Y. R., et al. (2011). Effect of drought on pigments, osmotic adjustment and antioxidant enzymes in six woody plant species in karst habitats of southwestern China. *Environ. Exp. Bot.* 71, 174–183. doi: 10.1016/j.envexpbot.2010.11.012

Liu, X., Yue, Y., Li, B., Nie, Y., Li, W., Wu, W. H., et al. (2007). A G protein-coupled receptor is a plasma membrane receptor for the plant hormone abscisic acid. *Science* 315, 1712–1716. doi: 10.1126/science.1135882

Liu, Y., Pan, Z., Zhuang, Q., Miralles, D. G., Teuling, A. J., Zhang, T., et al. (2015). Agriculture intensifies soil moisture decline in Northern China. *Sci. Rep.* 5:11261. doi: 10.1038/srep11261

Ma, Y., Szostkiewicz, I., Korte, A., Moes, D., Yang, Y., Christmann, A., et al. (2009). Regulators of PP2C phosphatase activity function as abscisic acid sensors. *Science* 324, 1064–1068. doi: 10.1126/science.1172408

Maehly, A. C., and Chance, B. (1954). The assay of catalases and per regulators of PP2C phosphatase activity function as abscisic acid sensors oxidases. *Methods Biochem. Anal.* 1, 357–424.

Maruyama, K., Urano, K., Yoshiwara, K., Morishita, Y., Sakurai, N., Suzuki, H., et al. (2014). Integrated analysis of the effects of cold and dehydration on rice metabolites, phytohormones, and gene transcripts. *Plant Physiol.* 164, 1759–1771. doi: 10.1104/pp.113.231720

Menconi, M., Sgherri, C. L. M., Pinzino, C., and Navari-Izzo, F. (1995). Activated oxygen production and detoxification in wheat plants subjected to a water deficit programme. *J. Exp. Bot.* 46, 1123–1130. doi: 10.1093/jxb/46.9.1123

Mustilli, A. C., Merlot, S., Vavasseur, A., Fenzi, F., and Giraudat, J. (2002). Arabidopsis OST1 protein kinase mediates the regulation of stomatal aperture by abscisic acid and acts upstream of reactive oxygen species production. *Plant Cell* 14, 3089–3099. doi: 10.1105/tpc.007906

Nakano, Y., and Asada, K. (1981). Hydrogen peroxide is scavenged by ascorbate-specific peroxidase in spinach chloroplasts. *Plant Cell Physiol.* 22, 867–880.

Pandey, S., Nelson, D. C., and Assmann, S. M. (2009). Two novel GPCR-type G proteins are abscisic acid receptors in *Arabidopsis*. *Cell* 136, 136–148. doi: 10.1016/j.cell.2008.12.026

Park, S. Y., Fung, P., Nishimura, N., Jensen, D. R., Fujii, H., Zhao, Y., et al. (2009). Abscisic acid inhibits type 2C protein phosphatases via the PYR/PYL family of START proteins. *Science* 324, 1068–1071. doi: 10.1126/science.1173041

Petrov, V., Hille, J., Mueller-Rueber, B., and Gechev, T. (2015). ROS-mediated abiotic-stress induced programmed cell death in plants. *Front. Plant Sci.* 6:69. doi: 10.3389/fpls.2015.00069

Pizzio, G. A., Rodriguez, L., Antoni, R., Gonzalez-Guzman, M., Yunta, C., Merilo, E., et al. (2013). The PYL4 A194T mutant uncovers a key role of PYR1-LIKE4/PROTEIN PHOSPHATASE 2CA interaction for abscisic acid signaling and plant drought resistance. *Plant Physiol.* 163, 441–455. doi: 10.1104/pp.113.224162

Saavedra, X., Modrego, A., Rodríguez, D., González-García, M. P., Sanz, L., Nicolás, G., et al. (2010). The nuclear interactor PYL8/RCAR3 of Fagus sylvatica FsPP2C1 is a positive regulator of abscisic acid signaling in seeds and stress. *Plant Physiol.* 152, 133–150. doi: 10.1104/pp.109.146381

Santiago, J., Rodrigues, A., Saez, A., Rubio, S., Antoni, R., Dupeux, F., et al. (2009). Modulation of drought resistance by the abscisic acid receptor PYL5 through inhibition of clade A PP2Cs. *Plant J.* 60, 575–588. doi: 10.1111/j.1365-313X.2009.03981.x

Seki, M., Ishida, J., Narusaka, M., Fujita, M., Nanjo, T., Umezawa, T., et al. (2002). Monitoring the expression pattern of around 7,000 *Arabidopsis* genes under ABA treatments using a foil-length cDNA microarray. *Funct. Integr. Genomics* 2, 282–291. doi: 10.1007/s10142-002-0070-6

Shanker, A. K., Maheswari, M., Yadav, S. K., Desai, S., Bhanu, D., Attal, N. B., et al. (2014). Drought stress responses in crops. *Funct. Integr. Genomics* 14, 11–22. doi: 10.1007/s10142-013-0356-x

Shen, Y. Y., Wang, X. F., Wu, F. Q., Du, S. Y., Cao, Z., Shang, Y., et al. (2006). The Mg-chelatase H subunit is an abscisic acid receptor. *Nature* 443, 823–826. doi: 10.1038/nature05176

Sivakumar, M. V. K., Das, H. P., and Brunini, O. (2005). Impacts of present and future climate variability and change on agriculture and forestry in the arid and semi-arid tropics. *Clim. Change* 70, 31–72. doi: 10.1007/s10584-005-5937-9

Skirycz, A., and Inzé, D. (2010). More from less: plant growth under limited water. *Curr. Opin. Biotechnol.* 21, 197–203. doi: 10.1016/j.copbio.2010.03.002

Sochor, J., Ruttkay-Nedecky, B., Babula, P., Adam, V., Hubalek, J., and Kizek, R. (2012). "Automation of methods for determination of lipid peroxidation," in *Lipid Peroxidation*, ed. A. Catala (Rijeka: In Tech).

Souza, R. P., Machado, E. C., Silva, J. A. B., Lagôa, A. M. M. A., and Silveira, J. A. G. (2004). Photosynthetic gas exchange, chlorophyll fluorescence and some associated metabolic changes in cowpea (*Vigna unguiculata*) during water stress and recovery. *Environ. Exp. Bot.* 51, 45–56. doi: 10.1016/S0098-8472(03)00059-5

Štajner, D., Orlovic, S., Popovic, B., Kebert, M., and Galic, Z. (2011). Screening of drought oxidative stress tolerance in Serbian melliferous plant species. *Afr. J. Biotechnol.* 10, 1609–1614.

Suzuki, N., Koussevitzky, S., Mittler, R., and Miller, G. (2012). ROS and redox signaling in the response of plants to abiotic stress. *Plant Cell Environ.* 35, 259–270. doi: 10.1111/j.1365-3040.2011.02336.x

Tian, X., Wang, Z., Li, X., Lv, T., Liu, H., Wang, L., et al. (2015). Characterization and functional analysis of pyrabactin resistance-like abscisic acid receptor family in rice. *Rice* 8, 28. doi: 10.1186/s12284-015-0061-6

Tyree, M. T., and Sperry, J. S. (1988). Do woody plants operate near the point of catastrophic xylem dysfunction caused by dynamic water stress? Answers from a model. *Plant Physiol.* 88, 547–580. doi: 10.1104/pp.88.3.574

Wang, J., Wu, B., Yin, H., Fan, Z., Li, X., Ni, S., et al. (2017). Overexpression of *CaAPX* induces orchestrated reactive oxygen scavenging and enhances cold and heat tolerances in tobacco. *Biomed Res. Int.* 2017:4049534. doi: 10.1155/2017/4049534

Wu, Z. G., Jiang, W., Chen, S. L., Mantri, N., Tao, Z. M., and Jiang, C. X. (2016). Insights from the cold transcriptome and metabolome of *Dendrobium officinale*: global reprogramming of metabolic and gene regulation networks during cold acclimation. *Front. Plant Sci.* 7:1653. doi: 10.3389/fpls.2016.01653

Yang, Y., Qi, M., and Mei, C. (2004). Endogenous salicylic acid protects rice plants from oxidative damage caused by aging as well as biotic and abiotic stress. *Plant J.* 40, 909–919. doi: 10.1111/j.1365-313X.2004.02267.x

Yoshida, R., Hobo, T., Ichimura, K., Mizoguchi, T., Takahashi, F., Aronso, J., et al. (2002). ABA-activated SnRK2 protein kinase is required for dehydration stress signaling in *Arabidopsis*. *Plant Cell Physiol.* 43, 1473–1483. doi: 10.1093/pcp/pcf188

Yoshimura, K., Miyao, K., Gaber, A., Takeda, T., Kanaboshi, H., Miyasaka, H., et al. (2004). Enhancement of stress tolerance in transgenic tobacco plants overexpressing *Chlamydomonas* glutathione peroxidase in chloroplasts or cytosol. *Plant J.* 37, 21–33. doi: 10.1046/j.1365-313X.2003.01930.x

Yu, J. L., Yang, L., Liu, X., Tang, R. J., Wang, Y., Ge, H. M., et al. (2016). Overexpression of poplar pyrabactin resistance-like abscisic acid receptors promotes abscisic acid sensitivity and drought resistance in transgenic *Arabidopsis*. *PLOS ONE* 11:e0168040. doi: 10.1371/journal.pone.0168040

Zeevaart, J. A. D., and Creelman, R. A. (1998). Metabolism and physiology of abscisic acid. *Annu. Rev. Plant Physiol. Plant Mol. Biol.* 39, 439–473. doi: 10.1146/annurev.pp.39.060188.002255

Zhao, Y., Chan, Z., Gao, J., Xing, L., Cao, M., Yu, C., et al. (2016). ABA receptor PYL9 promotes drought resistance and leaf senescence. *Proc. Natl. Acad. Sci. U.S.A.* 113, 1949–1954. doi: 10.1073/pnas.1522840113

Zhou, L., Wang, S., Chi, Y., Li, Q., Huang, K., and Yu, Q. (2015). Responses of photosynthetic parameters to drought in subtropical forest ecosystem of China. *Sci. Rep.* 5:18254. doi: 10.1038/srep18254

Zhu, J. K. (2002). Salt and drought stress signal transduction in plants. *Annu. Rev. Plant Biol.* 53, 247–273. doi: 10.1146/annurev.arplant.53.091401.143329

Conflict of Interest Statement: The authors declare that the research was conducted in the absence of any commercial or financial relationships that could be construed as a potential conflict of interest.

frontiers in Plant Science

REVIEW
published: 04 October 2017
doi: 10.3389/fpls.2017.01704

Cyclic Nucleotide Monophosphates and Their Cyclases in Plant Signaling

Chris Gehring[1,2]* *and Ilona S. Turek*[1,3]

[1] Biological and Environmental Science and Engineering, King Abdullah University of Science and Technology, Thuwal, Saudi Arabia, [2] Department of Chemistry, Biology and Biotechnology, University of Perugia, Perugia, Italy, [3] Leibniz Institute of Plant Biochemistry, Halle, Germany

The cyclic nucleotide monophosphates (cNMPs), and notably 3′,5′-cyclic guanosine monophosphate (cGMP) and 3′,5′-cyclic adenosine monophosphate (cAMP) are now accepted as key signaling molecules in many processes in plants including growth and differentiation, photosynthesis, and biotic and abiotic defense. At the single molecule level, we are now beginning to understand how cNMPs modify specific target molecules such as cyclic nucleotide-gated channels, while at the systems level, a recent study of the Arabidopsis cNMP interactome has identified novel target molecules with specific cNMP-binding domains. A major advance came with the discovery and characterization of a steadily increasing number of guanylate cyclases (GCs) and adenylate cyclases (ACs). Several of the GCs are receptor kinases and include the brassinosteroid receptor, the phytosulfokine receptor, the Pep receptor, the plant natriuretic peptide receptor as well as a nitric oxide sensor. We foresee that in the near future many more molecular mechanisms and biological roles of GCs and ACs and their catalytic products will be discovered and further establish cNMPs as a key component of plant responses to the environment.

Keywords: signaling, cGMP, cAMP, guanylate cyclase (GC) and adenylate cyclase (AC), receptor kinases, *Arabidopsis thaliana*

OPEN ACCESS

Edited by:
Gerald Alan Berkowitz, University of Connecticut, United States

Reviewed by:
Frantisek Baluska, University of Bonn, Germany
Zhi Qi, Inner Mongolia University, China

***Correspondence:**
Chris Gehring
c.a.gehring@molecular-signals.com

Specialty section:
This article was submitted to Plant Traffic and Transport, a section of the journal Frontiers in Plant Science

Received: *25 July 2017*
Accepted: *19 September 2017*
Published: *04 October 2017*

Citation:
Gehring C and Turek IS (2017) Cyclic Nucleotide Monophosphates and Their Cyclases in Plant Signaling. Front. Plant Sci. 8:1704. doi: 10.3389/fpls.2017.01704

INTRODUCTION

There is a growing awareness that cyclic nucleotide monophosphates (cNMPs) and their cyclases are universal signaling molecules across the tree of life (Schaap, 2005). They are also key to many plant responses and the novel biological roles of these molecules and their mechanisms of action are discovered at an increasing rate (Meier et al., 2009; Wong et al., 2015; Marondedze et al., 2016a). Here, we review some of the early work on the detection of cNMPs in plants and the discovery of the cyclases that catalyze formation of 3′,5′-cyclic adenosine or guanosine monophosphate (cAMP or cGMP) and pyrophosphate from their corresponding nucleoside 5′-triphosphate. We will also review recent approaches to elucidate systems responses to cNMPs in plants (e.g., Isner et al., 2012; Marondedze et al., 2013; Alqurashi et al., 2016). A summary of cGMP-dependent processes is provided in **Figure 1**.

A BRIEF SUMMARY OF THE ROLES OF cAMP AND cGMP IN PLANT FUNCTION

Despite the fact that cAMP and cGMP have been recognized as important second messengers in animals nearly half a century ago, the notion that the cNMPs signaling system is universal and operates in plants was a matter of debate until recently. The existence and physiological functions

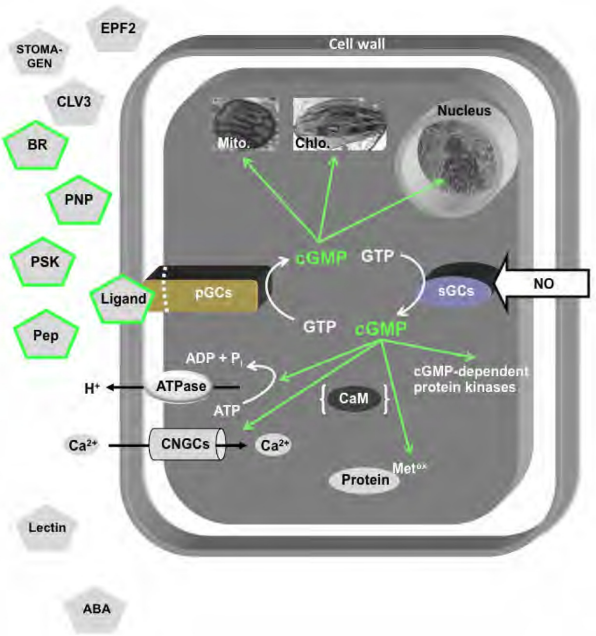

FIGURE 1 | Overview of cGMP-dependent processes in plant cells. Particulate guanylate cyclases (pGCs) or soluble guanylate cyclases (sGCs) catalyze the reaction from GTP to cGMP that in turn modulates processes in the cell membrane, the cytosol, the mitochondria (Mito.), the chloroplast (Chlo.), or the nucleus. Proton transport is modulated by ATPases, while cation transport, including Ca^{2+} uptake, is enabled by cyclic nucleotide-gated channels (CNGCs) and calmodulin (Gonzalez-Fontes et al., 2014). Cyclic nucleotide-dependent processes also affect the phosphoproteome and other post-translational processes, including methionine oxidation. Established ligands of GC-coupled receptors are represented by pentagrams with green borders and include the PNP receptor (AtPNP-R1), the Pep receptor (AtPepR1), the brassinosteroid receptor (AtBRI-GC), and the phytosulfokine receptor (AtPSKR1). Candidate GC-coupled receptors include a Stomagen receptor, a CLAV3 receptor, an EPF2 receptor, and a lectin receptor.

of cNMPs in higher plants have been questioned for long time mainly due to the fact that the cAMP and cGMP levels in plants appeared to be low (usually in the nanomolar range based on fresh weight) compared to those found in animals and lower eukaryotes (concentrations in the nano- to micromolar range) and often below the detection limits of analytical methods available in the past. Furthermore, reported amounts of cNMPs in different plants largely disregarded spatial and temporal variations of these secondary messengers. Arguably, the first convincing experimental evidence for the occurrence of cNMPs in higher plants came from a report that demonstrated changes in cNMPs levels during cell expansion and division in tobacco (*Nicotiana tabacum*) (Lundeen et al., 1973). Given the relatively low concentrations of cNMPs in plants, a second controversy concerned the biological significance of the effects exerted by non-physiological micromolar concentrations of exogenously applied cNMPs analogs on plant systems. However, numerous reports of nanomolar concentrations of cNMPs stimulating plant responses have since then overcome this point (e.g., Alqurashi et al., 2016; Marondedze et al., 2016a).

A growing body of evidence from plant electrophysiology and cell and molecular biology reveals that a considerable number of physiological processes in plants are correlated with alterations in cNMPs levels. Reports from several laboratories have shown direct effects of cNMPs on cation fluxes, including K^+, Na^+, and Ca^{2+}, sparking interest in these molecules as potential regulators of ion and water homeostasis. Both cAMP and cGMP cause elevation of cytosolic Ca^{2+} concentration, involving internal and external Ca^{2+} stores, in tobacco (*Nicotiana plumbaginofolia*) protoplasts (Volotovski et al., 1998) and down-regulate Na^+ influx and accumulation in Arabidopsis roots (Essah et al., 2003; Isner and Maathuis, 2011). Direct evidence for cAMP activation of hyperpolarization-activated Ca^{2+} channels in plasma membrane (PM) was provided in guard and mesophyll cells of *Arabidopsis thaliana* (Lemtiri-Chlieh and Berkowitz, 2004) and in pollen tube of Asian pear (*Pyrus pyrifolia*) (Wu et al., 2011). Cyclic GMP-dependent modulation of PM H^+-ATPase activity, which indirectly provides a driving force for the cellular uptake of cations, particularly K^+, and hence may significantly affect nutrient uptake and solute transport and could regulate cell volume, was reported in *Tradescantia multiflora* stem and leaf tissue (Suwastika and Gehring, 1999). K^+ and Na^+ fluxes modulated by cGMP by the activation of non-selective ion channels were observed in *Zea mays* roots (Pharmawati et al., 1999). Whole-cell patch-clamp current recordings in protoplasts from *Vicia faba* mesophyll cells revealed dose-dependent increases in the outward K^+ current upon intracellular application of cAMP (Li et al., 1994), whereas cGMP was suggested to directly affect K^+ fluxes in Arabidopsis guard cells (Pharmawati et al., 2001) and in intact tissue (Maathuis, 2006). Furthermore, both cNMPs were demonstrated to modulate K^+ and Ca^{2+} flux responses to H_2O_2 in Arabidopsis roots (Ordoñez et al., 2014). In analogy to animal systems, many functions of plant cNMPs are primarily mediated through cyclic nucleotide-gated channels (CNGCs), many of which have already been demonstrated as critical for plant responses to both biotic and abiotic cues (Kaplan et al., 2007; Jha et al., 2016). One of the CNGCs characterized in Arabidopsis, namely AtCNGC4, that is permeable to both Na^+ and K^+, is activated by both cAMP and cGMP and has been implicated in plant responses to biotic stress (Balague et al., 2003).

Ample evidence for the role of both cAMP and cGMP in several physiological processes, including cell cycle progression as well as cell proliferation, growth and differentiation, organelle development, seed germination, and finally, plant growth and flowering have been accumulated. Early studies revealed changes in cGMP concentration that occur during cell volume increases and division in excised pith tissues of tobacco (Lundeen et al., 1973). Stringent control of intracellular cAMP levels was observed during progression through the cell cycle of the tobacco BY-2 cells, with cAMP peaks observed in S phase and, to lesser extent, in G_1 phase (Ehsan et al., 1998). In contrast, reduced cAMP levels were noted at the beginning of G_1 phase in arrested cells (Ehsan et al., 1999). cGMP was also implicated in chloroplast development (Bowler et al., 1994a), which could be inhibited by high level of cGMP (Bowler et al., 1994b; Wu et al., 1996). Immunochemical and cytoenzymological detection

of cAMP and adenylate cyclase (AC) activity, respectively, was demonstrated in the developing tobacco chloroplasts (Witters et al., 2005), providing additional evidence for a general role of cNMPs in photosynthetic activity of higher plants, resembling well-characterized functions of these secondary messengers in lower plants. In addition to gibberellic acid (GA)-dependent elevation of cAMP concentration required for seeds germination, observed in common broomrape (*Orobanche minor*) (Uematsu et al., 2007) and phacelia (*Phacelia tanacetifolia*) seeds (Uematsu and Fukui, 2008), cGMP was identified as a positive regulator of Arabidopsis seed germination (Teng et al., 2010). In pollen, where tube grow and orientation (Prado et al., 2004) and targeting (Prado et al., 2008) are critical, the gaseous signaling molecule nitric oxide (NO) has a role too and as in other systems, cyclic nucleotides are implicated in downstream signals [for review see Domingos et al. (2015)]. In addition, cGMP was demonstrated to mediate adventitious root formation (Pagnussat et al., 2003), root gravitropism (Hu et al., 2005), and is vital for root growth and development by positive modulation of auxin-regulated signaling responses (Nan et al., 2014). Furthermore, cAMP was implicated in the regulation of symbiotic root nodule formation, with soybean (*Glycine max*) root nodules containing significant levels of cAMP, while low cAMP level was noted in leaves (Terakado et al., 1997), and low concentrations of this cNMP were demonstrated to induce self-incompatibility in lily (*Lilium longiflorum*) (Tezuka et al., 2007). Assigning guanylate cyclase (GC) activity to brassinosteroid receptor BRI1 (Kwezi et al., 2007) and phytosulfokine receptor PSKR1 (Kwezi et al., 2011) provided a link between cGMP signaling and regulation of multiple growth and developmental processes, including embryogenesis, cell proliferation and elongation, and vascular differentiation (Sauter, 2015; Wei and Li, 2016). Furthermore, cGMP has been also implicated in phytochrome-controlled induction of flowering of morning glory (*Pharbitis nil*) (Szmidt-Jaworska et al., 2008) and in programmed-cell death (PCD) (Clarke et al., 2000), again highlighting impact of cNMPs on nearly every aspect of plant life cycle.

It is evident that cNMPs are becoming increasingly recognized as modulators of plant metabolism and a recurrent theme that has emerged since the early descriptions of these fundamental secondary messengers is the importance of their interplay with plant hormones. For instance, GA treatment of cereal aleurone layers led to a transient increase in cGMP levels and the subsequent induction of α-amylase production that in turn causes the conversion of starch to sugar (Penson et al., 1996), whereas auxin and kinetin, which cause stomatal opening, also signal via this cNMP (Cousson and Vavasseur, 1998; Pharmawati et al., 2001). Elevated concentrations of cAMP coincide with the early stages of the response to phytoalexins and evoke production of an antifungal isocoumarin, 6-methoxymellein, in cultured carrot (*Daucus carota*) cells (Kurosaki et al., 1987; Kurosaki and Nishi, 1993). Furthermore, NO elicits many processes in plants [for review see Domingos et al. (2015)] and often does so together with cyclic nucleotides and notably cGMP, which in analogy to mammalian systems, has been strongly implicated in NO signaling in plants (Pfeiffer et al., 1994; Durner et al., 1998; Dubovskaya et al., 2011). Examples include calcium-dependent development of cell polarity in *Ceratopteris richardii* (Salmi et al., 2007), NO increases in mitochondrial respiration in Arabidopsis callus (Wang et al., 2010), and NO- and redox signaling in the phloem upon localized leaf wounding (Gaupels et al., 2016). Finally, cGMP mediates plant natriuretic peptides (PNPs) signal (Morse et al., 2004), pinpointing a general function of cNMPs in regulation of ion and solute homeostasis in plants.

Importantly, cNMPs are involved in perception of extracellular abiotic and biotic stimuli and subsequent amplification and transduction of the signals to corresponding responses. Numerous observations have provided incontrovertible evidence that cNMPs function in plant abiotic stress responses and this is often accomplished by regulation of the ion fluxes. Addition of membrane permeable cNMPs during growth assays of *A. thaliana* roots affected voltage-independent channels and reduced levels of Na^+ accumulation, thus improving plant salinity tolerance (Maathuis and Sanders, 2001). A rapid (<1 min) time-dependent increases in cellular cGMP levels also occur after the salt and osmotic stress treatments (Donaldson et al., 2004) and CNGC19 and CNGC20 were speculated to presumably be involved in these early responses (Kugler et al., 2009). Elevated cGMP was also noted in late (>2 h) response to ozone (Pasqualini et al., 2009), whereas increased cGMP level upon a 30 min-long heat stress was associated with CNGC16 (Tunc-Ozdemir et al., 2013). These increases point to physiological roles of cNMPs in abiotic stress responses. It is noteworthy that proteomic study also suggested that cAMP functions in responses to environmental threats, such as temperature, as well as in light signaling and regulation of photosynthesis (Thomas et al., 2013). Early studies revealed considerable fluctuations of cGMP levels occurring in response to light (Brown et al., 1989; Bowler et al., 1994b), and a direct effect of cGMP concentrations on the phytochrome signal transduction was elucidated by investigating *aurea* mutant of tomato that is deficient in phytochrome A, a photoreceptor responsible for regulating many morphogenesis responses, including flowering, seed germination, and diurnal rhythms; cGMP not only triggered the production of photoprotective compounds anthocyanins, but in combination with Ca^{2+} induced development of fully mature chloroplasts containing all the photosynthetic machinery (Bowler et al., 1994a). In line with these observations, recently reported interactors of cNMPs include several enzymes involved in Calvin cycle (Donaldson et al., 2016), implying specific roles of cNMPs in photosynthesis.

An impact of cNMPs on gas exchange can also be assumed based on early observations describing effect of cAMP analogs in stomata opening in *V. faba* (Curvetto et al., 1994), while cGMP analog was reported to induce stomata opening in a number of plants, including Arabidopsis (Pharmawati et al., 1998, 2001); this occurs downstream of abscisic acid (ABA)-induced changes in H_2O_2 and NO (Dubovskaya et al., 2011). Consistent with the notion of cNMPs involvement in photorespiration, several photorespiratory enzymes were observed among proteins identified as cAMP or cGMP interactors (Donaldson et al., 2016). Furthermore, differential effects of cGMP and 8-nitro-cGMP on stomata opening (Joudoi et al., 2013) were reported, whereas, similarly to cGMP, cyclic adenosine 5′-diphosphoribose

(cADPR) was shown to positively function in ABA and methyl jasmonate-induced stomatal closure in Arabidopsis (Hossain et al., 2014). Since stomata can be considered a frontline of plant interaction with the environment, their closure can be induced by adverse conditions, including not only drought and salt, but also pathogen attack, to reduce water loss and cell dehydration. Thus, function of cNMPs in plant responses to biotic stress appears plausible.

During the past two decades, the role of endogenous cAMP and cGMP in plant defense responses gained more recognition. cGMP was also reported to cause transcript increases of the defense-related genes encoding pathogenesis-related 1 and phenylalanine ammonia lyase proteins in tobacco (Durner et al., 1998) and to participate in signal transduction pathways activated by a group of danger-associated molecular patterns (DAMPs), such as AtPeps (Qi et al., 2010). NO has also a central role in defense against pathogens and the salicylic acid pathogen defense response pathways do not just include NO but also cGMP (Klessig et al., 2000) and this holds true for NO-triggered PCD (Clarke et al., 2000). In accordance with this finding, challenging *A. thaliana* with avirulent strain of *Pseudomonas syringae* results in cGMP accumulation (Meier et al., 2009). More recently it has been demonstrated that infection of *A. thaliana* with avirulent pathogens (and not avirulent strains) can cause a biphasic increase of cGMP downstream of NO. However, constitutive cGMP accumulation can compromise systemic acquired resistance (Hussain et al., 2016) and this would suggest that "swamping" the cell with a signaling molecule can cause disfunction. Accumulation of cGMP was also demonstrated in extrafascicular phloem, a defensive structure against herbivorous animals, in leaf wounded pumpkin (*Cucurbita maxima*) (Gaupels et al., 2016). Similarly, pathogen attack and mechanical wounding elevated cGMP content in *Hippeastrum hybrid* (Swiezawska et al., 2015). On the other hand, cAMP, apart from being implicated in activation of phytoalexin synthesis in sweet potato (*Ipomoea batatas*) (Oguni et al., 1976) and in early signaling events in the apoplastic oxidative burst (Bindschedler et al., 2001), was also reported to be elevated at the infection site initiation in pathogen-related cytosolic Ca^{2+} signaling (Ma et al., 2009). Moreover, production of elevated concentrations of cAMP by the administration of elicitors has been demonstrated in French bean (*Phaseolus vulgaris*) (Bolwell, 1992), carrot (*D. carota*) (Kurosaki and Nishi, 1993), alfalfa (*Medicago sativa*) exposed to *Verticillium alboatrum* glycoprotein (Cooke et al., 1994), Mexican cypress (*Cupressus lusitanica*) cell culture treated with yeast oligosaccharides (Zhao et al., 2004), and Arabidopsis treated with *Verticillium dahliae* toxins, resulting in improved disease resistance of the plants (Jiang et al., 2005). It is noteworthy that many signaling cascades generated in response to biotic stresses not only employ cNMPs, but also critically depend on CNGCs. For instance, AtCNGC4, activated by cAMP and cGMP, is induced as a result of pathogen infection and certain pathogen-related signals (Balague et al., 2003), whereas CNGC11 and CNGC12 activate multiple pathogen resistance responses and act as positive mediators of plant resistance against avirulent isolate of oomycete *Hyaloperonospora parasitica* (Yoshioka et al., 2006). Interestingly enough, recently several other CNGCs, including CNGC2 and CNGC4, have also been associated with plant responses to biotic stresses (Ali et al., 2007; Chin et al., 2013). In Arabidopsis, AtCNGC2 has recently been demonstrated to induce apoplastic Ca^{2+} influx in response to jasmonic acid (JA) and thus linking JA-induced cAMP increases to Ca^{2+}-dependent downstream signaling (Lu et al., 2016). The rapid (<5 min) JA-dependent cytosolic cAMP increases and concomitant increase in cytosolic Ca^{2+} are indeed consistent with cAMP being an AtCNGC2 ligand (Lu et al., 2016). It is noteworthy, that another recent report suggests that AtCNGC2 delivers Ca^{2+} from veins into leaf cells thereby preventing apoplastic Ca^{2+} accumulation but does not seem to have a direct influence on the hypersensitive response (Wang et al., 2017).

Furthermore, wounding stress was shown to lead to a rapid approximately five-fold increase in concentration of the non-canonical 2′,3′-isomers of cAMP and cGMP in *A. thaliana* leaves (Van Damme et al., 2014). These reports, taken together, strongly argue that both the host–pathogen recognition and the downstream processes are transduced by complex cNMP signatures and often include regulation of CNGCs. The role of cNMPs in both abiotic and biotic stress responses does not come as a surprise considering the fact that in biotic interactions pathogens modulate plant host ion and water homeostasis, inflicting abiotic stress conditions, to the detriment of the host (Gottig et al., 2008).

Since the low concentrations of cNMPs in higher plants definitely constituted a major problem in cNMP research in this system, it can be noteworthy to emphasize the impact of technological progress in the development of methods for extraction, purification, detection, and quantitation of cNMPs, with a very low limit of detection, on the advancement in investigation of plant cNMPs signaling witnessed over last few decades. Initial methods of cNMPs separation and detection, such as radio-immune assays, characterized by a femtomole dynamic range, suffered from lack of accuracy due to co-elution of interfering plant metabolites, including derivatives of cNMPs and hence significantly compromising the data. This problem was largely overcome due to the use of anti-cAMP or anti-cGMP antibodies in an immunopurification step, allowing more powerful sample clean-up. In the 1980s, chromatographic analyses in plant cNMPs analysis, including paper and thin-layer chromatographies, were replaced by high-performance liquid chromatography (LC) by virtue of its capability to separate the 3′,5′-cyclic nucleotides and their 2′,3′-isomers (Brown, 1983). Nevertheless, unambiguous demonstration of the identity of the putative cNMPs obtained in cell extracts and as the product of incubations with AC and guanylyl cyclase (GC) was accomplished by the use of physical techniques, mass spectrometry (MS) in particular. The fast atom bombardment (FAB) collision-induced dissociation (CID) tandem MS (MS/MS) not only allowed the unequivocal identification of cAMP and cGMP, but also demonstrated natural occurrence of cytidine, inosine, uridine, and 2′-deoxythymidine 3′,5′-cyclic monophosphate (cCMP, cIMP, cUMP, and cdTMP, respectively) in pea (*Pisum sativum*) (Newton et al., 1991) in the early 1990s. Due to its greater sensitivity, LC–electrospray ionization (ESI)–MS/MS set-up, which decreased detection limits to femtomole

level, gradually replaced FAB–MS/MS and is successfully used in cNMP detection and quantification studies until now, providing an excellent platform for large-scale investigation of cNMPs interactors and system-level analyses of proteins that are differentially expressed and/or post-translationally modified in a cNMP-dependent manner. Further advancement of separation techniques enabled analysis of 2′,3′-cNMPs in plants (Pabst et al., 2010) and facilitated studies on physiological relevance of both the canonical and non-canonical cNMPs in plants over the last decade (Van Damme et al., 2014).

The analytical chemistry methods developed for determination of cNMPs concentrations with fine enough spatial and temporal resolution that provides confidence in the biological significance of the results, although powerful, are labor intensive and costly in terms of infrastructure, require high levels of expertise and large amount of tissue. The enzyme immunoassays (EIAs), tailored for animal cells, used to determine contents of cAMP or cGMP in analyzed plant samples suffered greatly from lack of specificity and selectivity, often leading to inconsistent results (Newton and Smith, 2004). Newer enzyme-linked immunosorbent assays (ELISAs) are more specific for cNMPs but may under-report amounts of cNMPs present in plant cells (Meier et al., 2010), whereas a recently improved EIA method for cAMP detection in plant tissue was promised to be 10 times more sensitive than previously used methods (Lomovatskaya et al., 2011). The advent of biosensor-based techniques in cell biology, and in particular reporter systems used to record cNMP levels non-destructively in real time and with relatively high spatial and temporal resolutions, was a significant step forward in plant cNMPs research. However, in plant research, we are still quite distance away from the development and application of high-resolution sensing, e.g., with cytosolic Förster resonance energy transfer-based cGMP biosensors (Gotz et al., 2014) that are currently applied in medial research. Another obstacle that is intrinsic to plant work is the very small cytosolic compartment of cells where by far the biggest volume is taken up by the vacuole which is almost certainly not the place where cNMP-dependent signaling has a key role. Still, owing to the ease of use, the currently available plant reporters have significantly contributed to establishing the physiological functions of cNMPs in plants and these reporters also offer an affordable alternative to the advanced techniques of analytical chemistry.

In brief, firstly, the imaging of cAMP cellular distribution and quantification was reported in living pollen tubes (Moutinho et al., 2001) and it was achieved by microinjecting a cAMP fluorosensor. The pollen tube was chosen to investigate the role of cAMP not least because it is a large single cell that lends itself to microinjecting a fluorescent sensor dye into its cytoplasm. Secondly, reliable quantification of cytoplasmic cGMP concentrations in plant cells transiently and stably transformed with δ-FlincG in response to various external stimuli has also been reported (Isner and Maathuis, 2011). The reported δ-FlincG dissociation constant for cGMP was approximately 200 nM and was reported to result in a dynamic range spanning from approximately 20 nM to 2 μM. Thirdly, the development of luciferase-based promoter reporter systems. The principle here is that the promoter of a cGMP-inducible gene [e.g., OLIGOPEPTIDE TRANSPORTER X (OPTX)] is fused to a luciferase reporter gene (Wheeler et al., 2013) and luciferase activity is a proxy for cGMP and can be calibrated.

In summary, the development and application of sophisticated methods in the fields of immunocytochemistry, electrophysiology, and separation technologies combined with MS have assisted in the in-depth characterization of components of the plant cNMP-dependent signalosome.

THE DISCOVERY OF THE FIRST GCs IN HIGHER PLANTS

Despite the fact that by the year 2000 the presence of cNMPs in higher plants was established beyond reasonable doubt and numerous cAMP- and cGMP-dependent processes have been reported, the cyclases responsible for the formation of cNMPs have remained elusive. While basic local alignment search tool (BLAST) searches with annotated GCs from lower eukaryotes and animals did return candidate GC in cyanobacteria perhaps surprisingly, when ACs and GCs from lower or higher eukaryotes were used to query the newly available *A. thaliana* genome no plausible plant candidates were returned (Ludidi and Gehring, 2003). This suggested that plant cyclases had lost ancestral cyclases domains and evolved new ones, or more likely, that plant cyclases had evolved in such a way that only the key catalytic residues remained conserved and that those few key amino acid (aa) residues where beyond the detection limit of BLAST searches. In order to test the second hypothesis, we firstly determined the key aa residues with annotated roles in the catalytic process (Liu et al., 1997; Tucker et al., 1998). These have in part been determined based on the crystal structure of the rat type II AC C2 catalytic domain that was in turn used to homology model a mammalian AC C1–C2 domain pair, a homodimeric AC of *Dictyostelium discoideum*, a heterodimeric soluble GC (sGC), and a homodimeric membrane GC. These authors also docked Mg^{2+}-complexed adenosine triphosphate (ATP) or guanosine triphosphate (GTP) to the active site to inspect stereo-chemical constraints of the resulting conformation (Liu et al., 1997). The authors report that their "models are consistent with the activities of seven mutants" in the catalytic site where an aspartic acid (D) and glutamine (Q) of type I ACs can coordinate the Mg^{2+} ion. They also show that mutating D310 residue to serine (S) and (D) 310 to alanine (A) decreases the reduced V_{max} of the reaction as well as altering [Mg^{2+}] dependence. Furthermore, it was proposed that the purine moieties bind in hydrophobic pockets and that specificity is due to a lysine (K) and D in AC, and a glutamic acid (E), an arginine (R), and a cysteine (C) in GCs. It was also predicted that an asparagine (N)–R pair would stabilize the transition state. With these structural parameters in mind, we then inspected alignments of known catalytic centers of different types of nucleotide cyclases (McCue et al., 2000) before aligning catalytic centers of annotated, and in some cases, experimentally confirmed nucleotide cyclases in lower and higher eukaryotes (Ludidi and Gehring, 2003). From this alignment, we extracted a 14 aa-long core catalytic center search motif (**Figure 2**) and

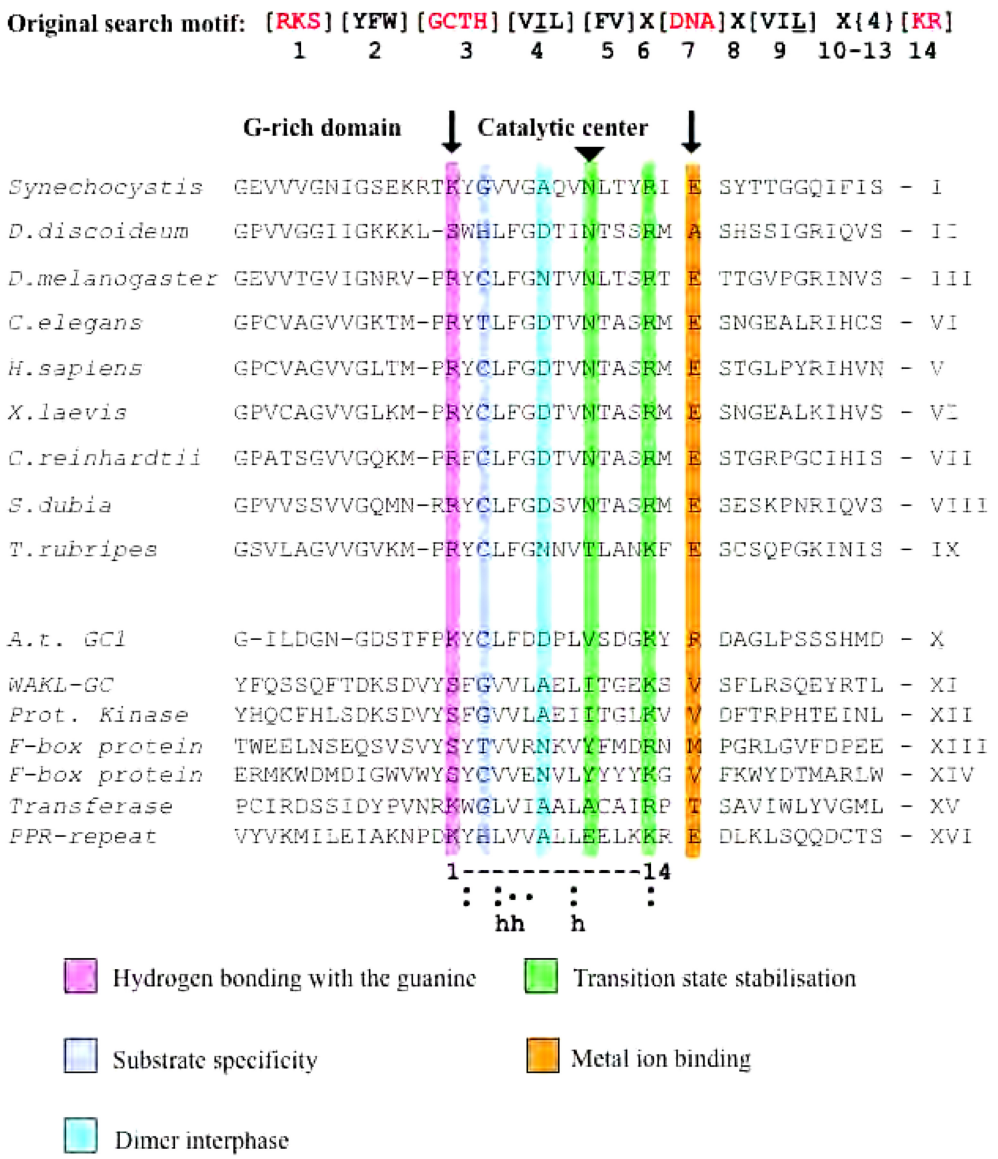

FIGURE 2 | Alignment of GC catalytic domains led to the original GC search. Alignment of catalytic centers of GC delineated by two solid arrows. The deduced 14 amino acid-long search motif is in bold, and substitutions are in square brackets; X represents any amino acid, and curly brackets define the number of amino acids. Red amino acids are functionally assigned residues of the catalytic center and the underlined amino acids in positions 4 and 9 are the third branched aliphatic amino acid not appearing in the alignment. The C-terminal residue implied in Mg^{2+}-binding or Mn^{2+}-binding was not included in the original search motif. The letter "h" stands for hydrophobic residues forming the hydrophobic pocket.

when used to query the Arabidopsis proteome, it returned seven candidate GCs, including AtCG1 (At5g05930) and AtWAKL10 (At1g79680).

A recombinant AtCG1 was first to be tested experimentally and shown to be capable to generate cGMP for GTP *in vitro* in the presence of Mg^{2+}. AtGC1 is a dual-domain 274 aa-long sGC with the catalytic center on the very N-terminus, but contrary to sGCs in animals, AtGC1 is not sensitive to NO and therefore represented a new type of sGC. The second domain has been predicted to be a peptidase family C39-like domain (IPR005074) typical for antibiotic bacteriocin-processing endopeptidases from bacteria where the cleavage is mediated by its ATP-binding cassette (ABC) transporter domain as part of the secretion process and this is supported by fold studies suggesting that AtGC1 is a member of a novel eukaryotic C proteinase family that might function as a protease (Ginalski and Zemojtel, 2004). While preliminary studies have confirmed the protease activity, the interrelationship between the GC activity and the protease activity as well as the biological function(s) has remained elusive.

We also tested AtWAKL1 that is a receptor type wall associated kinase-like molecule that can also generate cGMP *in vitro* as well as having kinase activity (Meier et al., 2010).

Furthermore, a co-expression and stimulus-specific expression analysis of AtWAKL10 has suggested that it is consistently co-expressed with extensively characterized pathogen defense-related genes and, much like these genes, is induced early and pronouncedly in responses to both a range of pathogens (including *Botrytis cinerea* and *P. syringae*) and their elicitors (Meier et al., 2010).

EXPANDING THE SEARCH AND DISCOVERY OF NOVEL CYCLASE IN HIGHER PLANTS

How many mononucleotide cyclases (MNCs; ACs and GCs) are there in the proteomes of higher plants? This question has remained unsolved, but several lines of evidence suggest that the number may be considerably higher than previously suspected and may in fact be >100. Firstly, we noted that *Chlamydomonas reinhardtii*, a unicellular green alga, contains >100 MNCs annotated on the basis of sequence homology with predicted and/or experimentally confirmed ACs and GCs. These MNCs come in >20 different domain combinations and configurations with 13 different partners including Heme NO/OXygen (H-NOX), periplasmic-binding protein, GAF-like and protein kinase-like domain, ATPase domain of HSP90, RNI-like, ribonuclease-H, duplicated hybrid motif, CheY-like, family AG protein-coupled receptors, homodimeric domain of SIG, SAM/pointed domain, and C proteinase (Meier et al., 2007). Still, while the dependence on cNMPs of biological processes such as sexual signaling by gametes (Pasquale and Goodenough, 1987) and nitrate assimilation (de Montaigu et al., 2010) have been described, the cyclases at the source of the signaling pathway have remained elusive.

Secondly, given the number and diverse nature of cNMP-dependent processes such as stomatal guard cell movement (Curvetto et al., 1994; Pharmawati et al., 1998; Joudoi et al., 2013), responses to light and temperature (Brown et al., 1989; Bowler et al., 1994b; Thomas et al., 2013), responses to pathogens (Bindschedler et al., 2001; Meier et al., 2009; Gaupels et al., 2016; Hussain et al., 2016) and Pep peptides (Qi et al., 2010), responses to NO and ozone (Clarke et al., 2000; Pasqualini et al., 2009), cation transport (Hoshi, 1995; Pharmawati et al., 1999; Maathuis, 2006; Ordoñez et al., 2014), the modulation of CNGCs (Ali et al., 2007; Zelman et al., 2012; Chin et al., 2013; Tunc-Ozdemir et al., 2013), and the specific cGMP-dependent protein phosphorylation (Marondedze et al., 2016a) and methionine oxidation (Marondedze et al., 2013), it seems highly unlikely that only a very small number of ACs and CGs is responsible for all of these complex reactions. It appears more likely that higher plants, much like Chlamydomonas, harbor a large number of diverse MNCs that are capable to deliver distinct spatial, temporal, and stimulus-specific transient signals.

Thirdly, Chlamydomonas MNCs do not seem to be closely related to proteins in *A. thaliana*. The lowest *e*-value of a Chlamydomonas MNC protein (or protein fragment) compared against Arabidopsis proteins is 0.009 and this protein is a putative ethylene-responsive DEAD box RNA helicase (At5G63120). Another three Chlamydomonas MNC proteins have BLAST *e*-values < 0.05 but >0.01. This makes the evolution of MNC from Chlamydomonas to Arabidopsis at best a matter of speculation only (Meier et al., 2007).

Given these considerations, we hypothesize that higher plants are likely to contain a large number of MNCs and that the most promising way forward was to use catalytic center motifs as a means to identify them. Modifications of the motif would be based on rational considerations and in some cases tested by site-directed mutagenesis of experimentally proven cyclases (Kwezi et al., 2007). This led to a derived more relaxed search motif ([R]X{5,20}[RKS][YFW][GCTH][VIL][FV]X{3}[VIL]X{4}[KR] X {1,2}[D]) that occurs in 27 *A. thaliana* proteins of which AtBRI1 (At4g39400), the receptor for the brassinosteroids, a class of plant hormones, was the first to be tested (Kwezi et al., 2007). AtBRI1 is a leucine-rich repeat receptor-like kinase (LRR-RLK) from which we have cloned and expressed a 114 aa-long recombinant protein (AtBRI1-GC) that harbors the GC domain. This domain can convert GTP to cGMP *in vitro*, a finding that suggested that AtBRI1 may belong to a novel class of GCs that contains both a cytosolic kinase and GC domain and we have subsequently shown that the GC activity of AtBRI1 enables brassinosteroid signaling by rapidly phosphorylating the downstream brassinosteroid signaling kinase 1 (BSK1) (Wheeler et al., 2017). Incidentally, AtBRI1 and other plant LRR-RLKs have a domain organization that is not dissimilar to that of animal atrial natriuretic peptide (ANP) receptors, NPR1 and NPR2 (Singh et al., 1988; Chinkers et al., 1989). Since ANPs bind specifically to PMs and elicit physiological responses (e.g., by stomatal opening) (Gehring et al., 1996) and plants also contain highly biologically active compounds that turned out to be functional homologs of ANPs, that also cause cGMP transients [for review see Gehring and Irving (2003) and Gehring and Irving (2013)], it was not entirely surprising when a recent report found and described the PNP receptor and showed that it contains a cytosolic GC domain that is activated by the ligand PNP (Turek and Gehring, 2016).

A second candidate tested in this group is AtPepR1 (At1g73080). It is a receptor for a family of peptide signaling molecules (AtPeps) that act as DAMPs in pathogen defense signaling cascades in plants (Qi et al., 2010). We showed that this LRR-RLK also has GC activity and that AtPep-dependent expression of biotic stress defense genes (*PDF1.2*, *MPK3*, and *WRKY33*) is linked to Ca^{2+} signaling pathway that in turn are associated with AtPeps and Pep receptors.

Interestingly, these 27 Arabidopsis proteins are highly significantly (*p*-value < $1e^{-5}$) enriched for the gene ontology (GO) categories of "phosphorus metabolic processes," "protein metabolic process," "cellular macromolecular metabolic process," and "biopolymer metabolic process." Furthermore, several proteins are annotated as LRR-RLKs and they include AtBRI1 (brassinosteroid insensitive 1; At4g39400), which is the receptor for brassinosteroids. What appears quite unusual about the domain architecture of this trans-membrane receptor kinase is that the GC domain is encapsulated in the cytoplasmic kinase domain, begging question of the evolutionary and functional relationship of these two domains. We have subsequently shown

that AtBRI1 has GC activity (Kwezi et al., 2007) and that cGMP enables brassinosteroid signaling by rapidly phosphorylating the downstream BSK1 (Wheeler et al., 2017).

Also included in the GC candidate list are three receptor kinases of the ERECTA family: At2g26330 ERECTA (ER), At5g62230 ERECTA-like1 (ERL1), and At5g07180 (ERL2) [for review see Ho et al. (2016), Ikematsu et al. (2017), and Lin et al. (2017)]. Arabidopsis *erecta* (*er*) mutants show altered organ shape and the ecotype Landsberg (Ler) is typified by compact inflorescences with flowers clustering at the top and also have round leaves with short petioles and siliques (Bowman, 1993). Furthermore, they include photomorphogenesis, phytohormone biosynthesis and signal transduction, and flower organ identity mutants. More recently, many of theses mutants have been identified as LRR-RLKs (Torii et al., 1996). At2g26330 (*ERECTA*) is a quantitative trait locus for transpirational efficiency due, in part, to its influence on epidermal and mesophyll development including stomatal density and porosity of leaves, and it has been shown to be required for callose deposition upon infection (Sanchez-Rodriguez et al., 2009) and implicated in the resistance to the soil borne bacterium *Ralstonia solanacearum*, the necrotrophic fungus *Plectosphaerella cucumerina*, and oomycetes from *Pythium irregulare* (Godiard et al., 2003; Llorente et al., 2005; Adie et al., 2007) as well as in thermotolerance (Shen et al., 2015). The second candidate, At5g62230 (*ERL1*), also encodes an RLK that, together with ER and ERL2, has a key role in the fate of protodermal cells to divide proliferatively and produce pavement cells or, alternatively, to undergo asymmetric divisions that will eventually form stomatal complexes. The third candidate, the RLK At5g07180 (*ERL2*), determines whether protodermal cells divide proliferatively to produce pavement cells or divide asymmetrically to generate stomatal complexes as well as for maintaining stomatal stem cell activity in order to prevent terminal differentiation into the guard mother cell (Staff et al., 2012). *In silico* identification of the candidate GC catalytic centers in these proteins may suggest that cGMP acts as a messenger in the developmental programming of stomatal formation. However, the biochemical proof of GC activity of these RLKs still awaits confirmation.

Furthermore, CLAVATA1 (CLV1; At4g20270) is another annotated LRR-RLK. It is expressed in the shoot apical meristem where stem cells are at their undifferentiated stage by inhibiting WUSCHEL (WUS) and FANTASTIC FOUR (FAF). *WUS* and *FAF2* expression is inhibited by the CLV3 peptide in wild-type plants and impaired with Ca^{2+} channel blockers and GC inhibitors. This inhibition was also observed in the DEFENSE NO DEATH 1 (*dnd1*) and 2 (*dnd2*) mutants that lack the CNGC 2 and 4, respectively (Chou et al., 2016). This may suggest that when CLV3 binds to the CLV1 receptor in the meristem, an increase in cGMP results and that may in turn activate CNGC2 channels and consequently increase cytoplasmic Ca^{2+}. Elevated Ca^{2+} concentrations have been reported to cause altered expression of *WUS* and *FAF2* and eventually change the fate of the meristem cell (Isner and Maathuis, 2016). Perception of CLV3 peptide by CLV1 activates mitogen-activated protein kinases (MPK) MPK3 and MPK6 signaling (Betsuyaku et al., 2011; Lee et al., 2011), that in turn is involved in mediating multiple developmental and stress responses, including responses to biotic cues. Interestingly enough, involvement of CLV1 in signaling and/or perception of CLV3/endosperm surrounding region (CLE)-like effector proteins secreted by plant-parasitic beet cyst nematodes was revealed since infection with *Heterodera schachtii* is reduced on *clv1* mutant and *CLV1* expression was induced in the nematode feeding sites (Replogle et al., 2013). More recent study investigated the function of both nematode A- and B-type CLE peptides in the regulation of cell proliferation at site of feeding, linking the function of CLE receptors, including CLV1 to the modulation of the vascular stem cell pathways (Guo et al., 2017).

In order to identify additional candidate GCs we have further modified the search motif ([R]X{5,40}[RKS][YFW][GCTH][VIL][FV]X{3}[VIL]X{4}[KR]X{2,3}[D]) and retrieved 107 candidates and subjected them to GO search. Of the significantly enriched terms, we chose these in the category of "trans-membrane receptor protein tyrosine kinase signaling pathway" [p-value: $2.7e^{-10}$; false discovery rate (FDR): $2.1e^{-09}$] and identified four candidates: At2g02220, phytosulfokine receptor 1 (AtPSKR1); At3g13065, strubbelig-receptor family 4 protein (SRF4); At5g58150, an uncharacterized LRR-RLK; and At5g65710, the HAESA-Like 2, HSL2. Of those, AtPSKR1 is perhaps the best studied GC. Not only was it shown that the recombinant complete kinase (cytoplasmic) domain of AtPSKR1 has serine/threonine kinase activity (approximate K_m of 7.5 M and V_{max} of 1800 nmol min^{-1} mg^{-1} protein), but also that this domain has a GC activity *in vitro*. It was further demonstrated that over-expression of the full-length AtPSKR1 receptor in *A. thaliana* leaf protoplasts caused a >20-fold increase in endogenous cGMP levels and, importantly, that the addition of the active sulfonated ligand, PSK, induces rapid increases in cGMP levels in protoplasts (Kwezi et al., 2011). This is entirely consistent with the idea that the cytosolic GC domain of the receptor is activated by the ligand and enables to downstream signal via cGMP and suggests that the receptor GCs where the catalytic GC center is embedded in functional kinases are in fact dual-functioning – moonlighting – enzymes (Irving et al., 2012). The arising question of the functional relationship of the two domains was also addressed and it was demonstrated firstly, that Ca^{2+} is the switch between the kinase and the cyclase activity in these moonlighting enzymes (Muleya et al., 2014) and secondly, that specific auto-phosphorylation and dimerization are essential mechanisms for ligand-mediated catalysis and signaling (Muleya et al., 2016). The remaining three candidates: SRF4, the un-annotated LRR-RLK, and HSL2 remain biochemically uncharacterized. SRF4 is likely to operate as a "positive regulator" of leaf size (Eyüboglu et al., 2007) but it is also transcriptionally activated by, e.g., ABA, drought, and the plant pathogen *Golovinomyces cichoracearum*. HSL2 participates in abscission and in particular floral abscission (Patharkar and Walker, 2015) and is induced by, e.g., ABA and the root-knot nematode *Meloidogyne incognita*.

SOLUBLE GCs AND NO SENSING

Nitric oxide is a gaseous reactive oxygen species (ROS) that has evolved as a signaling hormone in many physiological processes in animals and plants, and in animal systems NO-dependent sGCs have long been known and are well characterized (Knowles et al., 1989; Denninger and Marletta, 1999). In plants, NO has been demonstrated to operate as regulator of development functioning as a signaling molecule at each step of the life cycle. NO has also been implicated in biotic and abiotic stress signaling [for review see Domingos et al. (2015)]. However, despite the multitude of plant responses to NO, many of them concomitant with cGMP increases, there have until recently been no sensor molecules discovered that can link NO to the GC activation.

In animal systems, NO binds to the heme group localized at a domain termed H-NOX, and this binding activates the GC catalytic center leading to the generation of cGMP from GTP (Palmer et al., 1987; Bellamy et al., 2002). Mutational and structural studies have confirmed the histidine (H) residue as a proximal ligand for the docking to the iron core of the heme porphyrin moiety (Wedel et al., 1994; Zhao et al., 1998) and the binding results in a 5-coordinate complex (Stone et al., 1995) that becomes a nitrosyl complex when bound to NO (Stone and Marletta, 1994). It can then sever the proximal H–Fe bond and lead to the subsequent displacement of the heme moiety (Dai et al., 2012). Given the chemistry of the structurally highly conserved H-NOX reaction center (Boon et al., 2005), we have again built a consensus motif search term (HX{12}PX{14,16}YXSXR) and retrieved four candidate molecules presumably capable of NO binding (At1g62580, At4g01160, At5g19160, and At5g57690). One of the candidate molecules (AtNOGC1, At1g62580) also contains the key residues required for GC catalytic activity ([RKS]X[GCTHS]X{9,10}[KR]) and is annotated as a flavin monooxygenase (Mulaudzi et al., 2011). Electrochemistry revealed that the recombinant binds NO and has higher affinity for NO than for O_2 and that AtNOGC1 can generate cGMP from GTP *in vitro* in a NO- and time-dependent manner. More recently, it was also demonstrated that in NO-dependent stomatal closing nitration of cGMP (8-nitro-cGMP) is key and that in the *Atnogc1* mutant neither cGMP nor the cell permeant 8-bromo-cGMP induce stomatal closure (Joudoi et al., 2013) making AtNOGC1 an essential component in this signaling pathway.

FINDING ACs IN HIGHER PLANTS

Establishing the presence and functions of cAMP and ACs in plants and higher plants in particular has been a long and at times rather controversial process (Gehring, 2010). Until a few years ago a *Z. mays* protein that participates in pollen tube growth and reorientation has remained the only experimentally confirmed AC in plants (Moutinho et al., 2001). In order to systematically identify candidate ACs in *A. thaliana*, we decided to undertake searches with modified GC motifs (**Figure 2**) since the aa in position 3 confers substrate specificity (Tucker et al., 1998; Roelofs et al., 2001; Wong and Gehring, 2013a). In GCs the residues in position 3 are [C, T, G, or H] whereas in ACs they are [D] or [E] (**Figure 2**). We then queried the Arabidopsis proteome using this substituted motif ([RKS][YFW][DE][VIL]X(8,9)[KR]X(1,3)[DE]) and retrieved 341 candidates proteins (Al-Younis et al., 2015). We then narrowed the search by including an N-terminal [R] 5–20 aa upstream of position 1 since [R] is essential for pyrophosphate-binding (Liu et al., 1997). This extended AC motif identifies 14 candidates. Testing of AC activity is somewhat more convenient than testing for GC activity since one can make use of an *Escherichia coli* cyaA mutant SP850 strain deficient in the AC (cyaA) gene (Shah and Peterkofsky, 1991) for rescue-based selection. Several of the candidates have since been tested and shown to be capable to rescue the cyaA mutant. One of them is the *A. thaliana* K^+-uptake permease 7 (AtKUP7, At5g09400). In AtKUP7, an AC catalytic center containing cytosolic fragment has also been shown with tandem MS methods to generate cAMP from ATP (Al-Younis et al., 2015). The biological role of this molecule remains to be elucidated since it might act as a cAMP-dependent K^+-flux sensor and is still under investigation.

It is noteworthy that in Paramecium, cAMP formation has been reported to be linked to K^+ conductance, and this conductance is an intrinsic property of the AC (Weber et al., 2004). This multi-domain AC therefore functions as both an AC and a K^+ channel in which a S4 voltage-sensor is part of the N-terminus and a K^+ pore-loop occupies the C-terminus on the cytoplasmic side (Weber et al., 2004). AtKUP7 also has such dual domain architecture and may function as both K^+ transporter and an AC; however, AtKUP7 is likely to be a proton-coupled carrier rather than a K channel. The future will tell if cAMP production is dependent on K^+ fluxes and/or if cAMP can modulate K^+ fluxes.

PREDICTING NOVEL ACs AND GCs WITH THE SUPPORT OF STRUCTURAL MODELING

Molecular methods for the study of signal transduction have steadily developed together with technical advances (Irving and Gehring, 2013) and this is also reflected in the discovery and characterization of cNMPs and their cyclases. These advances include computational methods for large-scale sequence analyses of the ever-increasing number of fully sequenced (plant) genomes in the public domain and the growing number of published structures of MNCs, ACs, and GCs. These two resources have indeed allowed a computational approach to the identification of candidate MNCs in higher plants (Wong and Gehring, 2013b). A method to achieve accurate predictions of Arabidopsis candidate MNCs has been detailed and includes pattern searches with catalytic center motifs of ACs or GCs. It is also recommended that these centers of candidate MNCs are compared with orthologs of closely as well as more distantly related species since conservation, particularly in the key residues, to add confidence to the predication.

An example are the systemically mobile peptidic plant hormones (the PNPs) that elicit many physiological responses

at nanomolar concentrations (Ludidi et al., 2002; Maryani et al., 2003; Gottig et al., 2008; Gehring and Irving, 2013; Turek et al., 2014). The *A. thaliana* PNP-A (At2g18660) is a ligand of AtPNP-R1 (At1g33612) receptor (Turek and Gehring, 2016) that we have shown to be a ligand-activated receptor kinase with GC activity. The ortholog in tomato is a protein (K4D0Y5_SOLLC) that also contains the key residues essential for catalysis. And given that a Verticillium natriuretic peptide-like molecule is the ligand for the tomato Verticillium wilt immune receptor (C4NAS0| C4NAS0_SOLLC Verticillium wilt disease resistance protein), it does not come as a surprise that this receptor also comes with a GC motif and may conceivably be a GC as well (de Jonge et al., 2012).

Furthermore, it has also proven useful to subject candidate MNCs to structural modeling against structure templates of annotated MNCs and in addition, docking of the substrate, ATP or GTP, to ascertain if the catalytic center forms a cavity with the key residues for ATP of GTP interaction and the metal-binding residue [an example is shown in Wong and Gehring (2013a)]. Incidentally, such an approach can also be used to model mutations and predict if candidates are conceivably functional as cyclases (Wong et al., 2015).

IN SEARCH OF NOVEL BIOLOGICAL FUNCTIONS OF cNMPs AND MNCs

Systems-based approaches to biology have also contributed and continue to contribute to or understanding of the breadth and complexity of cNMP-dependent cellular processes. The cGMP-dependent signals and their role in phosphorylation was examined using a phosphoproteomics approach and it was shown that upon treatment of *A. thaliana* roots with membrane-permeable cGMP a number of plant hormone-dependent microsomal proteins changed their phosphorylation status thus linking plant hormone responses to hormone-dependent cGMP transients and cGMP-dependent downstream phosphorylation (Isner et al., 2012). More recently a quantitative cGMP-dependent phosphoproteome of *A. thaliana* suspension-cultured cells that were metabolically labeled with ^{15}N has revealed highly specific responses and points to hitherto unknown cGMP-dependent phosphorylation and dephosphorylation events (Marondedze et al., 2016a). A pathway analysis of the identified proteins revealed that seven of them are part of the spliceosome (Matera and Wang, 2014) and belong to four different spliceosome complexes. They include the pre-mRNA processing protein (At1g44910) and splicing factor PW1 (At1g60200) that belong to the U1 complex; the WD40 repeat protein (At2g32700) is part of the U4/U6 complex; the periodic tryptophan protein 2 (At1g15440, AtPWP2) belongs to the U5 complex; the UBP1-associated protein 2A (At3g56860), the RNA-binding protein 47C (At1g47500), and the R/S-rich splicing factor that are common spliceosome components. There is firm evidence that the alternative splicing and hence the spliceosome have an important role in biotic and abiotic stresses responses and that mutations in splicing factors and spliceosomal proteins are predicted to modulate the circadian clock and the highly complex plant defense responses (e.g., Staiger and Brown, 2013) and that the phosphorylation status of spliceosome components can affect splicing (Feng et al., 2008; Lipp et al., 2015) including in responses to stimuli. This points to a direct or indirect role of cGMP in splicing-mediated stress responses.

A recent study has used an affinity purification approach to identify cyclic nucleotide-binding proteins in *A. thaliana* (Donaldson et al., 2016). Of the 15 novel candidate cNMP-binding proteins (**Table 1**), several have key functions in the Calvin cycle and photorespiration pathway, and 8 of the 15 were shown to contain cyclic nucleotide-binding domains. What is particularly interesting is the fact that the identified proteins are post-translationally modified by NO, co-expressed, and annotated to function in responses to H_2O_2 and defense response (Donaldson et al., 2016). The activity of one of cGMP interacting proteins, glycolate oxidase 1 (At3g14420) is a photorespiratory enzyme that produces H_2O_2 in response to Pseudomonas, and was shown to be repressed by the combination of cGMP and NO treatment. This gave rise to the hypothesis that these cNMP-binding proteins (co-)operate as points of cross-talk between cyclic nucleotides, NO, and ROS signaling during defense responses (Donaldson et al., 2016).

TABLE 1 | List of candidate cNMP interacting proteins.

Accession	Annotation	GO categories
At1g09340	Chloroplast RNA (stem loop)-binding protein, CRB	1, 2, 3, 4, 5
At1g42970	Glyceraldehyde-3-phosphate dehydrogenase b subunit	2, 3, 4, 5
At1g56330	Secretion-associated Ras 1b; GTP-binding protein	1
At3g01500	β-Carbonic anhydrase βCA1; salicylic acid-binding	1, 2, 3, 4, 5
At3g12780	Nuclear phosphoglycerate kinase, PGK1	1, 2, 3, 4
At3g13920	Eukaryotic translation initiation factor 4A1	
At3g14420	Glycolate oxidase 1, GOX1	5
At3g60750	Transketolase, TKL1	3, 4, 5
At3g62560	Ras-related small GTP-binding family protein	
At4g02080	A member of ARF-like GTPase family	
At4g09650	ATP synthase δ-subunit; pigment defective	2, 3, 4, 5
At4g20360	RAB GTPase homolog E1B	
At4g27440	Light-dep. NADPH:protochlorophyllide oxidoreductase B	5
At4g37930	Serine hydroxymethyltransferase 1	1, 2, 3, 4
At5g50920	ATP-dependent Clp protease	4, 5

The GO analysis was performed in: http://bioinfo.cau.edu.cn/agriGO/. 1, GO:0009409: response to cold (FDA $6.3e^{-08}$); 2, GO:0009266: response to temperature stimulus (FDA $3.1e^{-07}$); 3, GO:0009628: response to abiotic stimulus (FDA $6.6e^{-06}$); 4, GO:0009526: plastid envelope (FDA $8.5e^{-12}$); and 5, GO:0009507: chloroplast (FDA $1.9e^{-05}$).

OUT-LOOK

The discovery of an increasing number of plant MNCs does suggest that cAMP and cGMP have critical and complex roles in plant development, physiology, and responses to the environment. This is also supported by the diversity of the domain organizations of the MNCs themselves, which include NO sensors, receptor kinases, and ion channels. Not only do these "moonlighting" MNCs have to be characterized at the single molecule level, it will also be necessary to use genetic tools to elucidate their biological functions and in particular the role the cNMPs play in the downstream responses. There are already indications that the cNMPs act together with other messengers such as Ca^{2+}. We can also expect to obtain further information on cNMP-dependent effects through investigations at the systems level, in particular extensive studies on cAMP- and cGMP-specific phosphorylation events, and the effect of the nucleotides on the metabolome. The recent report on Arabidopsis RNA-binding proteome has revealed that >20 RNA-binding proteins are spliceosome components (Marondedze et al., 2016b) and it will therefore be interesting to see if stress responses affect the RNA-binding proteome particularly since cGMP has been shown to cause specific cGMP-dependent phosphorylation of spliceosome components (Marondedze et al., 2016a).

In addition, there is increasing evidence that not only cAMP and cGMP function as messengers or modulators but also non-canonical nucleotides such as cCMP or cIMP. These molecules have long been known to be present in plants (Newton et al., 1999), and it has recently been demonstrated that particularly cIMP can induce significant ROS production. Incidentally, when homology models of experimentally confirmed plant GCs were probed with substrates other than GTP, it appears conceivable that they might function (Marondedze et al., 2017). This is of course not answering the question if there are cyclases that are specific for cCMP or cIMP.

A possibly the most intriguing unanswered question is where the plant 3′,5′-cyclic-nucleotide phosphodiesterases (PDEs) in higher plants are. Again, much like in the case of the cyclases, a BLAST search with an annotated *C. reinhardtii* PDE (A8HNW2_CHLRE) does not return any plausible candidate with reasonable similarity. However, recently a liverwort (*Marchantia polymorpha*) protein has been reported that has both AC and PDE domain and both activities (Kasahara et al., 2016). Incidentally, the molecule does contain an AC catalytic center motif ([RKS]X[CTGH]X{8,12}[KR]X{1,3}[DE]) but has no ortholog in Arabidopsis or other higher plants for that matter.

AUTHOR CONTRIBUTIONS

Both authors have made a substantial, direct and intellectual contribution to the work, and approved it for publication.

FUNDING

The cost for the publication of this article was covered by King Abdullah University of Science and Technology.

REFERENCES

Adie, B. A., Perez-Perez, J., Perez-Perez, M. M., Godoy, M., Sanchez-Serrano, J. J., Schmelz, E. A., et al. (2007). ABA is an essential signal for plant resistance to pathogens affecting JA biosynthesis and the activation of defenses in Arabidopsis. *Plant Cell* 19, 1665–1681. doi: 10.1105/tpc.106.048041

Ali, R., Ma, W., Lemtiri-Chlieh, F., Tsaltas, D., Leng, Q., Von Bodman, S., et al. (2007). Death don't have no mercy and neither does calcium: Arabidopsis Cyclic Nucleotide Gated Channel2 and innate immunity. *Plant Cell* 19, 1081–1095. doi: 10.1105/tpc.106.045096

Alqurashi, M., Gehring, C., and Marondedze, C. (2016). Changes in the *Arabidopsis thaliana* proteome implicate cAMP in biotic and abiotic stress responses and changes in energy metabolism. *Int. J. Mol. Sci.* 17:852. doi: 10.3390/ijms17060852

Al-Younis, I., Wong, A., and Gehring, C. (2015). The *Arabidopsis thaliana* K^+-uptake permease 7 (AtKUP7) contains a functional cytosolic adenylate cyclase catalytic centre. *FEBS Lett.* 589, 3848–3852. doi: 10.1016/j.febslet.2015.11.038

Balague, C., Lin, B., Alcon, C., Flottes, G., Malmstrom, S., Kohler, C., et al. (2003). HLM1, an essential signaling component in the hypersensitive response, is a member of the cyclic nucleotide-gated channel ion channel family. *Plant Cell* 15, 365–379. doi: 10.1105/tpc.006999

Bellamy, T. C., Wood, J., and Garthwaite, J. (2002). On the activation of soluble guanylyl cyclase by nitric oxide. *Proc. Natl. Acad. Sci. U.S.A.* 99, 507–510. doi: 10.1073/pnas.012368499

Betsuyaku, S., Takahashi, F., Kinoshita, A., Miwa, H., Shinozaki, K., Fukuda, H., et al. (2011). Mitogen-activated protein kinase regulated by the CLAVATA receptors contributes to shoot apical meristem homeostasis. *Plant Cell Physiol.* 52, 14–29. doi: 10.1093/pcp/pcq157

Bindschedler, L. V., Minibayeva, F., Gardner, S. L., Gerrish, C., Davies, D. R., and Bolwell, G. P. (2001). Early signalling events in the apoplastic oxidative burst in suspension cultured French bean cells involve cAMP and Ca^{2+}. *New Phytol.* 151, 185–194. doi: 10.1046/j.1469-8137.2001.00170.x

Bolwell, G. P. (1992). A role for phosphorylation in the down-regulation of phenylalanine ammonia-lyase in suspension-cultured cells of french bean. *Phytochemistry* 31, 4081–4086. doi: 10.1016/0031-9422(92)80418-E

Boon, E. M., Huang, S. H., and Marletta, M. A. (2005). A molecular basis for NO selectivity in soluble guanylate cyclase. *Nat. Chem. Biol.* 1, 53–59. doi: 10.1038/nchembio704

Bowler, C., Neuhaus, G., Yamagata, H., and Chua, N. H. (1994a). Cyclic GMP and calcium mediate phytochrome phototransduction. *Cell* 77, 73–81. doi: 10.1016/0092-8674(94)90236-4

Bowler, C., Yamagata, H., Neuhaus, G., and Chua, N. H. (1994b). Phytochrome signal transduction pathways are regulated by reciprocal control mechanisms. *Genes Dev.* 8, 2188–2202. doi: 10.1101/gad.8.18.2188

Bowman, J. L. (ed.). (1993). *Arabidopsis: An Atlas of Morphology and Development*. Berlin: Springer-Verlag.

Brown, E. G., Newton, R. P., Evans, D. E., Walton, T. J., Younis, L. M., and Vaughan, J. M. (1989). Influence of light on cyclic nucleotide metabolism in plants; effect of dibutyryl cyclic nucleotides on chloroplast components. *Phytochemistry* 28, 2559–2563. doi: 10.1016/S0031-9422(00)98040-3

Brown, P. R. (1983). Current high-performance liquid chromatographic methodology in analysis of nucleotides, nucleosides, and their bases. I. *Cancer Invest.* 1, 439–454. doi: 10.3109/07357908309020277

Chin, K., Defalco, T. A., Moeder, W., and Yoshioka, K. (2013). The Arabidopsis cyclic nucleotide-gated ion channels AtCNGC2 and AtCNGC4 work in the same signaling pathway to regulate pathogen defense and floral transition. *Plant Physiol.* 163, 611–624. doi: 10.1104/pp.113.225680

Chinkers, M., Garbers, D. L., Chang, M. S., Lowe, D. G., Chin, H. M., Goeddel, D. V., et al. (1989). A membrane form of guanylate cyclase is an atrial natriuretic peptide receptor. *Nature* 338, 78–83. doi: 10.1038/338078a0

Chou, H., Zhu, Y., Ma, Y., and Berkowitz, G. A. (2016). The CLAVATA signaling pathway mediating stem cell fate in shoot meristems requires Ca^{2+} as a secondary cytosolic messenger. *Plant J.* 85, 494–506. doi: 10.1111/tpj.13123

Clarke, A., Desikan, R., Hurst, R. D., Hancock, J. T., and Neill, S. J. (2000). NO way back: nitric oxide and programmed cell death in *Arabidopsis thaliana* suspension cultures. *Plant J.* 24, 667–677. doi: 10.1046/j.1365-313x.2000.00911.x

Cooke, C. J., Smith, C. J., Walton, T. J., and Newton, R. P. (1994). Evidence that cyclic AMP is involved in the hypersensitive response of *Medicago sativa* to a fungal elicitor. *Phytochemistry* 35, 889–895. doi: 10.1016/S0031-9422(00)90633-2

Cousson, A., and Vavasseur, A. (1998). Putative involvement of cytosolic Ca^{2+} and GTP-binding proteins in cyclic-GMP-mediated induction of stomatal opening by auxin in *Commelina communis* L. *Planta* 206, 308–314. doi: 10.1007/s004250050405

Curvetto, N., Darjania, L., and Delmastro, S. (1994). Effect of 2 cAMP analogs on stomatal opening in *Vicia faba* - possible relationship with cytosolic calcium-concentration. *Plant Physiol. Biochem.* 32, 365–372.

Dai, Z., Farquhar, E. R., Arora, D. P., and Boon, E. M. (2012). Is histidine dissociation a critical component of the NO/H-NOX signaling mechanism? Insights from X-ray absorption spectroscopy. *Dalton Trans.* 41, 7984–7993. doi: 10.1039/c2dt30147d

de Jonge, R., Van Esse, H. P., Maruthachalam, K., Bolton, M. D., Santhanam, P., Saber, M. K., et al. (2012). Tomato immune receptor Ve1 recognizes effector of multiple fungal pathogens uncovered by genome and RNA sequencing. *Proc. Natl. Acad. Sci. U.S.A.* 109, 5110–5115. doi: 10.1073/pnas.1119623109

de Montaigu, A., Sanz-Luque, E., Galvan, A., and Fernandez, E. (2010). A soluble guanylate cyclase mediates negative signaling by ammonium on expression of nitrate reductase in Chlamydomonas. *Plant Cell* 22, 1532–1548. doi: 10.1105/tpc.108.062380

Denninger, J. W., and Marletta, M. A. (1999). Guanylate cyclase and the NO/cGMP signaling pathway. *Biochim. Biophys. Acta* 1411, 334–350. doi: 10.1016/S0005-2728(99)00024-9

Domingos, P., Prado, A. M., Wong, A., Gehring, C., and Feijo, J. A. (2015). Nitric oxide: a multitasked signaling gas in plants. *Mol. Plant* 8, 506–520. doi: 10.1016/j.molp.2014.12.010

Donaldson, L., Ludidi, N., Knight, M. R., Gehring, C., and Denby, K. (2004). Salt and osmotic stress cause rapid increases in *Arabidopsis thaliana* cGMP levels. *FEBS Lett.* 569, 317–320. doi: 10.1016/j.febslet.2004.06.016

Donaldson, L., Meier, S., and Gehring, C. (2016). The arabidopsis cyclic nucleotide interactome. *Cell. Commun. Signal.* 14, 10. doi: 10.1186/s12964-016-0133-2

Dubovskaya, L. V., Bakakina, Y. S., Kolesneva, E. V., Sodel, D. L., Mcainsh, M. R., Hetherington, A. M., et al. (2011). cGMP-dependent ABA-induced stomatal closure in the ABA-insensitive Arabidopsis mutant *abi1-1*. *New Phytol.* 191, 57–69. doi: 10.1111/j.1469-8137.2011.03661.x

Durner, J., Wendehenne, D., and Klessig, D. F. (1998). Defense gene induction in tobacco by nitric oxide, cyclic GMP, and cyclic ADP-ribose. *Proc. Natl. Acad. Sci. U.S.A.* 95, 10328–10333. doi: 10.1073/pnas.95.17.10328

Ehsan, H., Reichheld, J. P., Roef, L., Witters, E., Lardon, F., Van Bockstaele, D., et al. (1998). Effect of indomethacin on cell cycle dependent cyclic AMP fluxes in tobacco BY-2 cells. *FEBS Lett.* 422, 165–169. doi: 10.1016/S0014-5793(97)01610-4

Ehsan, H., Roef, L., Witters, E., Reichheld, J. P., Van Bockstaele, D., Inze, D., et al. (1999). Indomethacin-induced G1/S phase arrest of the plant cell cycle. *FEBS Lett.* 458, 349–353. doi: 10.1016/S0014-5793(99)01152-7

Essah, P. A., Davenport, R., and Tester, M. (2003). Sodium influx and accumulation in Arabidopsis. *Plant Physiol.* 133, 307–318. doi: 10.1104/pp.103.022178

Eyüboglu, B., Pfister, K., Haberer, G., Chevalier, D., Fuchs, A., Mayer, K. F., et al. (2007). Molecular characterisation of the Strubbelig-Receptor Family of genes encoding putative leucine-rich repeat receptor-like kinases in *Arabidopsis thaliana*. *BMC Plant Biol.* 7:16. doi: 10.1186/1471-2229-7-16

Feng, Y., Chen, M., and Manley, J. L. (2008). Phosphorylation switches the general splicing repressor SRp38 to a sequence-specific activator. *Nat. Struct. Mol. Biol.* 15, 1040–1048. doi: 10.1038/nsmb.1485

Gaupels, F., Furch, A. C., Zimmermann, M. R., Chen, F., Kaever, V., Buhtz, A., et al. (2016). Systemic induction of NO-, redox-, and cGMP signaling in the pumpkin extrafascicular phloem upon local leaf wounding. *Front. Plant Sci.* 7:154. doi: 10.3389/fpls.2016.00154

Gehring, C. (2010). Adenyl cyclases and cAMP in plant signaling - past and present. *Cell Commun. Signal.* 8:15. doi: 10.1186/1478-811x-8-15

Gehring, C., and Irving, H. (2013). Plant natriuretic peptides: systemic regulators of plant homeostasis and defense that can affect cardiomyoblasts. *J. Investig. Med.* 61, 823–826. doi: 10.2310/JIM.0b013e3182923395

Gehring, C. A., and Irving, H. R. (2003). Natriuretic peptides - a class of heterologous molecules in plants. *Int. J. Biochem. Cell Biol.* 35, 1318–1322. doi: 10.1016/S1357-2725(03)00032-3

Gehring, C. A., Khalid, K. M., Toop, T., and Donald, J. A. (1996). Rat natriuretic peptide binds specifically to plant membranes and induces stomatal opening. *Biochem. Biophys. Res. Commun.* 228, 739–744. doi: 10.1006/bbrc.1996.1725

Ginalski, K., and Zemojtel, T. (2004). ECEPE proteins: a novel family of eukaryotic cysteine proteinases. *Trends Biochem. Sci.* 29, 524–526. doi: 10.1016/j.tibs.2004.08.003

Godiard, L., Sauviac, L., Torii, K. U., Grenon, O., Mangin, B., Grimsley, N. H., et al. (2003). ERECTA, an LRR receptor-like kinase protein controlling development pleiotropically affects resistance to bacterial wilt. *Plant J.* 36, 353–365. doi: 10.1046/j.1365-313X.2003.01877.x

Gonzalez-Fontes, A., Navarro-Gochicoa, M. T., Camacho-Cristobal, J. J., Herrera-Rodriguez, M. B., Quiles-Pando, C., and Rexach, J. (2014). Is Ca^{2+} involved in the signal transduction pathway of boron deficiency? New hypotheses for sensing boron deprivation. *Plant Sci.* 217-218, 135–139. doi: 10.1016/j.plantsci.2013.12.011

Gottig, N., Garavaglia, B. S., Daurelio, L. D., Valentine, A., Gehring, C., Orellano, E. G., et al. (2008). *Xanthomonas axonopodis* pv. citri uses a plant natriuretic peptide-like protein to modify host homeostasis. *Proc. Natl. Acad. Sci. U.S.A.* 105, 18631–18636. doi: 10.1073/pnas.0810107105

Gotz, K. R., Sprenger, J. U., Perera, R. K., Steinbrecher, J. H., Lehnart, S. E., Kuhn, M., et al. (2014). Transgenic mice for real-time visualization of cGMP in intact adult cardiomyocytes. *Circ. Res.* 114, 1235–1245. doi: 10.1161/CIRCRESAHA.114.302437

Guo, X., Wang, J., Gardner, M., Fukuda, H., Kondo, Y., Etchells, J. P., et al. (2017). Identification of cyst nematode B-type CLE peptides and modulation of the vascular stem cell pathway for feeding cell formation. *PLOS Pathog.* 13:e1006142. doi: 10.1371/journal.ppat.1006142

Ho, C. M., Paciorek, T., Abrash, E., and Bergmann, D. C. (2016). Modulators of stomatal lineage signal transduction alter membrane contact sites and reveal specialization among ERECTA kinases. *Dev. Cell* 38, 345–357. doi: 10.1016/j.devcel.2016.07.016

Hoshi, T. (1995). Regulation of voltage dependence of the KAT1 channel by intracellular factors. *J. Gen. Physiol.* 105, 309–328. doi: 10.1085/jgp.105.3.309

Hossain, M. A., Ye, W., Munemasa, S., Nakamura, Y., Mori, I. C., and Murata, Y. (2014). Cyclic adenosine 5'-diphosphoribose (cADPR) cyclic guanosine 3',5'-monophosphate positively function in Ca^{2+} elevation in methyl jasmonate-induced stomatal closure, cADPR is required for methyl jasmonate-induced ROS accumulation NO production in guard cells. *Plant Biol.* 16, 1140–1144. doi: 10.1111/plb.12175

Hu, X., Neill, S. J., Tang, Z., and Cai, W. (2005). Nitric oxide mediates gravitropic bending in soybean roots. *Plant Physiol.* 137, 663–670. doi: 10.1104/pp.104.054494

Hussain, J., Chen, J., Locato, V., Sabetta, W., Behera, S., Cimini, S., et al. (2016). Constitutive cyclic GMP accumulation in *Arabidopsis thaliana* compromises systemic acquired resistance induced by an avirulent pathogen by modulating local signals. *Sci. Rep.* 6:36423. doi: 10.1038/srep36423

Ikematsu, S., Tasaka, M., Torii, K. U., and Uchida, N. (2017). ERECTA-family receptor kinase genes redundantly prevent premature progression of secondary growth in the Arabidopsis hypocotyl. *New Phytol.* 213, 1697–1709. doi: 10.1111/nph.14335

Irving, H. R., and Gehring, C. (2013). Molecular methods for the study of signal transduction in plants. *Methods Mol. Biol.* 1016, 1–11. doi: 10.1007/978-1-62703-441-8_1

Irving, H. R., Kwezi, L., Wheeler, J., and Gehring, C. (2012). Moonlighting kinases with guanylate cyclase activity can tune regulatory signal networks. *Plant Signal. Behav.* 7, 201–204. doi: 10.4161/psb.18891

Isner, J. C., and Maathuis, F. J. (2011). Measurement of cellular cGMP in plant cells and tissues using the endogenous fluorescent reporter FlincG. *Plant J.* 65, 329–334. doi: 10.1111/j.1365-313X.2010.04418.x

Isner, J.-C., and Maathuis, F. J. M. (2016). cGMP signalling in plants: from enigma to main stream. *Funct. Plant Biol.* (in press). doi: 10.1071/FP16337

Isner, J. C., Nuhse, T., and Maathuis, F. J. (2012). The cyclic nucleotide cGMP is involved in plant hormone signalling and alters phosphorylation of *Arabidopsis thaliana* root proteins. *J. Exp. Bot.* 63, 3199–3205. doi: 10.1093/jxb/ers045

Jha, S. K., Sharma, M., and Pandey, G. K. (2016). Role of cyclic nucleotide gated channels in stress management in plants. *Curr. Genomics* 17, 315–329. doi: 10.2174/1389202917666160331202125

Jiang, J., Fan, L. W., and Wu, W. H. (2005). Evidences for involvement of endogenous cAMP in Arabidopsis defense responses to Verticillium toxins. *Cell Res.* 15, 585–592. doi: 10.1038/sj.cr.7290328

Joudoi, T., Shichiri, Y., Kamizono, N., Akaike, T., Sawa, T., Yoshitake, J., et al. (2013). Nitrated cyclic GMP modulates guard cell signaling in Arabidopsis. *Plant Cell* 25, 558–571. doi: 10.1105/tpc.112.105049

Kaplan, B., Sherman, T., and Fromm, H. (2007). Cyclic nucleotide-gated channels in plants. *FEBS Lett.* 581, 2237–2246. doi: 10.1016/j.febslet.2007.02.017

Kasahara, M., Suetsugu, N., Urano, Y., Yamamoto, C., Ohmori, M., Takada, Y., et al. (2016). An adenylyl cyclase with a phosphodiesterase domain in basal plants with a motile sperm system. *Sci. Rep.* 6:39232. doi: 10.1038/srep39232

Klessig, D. F., Durner, J., Noad, R., Navarre, D. A., Wendehenne, D., Kumar, D., et al. (2000). Nitric oxide and salicylic acid signaling in plant defense. *Proc. Natl. Acad. Sci. U.S.A.* 97, 8849–8855. doi: 10.1073/pnas.97.16.8849

Knowles, R. G., Palacios, M., Palmer, R. M., and Moncada, S. (1989). Formation of nitric oxide from L-arginine in the central nervous system: a transduction mechanism for stimulation of the soluble guanylate cyclase. *Proc. Natl. Acad. Sci. U.S.A.* 86, 5159–5162. doi: 10.1073/pnas.86.13.5159

Kugler, A., Kohler, B., Palme, K., Wolff, P., and Dietrich, P. (2009). Salt-dependent regulation of a CNG channel subfamily in Arabidopsis. *BMC Plant Biol.* 9:140. doi: 10.1186/1471-2229-9-140

Kurosaki, F., and Nishi, A. (1993). Stimulation of calcium influx and calcium cascade by cyclic AMP in cultured carrot cells. *Arch. Biochem. Biophys.* 302, 144–151. doi: 10.1006/abbi.1993.1192

Kurosaki, F., Tsurusawa, Y., and Nishi, A. (1987). The elicitation of phytoalexins by Ca^{2+} and cyclic AMP in carrot cells. *Phytochemistry* 26, 1919–1923. doi: 10.1016/S0031-9422(00)81729-X

Kwezi, L., Meier, S., Mungur, L., Ruzvidzo, O., Irving, H., and Gehring, C. (2007). The *Arabidopsis thaliana* Brassinosteroid Receptor (AtBRI1) contains a domain that functions as a guanylyl cyclase *in vitro*. *PLOS ONE* 2:e449. doi: 10.1371/journal.pone.0000449

Kwezi, L., Ruzvidzo, O., Wheeler, J. I., Govender, K., Iacuone, S., Thompson, P. E., et al. (2011). The Phytosulfokine (PSK) Receptor is capable of guanylate cyclase activity and enabling cyclic GMP-dependent signaling in plants. *J. Biol. Chem.* 286, 22580–22588. doi: 10.1074/Jbc.M110.168823

Lee, H., Chah, O. K., and Sheen, J. (2011). Stem-cell-triggered immunity through CLV3p-FLS2 signalling. *Nature* 473, 376–379. doi: 10.1038/nature09958

Lemtiri-Chlieh, F., and Berkowitz, G. A. (2004). Cyclic adenosine monophosphate regulates calcium channels in the plasma membrane of Arabidopsis leaf guard and mesophyll cells. *J. Biol. Chem.* 279, 35306–35312. doi: 10.1074/Jbc.M400311200

Li, W., Luan, S., Schreiber, S. L., and Assmann, S. M. (1994). Cyclic AMP stimulates K^+ channel activity in mesophyll cells of *Vicia faba* L. *Plant Physiol.* 106, 957–961. doi: 10.1104/pp.106.3.957

Lin, G., Zhang, L., Han, Z., Yang, X., Liu, W., Li, E., et al. (2017). A receptor-like protein acts as a specificity switch for the regulation of stomatal development. *Genes Dev.* 31, 927–938. doi: 10.1101/gad.297580.117

Lipp, J. J., Marvin, M. C., Shokat, K. M., and Guthrie, C. (2015). SR protein kinases promote splicing of nonconsensus introns. *Nat. Struct. Mol. Biol.* 22, 611–617. doi: 10.1038/nsmb.3057

Liu, Y., Ruoho, A. E., Rao, V. D., and Hurley, J. H. (1997). Catalytic mechanism of the adenylyl and guanylyl cyclases: modeling and mutational analysis. *Proc. Natl. Acad. Sci. U.S.A.* 94, 13414–13419. doi: 10.1073/pnas.94.25.13414

Llorente, F., Alonso-Blanco, C., Sanchez-Rodriguez, C., Jorda, L., and Molina, A. (2005). ERECTA receptor-like kinase and heterotrimeric G protein from Arabidopsis are required for resistance to the necrotrophic fungus *Plectosphaerella cucumerina*. *Plant J.* 43, 165–180. doi: 10.1111/j.1365-313X.2005.02440.x

Lomovatskaya, L. A., Romanenko, A. S., Filinova, N. V., and Dudareva, L. V. (2011). Determination of cAMP in plant cells by a modified enzyme immunoassay method. *Plant Cell Rep.* 30, 125–132. doi: 10.1007/s00299-010-0950-5

Lu, M., Zhang, Y., Tang, S., Pan, J., Yu, Y., Han, J., et al. (2016). AtCNGC2 is involved in jasmonic acid-induced calcium mobilization. *J. Exp. Bot.* 67, 809–819. doi: 10.1093/jxb/erv500

Ludidi, N., and Gehring, C. (2003). Identification of a novel protein with guanylyl cyclase activity in *Arabidopsis thaliana*. *J. Biol. Chem.* 278, 6490–6494. doi: 10.1074/Jbc.M210983200

Ludidi, N. N., Heazlewood, J. L., Seoighe, C., Irving, H. R., and Gehring, C. A. (2002). Expansin-like molecules: novel functions derived from common domains. *J. Mol. Evol.* 54, 587–594. doi: 10.1007/s00239-001-0055-4

Lundeen, C. V., Wood, H. N., and Braun, A. C. (1973). Intracellular levels of cyclic nucleotides during cell enlargement and cell division in excised tobacco pith tissues. *Differentiation* 1, 255–260. doi: 10.1111/j.1432-0436.1973.tb00120.x

Ma, W., Smigel, A., Verma, R., and Berkowitz, G. A. (2009). Cyclic nucleotide gated channels and related signaling components in plant innate immunity. *Plant Signal. Behav.* 4, 277–282. doi: 10.4161/psb.4.4.8103

Maathuis, F. J. (2006). cGMP modulates gene transcription and cation transport in Arabidopsis roots. *Plant J.* 45, 700–711. doi: 10.1111/j.1365-313X.2005.02616.x

Maathuis, F. J., and Sanders, D. (2001). Sodium uptake in Arabidopsis roots is regulated by cyclic nucleotides. *Plant Physiol.* 127, 1617–1625. doi: 10.1104/pp.010502

Marondedze, C., Groen, A. J., Thomas, L., Lilley, K. S., and Gehring, C. (2016a). A quantitative phosphoproteome analysis of cGMP-dependent cellular responses in *Arabidopsis thaliana*. *Mol. Plant* 9, 621–623. doi: 10.1016/j.molp.2015.11.007

Marondedze, C., Thomas, L., Serrano, N. L., Lilley, K. S., and Gehring, C. (2016b). The RNA-binding protein repertoire of *Arabidopsis thaliana*. *Sci. Rep.* 6:29766. doi: 10.1038/srep29766

Marondedze, C., Turek, I., Parrott, B., Thomas, L., Jankovic, B., Lilley, K. S., et al. (2013). Structural and functional characteristics of cGMP-dependent methionine oxidation in *Arabidopsis thaliana* proteins. *Cell Commun. Signal.* 11:1. doi: 10.1186/1478-811X-11-1

Marondedze, C., Wong, A., Thomas, L., Irving, H., and Gehring, C. (2017). Cyclic nucleotide monophosphates in plants and plant signaling. *Handb. Exp. Pharmacol.* 238, 87–103. doi: 10.1007/164_2015_35

Maryani, M. M., Morse, M. V., Bradley, G., Irving, H. R., Cahill, D. M., and Gehring, C. A. (2003). *In situ* localization associates biologically active plant natriuretic peptide immuno-analogues with conductive tissue and stomata. *J. Exp. Bot.* 54, 1553–1564. doi: 10.1093/jxb/erg174

Matera, A. G., and Wang, Z. (2014). A day in the life of the spliceosome. *Nat. Rev. Mol. Cell Biol.* 15, 108–121. doi: 10.1038/nrm3742

McCue, L. A., McDonough, K. A., and Lawrence, C. E. (2000). Functional classification of cNMP-binding proteins and nucleotide cyclases with implications for novel regulatory pathways in *Mycobacterium tuberculosis*. *Genome Res.* 10, 204–219. doi: 10.1101/gr.10.2.204

Meier, S., Madeo, L., Ederli, L., Donaldson, L., Pasqualini, S., and Gehring, C. (2009). Deciphering cGMP signatures and cGMP-dependent pathways in plant defence. *Plant Signal. Behav.* 4, 307–309. doi: 10.1111/j.1469-8137.2008.02711.x

Meier, S., Ruzvidzo, O., Morse, M., Donaldson, L., Kwezi, L., and Gehring, C. (2010). The arabidopsis wall associated kinase-like 10 gene encodes a functional guanylyl cyclase and is co-expressed with pathogen defense related genes. *PLOS ONE* 5:e8904. doi: 10.1371/journal.pone.0008904

Meier, S., Seoighe, C., Kwezi, L., Irving, H., and Gehring, C. (2007). Plant nucleotide cyclases: an increasingly complex and growing family. *Plant Signal. Behav.* 2, 536–539. doi: 10.1371/journal.pone.0000449

Morse, M., Pironcheva, G., and Gehring, C. (2004). AtPNP-A is a systemically mobile natriuretic peptide immunoanalogue with a role in *Arabidopsis thaliana* cell volume regulation. *FEBS Lett.* 556, 99–103. doi: 10.1016/S0014-5793(03)01384-X

Moutinho, A., Hussey, P. J., Trewavas, A. J., and Malho, R. (2001). cAMP acts as a second messenger in pollen tube growth and reorientation. *Proc. Natl. Acad. Sci. U.S.A.* 98, 10481–10486. doi: 10.1073/Pnas.171104598

Mulaudzi, T., Ludidi, N., Ruzvidzo, O., Morse, M., Hendricks, N., Iwuoha, E., et al. (2011). Identification of a novel *Arabidopsis thaliana* nitric oxide-binding molecule with guanylate cyclase activity *in vitro*. *FEBS Lett.* 585, 2693–2697. doi: 10.1016/j.febslet.2011.07.023

Muleya, V., Marondedze, C., Wheeler, J. I., Thomas, L., Mok, Y. F., Griffin, M. D., et al. (2016). Phosphorylation of the dimeric cytoplasmic domain of the phytosulfokine receptor. PSKR1, *Biochem. J.* 473, 3081–3098. doi: 10.1042/BCJ20160593

Muleya, V., Wheeler, J. I., Ruzvidzo, O., Freihat, L., Manallack, D. T., Gehring, C., et al. (2014). Calcium is the switch in the moonlighting dual function of the ligand-activated receptor kinase phytosulfokine receptor 1. *Cell Commun. Signal.* 12:60. doi: 10.1186/s12964-014-0060-z

Nan, W., Wang, X., Yang, L., Hu, Y., Wei, Y., Liang, X., et al. (2014). Cyclic GMP is involved in auxin signalling during Arabidopsis root growth and development. *J. Exp. Bot.* 65, 1571–1583. doi: 10.1093/jxb/eru019

Newton, R. P., Brenton, A. G., Ghosh, D., Walton, T. J., Langridge, J., Harris, F. M., et al. (1991). Qualitative and quantitative mass spectrometric analysis of cyclic nucleotides and related enzymes. *Anal. Chim. Acta* 247, 161–175. doi: 10.1016/S0003-2670(00)83811-8

Newton, R. P., Roef, L., Witters, E., and Van Onckelen, H. (1999). Tansley Review No. 106. Cyclic nucleotides in higher plants: the enduring paradox. *New Phytol.* 143, 427–455. doi: 10.1046/j.1469-8137.1999.00478.x

Newton, R. P., and Smith, C. J. (2004). Cyclic nucleotides. *Phytochemistry* 65, 2423–2437. doi: 10.1016/j.phytochem.2004.07.026

Oguni, I., Suzuki, K., and Uritani, I. (1976). Terpenoid induction in sweet potato roots by cyclic-3', 5'-adenosine monophosphate. *Agric. Biol. Chem.* 40, 1251–1252. doi: 10.1271/bbb1961.40.1251

Ordoñez, N. M., Marondedze, C., Thomas, L., Pasqualini, S., Shabala, L., Shabala, S., et al. (2014). Cyclic mononucleotides modulate potassium and calcium flux responses to H2O2 in Arabidopsis roots. *FEBS Lett.* 588, 1008–1015. doi: 10.1016/j.febslet.2014.01.062

Pabst, M., Grass, J., Fischl, R., Leonard, R., Jin, C., Hinterkorner, G., et al. (2010). Nucleotide and nucleotide sugar analysis by liquid chromatography-electrospray ionization-mass spectrometry on surface-conditioned porous graphitic carbon. *Anal. Chem.* 82, 9782–9788. doi: 10.1021/ac101975k

Pagnussat, G. C., Lanteri, M. L., and Lamattina, L. (2003). Nitric oxide and cyclic GMP are messengers in the indole acetic acid-induced adventitious rooting process. *Plant Physiol.* 132, 1241–1248. doi: 10.1104/pp.103.022228

Palmer, R. M., Ferrige, A. G., and Moncada, S. (1987). Nitric oxide release accounts for the biological activity of endothelium-derived relaxing factor. *Nature* 327, 524–526. doi: 10.1038/327524a0

Pasquale, S. M., and Goodenough, U. W. (1987). Cyclic AMP functions as a primary sexual signal in gametes of *Chlamydomonas reinhardtii*. *J. Cell Biol.* 105, 2279–2292. doi: 10.1083/jcb.105.5.2279

Pasqualini, S., Meier, S., Gehring, C., Madeo, L., Fornaciari, M., Romano, B., et al. (2009). Ozone and nitric oxide induce cGMP-dependent and -independent transcription of defence genes in tobacco. *New Phytol.* 181, 860–870. doi: 10.1111/j.1469-8137.2008.02711.x

Patharkar, O. R., and Walker, J. C. (2015). Floral organ abscission is regulated by a positive feedback loop. *Proc. Natl. Acad. Sci. U.S.A.* 112, 2906–2911. doi: 10.1073/pnas.1423595112

Penson, S. P., Schuurink, R. C., Fath, A., Gubler, F., Jacobsen, J. V., and Jones, R. L. (1996). cGMP is required for gibberellic acid-induced gene expression in barley aleurone. *Plant Cell* 8, 2325–2333. doi: 10.1105/tpc.8.12.2325

Pfeiffer, S., Janistyn, B., Jessner, G., Pichorner, H., and Ebermann, R. (1994). Gaseous nitric oxide stimulates guanosine-3',5'-cyclic monophosphate (cGMP) formation in spruce needles. *Phytochemistry* 36, 259–262. doi: 10.1016/S0031-9422(00)97057-2

Pharmawati, M., Billington, T., and Gehring, C. A. (1998). Stomatal guard cell responses to kinetin and natriuretic peptides are cGMP-dependent. *Cell Mol. Life Sci.* 54, 272–276. doi: 10.1007/s000180050149

Pharmawati, M., Maryani, M. M., Nikolakopoulos, T., Gehring, C. A., and Irving, H. R. (2001). Cyclic GMP modulates stomatal opening induced by natriuretic peptides and immunoreactive analogues. *Plant Physiol. Biochem.* 39, 385–394. doi: 10.1016/S0981-9428(01)01252-9

Pharmawati, M., Shabala, S. N., Newman, I. A., and Gehring, C. A. (1999). Natriuretic peptides and cGMP modulate K^+, Na^+, and H^+ fluxes in *Zea mays* roots. *Mol. Cell Biol. Res. Commun.* 2, 53–57. doi: 10.1006/mcbr.1999.0151

Prado, A. M., Colaco, R., Moreno, N., Silva, A. C., and Feijo, J. A. (2008). Targeting of pollen tubes to ovules is dependent on nitric oxide (NO) signaling. *Mol. Plant* 1, 703–714. doi: 10.1093/mp/ssn034

Prado, A. M., Porterfield, D. M., and Feijo, J. A. (2004). Nitric oxide is involved in growth regulation and re-orientation of pollen tubes. *Development* 131, 2707–2714. doi: 10.1242/dev.01153

Qi, Z., Verma, R., Gehring, C., Yamaguchi, Y., Zhao, Y., Ryan, C. A., et al. (2010). Ca^{2+} signaling by plant *Arabidopsis thaliana* Pep peptides depends on AtPepR1, a receptor with guanylyl cyclase activity, and cGMP-activated Ca^{2+} channels. *Proc. Natl. Acad. Sci. U.S.A.* 107, 21193–21198. doi: 10.1073/pnas.1000191107

Replogle, A., Wang, J., Paolillo, V., Smeda, J., Kinoshita, A., Durbak, A., et al. (2013). Synergistic interaction of CLAVATA1, CLAVATA2, and RECEPTOR-LIKE PROTEIN KINASE 2 in cyst nematode parasitism of Arabidopsis. *Mol. Plant Microbe Interact.* 26, 87–96. doi: 10.1094/mpmi-05-12-0118-fi

Roelofs, J., Meima, M., Schaap, P., and Van Haastert, P. J. M. (2001). The Dictyostelium homologue of mammalian soluble adenylyl cyclase encodes a guanylyl cyclase. *EMBO J.* 20, 4341–4348. doi: 10.1093/Emboj/20.16.4341

Salmi, M. L., Morris, K. E., Roux, S. J., and Porterfield, D. M. (2007). Nitric oxide and cGMP signaling in calcium-dependent development of cell polarity in *Ceratopteris richardii*. *Plant Physiol.* 144, 94–104. doi: 10.1104/pp.107.096131

Sanchez-Rodriguez, C., Estevez, J. M., Llorente, F., Hernandez-Blanco, C., Jorda, L., Pagan, I., et al. (2009). The ERECTA receptor-like kinase regulates cell wall-mediated resistance to pathogens in *Arabidopsis thaliana*. *Mol. Plant Microbe Interact.* 22, 953–963. doi: 10.1094/mpmi-22-8-0953

Sauter, M. (2015). Phytosulfokine peptide signalling. *J. Exp. Bot.* 66, 5161–5169. doi: 10.1093/jxb/erv071

Schaap, P. (2005). Guanylyl cyclases across the tree of life. *Front. Biosci.* 10, 1485–1498. doi: 10.2741/1633

Shah, S., and Peterkofsky, A. (1991). Characterization and generation of *Escherichia coli* adenylate cyclase deletion mutants. *J. Bacteriol.* 173, 3238–3242. doi: 10.1128/jb.173.10.3238-3242.1991

Shen, H., Zhong, X., Zhao, F., Wang, Y., Yan, B., Li, Q., et al. (2015). Overexpression of receptor-like kinase ERECTA improves thermotolerance in rice and tomato. *Nat. Biotechnol.* 33, 996–1003. doi: 10.1038/nbt.3321

Singh, S., Lowe, D. G., Thorpe, D. S., Rodriguez, H., Kuang, W. J., Dangott, L. J., et al. (1988). Membrane guanylate cyclase is a cell-surface receptor with homology to protein kinases. *Nature* 334, 708–712. doi: 10.1038/334708a0

Staff, L., Hurd, P., Reale, L., Seoighe, C., Rockwood, A., and Gehring, C. (2012). The hidden geometries of the *Arabidopsis thaliana* epidermis. *PLOS ONE* 7:e43546. doi: 10.1371/journal.pone.0043546

Staiger, D., and Brown, J. W. (2013). Alternative splicing at the intersection of biological timing, development, and stress responses. *Plant Cell* 25, 3640–3656. doi: 10.1105/tpc.113.113803

Stone, J. R., and Marletta, M. A. (1994). Soluble guanylate cyclase from bovine lung: activation with nitric oxide and carbon monoxide and spectral characterization of the ferrous and ferric states. *Biochemistry* 33, 5636–5640. doi: 10.1021/bi00184a036

Stone, J. R., Sands, R. H., Dunham, W. R., and Marletta, M. A. (1995). Electron paramagnetic resonance spectral evidence for the formation of a pentacoordinate nitrosyl-heme complex on soluble guanylate cyclase. *Biochem. Biophys. Res. Commun.* 207, 572–577. doi: 10.1006/bbrc.1995.1226

Suwastika, I. N., and Gehring, C. A. (1999). The plasma membrane H^+-ATPase from Tradescantia stem and leaf tissue is modulated *in vitro* by cGMP. *Arch. Biochem. Biophys.* 367, 137–139. doi: 10.1006/abbi.1999.1228

Swiezawska, B., Jaworski, K., Szewczuk, P., Pawelek, A., and Szmidt-Jaworska, A. (2015). Identification of a *Hippeastrum hybridum* guanylyl cyclase responsive to wounding and pathogen infection. *J. Plant Physiol.* 189, 77–86. doi: 10.1016/j.jplph.2015.09.014

Szmidt-Jaworska, A., Jaworski, K., and Kopcewicz, J. (2008). Involvement of cyclic GMP in phytochrome-controlled flowering of *Pharbitis nil*. *J. Plant Physiol.* 165, 858–867. doi: 10.1016/j.jplph.2007.02.010

Teng, Y., Xu, W., and Ma, M. (2010). cGMP is required for seed germination in *Arabidopsis thaliana*. *J. Plant Physiol.* 167, 885–889. doi: 10.1016/j.jplph.2010.01.015

Terakado, J., Okamura, M., Fujihara, S., Ohmori, M., and Yoneyama, T. (1997). Cyclic AMP in rhizobia and symbiotic nodules. *Ann. Bot.* 80, 499–503. doi: 10.1006/anbo.1997.0477

Tezuka, T., Akita, I., Yoshino, N., and Suzuki, Y. (2007). Regulation of self-incompatibility by acetylcholine and cAMP in *Lilium longiflorum*. *J. Plant Physiol.* 164, 878–885. doi: 10.1016/j.jplph.2006.05.013

Thomas, L., Marondedze, C., Ederli, L., Pasqualini, S., and Gehring, C. (2013). Proteomic signatures implicate cAMP in light and temperature responses in *Arabidopsis thaliana*. *J Proteomics* 83, 47–59. doi: 10.1016/J.Jprot.2013.02.032

Torii, K. U., Mitsukawa, N., Oosumi, T., Matsuura, Y., Yokoyama, R., Whittier, R. F., et al. (1996). The Arabidopsis ERECTA gene encodes a putative receptor protein kinase with extracellular leucine-rich repeats. *Plant Cell* 8, 735–746. doi: 10.1105/tpc.8.4.735

Tucker, C. L., Hurley, J. H., Miller, T. R., and Hurley, J. B. (1998). Two amino acid substitutions convert a guanylyl cyclase, RetGC-1, into an adenylyl cyclase. *Proc. Natl. Acad. Sci. U.S.A.* 95, 5993–5997. doi: 10.1073/Pnas.95.11.5993

Tunc-Ozdemir, M., Tang, C., Ishka, M. R., Brown, E., Groves, N. R., Myers, C. T., et al. (2013). A cyclic nucleotide-gated channel (CNGC16) in pollen is critical for stress tolerance in pollen reproductive development. *Plant Physiol.* 161, 1010–1020. doi: 10.1104/pp.112.206888

Turek, I., and Gehring, C. (2016). The plant natriuretic peptide receptor is a guanylyl cyclase and enables cGMP-dependent signaling. *Plant Mol. Biol.* 91, 275–286. doi: 10.1007/s11103-016-0465-8

Turek, I., Marondedze, C., Wheeler, J. I., Gehring, C., and Irving, H. R. (2014). Plant natriuretic peptides induce proteins diagnostic for an adaptive response to stress. *Front. Plant Sci.* 5:661. doi: 10.3389/fpls.2014.00661

Uematsu, K., and Fukui, Y. (2008). Role and regulation of cAMP in seed germination of *Phacelia tanacetifolia*. *Plant Physiol. Biochem.* 46, 768–774. doi: 10.1016/j.plaphy.2007.10.015

Uematsu, K., Nakajima, M., Yamaguchi, I., Yoneyama, K., and Fukui, Y. (2007). Role of cAMP in gibberellin promotion of seed germination in Orobanche minor Smith. *J. Plant Growth Regul.* 26, 245–254. doi: 10.1007/s00344-007-9012-9

Van Damme, T., Blancquaert, D., Couturon, P., Van Der Straeten, D., Sandra, P., and Lynen, F. (2014). Wounding stress causes rapid increase in concentration of the naturally occurring 2',3'-isomers of cyclic guanosine- and cyclic adenosine monophosphate (cGMP and cAMP) in plant tissues. *Phytochemistry* 103, 59–66. doi: 10.1016/j.phytochem.2014.03.013

Volotovski, I. D., Sokolovsky, S. G., Molchan, O. V., and Knight, M. R. (1998). Second messengers mediate increases in cytosolic calcium in tobacco protoplasts. *Plant Physiol.* 117, 1023–1030. doi: 10.1104/pp.117.3.1023

Wang, X., Li, J., Liu, J., He, W., and Bi, Y. (2010). Nitric oxide increases mitochondrial respiration in a cGMP-dependent manner in the callus from *Arabidopsis thaliana*. *Nitric Oxide* 23, 242–250. doi: 10.1016/j.niox.2010.07.004

Wang, Y., Kang, Y., Ma, C., Miao, R., Wu, C., Long, Y., et al. (2017). CNGC2 is a Ca^{2+} influx channel that prevents accumulation of apoplastic Ca^{2+} in the leaf. *Plant Physiol.* 173, 1342–1354. doi: 10.1104/pp.16.01222

Weber, J. H., Vishnyakov, A., Hambach, K., Schultz, A., Schultz, J. E., and Linder, J. U. (2004). Adenylyl cyclases from Plasmodium, Paramecium and Tetrahymena are novel ion channel/enzyme fusion proteins. *Cell. Signal.* 16, 115–125. doi: 10.1016/S0898-6568(03)00129-3

Wedel, B., Humbert, P., Harteneck, C., Foerster, J., Malkewitz, J., Bohme, E., et al. (1994). Mutation of His-105 in the beta 1 subunit yields a nitric oxide-insensitive form of soluble guanylyl cyclase. *Proc. Natl. Acad. Sci. U.S.A.* 91, 2592–2596. doi: 10.1073/pnas.91.7.2592

Wei, Z., and Li, J. (2016). Brassinosteroids regulate root growth, development, and symbiosis. *Mol. Plant* 9, 86–100. doi: 10.1016/j.molp.2015.12.003

Wheeler, J. I., Freihat, L., and Irving, H. R. (2013). A cyclic nucleotide sensitive promoter reporter system suitable for bacteria and plant cells. *BMC Biotechnol.* 13:97. doi: 10.1186/1472-6750-13-97

Wheeler, J. I., Wong, A., Marondedze, C., Groen, A. J., Kwezi, L., Freihat, L., et al. (2017). The brassinosteroid receptor BRI1 can generate cGMP enabling cGMP-dependent downstream signaling. *Plant J.* 91, 590–600. doi: 10.1111/tpj.13589

Witters, E., Valcke, R., and Van Onckelen, H. (2005). Cytoenzymological analysis of adenylyl cyclase activity and 3',5'-cAMP immunolocalization in chloroplasts of *Nicotiana tabacum*. *New Phytol.* 168, 99–108. doi: 10.1111/j.1469-8137.2005.01476.x

Wong, A., and Gehring, C. (2013a). The *Arabidopsis thaliana* proteome harbors undiscovered multi-domain molecules with functional guanylyl cyclase catalytic centers. *Cell Commun. Signal.* 11:48. doi: 10.1186/1478-811X-11-48

Wong, A., and Gehring, C. (2013b). Computational identification of candidate nucleotide cyclases in higher plants. *Methods Mol. Biol.* 1016, 195–205. doi: 10.1007/978-1-62703-441-8_13

Wong, A., Gehring, C., and Irving, H. R. (2015). Conserved functional motifs and homology modeling to predict hidden moonlighting functional sites. *Front. Bioeng. Biotechnol.* 3:82. doi: 10.3389/fbioe.2015.00082

Wu, J., Qu, H., Jin, C., Shang, Z., Wu, J., Xu, G., et al. (2011). cAMP activates hyperpolarization-activated Ca^{2+} channels in the pollen of *Pyrus pyrifolia*. *Plant Cell Rep.* 30, 1193–1200. doi: 10.1007/s00299-011-1027-9

Wu, Y., Hiratsuka, K., Neuhaus, G., and Chua, N. H. (1996). Calcium and cGMP target distinct phytochrome-responsive elements. *Plant J.* 10, 1149–1154. doi: 10.1046/j.1365-313X.1996.10061149.x

Yoshioka, K., Moeder, W., Kang, H. G., Kachroo, P., Masmoudi, K., Berkowitz, G., et al. (2006). The chimeric Arabidopsis CYCLIC NUCLEOTIDE-GATED ION CHANNEL11/12 activates multiple pathogen resistance responses. *Plant Cell* 18, 747–763. doi: 10.1105/tpc.105.038786

Zelman, A. K., Dawe, A., Gehring, C., and Berkowitz, G. A. (2012). Evolutionary and structural perspectives of plant cyclic nucleotide-gated cation channels. *Front. Plant Sci.* 3:95. doi: 10.3389/fpls.2012.00095

Zhao, J., Guo, Y., Fujita, K., and Sakai, K. (2004). Involvement of cAMP signaling in elicitor-induced phytoalexin accumulation in *Cupressus lusitanica* cell cultures. *New Phytol.* 161, 723–733. doi: 10.1111/j.1469-8137.2004.00976.x

Zhao, Y., Schelvis, J. P., Babcock, G. T., and Marletta, M. A. (1998). Identification of histidine 105 in the beta1 subunit of soluble guanylate cyclase as the heme proximal ligand. *Biochemistry* 37, 4502–4509. doi: 10.1021/bi972686m

Conflict of Interest Statement: The authors declare that the research was conducted in the absence of any commercial or financial relationships that could be construed as a potential conflict of interest.

frontiers in Plant Science

ORIGINAL RESEARCH
published: 04 October 2017
doi: 10.3389/fpls.2017.01732

ALA6, a P_4-type ATPase, Is Involved in Heat Stress Responses in *Arabidopsis thaliana*

Yue Niu, Dong Qian, Baiyun Liu, Jianchao Ma, Dongshi Wan, Xinyu Wang, Wenliang He and Yun Xiang**

MOE Key Laboratory of Cell Activities and Stress Adaptations, School of Life Sciences, Lanzhou University, Lanzhou, China

Maintaining lipid membrane integrity is an essential aspect of plant tolerance to high temperature. P_4-type ATPases are responsible for flipping and stabilizing asymmetric phospholipids in membrane systems, though their functions in stress tolerance are not entirely clear. Aminophospholipid ATPase6 (ALA6) is a member of the P_4-type ATPase family, which has 12 members in *Arabidopsis thaliana*. Here, we show that a loss-of-function mutant of ALA6 (*ala6*) exhibits clear sensitivity to heat stress, including both basal and acquired thermotolerance treatments. Overexpression of *ALA6* improves seedling resistance to heat stress, while mutated *ALA6* transgenic plants, in which the conserved functional site of the ALA family has a point mutation, are still susceptible to heat stress like *ala6* loss-of-function mutant. In addition, *ala6* displays higher ion-leakage during heat treatment, suggesting that the lipid flippase activity of ALA6 plays a vital role in heat stress responses. Transcriptome analysis reveals differences in gene expression between *ala6* and wild-type plants with or without heat stress. The differentially expressed genes are involved primarily in the physiological processes of stress response, cellular compartment maintenance, macromolecule stability and energy production. Our results suggest that ALA6 is crucial for the stability of membrane when plants suffer from high temperature stress.

Keywords: *Arabidopsis* P_4-type ATPase, Aminophospholipid ATPase6 (ALA6), *ALA6* T-DNA insertion mutant (*ala6*), lipid flippase, membrane, heat stress response

OPEN ACCESS

Edited by:
Yi Ma,
University of Connecticut,
United States

Reviewed by:
Shengcheng Han,
Beijing Normal University, China
Joshua Blakeslee,
The Ohio State University,
United States

****Correspondence:***
Yue Niu
niuy@lzu.edu.cn
Yun Xiang
xiangy@lzu.edu.cn

Specialty section:
This article was submitted to Plant Traffic and Transport, a section of the journal Frontiers in Plant Science

Received: *03 May 2017*
Accepted: *21 September 2017*
Published: *04 October 2017*

Citation:
Niu Y, Qian D, Liu B, Ma J, Wan D, Wang X, He W and Xiang Y (2017) ALA6, a P_4-type ATPase, Is Involved in Heat Stress Responses in Arabidopsis thaliana. Front. Plant Sci. 8:1732. doi: 10.3389/fpls.2017.01732

INTRODUCTION

The phospholipid bilayer of cell membranes is asymmetrical, as the abundance of various lipid species on one side differs from that on the other. Within the membrane leaflets, the positions of the phospholipids are not fixed. Phospholipids perform multiple intramolecular motions, including rotation and lateral diffusion, and can also flip-flop between the two leaflets (Pomorski and Menon, 2016). The ambient temperature has a direct effect on the rate and frequency of these movements, eventually altering membrane fluidity. Thus, maintenance of the thermodynamic balance of the

Abbreviations: AGP, Arabinogalactan protein; AOC, Allene oxide cyclase; BBX, B-box domain protein; Chl, Chlorophyll; DEG, Differentially expressed gene; EL, Electrolyte leakage; ERF, Ethylene response factor; FPKM, Fragments per kilobase of transcript per million fragments mapped; GUS, β-Glucuronidase; HSP, Heat shock protein; JA, Jasmonic acid; MGDG, Monogalactosyldiacylglycerol; PC, Phosphatidylcholine; PCR, Polymerase chain reaction; PE, Phosphatidylethanolamine; PS, Phosphatidylserine; PSII, Photosystem II; SLAH, Slow anion channel-associated homolog; UBQ, Ubiquitin; WRKY, Transcription factor with conserved amino acid sequence WRKYGQK.

membrane is vital for cell function, especially during abrupt temperature changes (Murata and Los, 1997; Vigh et al., 1998, 2007; Horváth et al., 2012).

Studies have revealed that lipid asymmetry via flip-flopping across membrane leaflets is involved in numerous functions of the membrane system, including formation and maintenance of cell shape; vesicle budding; membrane trafficking, impermeability, and rigidity; extra- and intracellular signaling; fertilization; apoptosis; and membrane-coupling protein regulation (Puts and Holthuis, 2009; Andersen et al., 2016). Generally, the chemical traits of phospholipids dictate that transbilayer exchange of polar lipids should occur slowly and rarely. In fact, lipid translocation across the two leaflets is greatly assisted by flippases/floppases and/or scramblases. The membrane proteins that carry out these lipid translocation processes are classified into two categories based on whether the lipid transportation across the bilayer is driven by ATP (Pomorski and Menon, 2006, 2016). P-type ATPases are found in all kingdoms of life and possess a conserved aspartic acid residue within the P-type motif DKTGT that mediates reversible phosphorylation and conformational changes during substrate transport (Pedersen and Carafoli, 1987). Based on substrate specificity and sequence characteristics, P-type ATPases are divided into five subclasses, P_1- through P_5-type ATPases (Palmgren and Axelsen, 1998). P_4-ATPases are flippases, which utilize the energy from ATP hydrolysis to transport specific phospholipids from the exoplasmic to the cytoplasmic face of the membrane against their concentration gradient (Coleman et al., 2009, 2013; Zhou and Graham, 2009; Lopez-Marques et al., 2014). These proteins are unique in that they flip "giant" phospholipids across membranes and are found only in eukaryotic cells (Paulusma and Elferink, 2010; Van Der Mark et al., 2013; Andersen et al., 2016). The first five P_4-ATPases (Neo1p, Drs2p, Dnf1p, Dnf2p, and Dnf3p) were found in yeast, and at least 14 such proteins (ATP8A1 to ATP11C) occur in mammals (Paulusma and Elferink, 2010; Sebastian et al., 2012; Van Der Mark et al., 2013; Andersen et al., 2016). Most P_4-ATPases have unique lipid specificities and subcellular localization. For example, Drs2p/ATP8A1 carries out PS and PE translocation in the late secretory pathway, while ATP8B2 and ATP10A were found to mediate PC asymmetry specifically (Ding et al., 2000; Alder-Baerens et al., 2006; Paterson et al., 2006; Xu et al., 2009; Zhou and Graham, 2009). Flippases with a relatively wide range of phospholipid specificities also exist, such as Dnf1p and Dnf2p, which can transport PC, lysophospholipids and synthetic alkylphospholipids in plasma membranes (Pomorski et al., 2003; Riekhof and Voelker, 2006; Baldridge et al., 2013).

Unlike those in yeast and mammals, the P_4-ATPase in the plant *Arabidopsis thaliana* was identified much later and its function remains unclear. There are12 P_4-ATPase proteins, ALA1 through ALA12 (Aminophospholipid ATPase subfamily) in *Arabidopsis* (Axelsen and Palmgren, 1998). Recent reports indicate that ALA2 internalizes PS in the endosomal system, whereas ALA3, localized in the Golgi apparatus, carries out flipping of a broad range of lipids, including PS, PE and PC (Poulsen et al., 2008; López-Marqués et al., 2010). ALA10 is located in the plasma membrane and internalizes various phospholipids, including lysoPC (Poulsen et al., 2015). With respect to biological function, ALA1 may play an important role in chilling tolerance (Gomès et al., 2000), while ALA2 may function with ALA1 in antiviral defense (Guo et al., 2017). ALA3 is involved in secretory processes of the Golgi apparatus at the root tip to regulate root growth (Poulsen et al., 2008). ALA6 and ALA7 are crucial for pollen fitness (McDowell et al., 2015). In addition, ALA10 has been found to function in leaf and root development, as well as in stomatal control (Poulsen et al., 2015; Botella et al., 2016). Some reports have also indicated that the physiological functions of several plant P_4-ATPases can be affected by changes in temperature (Gomès et al., 2000; McDowell et al., 2013, 2015; Botella et al., 2016). Nevertheless, the ways in which these flippases respond to some types of temperature stresses remain unclear.

In the present study, our results suggest that seedlings of a loss-of-function mutant of *ALA6* (*ala6*) grow normally at standard temperatures, while they wither, turn yellow and eventually die under basal and acquired thermotolerance treatments. Overexpression of *ALA6* can improve plant tolerance of high temperature, and *ALA6* point-mutated transgenic plants lacking a conserved aspartic acid residue are still sensitive to heat stress. In addition, the results of a transcriptome analysis and observation of increased ion-leakage and *Chl b*/*a* ratios in *ala6* plants during heat treatment further suggest that ALA6 may protect plant cells from heat stress via the maintenance of membrane stability and integrity.

MATERIALS AND METHODS

T-DNA Insertion Mutants

The *Arabidopsis thaliana* plants used here were in the Col-0 background. The T-DNA insertion mutant used in this experiment was *ala6* (SALK_150173), obtained from the Arabidopsis Biological Resource Center (Ohio State University[1]) with homozygous progeny determined via PCR screening (Alonso et al., 2003). The T-DNA insertion site is shown in **Figure 2A**, and all PCR primer sequences are given in Supplementary Table S1.

Plant Growth Conditions

Seeds were surface-sterilized in 20% bleach for 12–15 min, rinsed five times with sterile water, and sown on ½ MS medium containing ½ Murashige and Skoog salts (MS; PhytoTech, Lenexa, KS, United States), 1% (w/v) sucrose, and 0.8% (w/v) agar. Plates were incubated at 4°C for 3 days in the dark and then transferred to a growth chamber at 21 ± 2°C with long days (16-h light/8-h dark cycles). The growth chamber was illuminated with white light at ∼110 μmol m^{-2} s^{-1}.

Gene Cloning and Transgenic Line Creation

Full-length cDNAs of *ALA6* and *ALA6* with a point mutation in the N-terminal aspartic acid at position 426 were amplified

[1]http://abrc.osu.edu/

via PCR. These cDNA fragments were cloned into the pBIB binary vectors driven by the *ALA6* gene promoter. Four-week-old wild-type (WT) Col-0 and *ala6* mutant plants were transformed with *A. tumefaciens* (strain GV3101) using the floral dip method as described by Clough and Bent (1998). Homozygous transgenic plants were isolated on Basta. Four transgenic *Arabidopsis* lines were generated: complementary and overexpressing lines containing ALA6-autologous-promoter-ALA6, a tissue localization line containing the GUS gene driven by the ALA6-autologous-promoter, and a line expressing a point mutation in ALA6 driven by *ALA6* gene promoter. The point mutation was an A-to-C conversion at base 1277 relative to the start codon of the full-length *ALA6* cDNA (Supplementary Figure S1). All PCR primer sequences and vectors are shown in Supplementary Table S1.

Basal and Acquired Thermotolerance Treatments

Thermotolerance assays were performed on 14-day-old seedlings as previously described (Larkindale and Vierling, 2008; Mittler et al., 2012). The basal heat treatment consisted of incubation at 43.5°C for 45, 60, or 90 min. The acquired thermotolerance treatment consisted of incubation at 37°C for 1.5 h followed by recovery at 22°C for 2 h and then by heat shock at 43.5°C for 1, 1.5, or 2 h. Plants were then moved to a growth chamber for 30, 36, or 72 h prior to sample preparation, measurement or photography. All assays were repeated at least in triplicate.

Determination of Electrolyte Leakage

Fourteen-day-old seedlings were subjected to thermotolerance treatments and allowed to recover for 36 h. EL was determined as described by Sairam and Srivastava (2002). The sample (0.5 g) was placed in a 15-ml tube with 10 ml deionized water and incubated at 25°C for 2 h, and the conductivity in the solution was measured using a conductometer (R_1). Samples were then heated for 15 min in a boiling water bath, and conductivity was measured again after the samples cooled to 25°C (R_2). EL was calculated as the ratio of the initial conductivity to the conductivity after heating in boiling water ($EL\,(\%) = \left(R_1/R_2\right) \times 100\%$). All assays were repeated at least in triplicate.

Measurement of Chlorophyll Contents

Samples were collected from 50 to 100 mg leaves for chlorophyll extraction. Chlorophyll contents were measured using 95% ethanol as described previously (Woo et al., 2001). Leaf samples of 50–100 mg were placed in a test tube and pulverized in liquid nitrogen. The freeze-dried powder was incubated with 1 ml 95% ethanol in the dark at room temperature for 2–3 h. After dilution with solvent to 1.5 ml, the mixture was centrifuged at 13400 × *g* for 5 min. One milliliter of the supernatant was diluted 2- to 10-fold with 95% ethanol (OD value = 0.1–0.6), and the chlorophyll level was determined by a spectrophotometer at 665 and 649 nm. All steps above were performed at room temperature (25°C). The assay was repeated at least in triplicate. Chlorophyll contents were calculated using the following formulae: $Chl\,a = 13.7 \times OD_{665} - 5.76 \times OD_{649}$, $Chl\,b = 25.8 \times OD_{665} - 7.6 \times OD_{649}$, and $Chl\,a + b = 6.10 \times OD_{665} + 20.04 \times OD_{649}$. *Chl a* is the chlorophyll *a* content, *Chl b* is the chlorophyll *b* content, *Chl a+b* is the total chlorophyll content, and OD is the absorbance.

Semi-Quantitative RT-PCR

Fourteen-day-old WT and *ala6* seedlings grown on MS agar plates were collected, placed in tubes, and stored in liquid nitrogen. Total RNA was isolated using the MiniBEST Plant RNA Extraction Kit (Takara Biotechnology Co., Ltd., China). First-strand cDNA synthesis reaction was performed as Takara manual using Reverse Transcriptase M-MLV (RNase H-) (Takara Biotechnology Co., Ltd., China). PCR was carried out via a TP350 thermal cycler (Takara Bio Inc., Otsu, Japan) with the following program: 3 min at 94°C (1 cycle); 30 s at 94°C, 30 s at 53∼60°C and 30 s∼1.5 min at 72°C (28/32 cycles); and 5 min at 72°C (1 cycle). Each PCR reaction was replicated for three times. ACTIN2 was selected as a reference gene (see Supplementary Table S1 for primer sequences).

Quantitative PCR

Fourteen-day-old WT, *ala6* and COM seedlings grown on MS agar plates were treated at 43.5°C for 45 min and recovered for 30 h, then collected in liquid nitrogen. Total RNA was reverse-transcribed into cDNA by the methods above. qPCR was carried out using a Stratagene MX3005P Real-Time System (Agilent, United States) with SYBR Premix Ex Taq (Takara Biotechnology Co., Ltd., China) as manufacturer's instructions. Program for the reaction was as follows: 95°C for 30 s, 40 cycles of 95°C for 5 s, 60°C for 30 s. Melt curves (0.5°C increments in a 60–95°C range) were performed for each gene to assess the sample for non-specific targets and primer dimers. *UBQ11* was used as an internal control to normalize the expression of the target gene. A list of the primers used in these experiments is found in Supplementary Table S1. The $\Delta\Delta$Ct method was used to analyze relative transcript abundance (Rieu and Powers, 2009). The results were based on three independent experiments.

GUS Staining

To identify the tissue-specific localization of ALA6, independent plants from each GUS-transgenic line were selected and various tissues were stained (Jefferson et al., 1987). Samples were incubated in a solution of 2 mM 5-bromo-4-chloro-3-indolyl-β-D-glucuronide (X-gluc), 3mM $K_3(Fe(CN)_6)$, 3M $K_4(Fe(CN)_6)$, 0.2% Triton-X-100, and 50 mM KH_2PO_4/K_2HPO_4(pH 7.2) at 37°C in the dark for overnight. Samples were then rinsed in 95% ethanol to remove chlorophyll. The samples were observed and photographed via anatomic microscope (SMZ-168, Motic Inc.).

Transcriptome Analysis

Fourteen-day-old WT and *ala6* seedlings grown on MS agar plates were incubated at 43.5°C for 45 min and allowed to recover for 30 h. Gene expression analysis was performed by the Novogene Corporation, Beijing, China. RNA libraries were sequenced on a HiSeq 2500 instrument. TopHat version 2.0.12[2]

[2]http://tophat.cbcb.umd.edu/

was used for mapping against the *Arabidopsis* genome[3]. HTSeq v0.6.1 was used to determine the read numbers for each gene. Based on the length of each gene and the corresponding number of reads, the FPKM value of each gene was calculated. Three independent experiments were conducted, and only genes having consistent expression changes in the three microarray assays were reported. DEG analysis was performed using the DESeq R package (1.18.0) with an adjusted *P*-value (<0.05). In addition, Gene Ontology (GO) enrichment analysis of DEGs was carried out using the GOseq R package, in which results were corrected for gene length bias. GO terms with corrected *P*-values less than 0.05 were considered to be significantly enriched DEGs.

Statistical Analysis

Each experiment was repeated at least three times. Data were analyzed using one-way ANOVA with Turkey's multiple-comparison test under a 0.05 confidence coefficient.

RESULTS

Tissue Expression Pattern of *ALA6*

To analyze the tissue specificity of *ALA6*, its promoter region was fused to a *GUS* reporter gene and stably expressed in *Arabidopsis* plants. After staining, GUS signals were found throughout the young seedling except in the root tip, with particularly strong expression at the junction between the root and hypocotyl (**Figure 1A(a)**). In the leaf, the signal penetrated the veins and was especially strong in the leaf margin (**Figure 1A(b)**). In the flower and silique, staining was strong in the stigma, anther and base and tip of the silique; the signal was also particularly intense in pollen (**Figure 1A(c,d)**). Gene expressed in different tissues via semi RT-PCR analysis also showed that *ALA6* was expressed in reproductive organs more than that in vegetative tissues (**Figure 1B**). The expression of *ALA6* in numerous tissues suggests that ALA6 may be involved in multiple physiological activities in the plant.

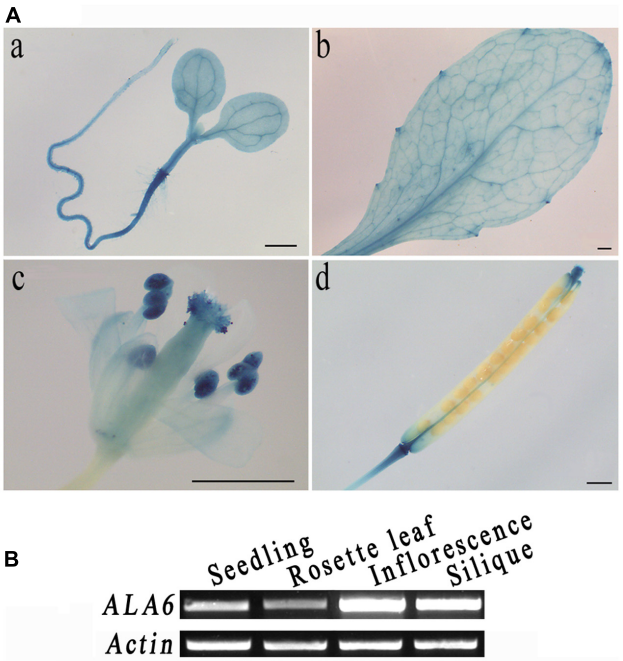

FIGURE 1 | Tissue-specific expression of *ALA6*. **(A) a**, 5-day-old seedling. **b**, rosette leaf. **c**, flower, stamen, and pistil. **d**, silique. **(B)** ALA6 expression in various tissues via RT-PCR assay.

Loss of Function of ALA6 Confers Hypersensitivity to Heat Stress in *Arabidopsis* Seedlings

To determine the function of ALA6, a T-DNA insertion mutant was obtained from the SALK collection (SALK_150173). The T-DNA was inserted into the first exon of *ALA6* (**Figure 2A**). The homozygous F2 progeny of *ala6* plants were screened (**Figure 2B**) and tested to determine *ALA6* expression levels, and it was found that the expression of *ALA6* in this T-DNA insertion line was completely suppressed (**Figure 2C**).

As ALA6 has been predicted to function in response to high temperature stress, two different experiments were performed to determine the heat-sensitive phenotype of *ala6* at a lethal temperature of 43.5°C (**Figure 3B**). As shown in **Figure 3A**, the first treatment consisted of incubation at high temperature for different lengths of time (45, 60, or 90 min) followed by recovery for 3 days. Compared to WT, *ala6* was extremely sensitive to heat stress. In the 45-min treatment, some *ala6* seedlings began to wilt, with leaves shrinking, curling, and yellowing. Seedlings also grew more slowly or died (**Figure 3A(b)**). After longer heat-treatments, the lethal effect of the *ala6* mutation was more obvious (**Figure 3A(c,d)**).

The second heat treatment consisted of exposure to a constant, non-lethal temperature (37°C) to allow acclimation, followed by incubation at an optimum temperature (22°C) prior to exposure to a lethal temperature (43.5°C) (**Figure 3B**). As shown in **Figure 3A(g,h)**, *ala6* remained sensitive to high temperature. Compared with the basal heat-treatment, both WT and *ala6* plants showed improved tolerance to high temperature after a brief period of acclimation. With preliminary heat acclimation, most WT seedlings survived, and approximately 50% of *ala6* seedlings turned yellow after 90 min at 43.5°C (**Figures 3A(g),C**). Without previous heat acclimation, only a few WT seedlings showed any viability, and all *ala6* seedlings were dead after 90 min at 43.5°C (**Figures 3A(d),C**). These results indicated that plants exposed to non-lethal temperatures in advance of abrupt exposure to high temperature showed improved responses to heat stress. In addition, it appeared that *ala6* was inherently heat-sensitive, showing susceptibility to heat treatment even after warm acclimation. ALA6 might play a crucial role in plant heat-tolerance.

Considering the conserved function of the ALA family in phospholipid transport, the membrane status of *ala6* plants under hyperthermia was investigated. WT and mutant seedlings

[3]www.arabidopsis.org

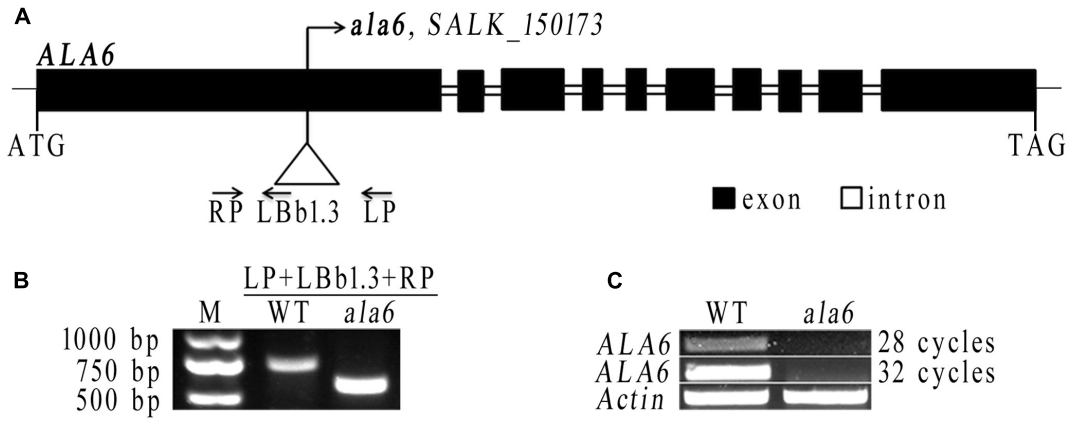

FIGURE 2 | The T-DNA insertion line of *ALA6*. **(A)** Diagram of the *ALA6* gene and the T-DNA insertion site. **(B)** Identification of homozygous *ala6* mutants, using the primers shown in **(A)**. **(C)** Semi-quantitative analysis demonstrates that *ALA6* is knocked-out in the *ala6* mutant. 28 cycles and 32 cycles are cycles in PCR amplification.

were grown on MS plates for 14 days and incubated at 43.5°C for 45 min, followed by a 36-h recovery under optimum conditions. After this treatment, the growth of all seedlings was affected. Seedlings were collected, and EL was quantified; the results were shown in **Figure 3D**. Heat treatment significantly increased the rate of EL in both WT and mutant plants. Leakage rates increase by 48.9 and 68.9% due to heat treatments in WT and *ala6* seedlings, respectively. Notably, the membrane status of *ala6* cells was altered more than that of WT cells, implying that ALA6 might protect plant cells from heat stress by regulating plasma membrane permeability and stability.

Changes in the contents of photosynthetic pigments (chlorophylls) and in *Chl b*/*a* ratios are useful indicators of stress and tolerance in plants (Zhang et al., 2008). We found that chlorophyll levels decreased during heat stress treatments in both WT and *ala6* mutant plants, indicating possible heat-induced damage to the photosynthetic activity of the chloroplasts (**Figure 3E**). In addition, the *chl b*/*a* ratio increased dramatically in *ala6* mutants after basal heat treatment, reaching a level 36.4% higher than in *ala6* mutants without treatment, whereas the ratio in WT increased only 28.2% (**Figure 3F**). These results indicated that a lack of ALA6 might increase the injurious impact of heat stress on membranous organelles.

The Intrinsic Function of ALA6 Is Critical for Thermotolerance

To confirm the function of *ala6* under high temperature, an exogenous *ALA6* gene (normal or deficient in conserved gene function) was expressed in *ala6* and WT plants. The complementation lines resulting from the former transformation were subjected to heat treatment, as shown in **Figure 4**, and it was found that the expression of *ALA6* could rescue the heat-lethal phenotype of the loss-of-function mutant. The growth of the complementation lines resembled that of WT plants, even after heat treatment. In addition, the *ALA6* overexpression lines exhibited greater vitality than WT plants (**Figures 4A,C**), showing that ALA6 was involved in intracellular responses to heat stress, and the heat-sensitive phenotype of *ala6* was due to the loss of function of ALA6.

P-type ATPases, including the ALA family in *Arabidopsis*, contain a motif that carries out phosphorylation during phospholipid transport; this motif contains an aspartic acid residue (Pedersen and Carafoli, 1987). To determine the relationship between the phospholipid transport activity of ALA6 and the heat stress response, transgenic lines containing a point mutation in the phosphorylation motif were generated. This mutation converted an A to a C in the codon encoding the conserved aspartic acid residue of ALA6. As expected, the transgenic lines showed a heat-hypersensitive phenotype like that of *ala6* under high-temperature treatment (**Figure 5A**). This result further demonstrated that the native phospholipid transport activity of ALA6 was implicated in heat-tolerance, and the specific phenotype of *ala6* was associated with a defect in its enzymatic activity. The levels of *ALA6* transcript in these transgenic lines were measured and were significantly higher than those of the WT (**Figures 4B**, **5B**). This observation was also supported by the survival rate shown in **Figures 4C**, **5C**.

Microarray Analysis Reveals ALA6-Related Genes

To investigate the underlying mechanism of heat sensitivity in *ala6*, we analyzed the RNA-seq data of WT and *ala6* *Arabidopsis* samples. A total of 426 DEGs were found to be related to ALA6 (**Figure 6A**). Of these, 286 genes showed down-regulated and 140 showed up-regulated expression in *ala6*. All the transcripts listed here exhibited twofold or larger changes in abundance. These DEGs were enriched in GO terms containing genes responsive to endogenous stimuli, chemical or organic substances, and biotic or abiotic stresses (shown in Supplementary Table S2). The top 30 DEGs that were annotated as stress response elements include various transcription factors,

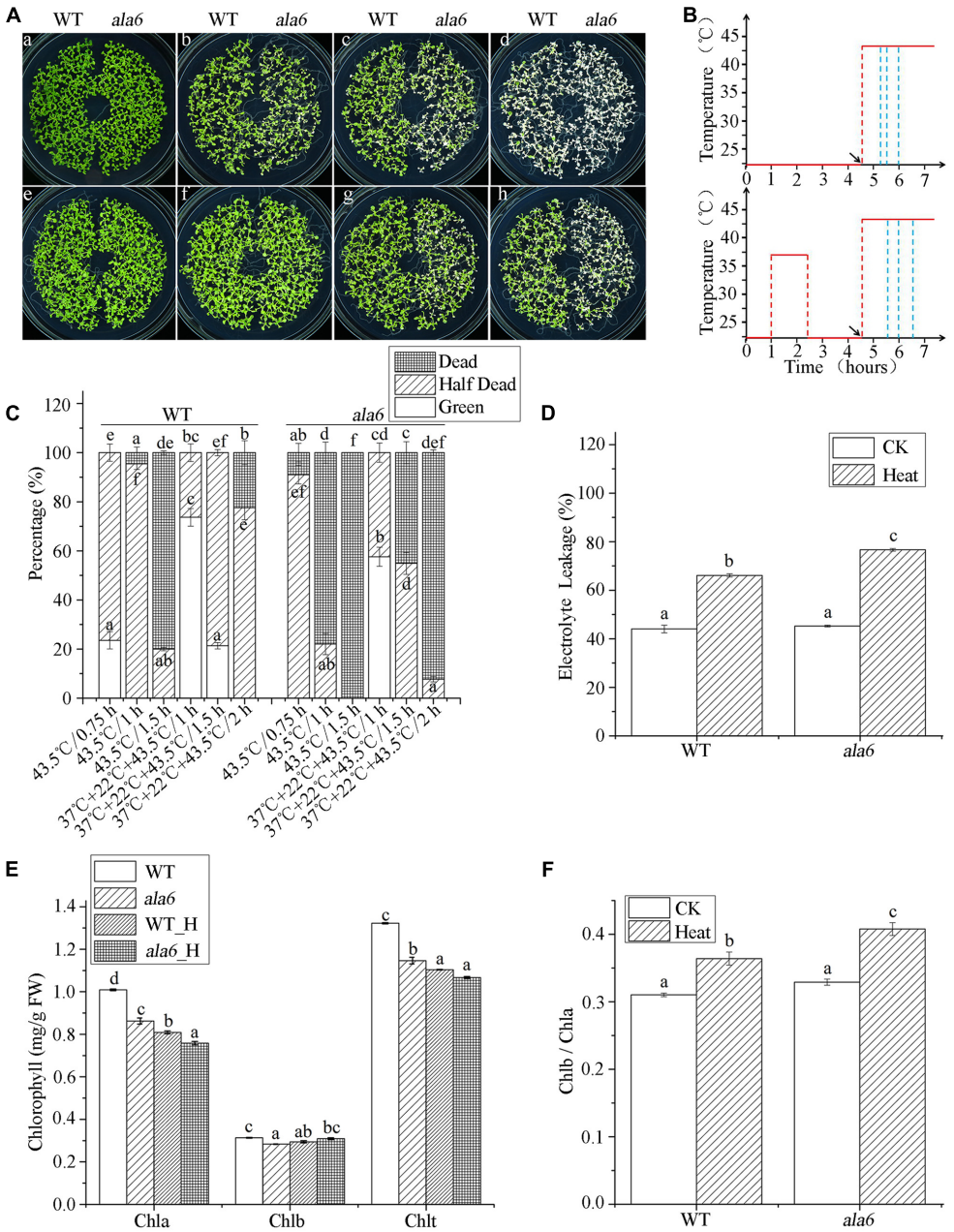

FIGURE 3 | *ala6* is hypersensitive to heat stress. **(A) a** and **e** are 14-day-old WT and *ala6* seedlings without thermal treatment; **b** was incubated at 43.5°C for 45 min; **c** and **f** were incubated at 43.5°C for 1 h received prior heat acclimation at 37°C for 1.5 h; **d** and **g** received the same treatments as c and f, respectively, but the heat shock time was 1.5 h; **h** received acclimation at 37°C prior to heat treatment for 2 h. **(B)** Schematic diagram for heat treatment corresponding to **(A)**; from top to bottom, linear graphs represent basal thermotolerance (no acclimation) and acquired thermotolerance (acclimation). Red lines indicate the temperatures and blue lines indicate different treatment times. Arrows illustrate the times of the heat shock at 43.5°C. **(C)** The percentage of seedlings, including dead, half-dead and alive. The six columns correspond to b, c, d, f, g, and h in **(A)** are calculated from three independent experiments (average results ±SE). Columns with different letters have significantly different values ($P < 0.05$). **(D)** Electrolyte leakage (%) of 14-day-old seedlings treated at 43.5°C for 45 min and allowed to recover for 36 h. **(E)** Chlorophyll contents (mg/g) of seedlings as in **(D)**. WT_H, wild type treated with heat stress; *ala6*_H, *ala6* treated with heat stress; Chla, chlorophyll a; Chlb, chlorophyll b; Chlt, total chlorophyll. **(F)** Chlb/Chla ratio of **(E)**. Results are calculated from three independent experiments (average results ±SE). Columns with different letters have significantly different values ($P < 0.05$).

membrane components and transporters (**Table 1**). These results indicated that ALA6 might be involved in multiple cellular responses.

To identify genes related to ALA6 under heat stress, the RNA-seq data of *Arabidopsis* WT and *ala6* samples with and without heat treatment were analyzed as described in the Section

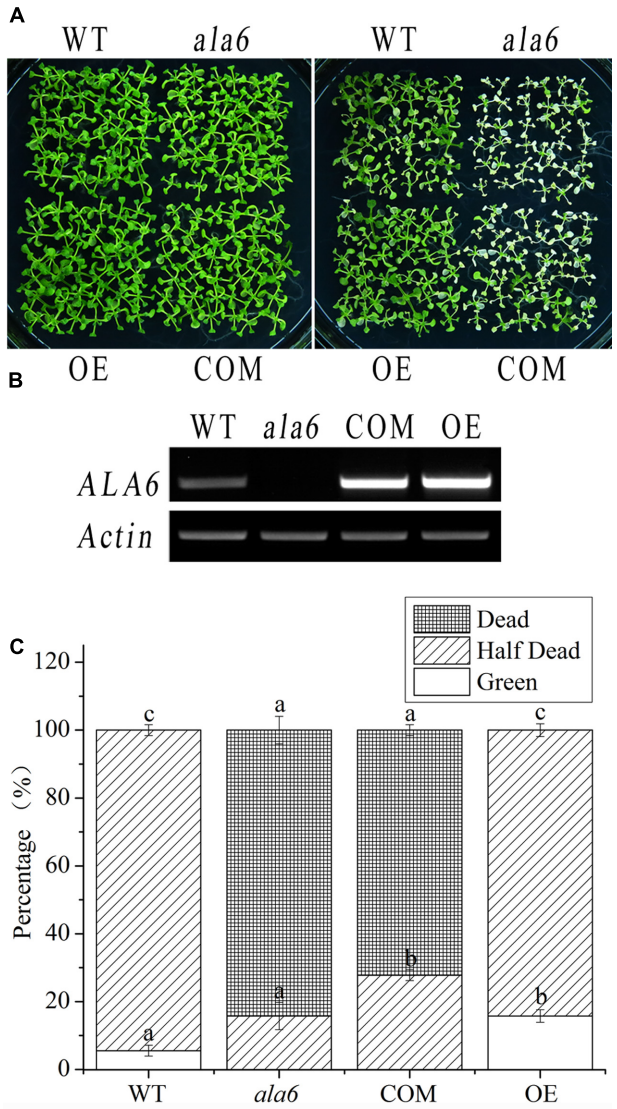

FIGURE 4 | Complementation and overexpression lines of *ALA6* under basal thermotolerance. **(A)** Phenotypes of complementation and overexpression lines under heat stress. WT, wild type; *ala6*, *ALA6* T-DNA insertion line; COM, complementation line of *ALA6*; OE, overexpression line of *ALA6*. **(B)** RT-PCR analysis of *ALA6* expression in complementary and overexpressed transgenic lines. **(C)** Survival rate of seedlings corresponding to **(A)**. Results are calculated from three independent experiments (average results ±SE). Columns with different letters have significantly different values ($P < 0.05$).

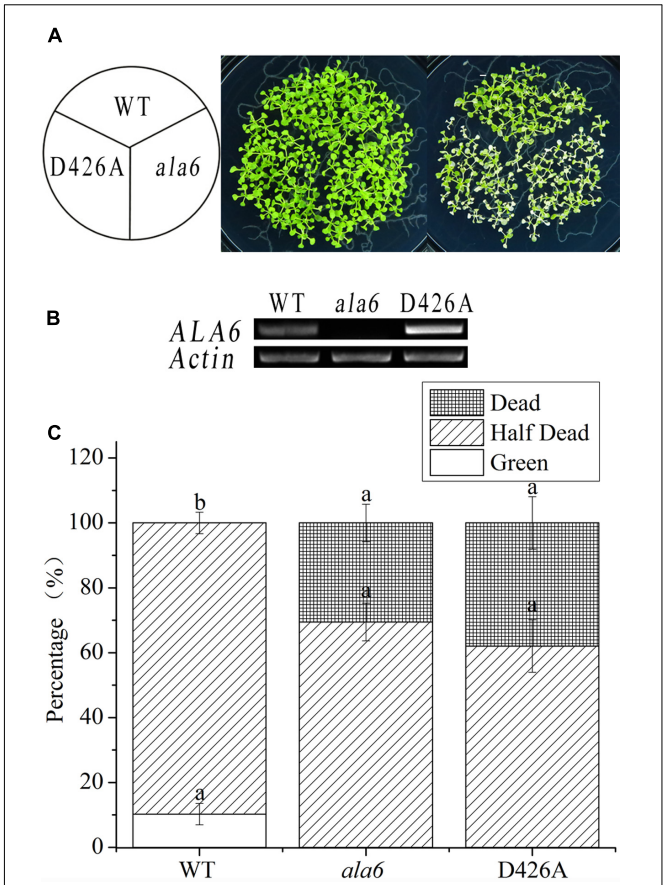

FIGURE 5 | Point-mutant lines of *ALA6* under basal thermotolerance. **(A)** Phenotype of point-mutant lines under heat stress. WT, wild type; *ala6*, *ALA6* T-DNA insertion line; D426A, conserved aspartic acid-point mutant line of ALA6. **(B)** RT-PCR analysis of the expression of *ALA6* in point-mutant transgenic lines. **(C)** Survival rate of seedlings corresponding to **(A)**. Results are calculated from three independent experiments (average results ±SE). Columns with different letters contain significantly different values ($P < 0.05$).

"Materials and Methods." Quantitative PCR analyzing the expression of several DEGs in WT, *ala6*, ALA6 complementary transgenic lines with or without heat stress also confirmed the results from RNA-seq data above (**Figure 7**). **Figure 6A** showed the DEGs for *ala6* vs. WT (a), WT with heat treatment vs. WT (b), *ala6* with heat treatment vs. *ala6* (c) and *ala6* with heat treatment vs. WT with heat treatment (d). It was believed that genes related to ALA6 under heat treatment should be found in b but not in c (**Figure 6A**). A total of 1058 DEGs were identified and implicated in heat stress responses related to ALA6. The top 30 DEGs in **Table 2** are involved in transcription factor activity, organelle components, and signal transduction and substrate transport. Of these genes, two transcription factors [*BBX14* (AT1G68520) and *ERF104* (AT5G61600)] had previously been implicated in stress response. And most of genes we screened were involved in photosynthesis-related activities (AT1G16720, AT4G12800, AT1G52870, AT2G30570, and AT1G06430) and transmembrane transport activity (AT5G49730, AT1G64720, AT5G46110, AT4G25570, and AT3G13062).

Differentially expressed genes from the basal heat treatment were subjected to GO enrichment analysis (**Figure 6B**). The genes associated with ALA6 under heat stress included 112 genes categorized as "response to endogenous stimulus" and 194 categorized as "response to stress." Other categories of enriched genes include "response to oxygen-containing compound" (141 genes), "defense response" (100 genes), "response to acid chemical" (92 genes), and "aromatic compound biosynthetic process" (160 genes). These results indicated that ALA6 might have versatile effects on cellular responses triggered by heat stress.

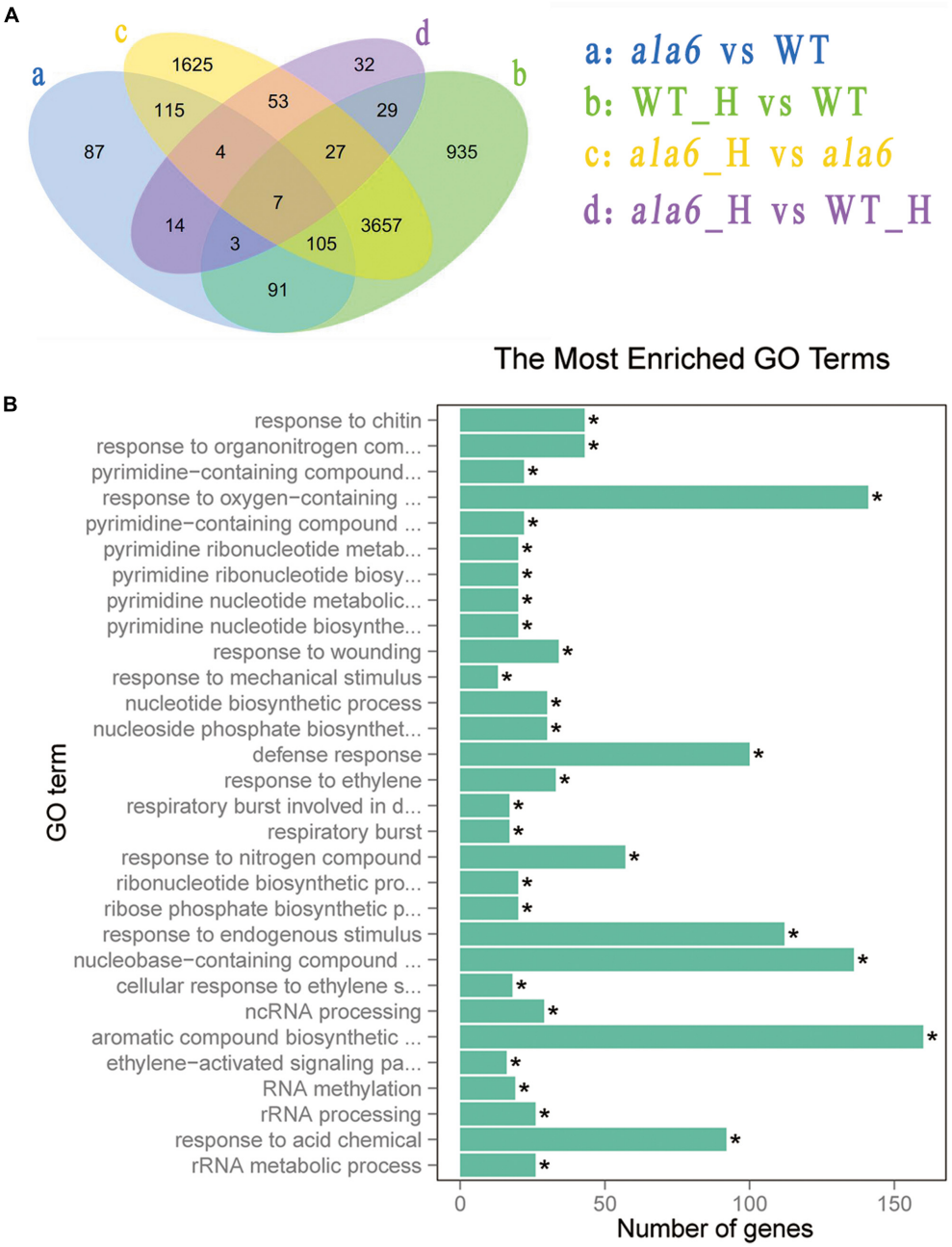

FIGURE 6 | Differentially expressed genes after basal thermotolerance. **(A)** Venn diagram indicates DEGs. DEGs for a: *ala6* vs. WT; b: WT with heat treatment vs. WT; c: *ala6* with heat treatment vs. *ala6*; d: *ala6* with heat treatment vs. WT with heat treatment. **(B)** GO enrichment for DEGs.

DISCUSSION

ALA6 Is Involved in Heat-Induced Cellular Responses via Maintenance of Membrane Stability

Temperature is a major environmental cue that has a rapid impact on cellular homeostasis, including both membrane stability and protein activity, and also has significant effects on plant development and growth. Because land plants are sessile, they are exposed to daily and seasonal temperature fluctuations (Saidi et al., 2011). To survive, plants evolved a series of mechanisms to respond to the ambient environment, including membrane-related stress signaling mechanisms for intact cell (Vigh et al., 2005, 2007). Stress-triggered changes in the lipid species of membranes could influence both the physical properties of the membrane and the distribution

and activity of membrane proteins (Vigh et al., 2005). P_4-type ATPases have recently been found to alter membrane lipid composition by transporting specific lipids, and some members of this protein family have been found to play crucial roles in stress responses in yeast and mammals (Axelsen and Palmgren, 2001; Sebastian et al., 2012). Among the 12 members of the P_4-type ATPase family in *Arabidopsis*, ALA1 was first reported to be implicated in cold tolerance (Gomès et al., 2000). In addition, pollen tube development in an *ala6/7* double mutant is described to be vulnerable under hot-day/cold-night temperature stress (McDowell et al., 2015). ALA3 has been demonstrated to participate in secretory processes of the Golgi apparatus, regulating root growth and reproductive development as well as tolerance to temperature stress (Poulsen et al., 2008; McDowell et al., 2013). Though ALA10 is responsible for root and leaf development independent of temperature, it can improve MGDG synthesis at low temperature (Poulsen et al., 2015; Botella et al., 2016). However, the functions of other members of this subclass have not been determined. In fact, the members of the ALA family that exhibit lipid substrate specificity have been shown to be involved in many physiological processes in a temperature-dependent manner. Considering the relatively close phylogenetic relationship among ALA family members 3–10 (Poulsen et al., 2015), we chose to investigate ALA6 and found that this protein is essential for responses to high temperature stress. As shown in **Figure 2A**, though a short-term acclimation can alleviate heat injury to seedlings, two heat treatments lead to the death of *ala6* seedlings, whereas WT seedlings survive. In addition, the partially sterile siliques of *ala6* plants under heat stress (data not shown) are comparable to the description given by McDowell et al. (2015). Since plants also suffer other stresses while acquiring thermotolerance via heat acclimation (Larkindale and Vierling, 2008; Mittler et al., 2012), this study shows that ALA6 can be implicated directly in heat stress-related intracellular responses rather than in other stresses. To determine whether the enzyme activity of phospholipid translocation is involved in the heat stress response, ALA6 with a point-mutation at a conserved functional site was analyzed and was confirmed not to rescue the heat-sensitive phenotype of an *ala6* knockout mutant (**Figure 5A**). Taken together with the greater EL and higher *Chl b*/*a* ratio of

TABLE 1 | Differentially expressed genes (DEGs) between WT and *ala6*.

Gene_id	FPKM_*ala6*	FPKM_WT	padj	Gene name	Description
AT1G54280	11.32	0.14	0	ALA6	ATPase E1-E2 type family protein/haloacid dehalogenase-like hydrolase family protein
AT1G25560	14.21	85.50	6.81*E*−275	TEM1	AP2/B3 transcription factor family protein
AT1G68840	17.46	90.52	1.48*E*−253	RAV2	Related to ABI3/VP1 2
AT5G21940	86.36	369.80	2.01*E*−233	–	Function unknown
AT2G40000	31.13	205.38	2.60*E*−224	HSPRO2	Ortholog of sugar beet HS1 PRO-1 2
AT1G23390	21.13	97.82	9.04*E*−222	–	Kelch repeat-containing F-box family protein
AT1G80440	36.24	160.52	2.97*E*−208	–	Galactose oxidase/kelch repeat superfamily protein
AT4G37610	17.23	90.47	1.18*E*−203	BT5	BTB and TAZ domain protein 5
AT1G73120	11.68	80.61	4.41*E*−175	–	
AT3G59940	62.83	225.29	1.64*E*−144	KFB50	Galactose oxidase/kelch repeat superfamily protein
AT5G60680	22.32	87.36	5.12*E*−140	–	Protein of unknown function, DUF584
AT3G46600	14.44	49.61	1.27*E*−138	–	GRAS family transcription factor
AT5G19120	78.50	218.55	1.62*E*−134	–	Eukaryotic aspartyl protease family protein
AT1G27730	11.42	59.58	1.85*E*−129	STZ	Salt tolerance zinc finger
AT4G05070	71.27	250.05	1.05*E*−128	–	Wound-responsive family protein
AT3G20340	12.07	63.50	1.56*E*−123	–	
AT1G68520	87.40	219.95	1.10*E*−122	BBX14	B-box type zinc finger protein with CCT domain
AT2G40140	24.02	82.13	5.15*E*−118	CZF1	Zinc finger (CCCH-type) family protein
AT5G37260	25.25	79.14	1.41*E*−107	CIR1	MYB family transcription factor Circadian 1
AT5G56550	11.66	80.83	1.35*E*−93	OXS3	Oxidative stress 3
AT5G61160	24.42	62.07	1.91*E*−83	AACT1	Anthocyanin 5-aromatic acyl transferase 1
AT5G24030	98.83	37.43	3.06*E*−83	SLAH3	SLAC1 homolog 3
AT1G80920	90.37	253.72	1.09*E*−81	J8	Chaperone DnaJ-domain superfamily protein
AT2G23130	114.40	37.32	9.69*E*−74	AGP17	Arabinogalactan protein 17
AT2G21210	13.92	47.65	4.39*E*−73	–	SAUR-like auxin-responsive protein family
AT1G32920	57.06	142.22	1.48*E*−69	–	
AT3G15450	149.28	423.60	1.58*E*−67	–	Aluminum induced protein with YGL and LRDR motifs
AT3G15630	86.45	183.59	2.66*E*−66	–	
AT5G67420	18.34	69.95	6.23*E*−66	LBD37	LOB domain-containing protein 37
AT5G18670	4.21	14.83	1.75*E*−65	BMY3	Beta-amylase 3

Gene_id: Gene identity; FPKM: Fragments Per Kilobase of transcript per Million fragments mapped; padj: P-value by adjustment.

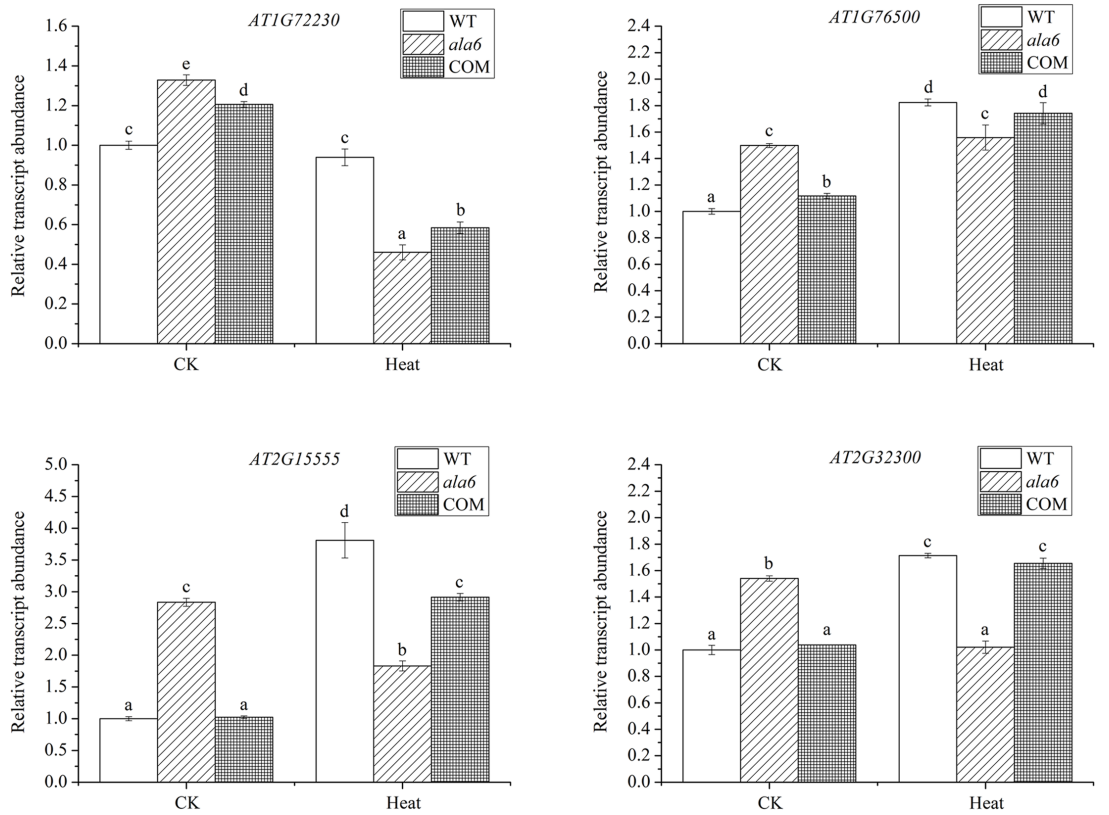

FIGURE 7 | Relative transcript abundance of DEGs randomly selected in WT, *ala6*, and ALA6 complementary lines with or without heat stress. Results are calculated from three independent experiments (average results ±SE). Columns with different letters contain significantly different values ($P < 0.05$).

ala6 mutants (Demidchik et al., 2014; Bi et al., 2016), this result implies that ALA6 might serve as a membrane stabilizer via altering membrane permeability, especially during heat stress.

ALA6 Can Induce Changes in the Expression of Heat Stress-Related Genes

Under high temperature, changes in lipid composition affect membrane dynamics and initiate the corresponding signal transduction pathways (Vigh et al., 1998). It has been reported that membrane fluidity can modulate the transcription of heat-inducible genes (Carratù et al., 1996; Horváth et al., 1998). To identify the downstream signaling triggered by *ALA6*, we analyzed gene expression in WT and *ala6* plants with and without heat shock. DEGs between WT and *ala6 Arabidopsis* were shown to be involved in many functions. Among the 286 down-regulated genes are numerous genes related to stress and hormone responses, including heat, cold, salt, drought, oxidative, and pathogen stress, as well as ethylene, abscisic acid, JA and salicylic acid in various other processes. These responses are involved in the control of gene expression by transcription factors, such as the F-box protein family, the B-box zinc finger protein family, *WRKY*s and *ERF*s (**Table 1**). For instance, the expression of *BBX14* (AT1G68520), a B-box-type zinc finger protein, was significantly lower in *ala6* than in WT *Arabidopsis*. Although the function of BBX14 is still unknown, expression of its homolog, *BBX18*, has been confirmed to be induced by heat shock and to affect seed germination and seedling survival negatively by suppressing the expression of heat-responsive genes (Wang et al., 2013). Other members of this family are also involved in responses to various biotic or abiotic stresses (Gangappa and Botto, 2014), likely explaining why *ala6* plants are sensitive to heat stress. In addition, it was found that 140 genes with up-regulated expression in *ala6* plant are responsible for various biological processes such as phosphorylation, substrate transport and synthesis, and lipid metabolism, but most of these genes have an integral membrane component (**Table 1** and Supplementary Table S2). Of these genes, only two fell within the top 30 DEGs with increased expression; these were *SLAH3* (AT5G24030) and *AGP17* (AT2G23130). The products of these genes both localize to the plasma membrane. SLAH3 is an anion channels involved in mediating ion homeostasis, while AGP17 is a glycosylphosphatidylinositol (GPI)-anchored protein involved in extracellular signal perception and interaction with proteins in lipid rafts (Gaspar et al., 2004; Zhang et al., 2016). The results imply that lack of ALA6 might not only lead to the alteration of membrane permeability

and integrity but also to corresponding changes in membrane proteins.

Interestingly, the expression of many chloroplast-related genes in the top 30 DEGs are shown to be up-regulated in *ala6*, whose functions depend greatly on membrane stability (**Table 2**; Boudière et al., 2014). A *HSP81-3* (*HSP90.3*, AT5G56010), which functions as a molecular chaperone, and *AOC*2 (AT3G25770), which has AOC activity, are among the most interesting genes we identified. The major functions of *HSPs* include preventing proteins from misfolding and disaggregation and protecting membranes that are exposed to high temperature (Banti et al., 2010). Proteins such as HSP20, HSP70, HSP90 and HSP101 have been shown to be components of the heat shock response and assist in thermotolerance by adjusting protein aggregation (Nieto-Sotelo et al., 2002; Cazalé et al., 2009; Fragkostefanakis et al., 2015; Yu et al., 2016). Thus, the decreased expression of *HSP* genes in an ALA6 loss-of-function mutant may also demonstrate that ALA6 plays an important role in heat-inducible signaling. Moreover, AOC2 catalyzes the biosynthesis of JA, for which a role in basal thermotolerance has been illustrated recently (Clarke et al., 2009; Stenzel et al., 2012). In conclusion, when plants are exposed to high temperature, it is speculated that ALA6 may have an effect on the membrane permeability and stability, and this alteration can induce changes in membrane proteins and eventually trigger heat-associated gene expression. However, the physiological functions and underlying mechanisms of these altered genes in *ala6* mutants require further study.

CONCLUSION

ALA6, a P_4-type ATPase of *Arabidopsis*, possesses the conserved structure and function of this family and serves as a phospholipid flippase to maintain membrane stability and fluidity under normal or adverse conditions. The seedlings of loss-of-function mutant *ala6* were found to wither, turn yellow and eventually die with exposure to basal thermotolerance or acquired thermotolerance treatments. Overexpression of *ALA6* can rescue this phenotype, while transgenic plants containing a point-mutation in a conserved region of *ALA6* show no response to heat stress. This suggests that ALA6 is

TABLE 2 | Genes related to ALA6 under basal thermotolerance.

Gene_id	FPKM_*ala6*	FPKM_WT	padj	Gene name	Description
AT4G01560	0.39	31.34	4.01*E*−236	MEE49	Ribosomal RNA processing Brix domain protein
AT1G16720	151.56	65.46	1.23*E*−186	HCF173	High chlorophyll fluorescence phenotype 173
AT1G52930	0.44	28.23	1.03*E*−180	–	Ribosomal RNA processing Brix domain protein
AT5G21940	91.16	369.80	1.33*E*−179	–	
AT4G12800	2143.26	1009.12	4.42*E*−179	PSAL	Photosystem I subunit l
AT5G56010	66.77	236.09	5.39*E*−179	HSP81-3	Heat shock protein 81-3
AT5G49730	51.63	18.26	1.62*E*−175	ATFRO6	Ferric reduction oxidase 6
AT1G64720	790.28	326.70	8.54*E*−172	CP5	Polyketide cyclase/dehydrase and lipid transport superfamily protein
AT1G68520	44.88	219.95	4.48*E*−171	BBX14	B-box type zinc finger protein with CCT domain
AT5G46110	595.47	329.87	5.18*E*−143	APE2	Glucose-6-phosphate/phosphate translocator-related
AT3G15630	43.84	183.59	4.89*E*−138	–	
AT2G30600	82.35	40.48	3.19*E*−132	–	BTB/POZ domain-containing protein
AT1G21130	364.42	192.73	2.53*E*−124	–	O-methyltransferase family protein
AT1G52870	116.67	56.31	9.62*E*−120	–	Peroxisomal membrane 22 kDa (Mpv17/PMP22) family protein
AT5G19120	70.83	218.55	3.29*E*−118	–	Eukaryotic aspartyl protease family protein
AT3G13180	0.80	14.02	7.62*E*−117	–	NOL1/NOP2/sun family protein/anti-termination NusB domain-containing protein
AT2G30570	2336.70	1219.77	1.44*E*−112	PSBW	Photosystem II reaction center W
AT4G34710	101.81	275.88	6.62*E*−110	ADC2	Arginine decarboxylase 2
AT5G35170	137.68	76.90	4.15*E*−109	–	Adenylate kinase family protein
AT3G25770	60.87	197.45	4.99*E*−109	AOC2	Allene oxide cyclase 2
AT5G61600	10.47	62.01	1.14*E*−108	ERF104	Ethylene response factor 104
AT3G20340	7.86	63.50	1.02*E*−106	–	
AT4G25570	335.27	194.81	1.78*E*−103	ACYB-2	Cytochrome b561/ferric reductase transmembrane protein family
AT1G06430	86.33	46.32	1.79*E*−103	FTSH8	FTSH protease 8
AT4G37300	357.03	209.52	2.41*E*−103	MEE59	Maternal effect embryo arrest 59
AT3G13062	71.42	34.92	1.33*E*−101	–	Polyketide cyclase/dehydrase and lipid transport superfamily protein
AT5G58330	197.06	113.47	1.69*E*−99	–	Lactate/malate dehydrogenase family protein
AT1G63780	0.34	14.25	1.03*E*−98	IMP4	Ribosomal RNA processing Brix domain protein
AT4G37610	22.21	90.47	8.19*E*−98	BT5	BTB and TAZ domain protein 5
AT1G58280	38.96	12.63	1.42*E*−96	–	Phosphoglycerate mutase family protein

Gene_id: Gene identity; FPKM: Fragments Per Kilobase of transcript per Million fragments mapped; padj: P-value by adjustment.

significant for response to high temperature stress. Moreover, *ala6* seedlings exhibit higher ion-leakage and lower chlorophyll content after heat treatment, indicating that ALA6 can protect membranes from the disordered state that results from heat stress. This protective effect involves the maintenance of membrane permeability, stability and integrity. In addition, transcriptome analysis shows that *ALA6* affects the expression of heat-inducible genes. Taken together, these evidences show that ALA6 plays an essential role in cellular responses to high temperature. In addition, characterization of ALA6 activity and its roles should further illuminate the mechanisms of the involvement of P_4-ATPase in stress responses.

ACCESSION NUMBER

RNA sequencing data is available at the National Center for Biotechnology Information (NCBI) data repository (accession PRJNA390831).

AUTHOR CONTRIBUTIONS

YN and YX designed research; YN, DQ, BL, JM, DW, XW, and WH performed research; YN, DQ, BL, JM analyzed data; and YN, DQ, and YX wrote the paper.

FUNDING

This work was supported by the National Natural Science Foundation of China (31400220) and the Fundamental Research Funds for the Central Universities (lzujbky-2014-92, lzujbky-2017-156, lzujbky-2017-k14).

SUPPLEMENTARY MATERIAL

The Supplementary Material for this article can be found online at: http://journal.frontiersin.org/article/10.3389/fpls.2017.01732/full#supplementary-material

REFERENCES

Alder-Baerens, N., Lisman, Q., Luong, L., Pomorski, T., and Holthuis, J. C. (2006). Loss of P4 ATPases Drs2p and Dnf3p disrupts aminophospholipid transport and asymmetry in yeast post-Golgi secretory vesicles. *Mol. Biol. Cell* 17, 1632–1642. doi: 10.1091/mbc.E05-10-0912

Alonso, J. M., Stepanova, A. N., Leisse, T. J., Kim, C. J., Chen, H., Shinn, P., et al. (2003). Genome-wide insertional mutagenesis of *Arabidopsis thaliana*. *Science* 301, 653–657. doi: 10.1126/science.1086391

Andersen, J. P., Vestergaard, A. L., Mikkelsen, S. A., Mogensen, L. S., Chalat, M., and Molday, R. S. (2016). P4-ATPases as phospholipid flippases-structure, function, and enigmas. *Front. Physiol.* 7:275. doi: 10.3389/fphys.2016.00275

Axelsen, K. B., and Palmgren, M. G. (1998). Evolution of substrate specificities in the P-type ATPase superfamily. *J. Mol. Evol.* 46, 84–101. doi: 10.1007/PL00006286

Axelsen, K. B., and Palmgren, M. G. (2001). Inventory of the superfamily of P-type ion pumps in *Arabidopsis*. *Plant Physiol.* 126, 696–706.

Baldridge, R. D., Xu, P., and Graham, T. R. (2013). Type IV P-type ATPases distinguish mono-versus diacyl phosphatidylserine using a cytofacial exit gate in the membrane domain. *J. Biol. Chem.* 288, 19516–19527. doi: 10.1074/jbc.M113.476911

Banti, V., Mafessoni, F., Loreti, E., Alpi, A., and Perata, P. (2010). The heat-inducible transcription factor *HsfA2* enhances anoxia tolerance in *Arabidopsis*. *Plant Physiol.* 152, 1471–1483. doi: 10.1104/pp.109.149815

Bi, A., Fan, J., Hu, Z., Wang, G., Amombo, E., Fu, J., et al. (2016). Differential acclimation of enzymatic antioxidant metabolism and photosystem II photochemistry in tall fescue under drought and heat and the combined stresses. *Front. Plant Sci.* 7:453. doi: 10.3389/fpls.2016.00453

Botella, C., Sautron, E., Boudiere, L., Michaud, M., Dubots, E., Yamaryo-Botté, Y., et al. (2016). ALA10, a phospholipid flippase, controls FAD2/FAD3 desaturation of phosphatidylcholine in the ER and affects chloroplast lipid composition in *Arabidopsis thaliana*. *Plant Physiol.* 170, 1300–1314. doi: 10.1104/pp.15.01557

Boudière, L., Michaud, M., Petroutsos, D., Rébeillé, F., Falconet, D., Bastien, O., et al. (2014). Glycerolipids in photosynthesis: composition, synthesis and trafficking. *Biochim. Biophys. Acta* 1837, 470–480. doi: 10.1016/j.bbabio.2013.09.007

Carratù, L., Franceschelli, S., Pardini, C. L., Kobayashi, G. S., Horvath, I., Vigh, L., et al. (1996). Membrane lipid perturbation modifies the set point of the temperature of heat shock response in yeast. *Proc. Natl. Acad. Sci. U.S.A.* 93, 3870–3875.

Cazalé, A. C., Clément, M., Chiarenza, S., Roncato, M. A., Pochon, N., Creff, A., et al. (2009). Altered expression of cytosolic/nuclear HSC70-1 molecular chaperone affects development and abiotic stress tolerance in *Arabidopsis thaliana*. *J. Exp. Bot.* 60, 2653–2664. doi: 10.1093/jxb/erp109

Clarke, S. M., Cristescu, S. M., Miersch, O., Harren, F. J., Wasternack, C., and Mur, L. A. (2009). Jasmonates act with salicylic acid to confer basal thermotolerance in *Arabidopsis thaliana*. *New Phytol.* 182, 175–187. doi: 10.1111/j.1469-8137.2008.02735.x

Clough, S. J., and Bent, A. F. (1998). Floral dip: a simplified method for *Agrobacterium*-mediated transformation of *Arabidopsis thaliana*. *Plant J.* 16, 735–743. doi: 10.1046/j.1365-313x.1998.00343.x

Coleman, J. A., Kwok, M. C., and Molday, R. S. (2009). Localization, purification, and functional reconstitution of the P4-ATPase Atp8a2, a phosphatidylserine flippase in photoreceptor disc membranes. *J. Biol. Chem.* 284, 32670–32679. doi: 10.1074/jbc.M109.047415

Coleman, J. A., Quazi, F., and Molday, R. S. (2013). Mammalian P4-ATPases and ABC transporters and their role in phospholipid transport. *Biochim. Biophys. Acta* 1831, 555–574. doi: 10.1016/j.bbalip.2012.10.006

Demidchik, V., Straltsova, D., Medvedev, S. S., Pozhvanov, G. A., Sokolik, A., and Yurin, V. (2014). Stress-induced electrolyte leakage: the role of K+-permeable channels and involvement in programmed cell death and metabolic adjustment. *J. Exp. Bot.* 65, 1259–1270. doi: 10.1093/jxb/eru004

Ding, J., Wu, Z., Crider, B. P., Ma, Y., Li, X., Slaughter, C., et al. (2000). Identification and functional expression of four isoforms of ATPase II, the putative aminophospholipid translocase. Effect of isoform variation on the ATPase activity and phospholipid specificity. *J. Biol. Chem.* 275, 23378–23386. doi: 10.1074/jbc.M910319199

Fragkostefanakis, S., Röth, S., Schleiff, E., and Scharf, K. D. (2015). Prospects of engineering thermotolerance in crops through modulation of heat stress transcription factor and heat shock protein networks. *Plant Cell Environ.* 38, 1881–1895. doi: 10.1111/pce.12396

Gangappa, S. N., and Botto, J. F. (2014). The BBX family of plant transcription factors. *Trends Plant Sci.* 19, 460–470. doi: 10.1016/j.tplants.2014.01.010

Gaspar, Y. M., Nam, J., Schultz, C. J., Lee, L. Y., Gilson, P. R., Gelvin, S. B., et al. (2004). Characterization of the *Arabidopsis* lysine-rich arabinogalactan-protein *AtAGP17* mutant(rat1) that results in a decreased efficiency of *agrobacterium* transformation. *Plant Physiol.* 135, 2162–2171.

Gomès, E., Jakobsen, M. K., Axelsen, K. B., Geisler, M., and Palmgren, M. G. (2000). Chilling tolerance in *Arabidopsis* involves ALA1, a member of a new family of putative aminophospholipid translocases. *Plant Cell* 12, 2441–2454.

Guo, Z., Lu, J., Wang, X., Zhan, B., Li, W., and Ding, S. W. (2017). Lipid flippases promote antiviral silencing and the biogenesis of viral and host siRNAs in

Arabidopsis. *Proc. Natl. Acad. Sci. U.S.A.* 114, 1377–1382. doi: 10.1073/pnas.1614204114

Horváth, I., Glatz, A., Nakamoto, H., Mishkind, M. L., Munnik, T., Saidi, Y., et al. (2012). Heat shock response in photosynthetic organisms: membrane and lipid connections. *Prog. Lipid Res.* 51, 208–220. doi: 10.1016/j.plipres.2012.02.002

Horváth, I., Glatz, A., Varvasovszki, V., Török, Z., Páli, T., Balogh, G., et al. (1998). Membrane physical state controls the signaling mechanism of the heat shock response in *Synechocystis* PCC 6803: identification of hsp17 as a "fluidity gene". *Proc. Natl. Acad. Sci. U.S.A.* 95, 3513–3518.

Jefferson, R. A., Kavanagh, T. A., and Bevan, M. W. (1987). GUS fusions: beta-glucuronidase as a sensitive and versatile gene fusion marker in higher plants. *EMBO J.* 6, 3901–3907.

Larkindale, J., and Vierling, E. (2008). Core genome responses involved in acclimation to high temperature. *Plant Physiol.* 146, 748–761.

Lopez-Marques, R. L., Poulsen, L. R., Bailly, A., Geisler, M., Pomorski, T. G., and Palmgren, M. G. (2014). Structure and mechanism of ATP-dependent phospholipid transporters. *Biochim. Biophys. Acta* 1850, 461–475. doi: 10.1016/j.bbagen.2014.04.008

López-Marqués, R. L., Poulsen, L. R., Hanisch, S., Meffert, K., Buch-Pedersen, M. J., Jakobsen, M. K., et al. (2010). Intracellular targeting signals and lipid specificity determinants of the ALA/ALIS P4-ATPase complex reside in the catalytic ALA alpha-subunit. *Mol. Biol. Cell* 21, 791–801. doi: 10.1091/mbc.E09-08-0656

McDowell, S. C., López-Marqués, R. L., Cohen, T., Brown, E., Rosenberg, A., Palmgren, M. G., et al. (2015). Loss of the *Arabidopsis thaliana* P4-ATPases ALA6 and ALA7 impairs pollen fitness and alters the pollen tube plasma membrane. *Front. Plant Sci.* 6:197. doi: 10.3389/fpls.2015.00197

McDowell, S. C., López-Marqués, R. L., Poulsen, L. R., Palmgren, M. G., and Harper, J. F. (2013). Loss of the *Arabidopsis thaliana* P4-ATPase ALA3 reduces adaptability to temperature stresses and impairs vegetative, pollen, and ovule development. *PLOS ONE* 8:e62577. doi: 10.1371/journal.pone.0062577

Mittler, R., Finka, A., and Goloubinoff, P. (2012). How do plants feel the heat? *Trends Biochem. Sci.* 37, 118–125. doi: 10.1016/j.tibs.2011.11.007

Murata, N., and Los, D. A. (1997). Membrane fluidity and temperature perception. *Plant Physiol.* 115, 875–879.

Nieto-Sotelo, J., Martínez, L. M., Ponce, G., Cassab, G. I, Alagón, A., Meeley, R. B., et al. (2002). MaizeHSP101plays important roles in both induced and basal thermotolerance and primary root growth. *Plant Cell* 14, 1621–1633.

Palmgren, M. G., and Axelsen, K. B. (1998). Evolution of P-type ATPases. *Biochim. Biophys. Acta* 1365, 37–45. doi: 10.1016/S0005-2728(98)00041-3

Paterson, J. K., Renkema, K., Burden, L., Halleck, M. S., Schlegel, R. A., Williamson, P., et al. (2006). Lipid specific activation of the murine P4-ATPase Atp8a1(ATPaseII). *Biochemistry* 45, 5367–5376. doi: 10.1021/bi052359b

Paulusma, C. C., and Elferink, R. P. (2010). P4 ATPases-the physiological relevance of lipid flipping transporters. *FEBS Lett.* 584, 2708–2716. doi: 10.1016/j.febslet.2010.04.071

Pedersen, P. L., and Carafoli, E. (1987). Ion motive ATPases I: ubiquity, properties and significance to cell function. *Trends Biochem. Sci.* 12, 146–150. doi: 10.1016/0968-0004(87)90071-5

Pomorski, T., Lombardi, R., Riezman, H., Devaux, P. F., van Meer, G., and Holthuis, J. C. M. (2003). Drs2p related P-type ATPases Dnf1p and Dnf2p are required for phospholipid translocation across the yeast plasma membrane and serve a role in endocytosis. *Mol. Biol. Cell* 14, 1240–1254. doi: 10.1091/mbc.E02-08-0501

Pomorski, T. G., and Menon, A. K. (2006). Lipid flippases and their biological functions. *Cell. Mol. Life Sci.* 63, 2908–2921. doi: 10.1007/s00018-006-6167-7

Pomorski, T. G., and Menon, A. K. (2016). Lipid somersaults: uncovering the mechanisms of protein-mediated lipid flipping. *Prog. Lipid. Res.* 64, 69–84. doi: 10.1016/j.plipres.2016.08.003

Poulsen, L. R., López-Marqués, R. L., McDowell, S. C., Okkeri, J., Licht, D., Schulz, A., et al. (2008). The Arabidopsis P4-ATPase ALA3 localizes to the Golgi and requires a beta-subunit to function in lipid translocation and secretory vesicle formation. *Plant Cell* 20, 658–676. doi: 10.1105/tpc.107.054767

Poulsen, L. R., López-Marqués, R. L., Pedas, P. R., McDowell, S. C., Brown, E., Kunze, R., et al. (2015). A phospholipid uptake system in the model plant *Arabidopsis thaliana*. *Nat. Commun.* 27, 7649. doi: 10.1038/ncomms8649

Puts, C. F., and Holthuis, J. C. (2009). Mechanism and significance of P4 ATPase-catalyzed lipid transport: lessons from a Na+/K+-pump. *Biochim. Biophys. Acta.* 1791, 603–611. doi: 10.1016/j.bbalip.2009.02.005

Riekhof, W. R., and Voelker, D. R. (2006). Uptake and utilization of lyso-phosphatidylethanolamine by *Saccharomyces cerevisiae*. *J. Biol. Chem.* 281, 36588–36596. doi: 10.1074/jbc.M608851200

Rieu, I., and Powers, S. J. (2009). Real-time quantitative RT-pcr: design, calculations, and statistics. *Plant Cell* 21, 1031–1033. doi: 10.1105/tpc.109.066001

Saidi, Y., Finka, A., and Goloubinoff, P. (2011). Heat perception and signalling in plants: a tortuous path to thermotolerance. *New Phytol.* 190, 556–565. doi: 10.1111/j.1469-8137.2010.03571.x

Sairam, R. K., and Srivastava, G. C. (2002). Changes in antioxidant activity in subcellular fraction of tolerant and susceptible wheat genotypes in response to long term salt stress. *Plant Sci.* 162, 897–904. doi: 10.1016/S0168-9452(02)00037-7

Sebastian, T. T., Baldridge, R. D., Xu, P., and Graham, T. R. (2012). Phospholipid flippases: building asymmetric membranes and transport vesicles. *Biochim. Biophys. Acta* 1821, 1068–1077. doi: 10.1016/j.bbalip.2011.12.007

Stenzel, I., Otto, M., Delker, C., Kirmse, N., Schmidt, D., Miersch, O., et al. (2012). ALLENE OXIDE CYCLASE (AOC) gene family members of *Arabidopsis thaliana*: tissue- and organ-specific promoter activities and in vivo heteromerization. *J. Exp. Bot.* 63, 6125–6138. doi: 10.1093/jxb/ers261

Van Der Mark, V. A., Elferink, R. P., and Paulusma, C. C. (2013). P4 ATPases: flippases in health and disease. *Int. J. Mol. Sci.* 14, 7897–7922. doi: 10.3390/ijms14047897

Vigh, L., Escribá, P. V., Sonnleitner, A., Sonnleitner, M., Piotto, S., Maresca, B., et al. (2005). The significance of lipid composition for membrane activity: new concepts and ways of assessing function. *Prog. Lipid Res.* 44, 303–344. doi: 10.1016/j.plipres.2005.08.001

Vigh, L., Maresca, B., and Harwood, J. (1998). Does the membrane's physical state control the expression of heat shock and other genes? *Trends Biochem. Sci.* 23, 369–374. doi: 10.1016/S0968-0004(98)01279-1

Vigh, L., Nakamoto, H., Landry, J., Gomez-Munoz, A., Harwood, J. L., and Horvath, I. (2007). Membrane regulation of the stress response from prokaryotic models to mammalian cells. *Ann. N. Y. Acad. Sci.* 1113, 40–51. doi: 10.1196/annals.1391.027

Wang, Q., Tu, X., Zhang, J., Chen, X., and Rao, L. (2013). Heat stress-induced *BBX18* negatively regulates the thermotolerance in *Arabidopsis*. *Mol. Biol. Rep.* 40, 2679–2688. doi: 10.1007/s11033-012-2354-9

Woo, H. R., Chung, K. M., Park, J. H., Oh, S. A., Ahn, T., Hong, S. H., et al. (2001). ORE9, an F-box protein that regulates leaf senescence in Arabidopsis. *Plant Cell* 13, 1779–1790. doi: 10.1105/TPC.010061

Xu, P., Okkeri, J., Hanisch, S., Hu, R. Y., Xu, Q., Pomorski, T. G., et al. (2009). Identification of a novel mouse P4-ATPase family member highly expressed during spermatogenesis. *J. Cell Sci.* 122, 2866–2876. doi: 10.1242/jcs.047423

Yu, J., Cheng, Y., Feng, K., Ruan, M., Ye, Q., Wang, R., et al. (2016). Genome-wide identification and expression profiling of tomatoHsp20gene family in response to biotic and abiotic stresses. *Front. Plant Sci.* 7:1215. doi: 10.3389/fpls.2016.01215

Zhang, A., Ren, H. M., Tan, Y. Q., Qi, G. N., Yao, F. Y., Wu, G. L., et al. (2016). S-type anion channels SLAC1 and SLAH3 function as essential negative regulators of inward K+ channels and stomatal opening in *Arabidopsis*. *Plant Cell* 28, 949–965. doi: 10.1105/tpc.15.01050

Zhang, X., Wollenweber, B., Jiang, D., Liu, F., and Zhao, J. (2008). Water deficits and heat shock effects on photosynthesis of a transgenic *Arabidopsis thaliana* constitutively expressing ABP9, a bZIP transcription factor. *J. Exp. Bot.* 59, 839–848. doi: 10.1093/jxb/erm364

Zhou, X., and Graham, T. R. (2009). Reconstitution of phospholipid translocase activity with purified Drs2p, a type-IV P-type ATPase from budding yeast. *Proc. Natl. Acad. Sci. U.S.A.* 106, 16586–16591. doi: 10.1073/pnas.0904293106

Conflict of Interest Statement: The authors declare that the research was conducted in the absence of any commercial or financial relationships that could be construed as a potential conflict of interest.

frontiers in Plant Science

ORIGINAL RESEARCH
published: 28 September 2017
doi: 10.3389/fpls.2017.01609

Transcriptome and Differential Expression Profiling Analysis of the Mechanism of Ca^{2+} Regulation in Peanut (*Arachis hypogaea*) Pod Development

Sha Yang[1†], Lin Li[2†], Jialei Zhang[1], Yun Geng[1], Feng Guo[1], Jianguo Wang[2], Jingjing Meng[1], Na Sui[3], Shubo Wan[4] and Xinguo Li[1*]*

[1] Biotechnology Research Center, Shandong Academy of Agricultural Sciences, Jinan, China, [2] College of Agronomy, Hunan Agricultural University, Changsha, China, [3] College of Life Sciences, Shandong Normal University, Jinan, China, [4] Shandong Provincial Key Laboratory of Crop Genetic Improvement, Ecology and Physiology, Shandong Academy of Agricultural Sciences, Jinan, China

Calcium not only serves as a necessary nutrient for plant growth but also acts as a ubiquitous central hub in a large number of signaling pathways. Free Ca^{2+} deficiency in the soil may cause early embryo abortion, which eventually led to abnormal development of peanut pod during the harvest season. To understand the mechanisms of Ca^{2+} regulation in pod development, transcriptome analysis of peanut gynophores and pods was performed by comparing the treatments between free Ca^{2+} sufficiency and free Ca^{2+} deficiency using Illumina HiSeq™ 2000. 9,903,082,800 nt bases are generated totally. After assembly, the average length of 102,819 unigenes is 999 nt, N50 is 1,782 nt. RNA-seq based gene expression profilings showed a large number of genes at the transcriptional level changed significantly between the aerial pegs and underground swelling pods under free Ca^{2+} sufficienct or deficiency treatments, respectively. Genes encoding key members of Ca^{2+} signaling transduction pathway, enzymes for hormone metabolism, cell division and growth, transcriptional factor as well as embryo development were highlighted. This information provides useful information for our further study. The results of digital gene expression (DGE) indicated that exogenous calcium might contribute to the development of peanut pod through its signal transduction pathway, meanwhile, promote the normal transition of the gynophores to the reproductive development.

Keywords: calcium, peanut, pod development, RNA-Seq, differential expression analysis

OPEN ACCESS

Edited by:
Gerald Alan Berkowitz, University of Connecticut, United States

Reviewed by:
Changai Wu, Shandong Agricultural University, China
Kun Wang, Michigan State University, United States
Daowen Wang, Institute of Genetics and Developmental Biology (CAS), China

***Correspondence:**
Shubo Wan
wansb@saas.ac.cn
Xinguo Li
xinguol@163.com

[†]These authors have contributed equally to this work as co-first authors.

Specialty section:
This article was submitted to Plant Traffic and Transport, a section of the journal Frontiers in Plant Science

Received: *02 June 2017*
Accepted: *04 September 2017*
Published: *28 September 2017*

Citation:
Yang S, Li L, Zhang J, Geng Y, Guo F, Wang J, Meng J, Sui N, Wan S and Li X (2017) Transcriptome and Differential Expression Profiling Analysis of the Mechanism of Ca^{2+} Regulation in Peanut (Arachis hypogaea) Pod Development. Front. Plant Sci. 8:1609. doi: 10.3389/fpls.2017.01609

INTRODUCTION

Peanut (*Arachis hypogaea* L.) is an economic crop that contributes 20% to the global oil production and 11% of the protein supply per year (Chen et al., 2014). Aerial flowering and underground development of fruit are special genetic characteristics of peanuts, and the ecological environment of dark, moist and mechanical stimulation is essential conditions for pod development. So, the ovule-carrying pegs (gynophores) must elongate to bury the fertilized ovule into the soil in order

to survive and reproduce (Arya et al., 2016). When gynophores are buried into the soil at 2–8 cm deep, the ovule swells to provide room for the embryo to grow. During this complex period, the peanut can directly absorb moisture, calcium, and other inorganic salts from the soil to maintain its reproductive development (Beringer and Taha, 1976). Calcium-deficient soil may result in the termination of pods expansion and eventually lead to embryo abortion. By contrast, peanuts will produce filled pods when sufficiently supplied with calcium (Jain et al., 2011). Therefore, the development of peanut pod is extremely sensitive to calcium, and free-Ca^{2+} deficiency in the field will greatly reduce the yield of peanut.

Ca^{2+}, a universal second messenger, plays an important role in plant growth and development, including cell division and apoptosis, polarity formation, differentiation and senescence (Hepler, 2005; Zhang et al., 2017). In our previous study, we reported that free-Ca^{2+} deficiency results in peanut dwarfism, and Ca^{2+}/CaM signal transduction pathway was involved in the turnover of PSII reaction center components to alleviate the damage of photoinhibition to PSII (Yang et al., 2013, 2015). However, little was known about the regulation of calcium on the development of peanut pods over the last century. With the development of molecular biological techniques, the transcriptome and proteomics benefited the peanut genomics research, and was applied in the seed development. Recently, several studies have compared genes and proteins between the aerial and underground peanut pods (Zhu et al., 2013). Chen et al. (2013) speculated that categories in the photosynthetic pathway were altered greatly in aerial gynophores, while the growth regulators such as IAA, ABA and kinetin may be the key factors contributing to the swelling of the subterranean pods. Other studies have explored changes in the gene expression at the different developmental stages of the gynophores. Xia et al. (2013) assembled 13 million short sequences into 72,527 unigenes to study peanut gynophores in three developmental stages. The results showed that numerous enzymes involved in plant hormone biosynthesis and signaling pathway, as well as light signaling, changed significantly when the ovary began to enlarge. These candidate genes and proteins have been identified to understand the regulation mechanisms that control the development of peanut pods and provide valuable resource to illustrate the specific mechanism of calcium signaling on pod development.

Digital gene expression (DGE) profiling, by comparing reads with the reference genome, can comprehensively and rapidly detect the specific gene expression of a particular species and distinguish the differences in the expression of poorly expressed genes (Glazinska et al., 2017). However, only reference transcripts from wild peanuts, not those of the cultivated peanut, have been published. Therefore, transcriptome profilings obtained from a mixture of all samples tested in our study will supply the data for the reference genome. Transcriptome sequencing can be used to sequence all mRNAs transcribed by eukaryotes, specific tissues, or cells in a particular state, and also analyze the structure of the genes and new transcripts produced (Sathiyanathan et al., 2017). This method has been widely applied in *Arabidopsis* and other model plants, e.g., rice and soybean, and has gradually become a useful tool in biological research.

In this study, RNA-Seq and digital gene profiling were combined to investigate and compare differentially expressed genes (DEGs) between aerial gynophores and underground pods grown under free-Ca^{2+}-sufficient or deficient Our objectives were to: (1) compare the DEGs of aerial gynophores between free Ca^{2+} sufficiency and free Ca^{2+} deficiency treatments, (2) identify candidate genes related to pod swelling affected by calcium, (3) find out the main regulatory pathways of calcium to promote pod development.

MATERIALS AND METHODS

Plant Materials and Treatments

The *Arachis hypogaea* "XiangHua 2008," a peanut cultivar from the Hunan Agriculture University, was used as material. The red soil overburden including exchangeable calcium 0.74 cmol(1/2 Ca^{2+})/kg in Gengyuan practice base, Hunan Province of China, was used for the free Ca^{2+} deficient treatment. The soil fertilized with 100 kg plaster (CaO) per 667 m^2 was used as free Ca^{2+} sufficiency treatment. CaO was applied before sowing.

The Method of Sampling

In peanut production, 15 days after pegging (DAP) was confirmed to be the most sensitive period for the free Ca^{2+} content in the soil. In this study, gynophores under free Ca^{2+}-deficient treatment 1 (GD1), free Ca^{2+}-deficient treatment 2 (GD2), free Ca^{2+}-sufficient treatment 1 (GS1), free Ca^{2+}-sufficient treatment 2 (GS2), as well as pods under free Ca^{2+}-deficient treatment 1 (PD1), free Ca^{2+}-deficient treatment 2 (PD2), free Ca^{2+}-sufficient treatment 1 (PS1), and free Ca^{2+}-sufficient treatment 2 (PS2), were harvested, frozen in liquid nitrogen and then stored at −70°C. The 8 samples were used to detect global changes in gene expression. Two biological replicates were used in this study. The mixed samples were used in transcriptome sequencing.

RNA Extraction and Sequencing

Total RNA was isolated from the harvested materials using the total RNA extraction Kit (TaKaRa, Inc., Dalian, China) according to the manufacturer's instructions. Agilent 2100 and NanoDrop were used to detect RNA quality and purity. Only high-quality RNA samples were chosen for RNA-seq analyses. Beads with Oligo (dT) were used to enrich for mRNA and the RNA was fragmented into short fragments. First-strand cDNA was synthesized using random hexamer primers and buffer, while dNTPs, RNaseH and DNA polymerase I were added to synthesize the second strand (Wang et al., 2009). After purification, the short fragments were then connected using sequencing adapters. Finally, the library was sequenced from directions on Illumina HiSeq™ 2000 System (Illumina, San Diego, CA). Data analysis and base calling were achieved by applying the Illumina instrument software. Whole dataset has been deposited in the NCBI Sequence Read Archive with accession number SRX1795063.

Digital Expression Profile Analysis

Differential expression profiling was conducted among the gynophores and pods under free- Ca^{2+}-deficient or sufficient treatments. Prior to further analysis, raw data should be filtered to decrease data noise and obtain clean data (Cock et al., 2010). Gene expression level was quantified by a software package RNASeq by Expectation Maximization (*RSEM*). *RSEM* computes maximum likelihood abundance estimates using the Expectation-Maximization (EM) algorithm for its statistical model, including the modeling of paired-end (PE) and variable-length reads, fragment length distributions, and quality scores, to determine which transcripts are isoforms of the same gene (Li and Dewey, 2011). Fragments per kilobase of exon per million fragments mapped (FPKM) method was used to calculate the expression level as follows: $FPKM = [10^6C/(NL/10^3)]$, where FPKM is the expression of gene A, C is the number of fragments uniquely aligned to gene A, N is the total number of fragments uniquely aligned to all genes, and L is the number of bases on gene A (Ning et al., 2013). The FPKM method can eliminate the influence of different gene lengths and sequencing discrepancy on the calculation of gene expression. The intensity values of each sample were further transformed on log2-scale and used to analyze differential expression. The probe sets with $P < 0.01$ in at least one of the comparisons were considered as DEGs for further analysis. The WEGO software was used to obtain gene ontology (GO) annotations for the DEGs, while pathway analyses were used to analyze KEGG and BLASTX ($E < 0.00001$) against the NCBI Nr database (Ye et al., 2006).

The contents of endogenous hormone indole acetic acid (IAA) and gibberellin (GA_3) were determined by enzyme linked immunosorbent assay (ELISA), which was performed as a commercial service in China agricultural university.

Quantitative Real Time PCR (qRT-PCR) Analysis

Gynophores and pod samples under the same treatments as those in RNA-seq were analyzed using qRT-PCR. cDNAs were reverse transcribed using the PrimeScript™ first-strand cDNA synthesis kit (K1622 Thermo scientific). The PCR was amplified using SYBR Premix Ex Taq™ following the manufacturer's instructions (TaKaRa, Inc., Dalian, China) with the qRT-PCR amplification instrument (ABI 7500, USA). The target gene primers (**Table S3**) were designed to detect the sample mRNA. Tua5-F and Tua5-R were used as controls to normalize the expression data (Yang et al., 2013). The relative gene expression was calculated using the $2^{-\Delta\Delta CT}$ method as described by Livak and Schmittgen (2001). For log_2-transformed FPKM values, the maximum expression level of each selected gene was considered to be 100, and the expression levels of the other genes were transformed accordingly (Zhang et al., 2016).

RESULTS

Transcriptome Sequencing and Data Analysis

Ca^{2+} deficiency in soil induces early embryo abortion in peanuts, and this process produces empty pods. This phenomenon was verified by the full pod number and dry weight of pods (**Table 1**). In our study, we attempted to reveal the molecular mechanism of the effect of free calcium on the development of peanut pods using a RNA-seq approach. A total of 99,030,828 clean reads with an average length of 90 bp, which corresponded to approximately 8.91 gigabase pairs (Gb) of raw data, were obtained. An overview of the sequencing and assembly is outlined in **Table S1**. 141,819 contigs with an average length of 391 bp were produced. Among these contigs, the length of 81,881 (57.73%) from 100 to 200 bp, 18,847 (13.28%) from 200 to 300 bp, 9256 (6.52%) from 300 to 400 bp, 5633 (3.97%) from 400 to 500 bp, and 26,202 (18.47%) were more than 500 bp in length. The results of the assembly showed 102,819 unigenes with a total length of 102.72 Mb and an average of 999 bp. Of these, the length of 46,924 (45.63%) were from 100 to 500 bp, 17,974 (17.48%) from 500 to 1,000 bp, 12,891 (12.53%) from 1,000 to 1,500 bp, 10,011 (9.73%) from 1,500 to 2,000 bp, and 15,019 (14.60%) were more than 2,000 bp (**Figure S1**). The length of assembled sequences is a criterion for successful assembly. We calculated the length distribution of contigs and unigenes, and the results showed that the Illumina sequencing solution was reproducible and reliable (**Figure S1**).

TABLE 1 | The effects of calcium treatment on peanut phenotype.

Treatment	Branch number	Dry weight of root and shem (g)	Full pod number	Dry weight of pods (g)
CK	11.67 ± 1.15a	9.82 ± 1.21a	9.33 ± 0.58a	23.65 ± 1.57a
NC_{12}	16.67 ± 1.15b	15.25 ± 1.37b	16.67 ± 1.15b	33.65 ± 1.68b

a, b means significant difference compared with CK and calcium-treated plants (NC12) using Student's t-test at P < 0.05.

Unigene Function Annotation

Functional annotation of unigenes gives protein functional annotation, COG functional annotation and Gene Ontology (GO) functional annotation. Unigenes were annotated with the databases of NR, NT, Swiss-Prot, KEGG, COG, and GO. Then the number of annotated unigenes was counted with each database (**Figure 1**). Analysis of species distribution showed that 42.2% of the unigenes were homologous with the sequence of *Glycine max*, and 13.8, 13.1 and 11.5% of the unigenes with the sequence of *Cicer arietinum*, *Phaseolus vulgaris*, and *Medicago truncatula*, respectively (**Figure 2**).

We use Blast2GO program with NR annotation to obtain the GO annotation of the unigenes. GO has three ontologies: molecular function, cellular component and biological process. Every GO-term belongs to a type of ontology (Conesa et al., 2005). **Figure S2** showed that the sequences were categorized into 55 functional groups according to the sequence homologies. We mapped the unigenes to the COG database to further predict the possible functions and statistics. In the 25 COG categories, general function prediction (7,524, 32.03%) represented the largest group, followed by transcription (4,202, 17.89%), and replication, recombination, and repair (4,128, 17.57%) (**Figure S3**).

A total of 14,985 sequences, containing 18,215 potential EST-SSRs, were detected with software MicroSAtellite (MISA). The quantity statistics of SSR classification showed that tri-nucleotide (40.86%) was the most abundant type of repeat motif,

followed by di-nucleotide (29.94%), mononucleotide (21.61%), hexa-nucleotide (2.67%), quad-nucleotide (2.53%), and penta-nucleotide (2.38%) repeat units (**Table S2**). Within the cSSRs detected, AG/CT represented the dominant type, followed by AAG/CTT, ATC/ATG, and AAT/ATT (**Figure S4**).

Digital Gene Expression (DGE) Profiling

Eight DGE libraries were created from four independent biological samples using gynophores and pods with free Ca^{2+}-deficient or -sufficient treatments as described in the method section. The clean reads (in millions) obtained from the different libraries were as follows: GD1, 14.91; GD2, 15.59; GS1, 14.54; GS2, 14.34; PD1, 16.02; PD2, 16.67; PS1, 14.19; and PS2, 12.84. The saturation analysis showed that when the number of reads reached a certain amount, the growth curve of detected genes tended to flatten in all libraries, indicating that the sequencing was saturated for gene identification (**Figure S5**).

GO annotation of the DEGs from two pairwise comparisons (GD/GS and PD/PS) was used to classify genes into different sub-categories belonging to the three main GO categories. In the biological process category, we identified three abundant sub-categories across both comparisons, namely, metabolic process, cellular process, and single organism process. Cell, cell part, and membrane were the main sub-categories identified in the cellular component category, while catalytic activity and binding dominated the molecular function category (**Figure 3**).

KEGG enrichment analysis allowed the mapping of DEGs to different pathways. The top 20 pathways in each pairwise comparison (mentioned above) are shown in **Figure S6**. DEGs were mainly enriched in photosynthesis, phagosome, glycolysis/gluconeogenesis, isoflavonoid biosynthesis, glycosylphosphatidylinositol (GPI)-anchor biosynthesis, carbon metabolism, and ABC transporters in GD-VD-GS. Meanwhile, circadian rhythm-plant,

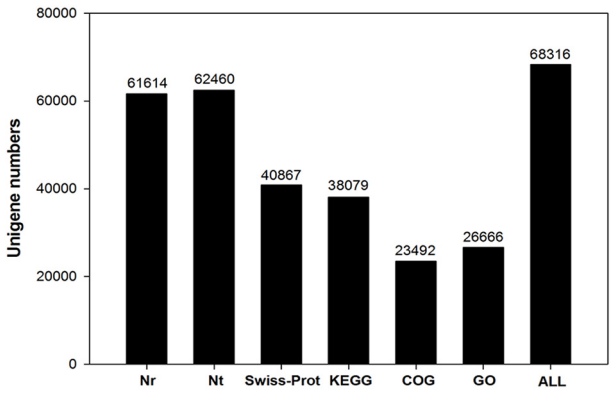

FIGURE 1 | The unigene number annotated in six public database searched.

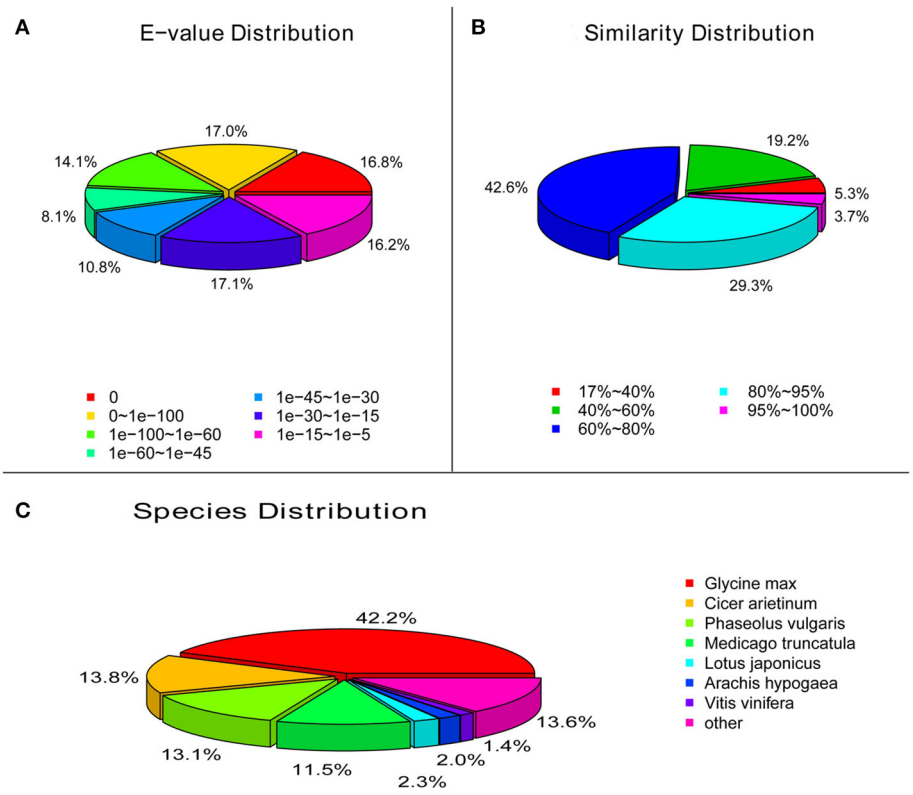

FIGURE 2 | Characteristics of similarity search of unigenes against Nr database. **(A)**, *E*-value of BLAST hits for each unigene. **(B)**, Similarity distribution of the top BLAST hits for each unigene. **(C)**, Species distribution of the top BLAST hits for each unigene in Nr database.

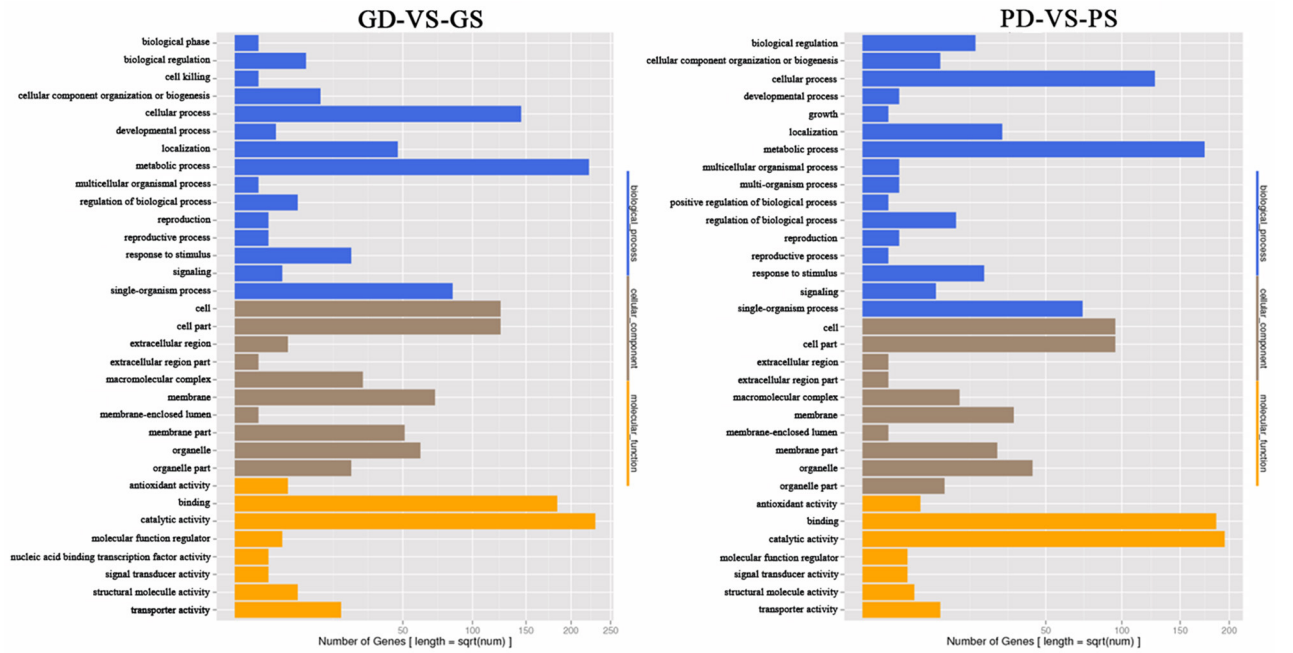

FIGURE 3 | GO annotation of the DEGs from the two pairwise comparisons (GD/GS, PD/PS).

plant hormone signal transduction, phagosome, isoflavonoid biosynthesis, glycolysis/gluconeogenesis, fatty acid metabolism, and biosynthesis of unsaturated fatty acids were mainly enriched in PD-VD-PS.

Analysis and qRT-PCR Validation of DGE Results

FPKM method was used to calculate the gene expression level. The reference transcripts of a progenitor of cultivated peanut (*Arachis ipaensis*) and our transcriptome data were used to generate an integrated reference library. For result list of each control-case pair, we draw scatter plots of all expressed genes, different color presents up-regulated, down-regulated or non-regulated genes. The total number of DEGs for each comparison was observed, and a histogram was drawn to show the number of significantly up-regulated or down-regulated genes in each control–case pair (**Figure 4**).

In order to confirm the transcriptome sequencing results, 10 DEGs in GS, GD, PS, and PD were selected randomly for qRT-PCR to analyze the expression levels. The selected genes participate in calcium signal transduction and phytohormone biosynthesis pathway, material biosynthesis, transcription factor and transporter. The consistency of trends between qRT-PCR and RNA-seq data indicated the credibility of the RNA-seq data (**Figure 5**).

Comparative Analysis of Genes between GD and GS

More than 20 unigenes annotated as transcription factors including NAC, WRKY, bHLH, and ethylene-responsive transcription factors were regulated in GS, while M1/AGAMOUS/DEFICIENS/SRF (MADS) transcription factor family were down-regulated in GS compared with GD. Contrary to the DEGs in pods, no significant difference in calcium-related genes between GD and GS was found, while the expression of some calcium-binding proteins (CBPs), and calcium-binding transcription factors were up-regulated in GS (**Table S4**).

The expression pattern of lipoxygenases (*LOX*) genes showed higher expression level in GS and the expression levels of 6 *LOX* genes were more than 2 times higher in GS than that in GD. Genes related to hormone response were screened out by GO analysis. Several DEGs involved in biosynthesis process and signaling pathway of gibberellin (GA), auxin, ABA, and brassinosteroid were up-regulated in GS at this stage. e. Numerous transporter-related genes were screened from DEGs based on GO analysis. Several energy- and substance-related transporter genes, including sugar transporter, carbohydrate transmembrane transporter, lipid transporter, protein transmembrane transporter, inositol transporter, zinc transporter, sulfate transporter, and nucleobase transporter were all up-regulated in GS. Meanwhile MFS transporter, ABC transporter and myo-inositol transporter had both up-regulated and down-regulated. Only the peptide/histidine transporter was down-regulated in GS (**Table S4**).

Differentially Expressed Genes between PD and PS

We identified the DEGs between PD and PS considering that calcium plays an important role in the development of

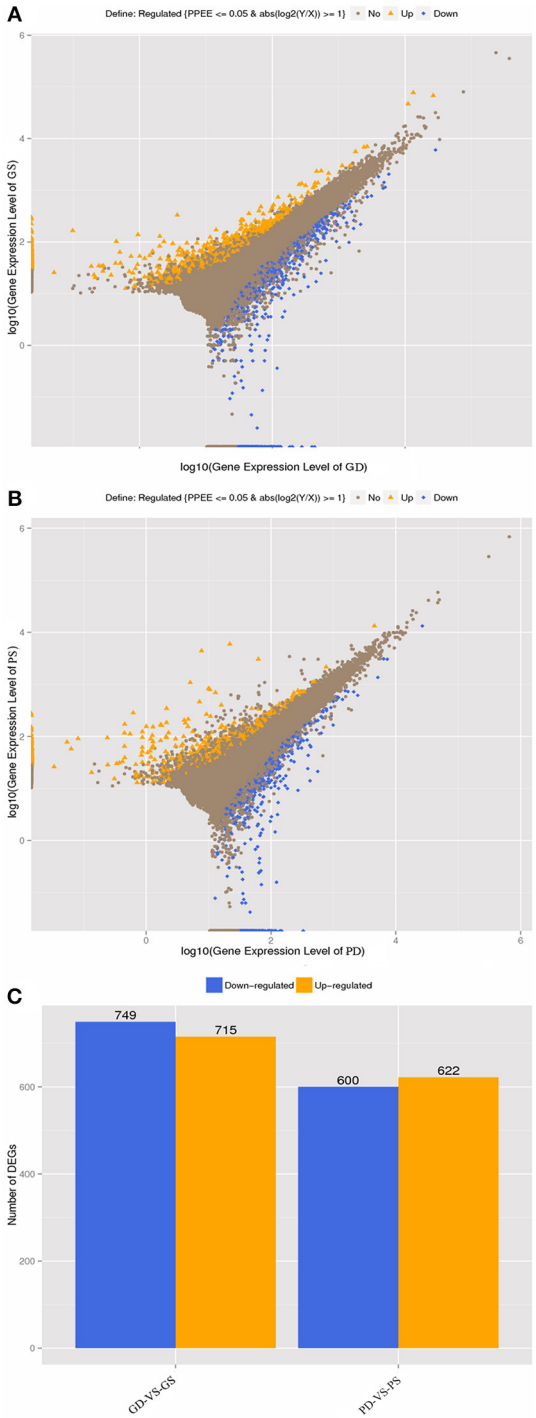

FIGURE 4 | Differentially expressed genes in GD, GS, PD, and PS. **(A)**, gene expression level (GD-vs.-GS). **(B)**, gene expression level (PD-vs.-PS). **(C)**, Statistic of differentially expressed genes between GD-vs.-GS and PD-vs.-PS, respectively.

peanut pods. Unigenes encoding proteins involved in calcium signaling transduction pathways such as calcium-dependent protein kinases (CDPKs), calcium-binding protein (CBP) and calmodulin (CaM)-binding protein were up-regulated under free Ca^{2+}-sufficient conditions. In particular, the expression of Ca^{2+}-related protein mitogen-activated protein kinase kinase kinase (MAPKKK) was also higher in PS than that in PD (**Table S5**).

Two categories of plant hormone-related genes (auxin and GA) showed significantly different expression between PD and PS. The auxin-related genes including 7 auxin response factors (ARFs) and 1 indole-3-acetic acid-amido synthetase were up-regulated in PS. Two selected DEGs, namely, GA 20-oxidase and GA receptor GID1, were up-regulated, while GA 2-oxidase, which is one of the key enzymes that catalyzes the inactivation of biological GA, was down-regulated in PS. Meanwhile, the ent-kaurenoic acid oxidase (KAO), an important enzyme in GA biosynthesis (Yamaguchi and Kamiya, 2000; Paparelli et al., 2013), was up-regulated under free Ca^{2+}-sufficient conditions. These results were in agreement with the high contents of IAA and GA_3 in PS (**Figure 6**). Thus, our results indicated that the up-regulated calcium-related genes increased GA level, which may play an important role in the early embryo development.

Genes encoding storage protein oleosin and some synthetases, such as tetrahydrocannabinolic acid synthase, long chain acyl-CoA synthetase, and callose synthase, exhibited higher level (5–8-folds) under free-Ca^{2+}-sufficient conditions. In addition, eight lipoxygenase were also up-regulated in PS. Previous studies indicated that lipoxygenase is the first key enzyme in the synthesis pathway of jasmonic acid, which plays an important role in the germination, growth, and stress resistance of plant seeds (Rahimi et al., 2016). GIGANTEA, a gene involved in circadian clock and phytochrome signaling (Cha et al., 2017), was down-regulated in PS (**Table S5**). This phenomenon may be due to the fact that this light response gene cannot play a regulatory role in the subterranean areas, because darkness is also a prerequisite for the normal development of peanut pods.

DISCUSSION

Early embryonic development is an important period for the formation of peanut yield and quality. Accumulating evidence illustrated that this complex process is regulated by light, endogenous hormones and environment stimuli. Ca^{2+} deficiency in this process leads to early embryo abortion in peanut, resulting in unfilled pod and reduced peanut yield. This phenomenon is a long-term concern in the acidic red-yellow soil in southern China (Zhang et al., 2007). *AhCYP707A4*A has been identified to regulate embryo abortion induced by Ca^{2+} deficiency using SSH cDNA libraries associated with library lift (SSHaLL) (Chen et al., 2015). However, SSHaLL is a less sensitive method that cannot detect the gene expression of whole species. Thus, this process provides limited information, and the underlying mechanism remains unclear.

De novo transcriptome sequencing facilitates the complete and rapid acquisition of almost all transcripts of a particular organ or tissue of a species based on high-throughput technologies. In this study, we characterized and compared gene expression profiles in gynophores and pods under free Ca^{2+}-sufficient or free Ca^{2+}-deficient treatment to identify candidate genes

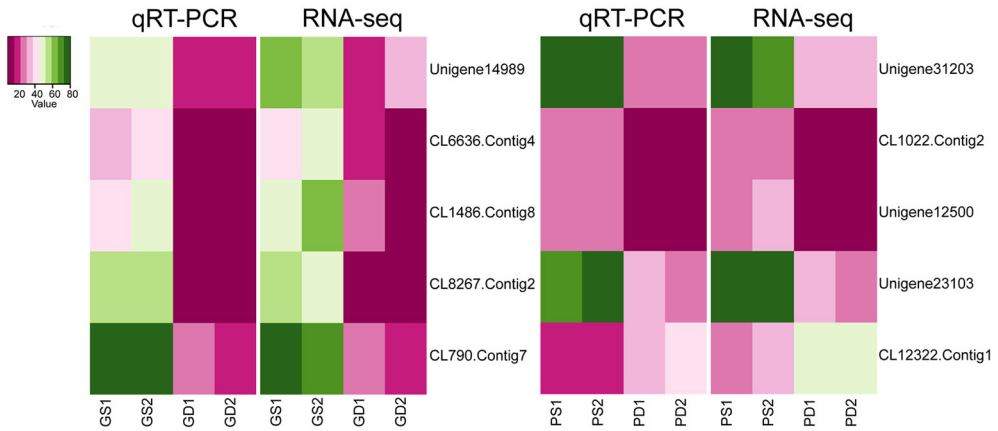

FIGURE 5 | qRT-PCR verification of expression of selected genes.

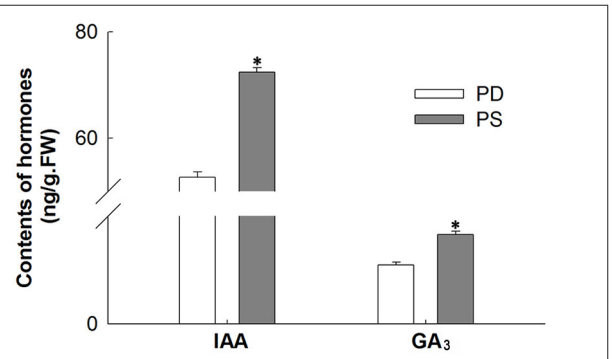

FIGURE 6 | Compare IAA and GA_3 contents between PS and PD. *Significant difference compared PD with PS using Student's *t*-test at $P < 0.05$.

related to Ca^{2+} regulation on pod development. Our project was sequenced on the platform of Illumina Hiseq 2000. A total of 9,903,082,800 nt bases were generated. For function annotation analysis, we obtained 61,614, 62,460, 40,867, 38,079, 23,492, and 26,666 unigenes annotated to the NR, NT, Swiss-Prot, KEGG, COG, GO database, respectively (**Figure 1**). The total number of SSR was 18,215 (**Figure S4**). These unigenes and the reference transcripts of *Arachis ipaensis* can serve as reference sequences to determine the regulation pathway of calcium on peanut pod development.

In recent years, with widespread application of sequencing technology, transcriptome and proteomics provide views to explore the mechanism of the development of aerial peg and swelling of underground pod (Chen et al., 2013). The mechanisms of calcium on the aerial and underground part of peanut have not been reported yet. In our study, MADS-box family was significantly up-regulated in gynophores under calcium-deficient condition (**Table S4**). MADS box transcription factors are mainly known as key regulators of seed and flower development in *Arabidopsis*. Overexpression of *OsMADS45* induces early flowering and premature senility of gynophores (Wang et al., 2013; Yu et al., 2017). Hence, calcium deficiency probably prevented the swelling of the gynophores to form a pod and resulted in abortion. LOXs, which are key genes that play important roles in the production of growth regulators and the mobilization of stored lipids during seed germination, exhibited differential transcription levels in GS and GD (Gao et al., 2011). The up-regulated expression of LOXs in GS is likely to provide sufficient nutrient preparation for pod development. Combined with the high expression of several energy- and substance-related transporter genes, which play critical roles in nutrient uptake and signal transduction (Leem et al., 2016), exogenous calcium probably promotes nutrient storage in the aerial gynophores, ascertaining the early development of pod.

Members of the Ca^{2+} signaling pathway, including CaM-binding protein, CDPK, and MAPKKK, were found to be highly expressed in PS (**Table S5**). CaM has no inherent catalytic activity, and requires the modulation of its downstream binding proteins to function (Leba et al., 2012; Poovaiah et al., 2013). Thus, CaM has an effect on transmitting the calcium signals to downstream proteins and regulating plant growth and development. CDPKs, which are calcium sensors, are also implicated in the growth of plants, such as pollen development and gravitropism, and their response to environment stresses, such as pathogens (Ormancey et al., 2017). The MAPK cascade consists of interlinked MAPK, MAPKK, and MAPKKK and such cascades play important roles in signal transduction of plant hormone, biotic stress and abiotic stress (Wang et al., 2017). By contrast, in aerial gynophores, no significant difference was found in the Ca^{2+} sensors between GD and GS, and only some CBPs and calcium-binding transcription factors were up-regulated in GS. It is probably interesting to investigate that calcium signal transduction pathway may participate in regulating the development of peanut pod.

Several studies have indicated that plant hormones, such as auxin, kinetin, ABA, and ethylene, can temporally and spatially coordinate the elongation of gynophore and swelling of pod (Jacobs, 1951; Ziv and Zamski, 1975; Shlamovitz et al., 1995). In this study, several enzymes in the synthesis pathway of GA were screened out to determine significant DEGs in pods between Ca^{2+}-sufficient and Ca^{2+}-deficient conditions,

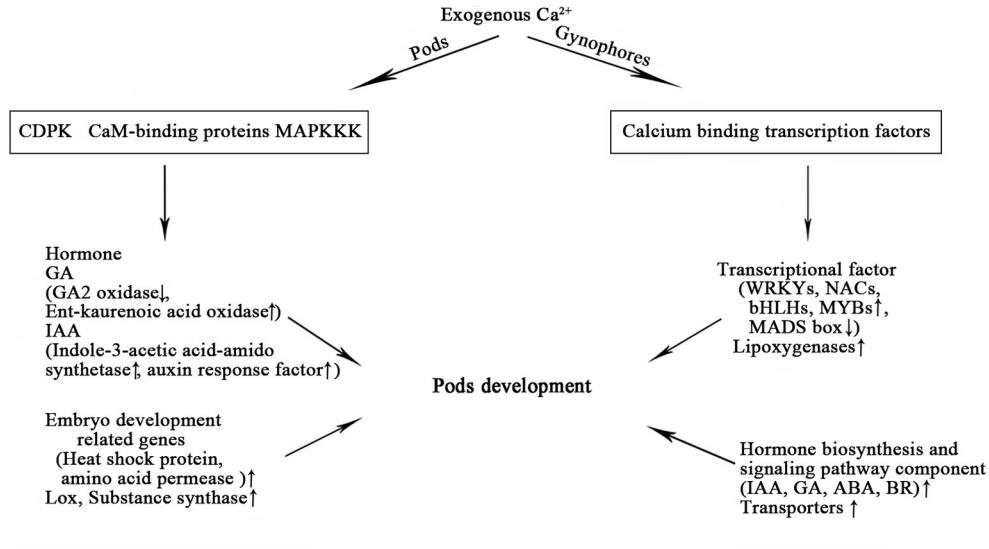

FIGURE 7 | Identified DEGs from gynophores and pods under free Ca^{2+} sufficient treatment and their functions during early pod development.

which were not found in gynophores. Low expression of GA_2-oxidase and high expression of ent-kaurenoic acid oxidase under sufficient exogenous calcium eventually led to high contents of GA (**Figure 6**). GA is reported to be required to enhance seed germination, and the increase in the synthesis of active GA contributes to the promotion of seed germination (Song et al., 2011). Therefore, calcium may promote peanut seed germination and development through GA biosynthesis pathway. This novel discovery has not been reported in previous studies. Auxin plays a critical role in plant organ development. Genes encoding auxin response factors (ARF) and indole-3-acetic acid-amido synthetase exhibited increased changes in the PS (**Table S5**). ARF is a transcription factor that activates or represses the expression of auxin response genes. In *Arabidopsis*, ARF5 can promote the development of cotyledon by recruiting DRN expression, and to a great extent, ABA function in seed germination depends on the TIR1/AFB-AUX/IAA-ARF–mediated auxin signaling pathway (Liu et al., 2013). Therefore, the mechanism by which auxin-related genes identified in our study respond to calcium signaling during peanut seed development needs further research. The change in these hormones under sufficient calcium condition is beneficial for the normal development of peanut pod. Thus, the results elucidate a crucial mechanistic role of calcium on pod development. On the one hand, calcium enhanced the storage of aerial nutrients. On the other hand, it activated calcium signaling pathways and hormone-related genes in embryonic development (**Figure 7**). All these elements ensure the normal development of pods.

CONCLUSION

In this study, we performed a comparative transcriptome and differential expression analysis of peanut gynophores and pods under free Ca^{2+} sufficient and deficient conditions, respectively. Transcription factors including WRKY, NAC, bHLH, and MADS-box transcription factors were found up-regulated in GS, while MADS transcription factor family were down-regulated in GS compared to GD. Genes involved in plant hormone biosynthesis and transporters were found to be differentially expressed in the GS and GD. Different from the aerial part of peanut, genes involved in calcium signaling transduction pathways were identified up-regulated in pods when free Ca^{2+} was sufficient. In addition, hormone and embryo-related genes also showed differentially expressed between PD and PS. To our best knowledge, we firstly provided mechanism of exogenous calcium on the aerial and underground parts of peanut at the early stage of seed development.

AUTHOR CONTRIBUTIONS

SW and XL designed the experiment and drafted the manuscript. SY and LL carried out most of the experiment, analyzed the transcriptome and digital gene expression data, wrote the methods part of the manuscript. JZ, FG, and JM performed experiments, JW, NS, and YG grew the plants and prepared the samples. All authors read and approved the final manuscript.

ACKNOWLEDGMENTS

This work was supported by Natural Science Foundation of Shandong Province (ZR2015YL077, BS2015SW020), Youth Scientific Research Foundation of Shandong Academy of Agricultural Sciences (2015YQN02, 2014QNM38, 2015YQN12), National Natural Science Foundation of China (31571581, 31571605), the Supporting Plan of National Science and Technology of China (2014BAD11B04), Major Projects of

Science and Technology Innovation in Shandong Academy of Agricultural Sciences (2014CXZ06-6).

SUPPLEMENTARY MATERIAL

The Supplementary Material for this article can be found online at: http://journal.frontiersin.org/article/10.3389/fpls.2017.01609/full#supplementary-material

Figure S1 | The length distribution of contigs and unigenes.

Figure S2 | GO classification analysis of unigenes in All-unigene. GO functions is showed in X-axis. The right Y-axis shows the number of genes which have the GO function, and the left Y-axis shows the percentage.

Figure S3 | Clusters of orthologous groups (COG) classification of Unigenes in All-Unigene.

Figure S4 | Quantity statistics of SSR classification. The X-axis is the repeat times of repeat units. The Y-axis is the number of SSRs.

Figure S5 | Sequence saturation analysis of eight samples. The X-axis shows the number of clean reads, units is 100 k, the Y-axis shows the number of genes, units is %.

Figure S6 | Scatter plot of top 20 KEGG pathways of two pairwise comparisons (GD/GS, PD/PS).

Table S1 | Summary for the transcriptome sequencing and assembly.

Table S2 | Summary of EST-SSR searching results.

Table S3 | Gene-specific primers used in quantitative real-time PCR.

Table S4 | Differentially expressed genes between GD and GS.

Table S5 | Differentially expressed genes between PD and PS.

REFERENCES

Arya, S. S., Salve, A. R., and Chauhan, S. (2016). Peanuts as functional food: a review. *J. Food Sci. Technol.* 53, 31–41. doi: 10.1007/s13197-015-2007-9

Beringer, H., and Taha, H. A. (1976). ^{45}Ca absorption by two cultivars of groundnut (*Arachis hypagea*). *Exp. Agric.* 12, 1–7. doi: 10.1017/S0014479700006992

Cha, J. Y., Kim, J., Kim, T. S., Zeng, Q., Wang, L., Lee, S. Y., et al. (2017). GIGANTEA is a co-chaperone which facilitates maturation of ZEITLUPE in the *Arabidopsis* circadian clock. *Nat. Commun.* 8:3. doi: 10.1038/s41467-016-0014-9

Chen, H., Zhang, C., Cai, T. C., Deng, Y., Zhou, S. B., Zheng, Y. X., et al. (2015). Identification of low Ca^{2+} stress-induced embryo apoptosis response genes in *Arachis hypogaea* by SSH-associated library lift (SSHaLL). *Plant Biotechnol. J.* 14, 682–698. doi: 10.1111/pbi.12415

Chen, X., Zhu, W., Azam, S., Li, H., Zhu, F., Li, H., et al. (2013). Deep sequencing analysis of the transcriptomes of peanut aerial and subterranean young pods identifies candidate genes related to early embryo abortion. *Plant Biotechnol. J.* 11, 115–127. doi: 10.1111/pbi.12018

Chen, Y. N., Wei, W. H., Ren, X. P., Zhao, X. Y., Zhou, X. J., Huang, L., et al. (2014). Construction of a high-quality genomic BAC library for Chinese peanut cultivar Zhonghua 8 with high oil content. *Bot. Stud.* 55:8. doi: 10.1186/1999-3110-55-8

Cock, P., Fields, C. J., Goto, N., Heuer, M. L., and Rice, P. M. (2010). The Sanger FASTQ file format for sequences with quality scores, and the Solexa/Illumina FASTQ variants. *Nucleic Acids Res.* 38, 1767–1771. doi: 10.1093/nar/gkp1137

Conesa, A., Gotz, S., Garcia-Gomez, J. M., Terol, J., Talon, M., and Robles, M. (2005). Blast2GO: a universal tool for annotation, visualization and analysis in functional genomics research. *Bioinformatics* 21, 3674–3676. doi: 10.1093/bioinformatics/bti610

Gao, G. L., Zhang, S. C., Wang, C. F., Yang, X., Wang, Y. Q., Su, X. J., et al. (2011). Arabidopsis *CPR5* independently regulates seed germination and postgermination arrest of development through LOX pathway and ABA signaling. *PLoS ONE* 6:e19406. doi: 10.1371/journal.pone.0019406

Glazinska, P., Wojciechowski, W., Kulasek, M., Glinkowski, W., Marciniak, K., Klajn, N., et al. (2017). *De novo* Transcriptome profiling of flowers, flower pedicels and pods of *Lupinus luteus* (Yellow Lupine) reveals complex expression changes during organ abscission. *Front. Plant Sci.* 8:641. doi: 10.3389/fpls.2017.00641

Hepler, P. K. (2005). Calcium: a central regulator of plant growth and development. *Plant Cell.* 17, 2142–2155. doi: 10.1105/tpc.105.032508

Jacobs, W. P. (1951). Auxin relationships in an intercalary meristem: further studies on the gynophore of *Arachis hypogaea* L. *Am. J. Bot.* 38, 307–310. doi: 10.2307/2438005

Jain, M., Pathak, B. P., Harmon, A. C., Tillman, B. L., and Gallo, M. (2011). Calcium dependent protein kinase (CDPK) expression during fruit development in cultivated peanut (*Arachis hypogaea*) under Ca^{2+}-sufficient and –deficient growth regimens. *J. Plant Physiol.* 168, 2272–2277. doi: 10.1016/j.jplph.2011.07.005

Leba, L. J., Perochon, A., Cheval, C., Ranty, B., Galaud, J. P., and Aldon, D. (2012). CML9, a multifunctional *Arabidopsis thaliana* calmodulin-like protein involved in stress responses and plant growth? *Plant Signal. Behav.* 7, 1121–1124. doi: 10.4161/psb.21308

Leem, K. H., Kim, M. G., Hahm, Y. T., and Kim, H. K. (2016). Hypoglycemic effect of *Opuntia ficus-indica* var. saboten is due to enhanced peripheral glucose uptake through activation of AMPK/p38 MAPK pathway. *Nutrients* 8:800. doi: 10.3390/nu8120800

Li, B., and Dewey, C. N. (2011). RSEM: accurate transcript quantification from RNA-Seq data with or without a reference genome. *BMC Bioinformatics.* 12:323. doi: 10.1186/1471-2105-12-323

Liu, X. D., Zhang, H., Zhao, Y., Feng, Z. Y., Li, Q., Yang, H. Q., et al. (2013). Auxin controls seed dormancy through stimulation of abscisic acid signaling by inducing ARF-mediated ABI3 activation in Arabidopsis. *Proc. Natl. Acad. Sci. U.S.A.* 110, 15485–15490. doi: 10.1073/pnas.1304651110

Livak, K. J., and Schmittgen, T. D. (2001). Analysis of relative gene expression data using real-time quantitative PCR and the 2(−delta delta C(T)) method. *Methods* 25, 402–408. doi: 10.1006/meth.2001.1262

Ning, L., Dawson, J. A., Thomson, J. A., Ruotti, V., Rissman, A. I., Smits, B. M. G., et al. (2013). EBSeq: an empirical Bayes hierarchical model for inference in RNA-seq experiments. *Bioinformatics* 29, 1035–1043. doi: 10.1093/bioinformatics/btt087

Ormancey, M., Thuleau, P., Mazars, C., and Cotelle, V. (2017). CDPKs and 14-3-3 Proteins: emerging duo in signaling. *Trends Plant Sci.* 22, 263–272. doi: 10.1016/j.tplants.2016.11.007

Paparelli, E., Parlanti, S., Gonzali, S., Novi, G., Mariotti, L., Ceccarelli, N., et al. (2013). Nighttime sugar starvation orchestrates gibberellin biosynthesis and plant growth in *Arabidopsis*. *Plant Cell.* 25, 3760–3769. doi: 10.1105/tpc.113.115519

Poovaiah, B. W., Du, L. Q., Wang, H. Z., and Yang, T. B. (2013). Recent advances in calcium/calmodulin-mediated signaling with an emphasis on plant-microbe interactions. *Plant Physiol.* 163, 531–542. doi: 10.1104/pp.113.220780

Rahimi, S., Kim, Y. J., Sukweenadhi, J., Zhang, D., and Yang, D. C. (2016). PgLOX6 encoding a lipoxygenase contributes to jasmonic acid biosynthesis and ginsenoside production in Panax ginseng. *J. Exp. Bot.* 67, 6007–6019. doi: 10.1093/jxb/erw358

Sathiyanathan, P., Tay, C. Y., and Stanton, L. W. (2017). Transcriptome analysis for the identification of cellular markers related to trabecular meshwork differentiation. *BMC Genomics* 18:383. doi: 10.1186/s12864-017-3758-7

Shlamovitz, N., Ziv, M., and Zamski, E. (1995). Light, dark and growth regulator involvement in groundnut (*Arachis hypogaea* L.) pod development. *Plant Growth Regul.* 16, 37–42. doi: 10.1007/BF00040505

Song, J., Guo, B. J., Song, F. W., Peng, H. R., Yao, Y. Y., Zhang, Y. R., et al. (2011). Genome-wide identification of gibberellins metabolic enzyme genes and expression profiling analysis during seed germination in maize. *Gene* 482, 34–42. doi: 10.1016/j.gene.2011.05.008

Wang, J. D., Lo, S. F., Li, Y. S., Chen, P. J., Lin, S. Y., Ho, T. Y., et al. (2013). Ectopic expression of OsMADS45 activates the upstream genes Hd3a and RFT1

at an early development stage causing early flowering in rice. *Bot. Stud.* 54:12. doi: 10.1186/1999-3110-54-12

Wang, L., Hu, W., Tie, W., Ding, Z., Ding, X., Liu, Y., et al. (2017). The MAPKKK and MAPKK gene families in banana: identification, phylogeny and expression during development, ripening and abiotic stress. *Sci. Rep*. 7:1159. doi: 10.1038/s41598-017-01357-4

Wang, Z., Gerstein, M., and Snyder, M. (2009). RNA-seq: a revolutionary tool for transcriptomics. *Nat. Rev. Genet.* 10, 57–63. doi: 10.1038/nrg2484

Xia, H., Zhao, C., Hou, L., Li, A. Q., Zhao, S. Z., Bi, Y. P., et al. (2013). Transcriptome profiling of peanut gynophores revealed global reprogramming of gene expression during early pod development in darkness. *BMC Genomics* 14:517. doi: 10.1186/1471-2164-14-517

Yamaguchi, S., and Kamiya, Y. (2000). Gibberellin biosynthesis: its regulation by endogenous and environmental signals. *Plant Cell Physiol.* 41, 251–257. doi: 10.1093/pcp/41.3.251

Yang, S., Wang, F., Wang, F., Meng, J. J., Li, X. G., Dong, S. T., et al. (2013). Exogenous calcium alleviates photoinhibition of PSII by improving the xanthophyll cycle in peanut (*Arachis hypogaea*) leaves during heat stress under high irradiance. *PLoS ONE* 8:e71214. doi: 10.1371/journal.pone.0071214

Yang, S., Wang, F., Guo, F., Meng, J. J., Li, X. G., and Wan, S. B. (2015). Exogenous calcium contributes to photoprotection and repair of photosystem II in peanut (*Arachis hypogaea* L.) leaves during heat stress under high irradiance. *J. Integr. Plant Biol.* 57, 486–495. doi: 10.1111/jipb.12249

Ye, J., Fang, L., Zheng, H., Zhang, Y., Chen, J., Zhang, Z., et al. (2006). WEGO: a web tool for plotting GO annotations. *Nucleic Acids Res*. 34, W293–W297. doi: 10.1093/nar/gkl031

Yu, L. H., Wu, J., Zhang, Z. S., Miao, Z. Q., Zhao, P. X., Wang, Z., et al. (2017). Arabidopsis MADS-box transcription factor AGL21 acts as environmental surveillance for seed germination by regulating ABI5 expression. *Mol. Plant* 10, 834–845. doi: 10.1016/j.molp.2017.04.004

Zhang, H. F., Wei, C. H., Yang, X. Z., Chen, H. J., Yang, Y. C., Mo, Y. L., et al. (2017). Genome-wide identification and expression analysis of calcium-dependent protein kinase and its related kinase gene families in melon (*Cucumis melo* L.). *PLoS ONE* 12:e0176352. doi: 10.1371/journal.pone.0176352

Zhang, J. C., Cai, N. B., Zhang, X. W., and Zhuang, W. J. (2007). Isolation and identification of specific expressed proteins from peanut (*Arachis hypogaea*) development/abortion embryo mediated by calcium. *Acta. Agronomica. Sinica*. 33, 814–819.

Zhang, Y., Wang, P. F., Xia, H., Zhao, C. Z., Hou, L., Li, C. S., et al. (2016). Comparative transcriptome analysis of basal and zygote-located tip regions of peanut ovaries provides insight into the mechanism of light regulation in peanut embryo and pod development. *BMC Genomics* 17:606. doi: 10.1186/s12864-016-2857-1

Zhu, W., Zhang, E. H., Li, H. F., Chen, X. P., Zhu, F. H., Hong, Y. B., et al. (2013). Comparative proteomics analysis of developing peanut aerial and subterranean pods identifies pod swelling related proteins. *J. Proteomics* 91, 172–187. doi: 10.1016/j.jprot.2013.07.002

Ziv, M., and Zamski, E. (1975). Geotropic responses and pod development in gynophore explants of peanut (*Arachis hypogaea* L.) cultured *in vitro*. *Ann. Bot*. 39, 579–583. doi: 10.1093/oxfordjournals.aob.a084968

Conflict of Interest Statement: The authors declare that the research was conducted in the absence of any commercial or financial relationships that could be construed as a potential conflict of interest.

frontiers in Plant Science

ORIGINAL RESEARCH
published: 27 September 2017
doi: 10.3389/fpls.2017.01688

ERECTA Regulates Cell Elongation by Activating Auxin Biosynthesis in *Arabidopsis thaliana*

Xiaoya Qu, Zhong Zhao and Zhaoxia Tian**

School of Life Sciences, University of Science and Technology of China, Hefei, China

The *ERECTA* family genes, *ERECTA (ER), ERECTA-LIKE1 (ERL1),* and *ERECTA-LIKE2 (ERL2),* encode leucine-rich repeat receptor-like kinases in *Arabidopsis thaliana.* Knocking out these three genes can cause severe phenotypes, which indicates that they play significant roles in plant growth and development. However, the molecular mechanism within remains unclear. Here we show that the short hypocotyl phenotypes of *er erl1 erl2* mutants are mainly due to the defects of cell elongation rather than the cell division. In contrast, in the *ERECTA* overexpression transgenic plants, the hypocotyl length is increased with elongated cells. Moreover, we show that the *er erl1 erl2* triple mutant contains a low level of auxin, and the expression levels of the key auxin biosynthesis genes are significantly reduced. Consistent with this observation, increasing exogenous or endogenous auxin levels could partially rescue the cell elongation defects of the *er erl1 erl2* triple mutant. Therefore, our results provide a molecular basis for auxin mediated *ERECTA* control of the hypocotyl length in *Arabidopsis thaliana*.

Keywords: *Arabidopsis*, *ERECTA*, auxin, hypocotyl length, cell elongation

OPEN ACCESS

Edited by:
Kai He,
Lanzhou University, China

Reviewed by:
Anja Thoe Fuglsang,
University of Copenhagen, Denmark
Yuxin Hu,
Institute of Botany (CAS), China

****Correspondence:***
Zhong Zhao
zhzhao@ustc.edu.cn
Zhaoxia Tian
zxtian@ustc.edu.cn

Specialty section:
This article was submitted to Plant Traffic and Transport, a section of the journal Frontiers in Plant Science

Received: *27 July 2017*
Accepted: *14 September 2017*
Published: *27 September 2017*

Citation:
Qu X, Zhao Z and Tian Z (2017) ERECTA Regulates Cell Elongation by Activating Auxin Biosynthesis in Arabidopsis thaliana. Front. Plant Sci. 8:1688. doi: 10.3389/fpls.2017.01688

INTRODUCTION

Plant cell size is one of the most important features in plant morphology, which is controlled strictly by the inheritance and influenced by the external environment. The cell size directly correlated with cell division and cell elongation. Schleiden and Schwann (1838-1839) established the "cell theory," which regard that the cell division and cell elongation activities determine the growth and development of living organism. Cell elongation is very important for the process of plant differentiation and morphogenesis of plant organs. The growth of hypocotyls in *Arabidopsis* is the elongation and division of hypocotyl cells in essence. In particular, the cell elongation growth plays a decisive role in hypocotyl length (Stuart et al., 1977; Fenwick et al., 1999). The hypocotyl is an important structure connecting root, shoot tip and leaves, and also an important channel for transporting water, nutrients and signaling molecules in *Arabidopsis*. At the same time, hypocotyls are very sensitive to endogenous signal molecules and external environment signal (Gray et al., 1998; Nozue et al., 2007; de Lucas et al., 2008; Christie et al., 2011; Sun et al., 2012). The morphological structure of *Arabidopsis thaliana* hypocotyl is simple, consisting of more than 20 cells in longitudinal direction, which is below cotyledons to the above of radicle. Because most of these cells are formed in the embryonic stage, only a few are produced by cell division after germination, suggests that the hypocotyl growth is mainly caused by the cell elongation (Gendreau et al., 1997). Therefore, the hypocotyl of *Arabidopsis* has become an important model system for studying plant cell elongation due to its simple structure and important physiological functions.

Plant hormones are important regulatory signal molecules of hypocotyl elongation, and auxin is one of the most important types. For a single cell, the main physiological function of auxin is to regulate cell elongation, and the effect of auxin on acceleration of cell elongation is very rapid, and the lag time from treatment to effectiveness is only about 10 min. Previous studies have found that mutants with excessive synthesis of auxin in light exhibit a longer hypocotyl length, while mutants with deficient synthesis of auxin have shorter hypocotyl length (Romano et al., 1991; Jensen et al., 1998; Zhao et al., 2001; Cheng et al., 2006). This indicates that an appropriate concentration of auxin is essential for the growth and development of hypocotyls. It has now been shown that the effect of auxin on hypocotyl length is achieved by stimulating the degradation of IAA3, which in turn causes the ARF transcription factor to be released (Vernoux et al., 2011; Oh et al., 2014). ARF transcription factors, especially ARF6 and ARF8, combine the signals from endogenous development and exogenous environments to control the elongation of hypocotyl cells by activating the expression of cell elongation factors such as *PRE*, *SAUR* family genes (Bai et al., 2012; Oh et al., 2014; Challa et al., 2016).

The intercellular communication is very important for the formation of normal tissues, organs and organisms of plants. The cell surface receptor protein kinase located on the cytoplasmic membrane plays a vital role in the initiation of cell signal transmission. The *ERECTA* (*ER*) gene in *Arabidopsis* encodes a leucine-rich repeat receptor-like protein kinase, whose protein structure consists of a hydrophobic signal peptide in the extracellular domain, a leucine repeat sequence for protein interaction, a single transmembrane domain, and intracellular serine/threonine kinase domain (Torii et al., 1996). *ERECTA* is widely expressed in plant tissues and plays an important role in plant development and responses to external environmental signals (Yokoyama et al., 1998; Shpak, 2013; Jorda et al., 2016; Gao et al., 2017). *ERECTA* knockout mutants show obvious dysplasia phenotypes, for instance, stem node, siliques and petiole become short and inflorescences are densely clustered. Although *Landsberg* deficit in *ERECTA* gene is widely used as an *Arabidopsis* ecotype, there is no in-depth study on how *ERECTA* gene mutations have led to such a markedly intense phenotype. In addition, *ERECTA*, as a multi-functional major gene in the plant, has two homologous genes *ERECTA LIKE 1* (*ERL1*) and *ERECTA LIKE 2* (*ERL2*), both of which have partial functional redundancy with *ERECTA*. The triple mutant *er erl1 erl2* intensifies *ERECTA* knockout mutant phenotype, and the plant is extremely dwarfed (Shpak et al., 2004). Previous studies have been shown that *ERECTA*, *ERL1* and *ERL2* play roles in the organ morphology and size determination in the reproductive stage of anthers and eggs by altering cell cycle progression (Shpak et al., 2004; Pillitteri et al., 2007). The mechanism of *ERECTA* gene family in cell-to-cell communication has been intensively studied in the stomatal development. *ERECTA* can recognize small peptide of the EPF/EPFL family, by forming a complex with TMM, affects stomatal development and differentiation by triggering MAPK cascade (Meng et al., 2012; Jewaria et al., 2013; Lin et al., 2017). However, the role of *ERECTA* family in the regulation hypocotyls remains unclear. Previous studies have shown that overexpression of *YUCCA5*, a member of *YUCCA* family of flavin monooxygenase in *Arabidopsis* auxin synthesis, inhibits mutant phenotype of *er-103* (one of the *ERECTA* mutants) (Woodward et al., 2005). In addition, *ERECTA* family regulates the transport of auxin by regulating the expression of *PIN1* at the initial stage of leaf primordia (Chen et al., 2013). However, the genetic interaction between the *ERECTA* family and auxin signaling in control of the hypocotyl development is still poorly understood.

In this study we found that, the hypocotyl lengths of single mutant *er-105* and triple mutant *er erl1 erl2* were significantly shorter than that of the wild type, whereas hypocotyls of ER-overexpressed plants was longer. We further showed that this change is due to a change in the length of a single cell in the hypocotyl rather than a change in the number of cells. In addition, we found that *DR5::GFP* signal of auxin reporter in the triple mutant *er erl1 erl2* was significantly reduced than that of wild type. Moreover, the transcriptional levels of auxin early response gene and the major auxin synthetase genes were significantly repressed in the *er erl1 erl2* triple mutant, suggesting that the auxin synthesis in the *er erl1 erl2* triple mutant is sabotaged. Consistent with the observation, the exogenous auxin and endogenous auxin were able to rescue the shortened hypocotyl and cell length phenotype of the *er erll erl2* triple mutant, indicating that these defects are due to the lack of auxin synthesis. Therefore we concluded that the *ERECTA* gene family controls the cell elongation in the hypocotyl by positively regulating the auxin biosynthesis in *Arabidopsis thaliana*.

MATERIALS AND METHODS

Plant Materials and Growth Conditions

All of the *Arabidopsis* lines used in this study were in the Col-0 background. The *ER* family mutants and overexpression plants have been described previously (Torii et al., 1996; Shpak et al., 2004; Shen et al., 2015). The seeds for *er-105*, *er-/- erl1+/- erl2-/-* mutant were kindly provided by Prof. Masao Tasaka (Nara Institute of Science and Technology). The seeds for *35S::ERECTA* were kindly provided by Prof. Zuhua He (Shanghai Institutes for Biological Sciences, Chinese Academy of Sciences). The seeds for *DR5::GFP-NLS* in wild type were kindly provided by Prof. Yuling Jiao (Institute of Genetics and Developmental Biology, Chinese Academy of Sciences). Other *Arabidopsis* seeds were obtained from self-preserved, genetic hybridization or agrobacterium-mediated transformation. All seeds were sterilized with 70% ethanol and 0.5% Tween for 10 min, followed by washing two times with 95% ethanol and air drying. After sterilization, seeds were sown onto 1/2 Murashige and Skoog (MS) medium containing 1% sucrose and 0.8% agar, then incubated at 4°C in darkness for 2 days, finally grown vertically at 21°C under long-day condition (16 h of light and 8 h of darkness).

Plasmid Construction

For construction of *pER::3 × VENUS-NLS*, a 1.4-kb upstream sequence of *ERECTA* before ATG was used as a promoter. For the

pERL1::3 × VENUS-NLS, a 4.1-kb upstream sequence of *ERL1* before ATG was used as a promoter. For the *pERL2::3 × VENUS-NLS*, a 3.6-kb upstream sequence of *ERL2* before ATG was used as a promoter. For construction of *pER::ER-GFP*, *pERL1::ERL1-GFP* and *pERL2::ERL2-GFP*, the genomic sequence of these three genes were amplified and used the same promoter we described above. The *pER::ER-GFP* construct was then transformed into the *er-105* mutant to rescue its defects, while other constructs were transformed into the Col-0. For p*ER::iaaM*, the 1.4-kb promoter of *ERECTA* was used to drive iaaM sequences that were obtained from Prof. Yunde Zhao (UC San Diego). This construct was then transformed into the *er-/- erl1+/- erl2-/-* mutant. The primer sequences used in the plasmid construction are listed in Supplementary Table S1.

Gene Expression Analysis

Whole seedlings were dissected and immediately transferred to liquid nitrogen. The Tripure Isolation Reagent (Roche) was used to isolate total RNA from the plant samples. The PrimeScriptTM RT Reagent Kit (TaKaRa) was used for cDNA synthesis. Quantitative PCR was performed with the Thermo PIKO REAL96 Real-Time PCR system using the GoTaq® qPCR Master Mix (Promega) with the following PCR conditions: 95°C for 5 min and 40 cycles of 95°C for 10 s, 57°C for 30 s and 72°C for 30 s, followed by 72°C for 10 min and 20°C for 10 s. *TUBULIN* was used to normalize the mRNA levels. Primers used for qRT-PCR are listed in Supplementary Table S1.

Propidium Iodide Staining

Propidium Iodide (PI) powder (Sigma) was dissolved with PBS solution to 5 mg/ml as a stock solution, which was stored in dark. The working solution was diluted to 5 μg/ml. The whole seedling was put into the solution for staining 10 min, then washed with water three times and then observed under the confocal microscope (OLYMPUS LSM1200).

Measurement

For the length of hypocotyls in the seedling stages, pictures were taken under the microscope; The Image J software was used for the measurement and statistical analysis. The cells in longitudinal direction from the top to the base of the hypocotyls epidermis were used for the measurement of each cell length, and 25 hypocotyls were used for biological repetitions, and the Image J software was used for the statistical analysis. The total cells number in the hypocotyls was counted directly under the microscope.

Exogenous Chemical Substance Treatment

IAA and yucasin powder (Sigma) were dissolved in the DMSO and diluted to 50 μM for IAA and 5 mM for yucasin as the stock solutions. The stock solutions were diluted 1000x and added to the corresponding 1/2MS media. The control group was added with the same amount of DMSO in the media. The plants were grown vertically at 21°C under long-day condition (16 h of light and 8 h of darkness).

Statistical Analysis

Where appropriate, statistical analyses were performed with analysis of variance (ANOVA) test. Otherwise, comparisons between two groups were conducted using Student's *t*-test. The *p*-value level was set to 5%.

RESULTS

The Hypocotyl Length Is Shortened in the *ERECTA* Family Mutants

One of the most striking defects in the *ERECTA* family mutants (*erf*) mutants is the dwarf phenotype (Shpak et al., 2004). The *er-105* single mutant showed reduced plant height comparing to that of wild type, whereas the plant height was increased in the *ERECTA* overexpressing plants (Supplementary Figure S1A) (Shen et al., 2015). In the *er erl1 erl2* triple mutant, we observed even severe phenotypes in the reduction of the plant height (Supplementary Figure S1A), suggesting that *ERECTA*, *ERL1* and *ERL2* were functionally redundant in control of the plant height. To further support these observations, we measured the plant height of the *35S::ERECTA*, *er-105* and *er erl1 erl2* plants. We observed a slight increase of the plant height in the *35S::ERECTA* plants, however, a significant decrease in the *er-105* and *er erl1 erl2* mutants (Supplementary Figure S1B).

Consistent with the observation of plant height, in the 6-day-old seedling, we observed that the length of hypocotyl in the *35S::ERECTA* plants was significantly increased comparing to that of wild type seedlings (**Figures 1A,B**). Conversely, the

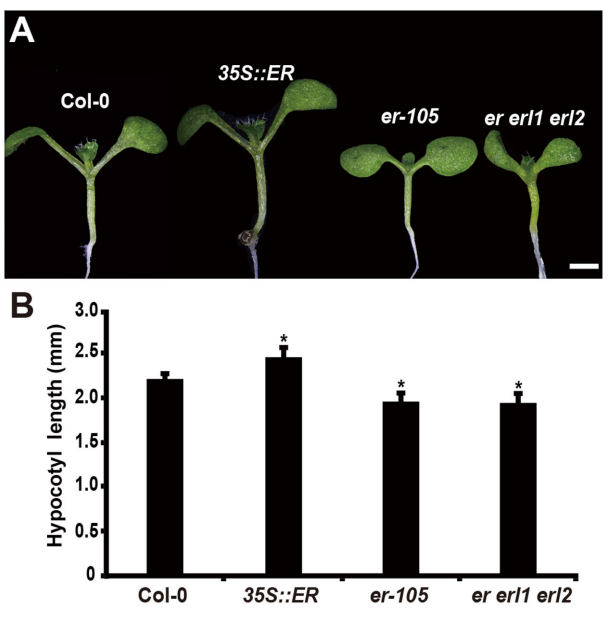

FIGURE 1 | Hypocotyl length is shorten in the *erf* mutants. **(A)** Six-day-old seedlings of the wild-type plant, *35S::ERECTA* transgenic plant, *er-105* mutant and *er erl1 erl2* mutant. **(B)** Average hypocotyl lengths of the 6-day-old seedlings in **(A)** ($n = 40$). Scale bar, 1 mm. $^*P < 0.05$, Student's *t*-test.

hypocotyl lengths in the *er-105* and *er er1 erl2* mutants were dramatically reduced (**Figures 1A,B**). We conclude that the *ERECTA* gene family are involved in the regulation of hypocotyl length in *Arabidopsis*.

Expression Patterns of *ERECTA* Gene Family in the Hypocotyl

Given the fact that disturbing the functions of *ERECTA* gene family causes the severe defects in the hypocotyl length, we assumed that *ERECTA* gene family are expressed in the hypocotyl cells. To test whether the *ERECTA* family genes are transcribed in the hypocotyl cells, we first performed the promoter activation analysis. To this end, we constructed *pER::3 × VENUS-NLS, pERL1::3 × VENUS-NLS, pERL2::3 × VENUS-NLS* transgenic plants. We observed evenly distributed fluorescence signals in the whole hypocotyl of these three transgenic plants (**Figures 2A–C**), suggesting that *ERECTA, ERL1* and *ERL2* genes are expressed in the whole hypocotyl of *Arabidopsis*.

Because *ERECTA* family genes encode leucine-rich repeat receptor-like kinases, we then test whether the ERECTA, ERL1 and ERL2 proteins are localized in the hypocotyl cells. We transformed the *pER::ER-GFP* construct into the *er-105* mutant and observed a fully rescue of the mutant defects. By the confocal microscopy, we observed that ERECTA proteins were strongly accumulated in the hypocotyls (**Figure 2D**).

To check the protein localization of two homologous genes of the *ERECTA*, the *pERL1::ERL1-GFP, pERL2::ERL2-GFP* transgenic plants were also analyzed under the confocal microscope. Consistent with the observation of ERECTA proteins, we found that the both of proteins, ERL1 and ERL2, were also localized in hypocotyls (**Figures 2E,F**).

The *ERECTA* Gene Family Controls the Cell Elongation of Hypocotyls

The organ size and shape of multicellular organism is directly related to the cells division and the size of cells. Therefore,

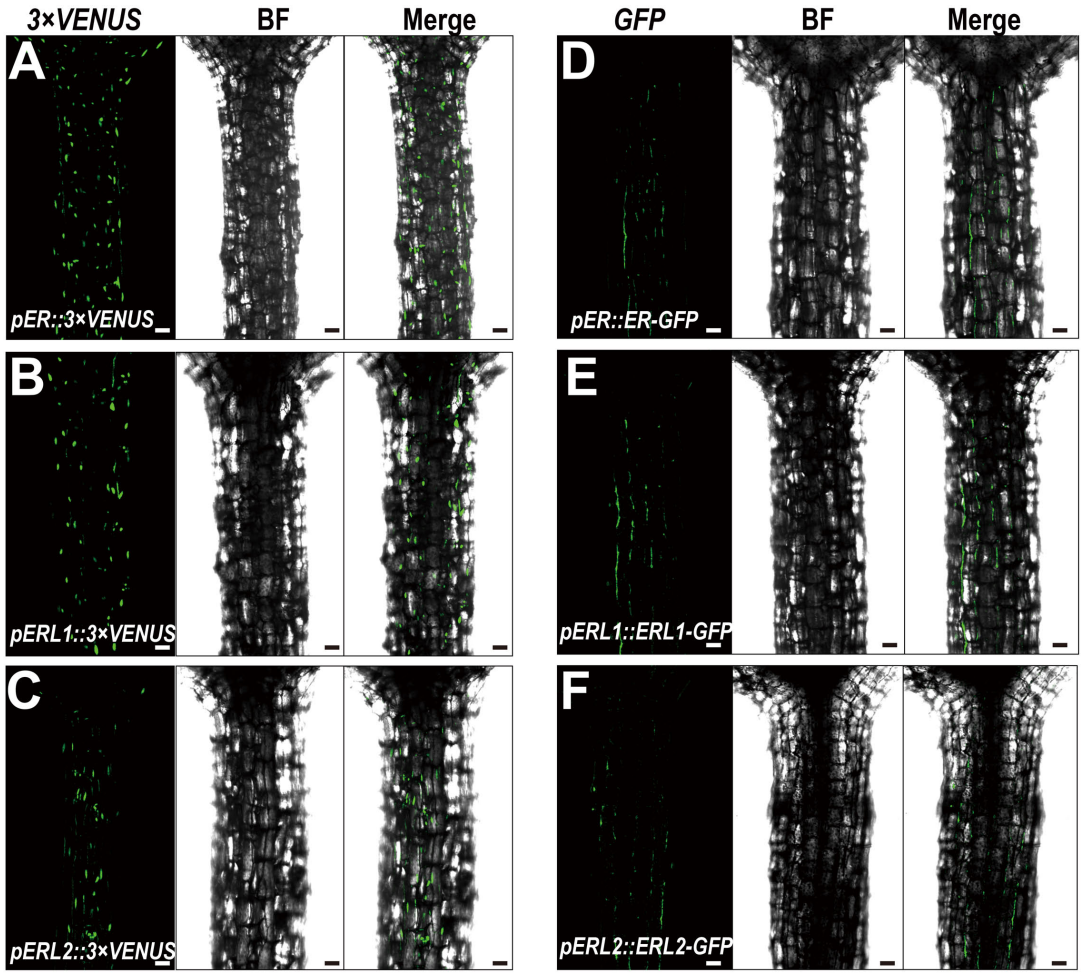

FIGURE 2 | Expression patterns of the *ERECTA* family genes in hypocotyls. **(A)** The expression of the *ERECTA* promoter in hypocotyls determined by the fluorescent signals of *pER::3 × VENNS-NLS*. **(B)** The expression of the *ERL1* promoter in hypocotyls determined by the fluorescent signals of *pERL1::3 × VENNS-NLS*. **(C)** The expression of the *ERL2* promoter in hypocotyls determined by the fluorescent signals of *pERL2::3 × VENNS-NLS*. **(D)** The localization of ERECTA proteins in hypocotyls. **(E)** The localization of ERL1 proteins in hypocotyls. **(F)** The localization of ERL2 proteins in hypocotyls. Scale bars, 50 μm.

the individual cell length and the total number of cells could determine the hypocotyl length in *Arabidopsis*. Previous studies have shown that *ERECTA* family genes may regulate cell number in some organs, including stomata, ovule and stamen (Shpak et al., 2004; Woodward et al., 2005; Pillitteri et al., 2007; Hord et al., 2008). However, whether the *ERECTA* family genes control the cells division and cell elongation in the hypocotyl is still unclear. To test this, we performed Propidium Iodide (PI) staining on the hypocotyls of the wild-type plants, *35S::ERECTA* plants, *er-105* single mutant plants, and *er erl1 erl2* triple mutant plants (**Figures 3A–D**). By the observation under the confocal microscope, we found that the individual cell size of hypocotyl in the *35S::ERECTA* overexpression plants was large than that of wild type plants (**Figure 3B**). On the contrary, we observed size largely reduced cells in the hypocotyls of the *er-105* single mutant and *er erl1 erl2* triple mutant plants comparing to that of wild type plants (**Figures 3C,D**). By the quantitative analysis of the average cells length in the middle column of the hypocotyl epidermis, we found that the average cells length in the *35S::ERECTA* overexpression plants was significantly increased, whereas it was remarkably decreased in the *er-105* and *er erl1 erl2* mutants (**Figure 3E**).

To test whether cells division is involved in the *ERECTA* family genes controlled hypocotyl elongation, we directly counted the total number of cells in the middle column of epidermis, and found that there were no significant difference in all the genotypes we test including the wild type, *35S::ERECTA*, *er-105* and *er erl1 erl2* plants (**Figure 3F**). We concluded that the *ERECTA* gene family regulates the hypocotyl length by controlling the cell elongation rather than the cell division.

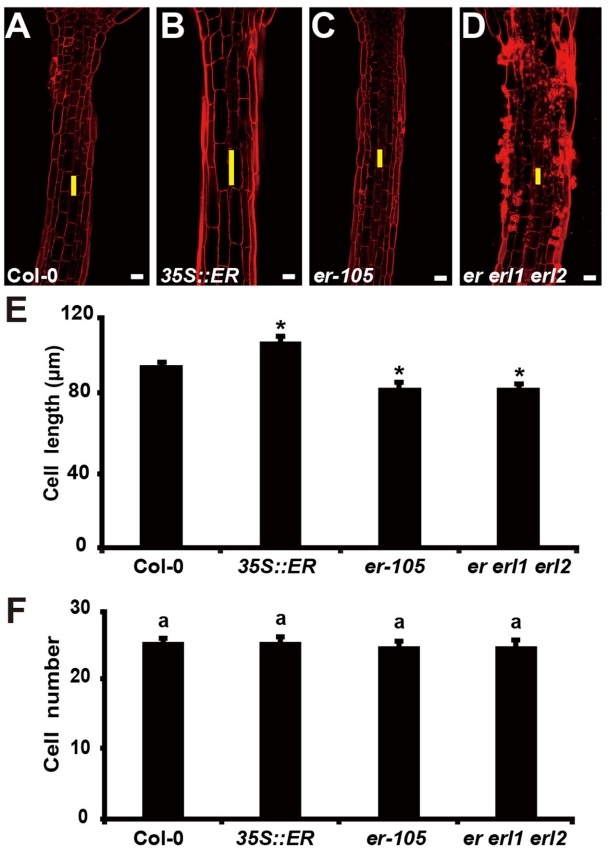

FIGURE 3 | The *ERECTA* family genes controls cell elongation in the hypocotyl. **(A–D)** PI staining of hypocotyls in the 6-day-old wild-type **(A)**, *35S::ERECTA* plant **(B)**, *er-105* mutant **(C)** and *er erl1 erl2* mutant **(D)**. **(E)** Average individual cell lengths of the hypocotyls in the 6-day-old wild-type, *35S::ERECTA* plant, *er-105* mutant and *er erl1 erl2* mutant ($n = 25$). **(F)** Total cell number in the hypocotyls of 6-day-old wild-type, *35S::ERECTA* plant, *er-105* mutant and *er erl1 erl2* mutant ($n = 25$). The yellow line represents the length of a single cell. Scale bars, 50 μm. ANOVA-test in **(F)**, same letters represent no statistically significant differences ($P < 0.05$). Student's *t*-test in **(E)**, $^*P < 0.05$.

Auxin Biosynthesis Is Down Regulated in the *erf* Mutants

Given the fact that the cell elongation was significantly reduced in the *erf* mutants, we then asked by what means does the *ERECTA* gene family regulate individual cell length in the hypocotyl? Previous studies have shown that the auxin plays an important role in regulation of cell elongation (Rayle and Cleland, 1992; Galinha et al., 2007). The endogenous auxin increased mutants exhibit hypocotyls-elongated phenotypes, whereas auxin deficient mutants have the reduced size of cells (Romano et al., 1991; Zhao et al., 2001; Cheng et al., 2006). To examine whether the auxin is involved in the *ERECTA* gene family mediated controls of cell elongation, two different auxin sensors, *DR5::GFP* and *DII-VENUS*, were applied to detect the endogenous auxin levels in the *er erl1 erl2* mutants. The *DR5::GFP* is a positive auxin sensor by which *GFP* transcriptions are activated by auxin (Ulmasov et al., 1997; Benkova et al., 2003). Under the confocal microscope, we observed evenly distributed fluorescence signals of *DR5::GFP* in the entire hypocotyl (**Figure 4A**), suggesting that the auxin was distributed in all the hypocotyl of *Arabidopsis*. However, we can barely detect the fluorescence signals in the *er erl1 erl2* mutant hypocotyl (**Figure 4B**), suggesting that the endogenous auxin levels were dramatically reduced in the triple mutant hypocotyl. To confirm this observation, the transgenic plants that harbored the negative auxin sensor *DII-VENUS* by which fluorescence proteins were degradated by auxin (Brunoud et al., 2012) were further analyzed. Consistent with the observation of *DR5::GFP*, there were only extremely weak signals can be detected in the wild type hypocotyl (**Figure 4C**), but stronger *DII-VENUS* signals in the *er erl1 erl2* triple mutants (**Figure 4D**). At the molecular level, we tested the transcriptional levels of auxin early response gene *IAA19*, which is commonly used to monitor the endogenous levels of auxin in *Arabidopsis*. We observed that the expression levels of *IAA19* in the *35S::ERECTA* transgenic plants were up regulated, whereas significantly down regulated in the *er-105* and *er erl1 erl2* triple mutants (**Figure 4E**). These data suggest that the *ERECTA* gene family is essential to maintain the endogenous auxin levels in the hypocotyl.

To shed light on the molecular mechanism underlying the ability of the *ERECTA* gene family controlling auxin

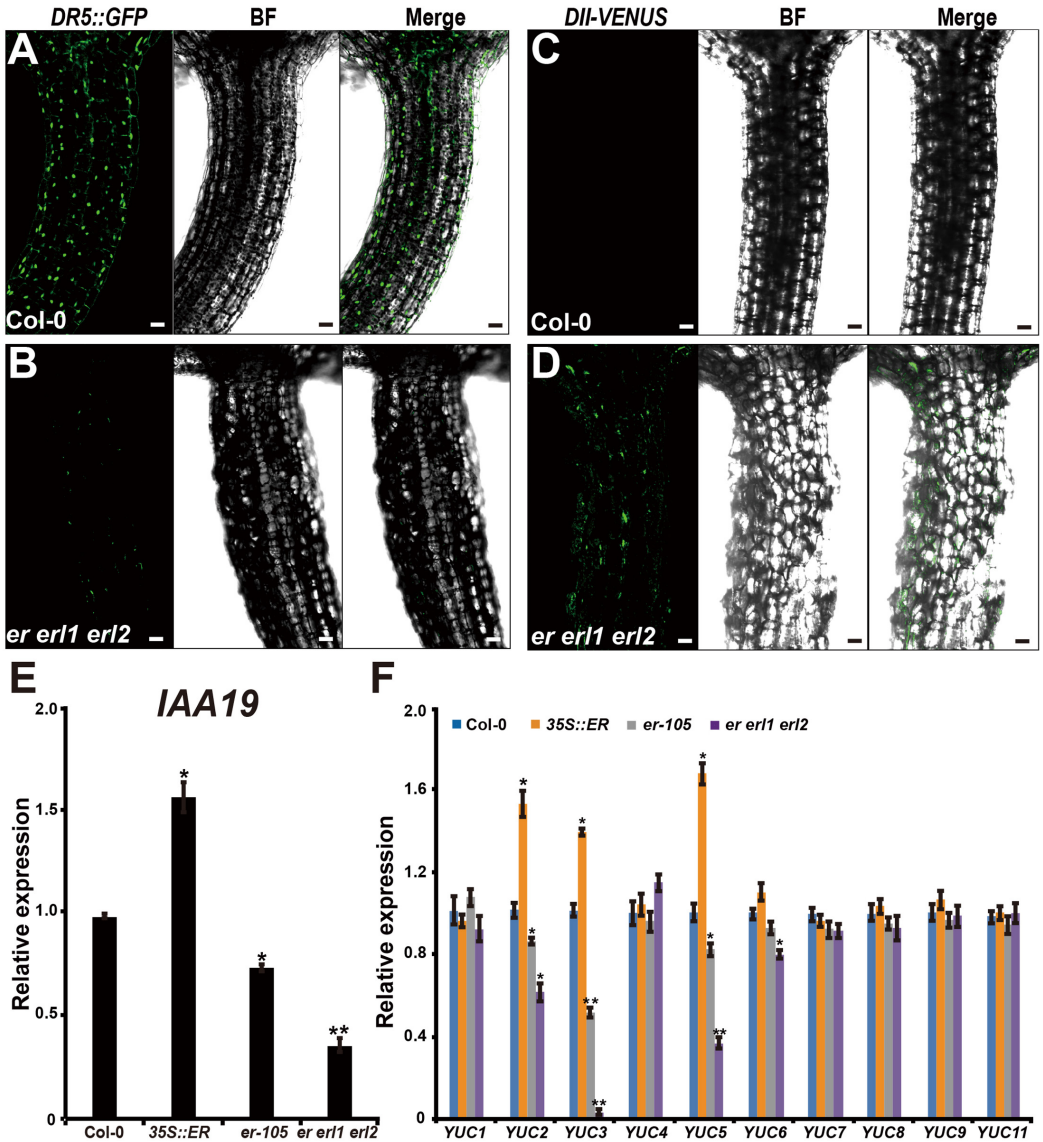

FIGURE 4 | The *ERECTA* family genes controls auxin biosynthesis in the hypocotyl. **(A)** The fluorescent signals of *DR5::GFP* in the wild-type hypocotyl. **(B)** The fluorescent signals of *DR5::GFP* in the *er erl1 erl2* mutant hypocotyl. **(C)** The fluorescent signals of *DII-VENUS* in the wild-type hypocotyl. **(D)** The fluorescent signals of *DII-VENUS* in the *er erl1 erl2* mutant hypocotyl. **(E)** The expression levels of *IAA19* in the wild-type, *35S::ERECTA, er-105* and *er erl1 erl2* hypocotyls. The 6-day-old hypocotyls of each genotype were used for the RNA extraction. **(F)** The expression levels of *YUC* family genes in the wild-type, *35S::ERECTA, er-105* and *er erl1 erl2* hypocotyls. The 6-day-old hypocotyls of each genotype were used for the RNA extraction. Scale bars, 50 μm. Error bars in the **(E,F)** indicate the SD of three biological repeats. $^{*}P < 0.05$, $^{**}P < 0.01$, Student's *t*-test.

levels in the hypocotyl, we examined the expression levels of the *YUCCA* family genes, which encodes the major auxin biosynthesis genes (Cheng et al., 2006). We observed that the transcriptional levels of *YUC2, YUC3* and *YUC5* were significantly increased in the *ERECTA* overexpression plants compared with wild type (**Figure 4F**). Conversely, these three key auxin biosynthesis genes were markedly decreased in the *er-105* and *er erl1 erl2* triple mutants; especially the expression levels of *YUC3* were drastically reduced in the *er erl1 erl2* triple mutants (**Figure 4F**). We draw the conclusion that the *ERECTA* gene family positively regulates auxin biosynthesis via activating the expressions of *YUC2, YUC3* and *YUC5* genes.

Exogenous Auxin Rescues the Cells Elongation Defects in *erf* Mutants

Given the fact that the *erf* mutants contain a very low amount of auxin and the key auxin biosynthesis genes are under the positive control of *ERECTA* gene family, we hypothesized exogenous increase of auxin might rescue the defects of cell elongation and short hypocotyl phenotypes of the *erf* mutants. While,

previous studies have shown that the high concentrations of auxin might inhibit the elongation of hypocotyls in wild-type *Arabidopsis* (Collett et al., 2000; Rashotte et al., 2003), which was also found in our experiments (data not shown). To exclude the possibility the high auxin inhibits the cell elongation in our test, we carefully select a very low concentration of IAA (50 nM), and performed our analysis. By applying this low concentration of IAA to the wild type seedlings, we did not observe any significant differences in term of the hypocotyl length comparing with the mock treatments (**Figures 5A,B**). However, this low concentration of IAA almost fully rescued the hypocotyl-shortened phenotypes of the *er-105* single mutants and *er erl1 erl2* triple mutants (**Figure 5A**). By quantifying the hypocotyl length, we observed significant increases of the hypocotyl length in the *er-105* and *er erl1 erl2* mutants upon the auxin treatments, which showed no differences to that of wild type seedlings (**Figure 5B**), suggesting that the hypocotyl-shortened defects in the *erf* mutants are due to the lacking of auxin, and the increase of exogenous auxin completely restores the mutant phenotypes. To further confirm this observation, we examine the cell elongation in the *erf* mutants after the auxin treatments. In the wild type hypocotyl, the 50 nM auxin treatments did not change the cell length comparing with the mock treatments (**Figures 6A,B**). However, in the *er-105* and *er erl1 erl2* mutants, the same amount of auxin effectively promoted the cell length to that of mock treatments (**Figure 6A**), and the cell length was significantly increased to the levels that comparable with the wild type seedlings (**Figure 6B**). To test the possibility whether the cell division was also involved in the rescue of *erf* mutants defects during the low auxin treatments, we directly counted the total number of cells in the middle column of epidermis with or without the low auxin treatments. We observed no significant difference among all the genotypes after the auxin treatments (Supplementary Figure S2). Therefore, we conclude that the hypocotyl-shortened phenotypes in the *erf* mutants are due to the cell elongation defects, which can be fully rescued by the treatments of exogenous auxin.

The *ERECTA* Gene Family Mediated Endogenous Auxin Biosynthesis Controls the Cell Elongation in Hypocotyls

Given the fact that the *ERECTA* gene family positively regulates auxin biosynthesis in the hypocotyl by activating the expressions

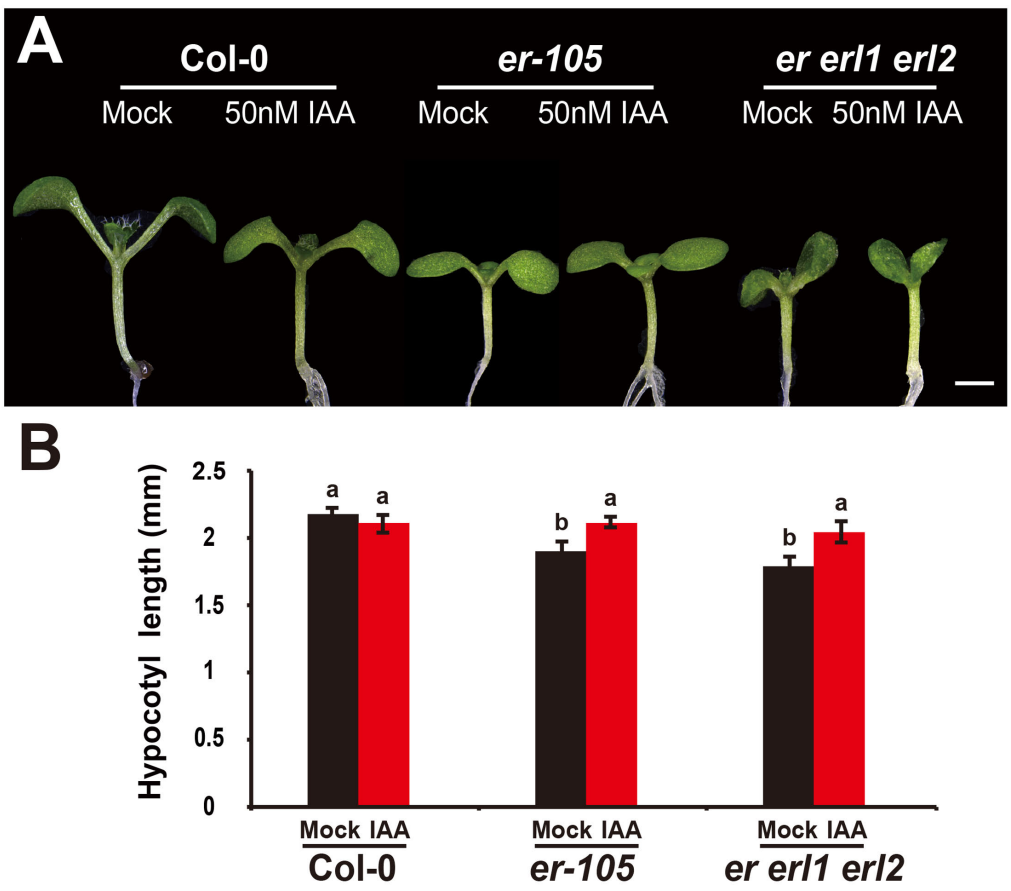

FIGURE 5 | The low auxin rescues the *erf* hypocotyl-shortened phenotypes. **(A)** Six-day-old seedlings of the wild type, *er-105* and *er erl1 erl2* mutant grown in the 1/2MS media with or without 50 nM IAA. **(B)** The hypocotyl lengths of the seedlings in **(A)** (n = 40). Scale bar, 1 mm. Different letters represent statistically significant differences ($P < 0.05$), ANOVA-test.

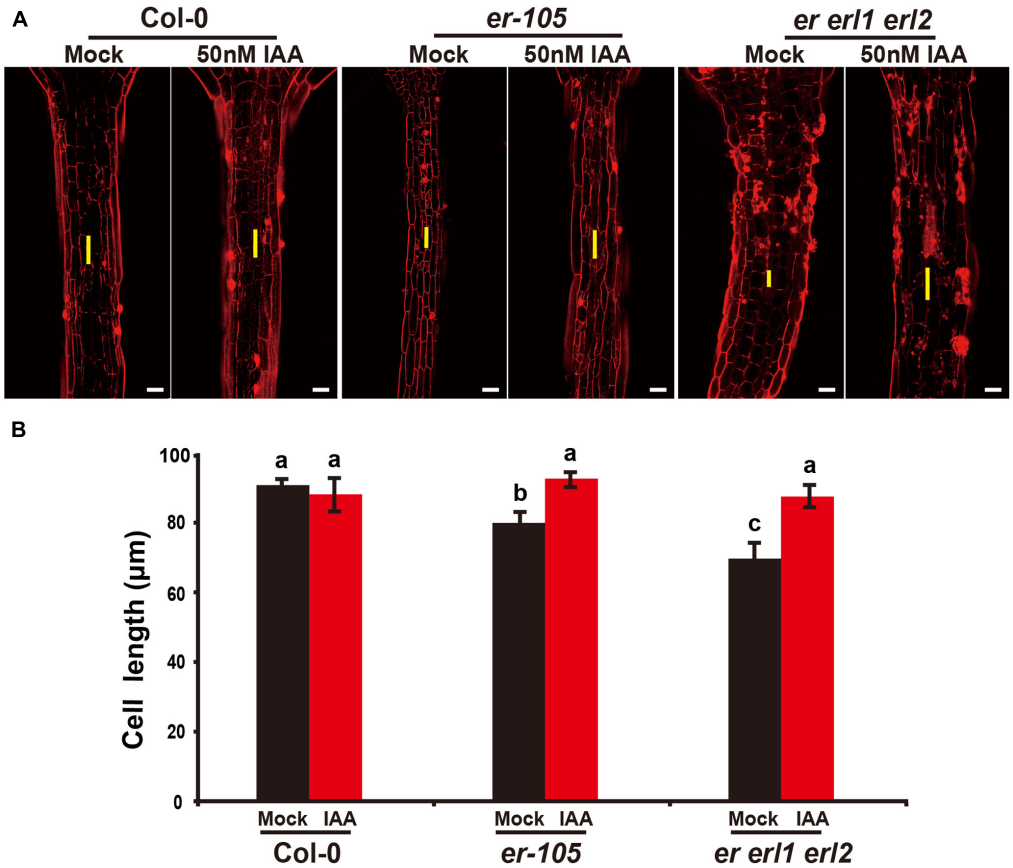

FIGURE 6 | Exogenous auxin rescues the cell elongation defects in the *erf* mutants. **(A)** PI staining of hypocotyls in the wild type, *er-105* and *er erl1 erl2* mutant grown in the 1/2MS media with or without 50 nM IAA. **(B)** The average cell lengths of the hypocotyls in the wild type, *er-105* and *er erl1 erl2* mutant grown in the 1/2MS media with or without 50 nM IAA. (n = 25). The yellow line represents the length of a single cell. Scale bars, 50 μm. Different letters represent statistically significant differences ($P < 0.05$), ANOVA-test.

of several *YUCCA* family genes, and the overexpression of *ERECTA* causes the elevated expressions of *YUC*s (**Figure 4F**), we then tested this interaction genetically. We treated the *35S::ERECTA* seedlings with the chemical yucasin, which have been shown to reduce the exogenous auxin levels by inhibiting the expression of *YUCCA* genes (Nishimura et al., 2014). We carefully select a low concentration of yucasin (5 μM) to perform the analysis, which showed no effect on the hypocotyl length in the wild type seedlings (Supplementary Figures S3A,B). While in the *35S::ERECTA* seedlings, the hypocotyl length was significantly decreased (Supplementary Figures S3A,B). Likely, the hypocotyl cell length of the wild type plants did not respond the low yucasin treatments. However, the cell length of the *35S::ERECTA* seedlings with increased *YUCCA* expressions, reduced dramatically upon the low yucasin treatments (Supplementary Figure S4), demonstrating that the *ERECTA* gene family controls the cell elongation in hypocotyls by positively regulating the auxin biosynthesis.

The bacterial auxin biosynthesis gene *iaaM*, which was firstly identified in the T-DNA of agrobacterium, is commonly used in plants to increase the endogenous auxin levels (Comai and Kosuge, 1982). To further investigate the mechanism by which the *ERECTA* gene family mediated auxin synthesis controls the cell elongation in hypocotyls, we expressed the *iaaM* gene under the control of the *ERECTA* promoter, and transformed the *pER:iaaM* construct into the *er*−/− *erl1*+/− *erl2*−/− mutants. By analyzing the expression levels of the *iaaM* and the *IAA19* genes in eight independent transgenic lines, we observed a correlation between these two genes, suggesting that the ectopically expressed *iaaM* increased the endogenous auxin levels in the *er erl1 erl2* triple mutant background (Supplementary Figure S5A). We measured the hypocotyl length of eight independent transgenic lines and selected three independent T1 transgenic lines with high expression of *iaaM* for the further analysis. (Supplementary Figure S5B), and observed that hypocotyls and individual cell lengths of *pER:iaaM* transgenic plants were higher than those of *er erl1 erl2* triple mutants (**Figures 7A–D**). Thus we conclude that the *ERECTA* gene family mediated endogenous auxin biosynthesis controls the cell elongation in hypocotyls.

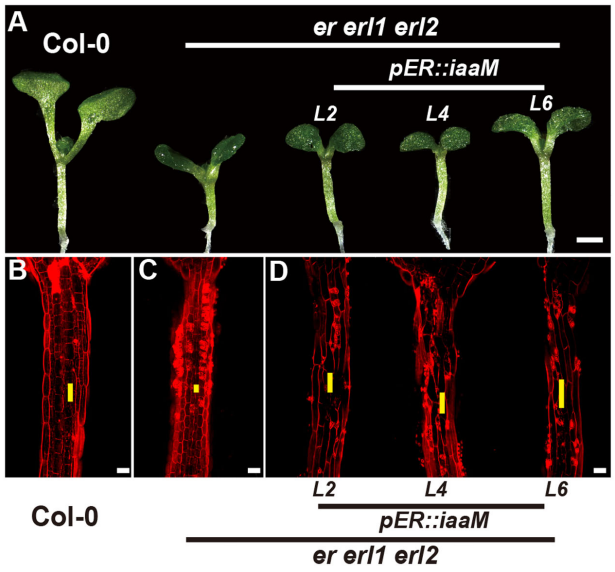

FIGURE 7 | The endogenous auxin rescues the *erf* mutant phenotypes in the hypocotyl. **(A)** Six-day-old seedlings of the wild type, the *er erl1 erl2* mutant and three independent *pER:iaaM* transgenic lines in the *er erl1 erl2* mutant background (*L2, L4 and L6*). **(B–D)** PI staining of hypocotyls in the wild type **(B)**, the *er erl1 erl2* mutant **(C)** and three independent *pER:iaaM* transgenic lines in the *er erl1 erl2* mutant background **(D)**. The yellow line represents the length of a single cell. Scale bar in **(A)**, 1 mm; scale bars in **(B–D)**, 50 μm.

DISCUSSION

The *ERECTA* family genes, which encode leucine-rich repeat receptor-like kinases, have been shown to regulate multiple developmental processes including stomatal formation, inflorescence architecture, and ovule development (Shpak et al., 2004, 2005; Lee et al., 2012). Woodward et al have previously shown that a dominant mutant, *super1-D*, which causes the overexpression of one of the *YUCCA* family genes *YUC5*, is epistatic to *er* mutants (Woodward et al., 2005). However, little is known about the genetic interaction between the *ERECTA* and auxin signaling in control of the hypocotyl development. In this study, we analyzed the endogenous auxin levels in the *erf* mutants by using two different auxin sensors, *DR5::GFP* and *DII-VENUS*. Our results show that the endogenous auxin levels were dramatically reduced in the hypocotyl of the *er erl1 erl2* triple mutant (**Figures 2A–D**). To further support this observation, we examined the expression levels of *IAA19* in the hypocotyl. We found that the *IAA19* transcripts are significantly reduced in the *er-105* and *er erl1 erl2* mutants, and increased in the *35S::ERECTA* transgenic plants (**Figure 4E**). To further investigate the mechanism by which the *ERECTA* family genes regulate auxin levels in the hypocotyl, we examined the key auxin biosynthesis genes. We observed that the transcriptional levels of *YUC2, YUC3* and *YUC5* were significantly decreased in the *er-105* and *er erl1 erl2* triple mutants, whereas increased in the *35S::ERECTA* transgenic plants (**Figure 4F**). Our data suggest that the *ERECTA* gene family positively regulates auxin biosynthesis by activating the key auxin biosynthesis genes.

Previous study has shown that the overexpression of *YUC5* in the wild type, *er-103* and *er-105* cause the same extent of increase of hypocotyls regardless of their genotypes (Woodward et al., 2005), which raises the question whether the *ERECTA* family genes regulate the cell elongation in the hypocotyl via auxin biosynthesis. By careful selection of a very low concentration, 50 nM of IAA fully rescued the short hypocotyl and cell elongation defects in the *er-105* and *er erl1 erl2* mutants, but have no significant effects in the wild type (**Figures 5**, **6**), suggesting that these defects of the *erf* mutants are caused by the auxin deficiency in the hypocotyl. Further support for this idea came from the observation that the elongated hypocotyl cells in the *35S::ERECTA* seedlings are completely suppressed by using the 5 μM yucasin treatments to inhibit *YUCCA* genes (Supplementary Figure S4). Our data demonstrate that the *ERECTA* gene family controls cell elongation by positively regulating auxin biosynthesis. Likely, during leaf margin morphogenesis, the ligand-receptor pair of EPFL2-ER has been shown to be essential for maintaining an appropriate auxin concentration (Tameshige et al., 2016).

The small-secreted peptide PSY1, together with its LRR receptor, positively regulates cell elongation in hypocotyls by triggering a signaling cascade (Mahmood et al., 2014), suggesting a crucial role of peptide ligand-receptor pair in the hypocotyl regulation. ERECTA with its ligands EPF/EPFL peptides family, participate multiple functions during plant development, for example, EPF1, EPF2 and EPFL9 in stomatal regulation, EPFL4, EPFL5 and EPFL6 in inflorescence development and EPFL2 in tooth development (Abrash et al., 2011; Uchida and Tasaka, 2013; Tameshige et al., 2016; Lin et al., 2017). Moreover, in the secondary growth of *Arabidopsis* hypocotyls, *ERECTA* and *ERL1* are very important in the xylem and phloem to prevent premature during sequential events in the secondary growth, suggesting that *ERECTA* family plays an important role in the morphogenesis of hypocotyls (Ikematsu et al., 2017). Therefore, we speculate that ERECTA family might regulate the cell elongation in hypocotyls with some members of the EPF/EPFL family or other ligands.

During the reproductive stage, the short internodes and pediceels phenotypes of the *erf* mutants in the inflorescences were mainly due to reduced cell proliferation (Shpak et al., 2003, 2004; Woodward et al., 2005). However, in the hypocotyl, mutations of the *ERECTA* gene family result in the defects specifically in the cell elongation rather than the cell division (**Figure 3**). This idea is further support by the early observation that, in *Arabidopsis*, hypocotyl elongation is mainly due to the cell elongation, while the number of cells is rather stable (Gendreau et al., 1997). These data suggest that the functions of *ERECTA* gene family in controlling of cell proliferation and cell elongation is highly tissue-specific, however, it remains to be shown how the functions of *ERECTA* gene family are specified in different tissues to fulfill their biological functions.

AUTHOR CONTRIBUTIONS

ZT, XQ, and ZZ designed the experiments, analyzed the data and wrote the paper. XQ performed the experiments.

FUNDING

This work was supported by the grant to ZT from the National Natural Science Foundation of China (31300248), and the grant to ZZ from the Ministry of Science and Technology of China (2013CB967300).

ACKNOWLEDGMENT

We thank Prof. Masao Tasaka, Prof. Zuhua He, Prof. Yuling Jiao, and Prof. Yunde Zhao for sharing seeds or plasmid.

SUPPLEMENTARY MATERIAL

The Supplementary Material for this article can be found online at: http://journal.frontiersin.org/article/10.3389/fpls.2017.01688/full#supplementary-material

REFERENCES

Abrash, E. B., Davies, K. A., and Bergmann, D. C. (2011). Generation of signaling specificity in *Arabidopsis* by spatially restricted buffering of ligand-receptor interactions. *Plant Cell* 23, 2864–2879. doi: 10.1105/tpc.111.086637

Bai, M. Y., Shang, J. X., Oh, E., Fan, M., Bai, Y., Zentella, R., et al. (2012). Brassinosteroid, gibberellin and phytochrome impinge on a common transcription module in *Arabidopsis*. *Nat. Cell Biol.* 14, U810–U878. doi: 10.1038/ncb2546

Benkova, E., Michniewicz, M., Sauer, M., Teichmann, T., Seifertova, D., Jurgens, G., et al. (2003). Local, efflux-dependent auxin gradients as a common module for plant organ formation. *Cell* 115, 591–602.

Brunoud, G., Wells, D. M., Oliva, M., Larrieu, A., Mirabet, V., Burrow, A. H., et al. (2012). A novel sensor to map auxin response and distribution at high spatio-temporal resolution. *Nature* 482, 103–106. doi: 10.1038/nature10791

Challa, K. R., Aggarwal, P., and Nath, U. (2016). Activation of YUCCA5 by the transcription factor TCP4 integrates developmental and environmental signals to promote hypocotyl elongation in *Arabidopsis*. *Plant Cell* 28, 2117–2130. doi: 10.1105/tpc.16.00360

Chen, M. K., Wilson, R. L., Palme, K., Ditengou, F. A., and Shpak, E. D. (2013). ERECTA family genes regulate auxin transport in the shoot apical meristem and forming leaf primordia. *Plant Physiol.* 162, 1978–1991. doi: 10.1104/pp.113.218198

Cheng, Y. F., Dai, X. H., and Zhao, Y. D. (2006). Auxin biosynthesis by the YUCCA flavin monooxygenases controls the formation of floral organs and vascular tissues in *Arabidopsis*. *Genes Dev.* 20, 1790–1799. doi: 10.1101/gad.1415106

Christie, J. M., Yang, H. B., Richter, G. L., Sullivan, S., Thomson, C. E., Lin, J. S., et al. (2011). phot1 Inhibition of ABCB19 primes lateral auxin fluxes in the shoot apex required for phototropism. *PLOS Biol.* 9:1001076. doi: 10.1371/journal.pbio.1001076

Collett, C. E., Harberd, N. P., and Leyser, O. (2000). Hormonal interactions in the control of *Arabidopsis* hypocotyl elongation. *Plant Physiol.* 124, 553–561. doi: 10.1104/pp.124.2.553

Comai, L., and Kosuge, T. (1982). Cloning and characterization of iaaM, a virulence determinant of *Pseudomonas-savastanoi*. *J. Bacteriol.* 149, 40–46.

de Lucas, M., Daviere, J. M., Rodriguez-Falcon, M., Pontin, M., Iglesias-Pedraz, J. M., Lorrain, S., et al. (2008). A molecular framework for light and gibberellin control of cell elongation. *Nature* 451, 480–484. doi: 10.1038/nature06520

Fenwick, K. M., Apperley, D. C., Cosgrove, D. J., and Jarvis, M. C. (1999). Polymer mobility in cell walls of cucumber hypocotyls. *Phytochemistry* 51, 17–22.

Galinha, C., Hofhuis, H., Luijten, M., Willemsen, V., Blilou, I., Heidstra, R., et al. (2007). PLETHORA proteins as dose-dependent master regulators of *Arabidopsis* root development. *Nature* 449, 1053–1057. doi: 10.1038/nature06206

Gao, Y., Wu, Y. J., Du, J. B., Zhan, Y. Y., Sun, D. D., Zhao, J. X., et al. (2017). Both light-induced SA accumulation and ETI mediators contribute to the cell death regulated by BAK1 and BKK1. *Front. Plant Sci.* 8:622. doi: 10.3389/fpls.2017.00622

Gendreau, E., Traas, J., Desnos, T., Grandjean, O., Caboche, M., and Hofte, H. (1997). Cellular basis of hypocotyl growth in *Arabidopsis thaliana*. *Plant Physiol.* 114, 295–305. doi: 10.1104/pp.114.1.295

Gray, W. M., Ostin, A., Sandberg, G., Romano, C. P., and Estelle, M. (1998). High temperature promotes auxin-mediated hypocotyl elongation in *Arabidopsis*. *Proc. Natl. Acad. Sci. U.S.A.* 95, 7197–7202. doi: 10.1073/pnas.95.12.7197

Hord, C. L. H., Suna, Y. J., Pillitteri, L. J., Torii, K. U., Wang, H. C., Zhang, S. Q., et al. (2008). Regulation of *Arabidopsis* early anther development by the mitogen-activated protein kinases, MPK3 and MPK6, and the ERECTA and related receptor-like kinases. *Mol. Plant* 1, 645–658. doi: 10.1093/mp/ssn029

Ikematsu, S., Tasaka, M., Torii, K. U., and Uchida, N. (2017). *ERECTA*-family receptor kinase genes redundantly prevent premature progression of secondary growth in the *Arabidopsis* hypocotyl. *New Phytol.* 213, 1697–1709. doi: 10.1111/nph.14335

Jensen, P. J., Hangarter, R. P., and Estelle, M. (1998). Auxin transport is required for hypocotyl elongation in light-grown but not dark-grown *Arabidopsis*. *Plant Physiol.* 116, 455–462. doi: 10.1104/pp.116.2.455

Jewaria, P. K., Hara, T., Tanaka, H., Kondo, T., Betsuyaku, S., Sawa, S., et al. (2013). Differential effects of the peptides stomagen, EPF1 and EPF2 on activation of MAP Kinase MPK6 and the SPCH protein level. *Plant Cell Physiol.* 54, 1253–1262. doi: 10.1093/pcp/pct076

Jorda, L., Sopena-Torres, S., Escudero, V., Nunez-Corcuera, B., Delgado-Cerezo, M., Torii, K. U., et al. (2016). ERECTA and BAK1 receptor like kinases interact to regulate immune responses in *Arabidopsis*. *Front. Plant Sci.* 7:897. doi: 10.3389/fpls.2016.00897

Lee, J. S., Kuroha, T., Hnilova, M., Khatayevich, D., Kanaoka, M. M., McAbee, J. M., et al. (2012). Direct interaction of ligand-receptor pairs specifying stomatal patterning. *Genes Dev.* 26, 126–136. doi: 10.1101/gad.179895.111

Lin, G. Z., Zhang, L., Han, Z. F., Yang, X. R., Liu, W. J., Li, E. T., et al. (2017). A receptor-like protein acts as a specificity switch for the regulation of stomatal development. *Genes Dev.* 31, 927–938. doi: 10.1101/gad.297580.117

Mahmood, K., Kannangara, R., Jorgensen, K., and Fuglsang, A. T. (2014). Analysis of peptide PSY1 responding transcripts in the two *Arabidopsis* plant lines: wild type and psy1r receptor mutant. *BMC Genomics* 15:441. doi: 10.1186/1471-2164-15-441

Meng, X. Z., Wang, H. C., He, Y. X., Liu, Y. D., Walker, J. C., Torii, K. U., et al. (2012). A MAPK cascade downstream of ERECTA receptor-like protein kinase regulates *Arabidopsis* inflorescence architecture by promoting localized cell proliferation. *Plant Cell* 24, 4948–4960. doi: 10.1105/tpc.112.104695

Nishimura, T., Hayashi, K., Suzuki, H., Gyohda, A., Takaoka, C., Sakaguchi, Y., et al. (2014). Yucasin is a potent inhibitor of YUCCA, a key enzyme in auxin biosynthesis. *Plant J.* 77, 352–366. doi: 10.1111/tpj.12399

Nozue, K., Covington, M. F., Duek, P. D., Lorrain, S., Fankhauser, C., Harmer, S. L., et al. (2007). Rhythmic growth explained by coincidence between internal and external cues. *Nature* 448, 358–361. doi: 10.1038/nature05946

Oh, E., Zhu, J. Y., Bai, M. Y., Arenhart, R. A., Sun, Y., and Wang, Z. Y. (2014). Cell elongation is regulated through a central circuit of interacting transcription factors in the Arabidopsis hypocotyl. *Elife* 3:e03031. doi: 10.7554/eLife.03031

Pillitteri, L. J., Bemis, S. M., Shpak, E. D., and Torii, K. U. (2007). Haploinsufficiency after successive loss of signaling reveals a role for *ERECTA*-family genes in *Arabidopsis* ovule development. *Development* 134, 3099–3109. doi: 10.1242/dev.004788

Rashotte, A. M., Poupart, J., Waddell, C. S., and Muday, G. K. (2003). Transport of the two natural auxins, indole-3-butyric acid and indole-3-acetic acid, in Arabidopsis. *Plant Physiol.* 133, 761–772. doi: 10.1104/pp.103.022582

Rayle, D. L., and Cleland, R. E. (1992). The acid growth theory of auxin-induced cell elongation is alive and well. *Plant Physiol.* 99, 1271–1274. doi: 10.1104/pp.99.4.1271

Romano, C. P., Hein, M. B., and Klee, H. J. (1991). Inactivation of auxin in tobacco transformed with the indoleacetic-acid lysine synthetase gene of *Pseudomonas-savastanoi*. *Genes Dev.* 5, 438–446. doi: 10.1101/gad.5.3.438

Shen, H., Zhong, X. B., Zhao, F. F., Wang, Y. M., Yan, B. X., Li, Q., et al. (2015). Overexpression of receptor-like kinase *ERECTA* improves thermotolerance in rice and tomato. *Nat. Biotechnol.* 33, 996–1003. doi: 10.1038/nbt.3321

Shpak, E. D. (2013). Diverse roles of *ERECTA* family genes in plant development. *J. Integr. Plant Biol.* 55, 1238–1250. doi: 10.1111/jipb.12108

Shpak, E. D., Berthiaume, C. T., Hill, E. J., and Torii, K. U. (2004). Synergistic interaction of three ERECTA-family receptor-like kinases controls *Arabidopsis* organ growth and flower development by promoting cell proliferation. *Development* 131, 1491–1501. doi: 10.1242/dev.01028

Shpak, E. D., Lakeman, M. B., and Torii, K. U. (2003). Dominant-negative receptor uncovers redundancy in the Arabidopsis ERECTA leucine-rich repeat receptor-like kinase signaling pathway that regulates organ shape. *Plant Cell* 15, 1095–1110. doi: 10.1105/tpc.010413

Shpak, E. D., McAbee, J. M., Pillitteri, L. J., and Torii, K. U. (2005). Stomatal patterning and differentiation by synergistic interactions of receptor kinases. *Science* 309, 290–293. doi: 10.1126/science.1109710

Stuart, D. A., Durnam, D. J., and Jones, R. L. (1977). Cell elongation and cell division in elongating lettuce hypocotyl sections. *Planta* 135, 249–255. doi: 10.1007/BF00384897

Sun, J. Q., Qi, L. L., Li, Y. N., Chu, J. F., and Li, C. Y. (2012). PIF4-mediated activation of *YUCCA8* expression integrates temperature into the auxin pathway in regulating *Arabidopsis* hypocotyl growth. *PLOS Genet.* 8:e1002594. doi: 10.1371/journal.pgen.1002594

Tameshige, T., Okamoto, S., Lee, J. S., Aida, M., Tasaka, M., Torii, K. U., et al. (2016). A secreted peptide and its receptors shape the auxin response pattern and leaf margin morphogenesis. *Curr. Biol.* 26, 2478–2485. doi: 10.1016/j.cub.2016.07.014

Torii, K. U., Mitsukawa, N., Oosumi, T., Matsuura, Y., Yokoyama, R., Whittier, R. F., et al. (1996). The Arabidopsis *ERECTA* gene encodes a putative receptor protein kinase with extracellular leucine-rich repeats. *Plant Cell* 8, 735–746. doi: 10.1105/tpc.8.4.735

Uchida, N., and Tasaka, M. (2013). Regulation of plant vascular stem cells by endodermis-derived EPFL-family peptide hormones and phloem-expressed ERECTA-family receptor kinases. *J. Exp. Bot.* 64, 5335–5343. doi: 10.1093/jxb/ert196

Ulmasov, T., Murfett, J., Hagen, G., and Guilfoyle, T. J. (1997). Aux/IAA proteins repress expression of reporter genes containing natural and highly active synthetic auxin response elements. *Plant Cell* 9, 1963–1971.

Vernoux, T., Brunoud, G., Farcot, E., Morin, V., Van den Daele, H., Legrand, J., et al. (2011). The auxin signalling network translates dynamic input into robust patterning at the shoot apex. *Mol. Syst. Biol.* 7:508. doi: 10.1038/msb.2011.39

Woodward, C., Bemis, S. M., Hill, E. J., Sawa, S., Koshiba, T., and Torii, K. U. (2005). Interaction of auxin and ERECTA in elaborating Arabidopsis inflorescence architecture revealed by the activation tagging of a new member of the YUCCA family putative flavin monooxygenases. *Plant Physiol.* 139, 192–203. doi: 10.1104/pp.105.063495

Yokoyama, R., Takahashi, T., Kato, A., Torii, K. U., and Komeda, Y. (1998). The Arabidopsis *ERECTA* gene is expressed in the shoot apical meristem and organ primordia. *Plant J.* 15, 301–310. doi: 10.1046/j.1365-313X.1998.00203.x

Zhao, Y. D., Christensen, S. K., Fankhauser, C., Cashman, J. R., Cohen, J. D., Weigel, D., et al. (2001). A role for flavin monooxygenase-like enzymes in auxin biosynthesis. *Science* 291, 306–309. doi: 10.1126/science.291.5502.306

Conflict of Interest Statement: The authors declare that the research was conducted in the absence of any commercial or financial relationships that could be construed as a potential conflict of interest.

frontiers in Plant Science

ORIGINAL RESEARCH
published: 14 July 2017
doi: 10.3389/fpls.2017.01241

Transcriptome Analysis of Calcium- and Hormone-Related Gene Expressions during Different Stages of Peanut Pod Development

Yan Li[1], Jingjing Meng[1], Sha Yang[1], Feng Guo[1], Jialei Zhang[1], Yun Geng[1], Li Cui[1], Shubo Wan[2] and Xinguo Li[1]**

[1] *Biotechnology Research Center, Shandong Academy of Agricultural Sciences, Jinan, China,* [2] *Shandong Provincial Key Laboratory of Crop Genetic Improvement, Ecology and Physiology, Shandong Academy of Agricultural Sciences, Jinan, China*

OPEN ACCESS

Edited by:
Yi Ma,
University of Connecticut, United States

Reviewed by:
Mei Yuan,
Shandong Peanut Research institute, China
Kunling Chen,
Institute of Genetics and Developmental Biology (CAS), China
Jianwei Gao,
Institute of Vegetables and Flowers, Shandong Academy of Agricultural Sciences, China

***Correspondence:**
Shubo Wan
wansb@saas.ac.cn
Xinguo Li
xinguol@163.com

Specialty section:
This article was submitted to Plant Traffic and Transport, a section of the journal Frontiers in Plant Science

Received: *21 March 2017*
Accepted: *30 June 2017*
Published: *14 July 2017*

Citation:
Li Y, Meng J, Yang S, Guo F, Zhang J, Geng Y, Cui L, Wan S and Li X (2017) Transcriptome Analysis of Calcium- and Hormone-Related Gene Expressions during Different Stages of Peanut Pod Development. Front. Plant Sci. 8:1241. doi: 10.3389/fpls.2017.01241

Peanut is one of the calciphilous plants. Calcium serves as a ubiquitous central hub in a large number of signaling pathways. In the field, free calcium ion (Ca^{2+})-deficient soil can result in unfilled pods. Four pod stages were analyzed to determine the relationship between Ca^{2+} excretion and pod development. Peanut shells showed Ca^{2+} excretion at all four stages; however, both the embryo of Stage 4 (S4) and the red skin of Stage 3 (S3) showed Ca^{2+} absorbance. These results showed that embryo and red skin of peanut need Ca^{2+} during development. In order to survey the relationship among calcium, hormone and seed development from gene perspective, we further analyzed the seed transcriptome at Stage 2 (S2), S3, and S4. About 70 million high quality clean reads were generated, which were assembled into 58,147 unigenes. By comparing these three stages, total 4,457 differentially expressed genes were identified. In these genes, 53 Ca^{2+} related genes, 40 auxin related genes, 15 gibberellin genes, 20 ethylene related genes, 2 abscisic acid related genes, and 7 cytokinin related genes were identified. Additionally, a part of them were validated by qRT-PCR. Most of their expressions changed during the pod development. Since some reports showed that Ca^{2+} signal transduction pathway is involved in hormone regulation pathway, these results implied that peanut seed development might be regulated by the collaboration of Ca^{2+} signal transduction pathway and hormone regulation pathway.

Keywords: peanut, calcium, hormone, pod development, transcriptome

INTRODUCTION

Peanut (*Arachis hypogaea* L.) is an important crop member of the legume family and a major source of plant oil, proteins, essential vitamins and minerals that can be used for human consumption, animal feed, bioenergy, and health products (Higgs, 2002; Li et al., 2010, 2011). Seed formation of peanut is a central stage of pod development. Some reports illustrated that seed development depends on the highly coordination between endogenous signal and environment stimuli (Sun, 2008). For instance, several plant hormones have long been known to play a significant role in peanut gynophore elongation and embryo differentiation, such as auxin (Jacobs, 1951; Moctezuma and Feldman, 1996), the ration of NAA and kinetin (Ziv and Zamski, 1975),

FIGURE 1 | Effects of soil free Ca^{2+} on peanut pod development. The experiments were conducted on a farmland with 4 g (free Ca^{2+}) kg^{-1} (dry soil). **(A)** Applied 120 kg CaO ha^{-1}. **(B)** Without CaO application.

ABA (Ziv and Kahana, 1988), ethylene (Shlamovitz et al., 1995), and so on. In addition, peanut needs more calcium relative to other plants. Free Ca^{2+} concentration in soil serious affects peanut fruiting and yield (Cox et al., 1982). During pod development, more than 90% calcium was directly absorbed from the soil by pod (Beringer and Taha, 1976). For plants, Ca^{2+} not only play roles as a nutrient element, but also as a second messenger in the regulation of diverse metabolic processes (Poovaih and Ready, 1993). As to the possible relationship between calcium signal transduction and plant hormones, Yang et al. (2015) reported that the expressions of most calmodulin-binding transcription activators of *M. Truncatula* (MtCAMTAs) were responsive to the four hormones, including IAA, salicylic acid (SA), jasmonic acid (JA), and ABA, which play critical roles in the regulation of nodule organogenesis in legumes. Additionally, it seems that the ripening of strawberry fruit are co-regulated by phytohormone and calcium signal transduction (Chen et al., 2016). Recent years, although there is a comprehensive understanding of calcium physiology related to peanut abiotic stress resistance, it is of vitally important to isolate and characterize more candidate genes for understanding some mechanisms regulating peanut pod development, especially Ca^{2+} and hormone regulating pathway.

With the development of molecular biological techniques, the genomic research has been conducted and made a considerable progress in model legume, e.g., soybean (Severin et al., 2010; Wilson and Grant, 2010; Woody et al., 2011) and *Medicago* (Cannon et al., 2005), but relatively less progress in peanut (Pandey et al., 2012; Zhang et al., 2012). The advent of rapid and high-throughput technology for quantification of the transcriptome (Malone and Oliver, 2011) benefited the peanut genomics research, and was used in the seed development and tissue expression of peanut (Zhang et al., 2012; Chen et al., 2013; Wang et al., 2013; Zhu et al., 2014). These researches make it probability to study the relationship of between calcium and peanut pod development by transcriptome method, and explore valuably candidate genes. In the present study, to better understand the roles of Ca^{2+} in pod development, we compared the transcriptome profile of peanut pod at different developmental stages, through which some potential candidate genes was identified to be related to calcium and hormone.

MATERIALS AND METHODS

Plant Materials and Treatments

Peanut cultivar, 'Huayu 22,' was provided by Biotechnology Research Center, Shandong Academy of Agricultural Science (SAAS, China). Free Ca^{2+} content in soil is 14 g (free Ca^{2+}) kg^{-1} (dry soil). The pods were collected at the 1st (Stage 1, abbr. S1), 5th (Stage 2, abbr. S2), 10th (Stage 3, abbr. S3), 20th (Stage 4, abbr. S4) day after the peg elongation into the soil. Four stage materials were used for Ca^{2+} excretion determination. The materials of S2, S3, and S4 were collected and immediately frozen in liquid nitrogen, and then

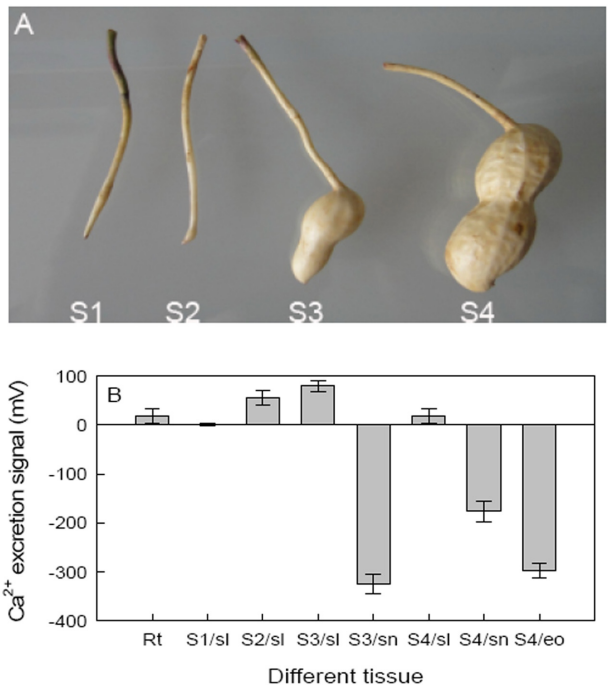

FIGURE 2 | Effects of calcium on peanut pod development and the Ca^{2+} excretion of different pod tissues. **(A)** Hair roots and four different pod developing stages were selected as detecting materials. **(B)** Ca^{2+} excretion was further detected on different tissues of these stages. Each value was averaged from more than three replicates (mean ± SD).

stored in a freezer at −80°C for comparative transcriptome analysis.

Calcium oxide (CaO) Application in Soil

Field experiments was conducted to observe effects of free Ca^{2+} in soil on pod development in Sanzhuang, Rizhao, Shandong Province in spring 2014 and 2015. Free Ca^{2+} content in soil is 4 g (free Ca^{2+}) kg^{-1} (dry soil). The 120 kg CaO ha^{-1} was applied in soil as Ca^{2+} treatment, and non-CaO treatment was as control. Each treatment had three replicates. CaO was applied before sowing.

Ca^{2+} Excretion Measured by Non-invasive Micro-test Technology (NMT)

Ca^{2+} excretion in pods of peanut were measured with NMT system (NMT100 Series, YoungerUSA LLC, Amherst, MA, United States; Xuyue (Beijing) Science and Technology Co., Ltd., Beijing, China) and iFluxes/imFluxes 1.0 (YoungerUSA, LLC, Amherst, MA, United States) Software. Steady-state ion fluxes were measured for 5–20 min. After that, the test treatment was applied and the ion flux in the meristematic zone (120 μm from the root/pod tip) was measured for further 10 min and recorded the data (Yue et al., 2012). And the roots and pods were treated with 40 μm Ca^{2+} solution. Each treatment was repeated at least three times and all tests were repeated at least six times.

Total RNA Isolation and mRNAs Purification

Total RNA was isolated and integrity confirmed using a 2100 Bioanalyzer (Agilent Technologies). Beads with oligo(dT) were used to isolate poly(A) mRNA from total RNA (Qiagen GmbH, Hilden, Germany).

Synthesis of cDNA and Sequencing

Following purification, the mRNA was fragmented using divalent cations under elevated temperature. Taking these short fragments as templates, the first-strand cDNA was synthesized using random hexamer primers and Superscript™ III (Invitrogen™, Carlsbad, CA, United States). The second strand cDNA was synthesized using buffer, dNTPs, RNaseH, and DNA polymerase I. Short fragments were purified with a QiaQuick PCR extraction kit (Qiagen) and resolved with EB buffer for end reparation and poly(A) addition. The short fragments were then connected using sequencing adapters. After agarose gel electrophoresis, suitable fragments were used as templates for PCR amplification. Finally, the library was sequenced from both directions on HiSeq 2000 System (illumina, San Diego, CA, United States) with 100 bp of data collected per run by applying TruSeq PE Cluster and TruSeq SBS Kits (illumina, San Diego, CA, United States). Data analysis and base calling were achieved by applying the illumina instrument software.

Transcriptome *De Novo* Assembly

The reference transcripts of a progenitor of cultivated peanut (*Arachis ipaensis*) were used to generate an integrated reference library. The processing and assembly of transcriptome data were performed with the application of modified Velvet to construct unique consensus sequences (Zerbino and Birney, 2008). The gene expression profile was developed by mapping trimmed transcriptome reads onto the unique consensus sequences by using SOAP2 (Li et al., 2009).

Annotation and Classification of Unigenes

Comparative transcriptomics analysis was conducted among the three different developmental stages. The intensity values of each sample were further transformed on $\log_2$-scale and used for differential expression analysis. The probe sets with a P-value < 0.01 and $>$ two-fold changes in at least one of the comparisons were considered as differentially expressed genes (DEGs) for further analysis. Unigenes were used for BLAST searches and annotation against an NCBI Nr protein database (NCBI non-redundant sequence database) by using an E-value cut-off of 10^{-5} (E-value < 0.00001). Unigenes sequences were further aligned by BLASTX to protein databases such as Swiss-Prot, KEGG, and COG, retrieving proteins with the highest sequence similarity with the given unigenes along with their protein functional annotations. If results of different databases conflicted, a priority order of Nr, Swiss-Prot, KEGG, and COG was followed. For unigenes that did not align to any of the above databases, EST Scan software (Iseli et al., 1999) was used to predict their coding regions and determine sequence

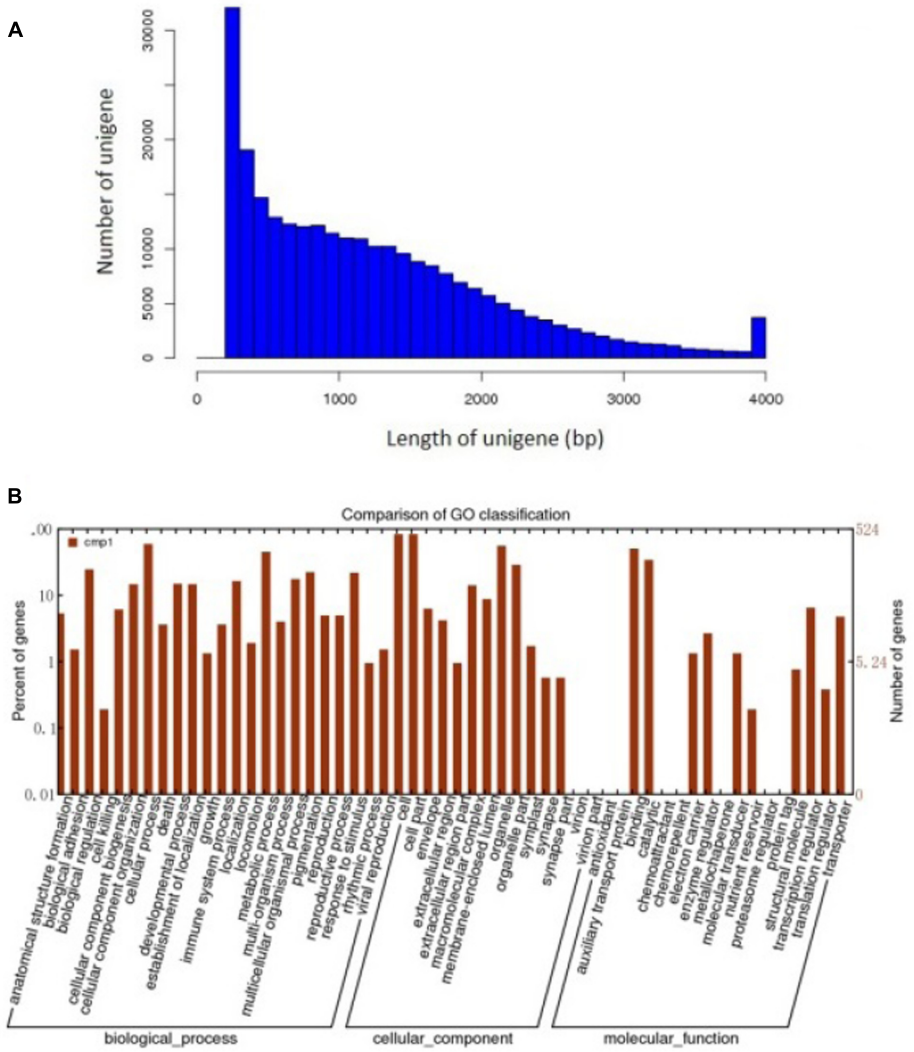

FIGURE 3 | Assembly and functional annotations of peanut seed transcriptomes. **(A)** Sequence lengths of 263,110 assembled peanut unigenes. **(B)** A histogram of unigene ontology classification.

direction. Unigenes aligned to databases with higher priority did not enter the next circle. The alignments were considered complete when all circles were finished. The coding region sequences were then determined for proteins with the highest ranks using BLAST. Unigenes that could not be aligned to any database were scanned by EST Scan (Iseli et al., 1999) to determine the nucleotide (50–30) and amino acid sequences of the coding regions. The Blast2 GO was used to obtain Gene Ontology (GO) annotations for the unigenes, as well as for KEGG and COG analysis (Conesa et al., 2005). The WEGO software was then used to perform GO functional classification of all unigenes to view the distribution of gene functions of the species at the macro level (Ye et al., 2006). It was mapped all of the annotated unigenes to GO terms in the database and calculated the number of unigenes associated with every term.

Real-Time Fluorescent Quantitative PCR Analysis

Total RNA was isolated and purified using TRIzol Reagent (Tiangen, China) according to the manufacture's instruction. The first-strand cDNA was synthesized by using Reverse Transcriptase M-MLV (Takara, Japan) according to the manufacturer's protocol. The PCR was amplified following the instruction of SYBR *Premix Ex Taq*^{TM} (Takara, Japan) with the fluorescent quantitative PCR amplification instrument (ABI 7500, United States). The target gene primers were used to detect the sample mRNA. Control reactions were carried out by using primers Tua5-F and Tua5-R to detect the transcript encoding ubiquitously expressed tua5 (Chi et al., 2012). All assays for a target gene were performed in triplicate synchronously under identical conditions.

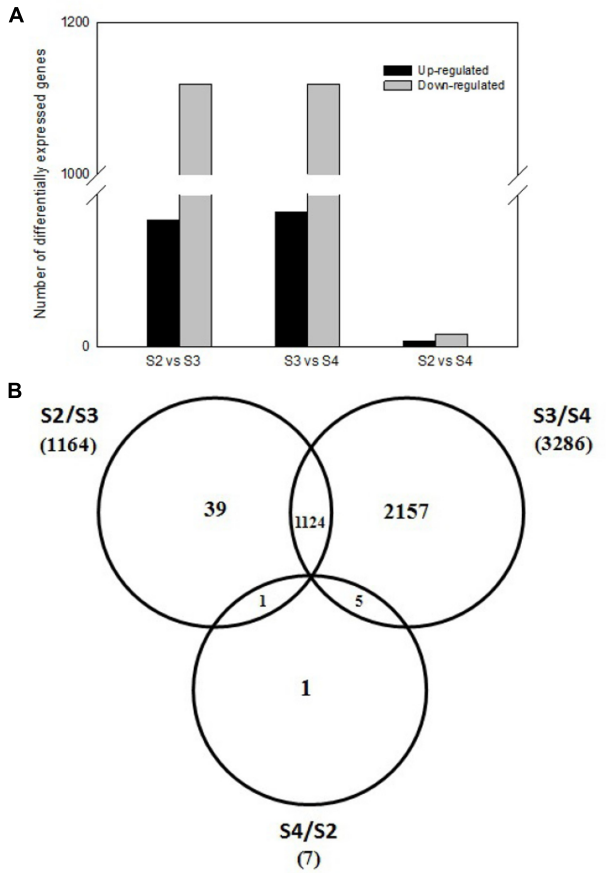

FIGURE 4 | Comparative analysis of three pod developmental stages. **(A)** Comparative analysis of different expressed genes between three pod developmental stages. **(B)** The number of differentially expressed genes between three pods development stages. The numbers of up-regulated and down-regulated genes are indicated at the 5th (S2), 10th (S3), 20th (S4) day after the peg elongation into the soil.

RESULTS

Effects of Calcium on Peanut Pod Development and Ca^{2+} Excretion of Different Pod Tissues

Peanut is one of the important oil crops for China, and its yield is often affected by all kinds of environmental factors, including free Ca^{2+} content in soil. When free Ca^{2+} is deficient in soil, it will cause unfilling of pods. **Figure 1** showed that pods were unfilled under 4 g (free Ca^{2+}) kg^{-1} (dry soil), and CaO application can benefit pod filling.

To assess the role of Ca^{2+} on pod development, hair root and four stages of pods were analyzed to determine Ca^{2+} excretion where: the peg just entered the soil (S1), tip of the peg initiated expansion (S2), beginning of pod reticulation (S3), and when the pod was clearly reticulated (S4), respectively, used to analyze (**Figure 2A**). The non-invasive microtest technique was used to detect net fluxes of Ca^{2+} at different seed tissues of different stages. Besides hair roots, peanut shells showed Ca^{2+} excretion at all four stages; however, both the embryo of S4 and the red skin of S3 and S4 showed Ca^{2+} absorbance. These results showed that embryo alone and embryo with red skin of peanut need Ca^{2+} during development (**Figure 2B**).

Assembly and Functional Annotations of Peanut Seed Transcriptomes

To further detect some mechanisms relate to the roles of Ca^{2+} in pod development. About 70 million high quality reads were obtained from the library. The average read size, Q30 percentage (sequencing error rate, 0.1%), and GC percentage for each library was 90 bp, >95%, and >40%, respectively. Clean reads from each library were used for assembly separately. And 263,110 unigenes were generated from library. The *de novo* assembly of all sequencing data using the modified Velvet was followed by the application of the SOAP2 program for unigene identification. The average sequence length of the unigenes was 1,235 bp and its range was 201–4,000 bp (**Figure 3A**).

The GO assignments were used to categorize the functions of the predicted peanut Unigenes. Based on the sequence homologies, the sequences were categorized into 45 functional groups (**Figure 3B**), contained three main categories of the GO classification (biological processes, cellular components, and molecular functions). The genes involved in cellular process and metabolic process were dominant in the "Biological Process" category. "Cell," "Cell part," and the "Organelle" are the top three abundant categories in "Cellular component," While "Binding," and "catalytic activity" are dominant in the "Molecular function" category (**Figure 3B**).

Comparative Analysis of Three Pod Developmental Stages

To investigate expression levels of stage-specific genes during pods development, we conducted comparative analysis of the transcriptome profiles among three pod development stages at 5th (S2), 10th (S3), 20th (S4) day after the peg elongation into the soil. As shown in **Figure 4A**, totally 1,169 DEGs were obtained between S2 and S3, including 50 up-regulated and 1,119 down-regulated genes. Similarly, 1,172 DEGs (including 53 up-regulated and 1,119 down-regulated genes), 7 DEGs (including two up-regulated and five down-regulated genes) were identified between S3 and S4, S2 and S4, respectively. In addition, some other stage-specific expression genes were also analyzed. Approximately 39, 2157, and 1 stage-specific expression genes were identified between S2 and S3, S3 and S4, S2 and S4, respectively (**Figure 4B**).

Calcium and Ca^{2+} Signal Related Unigenes and Their Functional Categories

Since deficient free Ca^{2+} in soil can cause unfilling of pods, some DEGs involved in biological process of Ca^{2+} binding and Ca^{2+}

TABLE 1 | The annotation of candidate genes related to calcium during pods development.

Gene ID	Uniprot No.	Gene description	Species	*E*-value
comp33933	Q8RYJ8	Putative calcium-binding protein CML19	*Oryza*	4.00*e* − 23
comp43665	Q9LE22	Probable calcium-binding protein CML27	*Arabidopsis*	5.00*e* − 55
comp36255	Q8L3R2	Probable calcium-binding protein CML41	*Arabidopsis*	9.00*e* − 37
comp50658	Q9ZQH1	Probable calcium-binding protein CML48	*Arabidopsis*	1.00*e* − 13
comp53390	Q9LF79	Calcium-transporting ATPase 8	*Arabidopsis*	0
comp51237	Q9FKP1	Cation/calcium exchanger 1	*Arabidopsis*	3.00*e* − 174
comp45295	Q9FKP2	Cation/calcium exchanger 2	*Arabidopsis*	1.00*e* − 50
comp14601	Q8LEM7	Calcineurin B-like protein 3	*Arabidopsis*	1.00*e* − 63
comp47042	O81223	Calcineurin B-like protein 4	*Arabidopsis*	8.00*e* − 100
comp47926	O65718	Cyclic nucleotide-gated ion channel 2	*Arabidopsis*	0
comp42319	P51074	Annexin-like protein RJ4	*Fragaria*	2.00*e* − 158
comp45239	Q940H6	Serine/threonine-protein kinase SRK2E	*Arabidopsis*	0
comp36540	Q96262	Plasma membrane-associated cation-binding protein 1	*Arabidopsis*	1.00*e* − 47
comp48463	Q93ZH2	Nuclear transcription factor Y subunit A-3	*Arabidopsis*	3.00*e* − 36
comp40687	P34913	Bifunctional epoxide hydrolase 2	*Homo*	2.00*e* − 19
comp49372	Q8LFG1	Probable alpha-amylase 2	*Arabidopsis*	1.00*e* − 149
comp52512	P14226	Oxygen-evolving enhancer protein 1	*Pisum*	0
comp38946	P16059	Oxygen-evolving enhancer protein 2	*Pisum*	2.00*e* − 151
comp46793	Q41932	Oxygen-evolving enhancer protein 3-2	*Arabidopsis*	3.00*e* − 81
comp48726	Q39254	Vacuolar cation/proton exchanger 2	*Arabidopsis*	8.00*e* − 6
comp45043	Q93Z81	Vacuolar cation/proton exchanger 3	*Arabidopsis*	2.00*e* − 151
comp47437	Q2HXL0	Respiratory burst oxidase homolog protein C	*Solanum*	0
comp51314	O48538	Respiratory burst oxidase homolog protein F	*Arabidopsis*	0
comp31869	Q39033	Phosphoinositide phospholipase C 2	*Arabidopsis*	8.00*e* − 50
comp50062	P17859	Phosphoinositide phospholipase C 2	*Arabidopsis*	8.00*e* − 50
comp41809	O82598	Aquaporin TIP1-3	*Arabidopsis*	2.00*e* − 129
comp33153	A5A7I7	Calcium-dependent protein kinase 4	*Solanum*	0
comp45958	Q9SSF8	Calcium-dependent protein kinase 30	*Arabidopsis*	0
comp44027	P28583	Calcium-dependent protein kinase SK5	*Glycine*	0
comp52882	Q6DN14	Multiple C2 and transmembrane domain-containing protein 1	*Homo*	2.00*e* − 10
comp50090	Q6DN12	Multiple C2 and transmembrane domain-containing protein 2	*Homo*	4.00*e* − 23
comp41514	O81270	Peroxygenase 1	*Arabidopsis*	1.00*e* − 107
comp51310	Q641Z6	EH domain-containing protein 1	*Rattus*	2.00*e* − 146
comp53583	Q8L493	Branched-chain-amino-acid aminotransferase-like protein 3	*Arabidopsis*	6.00*e* − 134
comp46176	O81916	Uncharacterized calcium-binding protein At1g02270	*Arabidopsis*	1.00*e* − 150
comp43596	Q8LBL1	Two-pore potassium channel 1	*Arabidopsis*	2.00*e* − 131
comp40656	Q9LDQ3	Putative cysteine-rich receptor-like protein kinase 35	*Arabidopsis*	6.00*e* − 78
comp52241	Q8L7E9	Protein MID1-COMPLEMENTING ACTIVITY 1	*Arabidopsis*	0
comp52082	Q94A4	Alpha-amylase 3, chloroplastic	*Arabidopsis*	0
comp52718	Q9C8E7	Glutamate receptor 3.3	*Arabidopsis*	0
comp43681	Q9LSQ6	Calcium-binding protein PBP1	*Arabidopsis*	4.00*e* − 37
comp34785	Q9LSQ6	Calcium-binding protein PBP1	*Arabidopsis*	3.00*e* − 43
comp49728	Q41142	Phospholipase D alpha 1	*Ricinus*	2.00*e* − 43
comp50171	Q9FYH7	Vacuolar-sorting receptor 6	*Arabidopsis*	4.00*e* − 13
comp50757	Q9FYH7	Vacuolar-sorting receptor 6	*Arabidopsis*	0
comp44749	Q93Z81	Vacuolar cation/proton exchanger 3	*Arabidopsis*	5.00*e* − 171
comp46345	P42055	Mitochondrial outer membrane protein porin of 34 kDa	*Solanum*	1.00*e* − 35
comp51265	Q9C9L5	Wall-associated receptor kinase-like 9	*Arabidopsis*	5.00*e* − 8
comp25145	F4JJJ3	NAD(P)H dehydrogenase B3, mitochondrial	*Arabidopsis*	0
comp48262	Q9BVG8	Kinesin-like protein KIFC3	*Homo*	4.00*e* − 60
comp49233	Q9FKI0	Fimbrin-like protein 2	*Arabidopsis*	0
comp45947	Q298L5	Mitochondrial Rho GTPase	*Sophophora*	5.00*e* − 87
comp42934	Q9S7C9	Putative DNA-binding protein ESCAROLA	*Arabidopsis*	5.00*e* − 6

TABLE 2 | The annotation of candidate genes related to hormone during pods development.

Gene ID	Uniprot No.	Gene description	Species	*E*-value
Auxin-related				
comp43478	Q6J163	Auxin-induced protein 5NG4	*Pinus*	4.00*e* − 8
comp47743	Q6J163	Auxin-induced protein 5NG4	*Pinus*	1.00*e* − 49
comp39204	Q6J163	Auxin-induced protein 5NG4	*Pinus*	3.00*e* − 15
comp51971	Q6J163	Auxin-induced protein 5NG4	*Pinus*	2.00*e* − 46
comp48589	Q6J163	Auxin-induced protein 5NG4	*Pinus*	6.00*e* − 77
comp44220	Q6J163	Auxin-induced protein 5NG4	*Pinus*	1.00*e* − 39
comp40373	Q6J163	Auxin-induced protein 5NG4	*Pinus*	5.00*e* − 29
comp48904	Q6J163	Auxin-induced protein 5NG4	*Pinus*	2.00*e* − 11
comp39544	Q6J163	Auxin-induced protein 5NG4	*Pinus*	1.00*e* − 42
comp44395	Q6J163	Auxin-induced protein 5NG4	*Pinus*	1.00*e* − 29
comp45206	Q6J163	Auxin-induced protein 5NG4	*Pinus*	2.00*e* − 56
comp49555	Q6J163	Auxin-induced protein 5NG4	*Pinus*	3.00*e* − 29
comp41016	Q6J163	Auxin-induced protein 5NG4	*Pinus*	2.00*e* − 64
comp43783	Q6J163	Auxin-induced protein 5NG4	*Pinus*	8.00*e* − 6
comp41488	Q6J163	Auxin-induced protein 5NG4	*Pinus*	5.00*e* − 47
comp46020	Q6J163	Auxin-induced protein 5NG4	*Pinus*	3.00*e* − 20
comp47084	Q6J163	Auxin-induced protein 5NG4	*Pinus*	1.00*e* − 28
comp34759	Q6J163	Auxin-induced protein 5NG4	*Pinus*	2.00*e* − 62
comp35338	Q6J163	Auxin-induced protein 5NG4	*Pinus*	5.00*e* − 7
comp45159	Q6J163	Auxin-induced protein 5NG4	*Pinus*	3.00*e* − 81
comp36946	Q6J163	Auxin-induced protein 5NG4	*Pinus*	1.00*e* − 129
comp43310	Q6J163	Auxin-induced protein 5NG4	*Pinus*	3.00*e* − 146
comp43748	Q8LAL2	Auxin-responsive protein IAA26	*Arabidopsis*	1.00*e* − 70
comp36524	Q9ZSY8	Auxin-responsive protein IAA27	*Arabidopsis*	8.00*e* − 91
comp35718	Q8H174	Auxin-responsive protein IAA31	*Arabidopsis*	3.00*e* − 31
comp50484	Q94BT2	Auxin-induced in root cultures protein 12	*Arabidopsis*	3.00*e* − 6
comp46184	Q94BT2	Auxin-induced in root cultures protein 12	*Arabidopsis*	8.00*e* − 15
comp44924	Q94BT2	Auxin-induced in root cultures protein 12	*Arabidopsis*	2.00*e* − 15
comp35357	Q9LF79	Auxin-induced protein 15A	*Glycine*	2.00*e* − 19
comp30777	P33081	Auxin-induced protein 15A	*Glycine*	1.00*e* − 20
comp36019	P33079	Auxin-induced protein 10A5	*Glycine*	8.00*e* − 13
comp36785	Q9FEL6	Auxin transporter-like protein 3	*Medicago*	0
comp45084	O24543	Auxin-induced protein 22E	*Vigna*	1.00*e* − 63
comp52994	Q9FGV1	Auxin response factor 8	*Arabidopsis*	7.00*e* − 133
comp46658	Q9XED8	Auxin response factor 9	*Arabidopsis*	0
comp28367	Q653H7	Auxin response factor 18	*Oryza*	7.00*e* − 63
comp45289	Q653H7	Auxin response factor 18	*Oryza*	1.00*e* − 162
comp33145	Q653H7	Auxin response factor 18	*Oryza*	7.00*e* − 47
comp32944	Q96247	Auxin transporter protein 1	*Arabidopsis*	9.00*e* − 163
comp41401	O04012	Auxin-binding protein ABP19	*Prunus*	5.00*e* − 74
Gibberellin-related				
comp53643	O04706	Gibberellin 20 oxidase 1-B	*Triticum*	1.00*e* − 121
comp46516	Q39111	Gibberellin 20 oxidase 2	*Arabidopsis*	2.00*e* − 129
comp44953	Q39111	Gibberellin 20 oxidase 2	*Arabidopsis*	8.00*e* − 80
comp45036	Q9SQ80	Gibberellin 2-beta-dioxygenase 1	*Pisum*	4.00*e* − 160
comp48090	Q9SQ80	Gibberellin 2-beta-dioxygenase 1	*Pisum*	6.00*e* − 162
comp43715	Q9XFR9	Gibberellin 2-beta-dioxygenase 2	*Arabidopsis*	6.00*e* − 17
comp47582	O49561	Gibberellin 2-beta-dioxygenase 8	*Arabidopsis*	4.00*e* − 46
comp40312	O49561	Gibberellin 2-beta-dioxygenase 8	*Arabidopsis*	3.00*e* − 51
comp44039	Q39103	Gibberellin 3-beta-dioxygenase 1	*Arabidopsis*	1.00*e* − 88
comp45509	Q9SVS8	Gibberellin 3-beta-dioxygenase 3	*Arabidopsis*	3.00*e* − 20

(Continued)

TABLE 2 | Continued

Gene ID	Uniprot No.	Gene description	Species	*E*-value
comp37867	P46690	Gibberellin-regulated protein 4	*Arabidopsis*	6.00*e* − 38
comp41469	P46690	Gibberellin-regulated protein 4	*Arabidopsis*	7.00*e* − 33
comp13386	Q9LFR3	Gibberellin-regulated protein 14	*Arabidopsis*	1.00*e* − 19
comp27867	F4IQJ4	Gibberellin-regulated protein 11	*Arabidopsis*	1.00*e* − 23
comp40799	Q9FDW1	Transcription factor MYB44	*Arabidopsis*	3.00*e* − 32
Ethylene-related				
comp35300	Q84QC2	Ethylene-responsive transcription factor ERF017	*Arabidopsis*	7.00*e* − 33
comp11865	Q8LBQ7	Ethylene-responsive transcription factor ERF034	*Arabidopsis*	9.00*e* − 23
comp45116	Q9SKT1	Ethylene-responsive transcription factor ERF053	*Arabidopsis*	5.00*e* − 43
comp34495	Q9LY05	Ethylene-responsive transcription factor ERF106	*Arabidopsis*	5.00*e* − 35
comp37722	Q9CA27	Ethylene-responsive transcription factor ERF118	*Arabidopsis*	5.00*e* − 20
comp53691	Q8LC30	Ethylene-responsive transcription factor RAP2-1	*Arabidopsis*	9.00*e* − 41
comp42029	P42736	Ethylene-responsive transcription factor RAP2-3	*Arabidopsis*	2.00*e* − 37
comp48452	Q6X5Y6	Ethylene-responsive transcription factor WRI1	*Arabidopsis*	3.00*e* − 37
comp44242	O80340	Ethylene-responsive transcription factor 4	*Arabidopsis*	9.00*e* − 9
comp42489	Q40477	Ethylene-responsive transcription factor 4	*Nicotiana*	2.00*e* − 22
comp37530	Q8L9K1	Ethylene-responsive transcription factor 13	*Arabidopsis*	2.00*e* − 34
comp47316	Q9SUQ2	Ethylene-responsive transcription factor CRF2	*Arabidopsis*	1.00*e* − 33
comp43675	Q9SUE3	Ethylene-responsive transcription factor CRF4	*Arabidopsis*	4.00*e* − 50
comp47833	Q9LVG2	AP2-like ethylene-responsive transcription factor TOE2	*Arabidopsis*	1.00*e* − 6
comp43442	Q38914	AP2-like ethylene-responsive transcription factor ANT	*Arabidopsis*	1.00*e* − 132
comp51344	Q38914	AP2-like ethylene-responsive transcription factor ANT	*Arabidopsis*	2.00*e* − 19
comp48832	Q1PFE1	AP2-like ethylene-responsive transcription factor AIL1	*Arabidopsis*	4.00*e* − 129
comp47962	Q52QU2	AP2-like ethylene-responsive transcription factor AIL6	*Arabidopsis*	5.00*e* − 14
comp50155	Q0WPQ2	Ethylene receptor 2	*Arabidopsis*	0
comp42987	Q8GWK2	AP2-like ethylene-responsive transcription factor At2g41710	*Arabidopsis*	2.00*e* − 148
Cytokinin-related				
comp44683	Q9ZW95	Cytokinin hydroxylase	*Arabidopsis*	6.00*e* − 72
comp14370	Q9FF18	Cytokinin hydroxylase	*Arabidopsis*	22.00*e* − 516
comp42133	Q9FF18	Cytokinin hydroxylase	*Arabidopsis*	2.00*e* − 175
comp42347	Q9FUJ1	Cytokinin dehydrogenase 7	*Arabidopsis*	3.00*e* − 41
comp40332	Q9FUJ1	Cytokinin dehydrogenase 7	*Arabidopsis*	1.00*e* − 166
comp53620	Q8L8B8	Cytokinin riboside 5'-monophosphate phosphoribohydrolase LOG3	*Arabidopsis*	4.00*e* − 130
comp38806	Q84MC2	Cytokinin riboside 5'-monophosphate phosphoribohydrolase LOG8	*Arabidopsis*	2.00*e* − 127
Abscisic acid-related				
comp38442	Q8RYD6	Abscisic acid insensitive 5-like protein 1	*Arabidopsis*	3.00*e* − 28
comp29840	Q9FH76	Abscisic acid 8'-hydroxylase 3	*Arabidopsis*	5.00*e* − 160

signaling were identified based on GO analysis. These potential candidate genes contained 53 Ca^{2+} or Ca^{2+} signal pathway related genes (**Table 1**). These genes were significant differentially expressed during seed and pod development, suggesting that Ca^{2+} and calcium related protein might be involved in seed development.

Hormone Related Unigenes and Their Functional Categories

Genes related to hormone response were screened out by GO analysis. There were 40 auxin related genes, 15 gibberellin related genes, 20 ethylene related genes, 2 abscisic acid related genes, and 7 cytokinin related genes (**Table 2**) showed significant differentially expression during seed and pod development.

Real-Time Fluorescent Quantitative PCR Analysis

In order to confirm the transcriptome sequencing results, Ca^{2+} and hormone related genes were selected from DEGs based on the GO analysis and used to real-time fluorescent quantitative PCR analysis. As shown in **Figure 5**, the expression pattern of 8 selected DEGs, which are related to Ca^{2+} signal pathway, were consistent with their respective microarrays data. Among these genes, two genes, which includes one CDPK gene (comp33153) and one uncharacterized calcium-binding protein At1g02270 (comp46176), were up-regulated at S4. The Serine/threonine-protein kinase SRK2E (comp45239) was up-regulated at S2, down-regulated at S3, and then up-regulated at S4. Three probable calmodulin like protein CMLs (comp33933, comp43665, and comp50658), one calcineurin

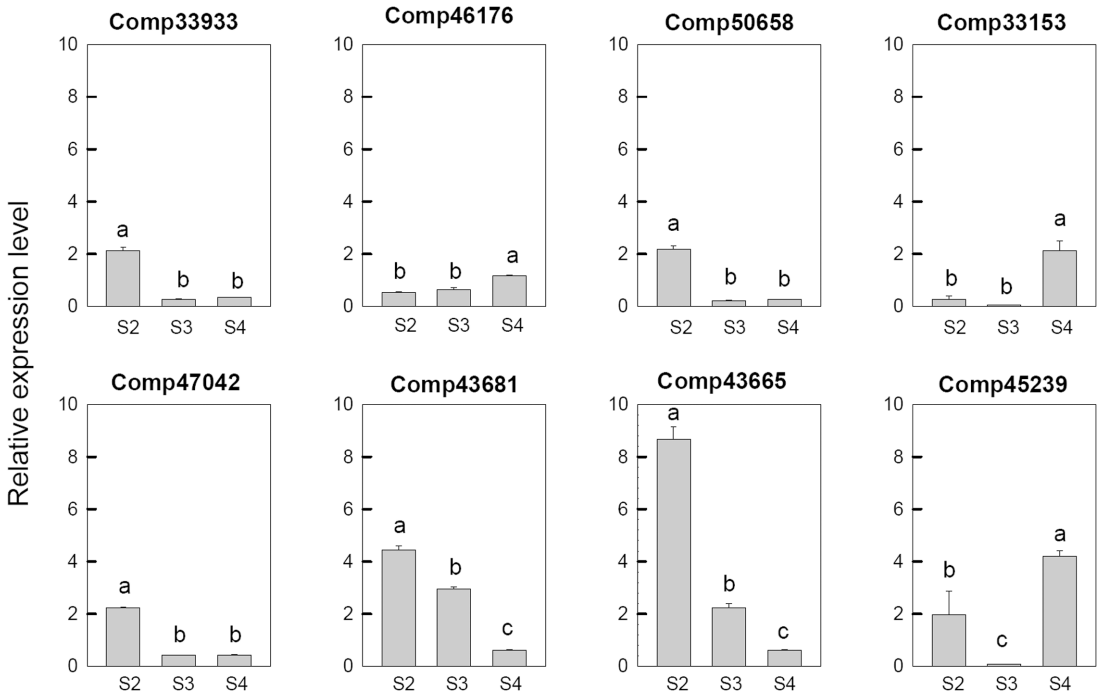

FIGURE 5 | Real-time fluorescent quantitative PCR analysis on mRNA transcription of the selected differentially expressed calcium related genes. These were the 5th (S2), 10th (S3), 20th (S4) day after the peg elongation into the soil. The ordinate axis greater than one means up-regulated, less than one was down-regulated.

B-like protein (comp47042) and one calcium-binding protein PBP1 (comp43681) were up-regulated at S2 and then down-regulated during the later stages.

Among the 12 selected auxin related genes, six genes, i.e., auxin-induced protein 5NG4 (comp43478), auxin-responsive protein IAA31 (comp35718), auxin-induced in root cultures protein 12 (comp50484), auxin-induced protein 15A (comp35357), auxin-induced protein 10A5 (comp36019), and auxin transporter-like protein 3 (comp36785), were down-regulated in S2 and then up-regulated during the later stages. Three auxin response factor 8 (comp52994, comp45289, and comp46658), one auxin-responsive protein IAA26 (comp36524) were down-regulated at S4. One auxin-induced protein 22E (comp45084) was down-regulated at S2, up-regulated at S3, and then down-regulated at S4 (**Figure 6**).

Among 11 selected gibberellin related genes, four genes, i.e., two gibberellin-regulated protein (comp41469, comp27867), two gibberellin 2-beta-dioxygenase (comp45036, comp43715), were down-regulated at S2 and then up-regulated at S4. One transcription factor MYB44 (comp40799), one gibberellin 20 oxidase (comp44953) and one gibberellin 3-beta-dioxygenase (comp44039) were up-regulated at S4. One gibberellin 20 oxidases (comp53643), one gibberellin 2-beta-dioxygenase (comp47582), one gibberellin 3-beta-dioxygenase (comp45509) and one gibberellin-regulated protein (comp13386) were up-regulated at S2, down-regulated at S3 and then up-regulated at S4 (**Figure 7**).

Seventeen selected ethylene related genes were analyzed. Two ethylene-responsive transcription factor RAP2 (comp53691 and comp42029), one ethylene-responsive transcription factor WRI1 (comp48452), three ethylene-responsive transcription factor ERF (comp34495, comp37722, and comp11865) and one AP2-like ethylene-responsive transcription factor AIL (comp47962) were down-regulated at S2 then up-regulated at S4. One ethylene-responsive transcription factor ERF (comp35300), one ethylene-responsive transcription factor (comp44242), two ethylene-responsive transcription factor CRF (comp47316 and comp43675) and one AP2-like ethylene-responsive transcription factor ANT (comp43442) were only down-regulated at S4. The AP2-like ethylene-responsive transcription factor TOE (comp47833) and ethylene-responsive transcription factor ERF (comp45116) were up-regulated at S4. AP2-like ethylene-responsive transcription factor At2g41710 (comp42987) and AP2-like ethylene-responsive transcription factor AIL1 (comp48832) were down-regulated at S2, up-regulated at S3, and then down-regulated at S4. The ethylene-responsive transcription factor 13 (comp37530) was up-regulated at S2 and S3, then down-regulated at S4 (**Figure 8**).

Among the four cytokinin related genes, cytokinin dehydrogenase (comp42347) was only up regulated at S4, cytokinin hydroxylase (comp44683) was down-regulated at S2 then up-regulated in later stage, cytokinin riboside 5′-monophosphate phosphoribohydrolase LOG3 (comp53620) was down-regulated from S3 and the Cytokinin riboside 5′-monophosphate phosphoribohydrolase LOG8 (comp38806) up-regulated from S3 (**Figure 9A**).

For the two abscisic acid related genes, the abscisic acid 8′-hydroxylase 3 (comp29840) was up-regulated at S3 and then

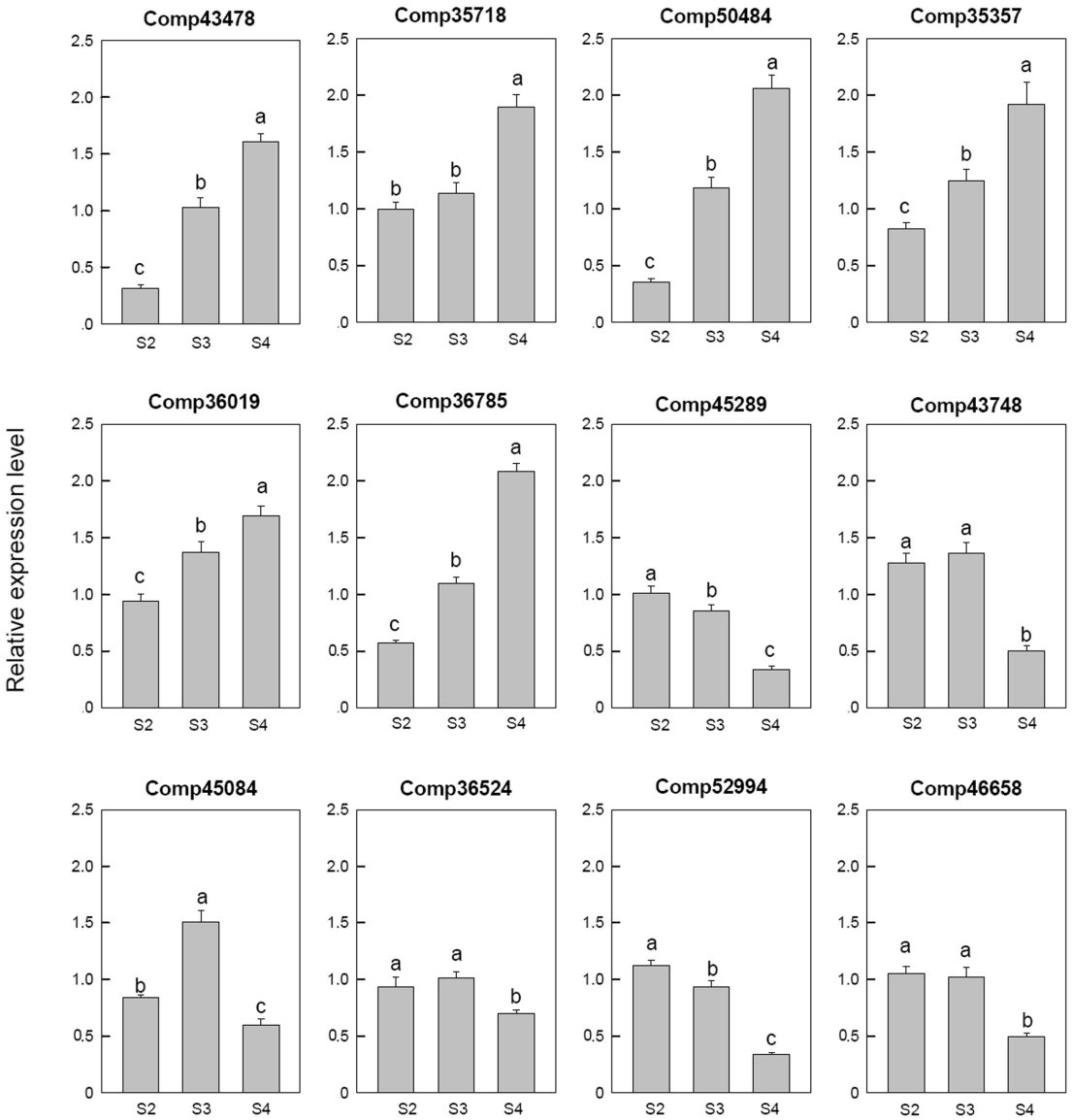

FIGURE 6 | Real-time fluorescent quantitative PCR analysis on mRNA transcription of the selected differentially expressed auxin related genes. These were the 5th (S2), 10th (S3), 20th (S4) day after the peg elongation into the soil. The ordinate axis greater than one means up-regulated, less than one was down-regulated.

down-regulated, however, the abscisic acid insensitive 5-like protein 1 (comp38442) was down-regulated at S2 (**Figure 9B**).

DISCUSSION

Calcium is not only an essential macroelement for plant growth, but also a second messenger involved in regulating diverse physiological processes (Poovaih and Ready, 1993). Peanut remains one of the most important oil-crops in the world, and Calcium is by far the most critical nutrient for this crop to achieve high yields. Calcium deficiency in soil can results in a decrease in yield, e.g., unfilled pods (Cox et al., 1982). Unfilled pods were also found in free Ca^{2+}-insufficient soil in the present work (**Figure 1**), and the pod yield would decreased by 20% or more. For pods, it seems that embryo alone or embryo with red skin are the main tissues need more Ca^{2+} (**Figure 2B**). It attracts us to pay more attention to investigate the mechanisms of how Ca^{2+} is involved in pod development.

As a powerful technique, transcriptome sequencing was used to observe global gene expression profiles and the physiological processes involved in various plants (Clarke and Zhu, 2006). As to fruit development, it has been applied to strawberry (Aharoni and O'Connell, 2002), tomato (Alba et al., 2005), pear (Fonseca et al., 2004), apple (Lee et al., 2007), and peanut seed development (Zhang et al., 2012; Zhu et al., 2014). But the relationship between calcium and peanut seed at different pods developmental stages was seldom mentioned. In the present work, 263,110

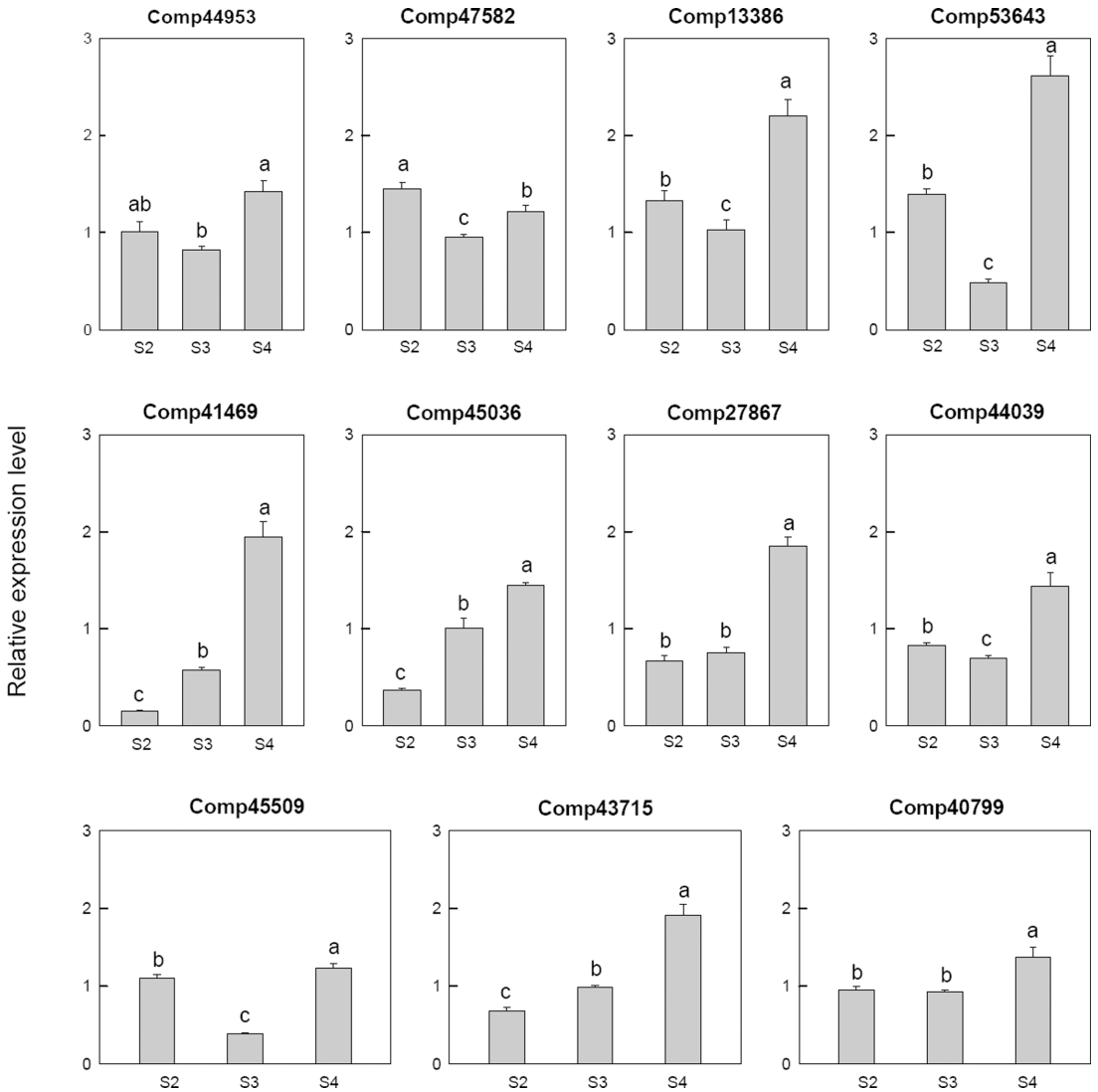

FIGURE 7 | Real-time fluorescent quantitative PCR analysis on mRNA transcription of the selected differentially expressed gibberellin related genes. These were the 5th (S2), 10th (S3), 20th (S4) day after the peg elongation into the soil. The ordinate axis greater than one means up-regulated, less than one was down-regulated.

unigenes were obtained from library. We identified 4,457 DEGs via sequencing analysis, and got 2,197 stage-specific expressed genes at different pod developmental stages (**Figure 4B**). It has been reported that free Ca^{2+} concentration in soil seriously affected peanut fruiting and yield, ovary handle and pods could absorb Ca^{2+} from soil, and transport it to both the developing seed and the vegetative organs, such as stem, leaves, etc. (Beringer and Taha, 1976). In this study, through Gene Ontology analysis, many DEGs involved in the Ca^{2+} responding and Ca^{2+} signal transduction, which were identified as potential candidate genes responsible for development of pods (**Table 1**). That is to say, calcium was related to pod development at the genetic levels.

Besides an important essential element, Ca^{2+} also acts as a secondary messenger in various biological processes. It has been shown that various Ca^{2+} transporters in plants (Dayod et al., 2010) and Ca^{2+} signal transduction protein were involved in gametogenesis, fertilization and early pollen tube growth (Tirlapur and Cresti, 1992). Interestingly, in the present study, we found some calcium-related unigenes at different pod developmental stages, and eight Ca^{2+} signaling-related genes were analyzed. These genes were calcium-dependent protein kinase (CDPK), calcineurin B-like protein (CBL), calmodulin like protein (CML), and some other Ca^{2+} signaling related genes. CDPKs were thought be involved in embryogenesis, seed development and germination of sandalwood (Anil et al., 2000) and in rice seed development (Morello et al., 2000). OsCDPK2 protein had a low level during early seed development, but had a high level which maintained in 20 days after fertilization (Frattini et al., 1999). Overexpression of the CDPK OsCDPK2 in transgenic rice disrupted seed development (Laura et al., 2000). In peanut, CDPK genes might be involved in pod development since they were up-regulated at 20th day after the peg elongation into

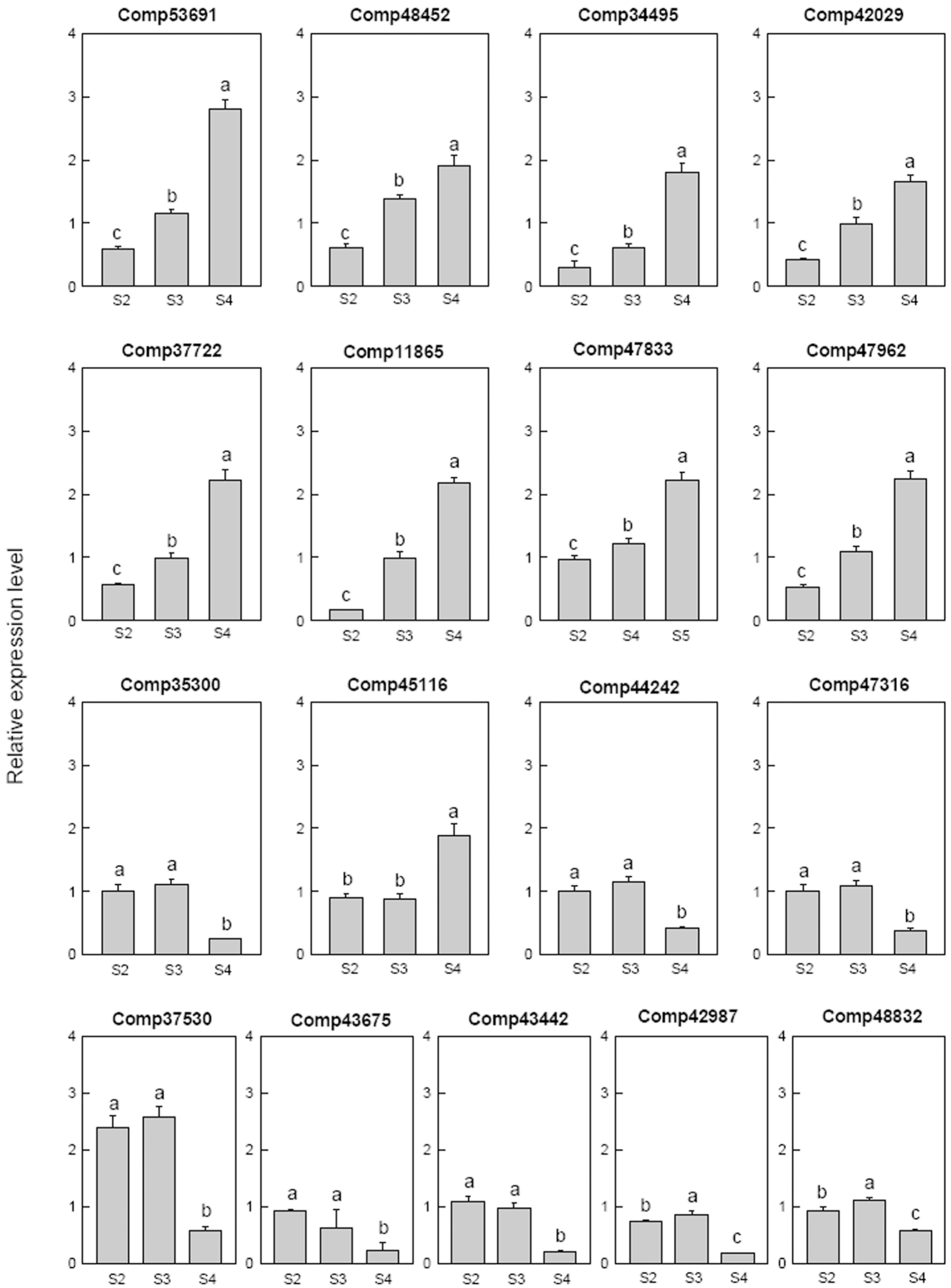

FIGURE 8 | Real-time fluorescent quantitative PCR analysis on mRNA transcription of the selected differentially expressed ethylene related genes. These were the 5th (S2), 10th (S3), 20th (S4) day after the peg elongation into the soil. The ordinate axis greater than one means up-regulated, less than one was down-regulated.

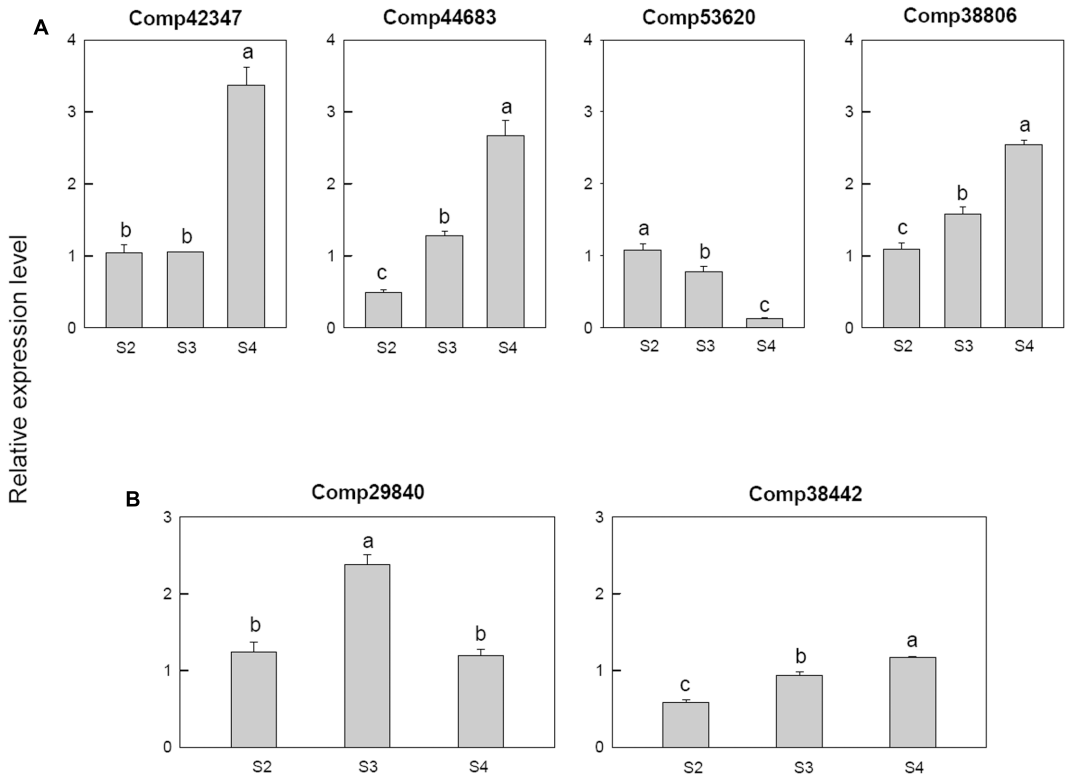

FIGURE 9 | Real-time fluorescent quantitative PCR analysis on mRNA transcription of the selected differentially expressed genes. **(A)** Cytokinin related genes, **(B)** abscisic acid related genes. These were the 5th (S2), 10th (S3), 20th (S4) day after the peg elongation into the soil. The ordinate axis greater than one means up-regulated, less than one was down-regulated.

the soil (**Figure 5**). However, some other calcium signal related genes, such as CBL, CML, and PBP1 were all down-regulated. These results implied that Ca^{2+}-signaling transduction pathway might be involved in pod development.

Auxin, gibberellin, abscisic acid, cytokinin, and ethylene have been implicated in regulating the peanut seed development and pod maturation (Jacobs, 1951; Ziv and Kahana, 1988; Shlamovitz et al., 1995; Moctezuma and Feldman, 1996; Ozga and Reinecke, 2003). Meanwhile, genes encoding key enzymes related to hormone metabolism showed significant changes in transcriptional level during peanut early pod development (Xia et al., 2013). In this study, a number of DEGs related to hormone response were identified at different pods developmental stages, e.g., auxin response factor, auxin-induced protein, auxin response factor, gibberellin-regulated protein, gibberellin 2-beta-dioxygenase, gibberellin 3-beta-dioxygenase, ethylene-responsive transcription factor, AP2-like ethylene-responsive transcription factor, cytokinin hydroxylase, cytokinin dehydrogenase, abscisic acid insensitive 5-like protein, and abscisic acid 8′-hydroxylase (**Table 2**). All these revealed that hormone response genes potentially played a crucial role in peanut seed development.

Seed development is a complex process, many physiological processes occurred during seed development (**Figure 3**), calcium and hormone seems to play important roles in this progress, respectively. It has been known that hormonal controls on cell division and expansion are active in the development of fruit. Many of phytohormonal pathways utilize changes in cytoplasmic calcium concentration ([Ca2C]cyt) as a secondary signal messenger (e.g., ABA, JA, auxin, GA, ethylene, brassinosteroids, and cytokinins) (Fortes et al., 2015). Recently, more and more reports showed that Ca^{2+} signal transduction pathway is involved in phytohormonal pathways. In Arabidopsis, a CPK4 is involved in modulating ABA signaling (Wang et al., 2017), meanwhile, CPK28 plays a role in balancing the phytohormones JA and GA in development (Matschi et al., 2015), and affects ethylene biosynthesis (Jin et al., 2017). Additionally, the calmodulin-like protein CML20, a functional Ca^{2+} sensor, negatively regulates ABA-induced stomatal movement in Arabidopsis (Wu et al., 2017), StCDPK3 in involved in the cross-talk between ABA and GA signaling at the onset of potato tuber development (Grandellis et al., 2016).

The present study provided basis for finding and screening calcium related gene and hormone response genes during peanut seed development. We speculated that besides being components of cell, such as membrane or something else, peanut seed development might be regulated by the collaboration of Ca^{2+} signal transduction pathway and hormone regulation pathway, or Ca^{2+} regulates pod development through modulating hormone since Ca^{2+} signal transduction pathway can modulate plant

hormone (Yang and Komatsu, 2000; Ullanat and Jayabaskaran, 2002; Mori et al., 2006), and it also might be related to the utilization calcium of auxin and ABA pathways as both a protein binding secondary messenger and in membrane transport mechanisms that modify turgor and solute accumulation to drive cell expansion and ripening (Hocking et al., 2016).

AUTHOR CONTRIBUTIONS

SW and XL planned and designed the research. YL, JM, FG, SY, JZ, YG, and LC performed experiments. YL collected data and conducted analysis. YL and XL wrote the manuscript.

ACKNOWLEDGMENTS

This work was supported by the National Natural Science Foundation of China (31571581, 31571605, 31601261, 31601261), the Natural Science Foundation of Shandong Province (ZR2015YL077 and BS2015SW020), the Postdoctoral Science Foundation of China (2016M592236), the Project of Significant Application of Agricultural Technology Innovation in Shandong Province, International Science and Technology Cooperation Program of China (2015DFA31190), the Supporting Plan of National Science and Technology of China (2014BAD11B04), the earmarked fund for Modern Agroindustry Technology Research System (CARS14).

REFERENCES

Aharoni, A., and O'Connell, A. (2002). Gene expression analysis of strawberry achene and receptacle maturation using DNA microarrays. *J. Exp. Bot.* 53, 2073–2087. doi: 10.1093/jxb/erf06

Alba, R., Payton, P., Fei, Z., McQuinn, R., Debbie, P., Martin, G. B., et al. (2005). Transcriptome and selected metabolite analyses reveal multiple points of ethylene control during tomato fruit development. *Plant Cell* 17, 2954–2965. doi: 10.1105/tpc.105.036053

Anil, V. S., Harmon, A. C., and Rao, K. S. (2000). Spatio-temporal accumulation and activity of calcium-dependent protein kinases during embryogenesis, seed development, and germination in sandalwood. *Plant Physiol.* 122, 1035–1043. doi: 10.1104/pp.122.4.1035

Beringer, H., and Taha, H. A. (1976). ^{45}Calcium absorption by two cultivars of groundnut (*Arachis hypogea*). *Exp. Agric.* 12, 1–7.

Cannon, S. B., Crow, J. A., Heuer, M. L., Wang, X., Cannon, E. K. S., Dwan, C., et al. (2005). Databases and information integration for the *Medicago truncatula* genome and transcriptome. *Plant Physiol.* 138, 38–46. doi: 10.1104/pp.104.059204

Chen, J., Mao, L., Mi, H., Lu, W., Ying, T., and Luo, Z. (2016). Involvement of three annexin genes in the ripening of strawberry fruit regulated by phytohormone and calcium signal transduction. *Plant Cell Rep.* 35, 733–743. doi: 10.1007/s00299-015-1915-5

Chen, X. P., Zhu, W., Azam, S., Li, H., Zhu, F., Li, H., et al. (2013). Deep sequencing analysis of the transcriptomes of peanut aerial and subterranean young pods identifies candidate genes related to early embryo abortion. *Plant Biotechnol. J.* 11, 115–127. doi: 10.1111/pbi.12018

Chi, X. Y., Hu, R. B., Yang, Q. L., Zhang, X. W., Pan, L. J., Chen, N., et al. (2012). Validation of reference genes for gene expression studies in peanut by quantitative real-time RT-PCR. *Mol. Genet. Genomics* 287, 167–176. doi: 10.1007/s00438-011-0665-5

Clarke, J. D., and Zhu, T. (2006). Microarray analysis of the transcriptome as a stepping stone towards understanding biological systems: practical considerations and perspectives. *Plant J.* 45, 630–650. doi: 10.1111/j.1365-313X.2006.02668.x

Conesa, A., Gotz, S., Garcia-Gomez, J. M., Terol, J., Talon, M., and Robles, M. (2005). Blast2GO: a universal tool for annotation, visualization and analysis in functional genomics research. *Bioinformatics* 21, 3674–3676. doi: 10.1093/bioinformatics/bti610

Cox, F. R., Adams, F., and Tucker, B. B. (1982). "Liming, fertilization, and mineral nutrition," in *Peanut Science and Technology*, eds H. E. Pattee and C. T. Young (Yoakum, TX: American Peanut Research and Education Society, Inc.), 139–163.

Dayod, M., Tyerman, S., Leigh, R., and Gilliham, M. (2010). Calcium storage in plants and the implications for calcium biofortification. *Protoplasma* 247, 215–231. doi: 10.1007/s00709-010-0182-0

Fonseca, S., Hackler, L., Zvara, A., Ferreira, S., Baldé, A., Dudits, D., et al. (2004). Monitoring gene expression along pear fruit development, ripening and senescence using cDNA microarrays. *Plant Sci.* 167, 457–469. doi: 10.1016/j.plantsci.2004.0.3.33

Fortes, A. M., Teixeira, R. T., and Agudelo-Romero, P. (2015). Complex interplay of hormonal signals during grape berry ripening. *Molecules* 20, 9326–9343. doi: 10.3390/molecules20059326

Frattini, M., Morello, L., and Breviario, D. (1999). Rice calcium-dependent protein kinase isoforms OsCDPK2 and OsCDPK11 show different responses to light and different expression patterns during seed development. *Plant Mol. Biol.* 41, 753–764. doi: 10.1023/A:1006316422400

Grandellis, C., Fantino, E., Muñiz García, M. N., Bialer, M. G., Santin, F., Capiati, D. A., et al. (2016). StCDPK3 phosphorylates in vitro two transcription factors involved in GA and ABA signaling in potato: StRSG1 and StABF1. *PLoS ONE* 11:e0167389. doi: 10.1371/journal.pone.0167389

Higgs, J. (2002). The beneficial role of peanuts in the diet-an update and rethink! Peanuts and their role in CHD. *Mol. Nutr. Food Sci.* 32, 214–218. doi: 10.1108/00346650210454190

Hocking, B., Tyerman, S. D., Burton, R. A., and Gilliham, M. (2016). Fruit calcium: transport and physiology. *Front. Plant Sci.* 7:569. doi: 10.3389/fpls.2016.00569

Iseli, C., Jongeneel, C. V., and Bucher, P. (1999). "ESTScan: a program for detecting, evaluating, and reconstructing potential coding regions in EST sequences," in *Proceedings of the International Conference on Intelligent Systems for Molecular Biology, ISMB*, Heidelberg, 138–148.

Jacobs, W. P. (1951). Auxin relationships in an intercalary meristem: further studies on the gynophore of *Arachis hypogaea* L. *Am. J. Bot.* 38, 307–310.

Jin, Y., Ye, N., Zhu, F., Li, H., Wang, J., Jiang, L., et al. (2017). Calcium-dependent protein kinase CPK28 targets the methionine adenosyltransferases for degradation by the 26S proteasome and affects ethylene biosynthesis and lignin deposition in Arabidopsis. *Plant J.* 90, 304–318. doi: 10.1111/tpj.13493

Laura, M., Milo, F., Silvia, G., Paul, C., and Diego, B. (2000). Overexpression of the calcium-dependent protein kinase OsCDPK2 in transgenic rice is repressed by light in leaves and disrupts seed development. *Transgenic Res.* 9, 453–462. doi: 10.1023/A:1026555021606

Lee, Y. P., Yu, G. H., Seo, Y. S., Han, S. E., Choi, Y. O., Daeil, K., et al. (2007). Microarray analysis of apple gene expression engaged in early fruit development. *Plant Cell Rep.* 26, 917–926. doi: 10.1007/s00299-007-0308-9

Li, R., Yu, C., Li, Y., Lam, T. W., Yiu, S. M., Kristiansen, K., et al. (2009). SOAP2: an improved ultrafast tool for short read alignment. *Bioinformatics* 25, 1966–1967. doi: 10.1093/bioinformatics/btp.336

Li, X., Hou, S., Su, M., Yang, M., Shen, S., Jiang, G., et al. (2010). Major energy plants and their potential for bioenergy development in China. *J. Environ Manage.* 46, 579–589. doi: 10.1007/s00267-010-9443-0

Li, X., Rezaei, R., Li, P., and Wu, G. (2011). Composition of amino acids in feed ingredients for animal diets. *Amino Acids* 40, 1159–1168. doi: 10.1007/s00726-010-0740-y

Malone, J. H., and Oliver, B. (2011). Microarrays, deep sequencing and the true measure of the transcriptome. *BMC Biol.* 9:34. doi: 10.1186/1741-7007-9-34

Matschi, S., Hake, K., Herde, M., Hause, B., and Romeis, T. (2015). The calcium-dependent protein kinase CPK28 regulates development by inducing growth phase-specific, spatially restricted alterations in jasmonic acid levels

independent of defense responses in Arabidopsis. *Plant Cell* 27, 591–606. doi: 10.1105/tpc.15.00024

Moctezuma, E., and Feldman, L. J. (1996). IAA redistributes to the upper side of gravistimulated peanut (*Arachis hypogaea*) gynophores. *Plant Physiol.* 111:S73.

Morello, L., Frattini, M., Christou, P., and Breviario, D. (2000). Overexpression of the calcium-dependent protein kinase OsCDPK2 in transgenic rice is repressed by light in leaves and disrupts seed development. *Transgenic Res.* 9, 453–462. doi: 10.1023/A:1026555021606

Mori, I. C., Murata, Y., Yang, Y., Munemasa, S., Wang, Y. F., Andreoli, S., et al. (2006). CDPKs CPK6 and CPK3 function in ABA regulation of guard cell S-type anion- and Ca^{2+}- permeable channels and stomatal closure. *PLoS Biol.* 4:e327. doi: 10.1371/journal.pbio.0040327

Ozga, J. A., and Reinecke, D. M. (2003). Hormonal interactions in fruit development. *J. Plant Growth Regul.* 22, 73–81. doi: 10.1007/s00344-003-0024-9

Pandey, M. K., Monyo, E., Ozias-Akins, P., Liang, X., Guimaraes, P., Nigam, S. N., et al. (2012). Advances in *Arachis* genomics for peanut improvement. *Biotechnol. Adv.* 30, 639–651. doi: 10.1016/j.biotechadv.2011.11.001

Poovaih, B. W., and Ready, A. S. (1993). Calcium and signal transduction in plants. *Crit. Rev. Plant Sci.* 12, 185–211.

Severin, A. J., Woody, J. L., Bolon, Y. T., Joseph, B., Diers, B. W., Farmer, A. D., et al. (2010). RNA-Seq Atlas of Glycine max: a guide to the soybean transcriptome. *BMC Plant Biol.* 10:160. doi: 10.1186/1471-2229-10-160

Shlamovitz, N., Ziv, M., and Zamski, E. (1995). Light, dark and growth regulator involvement in groundnut (*Arachis hypogaea* L.) pod development. *Plant Growth Regul.* 16, 37–42. doi: 10.1007/BF00040505

Sun, D. (2008). *Plant Breeding*. Beijing: China Agricultural Press, 424–443.

Tirlapur, U. K., and Cresti, M. (1992). Computer-assisted video image analysis of spatial variations in membrane-associated Ca^{2+} and calmodulin during pollen hydration, germination and tip growth in *Nicotiana tabacum* L. *Ann. Rot.* 69, 503–508.

Ullanat, R., and Jayabaskaran, C. (2002). Distinct light-, cytokinin- and tissue-specific regulation of calcium dependent protein kinase gene expression in cucumber (*Cucumis sativus*). *Plant Sci.* 162, 153–163. doi: 10.1016/S0168-9452(01)00546-5

Wang, P., Yang, Q., Sang, S., Chen, Y., Zhong, Y., and Wei, Z. (2017). Arabidopsis inositol polyphosphate kinase AtIpk2β is phosphorylated by CPK4 and positively modulates ABA signaling. *Biochem. Biophys. Res. Commun.* doi: 10.1016/j.bbrc.2017.06.060 [Epub ahead of print].

Wang, T., Chen, X. P., Li, H. F., Liu, H. Y., Hong, Y. B., Yang, Q. L., et al. (2013). Transcriptome identification of the resistance-associated genes (RAGs) to *Aspergillus flavus* infection in pre-harvested peanut (*Arachis hypogaea*). *Funct. Plant Biol.* 40, 292–303. doi: 10.1071/FP12143

Wilson, R. F., and Grant, D. (2010). *Soybean Genomics Research Program Accomplishments Report*. Available at: https://soybase.org/SoyGenStrat2007/SoyGenStratPlan2008-2012-Accomplishments%20v1.6.pdf

Woody, J. L., Severin, A. J., Bolon, Y. T., Joseph, B., Diers, B. W., Farmer, A. D., et al. (2011). Gene expression patterns are correlated with genomic and genic structure in soybean. *Genome* 54, 10–18. doi: 10.1139/G10-090

Wu, X., Qiao, Z., Liu, H., Acharya, B. R., Li, C., and Zhang, W. (2017). CML20, an *Arabidopsis* calmodulin-like protein, negatively regulates guard cell ABA signaling and drought stress tolerance. *Front. Plant Sci.* 8:824. doi: 10.3389/fpls.2017.00824

Xia, H., Zhao, C. Z., Hou, L., Li, A. Q., Zhao, S. Z., Bi, Y. P., et al. (2013). Transcriptome profiling of peanut gynophores revealed global reprogramming of gene expression during early pod development in darkness. *BMC Genomics* 14:517. doi: 10.1186/1471-2164-14-517

Yang, G., and Komatsu, S. (2000). Involvement of calcium-dependent protein kinase in rice (*Oryza sativa* L.) lamina inclination caused by brassinolide. *Plant Cell Physiol.* 41, 1243–1250.

Yang, Y., Sun, T., Xu, L., Pi, E., Wang, S., Wang, H., et al. (2015). Genome-wide identification of CAMTA gene family members in *Medicago truncatula* and their expression during root nodule symbiosis and hormone treatments. *Front. Plant Sci.* 6:457. doi: 10.3389/fpls.2015.00459

Ye, J., Fang, L., Zheng, H., Zhang, Y., Chen, J., Zhang, Z., et al. (2006). WEGO: a web tool for plotting GO annotations. *Nucleic Acids Res.* 34, W293–W297. doi: 10.1371/journal.pone.0060881

Yue, Y., Zhang, M., Zhang, J., Duan, L., and Li, Z. (2012). SOS1 gene overexpression increased salt tolerance in transgenic tobacco by maintaining a higher K^+/Na^+ ratio. *J. Plant Physiol.* 169, 225–261. doi: 10.1016/j.jplph.2011.10.007

Zerbino, D. R., and Birney, E. (2008). Velvet: algorithms for de novo short read assembly using de Bruijn graphs. *Genome Res.* 18, 821–829. doi: 10.1101/gr.074492.107

Zhang, J., Liang, S., Duan, J., Wang, J., Chen, S., Cheng, Z., et al. (2012). De novo assembly and characterisation of the transcriptome during seed development, and generation of genic-SSR markers in peanut (*Arachis hypogaea* L.). *BMC Genomics* 13:90. doi: 10.1186/1471-2164-13-90

Zhu, W., Chen, X. P., Li, H. F., Zhu, F. H., Hong, Y. B., Varshney, K. R., et al. (2014). Comparative transcriptome analysis of aerial and subterranean pods development provides insights into seed abortion in peanut. *Plant Mol. Biol.* 85, 395–409. doi: 10.1007/s11103-014-0193-x

Ziv, M., and Kahana, O. (1988). The role of the peanut (*Araschis hypogaea*) ovular tissue in the photo-morphogenetic response of the embryo. *Plant Sci.* 57, 159–164. doi: 10.1016/0168-9452(88)90082-9

Ziv, M., and Zamski, E. (1975). Geotropic responses and pod development in gynophore explants of peanut (*Arachis hypogaea* L.) cultured in vitro. *Ann. Bot. Fenn.* 39, 579–583. doi: 10.1093/oxfordjournals.aob.a084968

Conflict of Interest Statement: The authors declare that the research was conducted in the absence of any commercial or financial relationships that could be construed as a potential conflict of interest.

frontiers in Plant Science

ORIGINAL RESEARCH
published: 25 April 2017
doi: 10.3389/fpls.2017.00622

Both Light-Induced SA Accumulation and ETI Mediators Contribute to the Cell Death Regulated by *BAK1* and *BKK1*

*Yang Gao, Yujun Wu, Junbo Du, Yanyan Zhan, Doudou Sun, Jianxin Zhao, Shasha Zhang, Jia Li and Kai He **

Ministry of Education Key Laboratory of Cell Activities and Stress Adaptations, School of Life Sciences, Lanzhou University, Lanzhou, China

Receptor-like kinases BAK1 and BKK1 modulate multiple cellular processes including brassinosteroid signaling and PRR-mediated PTI in Arabidopsis. Our previous reports also demonstrated that *bak1 bkk1* double mutants exhibit a spontaneous cell death phenotype under normal growth condition. With an unknown mechanism, the cell death in *bak1 bkk1* is significantly suppressed when grown in dark but can be quickly induced by light. Furthermore, little is known about intrinsic components involved in *BAK1* and *BKK1*-regulated cell death pathway. In this study, we analyzed how light functions as an initiator of cell death and identified ETI components to act as mediators of cell death signaling in *bak1 bkk1*. Cell death suppressed in *bak1 bkk1* by growing in dark condition recurred upon exogenously treated SA. SA biosynthesis-related genes *SID2* and *EDS5*, which encode chloroplast-localized proteins, were highly expressed in *bak1-4 bkk1-1*. When crossed to *bak1-3 bkk1-1*, *sid2* or *eds5* was capable of efficiently suppressing the cell death. It suggested that overly produced SA is crucial for inducing cell death in *bak1 bkk1* grown in light. Notably, *bak1-3* or *bkk1-1* single mutant was shown to be more susceptible but *bak1-3 bkk1-1* double mutant exhibited enhanced resistance to bacterial pathogen, suggesting immune signaling other than PTI is activated in *bak1 bkk1*. Moreover, genetic analyses showed that mutation in *EDS1* or *PAD4*, key ETI mediator, significantly suppressed the cell death in *bak1-3 bkk1-1*. In this study, we revealed that light-triggered SA accumulation plays major role in inducing the cell death in *bak1 bkk1*, mediated by ETI components.

Keywords: Arabidopsis, *BAK1*, *BKK1*, cell death, light, SA, PTI, ETI

OPEN ACCESS

Edited by:
Yi Ma,
University of Connecticut, USA

Reviewed by:
Jianfeng Li,
Sun Yat-sen University, China
Xiaofeng Wang,
Northwest A&F University, China
Honghui Lin,
Sichuan University, China

****Correspondence:***
Kai He
hekai@lzu.edu.cn

Specialty section:
This article was submitted to Plant Traffic and Transport, a section of the journal Frontiers in Plant Science

Received: *01 March 2017*
Accepted: *06 April 2017*
Published: *25 April 2017*

Citation:
Gao Y, Wu Y, Du J, Zhan Y, Sun D, Zhao J, Zhang S, Li J and He K (2017) Both Light-Induced SA Accumulation and ETI Mediators Contribute to the Cell Death Regulated by BAK1 and BKK1. Front. Plant Sci. 8:622. doi: 10.3389/fpls.2017.00622

INTRODUCTION

Plant cells utilize plasma membrane (PM)-localized receptor-like kinases (RLKs) to communicate with each other and respond to environmental challenges in coordinating plant growth, development and stress adaptions. RLKs, the single-pass transmembrane proteins with an extracellular domain and a cytoplasmic kinase domain, play essential roles in transducing

apoplastic signals into intracellular responses. Leucine-rich repeat (LRR)-RLK family is the largest RLK subfamily containing at least 223 members (Gou et al., 2010), a number of which were found to regulate a variety of physiological processes, such as phytohormone signaling (Li and Chory, 1997; Li et al., 2002; Nam and Li, 2002), innate immunity (Gómez-Gómez and Boller, 2000; Zipfel et al., 2006), meristem maintenance (Clark et al., 1997), pollen development (Zhao et al., 2002; Albrecht et al., 2005; Colcombet et al., 2005), stomatal development (Shpak et al., 2005), pollen tube-egg recognition (Escobar-Restrepo et al., 2007) and cell death control (He et al., 2007, 2008; Kemmerling et al., 2007) etc. Arabidopsis SOMATIC EMBRYOGENESIS RECEPTOR-LIKE KINASE (SERK) family, containing SERK1-SERK5, has become one of the best functionally analyzed LRR-RLK subfamilies (Li, 2010). *SERK* was originally isolated in carrot and identified as a marker gene of somatic embryogenesis (Schmidt et al., 1997). In Arabidopsis, *SERKs* were found to regulate various signaling pathways, in which they often play redundant roles. *SERK1* and *SERK2* regulate porogenesis by maintaining a normal tapetum during pollen maturation (Albrecht et al., 2005; Colcombet et al., 2005); SERK1, SERK3/BRI1-ASSOCIATED KINASE 1 (BAK1), and SERK4/BAK1-LIKE 1 (BKK1) act as co-receptors of the brassinosteroid (BR) receptor BRASSINOSTEROID INSENSITIVE 1 (BRI1) to perceive BRs and initiate cellular signaling cascade (Li et al., 2002; Nam and Li, 2002; Karlova et al., 2006; He et al., 2007; Gou et al., 2012).

BAK1 is also engaged in plant innate immunity. A two-tiered system has been proposed to regulate plant innate immunity (Dodds and Rathjen, 2010). The first layer of immunity is activated after perceiving pathogen-associated molecular patterns (PAMPs) by pattern recognition receptors (PRRs) localized at the surface of a plant cell, known as PAMP-triggered immunity (PTI) (Macho and Zipfel, 2014). The second layer of immunity relies on recognition of pathogen-derived effectors by intracellular resistance (R) proteins in plants, known as effector-triggered immunity (ETI) (Jones and Dangl, 2006). PTI confers plant basal resistance to pathogens and ETI enables faster and stronger defense responses in plants, which is often accompanied with hypersensitive response (HR), a type of programmed cell death (PCD) (Jones and Dangl, 2006; Macho and Zipfel, 2014). Canonical R proteins are nucleotide-binding/leucine-rich repeat (NLR) receptors which fall into two groups, including CNLs, possessing a coiled-coil (CC) domain, and TNLs, containing a Toll-Interleukin-1 receptor (TIR) domain (Meyers et al., 1999; Cannon et al., 2002). EDS1 and PAD4, two lipase-like proteins, are required for TNL-mediated ETI; while NDR1, a PM-associated protein, functions as key mediator in CNL signaling (Aarts et al., 1998; Wiermer et al., 2005; Knepper et al., 2011). BAK1 was found to be involved in PAMP recognition and mediating PTI via associating with several PRR RLKs such as FLAGELLIN-SENSITIVE 2 (FLS2), the receptor for bacterial flagellin, EF-TU RECEPTOR (EFR), the receptor for bacterial elongation factor Tu (EF-Tu), and PEP1 RECEPTOR 1 (PEPR1), the receptor for plant endogenous PROPEP-derived Pep epitopes (Chinchilla et al., 2007; Heese et al., 2007; Schulze et al., 2010). *BAK1*, therefore, positively regulates PTI, the first tier of plant innate immunity.

Intriguingly, our previous studies revealed *BAK1*/*SERK3* and *BKK1*/*SERK4* also mediate a cell death pathway that is independent of the BR signaling pathway (He et al., 2007). A null double mutant, *bak1-4 bkk1-1*, exhibits an extremely strong cell lesion phenotype even on the sterilized medium under normal growth condition. The cell death symptom of *bak1-4 bkk1-1* emerged about 7 days after germination and eventually led to lethality within 2 weeks (He et al., 2007). The cell death phenotype we reported was in line with a simultaneous study of a different group showing that *bak1-4* single mutant exhibited a runaway cell death upon microbial pathogen inoculation (Kemmerling et al., 2007).

Salicylic acid (SA) was identified as an essential signal molecule in mediating plant defense responses (Vlot et al., 2009). Serving as a crucial signal for activating disease resistance including PTI and ETI, SA is rapidly synthesized upon pathogen invasions. Arabidopsis mutants that fail to sufficiently synthesize endogenous SA exhibit impaired innate immunity and enhanced susceptibility to pathogen treatments (Rogers and Ausubel, 1997; Nawrath and Métraux, 1999; Wildermuth et al., 2001; Nawrath et al., 2002). Given that *PR1* is a key marker gene of SA signaling, the extremely high expression of *PR1* suggested an exceedingly activated SA signaling in *bak1-4 bkk1-1* (He et al., 2007). In Arabidopsis, SA is synthesized through two distinct routes, the phenylalanine ammonia-lyase (PAL) pathway and the isochorismate (IC) pathway (Dempsey et al., 2011). Chorismate, the end product of the shikimate pathway, is used as the SA precursor in both pathways (Dempsey et al., 2011). In Arabidopsis, four PAL proteins (PAL1-4) are essential for catalyzing the reaction from phenylalanine to trans-cinnamic acid, a critical step for SA production (Mauch-Mani and Slusarenko, 1996; Chen et al., 2009; Huang et al., 2010). The PAL pathway occurs in cytoplasm and was proposed to account for only 5% of SA production (Métraux, 2002; Chen et al., 2009). The IC pathway, by contrast, takes place in chloroplast and contributes 95% of total cellular SA production (Wildermuth et al., 2001; Métraux, 2002; Garcion et al., 2008; Chen et al., 2009). Two redundant genes *ISOCHORISMATE SYNTHASE 1* (*ICS1*) and *ICS2* were identified to encode essential enzymes localized in chloroplasts to catalyze the conversion of chorismate to isochorismate, a key step of SA biosynthesis in the IC pathway (Garcion et al., 2008). Since *ICS2* only plays a marginal role in this reaction, *ICS1*, also known as *SALICYLIC ACID INDUCTION DEFICIENT 2* (*SID2*), functions as the determinate catalyzator of SA synthesis in IC pathway (Wildermuth et al., 2001; Garcion et al., 2008). Distinct from WT, *ics1*/*sid2* single mutant plants showed no obvious SA accumulation upon a variety of stress treatments such as UV light, ozone, or pathogen incubations (Nawrath and Métraux, 1999; Garcion et al., 2008). The majority of SA, therefore, appears to be produced in chloroplasts and subsequently transported to cytosol and other cellular compartments to fulfill its physiological roles. It has been previously reported that ENHANCED DISEASE SUSCEPTIBILITY 5 (EDS5), a member of Multidrug and Toxic Compound Extrusion (MATE) transporter family, also impacts

SA accumulation (Nawrath et al., 2002). EDS5 was suggested to be localized on plastid membrane and presumably function as an SA transporter in translocating SA from chloroplasts to cytosol (Serrano et al., 2013). Like *ics1*/*sid2*, *eds5* mutants also failed to efficiently accumulate SA when exposed to pathogens (Nawrath and Métraux, 1999).

Little progress has been made since *BAK1* and *BKK1* were discovered to be essential in mediating a cell death pathway. One earlier study indicated that another LRR-RLK, BAK1-INTERACTING RECEPTOR-LIKE KINASE 1 (BIR1), can interact with BAK1, and that *bir1* mutants displayed a cell death phenotype similar to that of the *bak1 bkk1* double mutants (Gao et al., 2009). A PM-localized copine-like protein, BONZAI1 (BON1), was identified as BAK1- and BIR1-interacting protein (Wang et al., 2011). The *bon1* mutant plants also exhibited a cell-death phenotype (Yang et al., 2006). However, the detailed mechanisms of *BIR1* and *BON1* in regulating cell death pathways and their connections to the *BAK1* and *BKK1*-regulated cell death pathway remain elusive. Key open questions still await answers. For instance, what are the primary factors responsible for initiating cell death in *bak1 bkk1* double mutant at early stage? Which biological processes are related to the cell death of *bak1 bkk1*? Our previous report suggested that light likely serves as a key factor in triggering cell death in *bak1-4 bkk1-1* (He et al., 2008). Distinct from the *bak1-4 bkk1-1* plants starting to exhibit lesion symptom at 7 days when grown under a long-day condition, *bak1-4 bkk1-1* grown in darkness did not display a cell death phenotype at 8 days (He et al., 2008). The mechanism regarding how light contributes to triggering cell death in *bak1 bkk1* has not been depicted. Despite the well establishment of BAK1 as an essential co-receptor of key PRRs in positively regulating PTI, the cell death occurring in *bak1 bkk1* seems to be unrelated to PTI. Overexpression or knocking-out of known BAK1-associated PRRs does not cause cell death in plants. Instead, the cell death phenotype of *bak1-4 bkk1-1* resembles HR, a typical defense response in ETI. It implies *BAK1* and *BKK1* play roles beyond PTI. However, whether ETI regulatory components are involved in the cell death pathway mediated by *BAK1* and *BKK1* remains unknown.

In this study, we carefully analyzed the light-triggered cell death in *bak1 bkk1* mutants. Our results indicated that SA accumulation in *bak1 bkk1* mutants may function as a primary initiator to trigger cell death. Genes encoding chloroplast-localized proteins SID2 and EDS5 that are essential for SA biosynthesis and accumulation were highly up-regulated in *bak1 bkk1* and played critical roles in cell death formation. Further analyses revealed that, despite maintaining their insensitivity to bacterial PAMP, *bak1 bkk1* mutants exhibited overly activated immunity, suggesting *BAK1* and *BKK1* mediate a different immunity signaling besides PTI. At last, our results showed that the loss-of-function mutation of *PAD4* or *EDS1*, key component mediating ETI, was capable of significantly suppressing the cell death of a weak double mutant, *bak1-3 bkk1-1*. These results provide genetic evidence suggesting the involvement of ETI in *BAK1* and *BKK1*-mediated cell death pathway.

MATERIALS AND METHODS

Plant Materials and Growth Conditions

All of the Arabidopsis lines used in this study are in the Col-0 ecotype except *pif1-1* (Col-3). T-DNA insertion lines *bak1-4* (SALK_116202), *bak1-3* (SALK_034523), *bkk1-1* (SALK_057955), *sid2-3* (SALK_088254), *eds5-2* (SALK_091541C), *pad4*-2 (SALK_089936), *eds1-3* (SALK_057149), *pif1-1* (CS66041), *pif3-1* (SALK_030753), *pif4-3* (SALK_140393C), *pif5-3* (SALK_087012C) were obtained from the Arabidopsis Biological Resource Center (ABRC). Multiple mutants were generated by genetic crossings. Homozygous plants were isolated via PCR with genotyping primers designed by http://signal.salk.edu/tdnaprimers.2.html. The wildtype and mutant plants were grown in greenhouse or illumination incubator at 22°C in dark condition or under long day cycle (16 h light/8 h dark). For SA treatment assay, seedlings were grown on 0.5× Murashige and Skoog medium with or without SA in dark condition and were analyzed at indicated days.

Trypan Blue Staining and DAB Staining

Tissue stainings with trypan blue and DAB were carried out as previously described (He et al., 2007).

Determination of Subcellular Distribution

The full length CDS of *SID2* and *EDS5* were amplified by RT-PCR and cloned into pBIB-BASTA-35S-GWR-GFP and pBIB-BASTA-35S-GWR-YFP, respectively. The two constructs were transformed into Agrobacterium tumefaciens strain GV3101. The transformed GV3101 were cultured in LB medium (supplemented 20 μM acetosyringone) about 12–16 h. Centrifuged and re-suspended the cultured cells with injection buffer (liquid MS medium containing 150 μM acetosyringone, 10 mM $MgCl_2$, 10 mM MES, pH 5.7) and adjusted to OD_{600} = 0.5. After quiescence for 2 h, the cultures were injected into the *N. benthamiana* mesophyll tissue. *N. benthamiana* protoplasts were isolated after 3 days of injection. YFP or GFP fluorescence signal was observed by Olympus FluoView FV1000 confocal microscope.

Gene Expression Analyses

For quantitative RT-PCR (qRT-PCR) assays, total RNA was extracted from the whole seedlings harvested under different time points. Two micrograms of total RNA was reversely transcribed in a 20 μl volume with M-MLV reverse transcriptase (Invitrogen). The fragments of target genes were amplified using SYBR Premix Ex Taq (TaKaRa). The thermal cycling program was 95°C for 30 s, followed by 40 cycles of 95°C for 5 s, 60°C for 30 s. *ACTIN2* (*At3G18780*) was used for normalization the relative expression level of each transcript, and the comparative $\Delta\Delta C_T$ method was employed to calculate the relative quantities of each amplified product. For identification of mutant alleles, total RNA was isolated from the leaves of 11-day-old plants grown in soil. Two micrograms of total RNA was reversely transcribed in a 20 μl volume using M-MLV reverse transcriptase (Invitrogen). The transcripts of specific genes were amplified with gene-specific primers. *ACTIN2* was used as a reference. The

primers used for qRT-PCR and semi-quantitative RT-PCR are listed in Table S1.

Measurements of SA Content

SA content measurements were carried out as previously described (Du et al., 2016).

Bacterial Infection Assays

Pst DC3000-LUX strain expressing *luxCDABE* operon was cultured in KB medium for 12 h. Centrifuged and re-suspended the cultured cells with 10 mM $MgCl_2$ and adjusted to OD_{600} = 0.2. The *Pst* DC3000-LUX suspension was sprayed onto the 3-week-old Arabidopsis plant lines indicated. All the sprayed plants were kept under a transparent lid to keep high humidity conditions. The plants were checked by a CCD camera to obtain the images of luciferase fluorescence at 30 h after inoculation. The experiments were repeated three times.

flg22 Treatments

Diluted flg22 with sterilized 0.5× Murashige and Skoog solution (pH5.7) to the concentration of 0.2 μM. Nine-day-old Col-0, *bak1-4 bkk1-1*, *bak1-4* and *bkk1-1* grown on 0.5× Murashige and Skoog medium were immersed with flg22 solution for 5, 15, and 30 min. Total protein was extracted from the seedlings harvested under different time points. The total protein extracts were separated by a 10% SDS-PAGE gel for western blot assay. P-p44/42 (Cell Signaling Technology) was used as the antibody. Equal loadings were tested by staining the SDS-PAGE gel with Coomassie brilliant blue G250.The experiments were repeated three times.

RESULTS

Initiation of the Cell Death in *bak1-4 bkk1-1* Was Light-Dependent

In order to elucidate the mechanism of light-induced cell death in *bak1 bkk1*, we analyzed *bak1-4 bkk1-1* mutant plants under a variety of light conditions. Consistent with our earlier results, dark-grown *bak1-4 bkk1-1* showed no clear cell death symptom 8 days after germination, similar to WT Col-0 plants (**Figure 1A**). Next, Col-0 and *bak1-4 bkk1-1* plants were first grown in dark for 4 days then transferred to a long-day condition (16 h light/8 h dark). *bak1-4 bkk1-1* started to exhibit cell death 2 days after transferring to light (**Figure 1A**). By contrast, no cell death was detected in dark-grown Col-0 subsequently treated by light (**Figure 1A**). These results indicated that dark condition prevented *bak1-4 bkk1-1* from forming cell death, which was quickly triggered by light. Cell death is often accompanied with ROS burst, which could be either the cause or consequence of cell death (Chaouch and Noctor, 2010). DAB staining was used to visualize the accumulation of H_2O_2. Col-0 did not accumulate H_2O_2 under either light or dark condition (**Figure 1B**). ROS burst was only detected in dark-grown *bak1-4 bkk1-1* after exposure to light (**Figure 1B**), displaying patterns similar to cell death formation (**Figure 1A**). Under light condition, the initiation of cell death was found to be 1 day prior to overaccumulation of ROS in *bak1-4 bkk1-1*. These results suggested that, instead of causing cell death, ROS burst may be the physiological consequence of cell death in *bak1-4 bkk1-1*.

Next, we examined whether the defense response of *bak1-4 bkk1-1* was also related to light. Utilizing qRT-PCR, a SA-responsive gene, *PR1*, and a cell death marker gene, *FOM1* (Bartsch et al., 2006; Li et al., 2013), were checked. Col-0 and *bak1-4 bkk1-1* grown in dark for 4 days then transferred to long-day condition for 1 or 2 days were analyzed. After being transferred to a long-day condition for 1 or 2 days, *PR1* in dark-grown *bak1-4 bkk1-1* increased about 17 or 600-fold, respectively, compared to the one in Col-0 (**Figure 2A**). In Col-0, *PR1* gene was kept at constantly low expression levels under both dark and light conditions (**Figure 2A**). *FMO1* expression was also significantly induced when dark-grown *bak1-4 bkk1-1* was exposed to light for 1 or 2 days (**Figure 2B**), consistent with trypan blue straining results (**Figure 1A**). As control *PR1* and *FOM1* genes were also analyzed in the seedlings grown in continuous dark. In contrast to the significantly increased expression of *PR1* and *FMO1* in dark-grown *bak1-4 bkk1-1* after light treatment, when grown in dark for 5 or 6 days, the expression of *PR1* and *FMO1* showed slight increases or almost no changes in *bak1-4 bkk1-1* compared to the ones in Col-0 (**Figures 2A,B**). Since *PR1*, a marker gene of SA signaling pathway, was highly expressed in *bak1-4 bkk1-1* upon light exposure, it was conjectured SA may contribute to the light-induced cell death mediated by *BAK1* and *BKK1*. The SA contents were measured in Col-0, *bak1-4*, *bkk1-1*, and *bak1-4 bkk1-1* seedlings grown in dark for 4 days and the seedling grown in dark for 4 days followed by exposure to long-day condition for 1 day. The free SA in Col-0 and single mutant plants grown in dark for 4 days was unchanged after transferring to a long-day condition for 1 day. In *bak1-4 bkk1-1* grown under dark for 4 days, free SA increased about 3-fold after growing the plants in long-day condition for 1 day, indicating a quick SA accumulation in *bak1-4 bkk1-1* upon light treatment (**Figure 2C**). Similarly, total SA in *bak1-4 bkk1-1* plants was also significantly increased when moved from dark to light condition (**Figure 2D**). Notably, high concentration of total SA was already detected in *bak1-4 bkk1-1* plants grown in dark before light treatment (**Figure 2D**). This result suggested that *BAK1* and *BKK1* may also regulate a pathway inactivating SA.

The majority of SA is synthesized in chloroplasts where SID2/ICS1 serves as a determinate enzyme (Wildermuth et al., 2001; Métraux, 2002; Garcion et al., 2008; Chen et al., 2009). A minor portion of SA is produced in cytoplasm, which is catalyzed by PALs (Métraux, 2002; Chen et al., 2009). To explicate why total SA was accumulated in *bak1-4 bkk1-1* even under a dark condition, we analyzed the expression levels of *PAL1-4* genes. In dark, the expression of all four *PAL* genes increased in *bak1-4 bkk1-1* compared to those in Col-0 (Figure S1). The elevated expression of *PAL* genes in *bak1-4 bkk1-1* may contribute to the accumulation of total SA in a dark condition, when free SA was still kept at low concentrations.

Interestingly, cell death eventually started to be detectable in *bak1-4 bkk1-1* at 12 days when grown in dark (Figure S2). These results indicated that the cell death phenotype was extensively

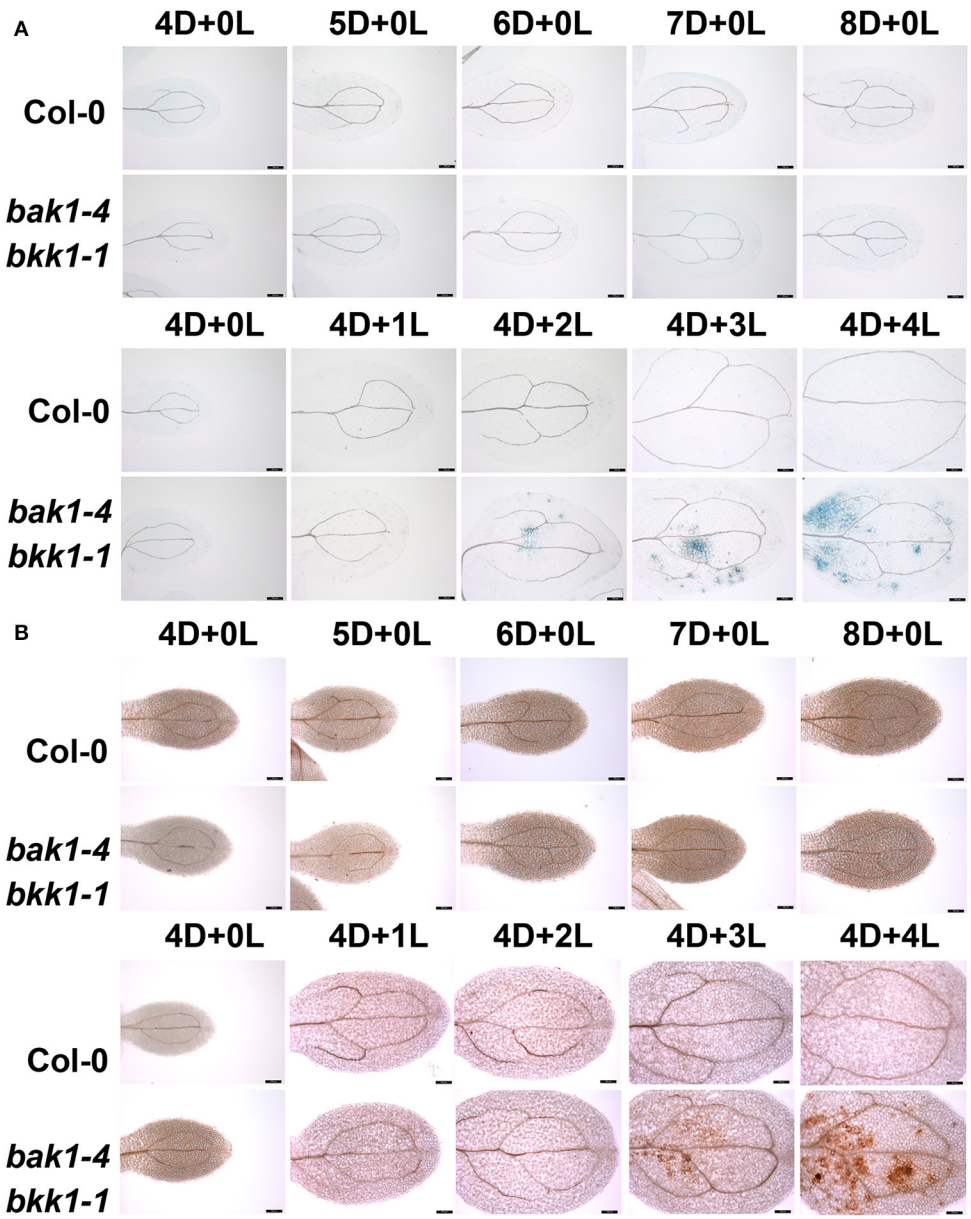

FIGURE 1 | Light initiates cell death in *bak1-4 bkk1-1*. Seedlings are grown in dark (D) for 4 days then relocated to long-day condition (L) for the indicated days (4D+1L, 4D+2L, 4D+3L, 4D+4L). Seedlings grown in dark (D) for the indicated days (4D+0L, 5D+0L, 6D+0L, 7D+0L, 8D+0L) are presented as control. The trypan blue staining assays indicate cell death symptom is induced in *bak1-4 bkk1-1* 2 days after the transfer from dark to light condition **(A)**. The DAB staining assays indicate ROS accumulation is detected in *bak1-4 bkk1-1* 3 days after the transfer from dark to light condition **(B)**. The scale bars represent 100 μm.

delayed but not completely abolished in *bak1-4 bkk1-1* when grown in dark.

Exogenously Applied SA Triggered Cell Death in *bak1-4 bkk1-1* in Dark

Given that the initiation of light-dependent cell death in *bak1-4 bkk1-1* was likely SA-related, we further analyzed the detailed role of SA in cell death induction. Trypan blue staining was used to detect cell death in Col-0 and *bak1-4 bkk1-1* grown on 1/2 MS medium supplemented with 0, 10, or 50 μM SA in dark condition. Col-0 showed no cell death when treated with 10 or 50 μM SA (**Figure 3A**). When grown on the medium supplemented with 50 μM SA in a dark condition, *bak1-4 bkk1-1* started to show cell death symptom 5 days after germination. When treated with 10 μM SA in dark, *bak1-4 bkk1-1* also exhibited obvious but less severe cell death symptom compared to those treated with 50 μM SA (**Figure 3A**). These results clearly demonstrated that cell death suppressed in *bak1-4 bkk1-1* by growing the seedlings in dark condition reappeared by exogenously treated SA. Therefore, SA seemed to reproduce the

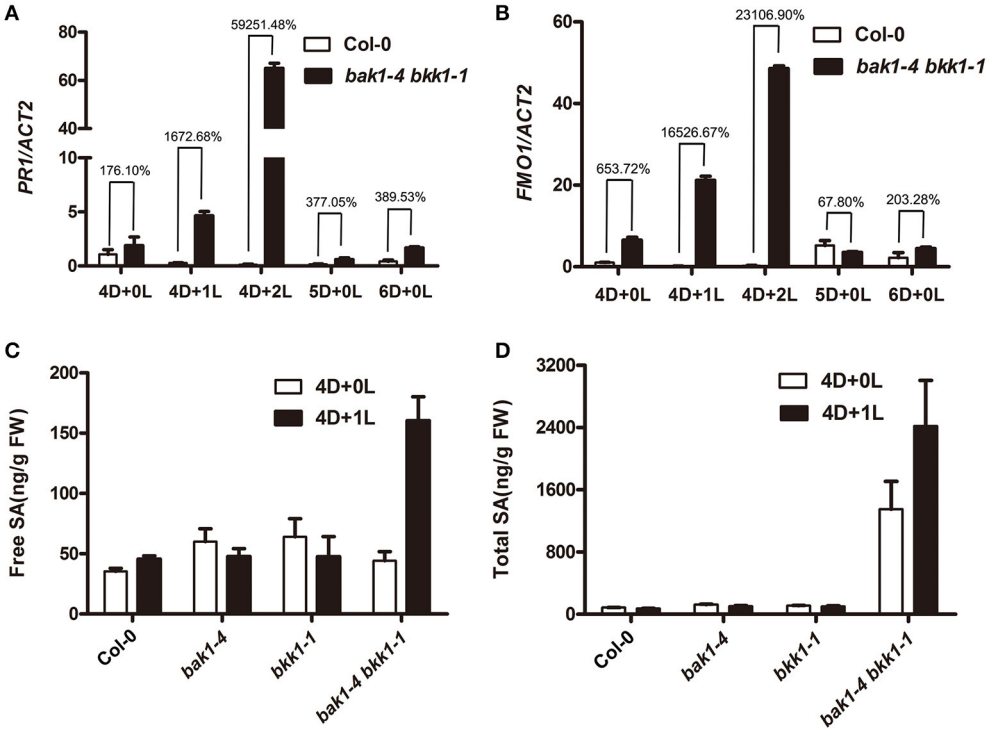

FIGURE 2 | The transcripts of *PR1* and *FMO1* and SA content in *bak1-4 bkk1-1* are significantly elevated upon light treatment. Quantitative RT-PCR assays demonstrate the expression of SA marker gene *PR1* **(A)** and cell death marker gene *FMO1* **(B)** is extensively up-regulated in *bak1-4 bkk1-1* by light. Free SA **(C)** and total SA **(D)** contents increase in *bak1-4 bkk1-1* 1 day after the transfer from dark to long-day condition. Seedlings grown in dark (D) for 4 days then relocated to long-day condition (L) for the indicated days (4D+1L, 4D+2L) and seedlings grown in dark (D) for the indicated days (4D+0L, 5D+0L, 6D+0L) are analyzed.

effect of light with regard to cell death induction in *bak1-4 bkk1-1*. ROS accumulation was also examined in Col-0 and *bak1-4 bkk1-1* plants upon SA treatment. This result suggested that $H_2O_2$was also accumulated in *bak1-4 bkk1-1* but not in Col-0 when SA was applied to the medium (**Figure 3B**). In dark condition, the ROS burst in *bak1-4 bkk1-1* appeared 1 day after the emergence of cell death symptom when treated with SA (**Figure 3**), similar to the patterns of light-induced cell death and ROS burst in *bak1-4 bkk1-1* (**Figure 1**).

The Expression of *SID2* and *EDS5* Was Highly Elevated in *bak1 bkk1*

SA-induced cell death in *bak1-4 bkk1-1* was light-independent, supporting light plays an indirect role in the induction of cell death in *bak1-4 bkk1-1*. SA accumulation may contribute to this process. We first analyzed whether light signaling pathways were involved in *BAK1* and *BKK1*-mediated cell death. A weak double mutant *bak1-3 bkk1-1* was crossed to several *pif* mutants to generate triple and quadruple mutant lines. *PIF* genes encode transcription factors mediating red light and blue light signaling pathways. *PIF1* usually functions redundantly with *PIF3*, and *PIF4* often plays an overlapping role with *PIF5*. Our genetic results demonstrated that none of *bak1-3 bkk1-1 pif1-1*, *bak1-3 bkk1-1 pif3-1,* or *bak1-3 bkk1-1 pif1-1 pif3-1* mutant plants displayed a phenotypic difference in cell death symptom compared to their background *bak1-3 bkk1-1* (Figure S3). Similarly, *bak1-3 bkk1-1 pif4-3*, *bak1-3 bkk1-1 pif5-3*, or *bak1-3 bkk1-1 pif4-3 pif5-3* mutant plants did not show alterations to *bak1-3 bkk1-1* with regard to cell death phenotype (Figure S4). These results suggested that the *PIF*-mediated light signalings may not contribute to the cell death initiation in *bak1 bkk1* under light condition. Thus, it was hypothesized that SA synthesis, mainly occurring in chloroplast and relying on light-dependent photomorphogenesis, plays a key role in the light-induced cell death in *bak1 bkk1*. Through data mining of our earlier microarray results that compare global gene expression patterns between Col-0 and *bak1-4 bkk1-1* seedlings, we noticed that two genes, *SID2* and *EDS5*, encoding critical components involved in SA biosynthesis and cytoplasmic accumulation, were dramatically up-regulated in *bak1-4 bkk1-1*. The microarray data indicated that the transcripts of *SID2* and *EDS5* in *bak1-4 bkk1-1* increased 19.86 and 5.78-fold, respectively, compared to the ones in Col-0. Interestingly enough, the protein products of these two genes were both suggested to locate to chloroplast. *SID2* encodes an isochorismate synthase catalyzing chorismate into isochorismate, a SA precursor, in chloroplast. *EDS5* encodes a MATE transporter, locating to the chloroplast envelope, and is suggested to function as an SA transporter mediating the translocation of chloroplast-synthesized SA to cytosol. Using a quantitative RT-PCR assay, we analyzed the expression patterns of *SID2* and *EDS5* in Col-0 and *bak1-4 bkk1-1* plants grown in dark condition for 4 days and the plants grown in dark for

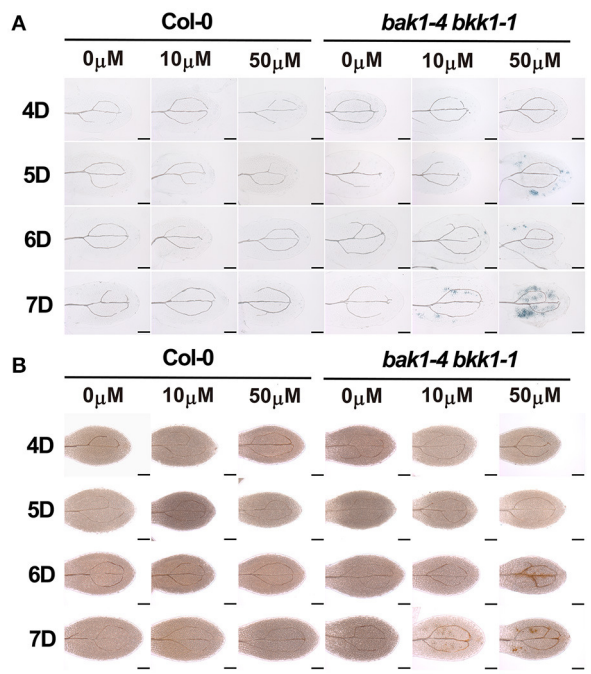

FIGURE 3 | Exogenously applied SA is sufficient to trigger cell death in *bak1-4 bkk1-1* in dark. The trypan blue staining assays indicate cell death formation in dark-grown *bak1-4 bkk1-1* on the 1/2 MS medium supplemented with 10 or 50 μM SA **(A)**. The DAB staining assays indicate ROS accumulation in dark-grown *bak1-4 bkk1-1* on the 1/2 MS medium supplemented with 10 or 50 μM SA **(B)**. Seedlings grown in dark (D) for the indicated days are presented (4D–7D). The scale bars represent 100 μm.

4 days then exposed in long-day condition for 1 or 2 days. *SID2* showed significantly high expression in *bak1-4 bkk1-1* (**Figure 4A**), indicating a robustly negative regulation on *SID2* expression by *BAK1* and *BKK1*. Treated with or without light condition, the transcripts of *SID2* increased about 30–40-fold in *bak1-4 bkk1-1* compared to those in Col-0 (**Figure 4A**), suggesting the inhibition on *SID2* expression by *BAK1* and *BKK1* was likely light-independent. In dark, the expression of *EDS5* increased about 2-fold in *bak1-4 bkk1-1* compared to the one in Col-0 (**Figure 4A**). Upon Light treatment, *EDS5* expression decreased in Col-0 but increased in *bak1-4 bkk1-1* (**Figure 4A**), suggesting *EDS5* is also suppressed by *BAK1* and *BKK1*, especially under light condition. When grown in dark for 5 or 6 days, *SID2* and *EDS5* in *bak1-4 bkk1-1* showed much lower levels of increases (**Figure 4A**). We next analyzed the subcellular locations of SID2 and EDS5 proteins. The cDNAs of *SID2* and *EDS5* were fused with *GFP* and *YFP*, respectively, and transiently expressed in *N. benthamiana*, driven by *35S* promoter. SID2-GFP was detected to be localized in chloroplast (**Figure 4B**). EDS5-YFP mainly located to the surface of chloroplast (**Figure 4B**), consistent with the previous report that EDS5 may function as an SA transporter at the chloroplast envelope. Taken together, our results indicated *SID2* and *EDS5*, encoding chloroplast-localized proteins essential for SA accumulation, were suppressed by *BAK1* and *BKK1* at transcriptional levels.

Mutation of *SID2* or *EDS5* Partially Suppressed the Cell Death in *bak1-3 bkk1-1*

In order to further dissect the function of *SID2* and *EDS5* in initiating cell death in *bak1 bkk1*, genetic approaches were employed. *bak1-3 bkk1-1* was crossed to *sid2-3* and *eds5-2* T-DNA insertion lines, respectively, to generate triple-mutants. RT-PCR results confirmed that *SID2* and *EDS5* were completely knocked out in *bak1-3 bkk1-1 sid2-3* and *bak1-3 bkk1-1 eds5-2*, respectively (Figure S5). Introduction of *sid2-3* into *bak1-3 bkk1-1* significantly suppressed the cell death symptom of *bak1-3 bkk1-1* when grown in soil for 3-week-old (**Figure 5A**). Trypan blue and DAB staining results confirmed *SID2* mutation greatly inhibited the cell death phenotype and ROS accumulation in 11-day-old *bak1-3 bkk1-1* (**Figures 5B–E,H–K**). In addition, the highly expressed *PR1* and *FMO1* in *bak1-3 bkk1-1* restored to WT-like levels in *bak1-3 bkk1-1 sid2-3* triple mutant, indicating *SID2* is essential for cell death induction in *bak1-3 bkk1-1* (**Figures 5N,O**). Similarly, the absence of *EDS5* also appeared to partially rescue the cell death phenotype of 3-week-old *bak1-3 bkk1-1* (**Figure 5A**). Trypan blue and DAB staining results verified that the cell death and ROS burst in 11-day-old *bak1-3 bkk1-1 eds5-2* was largely prevented (**Figures 5B–M**). The qRT-PCR results showed that the expression of *PR1* and *FMO1* was greatly suppressed in *bak1-3 bkk1-1 eds5-2* compared to the ones in *bak1-3 bkk1-1* (**Figures 5N,O**). Collectively, our genetic results indicated SA biosynthesis-related genes *SID2* and *EDS5* act as crucial components in promoting cell death in *bak1-3 bkk1-1*.

bak1 bkk1 Showed Enhanced Bacterial Resistance and Impaired PTI

Since it is established that BAK1 positively regulates PTI via interacting and collaborating with several PRRs, we further examined the basal defense in *bak1 bkk1*. Three-week-old soil-grown plants of Col-0, *sid2-3*, *eds5-2*, *bak1-3*, *bkk1-1*, *bak1-3 bkk1-1*, *bak1-3 bkk1-1 sid2-3,* and *bak1-3 bkk1-1 eds5-2* were sprayed with *P. syringae* pv *tomato* DC3000 (*Pst* DC3000)-LUX for 30 h before the images of luciferase florescence were taken. Single mutant *sid2-3* or *eds5-2* showed enhanced susceptibility to the bacterial pathogen, indicating the essential role of SA in mediating basal defense (**Figure 6A**). Similarly, single mutant *bak1-3* or *bkk1-1* also exhibited markedly reduced resistance to *Pst* DC3000, consistent with the notion that *BAK1* functions as a positive regulator in PTI (**Figure 6A**). Surprisingly, the double mutant *bak1-3 bkk1-1* showed enhanced resistance to *Pst* DC3000, different from either *bak1-3* or *bkk1-1* (**Figure 6A**). Compared to *bak1-3 bkk1-1*, *bak1-3 bkk1-1 sid2-3* or *bak1-3 bkk1-1 eds5-2* showed reduced bacterial resistance, suggesting SA was involved in the defense activation in *bak1-3 bkk1-1*. To confirm these results, we analyzed the activation status of MPK3/6 in various plants lines. MPK3/6 were identified as mediators in basal defense and receptor triggered immunity including PTI and ETI (Rasmussen et al., 2012; Tsuda et al., 2013). Activated MPK3/6 via phosphorylation indicate enhanced immune response. By using

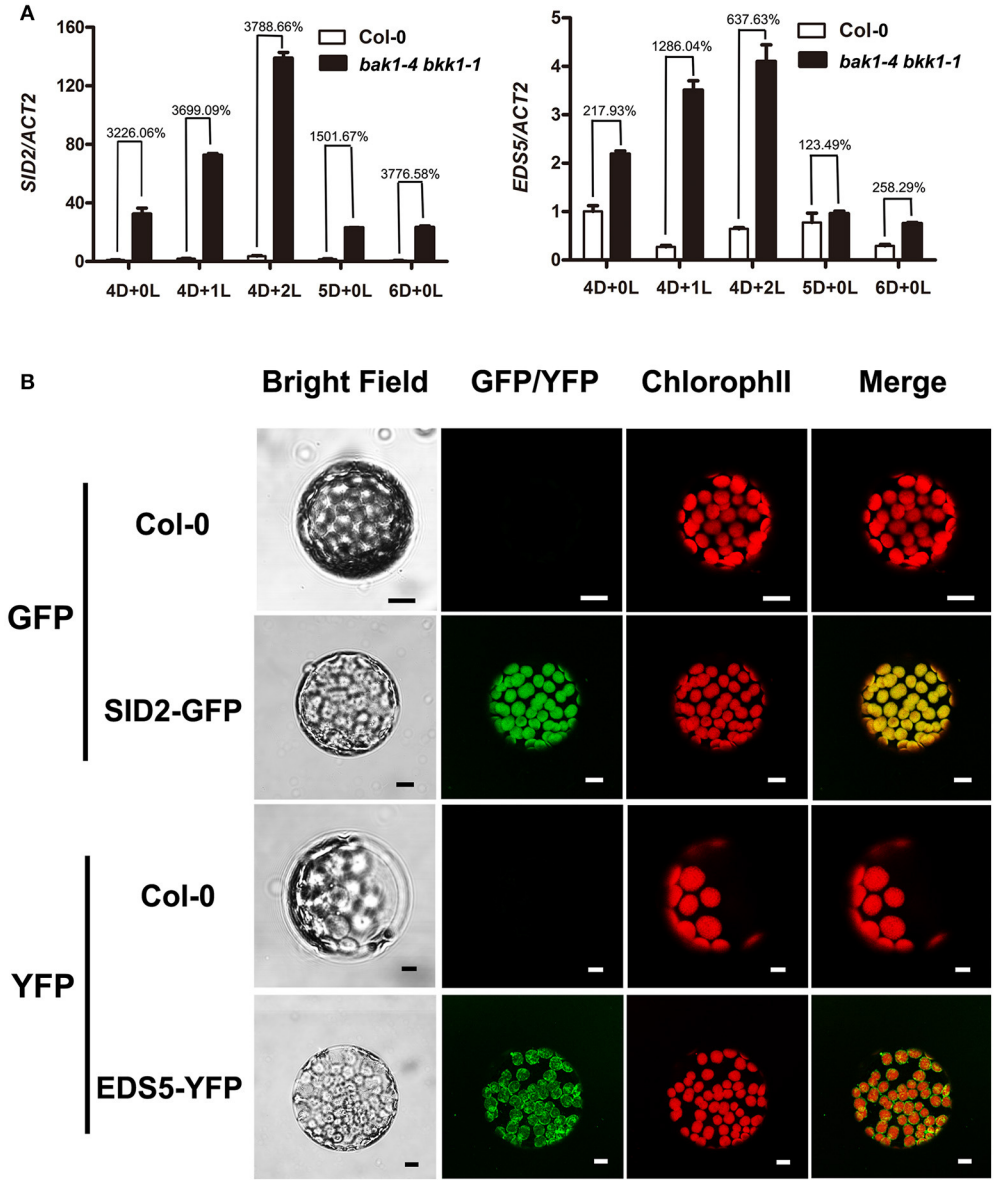

FIGURE 4 | *BAK1* and *BKK1* robustly suppress the expression of SA biosynthesis-related genes *SID2* and *EDS5*. Seedlings are grown in dark (D) for 4 days then relocated to long-day condition (L) for the indicated days (4D+0L, 4D+1L, 4D+2L). Seedlings grown in dark for 5 or 6 days (5D+0L or 6D+0L) are analyzed as control. Quantitative RT-PCR assays indicate both *SID2* and *EDS5* are significantly up-regulated in *bak1-4 bkk1-1* compared to those in Col-0 **(A)**. SID2-GFP and EDS5-YFP are detected to locate to the entire chloroplast and chloroplast surface, respectively, in *N. benthamiana* protoplasts **(B)**. The scale bars represent 10 μm .

a P-p44/42 antibody, phosphorylated MPK3/6 were detected in various plant lines. Consistent to *Pst* DC3000 treatment results, *bak1-3 bkk1-1* showed over-activated MPK3/6, which were less phosphorylated in *sid2-3*, *eds5-2*, *bak1-3*, *bak1-4,* or *bkk1-1*, compared to Col-0 (**Figure 6B**). In *bak1-3 bkk1-1 sid2-3* and *bak1-3 bkk1-1 eds5-2,* phosphorylated MPK3/6 were reduced compared to *bak1-3 bkk1-1*, suggesting the autoimmunity in *bak1-3 bkk1-1* is partially SA-dependent (**Figure 6B**). It was intriguing that *bak1-3* and *bkk1-1* single mutants were more susceptible but *bak1-3 bkk1-1* double mutant were more resistant to bacterial pathogen. We next analyzed PTI signaling in *bak1 bkk1* to examine whether PTI was responsible for the enhanced immunity in *bak1-4 bkk1-1*. Nine-day-old Col-0, *bak1-4 bkk1-1*, *bak1-4,* and *bkk1-1* were incubated with flg22, a 22-amino-acid peptide conserved in bacterial flagellin that is efficient to trigger FLS2-mediated immune signaling, for 5, 15, and 30 min before examining phosphorylated MPK3/6. Both of the single mutants *bak1-4* and *bkk1-1* showed reduced response to flg22 (**Figure 6C**). The response of double mutant *bak1-4 bkk1-1* to flg22 was dramatically reduced, demonstrating PTI in *bak1-4 bkk1-1* was nearly blocked (**Figure 6C**). Our results supported the

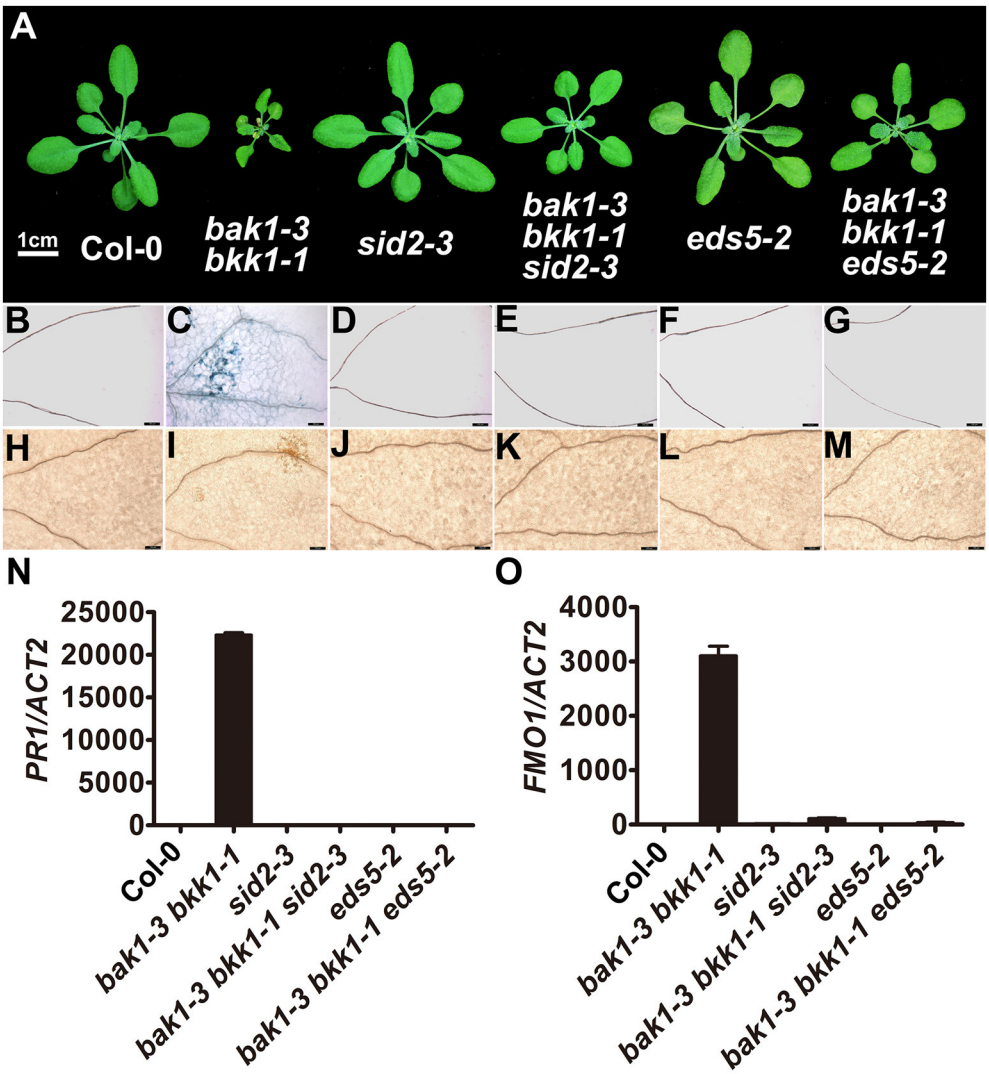

FIGURE 5 | The cell death in *bak1-3 bkk1-1* is significantly suppressed by the mutation in *SID2* or *EDS5*. The representative phenotypes of 3-week-old Col-0, *bak1-3 bkk1-1*, *sid2-3*, *bak1-3 bkk1-1 sid2-3*, *eds5-2,* and *bak1-3 bkk1-1 eds5-2* grown in soil are presented **(A)**.Trypan blue staining **(B–G)** and DAB staining **(H–M)** assays indicate the cell death and ROS accumulation in *bak1-3 bkk1-1* are largely prevented in *bak1-3 bkk1-1 sid2-3* and *bak1-3 bkk1-1 eds5-2*. Quantitative RT-PCR assays indicate the highly expressed *PR1* and *FMO1* in *bak1-3 bkk1-1* are restored to WT-like levels in *bak1-3 bkk1-1 sid2-3* and *bak1-3 bkk1-1 eds5-2* **(N,O)**. Scale bars represent 1 cm **(A)** and 100 μm **(B–M)**, respectively. 11-day-old seedlings are analyzed in **(B–O)**.

previous findings that *BAK1* is essential for PRR-mediated PTI and, more importantly, suggested that *bak1 bkk1* double mutants undergo an enhanced immune signaling other than PTI.

EDS1 and PAD4, Components Mediating ETI, Were Involved in the Cell Death in *bak1 bkk1*

EDS1-PAD4 complex acts as an essential component in mediating all tested TNL type R protein pathway in ETI (Wiermer et al., 2005). To understand whether ETI is involved in the cell death induction in *bak1 bkk1*, *bak1-3 bkk1-1* was crossed to *eds1-3* and *pad4-2*, respectively *eds1-3* was able to partially rescue the cell death of *bak1-3 bkk1-1*; while *pad4-2* dramatically suppressed the lesion symptom of *bak1-3 bkk1-1* (**Figure 7A**). Our genetic results thus implicated the autoimmunity in *bak1 bkk1* is likely ETI-related.

Given that EDS1 and PAD4 also function as upstream of SA pathway via regulating *ICS1*-generated SA biogenesis, we next tested whether the suppression of *bak1-3 bkk1-1* by *eds1* or *pad4* was SA-dependent. No clear cell death symptom was detected in 3-week-old *bak1-3 bkk1-1 sid2-3* (**Figure 5**). By contrast, 26-day-old *bak1-3 bkk1-1 sid2-3* started to exhibit detectable

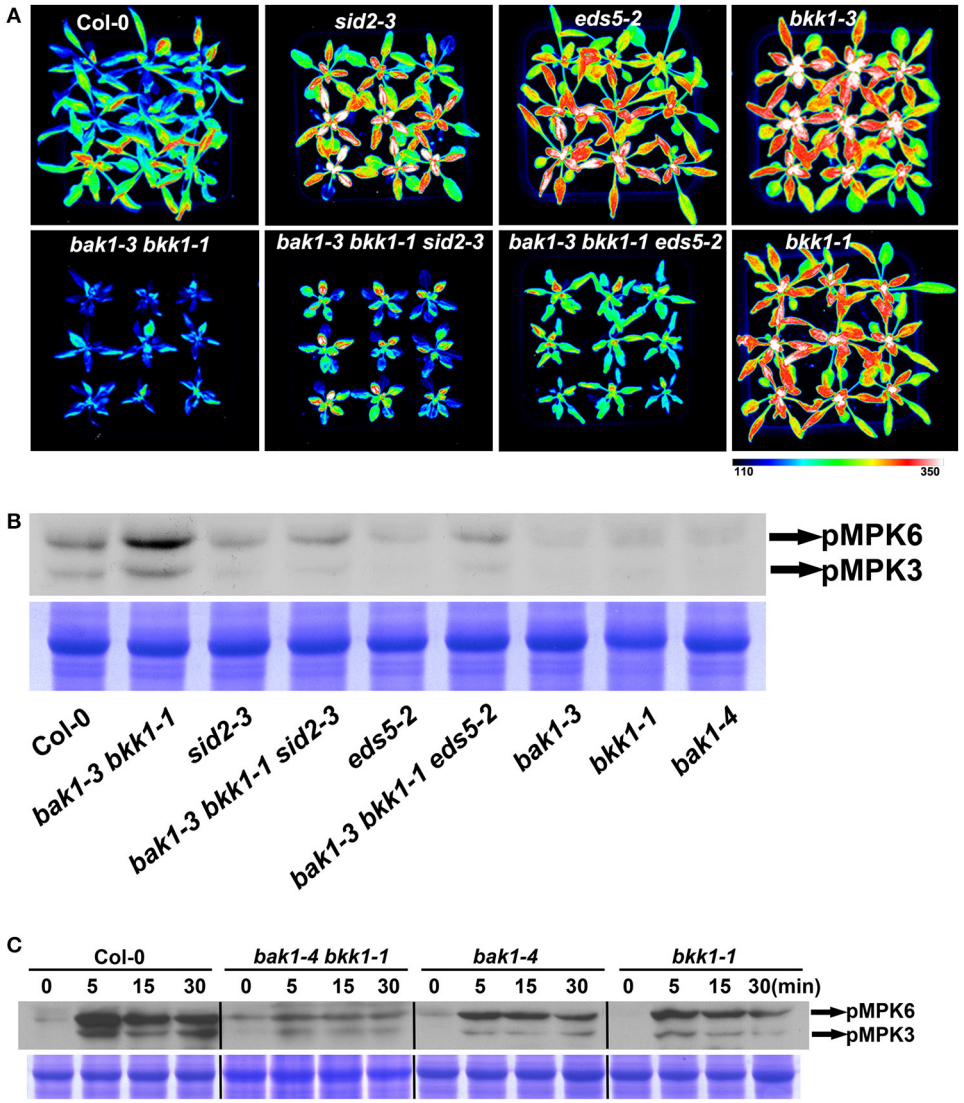

FIGURE 6 | *bak1-3 bkk1-1* shows enhanced resistance to bacterial pathogen. The image of 3-week-old Col-0, *bak1-3 bkk1-1*, *sid2-3*, *bak1-3 bkk1-1 sid2-3*, *eds5-2*, *bak1-3 bkk1-1 eds5-2*, *bak1-3,* and *bkk1-1* grown in soil is presented at 30 h after sprayed with *Pst* DC3000-LUX **(A)**. The western blot assay shows the phosphorylation levels of MPK3/MPK6 in 2-week-old Col-0, *bak1-3 bkk1-1*, *sid2-3*, *bak1-3 bkk1-1 sid2-3*, *eds5-2*, *bak1-3 bkk1-1 eds5-2*, *bak1-3*, *bak1-4,* and *bkk1-1* **(B)**. The western blot assay shows the phosphorylation levels of MPK3/MPK6 in 9-day-old Col-0, *bak1-4 bkk1-1*, *bak1-4,* and *bkk1-1* treated with flg22 **(C)**. Seedlings are grown in soil **(B)** and 0.5× Murashige and Skoog medium **(C)**, respectively.

lesion symptom, suggesting the cell death pathway was partially SA-dependent. The cell death of *bak1-3 bkk1-1 sid2-3* was further suppressed by *eds1* or *pad4*, suggesting EDS1 and PAD4 contributed to the BAK1 and BKK1-mediated cell death pathway other than, or in addition to, regulating SA accumulation (**Figure 7B**). Therefore, ETI mediated by EDS1 and PAD4 was proposed to be involved in BAK1-mediated cell death pathway. We also introduced a mutation of *NDR1*, a key mediator in CNL signaling, into *bak1-3 bkk1-1*. The triple mutant *bak1-3 bkk1-1 ndr1-1* exhibited identical cell death phenotype to *bak1-3 bkk1-1*, suggesting TNL type but not CNL type R proteins are likely involved in BAK1 and BKK1-mediated cell death pathway (Figure S6).

DISCUSSION

BAK1 was originally identified as a co-receptor of BRI1, positively regulating BR signal transduction. Genetic analyses revealed that *BAK1* and its closest homolog *BKK1* can also modulate a cell death pathway that is independent of the BR signaling pathway. This unexpected finding suggested the versatile roles of BAK1 in regulating plant growth and development, as well as adaptations to environmental stresses. Removal of both *BAK1* and *BKK1* in a single plant leads to cell lesion and ultimately a lethality phenotype under a normal growth condition, indicating the irreplaceable roles *BAK1* and *BKK1* play in the physiological events essential for plants to fulfill their life cycles. However,

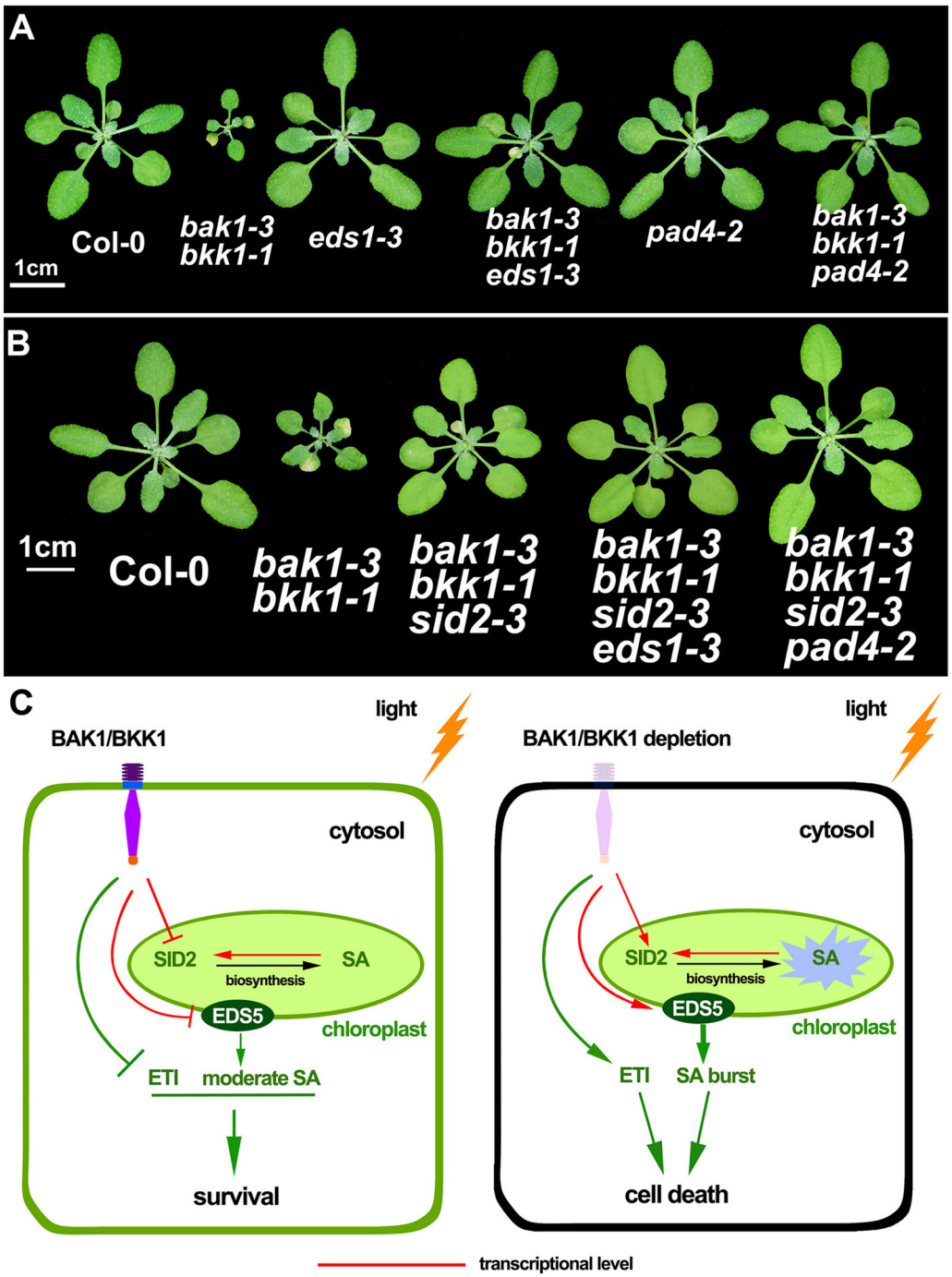

FIGURE 7 | The cell death in *bak1-3 bkk1-1* is significantly suppressed by the mutation in *EDS1* or *PAD4*. The representative phenotypes of 3-week-old Col-0, *bak1-3 bkk1-1*, *eds1-3*, *bak1-3 bkk1-1 eds1-3*, *pad4-2* and *bak1-3 bkk1-1 pad4-2* grown in soil are presented **(A)**. The representative phenotypes of 26-day-old Col-0, *bak1-3 bkk1-1*, *bak1-3 bkk1-1 sid2-3*, *bak1-3 bkk1-1 sid2-3 eds1-3,* and *bak1-3 bkk1-1 sid2-3 pad4-2* grown in soil are presented **(B)**. A hypothetical model for the cell death induction in *bak1 bkk1*. Under light condition, *BAK1* and *BKK1* repress *SID2* and *EDS5* at transcriptional levels, resulting in low concentrations of cellular SA. The absence of both *BAK1* and *BKK1* leads to highly expressed *SID2* and *EDS5*, causing overly produced endogenous SA in the chloroplast followed by SA transport to cytosol through EDS5. Positive feedback regulation of *SID2* by SA causes SA burst that ultimately triggers cell death. BAK1 and BKK1 also suppress ETI signaling mediated by EDS1-PAD4. Depletion of both BAK1 and BKK1 leads to release of the inhibition on ETI. Activated ETI induces cell death (HR) and confers plants enhanced resistance **(C)**.

the detailed mechanisms of *BAK1* and *BKK1* in mediating cell death are still beyond what we understand. After the finding of *BAK1*-mediated cell death, BAK1 was reported to be engaged in plant innate immunity through associating with PRRs such as FLS2, EFR and PEPR1 (Chinchilla et al., 2007; Heese et al., 2007; Schulze et al., 2010). Nevertheless, loss-of-function mutants of the BAK1-interacting PRRs only exhibit impaired innate immunity but no cell death symptom, suggesting the cell death mediated by BAK1 and BKK1 is unlikely directly related to PTI mediated by PRRs. In addition, a *BAK1* point mutation allele, *bak1-5*, was identified to display disrupted FLS2-mediated PTI, but *bak1-5 bkk1-1* showed no cell death (Schwessinger et al., 2011), suggesting that BAK1-mediated PTI pathway and BAK1-mediated cell death pathway belong to distinct signaling events.

Our previous research suggested dark growth condition largely suppressed the cell death symptom in *bak1-4 bkk1-1* and light treatment quickly induced lesion phenotype in dark-grown *bak1-4 bkk1-1*. How light serves as an initiator of cell death in *bak1 bkk1* mutants is still unclear. Furthermore, the downstream signaling components involved in cell death induction in *bak1 bkk1* are nearly unknown. Considering that PTI is not likely involved in the cell death of *bak1 bkk1*, ETI, the stronger immune response featured by quick cell death formation, is worth being investigated whether is related to *BAK1* and *BKK1*-mediated cell death pathway.

In this study, we analyzed the formation of cell death in *bak1 bkk1* upon light treatment. Our results indicated that cell death was undetectable in *bak1-4 bkk1-1* when grown in dark up to 12 days, while evident lesion symptom was induced in *bak1-4 bkk1-1* 2 days after being transferred from dark to light condition, accompanied with highly accumulated SA and ROS. Fascinatingly, dark-grown *bak1-4 bkk1-1* was capable of exhibiting obvious cell death when exogenous SA was applied, illustrating that light does not directly regulate cell death and SA might function downstream of light and play a central role in promoting the cell death in *bak1 bkk1*. qRT-PCR results revealed that two genes *SID2* and *EDS5*, critical in modulating SA biosynthesis, were significantly up-regulated in *bak1-4 bkk1-1*; and more interestingly, the protein products of both genes are located in chloroplasts. The mutation in either *SID2* or *EDS5* in *bak1-3 bkk1-1* remarkably rescued the cell death phenotype of the double mutant, suggesting chloroplast-localized SID2 and EDS5 are crucial for cell death formation in *bak1-3 bkk1-1*, likely via affecting SA accumulation. Furthermore, in a pathogen treatment assay, both *bak1-3* and *bkk1-1* single mutants were more susceptible to *Pst* DC3000 compared to Col-0, consistent to the notion that BAK1 functions as major contributor to the basal resistance to several pathogens including *Pst* DC3000 (Roux et al., 2011). Surprisingly, *bak1-3 bkk1-1* double mutant exhibited enhanced resistance to *Pst* DC3000, indicating the loss of either *BAK1* or *BKK1* causes impaired immunity but removing both *BAK1* and *BKK1* leads to triggering additional route of plant immunity instead. Genetic analyses supported this notion by showing that mutation in either *EDS1* or *PAD4*, key regulator mediating ETI, resulted in suppression of cell death in *bak1 bkk1*.

Based on the aforementioned results, we propose a hypothetic model. SA is not efficiently synthesized in *bak1 bkk1* in dark condition. Light-induced overexpression of *SID2* and *EDS5* in *bak1 bkk1* causes highly accumulated SA. Positive feedback regulation on SA biosynthetic genes by high concentrations of SA further enhances the SA biosynthesis and leads to SA burst that ultimately induce cell death in *bak1 bkk1*. In addition, BAK1 and BKK1 regulate a signaling pathway to inhibit ETI, which is mediated by EDS1-PAD4 complex, under normal growth conditions. When BAK1 and BKK1 are both depleted, ETI is activated to initiate cell death in plants, a faster and stronger defense response (**Figure 7C**).

Light has been reported to cause cell death when it is excessive (Szechyńska-Hebda and Karpiński, 2013); and UV light treatment often leads to lesions in plant tissues (Nawkar et al., 2013). Nevertheless, the light-dependent cell death found in *bak1 bkk1* seems to be distinct from the known light-induced cell death. The known light-induced lesion is caused by rapid ROS accumulation, a key cell death signal. In *bak1 bkk1* double mutants, the cell death symptom appears prior to the accumulation of ROS, indicating ROS is not the cause of the cell death. Instead, ROS accumulation is likely an effect of cell death in *bak1 bkk1*. Nevertheless, since ROS also serves as a feedback signal for SA biosynthesis (Torres et al., 2006), the ROS accumulation in *bak1 bkk1* may further deteriorate the cell death symptom. In addition, none of the multiple *bak1-3 bkk1-1 pif* mutant plants displayed altered lesion phenotype compared with *bak1-3 bkk1-1* (Figures S3, S4), suggesting light-induced cell death in *bak1 bkk1* is independent of *PIF*-mediated blue and red light signaling pathways (Castillon et al., 2007; Pedmale et al., 2016). Moreover, the effect of light on cell death initiation can be reproduced by SA treatment in *bak1 bkk1* in dark (**Figure 3**), suggesting light acts as an indirect factor to trigger cell death in *bak1 bkk1* and light signaling is not essential for this process.

Compared to those in Col-0, the transcripts of *SID2* increased about 30–40-fold in *bak1-4 bkk1-1*, demonstrating *SID2* expression is strongly inhibited by *BAK1* and *BKK1*. Even though the expression of *SID2* was indeed enhanced by light, the suppression of *SID2* by *BAK1* and *BKK1* seemed to be light-independent, indicated by similar multiple increases of *SID2* in dark-grown Col-0 and *bak1-4 bkk1-1* upon light treatment (**Figure 4A**). The expression of *EDS5* is suppressed by *BAK1* and *BKK1*. Compared to those in Col-0, *EDS5* transcripts increased about 2-fold in dark condition, but elevated around 12-fold 1 day after relocating to light condition in *bak1-4 bkk1-1*. This result suggested the expression of *EDS5* is synergistically controlled by light and *BAK1*and *BKK1* (**Figure 4**).

In PAL pathway of SA synthesis, four *PAL* genes were identified to encode enzymes facilitating production of the SA precursor in cytosol. Our results suggested the expression levels of *PAL* genes were also inhibited by *BAK1* and *BKK1*. It may explicate that high total SA content was detected under dark condition in *bak1-4 bkk1-1*. The *PAL*-dependent SA biosynthesis pathway may contribute to the cell death initiation in *bak1-4 bkk1-1* when grown in dark for an elongated period of time (Figures S1, S2). It is also possible that additional BAK1 and BKK1-mediated pathway that is SA-independent may contributes to the cell death signaling. Despite high concentration of total SA in *bak1-4 bkk1-1* in dark, the free SA

content was almost equal to that in Col-0. Thus, *BAK1* and *BKK1* might control an unknown SA regulation pathway conjugating SA to other components, serving as a mechanism of preventing toxicity caused by highly accumulated free SA (Dempsey et al., 2011).

A recent study indicated that *bak1* mutant exhibited enhanced resistance to *Pst* DC3000, through reprogramming PEPR-mediated defense signaling. Upon *Pst* DC3000 treatment, *PROPEP* genes were up-regulated at 24 hpi (hours post-inoculation) and *bak1* was more resistant at 3 dpi (days post-inoculation) (Yamada et al., 2016). It suggested the resistance to *Pst* DC3000 found in *bak1* is caused by activation of an additional immune response, the PEPR-mediated signaling. To wipe out the potential interference by secondary response in *bak1*, we examined the early responses of various plant lines to *Pst* DC3000 at 30 hpi. Instead, the single mutant *bak1-3* or *bkk1-1* was more susceptible to *Pst* DC3000, which is in line with previous studies showing that BAK1 serves as a co-receptor for multiple PRRs and the mutation of *BAK1* causes impaired PTI and reduced resistance (Chinchilla et al., 2007; Heese et al., 2007; Schulze et al., 2010; Roux et al., 2011; Schwessinger et al., 2011). It is interesting that *bak1-3 bkk1-1* double mutant was more resistant to *Pst* DC3000 (**Figure 6A**). In an flg22 treatment assay, we confirmed that the sensitivity of flagellin PAMP was almost abolished in *bak1-4 bkk1-1* (**Figure 6C**). Thus, *bak1 bkk1* double mutant maintains a dampened PTI but exhibits enhanced pathogen resistance. Therefore, additional immune signaling must be activated in *bak1-3 bkk1-1*. Our results showed that *eds1* or *pad4* can significantly suppress the cell death phenotype of *bak1-3 bkk1-1*, supporting the notion that ETI is inhibited by BAK1 and BKK1-mediated signaling (**Figure 7A**). It explained why *bak1-3 bkk1-1* was more resistant to pathogen. Although EDS1-PAD4 complex was known to regulate SA via affecting *ICS1*-generated SA biosynthesis, the suppression of *bak1-3 bkk1-1* by *eds1* or *pad4* appears to be SA-independent. *bak1-3 bkk1-1 sid2-3* showed lesion phenotype when grown for an extended period of time. *eds1* or *pad4* suppressed the cell death of *bak1-3 bkk1-1 sid2-3*, suggesting EDS1-PAD4 regulate BAK1-mediated cell death signaling via a SA-independent manner (**Figure 7B**). In a recent report, it was shown that the major function of EDS1 and PAD4 in mediating ETI is SA-independent (Rietz et al., 2011). This study was in line with our results showing that *sid2* only partially suppressed the cell death of *bak1-3 bkk1-1* and that *eds1* or *pad4* further enhanced the suppression of cell death in *bak1-3 bkk1-1 sid2-3*.

Pathogen-derived effectors target key components mediating PTI in plant cell. FLS2, EFR, or CERK1 (CHITIN ELICITOR RECEPTOR KINASE 1) was shown to be the substrate of several effectors such as Pto, a kinase inhibitor, PtoB, a ubiquitin ligase, and HopAO1, a tyrosine phosphatase (Göhre et al., 2008; Xiang et al., 2008; Gimenez-Ibanez et al., 2009; Macho et al., 2014). The association between PRRs and effectors leads to dysfunction or degradation of PRRs, a strategy of pathogens to suppress plant immunity and enhance pathogenesis. BAK1, the co-receptor of several key PRRs, is also the target of several effectors, including PtoB, HopF2, an ADP-ribosyltransferase, and HopB1, a protease (Shan et al., 2008; Zhou et al., 2014; Li et al., 2016). It seems to be an efficient way for invading pathogens to attack a co-receptor in order to interrupt multiple PRR-mediated immune signalings. In our model, BAK1 and BKK1 may serve as guard proteins to surveil pathogen invasions. Depletion of BAK1 and BKK1 caused by effector attacks activates ETI, the stronger immunity featured by induction of cell death (HR), to enhance plant resistance to pathogens (**Figure 7C**).

In this study, we investigated the mechanism of how light functions as a primary factor in initiating cell death in *bak1 bkk1*. Our results supported light-induced overly expressed SA biosynthetic genes play a central role in this process. We also found key ETI components contribute to the cell death formation in *bak1 bkk1*. Future studies will focus on whether R proteins, the initiators of ETI signaling, function as downstream substrates of BAK1 and BKK1 and are engaged in the cell death induction in *bak1 bkk1*.

AUTHOR CONTRIBUTIONS

KH, JL, and YG designed the experiments. YG, YW, JD, YZ, DS, JZ, and SZ performed the experiments. KH and YG analyzed the data and wrote the manuscript.

ACKNOWLEDGMENTS

We thank Dr. Guojing Li for providing technical support for SA measurements, and the Arabidopsis Biological Resource Center for other seed stocks. These studies were supported by the grant from the National Natural Science Foundation of China to KH (31471305), the Ministry of Agriculture of the People's Republic of China (2016ZX08009-003-002), the Fundamental Research Funds for the Central Universities to KH (lzujbky-2016-75), and the grant from the National Natural Science Foundation of China to JL (31530005 and 31470380).

SUPPLEMENTARY MATERIAL

The Supplementary Material for this article can be found online at: http://journal.frontiersin.org/article/10.3389/fpls.2017.00622/full#supplementary-material

REFERENCES

Aarts, N., Metz, M., Holub, E., Staskawicz, B. J., Daniels, M. J., and Parker, J. E. (1998). Different requirements for EDS1 and NDR1 by disease resistance genes define at least two R gene-mediated signalling pathways in Arabidopsis. *Proc. Natl. Acad. Sci. U.S.A.* 95, 10306–10311. doi: 10.1073/pnas.95.17.10306

Albrecht, C., Russinova, E., Hecht, V., Baaijens, E., and de Vries, S. (2005). The *Arabidopsis thaliana* SOMATIC EMBRYOGENESIS RECEPTOR-LIKE KINASES1 and 2 control male sporogenesis. *Plant Cell* 17, 3337–3349. doi: 10.1105/tpc.105.036814

Bartsch, M., Gobbato, E., Bednarek, P., Debey, S., Schultze, J. L., Bautor, J., et al. (2006). Salicylic acid–independent ENHANCED DISEASE SUSCEPTIBILITY1

signaling in Arabidopsis immunity and cell death is regulated by the monooxygenase FMO1 and the nudix hydrolase NUDT7. *Plant Cell* 18, 1038–1051. doi: 10.1105/tpc.105.039982

Cannon, S. B., Zhu, H., Baumgarten, A. M., Spangler, R., May, G., Cook, D. R., et al. (2002). Diversity, distribution, and ancient taxonomic relationships within the TIR and non-TIR NBS-LRR resistance gene subfamilies. *J. Mol. Evol.* 54, 548–562 doi: 10.1007/s0023901-0057-2

Castillon, A., Shen, H., and Huq, E. (2007). Phytochrome interacting factors: central players in phytochrome-mediated light signalling networks. *Trends Plant Sci.* 12, 514–521. doi: 10.1016/j.tplants.2007.10.001

Chaouch, S., and Noctor, G. (2010). Myo-inositol abolishes salicylic acid-dependent cell death and pathogen defence responses triggered by peroxisomal hydrogen peroxide. *New Phytol.* 188, 711–718. doi: 10.1111/j.1469-8137.2010.03453.x

Chen, Z., Zheng, Z., Huang, J., Lai, Z., and Fan, B. (2009). Biosynthesis of salicylic acid in plants. *Plant Signal. Behav.* 4, 493–496. doi: 10.4161/psb.4.6.8392

Chinchilla, D., Zipfel, C., Robatzek, S., Kemmerling, B., Nurnberger, T., Jones, J. D. G., et al. (2007). A flagellin-induced complex of the receptor FLS2 and BAK1 initiates plant defence. *Nature* 448, 497–500. doi: 10.1038/nature05999

Clark, S. E., Williams, R. W., and Meyerowitz, E. M. (1997). The *CLAVATA1* gene encodes a putative receptor kinase that controls shoot and floral meristem size in Arabidopsis. *Cell* 89, 575–585. doi: 10.1016/S0092-8674(00)80239-1

Colcombet, J., Boisson-Dernier, A., Ros-Palau, R., Vera, C. E., and Schroeder, J. I. (2005). Arabidopsis SOMATIC EMBRYOGENESIS RECEPTOR KINASES1 and 2 are essential for tapetum development and microspore maturation. *Plant Cell* 17, 3350–3361. doi: 10.1105/tpc.105.036731

Dempsey, D. A., Vlot, A. C., Wildermuth, M. C., and Klessig, D. F. (2011). Salicylic acid biosynthesis and metabolism. *Arabidopsis Book* 9:e0156. doi: 10.1199/tab.0156

Dodds, P. N., and Rathjen, J. P. (2010). Plant immunity: towards an integrated view of plant-pathogen interactions. *Nat. Rev. Genet.*11, 539–548. doi: 10.1038/nrg2812

Du, J., Gao, Y., Zhan, Y., Zhang, S., Wu, Y., Xiao, Y., et al. (2016). Nucleocytoplasmic trafficking is essential for BAK1 and BKK1-mediated cell-death control. *Plant J.* 85, 520–531. doi: 10.1111/tpj.13125

Escobar-Restrepo, J.-M., Huck, N., Kessler, S., Gagliardini, V., Gheyselinck, J., Yang, W.-C., et al. (2007). The FERONIA receptor-like kinase mediates male-female interactions during pollen tube reception. *Science* 317, 656–660. doi: 10.1126/science.1143562

Gao, M., Wang, X., Wang, D., Xu, F., Ding, X., Zhang, Z., et al. (2009). Regulation of cell death and innate immunity by two receptor-like kinases in Arabidopsis. *Cell Host Microbe* 6, 34–44. doi: 10.1016/j.chom.2009.05.019

Garcion, C., Lohmann, A., Lamodière, E., Catinot, J., Buchala, A., Doermann, P., et al. (2008). Characterization and biological function of the *ISOCHORISMATE SYNTHASE2* gene of Arabidopsis. *Plant Physiol.* 147, 1279–1287. doi: 10.1104/pp.108.119420

Gimenez-Ibanez, S., Hann, D. R., Ntoukakis, V., Petutschnig, E., Lipka, V., and Rathjen, J. P. (2009). AvrPtoB targets the LysM receptor kinase CERK1 to promote bacterial virulence on plants. *Curr. Biol.* 19, 423–429. doi: 10.1016/j.cub.2009.01.054

Göhre, V., Spallek, T., Häweker, H., Mersmann, S., Mentzel, T., Boller, T., et al. (2008). Plant pattern-recognition receptor FLS2 is directed for degradation by the bacterial ubiquitin ligase AvrPtoB. *Curr. Biol.* 18, 1824–1832. doi: 10.1016/j.cub.2008.10.063

Gómez-Gómez, L., and Boller, T. (2000). FLS2: an LRR receptor–like kinase involved in the perception of the bacterial elicitor flagellin in Arabidopsis. *Mol. Cell* 5, 1003–1011. doi: 10.1016/S1097-2765(00)80265-8

Gou, X., He, K., Yang, H., Yuan, T., Lin, H., Clouse, S. D., et al. (2010). Genome-wide cloning and sequence analysis of leucine-rich repeat receptor-like protein kinase genes in *Arabidopsis thaliana*. *BMC Genomics* 11:19. doi: 10.1186/1471-2164-11-19

Gou, X., Yin, H., He, K., Du, J., Yi, J., Xu, S., et al. (2012). Genetic evidence for an indispensable role of somatic embryogenesis receptor kinases in brassinosteroid signalling. *PLoS Genet.* 8:e1002452. doi: 10.1371/journal.pgen.1002452

He, K., Gou, X., Powell, R. A., Yang, H., Yuan, T., Guo, Z., et al. (2008). Receptor-like protein kinases, BAK1 and BKK1, regulate a light-dependent cell-death control pathway. *Plant Signal. Behav.* 3, 813–815. doi: 10.4161/psb.3.10.5890

He, K., Gou, X., Yuan, T., Lin, H., Asami, T., Yoshida, S., et al. (2007). BAK1 and BKK1 regulate brassinosteroid-dependent growth and brassinosteroid-independent cell-death pathways. *Curr. Biol.* 17, 1109–1115. doi: 10.1016/j.cub.2007.05.036

Heese, A., Hann, D. R., Gimenez-Ibanez, S., Jones, A. M., He, K., Li, J., et al. (2007). The receptor-like kinase SERK3/BAK1 is a central regulator of innate immunity in plants. *Proc. Natl. Acad. Sci. U.S.A.* 104, 12217–12222. doi: 10.1073/pnas.0705306104

Huang, J., Gu, M., Lai, Z., Fan, B., Shi, K., Zhou, Y.-H., et al. (2010). Functional analysis of the Arabidopsis *PAL* gene family in plant growth, development, and response to environmental stress. *Plant Physiol.* 153, 1526–1538. doi: 10.1104/pp.110.157370

Jones, J. D., and Dangl, J. L. (2006). The plant immune system. *Nature* 444, 323–329. doi: 10.1038/nature05286

Karlova, R., Boeren, S., Russinova, E., Aker, J., Vervoort, J., and de Vries, S. (2006). The Arabidopsis SOMATIC EMBRYOGENESIS RECEPTOR-LIKE KINASE1 protein complex includes BRASSINOSTEROID-INSENSITIVE1. *Plant Cell* 18, 626–638. doi: 10.1105/tpc.105.039412

Kemmerling, B., Schwedt, A., Rodriguez, P., Mazzotta, S., Frank, M., Qamar, S. A., et al. (2007). The BRI1-associated kinase 1, BAK1, has a brassinolide-independent role in plant cell-death control. *Curr. Biol.* 17, 1116–1122. doi: 10.1016/j.cub.2007.05.046

Knepper, C., Savory, E. A., and Day, B. (2011). The role of NDR1 in pathogen perception and plant defense signalling. *Plant Signal. Behav.* 6, 1114–1116. doi: 10.4161/psb.6.8.15843

Li, J. (2010). Multi-tasking of somatic embryogenesis receptor-like protein kinases. *Curr. Opin. Plant. Biol.* 13, 509–514. doi: 10.1016/j.pbi.2010.09.004

Li, J., and Chory, J. (1997). A putative leucine-rich repeat receptor kinase involved in brassinosteroid signal transduction. *Cell* 90, 929–938. doi: 10.1016/S0092-8674(00)80357-8

Li, J., Wen, J., Lease, K. A., Doke, J. T., Tax, F. E., and Walker, J. C. (2002). BAK1, an Arabidopsis LRR receptor-like protein kinase, interacts with BRI1 and modulates brassinosteroid signalling. *Cell* 110, 213–222. doi: 10.1016/S0092-8674(02)00812-7

Li, L., Kim, P., Yu, L., Cai, G., Chen, S., Alfano, J. R., et al. (2016). Activation-dependent destruction of a co-receptor by a *Pseudomonas syringae* effector dampens plant immunity. *Cell Host Microbe* 20, 504–514. doi: 10.1016/j.chom.2016.09.007

Li, Y., Chen, L., Mu, J., and Zuo, J. (2013). LESION SIMULATING DISEASE1 interacts with catalases to regulate hypersensitive cell death in Arabidopsis. *Plant Physiol.* 163, 1059–1070. doi: 10.1104/pp.113.225805

Macho, A. P., and Zipfel, C. (2014). Plant PRRs and the activation of innate immune signalling. *Mol. Cell* 54, 263–272. doi: 10.1016/j.molcel.2014.03.028

Macho, A. P., Schwessinger, B., Ntoukakis, V., Brutus, A., Segonzac, C., Roy, S., et al. (2014). A bacterial tyrosine phosphatase inhibits plant pattern recognition receptor activation. *Science* 343, 1509. doi: 10.1126/science.1248849

Mauch-Mani, B., and Slusarenko, A. J. (1996). Production of salicylic acid precursors is a major function of phenylalanine ammonia-lyase in the resistance of Arabidopsis to *Peronospora parasitica*. *Plant Cell* 8, 203–212. doi: 10.1105/tpc.8.2.203

Métraux, J.-P. (2002). Recent breakthroughs in the study of salicylic acid biosynthesis. *Trends Plant Sci.* 7, 332–334. doi: 10.1016/S1360-1385(02)02313-0

Meyers, B. C., Dickerman, A. W., Michelmore, R. W., Sivaramakrishnan, S., Sobral, B. W., and Young, N. D. (1999). Plant disease resistance genes encode members of an ancient and diverse protein family within the nucleotide-binding superfamily. *Plant J.* 20, 317–332. doi: 10.1046/j.1365-313X.1999.t01-1-00606.x

Nam, K. H., and Li, J. (2002). BRI1/BAK1, a receptor kinase pair mediating brassinosteroid signalling. *Cell* 110, 203–212. doi: 10.1016/S0092-8674(02)00814-0

Nawkar, G. M., Maibam, P., Park, J. H., Sahi, V. P., Lee, S. Y., and Kang, C. H. (2013). UV-induced cell death in plants. *Int. J. Mol. Sci.* 14, 1608–1628. doi: 10.3390/ijms14011608

Nawrath, C., Heck, S., Parinthawong, N., and Métraux, J.-P. (2002). EDS5, an essential component of salicylic acid–dependent signalling for disease resistance in Arabidopsis, is a member of the MATE transporter family. *Plant Cell* 14, 275–286. doi: 10.1105/tpc.010376

Nawrath, C., and Métraux, J. P. (1999). Salicylic acid induction-deficient mutants of Arabidopsis express *PR-2* and *PR-5* and accumulate high levels of camalexin after pathogen inoculation. *Plant Cell* 11, 1393–1404. doi: 10.2307/3870970

Pedmale, U. V., Huang, S.-S., Zander, M., Cole, B. J., Hetzel, J., Ljung, K., et al. (2016). Cryptochromes interact directly with PIFs to control plant growth in limiting blue light. *Cell* 164, 233–245. doi: 10.1016/j.cell.2015.12.018

Rasmussen, M. W., Roux, M., Petersen, M., and Mundy, J. (2012). MAP kinase cascades in Arabidopsis innate immunity. *Front. Plant Sci.* 3:169. doi: 10.3389/fpls.2012.00169

Rietz, S., Stamm, A., Malonek, S., Wagner, S., Becker, D., Medina-Escobar, N., et al. (2011). Different roles of Enhanced Disease Susceptibility1 (EDS1) bound to and dissociated from Phytoalexin Deficient4 (PAD4) in Arabidopsis immunity. *New Phytol.* 191, 107–119. doi: 10.1111/j.1469-8137.2011.03675.x

Rogers, E. E., and Ausubel, F. M. (1997). Arabidopsis enhanced disease susceptibility mutants exhibit enhanced susceptibility to several bacterial pathogens and alterations in *PR-1* gene expression. *Plant Cell* 9, 305–316. doi: 10.1105/tpc.9.3.305

Roux, M., Schwessinger, B., Albrecht, C., Chinchilla, D., Jones, A., Holton, N., et al. (2011). The Arabidopsis leucine-rich repeat receptor–like kinases BAK1/SERK3 and BKK1/SERK4 are required for innate immunity to hemibiotrophic and biotrophic pathogens. *Plant Cell* 23, 2440–2455. doi: 10.1105/tpc.111.084301

Schmidt, E. D., Guzzo, F., Toonen, M. A., and de Vries, S. C. (1997). A leucine-rich repeat containing receptor-like kinase marks somatic plant cells competent to form embryos. *Development* 124, 2049–2062.

Schulze, B., Mentzel, T., Jehle, A. K., Mueller, K., Beeler, S., Boller, T., et al. (2010). Rapid heteromerization and phosphorylation of ligand-activated plant transmembrane receptors and their associated kinase BAK1. *J. Biol. Chem.* 285, 9444–9451. doi: 10.1074/jbc.M109.096842

Schwessinger, B., Roux, M., Kadota, Y., Ntoukakis, V., Sklenar, J., Jones, A., et al. (2011). Phosphorylation-dependent differential regulation of plant growth, cell death, and innate immunity by the regulatory receptor-like kinase BAK1. *PLoS Genet.* 7:e1002046. doi: 10.1371/journal.pgen.1002046

Serrano, M., Wang, B., Aryal, B., Garcion, C., Abou-Mansour, E., Heck, S., et al. (2013). Export of salicylic acid from the chloroplast requires the multidrug and toxin extrusion-like transporter EDS5. *Plant Physiol.* 162, 1815–1821. doi: 10.1104/pp.113.218156

Shan, L., He, P., Li, J., Heese, A., Peck, S. C., Nürnberger, T., et al. (2008). Bacterial effectors target the common signalling partner BAK1 to disrupt multiple MAMP receptor-signalling complexes and impede plant immunity. *Cell Host Microbe* 4, 17–27. doi: 10.1016/j.chom.2008.05.017

Shpak, E. D., McAbee, J. M., Pillitteri, L. J., and Torii, K. U. (2005). Stomatal patterning and differentiation by synergistic interactions of receptor kinases. *Science* 309, 290–293. doi: 10.1126/science.1109710

Szechyńska-Hebda, M., and Karpiński, S. (2013). Light intensity-dependent retrograde signalling in higher plants. *J. Plant Physiol.* 170, 1501–1516. doi: 10.1016/j.jplph.2013.06.005

Torres, M. A., Jones, J. D. G., and Dangl, J. L. (2006). Reactive oxygen species signalling in response to pathogens. *Plant Physiol.* 141, 373–378. doi: 10.1104/pp.106.079467

Tsuda, K., Mine, A., Bethke, G., Igarashi, D., Botanga, C. J., Tsuda, Y., et al. (2013). Dual regulation of gene expression mediated by extended MAPK activation and salicylic acid contributes to robust innate immunity in *Arabidopsis thaliana*. *PLoS Genet.* 9:e1004015. doi: 10.1371/journal.pgen.1004015

Vlot, A. C., Dempsey, D. A., and Klessig, D. F. (2009). Salicylic acid, a multifaceted hormone to combat disease. *Annu. Rev. Phytopathol.* 47, 177–206. doi: 10.1146/annurev.phyto.050908.135202

Wang, Z., Meng, P., Zhang, X., Ren, D., and Yang, S. (2011). BON1 interacts with the protein kinases BIR1 and BAK1 in modulation of temperature-dependent plant growth and cell death in Arabidopsis. *Plant J.* 67, 1081–1093. doi: 10.1111/j.1365-313X.2011.04659.x

Wiermer, M., Feys, B. J., and Parker, J. E. (2005). Plant immunity: the EDS1 regulatory node. *Curr. Opin. Plant. Biol.* 8, 383–389. doi: 10.1016/j.pbi.2005.05.010

Wildermuth, M. C., Dewdney, J., Wu, G., and Ausubel, F. M. (2001). Isochorismate synthase is required to synthesize salicylic acid for plant defence. *Nature* 414, 562–565. doi: 10.1038/35107108

Xiang, T., Zong, N., Zou, Y., Wu, Y., Zhang, J., Xing, W., et al. (2008). Pseudomonas syringae effector AvrPto blocks innate immunity by targeting receptor kinases. *Curr. Biol.* 18, 74–80. doi: 10.1016/j.cub.2007.12.020

Yamada, K., Yamashita-Yamada, M., Hirase, T., Fujiwara, T., Tsuda, K., Hiruma, K., et al. (2016). Danger peptide receptor signaling in plants ensures basal immunity upon pathogen-induced depletion of BAK1. *EMBO J.* 35, 46–61. doi: 10.15252/embj.201591807

Yang, S., Yang, H., Grisafi, P., Sanchatjate, S., Fink, G. R., Sun, Q., et al. (2006). The *BON/CPN* gene family represses cell death and promotes cell growth in Arabidopsis. *Plant J.* 45, 166–179. doi: 10.1111/j.1365-313X.2005.02585.x

Zhao, D.-Z., Wang, G.-F., Speal, B., and Ma, H. (2002). The *EXCESS MICROSPOROCYTES1* gene encodes a putative leucine-rich repeat receptor protein kinase that controls somatic and reproductive cell fates in the Arabidopsis anther. *Genes Dev.* 16, 2021–2031. doi: 10.1101/gad.997902

Zhou, J., Wu, S., Chen, X., Liu, C., Sheen, J., Shan, L., et al. (2014). *Pseudomonas syringae* effector HopF2 suppresses Arabidopsis immunity by targeting BAK1. *Plant J.* 77, 235–245. doi: 10.1111/tpj.12381

Zipfel, C., Kunze, G., Chinchilla, D., Caniard, A., Jones, J. D., Boller, T., et al. (2006). Perception of the bacterial PAMP EF-Tu by the receptor EFR restricts Agrobacterium-mediated transformation. *Cell* 125, 749–760. doi: 10.1016/j.cell.2006.03.037

Conflict of Interest Statement: The authors declare that the research was conducted in the absence of any commercial or financial relationships that could be construed as a potential conflict of interest.

Advantages of publishing in Frontiers

OPEN ACCESS
Articles are free to read for greatest visibility and readership

FAST PUBLICATION
Around 90 days from submission to decision

HIGH QUALITY PEER-REVIEW
Rigorous, collaborative, and constructive peer-review

TRANSPARENT PEER-REVIEW
Editors and reviewers acknowledged by name on published articles

Frontiers
Avenue du Tribunal-Fédéral 34
1005 Lausanne | Switzerland

Visit us: www.frontiersin.org
Contact us: info@frontiersin.org | +41 21 510 17 00

REPRODUCIBILITY OF RESEARCH
Support open data and methods to enhance research reproducibility

DIGITAL PUBLISHING
Articles designed for optimal readership across devices

FOLLOW US
@frontiersin

IMPACT METRICS
Advanced article metrics track visibility across digital media

EXTENSIVE PROMOTION
Marketing and promotion of impactful research

LOOP RESEARCH NETWORK
Our network increases your article's readership